Design and synthesis of novel dual GSK3β/p38α MAPK inhibitors and their optimization towards GSK3β selectivity

Dissertation

der Mathematisch-Naturwissenschaftlichen Fakultät

der Eberhard Karls Universität Tübingen

zur Erlangung des Grades eines

Doktors der Naturwissenschaften

(Dr. rer. nat.)

vorgelegt von

Fabian Andreas Heider

aus Langenfeld (Rhld.)

Tübingen

2019

Gedruckt mit Genehmigung der Mathematisch-Naturwissenschaftlichen Fakultät der Eberhard Karls Universität Tübingen.

Tag der mündlichen Qualifikation: 05.07.2019

Dekan: Prof. Dr. Wolfgang Rosenstiel

1. Berichterstatter: Prof. Dr. Pierre Koch

2. Berichterstatter: Prof. Dr. Stefan A. Laufer

Meinen Eltern für ihre

immerwährende Unterstützung

„Il semble que la perfection soit atteinte non quand il n'y a plus rien à ajouter,

mais quand il n'y a plus rien à retrencher.“

(*It seems that perfection is attained not when there is nothing more to add, but when there is nothing more to remove.*)

- Antoine de Saint-Exupéry (1900 - 1944)

Acknowledgments

First and foremost, I want to thank my advisor Prof. Dr. Pierre Koch for giving me the opportunity to work independently on this project and for his supervision, support and guidance in the course of my doctoral studies.

I am equally grateful to Prof. Dr. Stefan A. Laufer for accepting me as a PhD student, for his scientific guidance and the financial support of the project. Also, I thank him for being the second examiner of this thesis.

Additionally, I would like to thank Prof. Dr. Frank M. Boeckler for the constructive and pleasant working atmosphere on the eighth floor and his readiness to help with suggestions, comments and the allocation of resources.

Furthermore, I want to thank both Prof. Dr. Harald Groß and Prof. Dr. Frank M. Boeckler for their participation as examiners in my thesis defense.

I am very grateful for Dr. Ahmed El-Gokha's mentorship and guidance in the first period of my PhD and for spreading good mood in the lab.

I want to thank Dr. Francesco Ansideri for our deep scientific discussions during coffee breaks, for being a great and always helpful labmate and his patience and passion for enzymatic assays.

I would like to express my gratitude to Stanislav Andreev for being a great colleague in the GSK3 project, for keeping his humour in every situation and for his kind and helpful nature.

Naturally, I want to thank everyone else involved in the AK Koch: Dr. Michael Eitel for bringing music, fun (and food) to the office/lab and Catharina Sessler for her valuable assistance with the compound management system and her contagious optimism.

I would like to thank Prof. Dr. Antti Poso, Dr. Roberta Tesch and Dr. Tatu Pantsar for their efforts in the molecular modelling and computational docking studies and the fruitful collaboration. Dr. Roberta Tesch is also acknowledged for her attempts on the co-crystallization of my compounds with GSK3β.

I owe many thanks to all current and former members of the AK Boeckler: Dr. Markus Zimmermann, Dr. Andreas Lange, Marcel Dammann, Sebastian Vaas, Marc Engelhardt, Erdem Veyisoglu and Susanne Hennig for making the eighth floor a great place to work. A special thanks goes to Dr. Johannes Heidrich for helping me several times with various problems, to Dr. Christoph Ernst for his assistance with certain purification methods and to Fabio Kipp for his sense of humour and for the entertaining last weeks in the lab.

My appreciation goes to all present and former colleagues of the AK Laufer for the constructive working atmosphere, their assistance and support in the use of laboratory equipment and the interesting scientific exchange: Dr. Matthias Gehringer, Dr. Michael Forster, Dr. Niklas Walter, Dr. Michael Juchum, Dr. Marcel Günther, Dr. Ellen Pfaffenrot, Dr. Silke Bauer, Dr. Fernando R. De Sá Alves, Dr. Ida D'Orazio, Dr. Heike Wentsch-Teltschik, Dr. Felix Muth, Dr. Roland Selig, Eva Döring, Bent Praefke, Juliander Reiner, Dirk Flötgen, Philip Kloevekorn, Theresa Kircher, Vanessa Haller, Teodor Dimitrov, Gregor Schmidberger and Florian Wittlinger. In particular, I would like to thank Mark Kudolo for his thoughtful opinions on many subjects and Gernot-Sebastian Haase for his support throughout the years and the entertaining stories.

I also gratefully acknowledge Katharina Bauer, Daniela Müller, Jens Strobach and Mark Kudolo for testing my compounds in various assays. I would also like to thank Eva Döring and Mark Kudolo for the performance of metabolism experiments with human liver microsomes. Moreover, I deeply appreciate the commitment of Gerd Helms towards the NMR spectrometers and his kind-hearted attitude.

I very much appreciate the assistance of Dr. Raimund Nieß and Kristine Schmidt with any organizational and bureaucratic matter.

I would like to thank Mechtild Seyboldt and Birgit Kailer for taking care with numerous shipments of chemicals and other deliveries.

Moreover, I would like to thank all my long- and short-term students and interns for their assistance in laboratory – especially Urs Haun whose master thesis was co-supervised by me.

A special thanks goes to Alexander Witte for the diverse distractions outside of the lab as well as to all my lifelong friends from the places I called "home" over the years. Without your support, this thesis would not have been possible.

I would like to express my deepest gratitude to my loving, encouraging and patient girlfriend Valeria whose faithful support at all stages of this doctoral thesis is much appreciated.

Finally, I would like to thank my parents and my brother for their constant and unconditional support in all my pursuits and their encouragement throughout my whole life.

Abstract / Summary of the thesis

Abberrant activity of glycogen synthase kinase 3β (GSK3β) has been implicated in the pathogenesis of neurodegenerative diseases like Alzheimer's disease (AD). On top of that, the kinase has been linked to a plethora of other pathological conditions like cancer, diabetes, bipolar disorders, schizophrenia and osteoporosis. The main aim of this thesis was the design and synthesis of novel GSK3β inhibitors exerting a possible positive effect on a variety of neurodegenerative diseases. As a secondary objective, the synthesis of dual targeting GSK3β/p38α mitogen-activated protein kinase (MAPK) inhibitors was pursued. The p38α MAPK is involved in proinflammatory processes and has therefore also emerged as a potential target for the treatment of neurodegenerative diseases. Inhibition of both kinases may have synergistic beneficial effects on the progression of many neurodegenerative diseases due to the pivotal impact of the two enzymes on the underlying disease mechanism and neuroinflammation. The first project of this thesis consisted of the optimization of a Tofacitinib-derived high throughput screening hit against GSK3β. Starting from the hit scaffold, a variety of more flexible derivatives were synthesized and investigated for their ability to inhibit the target kinase. In a second approach, dual GSK3β/p38α MAPK inhibiting pyridinylimidazole-based screening hits were optimized towards their inhibitory balance, metabolic stability and CNS penetration. The best dual inhibitor of the series inhibited GSK3β and p38α MAPK in the low double digit nanomolar range with a GSK3β/p38α MAPK ratio of 2.2 and displayed metabolic stability in human liver microsomes as well as modest CNS penetration in a mouse model. In the final project of this thesis, the obtained dual inhibitors were further optimized with the aim to shift the selectivity completely towards GSK3β. Different substituents at the imidazole-C2 and -C4 positions led to several inhibitors in the low single digit nanomolar range with an exquisite selectivity over p38α MAPK. Moreover, the inhibitors showed an excellent metabolic stability in human liver microsomes and a good overall kinome-selectivity in a diverse panel of 56 kinases. The in the course of this doctoral thesis prepared compounds can be used for further studying the direct influence of the two kinases on neurodegenerative diseases like AD.

Zusammenfassung

Fehlgeleitete Aktivität der Glykogensynthase-Kinase 3β (GSK3β) wurde in den letzten Jahren oft in Verbindung mit der Pathogenese von neurodegenerativen Erkrankungen wie Morbus Alzheimer (AD) gebracht. Auch an der Entstehung von weiteren schwerwiegenden Krankheiten wie Krebs, Diabetes mellitus, bipolaren Störungen, Schizophrenie und Osteoporose scheint die Kinase beteiligt zu sein. Ziel dieser Arbeit war das Design und die Synthese neuartiger GSK3β Inhibitoren mit möglichen positiven Effekten auf eine Reihe neurodegenerativer Erkrankungen. Des Weiteren wurde die Synthese dualer GSK3β/p38α Mitogen-aktivierte Protein Kinase (MAPK) Inhibitoren verfolgt. Die p38α MAPK ist an einer Reihe von proinflammatorischen Prozessen beteiligt und bietet sich daher als ein potentielles Target für die Behandlung neurodegenerativer Erkrankungen an. Die Hemmung beider Kinasen verspricht synergistische, positive Effekte bei einer Reihe von neurodegenerativen Erkrankungen, insbesondere AD, da beide Kinasen tief in die zugrundeliegenden Mechanismen dieser Erkrankungen eingreifen. Das erste Projekt dieser Arbeit bestand aus der Optimierung einer von Tofacitinib abgeleiteten Leitstruktur, welche in einem Hochdurchsatz-Screening gegen GSK3β identifiziert wurde. Ausgehend von dieser Struktur wurde eine Reihe von flexibleren Derivaten synthetisiert, welche dann auf ihre biologische Aktivität getestet wurden. Aus dem gleichen Screening wurden duale GSK3β/p38α MAPK Pyridinylimidazol-basierte Hemmstoffe identifiziert und im Hinblick auf ihre inhibitorische Balance, metabolische Stabilität und ZNS-Gängigkeit optimiert. Der beste duale Inhibitor dieser Serie hemmte GSK3β und p38α MAPK im niedrigen nanomolaren Bereich mit einem GSK3β/p38α MAPK Verhältnis von 2,2. Außerdem war der Inhibitor metabolisch stabil nach Inkubation mit humanen Lebermikrosomen und zeigte eine moderate ZNS-Penetration im Mausmodell. Im finalen Projekt dieser Arbeit, wurden die erhaltenen dualen Inhibitoren weiter optimiert und die Selektivität wurde in Richtung GSK3β verschoben. Austausch am Imidazol-C2 und -C4 führte zu mehreren Inhibitoren im einstellig nanomolaren Bereich mit sehr guter Selektivität gegenüber p38α MAPK. Die Verbindungen zeigten wieder eine exzellente metabolische Stabilität und eine gute Kinomselektivität in einem Panel von 56 Kinasen. Die im Rahmen dieser Arbeit hergestellten Verbindungen ermöglichen es den Einfluss der beiden Kinasen auf neurodegenerative Erkrankungen wie AD weiter zu erforschen.

Table of contents

List of abbreviations

AD	Alzheimer’s disease
ALK	Anaplastic lymphoma kinase
ALS	Amyotrophic lateral sclerosis
APC	Adenomatosis polyposis coli
APP	Amyloid precursor protein
ATP	Adenosine triphosphate
BBB	Blood–brain barrier
Boc	*tert*-Butyloxycarbonyl
BTK	Bruton's tyrosine kinase
$CDCl_3$	Deuterated chloroform
CDK	Cyclin-dependent kinase
CK	Casein kinase
CNS	Central nervous system
CTE	Chronic traumatic encephalopathy
CYP	Cytochrome P450
DCC	*N,N'*-Dicyclohexylcarbodiimide
DIPEA	*N,N*-Diisopropylethylamine (= Hünig's base)
EGFR	Epidermal growth factor receptor
ELISA	Enzyme-linked immunosorbent assay
EMA	European Medicines Agency
ERK	Extracellular signal–regulated kinase
ESI	Electrospray ionization
FDA	(United States) Food and Drug Administration
GS	Glycogen synthase
GSK3	Glycogen synthase kinase 3
HD	Huntington’s disease
HLM	Human liver microsomes
HR	Hydrophobic region
HTS	High-throughput screening

IL	Interleukin
IRS	Insulin receptor substrate
JAK	Janus kinase
JNK3	c-Jun N-terminal kinase 3
LiHMDS	Lithium hexamethyldisilazide
MAPK	Mitogen-activated protein kinase
NBS	*N*-Bromosuccinimide
NFTs	Neurofibrillary tangles
NSCLC	Non-Small Cell Lung Cancer
PD	Parkinson's disease
$Pd_2(dba)_3$	Tris(dibenzylideneacetone)dipalladium(0)
$Pd(dppf)Cl_2 \cdot DCM$	[1,1′-Bis(diphenylphosphino)ferrocene]dichloro-palladium(II) in complex with dichloromethane
PHF	Paired helical filaments
PI3K	Phosphoinositide 3-kinase
PKB	Protein kinase B (also known as AKT)
PP2A	Protein phosphatase 2A
PS-1	Presenilin-1
PSP	Progressive supranuclear palsy
PyBOP	(Benzotriazol-1-yloxy)tripyrrolidinophosphonium hexafluorophosphate
SAR	Structure-activity relationship
S_NAr	Nucleophilic aromatic substitution
τ protein	Microtubule-associated protein tau
TFA	Trifluoroacetic acid
THP	Tetrahydropyran
TNF	Tumor necrosis factor
Tos	Toluenesulfonyl
XantPhos	4,5-Bis(diphenylphosphino)-9,9-dimethylxanthene
XPhos	2-Dicyclohexylphosphino-2′,4′,6′-triisopropylbiphenyl

List of publications

Publication I

Heider, F.; Haun, U.; Döring, E.; Kudolo, M.; Sessler, C.; Albrecht, W.; Laufer, S.; Koch, P. – From 2-Alkylsulfanylimidazoles to 2-Alkylimidazoles: An Approach towards Metabolically More Stable p38α MAP Kinase Inhibitors. *Molecules* **2017**, *22* (10), 1729.

Publication II

Heider, F.; Ansideri, F.; Tesch, R.; Pantsar, T.; Haun, U.; Döring, E.; Kudolo, M.; Poso, A.; Albrecht, W.; Laufer, S. A.; Koch, P. – Pyridinylimidazoles as dual glycogen synthase kinase 3β/p38α mitogen-activated protein kinase inhibitors. *European Journal of Medicinal Chemistry* **2019**, *175*, 309-329.

Publication III

Heider, F.; Pantsar, T.; Kudolo M.; Ansideri, F.; De Simone, A.; Andrisano, V.; Pruccoli, L.; Schneider, T.; Goettert, M.; Tarozzi, A.; Laufer, S.; Koch, P. – Pyridinylimidazoles as GSK3β Inhibitors: The Impact of Tautomerism on Compound Activity via Water Networks. *ACS Medicinal Chemistry Letters*, **2019**, *10*, 1407-1414.

Author contributions

Publication I

From 2-Alkylsulfanylimidazoles to 2-Alkylimidazoles: An Approach towards Metabolically More Stable p38α MAP Kinase Inhibitors

Fabian Heider

- Design of the experiments and synthesis planning
- Supervision of the synthetic efforts
- Interpretation of the biological and metabolism data
- Writing of the manuscript and the supporting information

Urs Haun

- Synthesis of the compounds

Eva Döring

- Planning and execution of the human liver microsomes metabolism experiments

Mark Kudolo

- Performance of the p38α MAPK ELISA assay

Catharina Sessler

- Conducting the fluorescence polarization assay for p38α MAPK

Dr. Wolfgang Albrecht

- Scientific support of the project

Prof. Dr. Stefan Laufer

- Scientific support of the project
- Coordination and supervision of the p38α ELISA assay performance as well as the metabolism experiments

Prof. Dr. Pierre Koch

- Generation, coordination and financing of the project
- Writing of the manuscript
- Final approval of the manuscript

Publication II

Pyridinylimidazoles as dual Glycogen Synthase Kinase 3β/p38α Mitogen-activated Protein Kinase Inhibitors

Fabian Heider

- Design of the experiments
- Synthesis of the majority of compounds (82 %)
- Supervision of the synthesis of the remaining compounds
- Interpretation of the biological and metabolism data
- Writing of the manuscript and the supporting information

Dr. Francesco Ansideri

- Performance of the GSK3α/β ADP Glo assay

Dr. Roberta Tesch

- Performance of the majority of docking/computational experiments (75 %)
- Creation of the majority of figures

Dr. Tatu Pantsar

- Performance of some docking/computational experiments (25 %)
- Adjustments of some figures
- Design and preparation of the table of contents graphic
- Writing of the experimental part in regard to computational methods
- Proofreading of the manuscript

Urs Haun

- Synthesis of some compounds (18 %)

Eva Döring

- Planning and execution of the human liver microsomes metabolism experiments

Mark Kudolo

- Performance of ADP-Glo assay to characterize the inhibitors as ATP-competitive

Prof. Dr. Antti Poso

- Coordination and supervision of the docking/computational experiments

Dr. Wolfgang Albrecht

- Scientific support of the project

Prof. Dr. Stefan Laufer

- Scientific support of the project
- Coordination and supervision of the p38α MAPK ELISA assay performance

Prof. Dr. Pierre Koch

- Generation, coordination and financing of the project
- Writing of the manuscript
- Final approval of the manuscript

Publication III

Pyridinylimidazoles as GSK3β Inhibitors: The Impact of Tautomerism on Compound Activity via Water Networks

Fabian Heider

- Design of the experiments
- Synthesis of the compounds
- Interpretation of the biological and metabolism data
- Writing of the manuscript and the supporting information

Dr. Tatu Pantsar

- Performance of the docking/computational experiments
- Proofreading of the manuscript
- Writing of the manuscript

Mark Kudolo

- Planning and execution of the human liver microsomes metabolism experiments

Dr. Francesco Ansideri

- Performance of the GSK3α/β ADP Glo assay

Dr. Angela De Simone

- Performance of the ESI-QTOF GSK3β assay

Dr. Letizia Pruccoli

- Performance of the neuronal cell assay

Dr. Taiane Schneider

- Performance of the cell viability assays

Prof. Dr. Marcia Goettert

- Coordination and supervision of the cell viability assay perfomance

Prof. Dr. Andrea Tarozzi

- Coordination and supervision of the neuronal cell assay perfomance

Prof. Dr. Vincenza Andrisano

- Coordination and supervision of the ESI-QTOF GSK3β assay perfomance

Prof. Dr. Stefan Laufer

- Scientific support of the project
- Coordination and supervision of the p38α MAPK ADP Glo assay performance

Prof. Dr. Pierre Koch

- Generation, coordination and financing of the project
- Writing of the manuscript
- Final approval of the manuscript

1 Introduction

1.1 Alzheimer's disease

In November 1906, the German psychiatrist Alois Alzheimer presented his talk "Über eine eigenartige Erkrankung der Hirnrinde" ("About a peculiar disease of the cerebral cortex") at a conference in Tübingen.[1] His presentation included a detailed description of the observations he made during the examination of his patient Auguste Deter. The 51-year-old woman suffered, among other symptoms, from memory impairment, confusion and sleep disorders. Her mental state deteriorated quickly and after her death, Alzheimer was able to investigate her brain meticulously. The autopsy revealed histological anomalies we know today as amyloid plaques and neurofibrillary tangles. In 1910 this pathological condition was termed Alzheimer's disease (AD) and today the disease still presents one of the major medical challenges of the 21st century. AD is the most common form of dementia accounting for roughly 60% of all cases worldwide.[2] Other important forms of dementia include vascular (~30%), Lewy body or frontotemporal dementia. The number of patients affected by any of these diseases is expected to rise constantly, from 50 million in 2018 to an estimated number of 150 million by 2050.[3] AD not only causes dreadful human suffering but also significant economic damage in the range of 1 trillion US dollars per year. Although the disease was discovered more than 110 years ago, today's treatment options can only be described as insufficent. Currently, there are just four chemical entities with two different modes of action approved by the FDA to treat AD. Donepezil (*Aricept*®), galantamine (*Razadyne*®) and rivastigmine (*Exelon*®) work as cholinesterase inhibitors thereby increasing the concentration of acetylcholine in the synaptic cleft. Since many symptoms of AD are related to a deficiency in the cholinergic transmission resulting from neuronal cell death, a cholinergic drug is able to briefly delay or attenuate symptoms. Memantine (*Namenda*®) is a NMDA receptor antagonist able to slow the clinical progression of AD in some patients for up to six months.[4] While a modulating effect on the dysbalanced glutamatergic system is postulated for memantine, its exact mechanism of action remains subject of scientific discussions.[5] Besides that, there are no more drugs available which in part is a result of the still poor understanding of the pathophysiology of AD.

In 1984 researchers identified the amyloid beta (Aβ) peptide as a main actor in the development of the disease.[6] Two years later, hyperphosphorylation of the microtubule-associated protein tau (τ protein) in AD patients was discovered.[7] These findings were the basis for the amyloid cascade hypothesis which implies that the deposition of Aβ plaques in the brain is a key event in the pathogenesis of AD, leading to neurofibrillary tangles, neuronal cell death and eventually dementia.[8]

In short, Aβ plaques are the result of the enzymatic processing of an integral membrane glycoprotein called amyloid precursor protein (APP). There are two different possible pathways for the degradation of APP: the amyloidogenic or the non-amyloidogenic pathway (*Figure 1.1*). In the non-amyloidogenic pathway, APP is cleaved by the aspartic protease α-secretase and subsequently by γ-secretase to give soluble p3 peptides. However, in the amyloidogenic pathway, β-secretase cuts APP into the soluble ectodomain sAPPβ and the c-terminal fragment CTFβ/C99. Cleavage of this fragment by γ-secretase leads to Aβ peptides of different lengths.[9] The longer $A\beta_{42}$ is perceived as the most amyloidogenic form, but $A\beta_{40}$ is also found in senile plaques. Once Aβ peptides start to accumulate extracellularly, they tend to form small, still soluble aggregates called Aβ oligomers. Nowadays these Aβ oligomers are recognized as the most neurotoxic form of Aβ.[10]

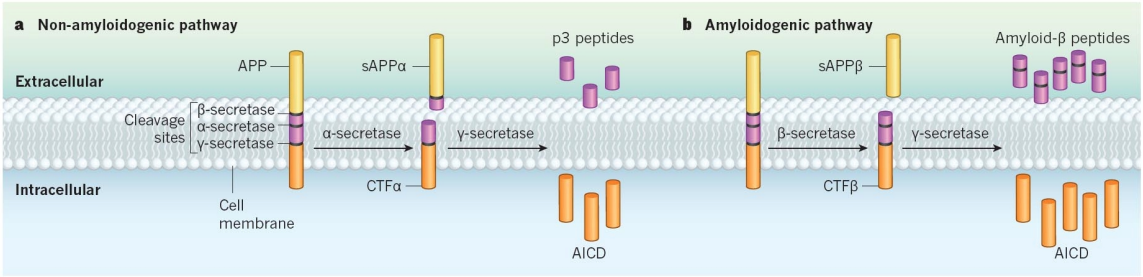

Figure 1.1. The non-amyloidogenic and amyloidogenic pathway according to CANTER, PENNEY AND TSAI. Reprinted by permission from Springer Nature,[9] Copyright (2016).

Gradual deposition of Aβ oligomers and the formation of solid plaques impairs synaptic functions and slowly leads to neuroinflammatory processes causing changes in kinase/phosphatase activities and oxidative stress (*Figure 1.3*).[11] Experimental evidence indicates that Aβ accumulation induces the formation of another hallmark of AD: neurofibrillary tangles (NFTs).[12,13] NFTs are aggregates of hyperphosphorylated τ protein. There are many more neurodegenerative diseases (referred to as “tauopathies”)

whose common feature is the accumulation of τ proteins in the brain, e.g. chronic traumatic encephalopathy (CTE), Pick's disease or progressive supranuclear palsy (PSP). All tauopathies share the pathogenic role of altered τ protein but the extent and localization varies and the underlying factors in the development of the diseases are not understood, yet.[14] In healthy individuals, τ proteins are responsible for the assembly and stability of neuronal microtubules. Abnormal phosphorylation through kinases like glycogen synthase kinase 3β (GSK3β), cyclin-dependent kinase (CDK) 5 and mitogen-activated protein kinases (MAPKs) inhibits microtubule assembly activity and prompts self-association of τ proteins into paired helical filaments (PHF).[15] These PHF grow over time to give polymerized NFTs and the lack of available soluble τ protein leads to disintegration of microtubules and axonal degeneration. Additionally, some forms of aberrant τ proteins (hyperphosphorylated, oligomeric or aggregated) may have toxic effects similar to Aβ but the exact molecular mechanism of toxicity caused by those abnormal τ species has not been elucidated, yet.[16] It has been postulated for instance that intermediate τ aggregates represent the most cytotoxic form and that insoluble PHF might be merely the product of a neuronal detoxification process.[17] Following this line of argumentation, the observed tangles might be the result of damage already dealt and not necessarily the driver of neuronal cell death.

This example shows the difficulties of investigating whether a causal link exists between the development of AD and certain histological anomalies in the brain and how challenging it is to validate an AD drug target given the number of cellular processes that are only poorly understood.

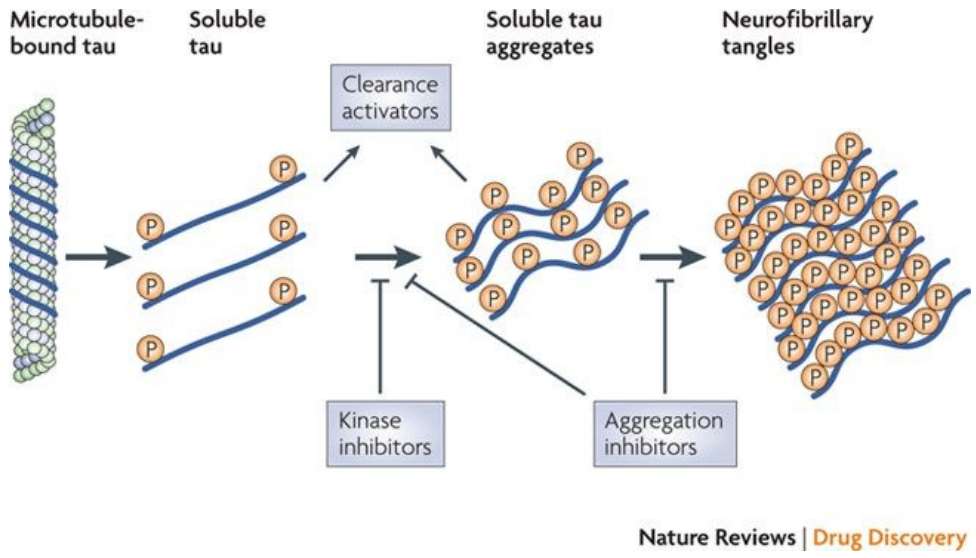

Figure 1.2. Tau pathology and possible intervention sites according to CITRON. Reprinted by permission from Springer Nature,[18] Copyright (2010).

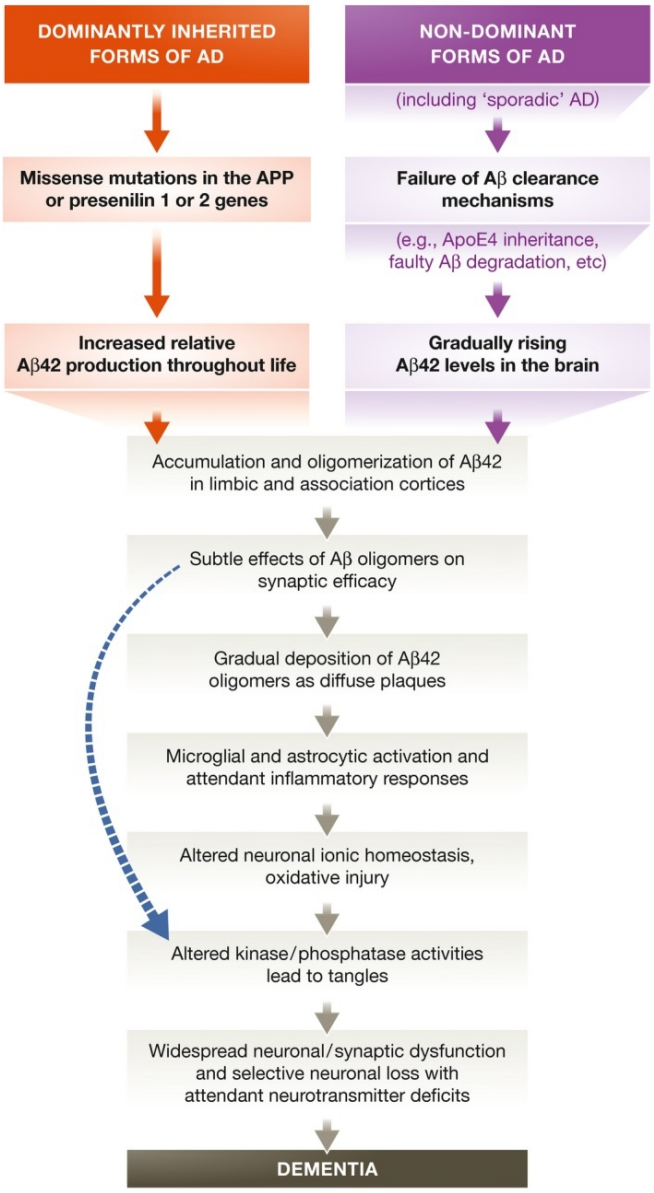

Figure 1.3. "The sequence of major pathogenic events leading to AD proposed by the amyloid cascade hypothesis" by SELKOE AND HARDY is licensed under CC BY 4.0.[11] This depiction provides an overview of neuronal events in the pathogenesis of AD, ultimately leading to dementia.

One of the less controversial statements about the pathogenesis of AD, is that the pathophysiological transformations in the brain start many years prior to a clinical manifestation.[19] This observation has direct consequences for any therapeutic approach. On the one hand it underlines the urgent need for early biomarkers enabling the detection of patients prior to developing symptoms and on the other hand it might mean that treatment is already needed years before any memory loss is perceived. Therefore, any new drug will be chronically administered for many years, making a favorable risk–benefit ratio with few side-effects an inevitable need for new pharmaceuticals.

1.2 Protein Kinases

1.2.1 The human kinome

Protein kinases are enzymes catalyzing the transfer of a γ-phosphate group from a nucleoside triphosphate to a substrate. Phosphorylation is the most common post-translational modification of proteins[20] but the list of possible substrates also contains lipids, sugars and nucleosides.[21] The direct antagonists of kinases are phosphatases which catalyze the opposite reaction, the hydrolysis of a phosphoester bond thereby removing the phosphate moiety from the substrate.[22] In living cells, a finely tuned system of phosphorylation and dephosphorylation is involved in almost every cellular signaling pathway. Kinases are therefore essential for the maintenance and regulation of many important cellular processes. Unsurprisingly, aberrant kinase activity has been linked to severe diseases like cancer[23], neurodegenerative disorders[24] and chronic inflammatory diseases.[25] The human genome project revealed that there are 518 genes encoding for protein kinases, resulting in more than 1,000 actual proteins as a result of different mutations and splicing variations.[26] The entirety of all kinases is often referred to as the "kinome". MANNING *et al.* proposed a way to categorize kinases according to their phylogenetic relationship as well as their sequence similarity (*Figure 1.4*).[27] Ultimately, all 478 eukaryotic protein kinases have been categorized into seven major groups, separated from the 40 atypical protein kinases, which form an extra group:

- **AGC group** (protein Kinase **A**, **G**, and **C** families):
  contains many cytoplasmic serine/threonine kinases which are often regulated by second messenger molecules
- **CAMK group** (Ca^{2+}/**ca**l**m**odulin-dependent **k**inase families):
  despite the name, some families of non-calcium regulated kinases are also included e.g. the proto-oncogene Pim-1 kinase
- **CK1 group** (**c**asein **k**inase **1** family)
  highly conserved group across all species
- **CMGC group** (**c**yclin-dependent kinases, **m**itogen-activated protein kinases, **g**lycogen synthase kinases and **C**DK-like kinases)
  contains mostly serine/threonine kinases including GSK3β and p38α MAPK relevant for this work

- **TK group** (**t**yrosine **k**inase)
  as the name suggests, this group includes non-receptor tyrosine kinases (also called cytosolic tyrosine kinases) and receptor tyrosine kinases;
  both subgroups contain prominent examples of kinases targeted by kinase inhibitors on the market like the janus kinase (JAK) or the epidermal growth factor receptor (EGFR)
- **TKL group** (**t**yrosine **k**inase-**l**ike)
  contains predominantly serine/threonine kinases in a variety of diverse and only weakly related families
- **STE group** (homologs of yeast **ste**rile kinase 7, 11 and 20 families):
  some upstream activators and regulators of MAPKs can be found in this group
- **Atypical protein kinases**
  atypical protein kinases usually possess protein kinase activity despite the lack of a sequence similarity to the eukaryotic protein kinase domain

The kinome tree is further divided into families and subfamilies, giving a detailed outline about the relationship of the kinases to one another. A second, less precise classification system is based on the substrates of the kinases. Typically, kinases phosphorylate hydroxyl groups of either serine, threonine or tyrosine residues of other proteins and classification according to their substrates leads to three groups, namely serine/threonine kinases, tyrosine kinases and dual-specificity kinases (hence targeting all three residues).

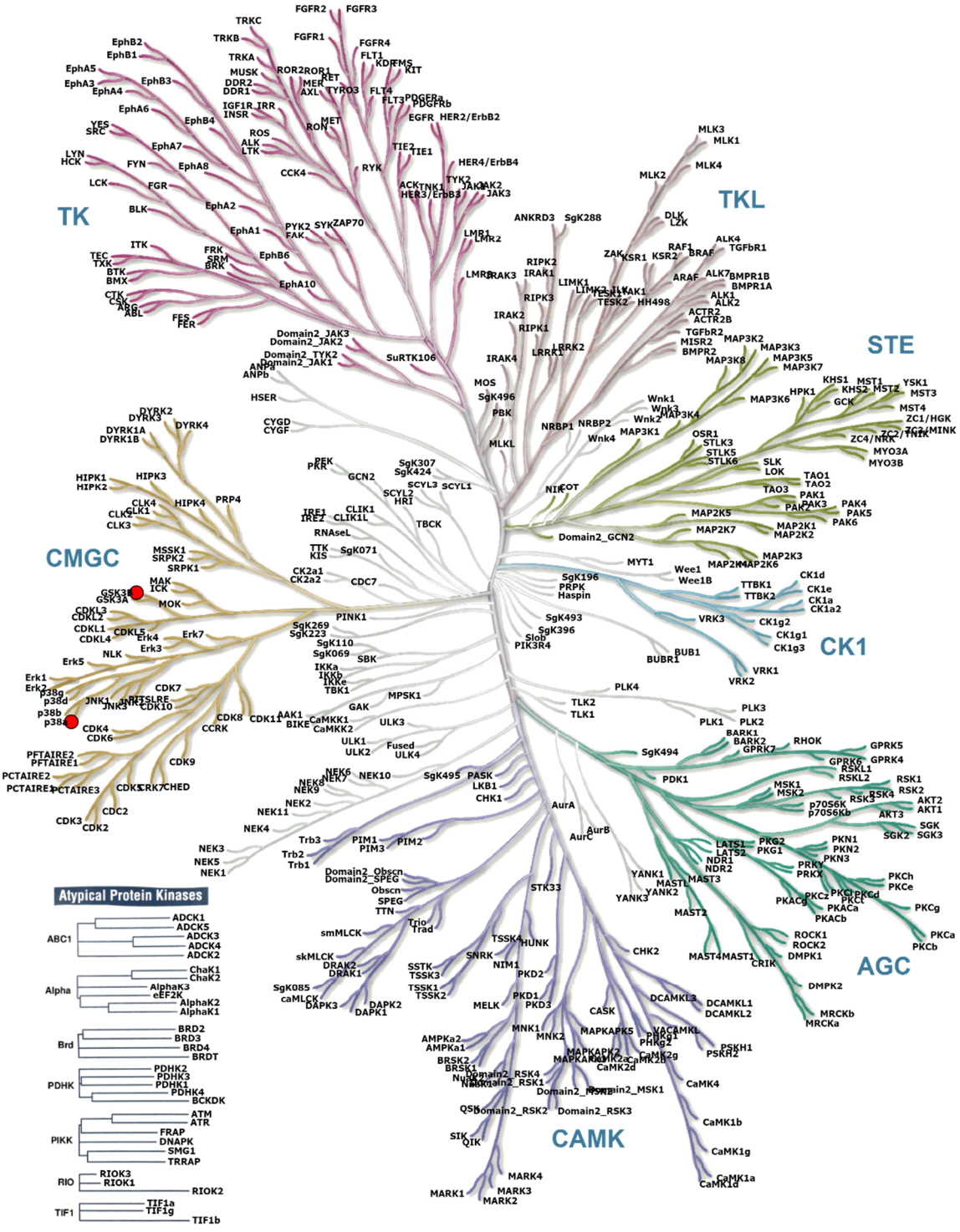

Figure 1.4. Human kinome phylogenetic tree according to MANNING *et al.*[27] The figure was created using the interactive online tool KinMap.[28] The red dots mark the two kinases GSK3β and p38α MAPK.

1.2.2 Structural features of protein kinases

The catalytic core (also called kinase domain) of eukaryotic protein kinases typically consists of about 250 to 300 amino acids and is folded into a two-lobed structure which consist of a smaller N-terminal domain (N-lobe) and a larger C-terminal domain (C-lobe) (*Figure 1.5*). Both lobes are connected by a flexible amino acid stretch in the central part, the so-called hinge region. The N-lobe is comprised of five stranded β-sheets and one helical subdomain, the universally conserved αC-helix, while the C-lobe is predominantly build from α-helices.[29] Based on sequence alignments, HANKS AND HUNTER divided the structure further into 12 highly conserved subdomains.[30] Subdomains I – IV are located in the N-lobe, whereas subdomains VIa – XI are situated in the C-terminal part. The kinase hinge region is part of the subdomain V. Subdomain I contains the glycine-rich loop, a Gly-X-Gly-X-X-Gly consensus motif, which arranges the γ-phosphate of ATP for catalysis. Subdomain II possesses a conserved lysine within the β-strand 3, which is crucial for kinase activity as it is forming interactions with the α- and β-phosphate of ATP thereby anchoring the ATP in the binding cleft. Subdomain III is portrayed by the large αC-helix and participates in the formation of a salt bridge between a Glu of the αC-helix and the lysine from subdomain II. Subdomain IV seems to be less important for the catalysis. As already mentioned above, subdomain V connects the N- and C-terminal lobe and plays an important role for the binding of ATP. The adenine ring is usually bound to the hinge via a bidentate hydrogen bond donor-acceptor motif. Similar to IV, subdomain VIa is not directly involved in the catalytic process and serves merely as a support structure.[30] The following subdomain VIb contains the catalytic loop characterized by the His-Arg-Asp-Leu-Lys-X-X-Asn motif. The name results from the important aspartic acid residue which acts as the catalytic base, extracting a proton from the hydroxyl group of the substrate. A conserved asparagine within the same loop binds a Mg^{2+} ion that also interacts with the α- and γ-phosphate of ATP. The regulatory DFG-motif (Asp-Phe-Gly) is situated in subdomain VII and because the Asp residue complexes a second Mg^{2+} ion, it is sometimes also referred to as the magnesium positioning loop.[31] The activation loop is located between subdomain VII and VIII and as the name implies, phosphorylation of certain amino acids in this region often leads to increased kinase activity.[32,33] Subdomain VIII plays an important role in substrate recognition and includes another highly conserved motif called APE (Ala-Pro-Glu). Subdomain IX contains the large, hydrophobic αF-helix[34] which includes an almost invariant aspartate residue. The last two

subdomains X and XI are less conserved and seem to play only a minor role in the catalysis.

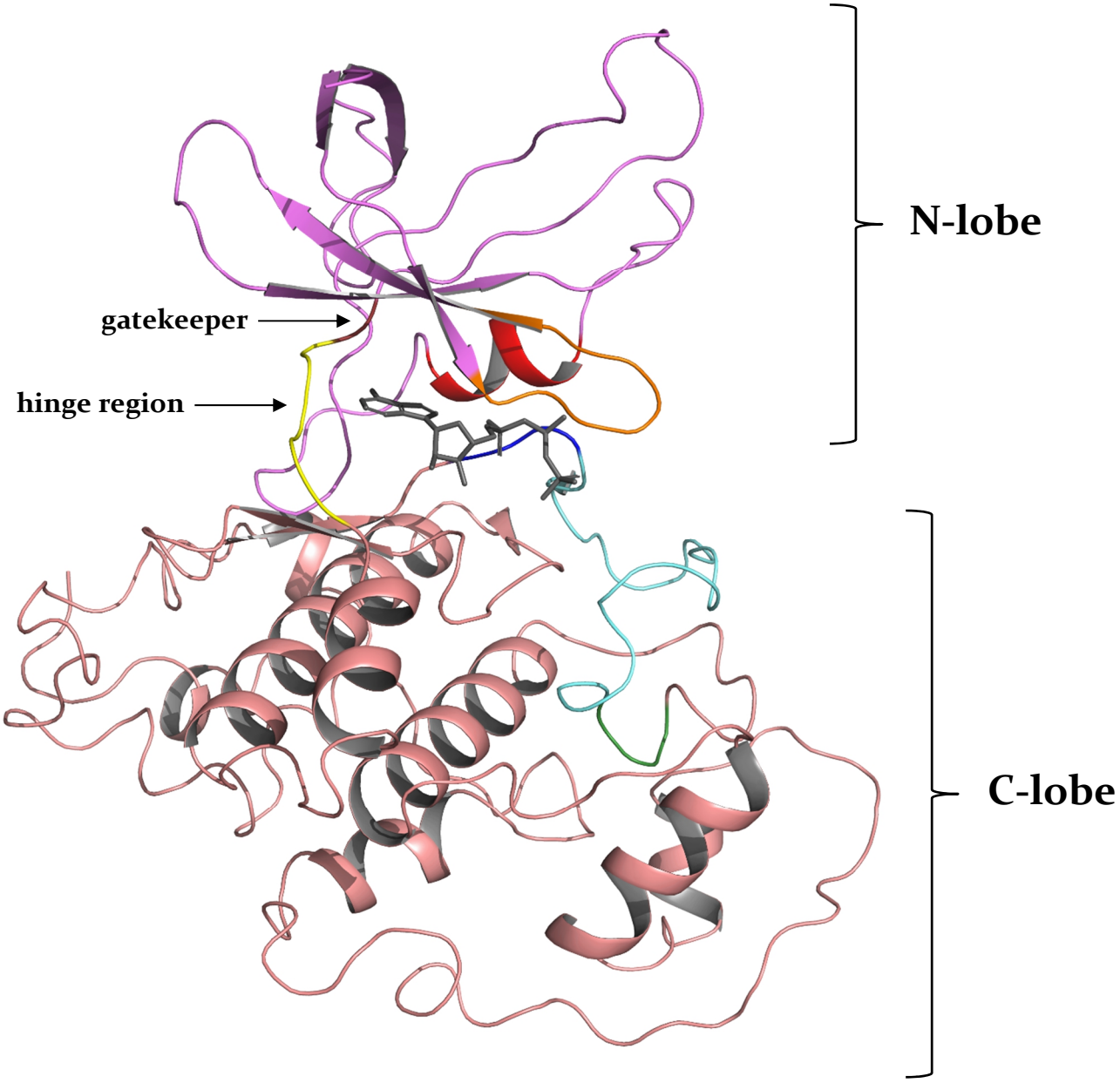

Figure 1.5. Structure of GSK3β in complex with adenylyl-imidodiphosphate which is displayed in dark grey (*PDB code:* 1PYX). Important features are highlighted in the following colors: P-loop (orange), αC-helix (red), gatekeeper residue (brown), hinge region (yellow) and the activation loop (cyan) is sandwiched between the DFG-motif (dark blue) and the APE-motif (green).

Schematic breakdown of the protein kinase ATP binding pocket:

TRAXLER *et al.* developed a general pharmacophore model of the protein kinase ATP binding site, which is applicable for the design of ATP competitive kinase inhibitors.[35] The model classifies the ATP binding cavity into five different regions (*Figure 1.6*):

Adenine region:

This hydrophobic region is – as the name suggests – accommodating the adenine ring of ATP which is usually engaged in a hydrogen bond donor-acceptor system with amino acids of the hinge region. The great majority of ATP competitive inhibitors also occupy this region and form one or often more hydrogen bonds with the hinge region.

Hydrophobic region I (HR I):

Access to this pocket is controlled by the so-called "gatekeeper" amino acid. As the endogenous ligand ATP is not addressing this region, this subsite is less conserved and therefore often exploited by medicinal chemists in order to gain additional inhibitory potency and selectivity, hence this region is sometimes also referred to as "selectivity pocket". The size of this pocket is varying from kinase to kinase depending on the size and flexibility of the gatekeeper amino acid (e.g. relatively small Thr106 in p38α MAPK compared to a large Phe80 in CDK2).

Hydrophobic region II (HR II):

This solvent exposed cavity is located adjacent to the adenine region and is also not addressed by ATP. As a consequence, this region is often targeted to improve binding affinity and selectivity of the inhibitors. In addition, its contact with the solvent exposed front region is sometimes used to enhance the pharmacokinetic properties of the molecules, for example by introducing soluble groups like morpholino or piperazine moieties reaching into this area.

Ribose pocket:

The ribose pocket (also known as sugar pocket) is a hydrophilic region which is occupied by ribose during the binding of ATP. Inhibitors often form hydrogen bonds with amino acids in this area, which usually anchor the ribose hydroxyl groups (e.g. Gln185 in GSK3β).

Phosphate region:

This region is in contact with the solvent exposed front and accommodates the triphosphate tail of ATP. Therefore, it is a quite hydrophilic and highly conserved area of the binding cleft.

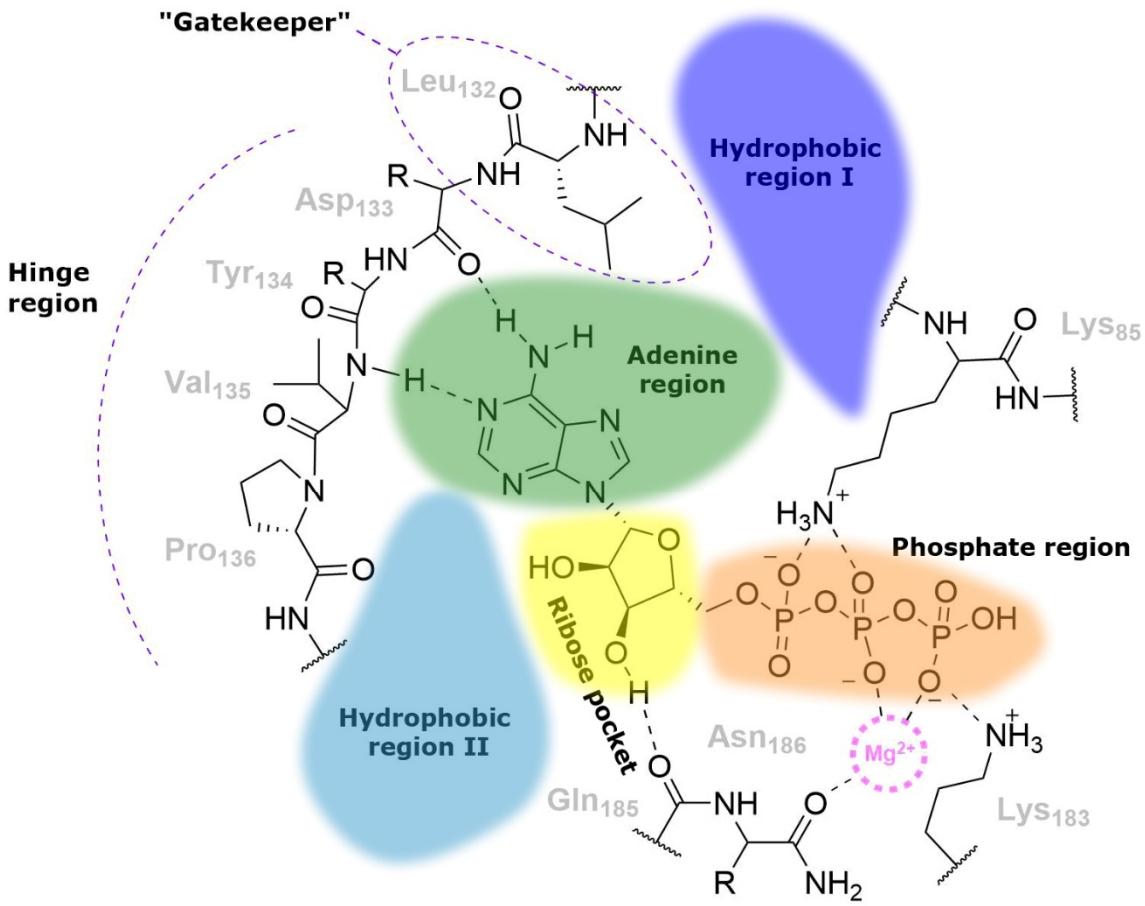

Figure 1.6. Schematic overview of ATP in the binding pocket of GSK3β based on TRAXLER'S pharmacophore model;[35] water molecules, the 2nd Mg^{2+} atom and Asp200 are omitted in this scheme for clarity.

1.2.3 Types of kinase inhibitors

Attempts to assign protein kinase inhibitors according to their different binding modes resulted in a classification system categorizing them from type I to VI:[36]

Type I inhibitors:

Type I inhibitors bind to the ATP binding site in the active conformation (DFG-in state) of the kinase. Therefore, all type I inhibitors are ATP competitive. Typically, one or more hydrogen bonds with the hinge region are formed by a heterocyclic core occupying the "adenine region". Moreover, the HR I and HR II are often addressed in order to gain a favorable selectivity profile and to improve physicochemical properties. Although this class of compounds is often considered to be rather unselective, some highly selective molecules have been described over the years.[37]

Type II inhibitors:

Type II inhibitors bind to the inactive conformation of the kinase (DFG-out state). They interact in a similar way with the adenine region of the binding pocket as type I inhibitors but most importantly these compounds also interact with a hydrophobic "deep pocket" proximal to the gatekeeper residue, which is only opened in the DFG-out conformation. The term DFG-out originates from the conformational change of the DFG-Phe, which shifts ~ 9 Å towards the ATP binding cleft, away from the αC-helix. The serendipitous discovery of this conformation during the development of Imatinib (*Glivec*®) fueled the hope for more selective kinase inhibitors because the amino acids of the deep pocket are usually less conserved than the ATP binding pocket itself.[38] However, this assumptions could not be supported by a closer analysis and comparison of approved type I and II inhibitors.[39] The approved type II inhibitors Ponatinib (*Iclusig*®) and Sunitinib (*Sutent*®) are two examples of rather promiscuous inhibitors.[40,41]

Type I½ inhibitors:

As the name suggests, this class can be described as a hybrid between type I and II inhibitors. Type I½ inhibitors bind to the hinge region like type I inhibitors and interact at the same time with the αC-helix-Glu and the DFG-Asp backbone. However, they are unable to reach the "deep pocket" which would stabilize the DFG-out state, meaning that they are able to bind the kinase in any DFG conformation state. As type I½ inhibitors disrupt the important regulatory spine (R-Spine) due to their interference with the DFG-motif, it is possible to achieve significantly increased target residence times at the kinase.[42] As a result, this class of inhibitors shows strongly reduced ATP-dependency despite their binding to the ATP cleft.

Type III inhibitors:

According to SIMARD *et al.* allosteric kinase inhibitors can be split into two types: type III and IV. Type III inhibitors are defined as allosteric inhibitors that bind to a site adjacent to the ATP binding cleft but do not interfere with it directly.[43] Because ATP and the inhibitor can both bind at the same time, they are considered to be non-ATP competitive binders. The evident advantage of this type of inhibitor is the possibility to achieve a high level of selectivity but on the other hand rational drug design approaches towards type III (or any other allosteric) inhibitors has proven to be very difficult.[44]

Today, there are only two FDA-approved type III inhibitors on the market: Cobimetinib (*Cotellic*®)[45] and Trametinib (*Mekinist*®)[46], both inhibiting MEK.

Type IV inhibitors:

As mentioned, type IV inhibitors are also allosteric inhibitors, but the interaction occurs at a binding site not connected to the ATP pocket. One classic example of type IV inhibitors is the Bcr-Abl inhibitor GNF-2[47] but also all three FDA-approved mammalian target of rapamycin (mTOR) inhibitors can be classified as type IV inhibitors: Everolimus (*Afinitor*®), Sirolimus (*Rapamune*®) and Temsirolimus (*Torisel*®).[36] This class of binders holds the same advantages and drawbacks as described for type III inhibitors. While the advantages in terms of e.g. (intra-family) selectivity are obvious, drug discovery projects often struggle in the deliberate design of allosteric inhibitors since the hydrophobic environment of most allosteric pockets makes it difficult to render drug-like molecules with good binding affinity. Another issue is the lack of suitable assays to discover allosteric inhibitors in screenings.

Type V inhibitors:

Type V inhibitors are by definition bivalent inhibitors, binding to two different regions of the kinase.[48] As an example, LECHTENBERG *et al.* recently published a potent combination of a small molecule targeting the ATP binding pocket of the extracellular signal–regulated kinase (ERK) 1/2 and a peptide targeting the hydrophobic D-recruitment site. The compound has an IC_{50} value against ERK1/2 in the low nanomolar range but suffers from a high molecular weight of almost 3000 Da and a surprising lack of selectivity, proving that on top of the poor drug-like properties, bivalent inhibitors do not automatically guarantee selectivity.[49]

Type VI inhibitors (Covalent inhibitors):

Type VI inhibitors bind covalently to a reactive residue within the active site of the kinase. Often the nucleophilic –SH group of a cysteine is targeted with an "electrophilic warhead". Covalent kinase inhibitors have been a hot topic for the last couple of years in kinase drug discovery efforts. Originally, concerns about toxicity due to unwanted reactivity impeded the development of type VI inhibitors, but once proof-of-concept studies showed success in clinic trials, the general opinion shifted. In October 2018, there were six covalent FDA-approved inhibitors on the market: Afatinib (*Gilotrif*®), Neratinib

(*Nerlynx*®), Osimertinib (*Tagrisso*®) and Dacomitinib (*Vizimpro*®) inhibiting EGFR-mutants as well as Ibrutinib (*Imbruvica*®) and Acalabrutinib (*Calquence*®) inhibiting BTK. Over the years a wide variety of electrophilic groups has been utilized as warheads in the design of kinase-targeting inhibitors. The most commonly used warhead is acrylamide followed by other α,β-unsaturated carboxamides.[50] But also cyanoacrylamides, α,β-unsaturated sulfonamides, haloketones and sulfonyl fluorides have been successfully applied as electrophiles.[51] Most covalent inhibitors are designed to target cysteine residues,[52] but in some cases also lysine has been successfully addressed.[53] Additionally, soon it might be possible to also specifically target methionine residues in the kinome as LIN *et al.* presented oxaziridines as chemoselective warheads targeting methionine in the proteome.[54] However, until today this concept has not been applied to any kinase, yet. One advantage of covalent inhibitors is the ability to achieve high selectivity since only a limited number of kinases possess cysteine residues in the proximity of the binding pocket.[52] Another advantage is the prolonged residence time of the compounds leading to the decoupling of the pharmacodynamic effects from the pharmacokinetic properties of the molecules. Nonetheless a generalization of (dis)advantageous assumptions is not advised in any case. As an example, proteomic profiling of Osimertinib, a 3rd generation EGFR inhibitor, showed several non-kinase off-targets *in vivo*, something that has not been seen in *in vitro* experiments before due to the fact that lysosomal accumulation of Osimertinib occurs only in cells.[55] Moreover, the hope of reduced risk for emerging drug resistance against covalent inhibitors was postulated but not fulfilled.[56] Especially in cancer cells, the instable genome and the high selective pressure applied by the kinase inhibitors quickly leads to drug resistance. While covalent inhibitors have been introduced in order to fight therapy-induced resistance against non-covalent kinase inhibitors like e.g. the 1st generation EGFR inhibitor Gefinitib (*Iressa* ®),[57] cysteine point mutations have been observed in the clinic for all approved covalent EGFR and BTK inhibitors, thus preventing the formation of a covalent bond.[58,59] Still, covalent kinase inhibitors have become indispensable as pharmacological tool compounds and drugs with further growing importance.

1.2.4 Protein kinase inhibitors as established drug targets – limitations and opportunities

For a long time, kinases were thought to be "undruggable" targets because of their high homology in the ATP binding site. It seemed impossible to achieve a reasonable selectivity within the kinome, resulting in a manageable side-effect profile. However, the approval of Imatinib (*Glivec*®) in 2001 for the treatment of chronic myelogenous leukemia and its extraordinary success in the clinic changed the prevailing opinion. As of December 2018, there are 47 FDA-approved kinase inhibitors on the market. While the great majority of these drugs is used to treat cancer, some are also prescribed for the treatment of chronic inflammatory diseases like rheumatoid arthritis. Obviously, the long-term risk-benefit ratio is much more important when chronic conditions like psoriasis, inflammatory bowel disease or AD are treated. Thus, off-target selectivity has to be reduced to a bare minimum, while most of the kinase inhibitors against cancer show a more promiscuous behavior in the kinome. In fact, a retrospective analysis by KARAMAN *et al.* showed that a lot of marketed kinase inhibitors were less selective than originally thought but clinically these inhibitors still possess an acceptable risk-benefit ratio.[60] However, over the years a lot of concepts for the development of highly selective kinase inhibitors have been presented and successfully applied to the effect that off-target related side-effects are no longer an obstacle in the development of chronically administered kinase inhibitors.

The treatment of central nervous system (CNS) diseases with kinase inhibitors has been mostly neglected in the last two "golden" decades of kinase inhibitors. As of today, there is no approved inhibitor with a CNS indication on the market. Although several kinase targets have been validated for a number of CNS disorders, there are a number of complications along the way. The greatest challenge for every CNS drug is certainly the necessity to penetrate the blood−brain barrier (BBB). Over the last years the understanding and theoretical knowledge about this process has rapidly advanced and concepts similar to Lipinski's famous rule-of-five have been established for BBB penetration but the design of potent and BBB crossing inhibitors still remains a big challenge.[61] Nevertheless, a number of inhibitors meeting those criteria have been reported and are currently evaluated in clinical trials.[62,63]

1.3 Glycogen synthase kinase 3

1.3.1 The GSK3 family

GSK3 is a serine/threonine protein kinase which was first isolated from rabbit skeletal muscle in 1980 at the University of Dundee. Identification of glycogen synthase (GS) as a substrate of this new kinase led to the name, since protein kinase A and phosphorylase kinase were already known as glycogen synthase kinases 1 and 2, respectively.[64] In humans, there are two genes encoding for two structurally closely related isoforms named GSK3α (gene locus: *19q13.1–2;* 51 kDa) and GSK3β (gene locus: *3q13.3;* 47 kDa). Both isoforms share an overall similarity in the catalytic kinase domain of 97%.[65] The main difference between the two isoforms is an extended glycine-rich N-terminal domain in GSK3α accounting for its slightly higher mass (*Figure 1.7*). Additionally, MUKAI *et al.* discovered a splice-variant called GSK3β2 containing a 13 amino acid insert in the catalytic domain.[66] This splice-variant seems to be neuron-specific[67], has a slightly different substrate preference[68] and is possibly required for axon growth.[69] Although the functional differences are not yet fully resolved, they seem to be marginal in regards to drug discovery efforts. It is worth mentioning that no crystal structure of the human GSK3α has been solved yet, while more than 75 crystal structures of the human GSK3β were available in the Protein Data Bank in December 2018.[70]

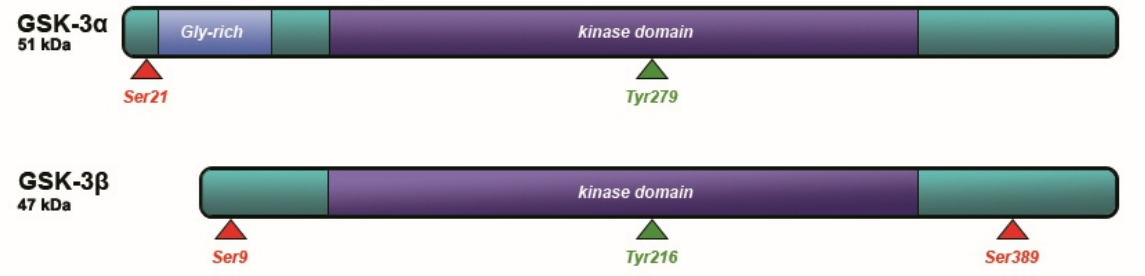

Figure 1.7. Schematic comparison of GSK3α with its extended glycine-rich N-terminal domain and GSK3β. Figure modified according to DOBLE AND WOODGETT.[71] Inhibitory/activating phosphorylation sites are marked with red and green arrows, respectively.[72–74]

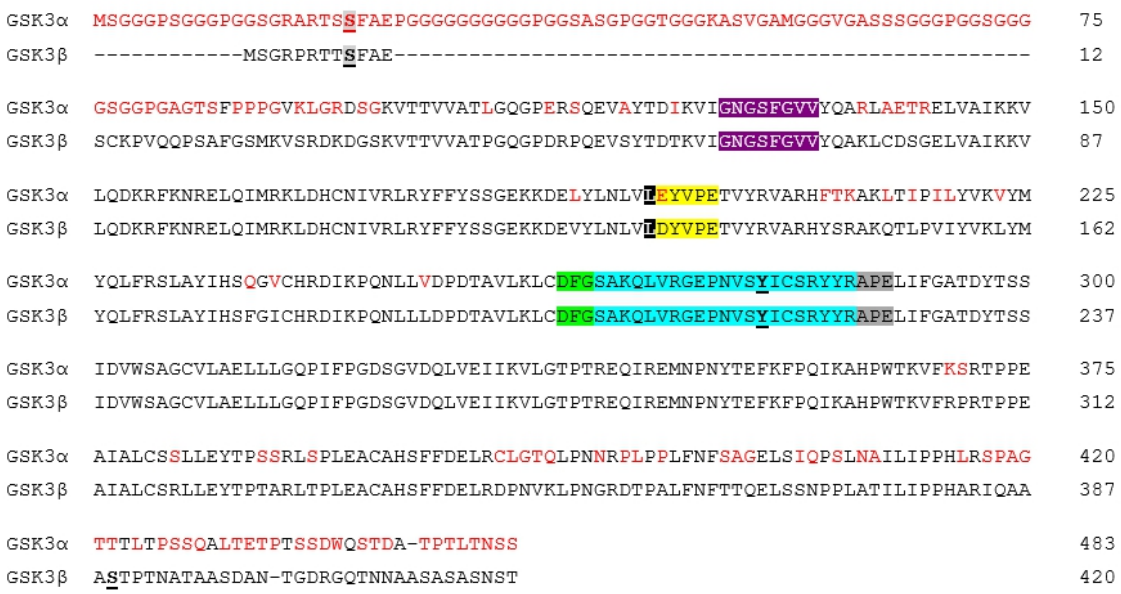

Figure 1.8. Sequence alignment of GSK3α and GSK3β. Residue differences between the two isoforms are marked red. The important regions of the kinases are highlighted with colors: P-loop (purple), gatekeeper residue (black), hinge region (yellow), DFG-motif (green), activation loop (light blue) and APE-motif (grey). Phosphorylation sites are boldly underlined.

Despite their high structural similarity, the two isoforms are not completely functionally redundant. Experiments with knockout mice showed that GSK3α$^{-/-}$ mice are viable while GSK3β$^{-/-}$ animals die in-utero due to defects in heart and skeletal development.[75,76] In other signaling pathways, the two isoforms seem to have overlapping functions e.g. in the Wnt/β-catenin signaling pathway, studies found both isoforms to be completely redundant.[77] Therefore the next sections (*1.3.2* to *1.3.4*) refer to both isoforms and differences are distinctly mentioned.

1.3.2 The peculiarities of GSK3

GSK3 is in general a rather unique kinase for several reasons: For a start, the kinase is constitutively active as the result of an autophosphorylation event taking place after translation in the activation loop at Tyr279 (GSK3α) and Tyr216 (GSK3β).[78] However, even without this activating phosphorylation, GSK3 has a substantial basal activity since the activation loop adopts by default a conformation analogous to the one observed in other kinases (e.g. CDK2 or ERK2) after a phosphorylation in their activation segment took place.[79,80] Another exceptional feature of the kinase is that most substrates require a "priming phosphate" on a serine or threonine

residue four amino acids C-terminal before the actual site of phosphorylation.[81] This pre-phosphorylation is carried out by other kinases and sets up a **Ser/Thr**-X-X-X-Ser/Thr(P) recognition pattern for GSK3. The eponymous substrate GS is a perfect example to illustrate this mechanism as it contains several Ser-X-X-X-Ser motifs in a row (*Figure 1.9*). Casein kinase (CK) 2 acts as the "priming kinase" in this case, phosphorylating GS at a specific serine residue. GSK3 is then able to bind the primed phosphate and can in turn phosphorylate at the P+4 position. Because GS has three additional serine residues – always in the P+4 position – this process is repeated sequentially by GSK3 until all five serine residues are phosphorylated.[82]

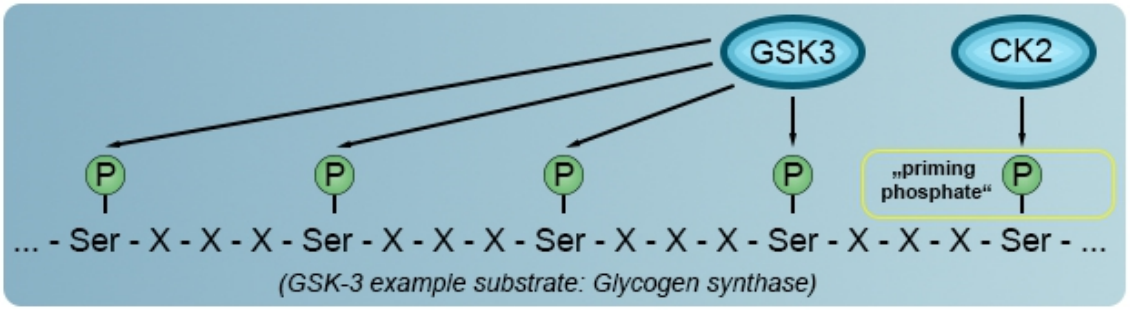

Figure 1.9. Schematic overview of the primed phosphorylation mechanism modified from COHEN AND FRAME.[83]

Tight regulation of any kinase activity is essential to maintain the carefully balanced homeostasis in all cell signaling pathways. This is in part done by phosphorylation at Ser21 (GSK3α) and Ser9 (GSK3β) as this leads to an inhibitory mechanism. Thereby, the N-terminal phosphorylated residue of the protein acts as a pseudosubstrate for GSK3, occupying the binding site normally used by primed substrates.[84] Some kinases that phosphorylate GSK3 at those specific sites have been identified. In response to the insulin signaling pathway, e.g. protein kinase B (PKB) inactivates GSK3 through Ser21/Ser9 phosphorylation but also p70 ribosomal S6 kinase and MAPK-activated protein kinase 1 have been described to target GSK3.[85] Aside from Ser9, THORNTON *et al.* found evidence for a possible, second inactivating phosphorylation at Ser389 of GSK3β. According to the authors this phosphorylation is mediated by p38α MAPK and leads to a substantial decrease of GSK3β (but not GSK3α) activity in mouse tissues.[74] However, the *in vivo* implications for humans remain questionable since for example GSK3β mediated hyper-phosphorylation of τ proteins occurs despite this postulated p38α MAPK-dependant inhibitory mechanism.

Not all substrates of GSK3 necessarily need to be primed in order to be recognized, meaning some substrates are decoupled from this inhibitory regulation mechanism.[86] *Table 1.1* gives a small overview of some known GSK3 substrates. Over the years far more than 100 substrates have been reported in the scientific literature but only a fraction has been validated with appropriate methods.[87]

Table 1.1. Selected GSK3 substrates

Metabolic and signaling proteins	Structural proteins	Transcription factors
APC[88]	CLASP[89]	β-catenin[90]
APP[91]	MAP1B[92]	c-jun[93]
ATP citrate lyase[94]	MAP2C[95]	c-myc[96]
Axin[97]	τ protein[98]	CREB-1[99]
eIF2B[100]	Telokin[101]	NFAT[102]
Glycogen synthase[103]		NF-κB (p65/p105)[104]
Insulin receptor substrate-2[105]		Notch[106]
Presenilin-1[107]		p53[108,109]
		STAT3/5[110]

1.3.3 Wnt/β-catenin dependent pathway

The Wnt signaling pathway is a highly conserved pathway that regulates essential processes during the embryonic development like "cell proliferation, cell fate determination, cell differentiation and cell polarity".[111] In adults it is linked to tissue homeostasis by somatic stem cell regulation and aberrant Wnt signaling has been associated with certain types of cancer.[112] In addition to the so called β-catenin dependent (canonical) pathway, there are also two β-catenin independent (non-canonical) pathways: the non-canonical Wnt/planar cell polarity pathway and the non-canonical Wnt/calcium pathway. All of these pathways are activated by Wnt ligands, which are highly post-translationally modified proteins.[113] In the "off-state" of the β-catenin dependent pathway, no Wnt ligand is binding to the extra-cellular receptor frizzled. A cytoplasmic "β-catenin destruction complex" comprised of the proteins adenomatosis polyposis coli

(APC), Axin, GSK3, protein phosphatase 2A (PP2A), CK1 and β-TrCP is responsible for the ubiquitination and subsequent proteasomal degradation of β-catenin (*Figure 1.10*).[114]

If a Wnt ligand binds to the seven transmembrane frizzled receptor and its co-receptor LRP5/6, the canonical pathway is activated whereupon the protein dishevelled is recruited intracellularly. In a complicated cascade, Axin and the β-catenin destruction complex translocate to the membrane and hyperphosphorylation of dishevelled by CK1 ultimately leads to the inactivation of the protein complex.[115] Now β-catenin starts to accumulate in the cell and translocates to the nucleus where it acts as transcriptional co-activator of other transcription factors like TCF/LEF, modifying the expression of a plethora of downstream genes (*Figure 1.10*).[116]

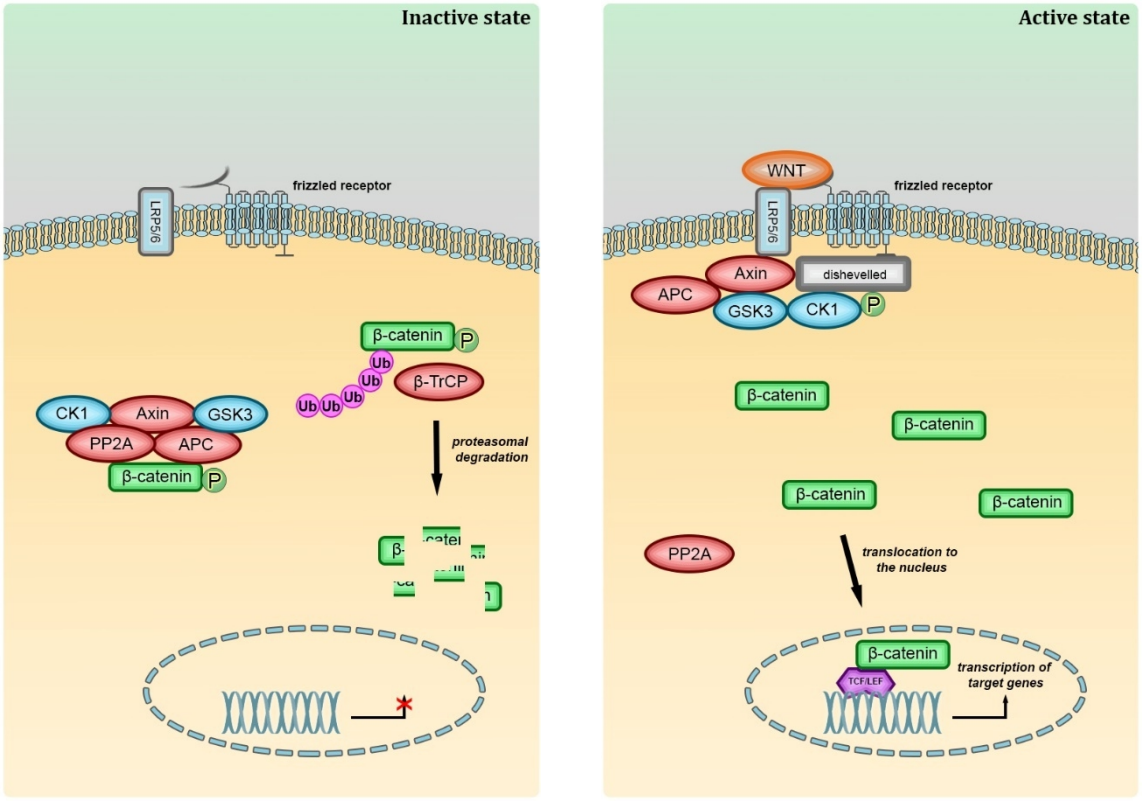

Figure 1.10. Inactive and active state of the Wnt/β-catenin dependent pathway.

Since β-catenin is a proto-oncogene, certain mutations can lead to an accumulation of β-catenin in the cells (and in the nucleus). This upregulation leads to the continuous transcription of the downstream target genes, which include certain oncogenes that promote carcinogenesis and tumor progression.[117] β-Catenin upregulation has been measured in several types of cancers but seems to be especially present in colorectal

malignancies.[118] Naturally, there are concerns that potent GSK3 inhibitors might also promote cancer as a result of this mechanism. However, studies found that a reduction of the total GSK3 (both isoforms) activity by 75% is necessary to measure significant differences in the β-catenin levels. Interestingly, COHEN *et al.* even observed a lower cancer prevalence in psychiatric patients treated with the GSK3 inhibitor lithium carbonate over a period from 1 to 18 years (*Section 1.3.5*).[119] In order to avoid any feared adverse drug events, finding the appropriate dose of the inhibitor is a key requirement. Another approach to minimize such risks has been proposed by researchers at AstraZeneca, who aim at the combination of GSK3β inhibitors with novel tissue-targeted drug delivery systems to limit any off-target effects.[120]

1.3.4 The role of GSK3β in the insulin signaling pathway

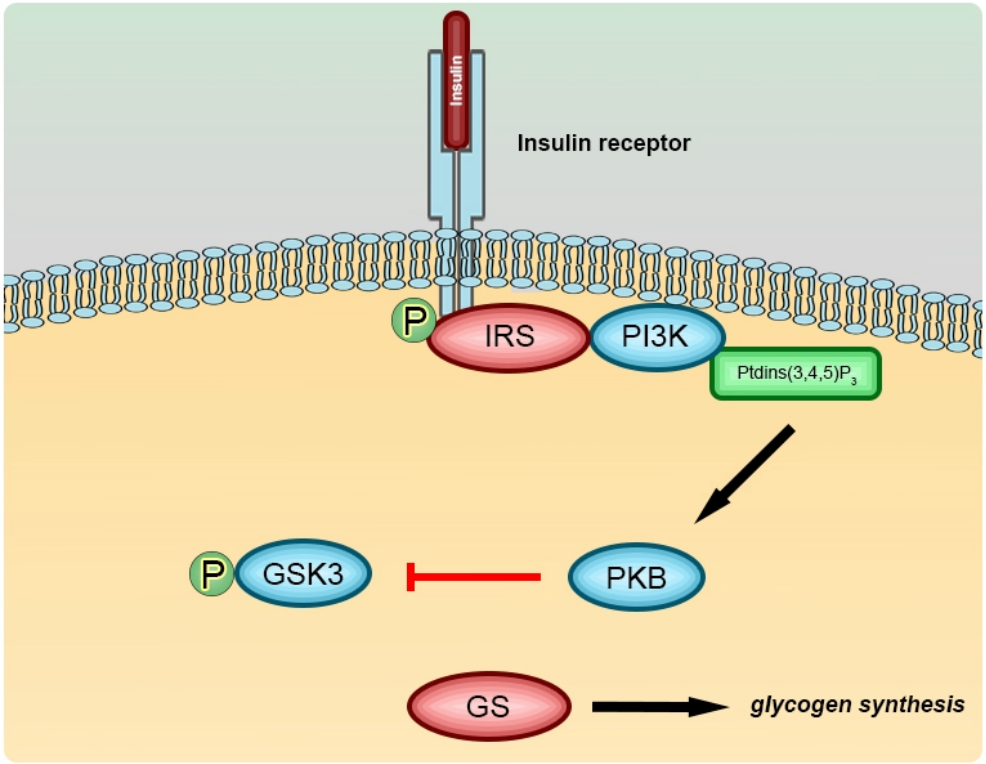

Figure 1.11. Insulin signaling pathway and the fate of GSK3 in case of insulin receptor activation. When the insulin receptor is not activated by a ligand, GSK3 is phosphorylating GS thereby inhibiting the synthesis of glycogen (not seen in the picture).[121]

Insulin is a hormone released by the β-cells of the pancreatic islets and, upon release, enabling among other metabolic effects, glucose uptake into cells and conversion of

glucose to glycogen by activation of GS. Once the transmembrane insulin receptor is activated by its endogenous ligands (insulin, IGF-I or IGF-II), autophosphorylation within the intracellular TK domain occurs which in turn leads to the recruitment and phosphorylation of insulin receptor substrates (IRS). Phosphorylated IRS can be bound by numerous interaction partners, one of them being the phosphoinositide 3 kinase (PI3K).[122] Activated PI3K is recruited to the plasma membrane where it catalyzes the reaction of phosphatidylinositol-4,5-bisphosphate (Ptdins(4,5)P_2) to phosphatidylinositol-3,4,5-trisphosphate (Ptdins(3,4,5)P_3). An important downstream effector of Ptdins(3,4,5)P_3 is protein kinase B (PKB; also known as AKT) which inactivates GSK3 through the previously explained serine phosphorylation (*Section 1.3.2*). Phosphatases can now activate GS through dephosphorylation, stimulating the insulin-induced synthesis of glycogen.[84]

In addition to the Wnt and insulin pathways, GSK3 also plays a role in reelin signaling[123], the hedgehog pathway[124], notch signaling[125], dopamine signaling[126], TGFβ signaling[127] and many more signaling pathways. Due to the extreme complexity of most pathways and their interconnection, the exact role of GSK3 is not always completely elucidated yet. Since a comprehensive study of all GSK3 connected pathways is not within the scope of this thesis, further details about the aforementioned signaling cascades are omitted and the reader is asked to resort to the extensive scientific literature on this topic.

1.3.5 Previously reported GSK3β inhibitors and their diverse applications

Over the years, GSK3β has become one of the most popular drug targets out of the kinome. Almost every major pharmaceutical company pursued a GSK3β project resulting in a myriad of inhibitors covering a wide variety of chemical space and physicochemical properties.

Lithium chloride was the first inhibitor described for GSK3β with an IC_{50} of 1-2 mM.[128] Direct competition of Li^+ with Mg^{2+} as well as an indirect mechanism via upregulation of other pathways leading to an increased Ser9 phosphorylation have been proposed.[128,129] This is interesting as lithium salts have been prescribed for the treatment of bipolar disorders for more than 50 years. Lithium carbonate for instance is used as a “mood stabilizer” but the exact mechanism of action is still unknown and a connection to its capability of inhibiting GSK3β is likely.[130] But lithium salts are by far not the only

naturally occurring inhibitors. Plenty of natural products and derivatives thereof are known to inhibit GSK3β but often a lack of potency and/or selectivity obstructs their use as drug or pharmacological probe.[131] However, the discovery of 6-bromoindirubin isolated from sea snails as a potent GSK3β inhibitor (IC_{50}: 45 nM) and subsequent synthetic efforts led to the improved and cell-permeable 6-bromoindirubin-3′-oxime (**BIO**) (IC_{50}: 5 nM) which has been used as a pharmacological tool compound for a long time despite its questionable selectivity profile.[132] Today, the ChemicalProbes portal[133] recommends the use of the potent aminopyrimidine **CHIR99021** (IC_{50}: 6.7 nM) for *in vitro* and cell models.[134] The compound was designed as a potential type 2 diabetes treatment exploiting the antihyperglycemic effects of a GSK3β inhibition and shows a much better overall kinome selectivity profile than **BIO**.[135,136]

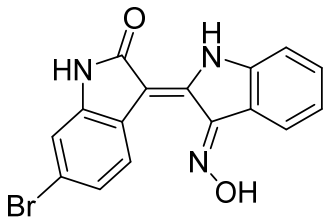

BIO

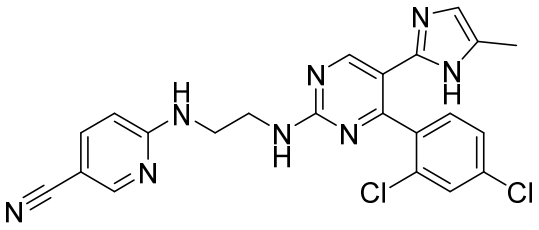

CHIR99021

Figure 1.12. Pharmacological tool compounds of GSK3β: **BIO**[132] and **CHIR99021**.[135]

Despite a great number of potent small molecule inhibitors, only a few have made it into clinical trials suggesting that preclinical toxicity is a major factor that has to be carefully monitored.[120,137] One of the few exceptions is the non-ATP competitive and irreversible inhibitor **Tideglusib**.[138] Not only was **Tideglusib** tested in two phase II clinical trials for the treatment of AD[139] and progressive supranuclear palsy (PSP)[140], but also did the outcome demonstrate that the drug was safe to use over the 52-week course of the PSP study. However, the trials did indicate a lack of efficacy in both cases. **Tideglusib** is currently also under investigation (under the synonym **AMO-02**) in another phase II study for the treatment of congenital myotonic dystrophy and has received fast track designation by the FDA.[141,142] Another small-molecule GSK3β inhibitor in clinical trials is **LY2090314** (IC_{50}: 1.3 nM), developed by Eli Lilly and Company.[143] A phase I dose-escalation study in combination with the cytostatics pemetrexed and carboplatin proved temporary upregulation of β-catenin levels in peripheral blood cells at 40 mg of **LY2090314** – indicating that on-target binding occurs in humans.[144] The same compound

was investigated in an open-label phase II trial with acute myeloid leukemia patients and showed a sufficient safety profile but overall limited clinical success.[145]

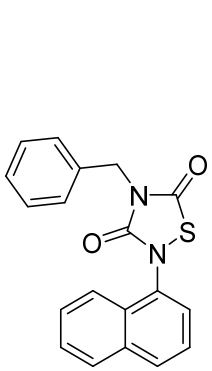

Tideglusib

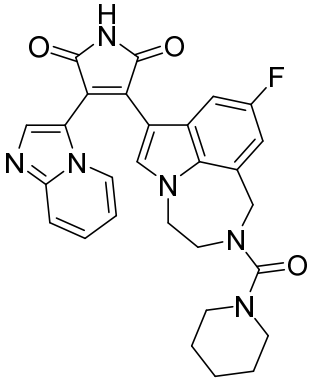

LY2090314

Figure 1.13. GSK3β inhibitors currently in clinical trials (as of November 2018).

Now it should be noted that all of the until here discussed inhibitors are more or less equipotent towards both GSK3 isoforms. There have been some reports in literature about molecules slightly selective towards one GSK3 isoform[146] but the general perception is that there is still a lack of sufficiently isoform-selective inhibitors especially when considering *in vivo* efficacy in mammalian (cell) models.

Recently WAGNER *et al.* published the two modestly isoform selective compounds **BRD3731** (GSK3α, IC_{50}: 215 nM; GSK3β, IC_{50}: 15 nM) and **BRD0705** (GSK3α, IC_{50}: 515 nM; GSK3β, IC_{50}: 66 nM) (*Figure 1.14*).[147] According to the authors, only a tiny difference in the hinge regions (Glu196 in GSK3α versus Asp133 in GSK3β; *Figure 1.8*) changes the conformation and size of a small selectivity pocket adjacent to the hinge region. The neopentyl moiety of **BRD3731** occupies this pocket in GSK3β while the cavity in GSK3α is too small to accommodate such bulky residues. **BRD0705** is currently evaluated as a potential drug for the therapy of acute myeloid leukemia.[148]

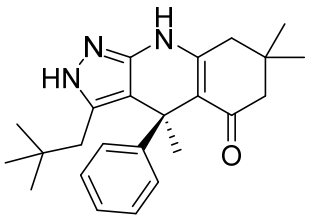

BRD3731

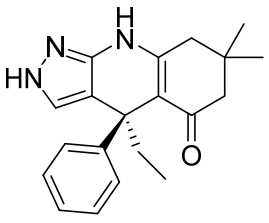

BRD0705

Figure 1.14. Modestly isoform selective GSK3 inhibitors.

Some envisaged applications for GSK3β inhibitors have already been mentioned before but on top of bipolar disorders, diabetes, cancer and a variety of neurodegenerative diseases (*Section 1.3.6*), over the years plenty of other possible diseases and ailments have been proposed as application areas. The list includes for example schizophrenia[149], osteoporosis[150], sepsis[151], heart failure[152] and even alcohol dependence.[153] A particularly interesting application for small-molecule GSK3β inhibitors was recently proposed by NEVES *et al*. Collagen sponges were soaked with a GSK3β inhibitor (either **BIO**, **CHIR99021** or **Tideglusib**) and used to fill carious lesions in mice. Local activation of the Wnt/β-catenin signaling pathway led to an increased expression of Axin-2 which ultimately promoted odontoblast-like cells to produce a natural, reparative dentine.[154] Biological regeneration of carious teeth seems to be possible with this method and since the inhibitors were only used locally and in very low doses, the risk of adverse drug effects is presumably very small.

Another fairly different use of GSK3 inhibitors has arisen from their ability to modulate embryonic stem cells.[155] **CHIR99021** for example enhances self-renewal of embryonic stem cells as well as their viability.[156] Also functional hepatocytes were generated from human adipose stem cells with the help of **CHIR99021**.[157] Therefore, GSK3 inhibitors could be an important component of tissue engineering techniques and other methods in the area of regenerative medicines.

1.3.6 Connections between GSK3β and AD

In 2008, HOOPER, KILLICK AND LOVESTONE postulated "the GSK3 hypothesis of Alzheimer's disease".[158] Therein the authors claimed a central role for GSK3 in the pathogenesis of AD and indeed, much evidence supporting this theory has accumulated over the years.

Post-mortem brain sample analysis showed overexpression of GSK3 in AD patients but direct evidence of increased enzymatic activity is still missing as it cannot be determined from dead neuronal tissue.[159,160] However, there is plenty of indirect evidence present: among the confirmed substrates of GSK3 (*Table 1.1*) there are many proteins directly involved in the AD pathology e.g. APP, presenilin-1 (PS-1) and τ protein. PS-1 is part of the γ-secretase multiprotein complex and mutations of PS-1 are strongly linked to familiar forms of AD.[161,162] Phosphorylation of PS-1 by GSK3β at Ser353 and Ser357[107] resulted in an unfavorable $A\beta_{42}/A\beta_{40}$ ratio and PS-1 phosphorylation was also increased in AD brain samples.[163] Furthermore, UEMURA *et al.* found changes in the localization and function of PS-1 upon GSK3β mediated phosphorylation.[164]

Elevated levels of Aβ led to increased GSK3β activity in rat neurons.[165] A possible mechanism for this observation is the interaction of Aβ with the insulin signaling pathway (*Section 1.3.4*). Aβ oligomers are responsible for the internalization of insulin receptors from the cell membrane and the consequential reduction of insulin signaling prevents PKB from transmitting an inhibitory phosphorylation on GSK3β, thus leading to increased activity.[166] Upregulated GSK3β on the other hand is mediating a plethora of detrimental effects including transcription of proinflammatory genes driving neuroinflammation[167], enhanced apoptosis[168] and τ hyperphosphorylation (*see below*). PHIEL *et al.* claimed that GSK3α promotes the generation of $A\beta_{40}$ and $A\beta_{42}$ peptides from APP but not GSK3β.[169] However, according to LY *et al.* inhibition of GSK3β mediates a decreased β-secretase gene transcription and expression, thereby reducing the production of Aβ.[170] While the isoform specific roles in the pathogenesis of AD are not elucidated yet[171], those findings establish a direct link between GSK3 and a main hallmark of AD (plaques). But GSK3β is also strongly involved in the formation of a second hallmark of AD called NFTs (details about the formation of NFTs are explained in *Section 1.1*). GSK3β is one of the main actors responsible for the hyperphosphorylation of τ proteins, thus the name “human tau protein kinase I” can sometimes be found as a synonym.[172] Consequently, upregulation of GSK3β in transgenic mice led to increased τ hyper-phosphorylation, NFT formation and signs of neurodegeneration.[173] Conversely, *in vitro*

inhibition of GSK3β in cultures of cortical neurons reduced τ hyperphosphorylation.[174] Furthermore, intracellular accumulation of GSK3β is regionally codistributed with hyperphosphorylated τ proteins and NFTs, indicating a causal connection.[175] On top of strong evidence for playing a pivotal role in the genesis of two pathological hallmarks of AD, GSK3β also influences certain pathways of the CNS immune system. As a result of dysregulated kinase activity, proinflammatory cytokines may gain the upper hand e.g. through NF-κB signaling.[176] Active GSK3β leads to translocation of NF-κB and CREB to the nucleus which in turn favors the transcription of proinflammatory cytokines.[177,178] This is just one of the few – often poorly understood – mechanisms by which GSK3β is involved in neuroinflammatory processes.

The direct impact of the kinase on PS-1 and Aβ processing or τ phosphorylation alone would make GSK3β an interesting drug target for AD. But when the combined contribution of the kinase to neurodegeneration is summed up (*Figure 1.15*), this enzyme can only result as one of the most promising targets for the treatment of AD currently known.

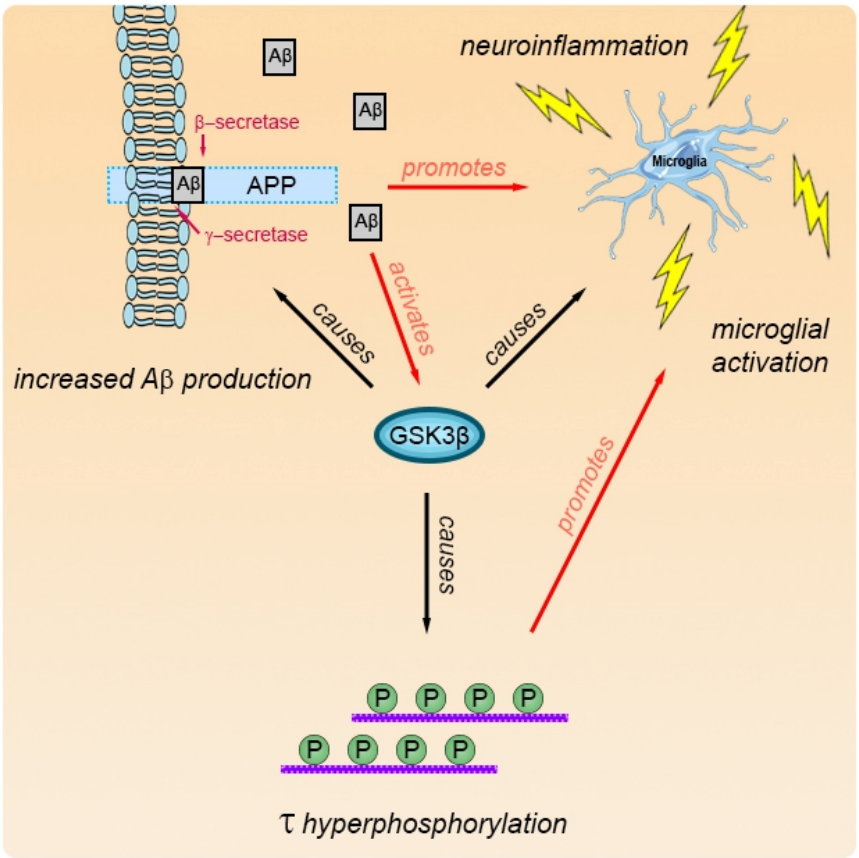

Figure 1.15. Schematic view of the most important links between GSK3β and certain pathological hallmarks of Alzheimer's disease modified from HOOPER, KILLICK AND LOVESTONE.[158]

1.4 Mitogen-activated protein kinase 14 (p38α MAPK)

1.4.1 The p38 MAPK family

The mitogen-activated protein kinase 14, also called p38α MAPK, is a serine/threonine protein kinase belonging to the p38 MAPK family and it was first described in 1994.[179] Further members of the family are the β, γ and δ isoforms. However, in terms of drug discovery efforts, the α isoform is by far the most targeted kinase of this family because of its important role in the biosynthesis of proinflammatory cytokines like interleukin (IL)–1β, IL-6 and tumor necrosis factor (TNF)–α.[180] Having recognized the potential of p38α MAPK inhibitors for the treatment of chronic inflammatory diseases like rheumatoid arthritis, a race from bench to bedside was started. Between 1996 and 2005 alone, more than 234 patents related to p38α MAPK inhibitors have been claimed.[181] Numerous p38α MAPK inhibitors have been evaluated in clinical trials and while no inhibitor made it to market yet[182], the extensive research certainly made p38α MAPK one of the most well-studied kinases.

1.4.2 The p38α MAPK signaling pathway

The p38α MAPK signaling pathway (*Figure 1.16*) is activated by a variety of extracellular triggers like oxidative stress, UV light, inflammatory cytokines or growth factors like TGF-β.[183] Like in all MAPK signaling cascades, first the upstream MAPKKK is activating the two MAPKKs MKK3 and MKK6 which then phosphorylate p38α MAPK twice on a conserved Thr-X-Tyr motif within the activation loop.[184] The now active kinase has a plethora of downstream substrates like other kinases, τ protein or cytosolic phospholipase A2. After nuclear translocation, a wide variety of transcription factors is influenced by p38α MAPK leading to an upregulation of predominantly proinflammatory cytokines like TNF-α and IL-1.

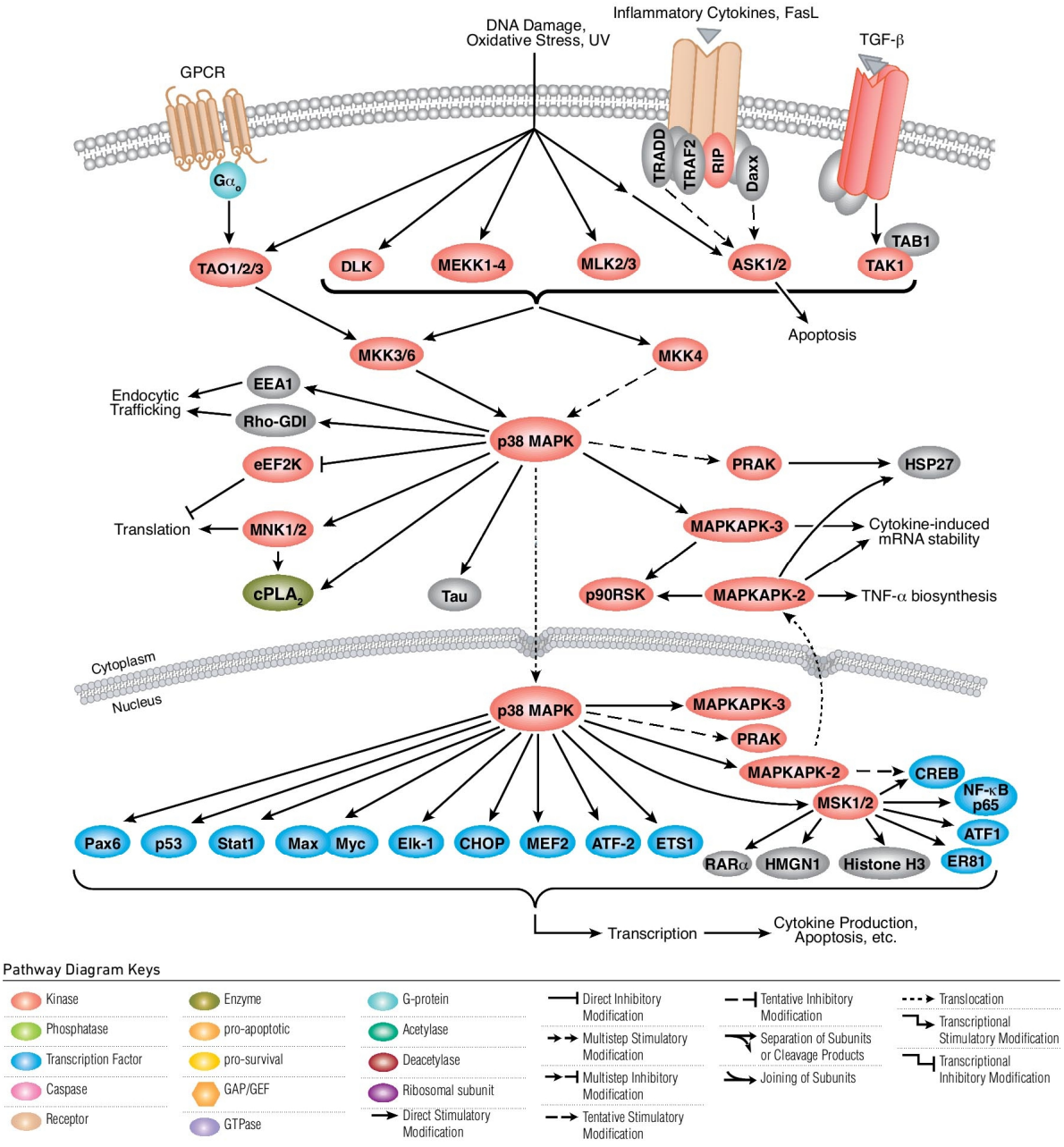

Figure 1.16. The p38α MAPK signaling pathway in detail. Illustration reproduced by courtesy of Cell Signaling Technology, Inc. (http://www.cellsignal.com/).

1.4.3 The involvement of p38α MAPK in AD

Soon after its discovery, upregulated levels of p38α MAPK were detected in AD patients and a link to neuroinflammation was suspected.[185] The definition of neuroinflammation is the presence of inflammatory responses within the brain and/or the spinal cord. Since the CNS is protected by the BBB most elements of the immune system cannot enter this highly sealed off area. Therefore, the CNS has its own neuroimmune system mainly consisting of microglia and astrocytes.[186] Microglia are the equivalent of macrophages in the CNS and as such vital for the primary immune response. Activation of microglia upon injury, infections or other stimuli leads to the release of proinflammatory cytokines and migration of the microglia towards the affected areas of the brain.[187] Particularly the microglial p38α MAPK seems to be a key contributor to cytokine upregulation after exposure to microglial activators (e.g. Aβ oligomers).[188] Prolonged inflammation and continuously high levels of TNF-α, IL-1 and reactive oxygen species ultimately induces apoptosis and neuronal degeneration. The role of p38α MAPK in these mechanisms has been investigated meticulously in the last few years and evidence for a pivotal involvement of p38α MAPK in neurodegeneration has been piling up. COLIÉ *et al.* specifically downregulated p38α MAPK in neurons of 5xFAD mice (transgenic mice that rapidly accumulate high levels of Aβ42 in the brain). Compared to normal 5xFAD, these "5xFAD/p38αΔ-N" termed mice showed an improved memory and neurogenesis, reduced levels of neuroinflammation and decreased Aβ accumulation.[189]

Aside from the massive impact of p38α MAPK on neuroinflammation, the kinase is suspected to be involved in the hyperphosphorylation of τ proteins. *In vitro* studies suggested that τ protein is a direct substrate of p38α MAPK[190,191] and further analysis of human brain samples indicated that p38α MAPK may phosphorylate τ proteins *in vivo*, too.[192] A study of ZHU *et al.* showed at least big differences in the expression patterns and amount of total p38α MAPK between samples of AD patients compared to age-matched control subjects. Furthermore, immunoprecipitation of p38α MAPK led to co-sedimentation of τ PHF suggesting a close association of both proteins *in vivo*.[192] In a newer study with "htau mice" which simulate a general tauopathy[193], treatment with a brain-penetrant, selective p38α MAPK inhibitor significantly diminished τ protein phosphorylation and signs of insoluble τ aggregates on top of the expected reduction of proinflammatory cytokine release.[194]

In humans, just recently results of the first phase II clinical trial against AD with the selective, brain-penetrant small-molecule inhibitor **Neflamapimod**/**VX-745**[195] (*Figure 1.17*) have been published by EIP Pharma LLC and further investigations have been announced.[196,197]

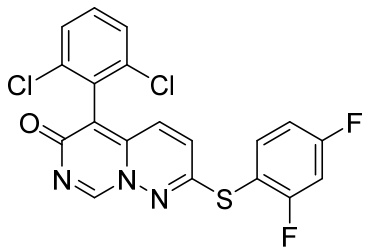

Figure 1.17. **Neflamapimod** (originally named **VX-745**)[195] is a selective, orally bioavailable and CNS-penetrating p38α MAPK inhibitor, developed by Vertex Pharmaceuticals.

In the exploratory clinical study, 16 patients with mild AD were enrolled and treated with either 40 or 125 mg of **Neflamapimod** twice daily for 12 weeks. The results were assessed by PET scans and a Wechsler Memory Scale test measuring Aβ plaque burden and the episodic memory, respectively. The small sample size makes it hard to draw solid conclusions but the sponsor of the study feels confident enough to pursue further clinical trials as there were statistically significant increases in the Wechsler Memory Scale test and no severe adverse events were observed.[197]

1.5 Potential synergistic effects of dual GSK3β/p38α MAPK inhibitors in a variety of neurodegenerative diseases

While AD certainly is the most common neurodegenerative disease, there are many more incurable neurological disorders which ultimately lead to neuronal cell death. The list includes but is not limited to Parkinson's disease (PD), amyotrophic lateral sclerosis (ALS), Huntington's disease (HD) and all prion diseases. Substantial evidence has arisen that GSK3β and p38α MAPK both play an important role in the pathogenesis or the course of many neurodegenerative diseases. PD for example is characterized by the progressive degeneration of dopaminergic neurons in the substantia nigra pars compacta. Histopathological changes like Lewy bodies comprised of aggregated α-synuclein can be observed in the affected brain areas.[198] The abundant soluble protein α-synuclein is usually unstructured but it can, under certain conditions, change its conformation into α-helical structures that are prone to aggregation. α-Synuclein in turn is a GSK3β substrate and kinase inhibition has shown beneficial effects on α-synuclein aggregation in cellular models.[199] In a 1-Methyl-4-phenyl-1,2,3,6-tetrahydropyridin (MPTP) model of PD, GSK3β inhibition prevented dopaminergic neurons from apoptosis, demonstrating the pivotal role of the kinase in the disease progression.[200] For HD and ALS similar observations about an involvement of GSK3β have been made.[201–203] But also the family of p38 MAPKs is able to contribution to the progression of PD and ALS in a direct, detrimental manner, as pharmacological studies have shown.[204,205] On top of that basically any persistent neural inflammation is in some way dependent on p38α MAPK activity. As a general mediator of inflammation in all neurodegenerative disorders, p38α MAPK is an attractive target for the attenuation of these inflammatory processes.[206]

Regarding their involvement in AD, each kinase has been extensively discussed in *Sections 1.3.6* and *1.4.3*, respectively, and a schematic overview can be found in *Figure 1.18*. A question that remains open is the relationship between the two kinases. As mentioned in *Sections 1.3.2*, THORNTON *et al.* found evidence for a possible, inactivating phosphorylation of GSK3β (Ser389) mediated by p38α MAPK.[74] However, these studies were only performed *in vitro* and in mice, meaning the implications for healthy humans

or AD patients are unclear. Since overactivation of p38α MAPK in AD brains does not seem to prevent GSK3β mediated hyperphosphorylation of τ proteins the significance of the observed p38α MAPK-dependant inhibitory mechanism remains questionable.

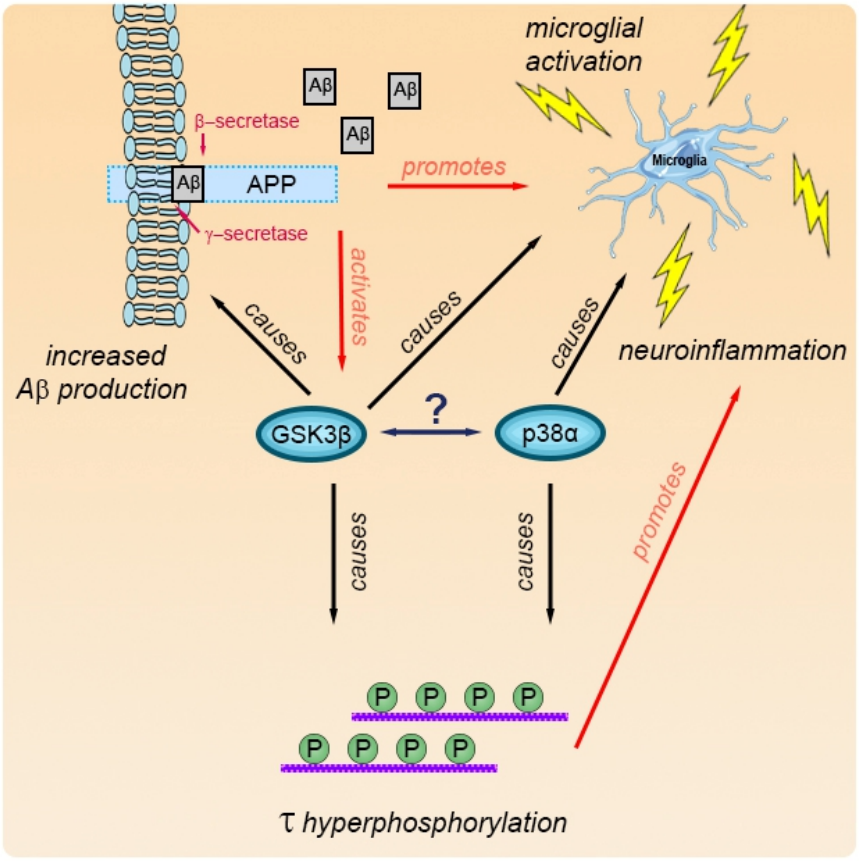

Figure 1.18. Schematic overview of the involvement of GSK3β and p38α MAPK in the progression of AD.

In summary, GSK3β and p38α MAPK have both been identified as crucial components of many neurodegenerative diseases. The inhibition of only one single kinase in these multifactorial disease cascades seems to be inefficient due to the considerable number of involved proteins. Targeting the hallmarks of neurodegenerative diseases with a dual approach should result in synergistic effects since escape mechanisms can be prevented from the start and multiple involved pathways are targeted at once.

2 Aims

2.1 Aims and objectives of the thesis

Until today there is still no therapy to prevent, slow or cure the progression of AD. Therefore, there is a high unmet medical need for new therapies and treatment options.[207] As previously mentioned, GSK3β is a key enzyme in the disease progression of AD and presents hence an attractive drug target. Similarly, p38α MAPK plays a vital role in the associated neuroinflammatory processes. Thus, inhibition of one or both kinases presents a viable option for the development of novel treatment options (*Section 1.5*).

The main aims of this thesis were:

(A) the design and synthesis of a potent, preferably (isoform-)selective and brain penetrant GSK3β inhibitor with good kinome-wide selectivity
as well as the
(B) the design and synthesis of a potent, preferably (isoform-)selective and brain penetrant dual p38α MAPK/GSK3β inhibitor

The first approach would focus on the aforementioned synergistic effects of a dual inhibition of the two pivotal kinases in the development of AD. The second option would allow the use of a novel GSK3β inhibitor alone or in combination with a suitable already known p38α MAPK inhibitor.

During the course of this thesis, both aims were pursued separately in different projects. First, the results of a high-throughput screening (HTS) against GSK3β were carefully analyzed. The Tofacitinib-derived compound **FM-064** (*Figure 2.1*) was a promising hit structure, which at the tested compound concentration of 5.5 µM displayed an inhibition of 87 %. A radiometric validation assay at ProQinase GmBH (Freiburg) determined an IC_{50} value of 5.29 µM. As a starting point of this work, **FM-064** should be subjected to a variety of different modifications in order to obtain first insights into the structure–activity relationship (SAR) of this novel hit compound.

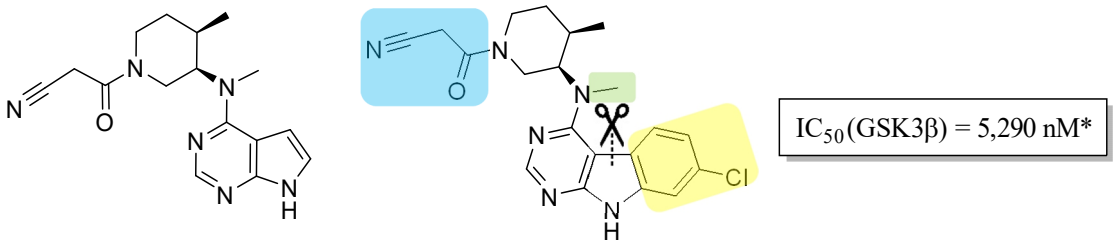

Tofacitinib **FM-064**

Figure 2.1. Structures of **Tofacitinib** and the derived hit compound **FM-064**.

* determined at ProQinase GmbH (Freiburg) using a FlashPlate-based radiometric assay

The 7*H*-pyrrolo[2,3-*d*]pyrimidine core structure is acting as the hinge binding motif in **Tofacitinib** and the same binding mode was expected for **FM-064** in regard to GSK3β. Possible sites of modifications included the exchange or removal of the cyanoacetamide moiety (cyan*; Figure 2.1*), alterations at the exocyclic *N*-methyl group (green; *Figure 2.1*) and different substituent patterns at the annealed phenyl ring (yellow; *Figure 2.1*). Since ANDREEV already started with the preparation of the first analogues during his master thesis[208], the responsibilities were split among the participants in the project. All modifications on the tricyclic core scaffold are therefore subject of a distinct PhD thesis. Instead the focus of this work lies solely on the ring-opened analogues (as indicated by the scissor in *Figure 2.1*) leading from the 9*H*-pyrimido[4,5-*b*]indole core to an anilinopyrimidine analogue. The more flexible, ring-opened derivatives were then modified at the different suggested sites as outlined above (*Section 3.1*).

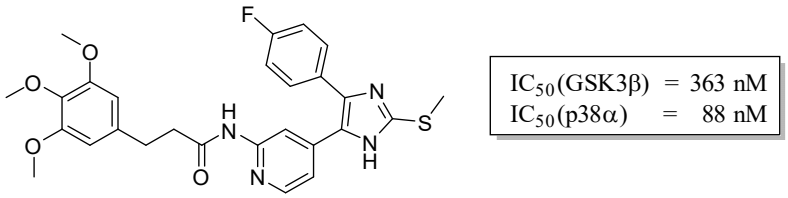

RN4186

Figure 2.2. Hit structure **RN4186** already displayed a reasonable inhibitory potency towards GSK3β and p38α MAPK.

Another interesting hit structure extracted from the HTS was the pyridinylimidazole **RN4186** (*Figure 2.2*). The compound is a known, potent p38α MAPK inhibitor and was independently reported by HALEKOTTE *et al.* as a potential CK1δ inhibitor during the preparation of this work.[209] Optimization of this hit structure towards a better balanced

dual GSK3β/p38α MAPK inhibitor according to aim **(B)** was then planned, starting with the detailed analysis of further pyridinylimidazoles containted in the screening (*Section 3.2.3*). Subsequently, the knowledge gained was used for the design and synthesis of a series of differently substituted *N*-(4-(4-(4-fluorophenyl)-2-(methylthio)-1*H*-imidazol-5-yl)pyridin-2-yl)amides.

Using the knowledge and SARs obtained during the development of the dual GSK3β/p38α MAPK inhibitors, a GSK3β selective inhibitor according to aim **(A)** should be developed containing the pyridinylimidazole core scaffold. In particular, the HR I of GSK3β ought to be probed with different substituents in combination with different modifications at the imidazole-C2 position (*Section 3.2.5*). The lipophilic ligand efficacy of the novel inhibitors was closely monitored to avoid "molecular obesity" to support CNS penetration and a gain of potency through specific protein-ligand interactions.[210]

In another project, it was planned to enhance the metabolic stability of the two known p38α MAPK inhibitors **ML3403** and **LN950** (*Figure 3.8*) by replacing their metabolic hotspot with a more stable group (*Section 3.2.2*).

Beyond this, some bioisosteric replacements in potent pyridinylimidazoles were conducted to show the feasibility of such an approach. Those "proof-of-concept" studies should demonstrate that not only imidazoles are tolerated by the targeted kinases, but also different heterocycles might be used as a di- or trisubstituted backbone structure to avoid certain issues associated with the imidazole ring (*Section 3.3.6*).

3 Results and Discussion

3.1 Project I: Pyrimidine derivates

3.1.1 From Tofacitinib to GSK3β

Tofacitinib (*Xeljanz*®), also known as CP-690,550[211], is a JAK1/JAK3 inhibitor developed by Pfizer Inc. It was approved by the FDA (2012) and EMA (2017) for the treatment of moderate to severe rheumatoid arthritis and has recently also been approved for the treatment of psoriatic arthritis by the FDA. In an HTS against GSK3β, the Tofacitinib-derived tricyclic compound **FM-064** (*Figure 3.1*) was identified as a hit structure showing 1% residual enzyme activity at 10 µM and 13% residual enzyme activity at 5.5 µM in a validation assay. **Tofacinitib** itself did not show any detectable inhibition of GSK3β at 1 µM in a reported selectivity screening.[212] **FM-064** originated from DR. MICHAEL FORSTER'S diploma thesis[213] adressing JAK3 inhibitors and was continued in the master thesis of ANDREEV, who further characterized the hit structure towards GSK3β.[208] The project continued in Andreev's PhD thesis simultaneously to this work, resulting amongst other compounds in the simplified structure **SA01-024** (*Figure 3.1*) with an IC_{50} of 1.86 µM.

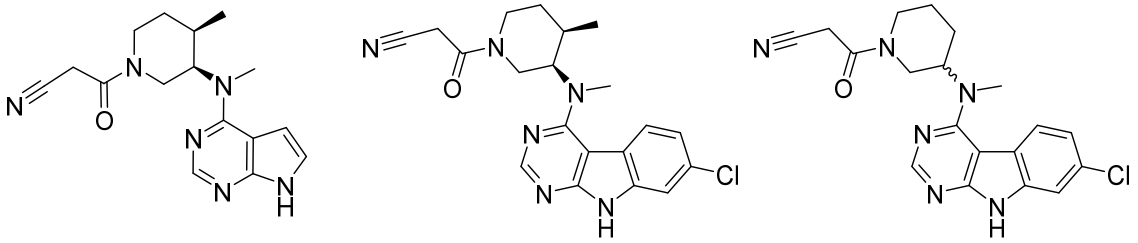

Figure 3.1. Structures of **Tofacitinib**, the derived hit compound **FM-064** and the resulting simplified structure **SA01-024**.

While the methyl group on the piperidine ring is occupying the so-called "JAK selectivity pocket" in JAK3, it was shown to be non-essential for activity against GSK3β. Therefore, in the initial SAR investigations, the racemic *N*-Boc-3-(methylamino)piperidine sidechain was utilized for the synthesis of all derivatives.

It was decided to examine the importance of the tricyclic ring system by cutting the central bond between the C4a and C4b atom in the 9*H*-pyrimido[4,5-*b*]indole core scaffold (*Figure 3.2.*).

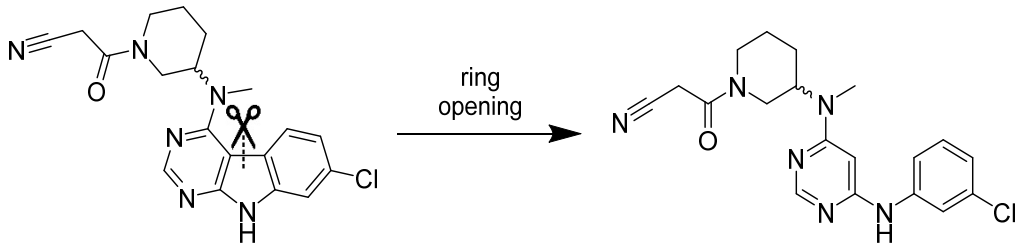

SA01-024 **1**

Figure 3.2. Dismembering the structure of **SA01-024** leads to compound **1**.

The aminopyrimidine motif represents a privileged kinase inhibitor scaffold resulting from its ability to form a bidentate hydrogen bond acceptor/donor system. **Imatinib** and **Ceritinib** are two FDA-approved kinase inhibitors each containing a 2-anilinopyrimidine but in literature also several 4-anilinopyrimidines are reported as potent kinase inhibitors (*Figure 3.3*).[214–216] Our hypothesis was that derivatives with increased flexibility might adjust better to the topology of the binding pocket or provide at least additional information about the general SARs.

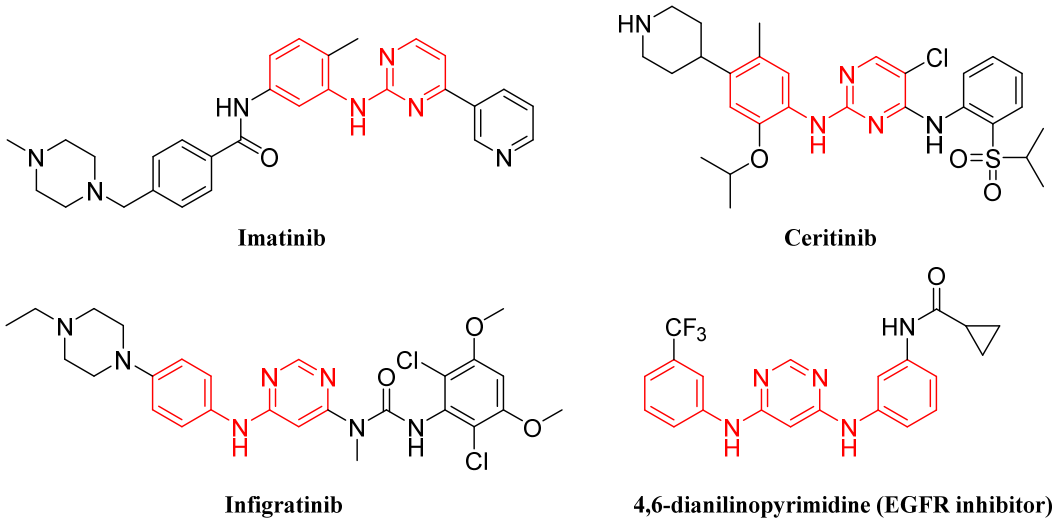

Imatinib **Ceritinib**

Infigratinib **4,6-dianilinopyrimidine (EGFR inhibitor)**

Figure 3.3. 2-Anilinopyrimidine-containing drug **Imatinib** and the 2,4-dianilino-pyrimidine **Ceritinib** are approved by the FDA for the treatment of leukemia and NSCLC, respectively. **Infigratinib** is a pan-FGFR inhibitor with a phenylurea moiety attached to the 4-anilinopyrimidine.[215] Another 4,6-dianilinopyrimidine was reported by ZHANG *et al.* as an EGFR inhibitor, which originated from a combinatorial kinase-directed library.[214]

Preliminary docking experiments with compound **1** in GSK3β (*PDB code:* 4PTC) using Schrödinger Small-Molecule Drug Discovery Suite 2015-4* suggested a reasonable hinge binding mode with the typical bidentate hydrogen bond acceptor/donor setup. The backbone amide of Val135 donates its hydrogen to the pyrimidine-N3, while the carbonyl of Val135 accepts a hydrogen from the pyrimidine-4-amine (*Figure 3.4, 2D representation*). Rational poses were obtained for both stereoisomers of **1**. Docking of the lead compound **SA01-024** resulted in similar binding modes. Most importantly, the hinge binding mode was always postulated as described above by the Glide docking tool. Interestingly, superimposition of the docked poses revealed (*R*)-**1** and (*S*)-**SA01-024** to be almost aligned and forming an additional hydrogen bond between the nitrile moiety and Thr138 (*Figure 3.4, PyMOL figure*). Those interactions were not seen for (*S*)-**1** and (*R*)-**SA01-024** as their nitrile groups were orientated more towards the solvent exposed front region. No direct clashes with the gatekeeper (Leu132) were observed in any pose, as there was always at least a distance of 4 Å between Leu132 and the pyrimidine rings. However, the gatekeeper prevents the aminopiperidine sidechains from rotating 90 to 180 ° away from the aromatic ring systems – two conformations that have been identified as favorable in *ab initio* calculations with **SA01-024**. The biggest difference was seen in the angles between the planes of the rings. While the tricyclic core of **SA01-024** was obviously planar, compound **1** showed angles between 27 ° and 45 °, depending on the pose (*ring angles measured between chlorophenyl and pyrimidine ring*).

The lack of a crystal structure of GSK3β co-crystallized with **FM-064**, **SA01-024** or a closely related compound as ligand was one of the reasons why computer-aided drug design strategies like structure-based lead optimization were not regarded as useful at the beginning of the project. Another reason was the scarcity of credible SARs. For example, it was unknown which stereoisomer was the eutomer and whether the nitrile group was adding a substantial contribution to the binding affinity. The necessity of the exocyclic amide moiety on the piperidine ring was equally unclear as the impact of the chloro atom. Furthermore, the high flexibility of the aminopiperidine sidechain proved to be challenging for most of the computational docking techniques.

---

* Maestro 10.4 (Schrödinger, LLC) with OPLS_2005 force field.
Prior to docking, all ligands were prepared using LigPrep with default settings.
The protein was processed using the Protein Preparation Wizard with default settings and the receptor grid was defined by the co-crystallized ligand. Glide docking was performed with XP precision.
The figures were prepared with PyMOL 2.0.7 (Schrödinger, LLC).

Altogether, the decision was made to generate some general SAR data first by synthesizing a variety of compounds addressing the aforementioned questions and re-evaluate the usefulness of computational docking methods at a later stage of the project.

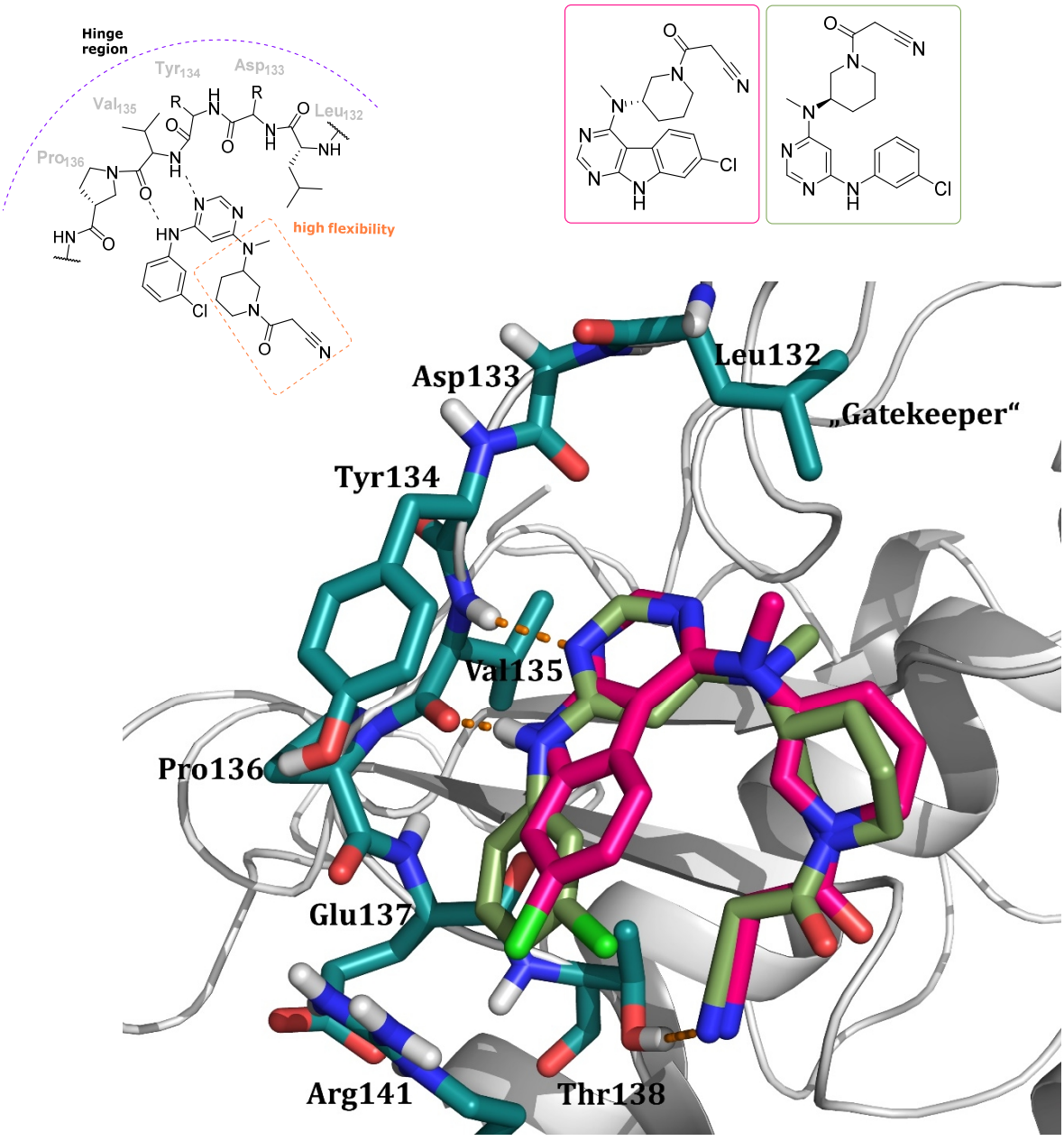

Figure 3.4. *Top left:* 2D representation of the interaction between GSK3β and **1**. *Below:* Overlay of (*S*)-**SA01-024** (magenta) and (*R*)-**1** (green) in GSK3β (*PDB code:* 4PTC). The glycine-rich-loop cartoon representation has been omitted for clarity. Hydrogen bonds are shown as orange dashes.

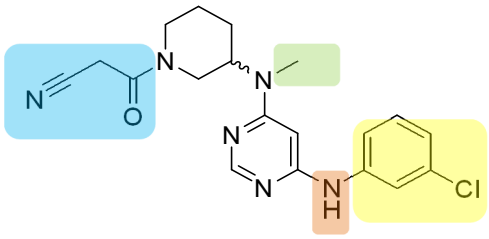

Figure 3.5. Modification sites for compound **1**.

The simplified hit structure **SA01-024** and its ring-opened derivative **1** offered plenty of areas suitable for derivatization, exchange or removal of moieties to evaluate the influence of each region on the binding affinity of the molecule.

An initial strategy consisted of derivatizing the nucleophilic nitrogen of the piperidine ring by replacing the cyanoacetamide moiety (*Figure 3.5*; *cyan*) with a variety of other amides. The carboxylic acids used in the amide coupling were chosen so that they contained one or more hydrogen bond acceptors, as it was suspected that the nitrile might act as a hydrogen bond acceptor, too. Additionally, the complete removal of the amide and installation of the corresponding propanenitrile was attempted to reveal the influence of the rather rigid, planar amide bond.

Another series of derivatives was planed, wherein the 3-chlorophenyl substituent (*Figure 3.5*; *yellow*) was exchanged against other phenyl rings with different substituents in the 3-position. Introduction of aminoheterocycles, differently-sized amides or phenyl ureas attached to the pyrimidines was then a way to retain the suspected hinge binding motif while exploring the surrounding SARs. The removal of the 3-chlorophenyl ring, leaving a simple methylamine, was also supposed to reveal more insights into the binding mode.

Modifications on the *N*-methylpiperidine part (*Figure 3.5*; *green*) were not prioritized but the removal of the methyl group would lead to increased polarity of the molecules and another potential hydrogen bond donor site.

Finally, the replacement of the aniline nitrogen (*Figure 3.5*; *orange*) will be discussed in detail in *Section 3.1.3*.

3.1.2 Synthesis of amino-/amido-/anilinopyrimidines

Starting from commercially available 4,6-dichloropyrimidine, a nucleophilic aromatic substitution (S_NAr) with 3-chloroaniline led to the mono-substituted anilinopyrimidine **4**, which was obtained in high yields (*Scheme 3.1*). The introduction of the first amino group deactivated the pyrimidine, making a second S_NAr unfavorable. Literature procedures proposed the use of harsh reaction conditions like high temperatures, prolonged heating for days or the addition of strong acids. Since the *tert*-butyloxycarbonyl (Boc) protecting group is fairly unstable under elevated temperatures and acidic conditions, all of the mentioned conditions tend to be problematic in combination with *N*-Boc-3-(methylamino)piperidine as the second reactant. While a deprotection of the Boc group after the formation of the desired product would be without consequences, an earlier formation of the unprotected piperidine (i.e. before/during the reaction) would certainly lead to unwanted side-products as the intracyclic nitrogen atom is more nucleophilic than the exocyclic *N*-methyl. In search of alternatives, neat heating of both reactants as proposed in a patent was examined.[217] The reaction led to the desired disubstituted pyrimidine but during the heating to 150 °C, the Boc group was indeed cleaved as expected and a significant amount of a not further characterized side-product was formed. Furthermore, the purification process was complicated and tedious, making the reaction unsuitable as a general procedure due to its doubtful reproducibility. The unsubstituted piperidine ring was coupled with cyanoacetic acid using benzotriazol-1-yl-oxytripyrrolidinophosphonium hexafluorophosphate (PyBOP) as coupling reagent and *N*,*N*-diisopropylethylamine (DIPEA) as a base to afford the ring-openend analogue (**1**) of the lead compound **SA01-024**.

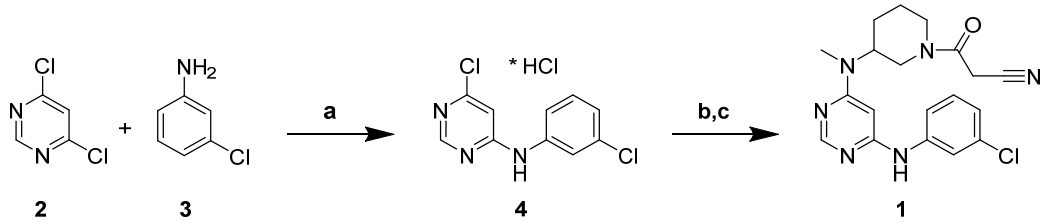

Scheme 3.1. Synthesis of compound **1**: (a) conc. HCl, iPrOH, 85 °C, 83%; (b) *N*-Boc-3-(methylamino)piperidine, neat, 150 °C; (c) cyanoacetic acid, PyBOP, DIPEA, DCM, rt, 15 % (*over 2 steps*).

Among the examinded alternatives to a S_NAr under harsh conditions, the Buchwald-Hartwig amination was found to be the most suitable one. This C-N bond forming,

palladium-catalyzed cross-coupling reaction can be employed under mild conditions, also tolerating acid labile reactants. In 1995, Stephen L. Buchwald and John F. Hartwig each independently discovered a cross-coupling reaction of aryl bromides with amines using a bis(tri-o-tolylphosphine)palladium(0) catalyst/ligand system in the presence of a base.[218,219] Originally the scope of the reaction was limited in terms of suitable substrates, solvents and bases. Using novel phosphine ligands, today also aryl chlorides, iodides and triflates can react with a broad repertoire of amines using a variety of different reaction conditions. As a result, the Buchwald-Hartwig amination has become an indispensable tool for chemists in the last two decades and is one of the most frequently used reactions in medicinal chemistry.[220]

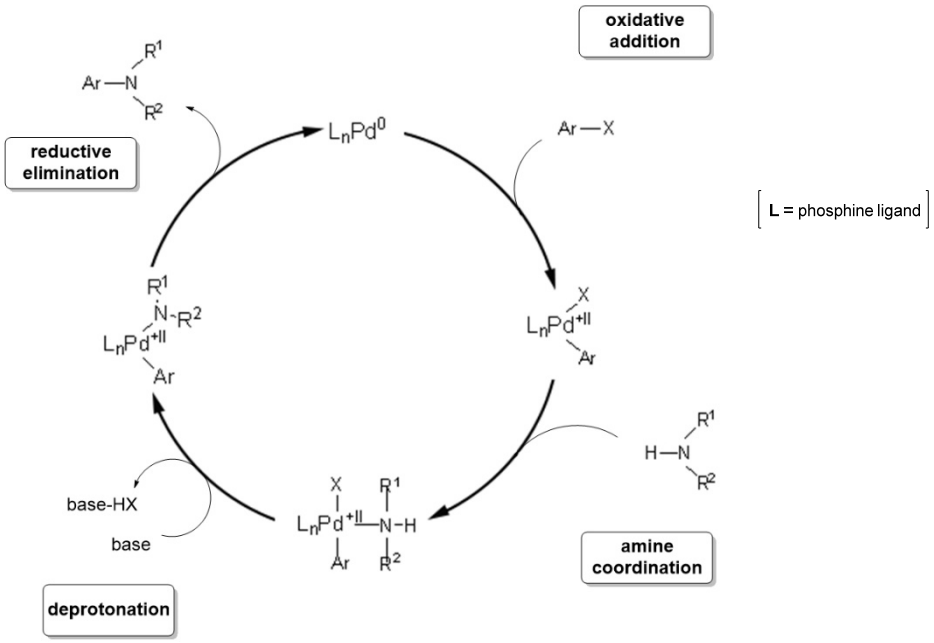

Figure 3.6. Catalytic cycle of Buchwald-Hartwig amination.

The catalytic cycle of the of Buchwald-Hartwig amination is similar to the general cycle of all Pd-catalyzed cross-couplings. First the oxidative addition of the aryl halide to the Pd^0 species takes place. In the second step, coordination of the amine to the palladium occurs followed by deprotonation through the base. Finally, the reductive elimination yields the aryl amine product and regenerates the catalyst. Instead of the reductive elimination a β-hydrogen elimination may occur as side-reaction (*not shown in Figure 3.6*) which produces the hydrodehalogenated arene and an imine. However, with the right choice of ligands this side-reaction can be completely avoided.[221,222]

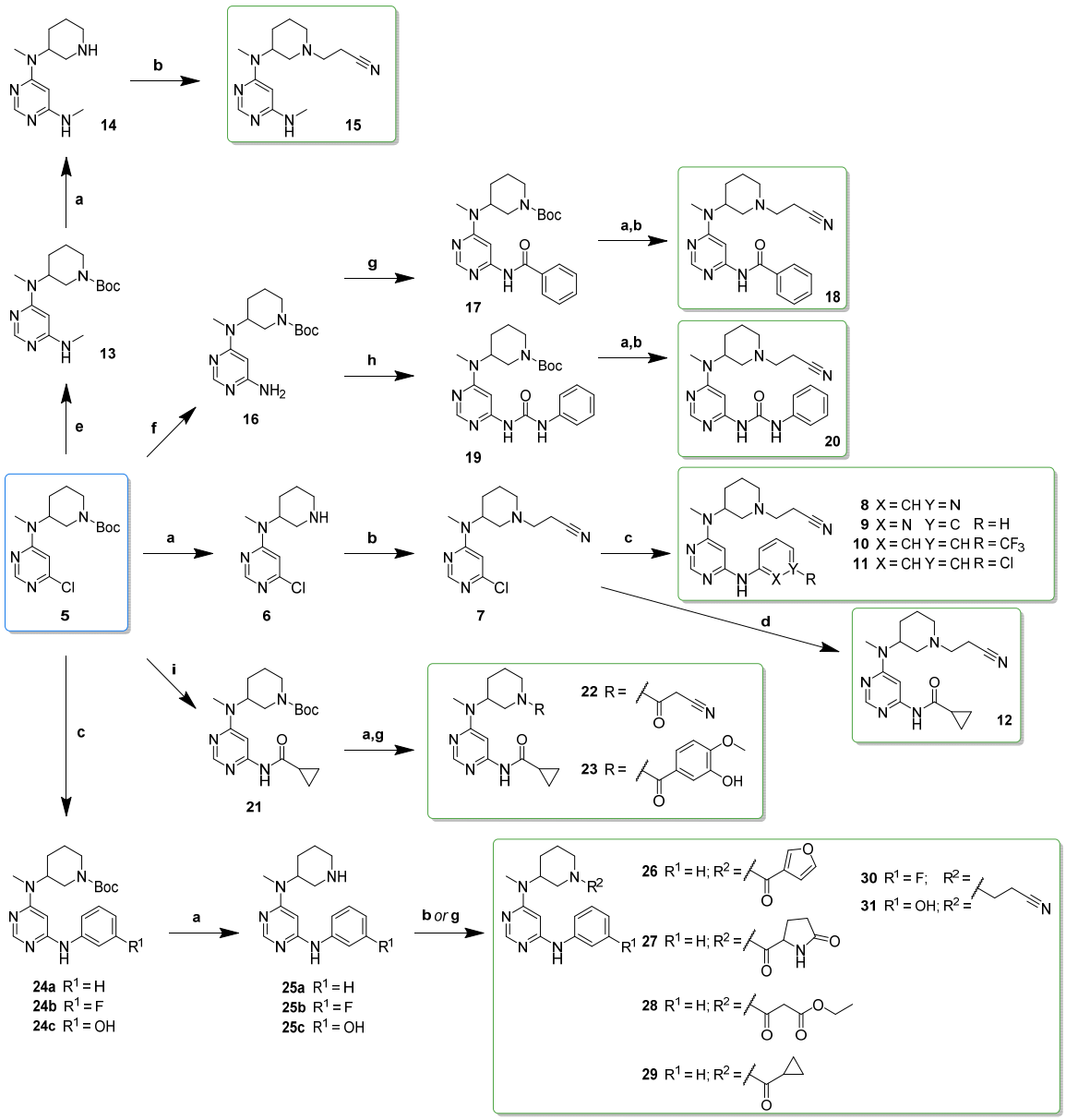

Scheme 3.2. Comprehensive overview of all syntheses starting from key intermediate **5**: (a) TFA in DCM (1:5 ratio), rt, 92-100 %; (b) acrylonitrile, (*sometimes* Et_3N), MeOH, rt, 33-62 %; (c) 2-aminopyridine *or* 3-aminopyridine *or* 3-substituted aniline, $Pd_2(dba)_3$, XPhos, NaO*t*Bu, DMF, 80 °C, 35-84 %; (d) cyclopropanecarboxamide, $Pd_2(dba)_3$, XantPhos, Cs_2CO_3, DMF, 90 °C, 30 %; (e) 2 M methylamine in MeOH, 95-120 °C, 83 %; (f) $Pd_2(dba)_3$, (*t*-Bu)$_3$P·HBF$_4$, 0.5 M LiHMDS in 1,4-dioxane, 80 °C, 73 %; (g) corresponding carboxylic acid, PyBOP, DIPEA, DCM, rt, 20-81 %; (h) phenyl isocyanate, toluene, 90 °C, 62 %; (i) cyclopropanecarboxamide, $Pd_2(dba)_3$, XantPhos, Cs_2CO_3, DMF, 110 °C, 78 %.

Since the plan was to exchange the 3-chloroaniline moiety against different substituents, in the first step 4,6-dichloropyrimidine was subjected to a S_NAr with *N*-Boc-3-(methylamino)piperidine, resulting in the key intermediate **5**. Starting from **5** a variety of reactions was employed to obtain an array of differently 4,6-substituted pyrimidines with the aim to generate some general SAR data (*Scheme 3.2*).

The S_NAr of **5** with methylamine as a nucleophile proceeded smoothly (**13**) once the reaction was heated for a prolonged time. Deprotection in diluted trifluoroacetic acid and a subsequent Michael reaction with acrylonitrile gave the final product **15**. As already mentioned, with weaker nucleophiles or where harsh conditions were not applicable, the Buchwald-Hartwig amination was used as an effective alternative. For example, key intermediate **5** was coupled with various anilines using an tris(dibenzylideneacetone)-dipalladium(0)/XPhos system in DMF to yield the still Boc-protected products (**24a**-**24c**). After deprotection, the intermediates were derivatized at the intracyclic nitrogen of the piperidine ring utilizing PyBOP and different carboxylic acids (**26**-**29**). Preliminary test results indicated that an exchange of the cyanoacetamide moiety against other amides seemed potentially unfavorable. New developments in the derivatization of the lead compound **SA01-024** also revealed that the replacement of a cyanoacetamide moiety through propanenitrile was possibly beneficial and should be further investigated.[223] For this reason, the other two derivatives **25b** and **25c** which resulted from 3-fluoroaniline and 3-aminophenol, respectively, were only subjected to a Michael addition with acrylonitrile. Once the propanenitrile moiety was established as the most effective substituent on the piperidine ring, intermediate **5** was deprotected and the piperidine was reacted with acrylonitrile to give the versatile intermediate **7**. Using Buchwald-Hartwig amination with 2- and 3-aminopyridine, 3-(trifluoromethyl)aniline and 3-chloroaniline led to the respective final compounds in moderate to very good yields. Most likely side-reactions like homocoupling or polymerization were responsible for the lower yield observed, when 3-chloroaniline was used as reactant (35 %, **11**). Once more starting from **7**, a Buchwald-Hartwig reaction using XantPhos as phosphine ligand and cyclopropanecarboxamide as reactant yielded the 4-(cyclopropanecarboxamido)-pyrimidine derivative **12**. Applying similar reaction conditions to key intermediate **5** gave the still Boc-protected 4-(cyclopropanecarboxamido)pyrimidine derivative (**21**) in much higher yields (78 % here vs. 30 % for **12**). Again, deprotection and in this case derivatization with PyBOP and carboxylic acids gave two final compounds (**22** and **23**). A second way to form amidopyrimidines was created after a procedure reported by

GEHRINGER *et al.*, in which lithium hexamethyldisilazide (LiHMDS) was used as an ammonia equivalent in a Buchwald-Hartwig coupling.[224] The formed aryl bissilylamine was hydrolyzed with aqueous HCl during the work-up, resulting in the free aminopyrimidine **16**. From **16**, a benzamidopyrimidine derivative (**18**) was synthesized using again PyBOP as an amide coupling reagent followed by the standardized deprotection and a Michael addition with acrylonitrile. Urea formation in decent yields was achieved by heating **16** and phenyl isocyanate in toluene for 16 hours. Deprotection and Michael addition again produced a final compound, this time with a urea moiety as the hinge binding motif (**20**).

Modifications on the exocyclic *N*-methyl nitrogen atom were limited to the removal of the methyl group. The synthetic route was straightforward, starting again with an S_NAr between 4,6-dichloropyrimidine and in this case 3-fluoroaniline. Using the established Buchwald conditions, the commercially available racemic *N*-Boc-3-aminopiperidine was reacted with **32** in acceptable yields. The final product (**34**) was obtained after deprotection and the previously described Michael addition (*Scheme 3.3*).

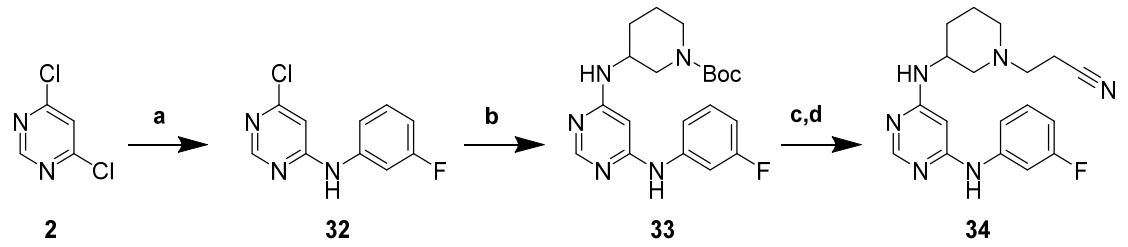

Scheme 3.3. Synthesis of compound **32**: (a) 3-fluoroaniline, DIPEA, *n*-BuOH, 120 °C, 62 %; (b) *N*-Boc-3-aminopiperidine, $Pd_2(dba)_3$, XPhos, NaO*t*Bu, DMF, 80 °C, 42 %; (c) TFA in DCM (1:5 ratio), rt; (d) acrylonitrile, MeOH, rt, 59 % (*over 2 steps*).

Clearly, 2,4-substituted pyrimidines are an overrepresented structural class in kinase scaffolds and literature reports when compared with its 4,6-analogue (e.g. *Figure 3.3; Imatinib and Ceritinib*). A SciFinder comparision between these two closely related heterocyclic core structures reveals a roughly 5-fold difference in favor of the 2,4-diaminopyrimidine (as of December 2018). Thus, a "flipped" phenyl analogue of compound **10** was synthesized and likewise tested in our assay. Synthesis started accordingly from 2,4-dichloropyrimidine and the first S_NAr with *N*-Boc-3-(methylamino)piperidine gave the desired regioisomer in a very good yield (*Scheme 3.4*).

The remaining steps to compound **35** were carried out analogues to the synthesis of the 4,6-derivatives.

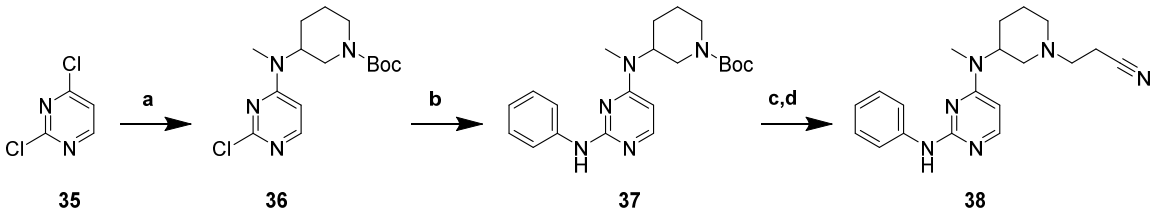

35 **36** **37** **38**

Scheme 3.4. Synthesis of 2,4-diaminopyrimidine **38**: (a) *N*-boc-3-(methylamino)-piperidine, DIPEA, iPrOH, 85 °C, 81 %; (b) aniline, $Pd_2(dba)_3$, XPhos, NaO*t*Bu, DMF, 80 °C, 51 %; (c) TFA in DCM (1:5 ratio), rt; (d) acrylonitrile, MeOH, rt, 68 % (*over 2 steps*).

Unfortunately, in the end all of the tested compounds were inactive or only very weakly active against GSK3β and no solid SAR conclusions could be drawn on the basis of the synthesized molecules (*Table 3.1 and Table 3.2 for detailed overview*). ELISA assays for p38α MAPK, c-Jun N-terminal kinase 3 (JNK3) and JAK3 at 10 μM concentration of compound revealed also no meaningful inhibition.

Despite a lot of effort, we were unable to obtain a co-crystal structure of GSK3β in complex with any (fused or ring-opened) 9*H*-pyrimido[4,5-*b*]indole derivative. Therefore, well reasoned predictions about binding mode and other certain peculiarities of this compound class are impossible. However, the ring-opened, novel compounds presented here have a distinctly higher degree of flexibility enabled by the additional rotational bond between the two aromatic rings. This seems to result in low-energy conformations of the molecules, which are highly unfavorable in regard to the overall binding affinity.

Table 3.1. Biological activity of the synthesized anilinopyrimidines.

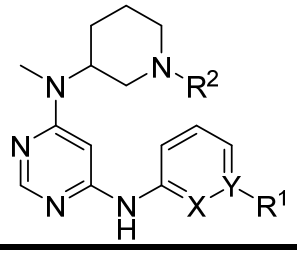

inhibition in % at 10 µM or * = IC_{50} values in µM

ID	R^1	R^2	X	Y	GSK3β	p38α MAPK	JNK3	JAK3
1	Cl	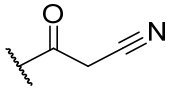	CH	C	>100 µM*	33 %	0 %	0 %
26	H	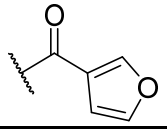	CH	C	7 % †	49 %	8 %	4 %
27	H	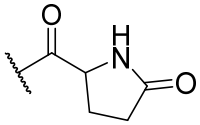	CH	C	24 % †	9 %	9 %	5 %
28	H	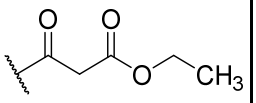	CH	C	4 % †	33 %	2 %	16 %
29	H	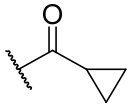	CH	C	1 % †	2 %	0 %	13 %
11	Cl	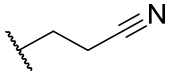	CH	C	24 % †	18 %	16 %	0 %
10	CF_3	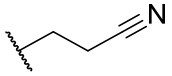	CH	C	10 % †	31 %	12 %	25 %
30	F	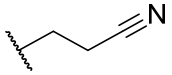	CH	C	>100 µM*	17 %	7 %	19 %
31	OH	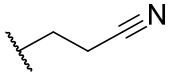	CH	C	>100 µM*	13 %	16 %	1 %
8	-	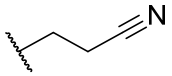	CH	N	44 % †	21 %	14 %	14 %
9	H	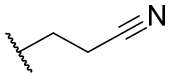	N	C	>100 µM*	12 %	18 %	0 %

* = IC_{50} values determined at ProQinase GmbH (Freiburg) using a FlashPlate-based radiometric assay

† = tested in an ADP-Glo assay at a concentration of 10 µM[225]

‡ = tested in an ELISA assay at a concentration of 10 µM

detailed ELISA assay conditions are described in each reference individually for p38α MAPK[226]*, JNK3*[227] *and JAK3*[228]

Table 3.2. Biological activity of the synthesized amidopyrimidines, phenylurea **18**, methylaminopyrimidine **13** and anilinopyrimidines **32** and **35**.

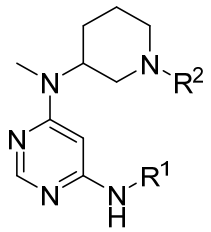

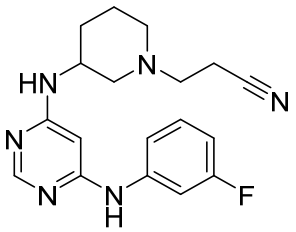

34

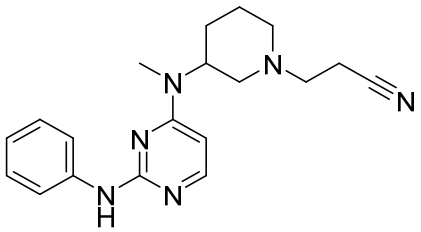

38

inhibition in % at 10 µM or * = IC_{50} values in µM

ID	R^1	R^2	GSK3β	p38α MAPK‡	JNK3‡	JAK3‡
23	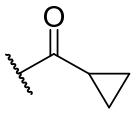	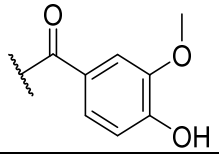	24 % †	23 %	3 %	23 %
22	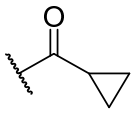	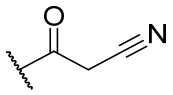	22 % †	44 %	10 %	13 %
12	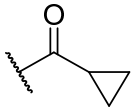	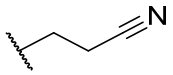	>100 µM*	21 %	1 %	0 %
18	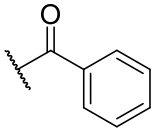	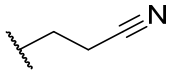	>100 µM*	n.d.	n.d.	0 %
20	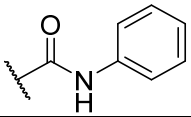	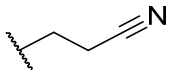	15 % †	33 %	n.d.	22 %
15		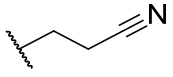	>100 µM*	12 %	9 %	28 %
34	-	-	>100 µM* 29 % †	42 %	n.d.	6 %
38	-	-	10 % †	n.d.	n.d.	n.d.

n.d. = not determined

* = IC_{50} values determined at ProQinase GmbH (Freiburg) using a FlashPlate-based radiometric assay

† = tested in an ADP-Glo assay at a concentration of 10 µM[225]

‡ = tested in an ELISA assay at a concentration of 10 µM

detailed ELISA assay conditions are described in each reference individually for p38α MAPK[226]*, JNK3*[227] *and JAK3*[228]

3.1.3 Synthesis of phenoxypyrimidines

Although the assumed hinge binding motif of the simplified 9*H*-pyrimido[4,5-*b*]indole derivative **SA01-024** involves a hydrogen bond acceptor/donor motif (*Figure 3.4*), a series of phenoxypyrimidines was planned to validate our hinge binding theory. If correct, the loss of one hydrogen bond donor would be reflected in a loss of activity compared to the anilinopyrimidines. It should be noted that at the start of the project, no in-house assay for GSK3β kinase activity was established, yet. Therefore, at the time of the synthesis of this series, it was not yet known that the anilinopyrimidines series displayed only poor inhibitory potency per se. A comparison between both series for our purposes then turned out to be ineffectual. Nevertheless, the compounds were tested at ProQinase GmbH (Freiburg) in a FlashPlate-based radiometric GSK3β assay. In-house screening at 10 µM against p38α MAPK, JNK3 and JAK3 generated additional data to characterize the compounds.

A straightforward synthetic route was planned, starting again from 4,6-dichloropyrimidine. Two successive S_NAr enabled the preparation of intermediates **41a** and **41b** in good yields. Using the well-established deprotection conditions followed by amide coupling with PyBOP or the previously described Michael addition with acrylonitrile gave the final products **42-48** (*Scheme 3.5*).

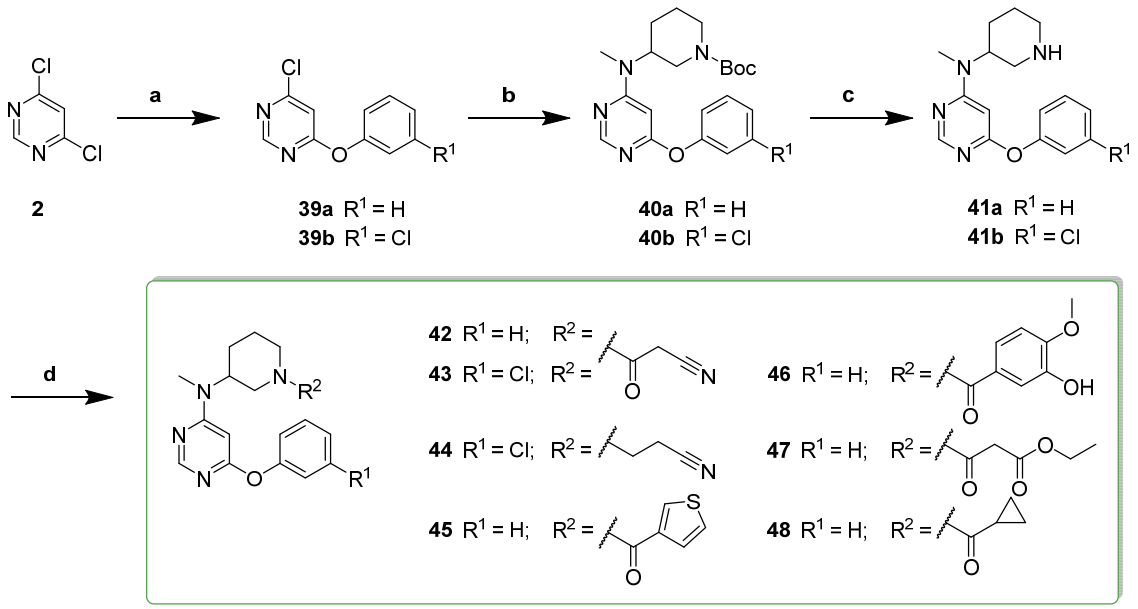

Scheme 3.5. Synthetic route to compounds **42-48**: (a) phenol, K_2CO_3, DMF, rt, 65 % *or* 3-chlorophenol, K_2CO_3, NaI, MeCN, rt, 97 %; (b) *N*-boc-3-(methylamino)piperidine, DIPEA, DMF, 80 °C, 56-71 %; (c) TFA in DCM (1:5 ratio), rt, 81-83 %; (d) carboxylic acid, PyBOP, DIPEA, DCM, rt, 23-81 % *or* acrylonitrile, MeOH, rt, 94 %.

In order to examine yet another hinge binding motif, a 6-aroylpyrimidine (**50**) was synthesized starting again from key intermediate **5**. Deprotonation of 3-fluorophenylacetonitrile is achieved with sodium hydride as strong base and the resulting stabilized benzylic carbanion then displaces the chlorine at the pyrimidine-C6. *In situ* oxidation led to a 6-(3-fluorobenzoyl)pyrimidine derivative (**49**) which was subjected to deprotection followed by a Michael addition to finally yield **50**.

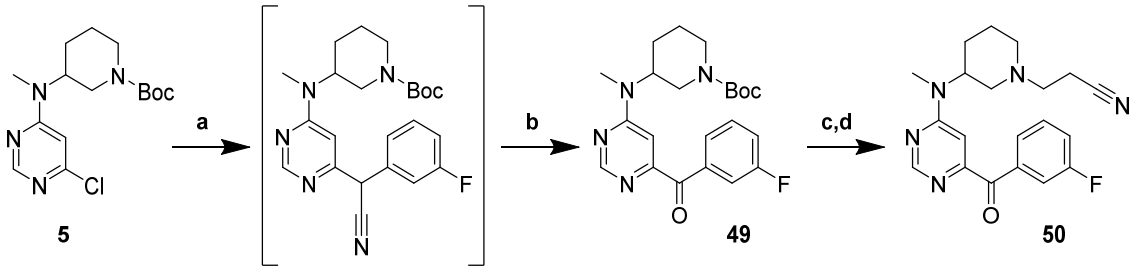

Scheme 3.6. Synthesis of compound **50**: (a) 3-fluorophenylacetonitrile, NaH, DMF, -20 °C → rt; (b) atmospheric O_2; (c) TFA in DCM (1:5 ratio), rt; (d) acrylonitrile, MeOH, rt, 76 % (*over 4 steps*).

As already expected all compounds were basically inactive with an $IC_{50} > 10$ µM against our desired target. Screening against an in-house kinase panel at a concentration of 10 µM from different families showed some very weak inhibition of p38α MAPK and none in a JNK3 ELISA assay. Moreover, the tyrosine kinase JAK3 was also not affected by the molecules. Only compounds **43**, **44** and **50** showed a weak measurable effect, likely due to their given similarity to the original lead structure **Tofacitinib** (which is a potent JAK1/JAK3 inhibitor).

Table 3.3 Biological activity of the synthesized phenoxypyrimidines and 3-fluorobenzoylpyrimidine **47**.

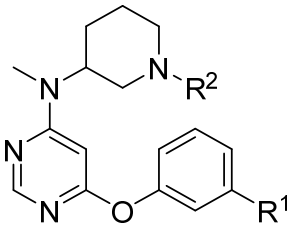

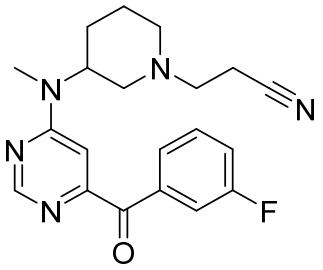

50

inhibition in % at 10 µM or * = IC_{50} values in µM

Cpd	R^1	R^2	GSK3β	p38α MAPK‡	JNK3‡	JAK3‡
42	H	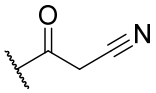	>100 µM*	38 %	0 %	n.d.
45	H	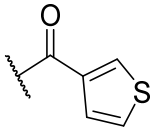	>100 µM*	42 %	0 %	4 %
46	H	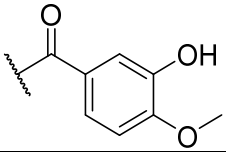	>100 µM*	39 %	0 %	0 %
47	H	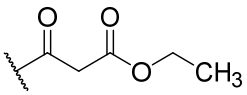	>100 µM*	11 %	4 %	5 %
48	H	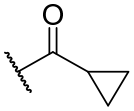	>100 µM*	37 %	0 %	0 %
43	Cl	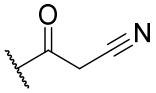	>100 µM*	43 %	0 %	19 %
44	Cl	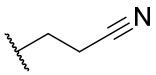	15 % †	n.d.	8 %	18 %
50	-	-	>100 µM*	17 %	7 %	19 %

n.d. = not determined

* = IC_{50} values determined at ProQinase GmbH (Freiburg) using a FlashPlate-based radiometric assay

† = tested in an ADP-Glo assay at a concentration of 10 µM[225]

‡ = tested in an ELISA assay at a concentration of 10 µM (conditions see legend *Table 3.2*)

3.1.4 Synthesis of the simplified Tofacitinib derivative

Another idea to generate first SAR insights was the removal of the annelated 3-chlorophenyl from our starting structure **SA01-024**. A closely related analogue of the original lead structure **Tofacitinib** should provide some clarity about the significance of the tricyclic core structure. The synthesis of the simplified **Tofacitinib** derivative (**54**) was started from commercially available 4-chloro-7*H*-pyrrolo[2,3-*d*]pyrimidine which was protected with a tosyl group to facilitate the following S_NAr with *N*-Boc-3-(methylamino)piperidine as described by ANDREEV.[208] Deprotection of the tosyl group was achieved in a basic environment whereas the Boc-group was cleaved with diluted trifluoroacetic acid. Finally, acrylonitrile was used to substitute the deprotected piperidine nitrogen in a Michael reaction. In our in-house GSK3β ADP-Glo assay compound **54** showed an IC_{50} of 2.99 µM. Compared to the tricyclic hit structure (IC_{50} = 1.86 µM) the removal of the ring leads to a ~ 2-fold decrease of inhibition. Changes in this rather small magnitude allow the conclusion that the annelated ring is not involved in any kind of directed interactions with the kinase. Also, it does not seem to sterically force the piperidine ring into a favorable conformation. However, unspecified lipophilic interactions might be leading to the slightly better potency of the inhibitor.

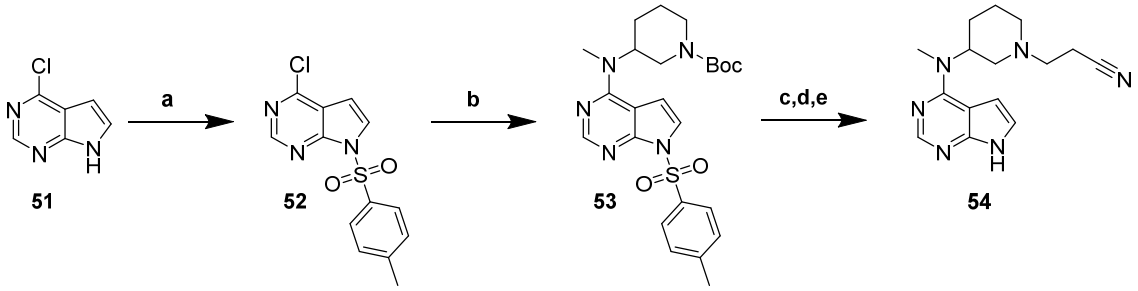

Scheme 3.7. Synthesis of compound **54**: (a) NaH, tosyl chloride, THF, 0 °C → rt, 92 %; (b) *N*-Boc-3-(methylamino)piperidine, DIPEA, DMF, 70 °C, 65 %; (c) NaO*t*Bu, THF, rt; (d) TFA in DCM (1:5 ratio), rt; (e) acrylonitrile, MeOH, rt, 35 % (*over 3 steps*).

3.2 Project II: Pyridinylimidazoles

3.2.1 History of pyridinylimidazoles in drug discovery

Trisubstituted pyridinylimidazoles have been known as anti-inflammatory drugs since **SKF-86002** and **SB-203580** (*Figure 3.7*) were disclosed in 1987 and 1995 by SmithKline Beecham, respectively.[229,230] At first the pharmacological target of the compounds was unknown but researchers at the company eventually managed to isolate and identify the p38α MAPK as an important kinase related to inflammatory processes.[179] The fact that, when binding to p38α MAPK, the inhibitors adopt a three-dimensional shape which distantly resembles the form of a tear led to the term "teardrop binders", which sometimes is used to refer to this structural class of compounds. The high versatility of this scaffold enabled the synthesis of multiple different pyridinylimidazole-based inhibitors, targeting several kinases next to p38α MAPK such as CK1δ/CK1ε[209], JNK3[231], triple mutant EGFR[232], B-Raf[233], ALK5[234] and TIE2 kinase[235]. A recent review by KOCH AND ANSIDERI presents a general overview of the synthesis and biological activity of pyridinylimidazoles against different kinases.[236]

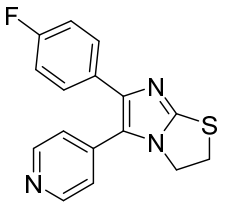

SKF-86002

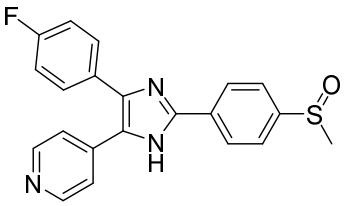

SB-203580

Figure 3.7. Prototypical trisubstituted pyridinylimidazoles and recognized p38α MAPK inhibitors **SKF-86002** and **SB-203580**.[230]

3.2.2 Improving the metabolic stability of 2-methylsulfanylimidazoles

The results of this project were published in Publication I.

Potential drawbacks of the 2-methylsulfanylimidazole scaffold are the occurring metabolic oxidation of the sulfur and the potential inhibition of cytochrome P450 (CYP) enzymes. CYPs are hemeproteins which prevalenty catalyze monooxygenase reactions in the liver. They are heavily involved in drug metabolism accounting for up to 75% of all metabolism reactions in humans and changes in their activity can lead to severe adverse drug reactions or treatment failure.[237] Imidazoles (and *N*-containing heterocycles in general) are known to be potential CYP inhibitors – a property that is even used therapeutically: **Fadrozole** contains a tetrahydroimidazo[1,5-*a*]pyridine and acts as a CYP19A1 (aromatase) inhibitor by coordinating to the heme iron. It was approved in 1995 in Japan to treat estrogen-dependent breast cancer.[238]

There are several ways to minimize the risk of CYP-associated liabilities. Reducing lipophilicity is a reasonable approach since unwanted CYP inhibition is often associated with high log P values.[239] Another way is the introduction of bulky or interfering moietys next to the *N*-atoms so that the coordination to the heme iron is hindered. The most logical option is of course the removal of the disturbing heterocycle. Simple omission of the imidazole in this case was impossible as it was the structural backbone of the molecule. Therefore, a bioisosteric replacement of the imidazole represented an interesting possibility which is discussed in *Section 3.2.6*. Issues like CYP-mediated liver toxicity became already obvious during the development of the triaryl pyridinylimidazole **SB-203580**. LAUFER *et al.* introduced a sulfur at the imidazole-C2 partially in order to reduce these toxic effects. However, this modification alone was not sufficient and only when a bulky tetramethylpiperidinyl moiety was introduced at the imidazole-N1, CYP inhibition was substantially reduced.[240] As already mentioned, those 2-thioimidazole derivatives are prone to oxidation by metabolic enzymes such as CYPs. The resulting sulfoxides are potent active metabolites which have been studied and characterized in detail as p38α MAPK inhibitors.[241–243] However, in the GSK3β assay all tested sulfoxide metabolites were 3 to 6-fold less active than their parent compounds indicating a potential problem. The 2-methylsulfanylimidazoles acting as dual GSK3β/p38α MAPK inhibitors (*Publication II*) displayed in fact decent stability (degradation of 50% over 4 h) in preliminary experiments with human liver microsomes (HLM) but in the follow-up *in vivo* experiments in mice, rapid metabolism to the sulfoxides was observed. In order to

improve the metabolic stability of the compounds and to assess the influence of the 2-thio moiety in regard to pharmacokinetic properties (e.g. cellular permeability) as well as CYP inhibition, 2-alkylimidazole derivatives of the known potent p38α MAPK inhibitors **ML3403**[240] and **LN950**[244] were synthesized (*Figure 3.9*).

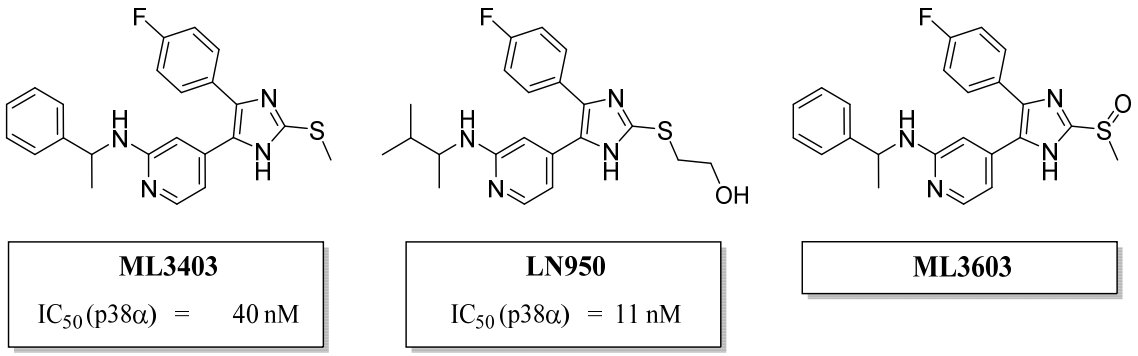

Figure 3.8. Previously reported potent inhibitors of p38α MAPK: **ML3403**[245], **LN950**[244], and its active metabolite **ML3603**.[242]

All synthesized 2-alkylimidazoles were metabolically stable over a period of 4 h when incubated with HLM. They displayed a similar inhibitory activity as their corresponding 2-methylsulfanylimidazole counterparts when tested against the isolated p38α MAPK enzyme in an ELISA assay.[226] The complete findings of this exploratory study can be found in Publication I (*Appendix*).

3.2.3 High-throughput screening and hit identification

The results of this project were published in Publication II.

Selected compounds of our in-house library containing more than 4000 molecules were screened against GSK3β at a compound concentration of 5.5 µM in a HTS. This led to the identification of some pyridinylimidazole-type inhibitors which showed a promising activity of more than 80 % inhibition at the tested concentration. This result was somewhat surprising since GSK3β was not seen as an off-target in selectivity screens previously performed for other pyridinylimidazoles.

Table 3.4. Top 5 pyridinylimidazole-type screening hits against GSK3β.

ID	Structure	Inhibition at 5.5 µM	Ref.
55 (**RN4186**)	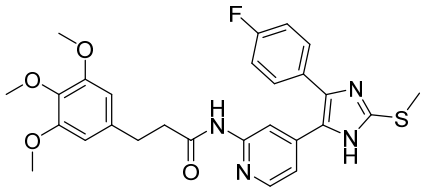	95 %	209
56	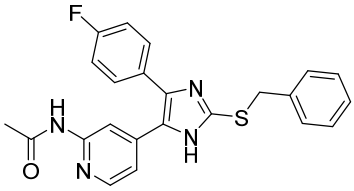	88 %	-
57	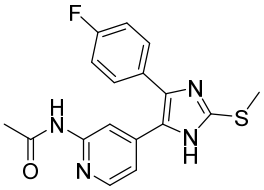	86 %	243
58	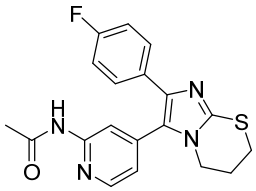	84 %	-
59	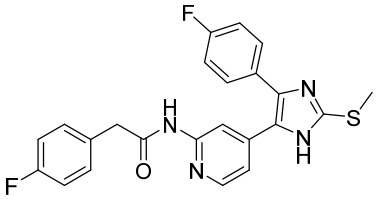	83 %	246

A closer analysis of all 269 pyridinylimidazole-type structures extracted from the screening, revealed that eleven out of the twelve best hits possessed an amide moiety at the pyridine-C2 position, seven were 2-methylsulfanylimidazoles and the ratio of tri- to tetrasubstituted imidazoles was seven to five. The first finding was rather unexpected since most of the included pyridinylimidazoles either possessed an amino moiety at the pyridine-C2 or similar to **SB-203580** no substituent on the pyridine at all. From the five best hits (*Table 3.4*), p38α MAPK inhibition data on two compounds (**57** and **59**) were

already published with values of 37 nM and 9 nM, respectively.[243] Gratifyingly, the screening contained multiple examples of "matched molecular pairs" that differ structurally from each other only at a single site.[247] By comparing the inhibitory potency of these pairs, well-grounded assumptions about the importance of certain functional groups in the structures could be deduced. Compound **57** had at least 12 derivatives with modifications at the imidazole-N1 included in the HTS. Often short alkyl chains (ethyl/propyl) with a halogen or hydroxyl group at the end were introduced in this position. But also, a tetrahydropyranyl group or 3-propanonic acid were among the functionalizations. However, all derivatives were substantially less active than **57**, indicating the importance of the unsubstituted imidazole nitrogen. Most of the compounds in our library contained an S-methyl moiety at the imidazole-C2 position. Due to this bias it was no surprise that many hits contained this motif. Interestingly the 2nd best hit (**56**) possessed a S-benzyl group in this position, which indicated a certain tolerance of bulkier groups towards this zone and thereby space for modifications. A known metabolic pathway of 2-methylsulfanylimidazoles is the CYP-mediated oxidation to the corresponding 2-methylsulfinylimidazole.[243] The few sulfoxides included in the screening were always showing decreased inhibition of GSK3β compared to their parent compounds. This finding urged us to keep an eye on the prevalence of metabolites and their activity during the development of the inhibitors. The most important suggestion from the data referred to the pyridine-C2 position. As already mentioned, the best inhibitors were all in possession of an amide moiety in this position. Exchange of the acetamide of **57** against simple isopropyl- or cyclopropylamines resulted in a massive loss of potency and the same decrease was seen for almost any amine. In contrast, different amides had a quite diversified impact on the enzyme, depending on the size and properties of the moiety attached adjacent to the amide group. This region demonstrated potentially great promise for improvements and previous synthetic efforts were mostly concentrated on different amines, making it reasonable to start expanding the SARs around the *N*-(pyridin-2-yl)amide moiety. The as well desired effect of p38α MAPK inhibition was also not impaired by the exchange of amines through amides at the pyridine-C2 position, as demonstrated by the data published for **57** and **59**. On top of that, even bulky residues can be accommodated by p38α MAPK since the HR II is solvent-exposed and therefore quite spacious. Because the pyridine core was considered to be essential for binding to the hinge region of both kinases, any changes here were ruled out for the first iterative synthetic cycles. The influence of the 4-flurorophenyl residue was

impossible to interpret as the vast majority of structures in the screening library possessed this structural feature. Additionally, the importance of an aryl ring in the imidazole-C4 position for p38α MAPK inhibition had been previously noticed.[231]

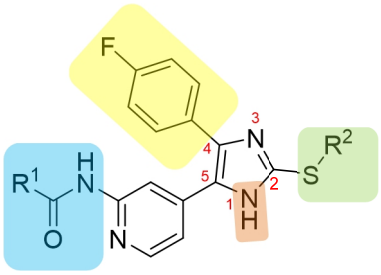

Figure 3.9. Possible modification sites of the core pyrid–inylimidazole are colored.

In summary, the best starting point for derivatization was found to be in the pyridine-C2 position. The synthesis of a series of different amides (blue; *Figure 3.9*) varying in size and carrying different additional functional groups seemed a promising approach to gain first SAR for this compound class in connection with GSK3β. Derivatization of the imidazole-N1 and imidazole-C4 were disregarded for the moment for reasons explained in the paragraph above. Lastly a closer look was taken on the differences between S-methyl and S-benzyl (green; *Figure 3.9*), hence a small series of 2-benzylsulfanyl-imidazoles was planned to assess the potential of certain amide functions in combination with the S-benzyl moiety. As a consequence of the observed metabolic liabilities (*Section 3.2.2*), an additional series of 2-alkylimidazoles was synthesized and biologically evaluated in the enzymatic assays.

3.2.4 Optimization of dual GSK3β/p38α MAPK inhibitors

The results of this project were published in Publication II.

A retrosynthetic analysis of the screening hits offered two possibilities for the introduction of the crucial amide moiety at the pyridine-C2 (*Scheme 3.8*). The preparation of the 2-chloropyridine precursor **60** had been already described as a high-yielding four-step synthesis.[248] Using non-optimized Buchwald-Hartwig conditions with the unprotected imidazole **60** and various (cyclo)alkylamides resulted in the corresponding *N*-(pyridin-2-yl)amides with yields up to ~ 60 %. According to literature research, this is the first time a successful Buchwald-Hartwig reaction has been reported for an unprotected trisubstituted 2-methylsulfanylpyridinylimidazole bearing a halogen moiety at the pyridine-C2 position.

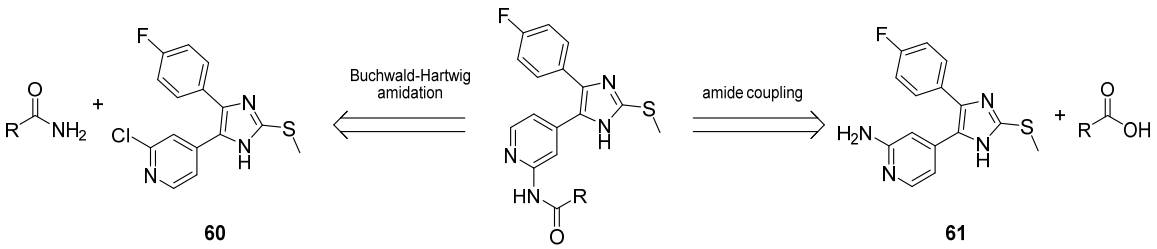

Scheme 3.8. Retrosynthetic approach towards the desired *N*-(pyridin-2-yl)amides.

However, the reaction suffered from inconsistent yields depending on the amides used and the need of rather expensive catalysts/ligands. Thus, the direct preparation of the desired compounds from intermediate **61** presented a more appealing option. Compound **61** itself can be synthesized for example starting from the corresponding 2-fluoropyridine derivative of **60** using ammonia under harsh SNAr conditions in a high-pressure reactor. As an alternative option, a slightly modified synthetic route from KOCH *et al.* was chosen for the preparation of **61**.[244] Starting from *tert*-butyl *N*-(4-methylpyridin-2-yl)carbamate a concise six-step synthesis derived from led to the key intermediate **61** in a good overall yield of 34 % calculated over 7 steps (*Scheme 3.9*). Finally, the desired amide moieties were introduced by direct reaction of **61** with acid chlorides or via carboxylic acids in combination with an amide coupling reagent. In this manner, a variety of distinctively substituted *N*-(pyridin-2-yl)amides were synthesized and evaluated in the biological *in vitro* assays against GSK3β and p38α MAPK.

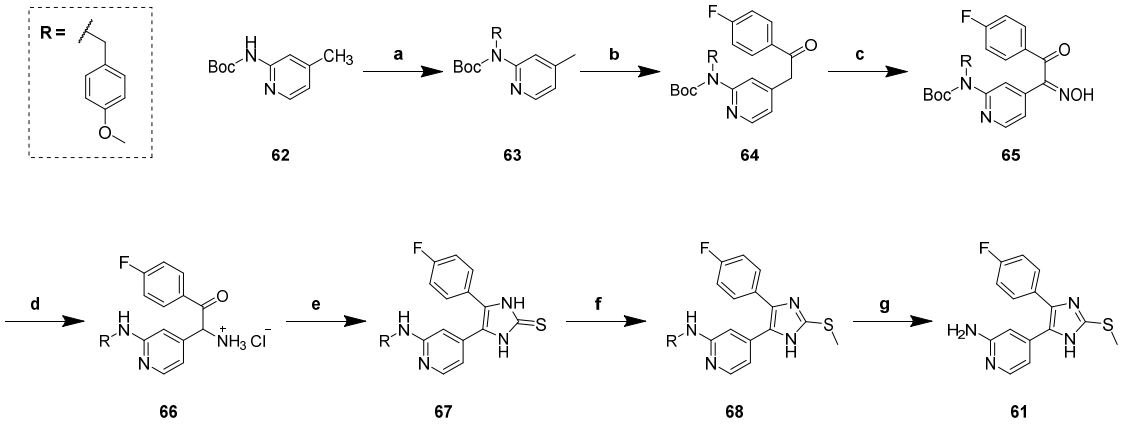

Scheme 3.9. Synthesis of key intermediate **61**: (a) NaH, 4-methoxybenzyl chloride, DMF, 0 °C, quant.; (b) NaHMDS, ethyl 4-fluorobenzoate, THF, 0 °C, 67 %; (c) $NaNO_2$, acetic acid, rt, quant.; (d) H_2, Pd/C 10 %, HCl in MeOH (sat. soln), 45 °C; (e) KSCN, DMF, 160 °C, 62 % (*over 2 steps*); (f) CH_3I, NaO*t*Bu, MeOH, 55 °C, 84 % (g) TFA, 45 °C, 97 %.

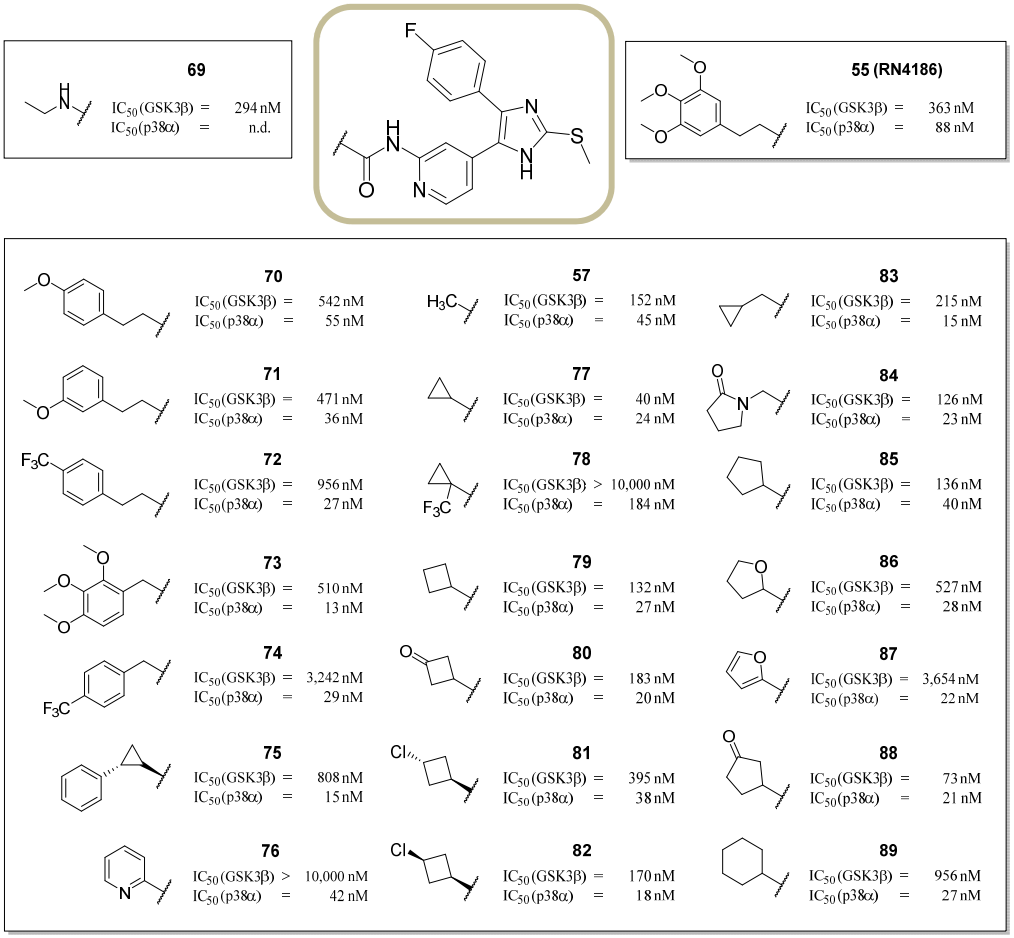

Figure 3.10. Biological evaluation of the synthesized compounds against GSK3β and p38α MAPK.

A synthesized, small series of five 2-benzylsulfinylimidazoles (*not shown here*; Publication II, *Appendix*) displayed – despite the promising hit structure **56** – only moderate to weak activity against GSK3β and the series was therefore not further developed. The ethylurea derivative **69** was also not displaying a much enhanced binding affinity and the focus was consequently put entirely on amide derivates. Among the synthesized compounds (*Figure 3.10*) were numerous inhibitors with an improved inhibitory potency against GSK3β going from the low triple, down to the double digit nanomolar range (e.g. **77**, **79**, **84** and **88**). The GSK3β/p38α MAPK ratio was also improved in some compounds compared to the hit structure **55** (ratio of 4.1). The well-balanced dual inhibitor **77** showed a GSK3β/p38α MAPK ratio of 1.7 and was at the same time the most potent compound from this series regarding GSK3β. Thus, the inhibitor was further evaluated towards its metabolic stability by *in vitro* experiments with HLM. Due to previous studies on the metabolic stability of similar 2-methylsulfanylimidazoles, it was known that the imidazole-C2 position is a "metabolic hotspot" for oxidation (*Section 3.2.2*). As expected, the HLM experiments resulted in the generation of the corresponding 2-alkylsulfinylimidazole (**90**) as the main metabolite. The compound was also synthesized and subjected to both inhibition assays where it showed a 6-fold reduced activity versus GSK3β while its activity versus p38α MAPK was only reduced by ~ 2-fold. This shift of the GSK3β/p38α MAPK ratio from 1.7 to 5.4 was seen critical as the steady formation of the active metabolite **90** *in vivo* would lead to an unwanted inhibitory dysbalance over time.

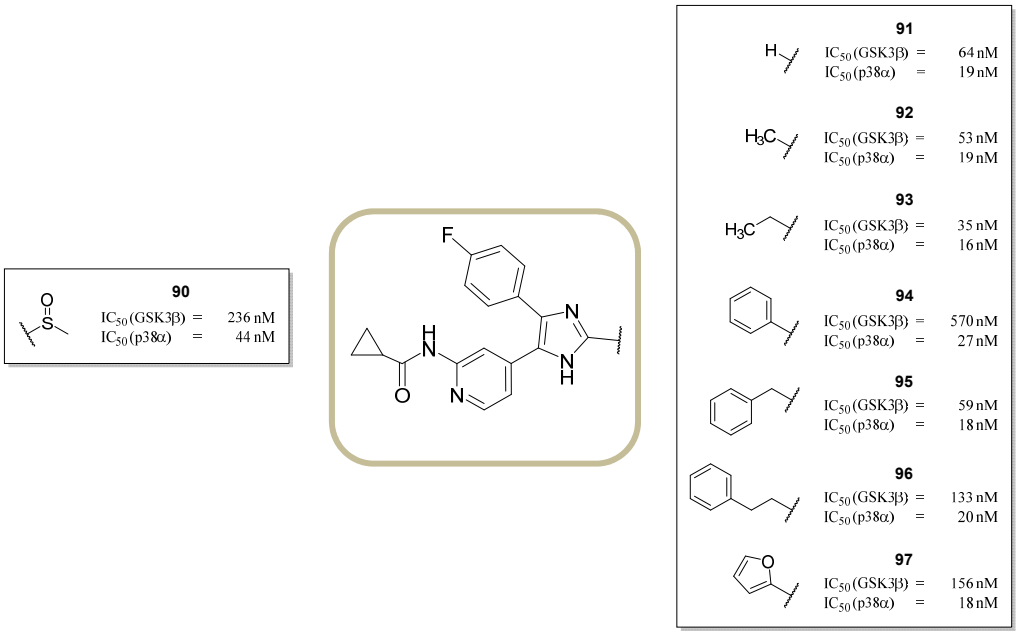

Figure 3.11. Biological evaluation of the metabolite **90** and the metabolically stable 2-alkylimidazole compounds **91-97** against GSK3β and p38α MAPK.

Based on the experiences gained during the improvement of **ML3403** and **LN950** (*Section 3.2.2*), a series of 2-alkylimidazoles (**91**-**97**) were synthesized by Urs Haun with the aim of creating metabolically more stable, potent, dual GSK3β/p38α MAPK inhibitors.[249] The concept was successfully realized as compound **93** was unaffected over a 4 h period of incubation with HLM. Compounds **77** and **93** were additionally tested in mice for their ability to cross the BBB. The active metabolite of **77** (= **90**) and **93** showed a moderate CNS-penetration proving the general suitability of this compound class to act as CNS drugs. Furthermore, the inhibition of LPS-stimulated TNF-α release from human whole blood (which is p38α MAPK-dependant)[250] was determined for **77** (541 nM) and **93** (317 nM) as well as their *in vitro* CYP and human Ether-a-go-go-related gene (hERG) channel inhibition profile (*Table 3.5*). Unintentitional inhibition of the hERG channel has been associated with QT prolongation, a dangerous cardiac side-effect. Compounds with hERG IC_{50} values above 10 µM are usually considered to be safe with respect to this adverse effect.[251] Details about the dangers of unwanted CYP inhibition have been already outlined in Section *3.2.2*.

Table 3.5. Evaluation of potential hERG and CYP liabilites.

	% inhibition at compound conc. of 10 µM					
Cpd	**hERG**	**CYP1A2**	**CYP2C9**	**CYP2C19**	**CYP2D6**	**CYP3A4**
77	30.1	88.4	77.7	56.1	14.6	75.6
93	43.3	83.6	83.6	81.7	58.3	75.1

Finally, GSK3 isoform selectivity was determined by subjecting a selected set of compounds also to the ADP-Glo GSK3α assay. Comparing the absolute IC_{50} values of **77** and **93**, the inhibitors showed a 7.5-fold and 8.5-fold selectivity towards the β isoform, respectively. To make definite statements about the discrimination of pyridinylimidazoles between the α and β isoforms, the determination of the K_i values would be beneficial.

A deeper analysis of all data and detailed descriptions of the experimental procedures performed can be found in Publication II (*Appendix*).

3.2.5 From dual-targeting to GSK3β-targeting inhibitors

The results of this section were published in Manuscript I.

Compound **98** (*Figure 3.12*) originated as a simplified derivative from the potent dual GSK3β/p38α MAPK inhibitor **77** and its metabolically more stable 2-alkylimidazole derivative **93**, during the development of the dual-targeting inhibitors (*Section 3.2.4*).

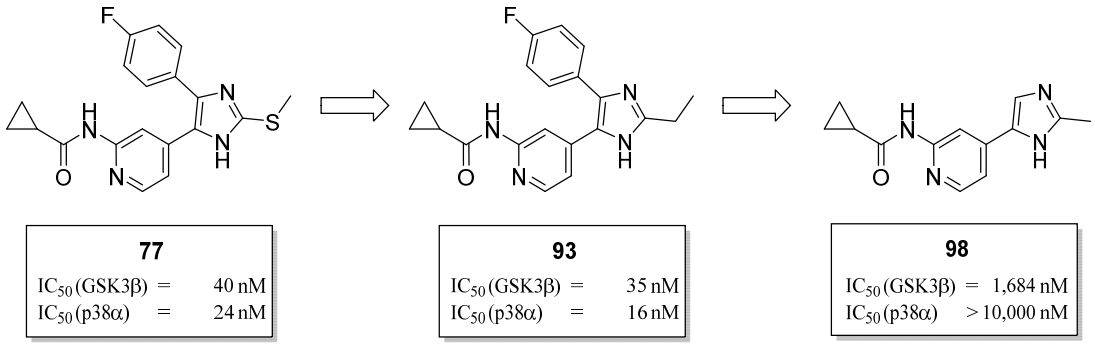

Figure 3.12. The potent dual GSK3β/p38α MAPK inhibitor **77** was derivatized to give the metabolically more stable 2-alkylimidazole **93**. Removal of the 4-fluorophenyl ring occupying HR I, resulted in **98**.

While the inhibitory potency of **98** versus GSK3β is decreased by a factor of ~ 45, a complete loss of activity against p38α MAPK was observed. Those dramatic changes can be attributed to the removal of the 4-fluorophenyl ring targeting the HR I. ANSIDERI *et al.* showed the influence of different aromatic and (cycloc)aliphatic moieties at the imidazole-C4 position on the inhibition of p38α MAPK and the closely related JNK3.[231] Thus, it was known that pyridinylimidazole-based p38α MAPK inhibitors prefer an aromatic ring reaching into HR I instead of smaller, non-aromatic residues. Regarding GSK3β, the influence and importance of the 4-fluorophenyl ring was not elucidated yet. The interesting inhibitory dysbalance of **98**, made the molecule a good starting point for further derivatizations with the aim of synthesizing a GSK3β selective di- or trisubstituted pyridinylimidazole. It was planned to probe the HR I of GSK3β with different aromatic and (cyclo)aliphatic moieties in order to deduce the best fitting residue with good inhibitory potency and selectivity over p38α MAPK (*Figure 3.13*). At the same time, the log P values and the lipophilic ligand efficacy of the synthesized compounds were calculated.[252] Decreased lipophilicity is generally associated with lower attrition rates in clinical trials due to less toxicity issues (e.g. reduced CYP interactions) and better pharmacokinetic properties.[253] Futhermore, log P values in the range of 0-3 have been

appraised as beneficial for the crossing of the BBB.[254] As a result, the focus was to avoid "molecular obesity" and the gain of potency solely through lipophilic interactions.[210]

The target molecules were constructed using a building block strategy beginning from the cost-efficient 2-methylimidazole (< 0.16 €/g). In this synthetic route the di- and trisubstituted imidazoles were build up gradually applying Pd-catalyzed C–C cross-coupling reactions (*Scheme 3.10*). Utilizing this strategy enables easy access to flexible variations in different parts of the molecules: probing the HR I with different aryl groups at the imidazole-C4 is as well possible as testing differently substituted pyridines or even other heterocycles as hinge binders.

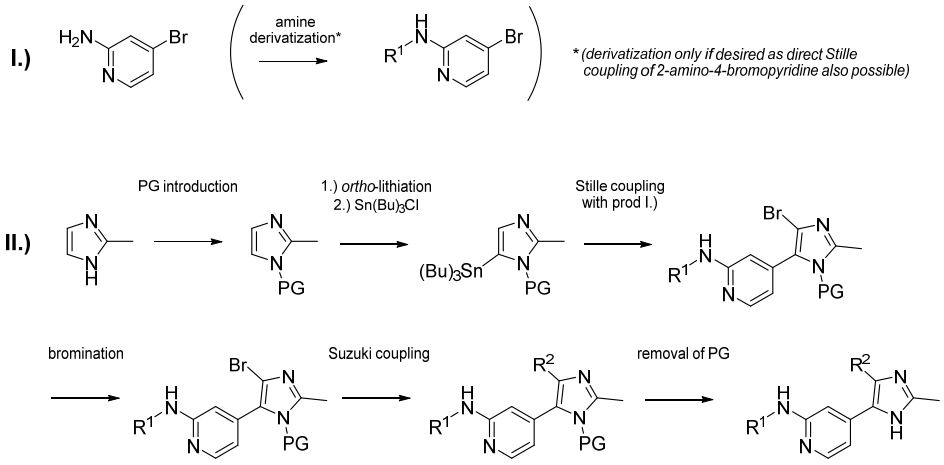

Scheme 3.10. General scheme of the flexible synthetic strategy towards differently substituted 2-methylimidazoles. **PG** = protecting group.

A lot of different synthetic stragies utilizing Pd-catalyzed C–C cross-coupling reactions towards pyridinylimidazole kinase inhibitors have been reported over the years (e.g. LIEDTKE *et al.*[248], GÜNTHER *et al.*[232], JUCHUM *et al.*[255] and SELIG *et al.*[256]). However, none of these routes were designed for the fast derivatization of the pyridine-C4 position, while maintaining a determined moiety towards the HR II. Many more Pd-catalyzed C–C cross-coupling strategies towards trisubstituted imidazoles have been described in literature but often the products are rather easily accessible triarylimidazoles (like **SB-203580**) or the synthetic procedures are incompatible with the azaheterocycle needed as integral part of the hinge binding motif – especially if this heterocycle is further substituted (e.g. as *N*-(pyridin-2-yl)amide or pyridine-2-amine).[257–261] One limitation of this route that has yet to be overcome, is that despite a plethora of different catalysts/ligand systems tested, couplings with (cyclo)alkylboronic acids were unsuccessful until now.

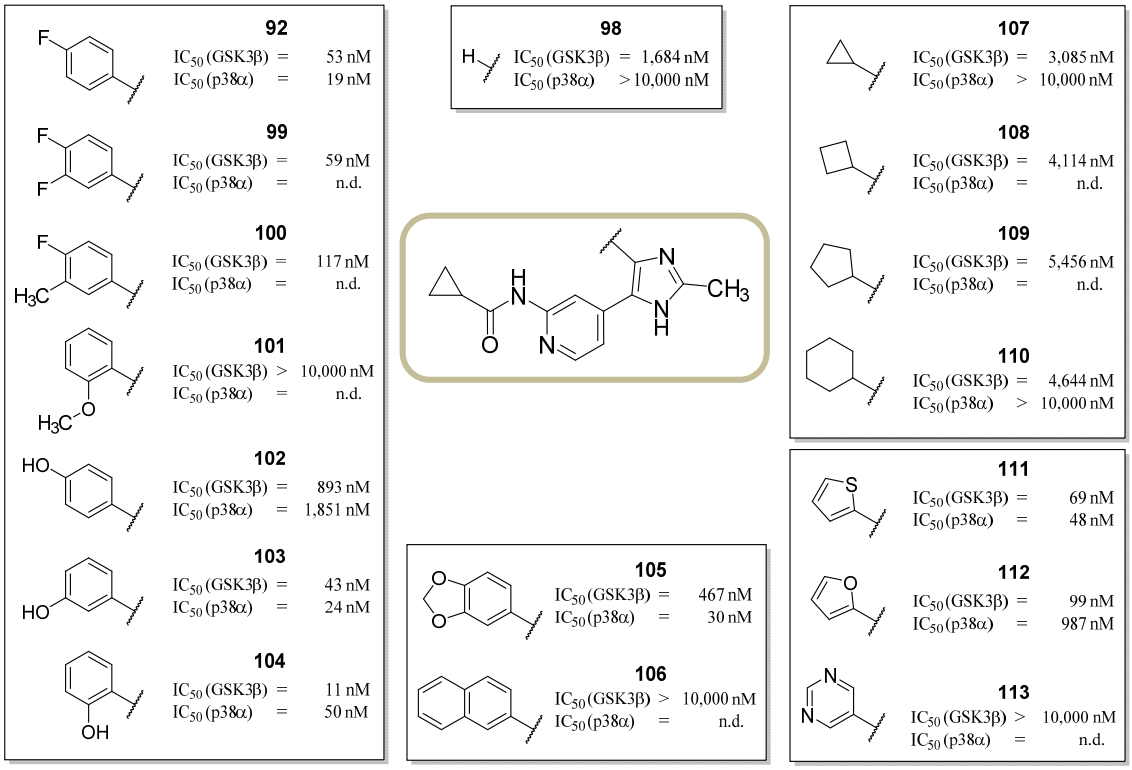

Figure 3.13. Biological evaluation of 2-methylimidazoles bearing different substituents targeting the HR I of GSK3β.

All prepared substances were again measured in the ADP Glo GSK3β assay and the most promising compounds were evaluated in an ADP Glo p38α MAPK assay which showed good correlation with the previously used ELISA p38α MAPK assay concerning the comparability of the IC_{50} values (*Figure 3.13*). Overall, a very similar profile of moieties is tolerated by both kinases. Aromatic rings filling the HR I are mandatory for submicromolar potency even if GSK3β is slightly more tolerant towards cycloaliphatic groups. Bigger moieties (**105** and **106**) are much better tolerated by p38α MAPK probably due to the larger HR I resulting from different gate keeper moieties (Leu in GSK3β; Thr in p38α MAPK). Similar to **106**, Ansideri *et al.* recently reported a 4-(4-(naphthalen-2-yl)-1*H*-imidazol-5-yl)pyridine with an IC_{50} value of 16 nM versus p38α MAPK, underlining the fact that there is plenty of space for bulky residues in the HR I of this kinase.[231] Introduction of *ortho*-, *meta*- and *para*-hydroxyphenyl rings led to the improved compound **104** with a 4.5-fold selectivity towards GSK3β. Even more selectivity was observed for compound **112**, which displayed a 10-fold selectivity towards GSK3β. Several more, rather well-balanced dual inhibitors were obtained (e.g. **103** and **111**). However, overall these findings confirmed that substitution of the imidazole-C4 with aromatic moities is not beneficial when pursuing selectivity away from p38α MAPK.

Thus, another strategy to generate more potent GSK3β inhibitors without an aromatic ring towards the HR I had to be fabricated. A computational docking approach revealed an opportunity to target a conserved lysine in GSK3β (Lys85) by exchanging the 2-methyl group against a 2-carboxamide (*Figure 3.14*). This Lys is forming a crucial salt bridge with Glu97 and is highly conserved throughout the kinome.[262] However, due to its flexibility and because of minor shifts in other areas of the kinases, the position of this salt bridge and thus the position of the Lys85 can vary substantially. For example, in p38α MAPK using pyridinylimidazoles as inhibitors, the corresponding Lys53 is forming a charge-assisted hydrogen bond with the imidazole nitrogen in close proximity.[263] Hence, despite the conservation, a good selectivity profile is achievable especially when other parts of the molecules are considered as well.

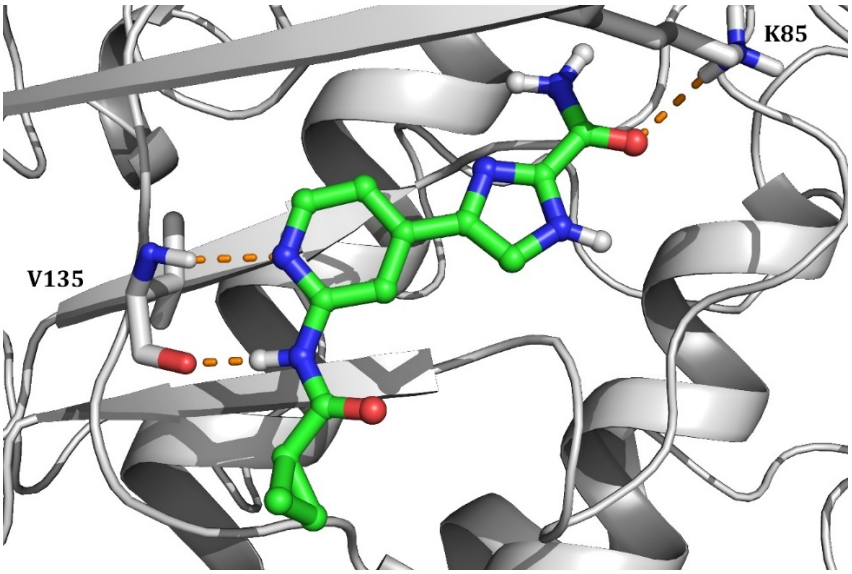

Figure 3.14. Docking pose of **114** in GSK3β (*PDB code:* 4PTC). The glycine-rich-loop cartoon representation has been omitted for clarity. Lysine 85 (*upper right side*) and Valine 135 (*left side*; in the hinge region) are depicted in stick representation. Hydrogen bonds are shown as orange dashes.

The synthesis and biological evaluation of the computationally designed and docked compound **114** resulted in a potent GSK3β inhibitor with a favorable selectivity profile in our in-house panel. The inhibitor was not only selective over p38α MAPK but showed also a ~ 30-fold selectivity over JNK3, which is also targeted by a variety of pyridinylimidazoles (*Figure 3.15*).[264]

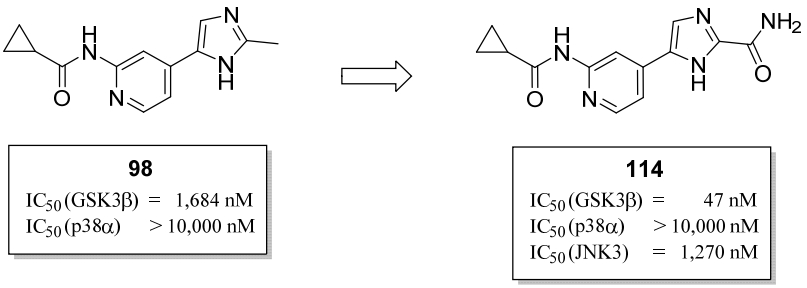

Figure 3.15. Exchange of the 2-methyl group (**98**) against a 2-carboxamide (**114**) led to an impressive improvement in GSK3β inhibition while the selectivity over p38α MAPK was maintained.

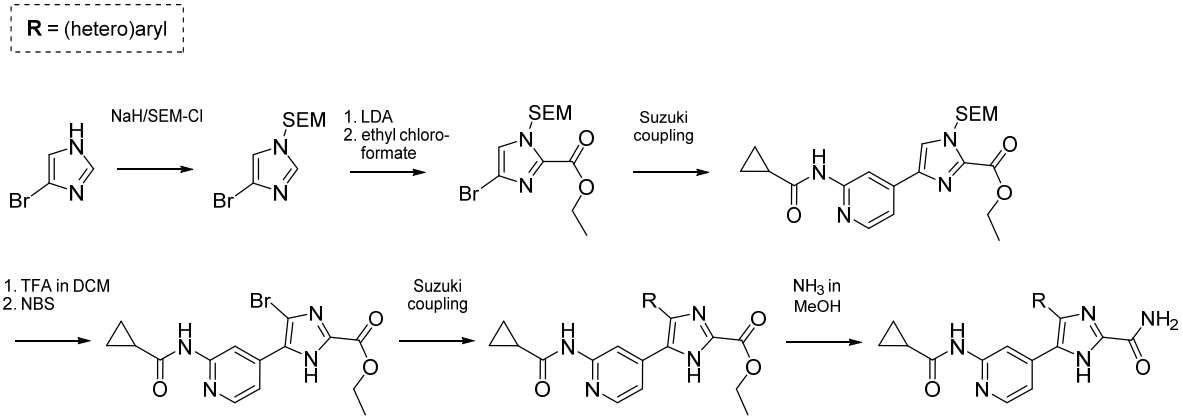

Scheme 3.11. General synthetic strategy towards imidazole-2-carboxamides.

The general synthetic route to the 2-methylimidazoles (*Scheme 3.10*) was slightly modified and with the new procedure (*Scheme 3.11*), di- and trisubstituted imidazole-2-carboxamides could be synthesized in a flexible fashion. After the hydrolysis of the ester moiety in theory different derivatizations at the imidazole-C2 position are also possible.

From various synthesized 2-methylimidazole compounds with a variety of different aromatic rings in the HR I, it was obvious that selectivity over p38α MAPK could not be expected from compounds **115-119**. Nevertheless, some interesting observations could be conceived from the biological evaluation of these 4,5-diarylimidazoles. Compared to the 2-methylimidazole **101**, compound **118** for example is showing a remarkably improved inhibitory activity. Even more striking are the results for the derivatives **120**, **121** and **122**.

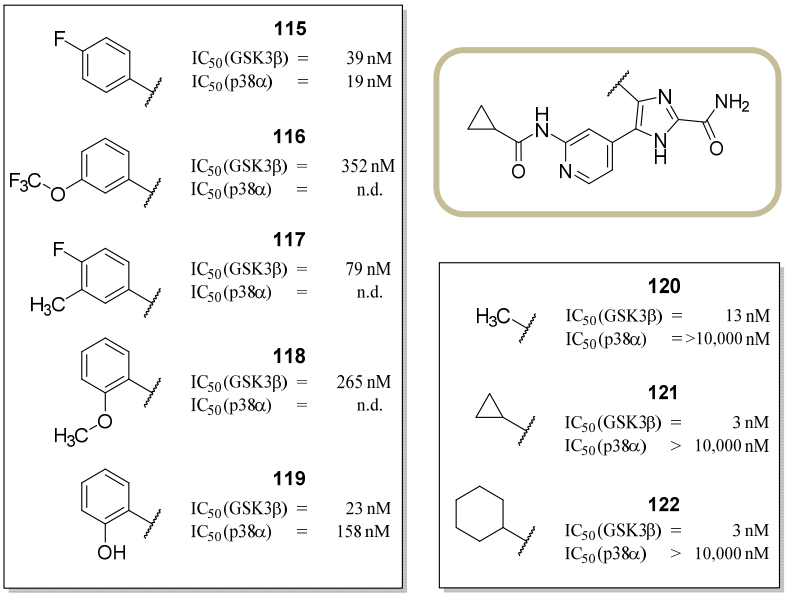

Figure 3.16. Biological evaluation of the prepared imidazole-2-carboxamides.

The inhibitors all displayed high potency versus GSK3β while they were virtually inactive on p38a MAPK. Compounds **104**, **121** and **122** were further evaluated towards their metabolic stability by *in vitro* incubation with HLM. All inhibitors showed excellent metabolic stability in this preliminary pharmacokinetic experiment. Compound **121** was also subjected to a selectivity screen at a concentration of 500 nM against a panel of 57 kinases from diverse families across the kinome. Only MLK1 and the two closely related kinases CDK2 and CDK9 were showing a residual activity of less than 25 %.

The complete, extensive synthetic work and the biological evaluation of all novel compounds can be found in Manuscript I (*Appendix*).

3.2.6 Bioisosteric replacement of the imidazole ring leads to pyridinyloxazoles

The term "bioisoster" is an extension to the original concept of "isosteres" developed by Langmuir in 1919.[265] Bioisosters are molecules "that possess near-equal molecular shapes and volumes, approximately the same distribution of electrons, and which exhibit similar physical properties".[266] More importantly, bioisosteres exhibit the same biological effects on the pharmacological target in terms of agonism, antagonism or modulation. The decision to use an oxazole replacing the imidazole was made based on several considerations:

a) Oxazoles were easily synthetically accessible from available starting material.
b) While the exchange of one atom (N → O) in the ring was considered a minor one with only a small impact on most of the molecular properties (including potency against both kinases), oxazoles are clearly less frequently detected as CYP inhibitors.[267]
c) Multiple di- and trisubstituted oxazoles have been reported in literature as kinase inhibitors – often including their pharmacokinetic profiles, which indicated the suitability of this scaffold in terms of general drug-likeness, metabolic stability and toxicity risk assessment.[268–270]
d) Simultaneously the 2-methylsulfanyl moiety of **77** (*Figure 3.17*) should be exchanged against a metabolically more stable 2-alkyl group analogous to *Section 3.2.2*.

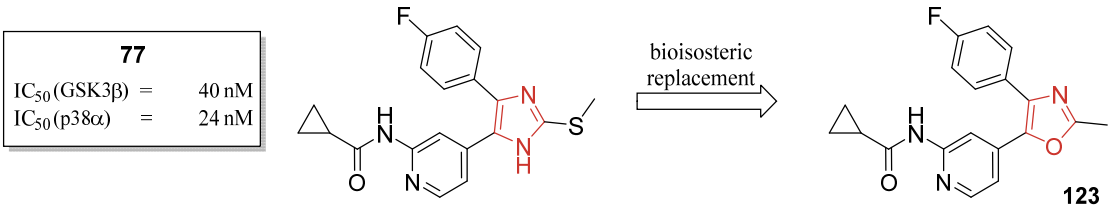

Figure 3.17. The potent dual GSK3β/p38α MAPK inhibitor **77** was chosen as the starting compound for a bioisosteric replacement of the heterocyclic core.

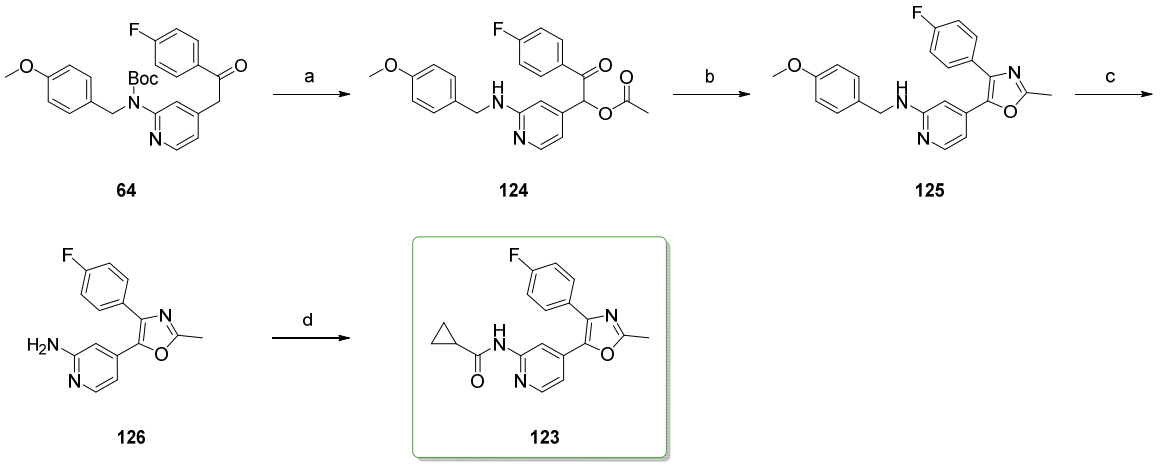

Scheme 3.12. Synthetic route to trisubstituted oxazole **123**: (a) $Pb(OAc)_4$, AcOH, 120 °C, 53 %; (b) NH_4OAc, AcOH, 120 °C, 58 %; (c) TFA in DCM (1:1 ratio), 50 °C, 78 %; (d) cyclopropanecarbonyl chloride, pyridine, rt, 73 %.

The synthesis was started from a precursor (**64**) originally used for the synthesis of the trisubstituted imidazole **77** (*Scheme 3.12*). A possible mechanism for the α-acetoxylation of **64** with lead(IV) acetate is depicted in *Scheme 3.12*. The enol state of the ketone forms an enol–lead(IV) acetate intermediate, which undergoes rearrangement to give **124** in fair yield. Deprotection under strongly acidic conditions with gentle heating gave the free aminopyridine (**126**) which was finally reacted with cyclopropanecarbonyl chloride to afford the trisubstituted oxazole **123**.

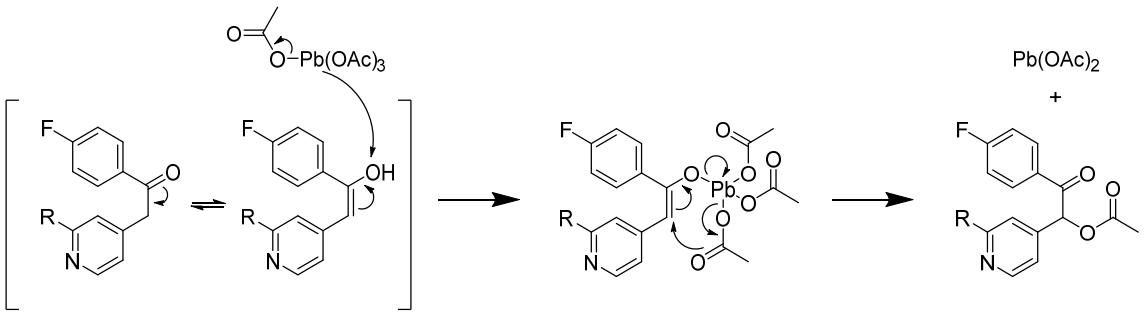

Scheme 3.13. Mechanism of the α-acetoxylation of enolizable ketones with lead(IV) tetraacetate.

Taking into account the introduction of two protecting groups for the 2-aminopicoline and the following condensation to obtain ethanone **64**, a faster and more flexible approach was needed to simplify the synthesis (*Scheme 3.14*). To evaluate the new synthetic route, two new oxazoles were synthesized in which the 4-fluorophenyl ring was exchanged against a 3-(trifluoromethyl)phenyl and a 3-(trifluoromethoxy)phenyl ring, respectively.

First, the commercially available acetophenones (**127a-b**) were treated with bromine in DCM. Cyclization was achieved by heating the intermediates **128a** and **128b** with acetamide. Ultimately, bromination of the heterocycles followed by Suzuki coupling with boronic acid ester **131** yielded the final oxazoles in high yields. The resulting three oxazoles were all tested in the ADP-Glo GSK3β assay (*Table 3.5*). Compound **123** convincingly showed the same inhibitory potency as **77**, proving that the bioisosteric exchange is not detrimental to inhibitory potency. In case of compounds **132** and **133**, the much lower potency can be explained with the unfavorable and too bulky 3-substituents on the phenyl ring occupying the HR I. In conclusion, it was shown that the bioisosteric replacement of the central imidazole core by an oxazole can be done without loosing affinity to both targets (**123**). This general strategy might be useful when pharmacokinetic and toxicological issues possibly need to be adressed at a later stage of the development.

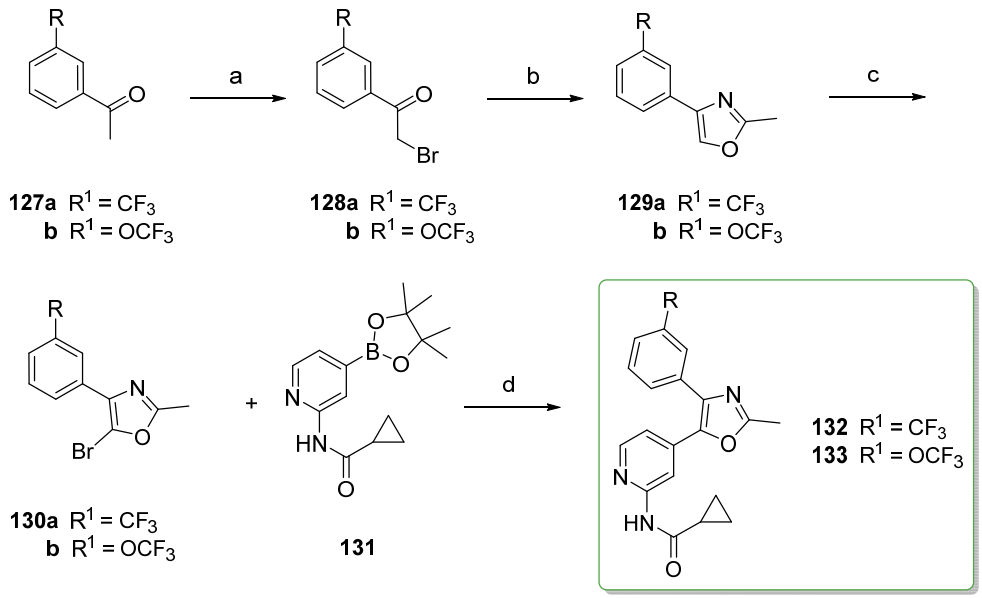

Scheme 3.14. Synthetic route to oxazoles **132** and **133**: (a) Br_2, DCM, rt, 82-85 %; (b) acetamide, 140 °C, 56 %; (c) NBS, AcOH, rt, 53-62 %; (d) $PdCl_2(PPh_3)_2$, K_2CO_3, DMF/H_2O (4:1), 85 °C, 83-88 %.

Table 3.6. Biological evaluation of synthesized oxazoles.

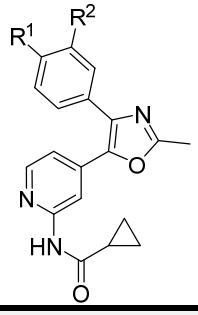

Cpd	R^1	R^2	GSK3β* ± SEM	p38α MAPK†
123	F	H	0.038 µM ± 0.001	0.073 µM
132	H	CF_3	0.934 µM ± 0.074	-
133	H	OCF_3	2.311 µM ± 0.206	-

* = IC_{50} values determined in an ADP-Glo assay[225]; n = 2;
† = (n = 1)

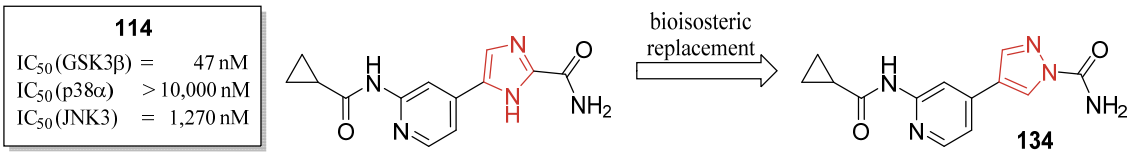

Figure 3.18. The potent GSK3β selective inhibitor **114** (*Manuscript I*) was chosen as the starting point for a bioisosteric replacement of the heterocyclic core.

Another small bioisosteric replacement study was performed with compound **114** (*Figure 3.18*), a GSK3β selective inhibitor resulting from the efforts of shifting the selectivity of dual GSK3β/p38α MAPK inhibitors towards GSK3β (*Section 3.2.5*). Substitution of the imidazole-2-carboxamide against a pyrazole-1-carboxamide (**134**) should again prove the viability of a bioisosteric replacement to remove e.g. potential CYP inhibition if needed. RITCHIE *et al.* reported an analysis of compounds containing a variety of heterocycles taken from the GlaxoSmithKline corporate database. The influence of those heterocycles on solubility, protein binding and CYP inhibition was statistically evaluated.[267] Pyrazoles were, similar to oxazoles, statistically less prone to inhibit CYPs and the introduction of a carboxamide was synthetically feasible. Therefore, 2-amino-4-bromopyridine was reacted with cyclopropanecarbonyl chloride to afford the precursor **129**. Suzuki coupling

with the commercially available THP-protected pyrazole boronic ester and subsequent deprotection under acidic conditions lead to **131** (*Scheme 3.15*). Introduction of the amide was achieved with sodium cyanate yielding the urea derivative **128**.

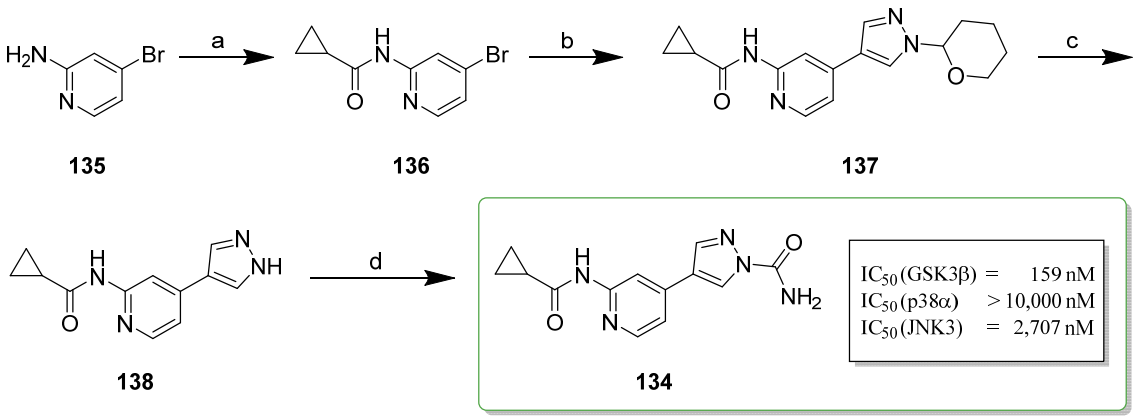

Scheme 3.15. Synthetic route to pyrazole-1-carboxamide **134**: (a) cyclopropanecarbonyl chloride, pyridine, DCM, rt, 84 %; (b) 1-(tetrahydro-2*H*-pyran-2-yl)-1*H*-pyrazole-4-boronic acid pinacol ester, K_2CO_3, Pd(dppf)Cl_2·DCM, 1,4-dioxane/H_2O (6:1), 95 °C, 30 %; (c) 4 M HCl in 1,4-dioxane, MeOH, rt, 64 %; (d) NaOCN, AcOH/H_2O, rt, 48 %.

Compound **134** was tested in three available in-house assays and displayed a slightly decreased yet still good inhibitory potency against GSK3β with an IC_{50} of 159 nM. The desired selectivity over p38α MAPK was retained and the also closely related kinase JNK3 was only weakly inhibited with an IC_{50} of 2,707 nM. This proof-of-concept experiment showed one more time, that a bioisosteric replacement of the imidazole can be realized without substantial loss of potency. To evaluate potential benefits regarding pharmacokinetic and/or pharmacodynamic properties, further experiments are still needed.

4 Experimental part

4.1 Instruments and methods

HPLC

Method A Agilent 1100 Series HPLC system, equipped with an UV DAD detector, detection at 218 nm, 254 nm and 280 nm.
XBridge™ 5 µm C18 column 130 Å, 150 mm x 4.6 mm;
oven temperature: 30 °C; injection volume: 10 µL;
flow rate: 1.5 mL / min; gradient: 0.01 M KH_2PO_4, pH 2.3 (solvent A), methanol (solvent B), 45% B to 85% B in 9 min; 85% B for 6 min; stop time 15 min.

Method B Hewlett Packard 1090 Series II LC, equipped with an UV DAD detector, detection at 230 nm and 254 nm.
Phenomenex Luna® 5 µm C8(2) column 100 Å, 150 mm x 4.6 mm;
oven temperature: 35 °C; injection volume: 5 µL;
flow rate: 1.5 mL / min; gradient: 0.01 M KH_2PO_4, pH 2.3 (solvent A), methanol (solvent B), 40% B to 85% B in 8 min; 85% B for 5 min; 85% B to 40% B in 1 min; 40% B for 2 min; stop time 16 min.

TLC Merck fluorescent silica gel 60 F_{254} plates

TLC-MS Advion Expression S electrospray ionization mass spectrometer connected with an Advion Plate Express

NMR Bruker Avance III HD at 300 Mhz
or
Bruker Avance III HDX at 400 Mhz

4.2 General procedures

General Procedure A (Buchwald-Hartwig-Amination)

The amine (1 – 1.5 eq.), $Pd_2(dba)_3$ (0.08 - 0.16 eq.), XPhos (0.1 – 0.3 eq) and a base (3 eq.) were dissolved under an atmosphere of argon in anhydrous DMF (0.2 M). The reaction mixture was then stirred for 18 h at 80 °C unless otherwise indicated. The mixture was allowed to cool to room temperature and then quenched with saturated aqueous NH_4Cl solution. It was extracted with EtOAc (3x) and the combined organic phases were washed with saturated aqueous NH_4Cl solution (2x) and brine (1x). After drying over anhydrous Na_2SO_4 the solvent was removed under reduced pressure.

General Procedure B (Boc deprotection)

The *N*-Boc protected compound was dissolved in a 5:1 mix of DCM and TFA (0.1 M). The solution was stirred at room temperature until reaction control showed full conversion (usually 3 - 10 h). Then the solvent was removed under reduced pressure and saturated aqueous $NaHCO_3$ solution was added (until pH = 7), before the product was extracted with EtOAc (3 – 6x). The organic phases were combined, dried over anhydrous Na_2SO_4 and then removed under reduced pressure.

General Procedure C (DCC coupling)

The amine was dissolved in anhydrous DCM (0.1 M) under an atmosphere of argon and 1.1 eq. of the acid was added. Then 1.1 eq. of a 0.5 M solution of DCC in anhydrous DCM were added to the reaction mixture in 2 portions at intervals of 5 minutes. After 4 h of stirring at room temperature, a precipitate was filtered off and washed with DCM (30 mL). The filtrate was collected and removed under reduced pressure.

General Procedure D (PyBOP coupling)

The amine and 3 eq. of DIPEA were dissolved in anhydrous DCM (0.1 M). The same amount of solvent was used to dissolve 1.2 eq. of the carboxylic acid and 1.2 eq. of PyBOP, together in a separate vial. After 5 min of stirring at room temperature, the

mixtures were combined and further stirred without heating for 3 h before the solvent was evaporated in vacuo and H_2O was added. It was extracted with EtOAc (3x) and the combined organic phases were washed with saturated $NaHCO_3$ solution (1x) and brine (1x). After drying over anhydrous Na_2SO_4, the solvent was removed under reduced pressure.

4.3 Preparations

tert-Butyl 3-((6-chloropyrimidin-4-yl)(methyl)amino)piperidine-1-carboxylate (5)

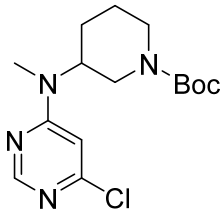

Molecular formula: $C_{15}H_{23}ClN_4O_2$

Molecular weight: 326.83

4,6-Dichloropyrimidine (650 mg, 4.36 mmol), *N*-Boc-3-(methylamino)piperidine (940 mg, 4.36 mmol) and DIPEA (890 µL, 5.24 mmol) were dissolved in iPrOH (22 mL). The mixture was stirred at 85 °C for 24 h before the solvent was removed under reduced pressure. Purification by flash chromatography (SiO_2, *n*-hexane/EtOAc 70:30) afforded 1.19 g (82.3 %) of an off-white solid. ^{1}H NMR (300 MHz, $CDCl_3$) δ 1.44 (s, 9H), 1.56 - 1.93 (m, 4H), 2.61 (t, *J* = 12.1 Hz, 1H), 2.76 (dd, *J* = 12.3, 11.4 Hz, 1H), 2.93 (s, 3H), 3.92 - 4.20 (m, 2H), 4.36 (br. s., 1H), 6.43 (s, 1H), 8.36 (d, *J* = 0.7 Hz, 1H). ^{13}C NMR (75 MHz, $CDCl_3$) δ 24.6, 27.9, 28.3, 29.9, 43.5, 45.8, 51.8, 79.9, 101.4, 154.6, 157.7, 159.8, 162.6. TLC-MS (ESI) *m/z*: 325.1 $[M - H]^-$. HPLC (A): t_R = 7.27 min.

6-Chloro-*N*-methyl-*N*-(piperidin-3-yl)pyrimidin-4-amine (6)

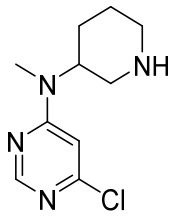

Molecular formula: $C_{10}H_{15}ClN_4$

Molecular weight: 226.71

The title compound was synthesized according to **General Procedure B** starting from compound **5** (1.48 g, 4.5 mmol) to afford 0.98 g (95.5 %) of a light yellow solid. ^{1}H NMR (300 MHz, MeOD) δ 1.86 - 2.20 (m, 4H), 2.97 - 3.12 (m, 1H), 3.22 (s, 3H), 3.33 - 3.47 (m, 3H), 5.32 (br. s, 1H), 7.30 (br. s., 1H), 8.69 (s, 1H). ^{13}C NMR (75 MHz, MeOD) δ 22.9, 26.6, 32.3, 44.6, 45.2, 52.6, 105.0, 150.4, 153.4, 164.5. TLC-MS (ESI) *m/z*: 227.2 $[M + H]^+$. HPLC (A): t_R = 1.30 min.

3-(3-((6-Chloropyrimidin-4-yl)(methyl)amino)piperidin-1-yl)propanenitrile (7)

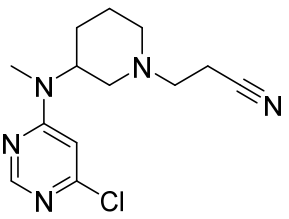

Molecular formula: $C_{13}H_{18}ClN_5$

Molecular weight: 279.77

Compound **6 (**812 mg, 3.58 mmol) was dissolved in anhydrous MeOH (14 mL) before acrylonitrile (890 µL, 10.75 mmol) was added. The mixture was stirred at room temperature for 24 h. Because the reaction control showed incomplete conversion, another portion of acrylonitrile (500 µL, 7.63 mmol) and Et_3N (500 µL, 6.81 mmol) were added and the mixture was stirred for 24 more h. The solvent was removed under reduced pressure and the residue was purified by flash chromatography (SiO_2, DCM:EtOH 95:5) to afford 503 mg (50.2 %) of an off-white solid. ^{1}H NMR (300 MHz, $CDCl_3$) δ 1.48 - 1.90 (m, 4H), 1.99 - 2.27 (m, 2H), 2.47 - 2.58 (m, 2H), 2.70 - 2.79 (m, 2H), 2.81 - 2.99 (m, 5H), 4.60 (br. s., 1H), 6.45 (s, 1H), 8.38 (d, *J* = 0.7 Hz, 1H). TLC-MS (ESI) *m/z*: 280.0 $[M + H]^+$. HPLC (A): t_R = 1.38 min.

3-(3-(Methyl(6-(pyridin-3-ylamino)pyrimidin-4-yl)amino)piperidin-1-yl)propanenitrile (8)

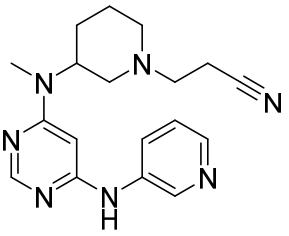

Molecular formula: $C_{18}H_{23}N_7$

Molecular weight: 337.43

The title compound was synthesized according to **General Procedure A** starting from compound **7** (80 mg, 0.29 mmol), 3-aminopyridine (40 mg, 0.37 mmol), XPhos (14 mg, 0.029 mmol), $Pd_2(dba)_3$ (13 mg, 0.014 mmol) and NaO*t*Bu (82 mg, 0.86 mmol). The product was purified by flash chromatography (SiO_2, *n*-hexane:EtOAc 80:20 → 0:100) to afford 64 mg (66.3 %) of an orange solid. ^{1}H NMR (300 MHz, $CDCl_3$) δ 1.48 - 1.62 (m, 1H), 1.62 - 1.87 (m, 3H), 1.97 - 2.09 (m, 1H), 2.09 - 2.20 (m, 1H), 2.46 - 2.57 (m, 2H), 2.64 - 2.79 (m, 2H), 2.81 - 2.94 (m, 5H), 4.54 (br. s., 1H), 5.82 (s, 1H), 7.30 (t, *J* = 4.1 Hz, 1H), 7.91 (d, *J* = 8.2 Hz, 2H), 8.22 - 8.41 (m, 2H), 8.61 (br. s., 1H). ^{13}C NMR (75

MHz, $CDCl_3$) δ 16.0, 24.5, 27.6, 29.8, 51.7, 52.8, 53.3, 55.5, 82.8, 118.8, 123.7, 128.1, 136.6, 142.7, 144.0, 157.5, 160.6, 162.5. TLC-MS (ESI) *m/z*: 338.3 $[M + H]^+$ *m/z*: 336.1 $[M - H]^-$. HPLC (A): t_R = 1.50 min, purity: 100.0 % (*254 nm*).

3-(3-(Methyl(6-(pyridin-2-ylamino)pyrimidin-4-yl)amino)piperidin-1-yl)propanenitrile (11)

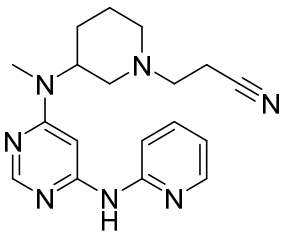

Molecular formula: $C_{18}H_{23}N_7$

Molecular weight: 337.43

The title compound was synthesized according to **General Procedure A** starting from compound **7** (69 mg, 0.25 mmol), 2-aminopyridine (35 mg, 0.37 mmol), XPhos (12 mg, 0.025 mmol), $Pd_2(dba)_3$ (11 mg, 0.012 mmol) and NaO*t*Bu (71 mg, 0.74 mmol). The product was purified by flash chromatography (SiO_2, *n*-hexane:EtOAc 80:20 → 0:100) to afford 54 mg (64.9 %) of an orange solid. ^{1}H NMR (300 MHz, $CDCl_3$) δ 1.43 - 1.63 (m, 1H), 1.68 - 1.85 (m, 3H), 2.02 (td, *J* = 11.0, 2.8 Hz, 1H), 2.15 (t, *J* = 10.4 Hz, 1H), 2.45 - 2.55 (m, 2H), 2.66 - 2.76 (m, 2H), 2.86 (d, *J* = 10.4 Hz, 2H), 2.93 (s, 3H), 4.64 (br. s., 1H), 6.9 (dd, *J* = 6.8, 5.3 Hz, 1H), 6.99 (s, 1H), 7.32 (d, *J* = 8.3 Hz, 1H), 7.53 - 7.63 (m, 1H), 8.29 (dd, *J* = 4.9, 1.2 Hz, 1H), 8.34 (d, *J* = 0.6 Hz, 1H), 8.70 (br. s., 1H). ^{13}C NMR (75 MHz, $CDCl_3$) δ 16.0, 24.6, 27.7, 30.0, 51.6, 52.9, 53.6, 55.7, 86.4, 112.9, 116.8, 118.9, 137.8, 147.7, 154.0, 157.2, 159.0, 162.9. TLC-MS (ESI) *m/z*: 338.1 $[M + H]^+$ *m/z*: 335.9 $[M - H]^-$. HPLC (A): t_R = 1.62 min, purity: 99.1 % (*254 nm*).

3-(3-(Methyl(6-((3-(trifluoromethyl)phenyl)amino)pyrimidin-4-yl)amino)piperidin-1-yl)propanenitrile (10)

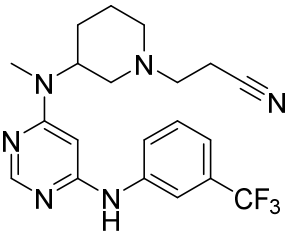

Molecular formula: $C_{20}H_{23}F_3N_6$

Molecular weight: 404.44

The title compound was synthesized according to **General Procedure A** starting from compound **7** (80 mg, 0.29 mmol), 3-(trifluoromethyl)aniline (69 mg, 0.43 mmol), XPhos (14 mg, 0.029 mmol), $Pd_2(dba)_3$ (13 mg, 0.014 mmol) and NaO*t*Bu (82 mg, 0.86 mmol). The product was purified by flash chromatography (SiO_2, *n*-hexane:EtOAc 80:20 → 20:80) to afford 56 mg (48.4 %) of a light yellow solid. ^{1}H NMR (300 MHz, $CDCl_3$) δ 1.42 - 1.60 (m, 1H), 1.61 - 1.85 (m, 3H), 2.02 (td, *J* = 11.2, 2.2 Hz, 1H), 2.13 (t, *J* = 10.6 Hz, 1H), 2.44 - 2.54 (m, 2H), 2.63 - 2.76 (m, 2H), 2.79 - 2.91 (m, 5H), 4.53 (br. s., 1H), 5.86 (s, 1H), 7.30 (d, *J* = 7.6 Hz, 1H), 7.44 (t, *J* = 7.8 Hz, 1H), 7.50 - 7.56 (m, 1H), 7.66 (s, 1H), 7.95 (d, *J* = 10.6 Hz, 1H), 8.28 (s, 1H). ^{13}C NMR (75 MHz, $CDCl_3$) δ 16.0, 24.5, 27.6, 29.8, 51.7, 52.8, 53.3, 55.6, 82.7, 117.5 (q, $^3J_{CF3}$ = 3.7 Hz), 118.8, 119.6 (q, $^3J_{CF3}$ = 4.0 Hz), 123.9 (q, $^1J_{CF3}$ = 272.7 Hz), 124.2, 129.8, 131.5 (q, $^2J_{CF3}$ = 32.6 Hz), 140.3, 157.6, 160.5, 162.6. TLC-MS (ESI) *m/z*: 405.2 $[M + H]^+$ *m/z*: 403.0 $[M - H]^-$. HPLC (A): t_R = 5.78 min, purity: 99.0 % (*254 nm*).

3-(3-((6-((3-Chlorophenyl)amino)pyrimidin-4-yl)(methyl)amino)piperidin-1-yl)propanenitrile (11)

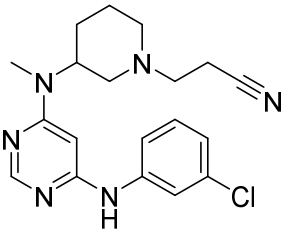

Molecular formula: $C_{19}H_{23}ClN_6$

Molecular weight: 370.89

The title compound was synthesized according to **General Procedure A** starting from compound **7** (110 mg, 0.39 mmol), 3-chloroaniline (150 mg, 1.18 mmol), XPhos (19 mg, 0.039 mmol), $Pd_2(dba)_3$ (18 mg, 0.019 mmol) and NaO*t*Bu (113 mg, 1.18 mmol). The product was purified twice by flash chromatography (SiO_2, *n*-hexane:EtOAc 80:20 → 0:100 & SiO_2, DCM:EtOH 98:2 → 96:4) to afford 51 mg (35.3 %) of a white solid. ^{1}H NMR (300 MHz, $CDCl_3$) δ 1.43 - 1.61 (m, 1H), 1.62 - 1.87 (m, 3H), 2.03 (td, *J* = 11.2, 2.4 Hz, 1H), 2.14 (t, *J* = 10.6 Hz, 1H), 2.46 - 2.56 (m, 2H), 2.68 - 2.77 (m, 2H), 2.81 - 2.90 (m, 5H), 4.56 (br. s., 1H), 5.83 - 5.90 (m, 1H), 7.05 (dt, *J* = 7.5, 1.7 Hz, 1H), 7.19 - 7.31 (m, 2H), 7.43 (t, *J* = 1.9 Hz, 1H), 8.05 (s, 1H), 8.25 - 8.32 (m, 1H). ^{13}C NMR (75 MHz, $CDCl_3$) δ 15.9, 24.5, 27.6, 29.8, 51.6, 52.7, 53.3, 55.6, 82.5, 118.8, 119.3, 121.1, 123.2, 130.2, 134.7, 140.9, 157.6, 160.6, 162.5. TLC-MS (ESI) *m/z*: 371.0 $[M + H]^+$ *m/z*: 368.9 $[M - H]^-$. HPLC (B): t_R = 3.88 min, purity: 98.5 % (*254 nm*).

N-(6-((1-(2-Cyanoethyl)piperidin-3-yl)(methyl)amino)pyrimidin-4-yl)cyclopropanecarboxamide (12)

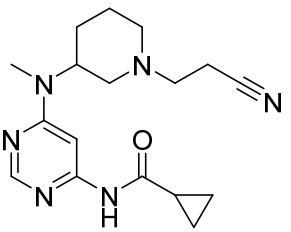

Molecular formula: $C_{17}H_{24}N_6O$

Molecular weight: 328.42

Compound **7** (85 mg, 0.30 mmol), cyclopropanecarboxamide (39 mg, 0.46 mmol), XantPhos (18 mg, 0.030 mmol), $Pd_2(dba)_3$ (14 mg, 0.015 mmol) and Cs_2CO_3 (297 mg, 0.91 mmol) were dissolved in anhydrous DMF (8 mL) under an atmosphere of argon. The reaction mixture was stirred at 90 °C for 18 h. After cooling to room temperature, the reaction was quenched with saturated NH_4Cl solution. It was extracted with EtOAc (3x) and the combined organic phases were washed with saturated NH_4Cl solution (2x) and brine (1x). After drying over anhydrous Na_2SO_4 the solvent was removed under reduced pressure. The product was purified by flash chromatography (SiO_2, *n*-hexane:EtOAc 80:20 → 20:80) to afford 30 mg (30.1 %) of a brownish solid. ^{1}H NMR (300 MHz, $CDCl_3$) δ 0.82 - 0.91 (m, 2H), 1.02 - 1.11 (m, 2H), 1.39 - 1.56 (m, 1H), 1.57 - 1.70 (m, 1H), 1.75 (d, *J* = 2.6 Hz, 3H), 2.00 (td, *J* = 10.9, 2.8 Hz, 1H), 2.14 (t, *J* = 10.5 Hz, 1H), 2.43 - 2.54 (m, 2H), 2.63 - 2.76 (m, 2H), 2.78 - 2.88 (m, 2H), 2.88 - 2.97 (m, 3H), 4.36 - 4.99 (m, 1H), 7.39 (s, 1H), 8.31 (s, 1H), 10.13 (br. s., 1H). ^{13}C NMR (75 MHz, $CDCl_3$) δ 8.5, 15.6, 15.8, 24.4, 27.5, 30.0, 51.5, 52.6, 53.4, 55.5, 90.0, 118.7, 156.9, *(C^4-Pyrim. missing)*, 163.1, 173.7. TLC-MS (ESI) *m/z*: 329.1 $[M + H]^+$ *m/z*: 327.0 $[M - H]^-$. HPLC (A): t_R = 1.46 min, purity: 99.6 % (*254 nm*).

tert-Butyl 3-(methyl(6-(methylamino)pyrimidin-4-yl)amino)piperidine-1-carboxylate (13)

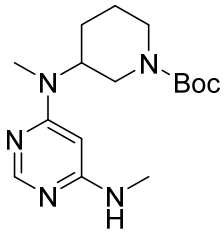

Molecular formula: $C_{16}H_{27}N_5O_2$

Molecular weight: 321.43

Compound **5** (150 mg, 0.46 mmol) was dissolved in 2 M methylamine in MeOH solution (5 mL) and stirred at 95 °C for 18 h. Reaction control did not show complete conversion

so the reaction vessel was heated up to 120 °C and stirred for 30 more h. The solvent was then removed under reduced pressure to afford 122 mg (82.7 %) of the title compound. ^{1}H NMR (300 MHz, $CDCl_3$) δ 1.46 (s, 9H), 1.60 - 1.73 (m, 2H), 1.78 (ddd, *J* = 8.3, 5.7, 2.8 Hz, 1H), 1.83 - 1.97 (m, 2H), 2.62 (t, *J* = 11.1 Hz, 1H), 2.75 (t, *J* = 11.8 Hz, 1H), 2.86 - 2.93 (m, 6H), 4.10 (br. s., 1H), 4.44 (br. s., 1H), 4.79 (d, *J* = 4.8 Hz, 1H), 5.35 (br. s., 1H), 8.15 (d, *J* = 0.6 Hz, 1H). TLC-MS (ESI) *m/z*: 320.1 $[M - H]^-$. HPLC (A): t_R = 4.09 min.

N^4,*N*^{6}-Dimethyl-*N*^{4}-(piperidin-3-yl)pyrimidine-4,6-diamine (14)

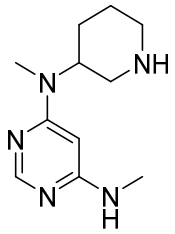

Molecular formula: $C_{11}H_{19}N_5$

Molecular weight: 211.31

The title compound was synthesized according to **General Procedure B** starting from compound **13** (122 mg, 0.38 mmol) to afford 80 mg (95.4 %) of a solid. ^{1}H NMR (300 MHz, $CDCl_3$) δ 1.62 - 1.75 (m, 2H), 1.79 - 1.92 (m, 2H), 2.54 (td, *J* = 12.3, 2.8 Hz, 2H), 2.72 (t, *J* = 11.6 Hz, 1H), 2.83 - 2.95 (m, 6H), 3.03 - 3.13 (m, 2H), 4.37 - 4.63 (m, 1H), 4.75 (d, *J* = 4.6 Hz, 1H), 5.32 (s, 1H), 8.14 (d, *J* = 0.7 Hz, 1H). TLC-MS (ESI) *m/z*: 210.1 $[M - H]^-$. HPLC (A): t_R = 1.36 min.

3-(3-(Methyl(6-(methylamino)pyrimidin-4-yl)amino)piperidin-1-yl)propanenitrile (15)

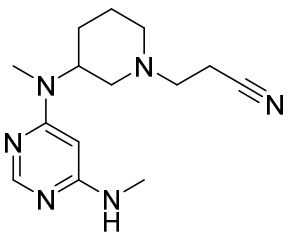

Molecular formula: $C_{14}H_{22}N_6$

Molecular weight: 274.37

Compound **13** (75 mg, 0.34 mmol) was dissolved in anhydrous MeOH (8 mL) before Et_3N (48 µL, 0.34 mmol) and acrylonitrile (22 µL, 0.34 mmol) were added dropwise. The mixture was stirred at room temperature for 17 h and the solvent was removed under reduced pressure. Purification by flash chromatography (SiO_2, DCM:EtOH 97:3)

afforded 58 mg (61.8 %) of a white solid. ^{1}H NMR (300 MHz, $CDCl_3$) δ 1.40 - 1.57 (m, 1H), 1.59 - 1.81 (m, 3H), 1.98 (td, *J* = 11.1, 2.8 Hz, 1H), 2.08 (t, *J* = 10.6 Hz, 1H), 2.42 - 2.52 (m, 2H), 2.58 - 2.75 (m, 2H), 2.77 - 2.83 (m, 3H), 2.84 (s, 2H), 2.86 (s, 3H), 4.52 (br. s., 1H), 5.27 (s, 2H), 8.09 (s, 1H). ^{13}C NMR (75 MHz, $CDCl_3$) δ 15.9, 24.6, 27.8, 28.4, 29.8, 51.5, 52.9, 53.5, 55.6, 79.4, 118.9, 157.3, 162.5, 163.8. TLC-MS (ESI) *m/z*: 275.0 $[M + H]^+$ *m/z*: 272.9 $[M - H]^-$. HPLC (A): t_R = 1.03 min, purity: 100.0 % (*254 nm*).

tert-Butyl 3-((6-aminopyrimidin-4-yl)(methyl)amino)piperidine-1-carboxylate (16)

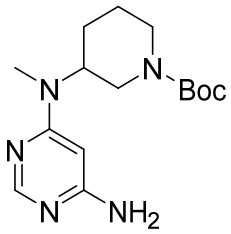

Molecular formula: $C_{15}H_{25}N_5O_2$

Molecular weight: 307.40

The title compound was synthesized according to a slightly modified procedure taken from GEHRINGER *et al*.[224] Compound **5** (600 mg, 1.84 mmol), tri-*tert*-butylphosphonium tetrafluoroborate (106 mg, 0.37 mmol) and $Pd_2(dba)_3$ (168 mg, 0.18 mmol) were combined in a Schlenk tube. Under an atmosphere of argon, 0.5 M LiHMDS in 1,4-dioxane (7.24 mL, 3.62 mmol) was added and the mixture was stirred at 80 °C for 20 h. The reaction was allowed to cool to room temperature before 2 M aqueous HCl solution (20 mL) was added and the reaction was stirred at room temperature for 30 min. After neutralization with $NaHCO_3$ solution the aqueous phase was extracted with DCM (4 x 30 mL). The combined organic layers were dried over anhydrous Na_2SO_4 and the solvent was removed under reduced pressure. Purification by flash chromatography (SiO_2, EtOAc:MeOH:Et_3N 94:4:2) afforded 412 mg (73.0 %) of a golden solid. ^{1}H NMR (300 MHz, $CDCl_3$) δ 1.44 (s, 9H), 1.53 - 1.68 (m, 2H), 1.69 - 1.79 (m, 1H), 1.80 - 1.90 (m, 1H), 2.50 - 2.65 (m, 1H), 2.72 (t, *J* = 11.8 Hz, 1H), 2.85 (s, 3H), 4.05 (br. s., 2H), 4.38 (br. s., 1H), 4.74 (br. s., 2H), 5.50 (s, 1H), 8.15 (d, *J* = 0.6 Hz, 1H). TLC-MS (ESI) *m/z*: 308.0 $[M + H]^+$ *m/z*: 305.9 $[M - H]^-$. HPLC (A): t_R = 3.88 min.

tert-Butyl 3-((6-aminopyrimidin-4-yl)(methyl)amino)piperidine-1-carboxylate (17)

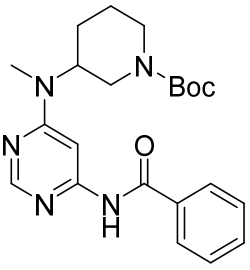

Molecular formula: $C_{22}H_{29}N_5O_3$

Molecular weight: 411.51

Compound **16** (85 mg, 0.28 mmol), benzoic acid (46 mg, 0.37 mmol), PyBOP (193 mg, 0.37 mmol) and DIPEA (145 µL, 0.83 mmol) were dissolved in anhydrous DCM (6 mL) and treated according to **General Procedure D**. The product was purified by flash chromatography (SiO_2, DCM:EtOH 98:2) to afford 60 mg (52.6 %) of the title compound. ^{1}H NMR (300 MHz, $CDCl_3$) δ 1.47 (s, 9H), 1.69 (d, *J* = 6.7 Hz, 2H), 1.85 - 1.99 (m, 2H), 2.63 (t, *J* = 11.3 Hz, 1H), 2.81 (t, *J* = 11.8 Hz, 1H), 3.01 (s, 3H), 4.10 (br. s., 2H), 4.64 (br. s., 1H), 7.44 - 7.61 (m, 3H), 7.67 (s, 1H), 8.00 - 8.06 (m, 2H), 8.08 - 8.14 (m, 1H), 8.30 (s, 1H). TLC-MS (ESI) *m/z*: 412.2 $[M + H]^+$ *m/z*: 410.0 $[M - H]^-$. HPLC (A): t_R = 6.29 min.

N-(6-((1-(2-Cyanoethyl)piperidin-3-yl)(methyl)amino)pyrimidin-4-yl)benzamide (18)

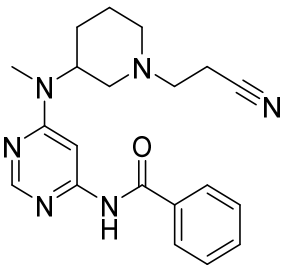

Molecular formula: $C_{20}H_{24}N_6O$

Molecular weight: 364.45

Compound **17** (60 mg, 0.15 mmol) was treated according to **General Procedure B**. After drying in vacuo, the product was dissolved in in anhydrous MeOH (5 mL) and acrylonitrile (25 µL, 0.38 mmol) was added. The mixture was stirred at room temperature for 16 h before the solvent was removed under reduced pressure. The product was purified by flash chromatography twice (SiO_2, DCM:EtOH 97:3 & SiO_2, *n*-hexane/EtOAc 100:0 → 0:100) to afford 20 mg (37.9 %) of a light yellow solid. ^{1}H NMR (300 MHz, $CDCl_3$) δ 1.56 (dd, *J* = 11.7, 4.7 Hz, 1H), 1.65 - 1.87 (m, 3H), 2.05 (td, *J* = 11.0, 3.3 Hz, 1H), 2.18 (t, *J* = 10.6 Hz, 1H), 2.49 - 2.57 (m, 2H), 2.71 - 2.79 (m, 2H), 2.88 (d, *J* = 11.0 Hz,

2H), 2.99 (s, 3H), 4.72 (br. s., 1H), 7.46 - 7.54 (m, 2H), 7.54 - 7.62 (m, 2H), 7.86 - 7.95 (m, 2H), 8.23 (d, *J* = 0.9 Hz, 1H), 8.80 (s, 1H). ^{13}C NMR (75 MHz, $CDCl_3$) δ 15.9, 24.5, 27.6, 30.2, 51.7, 52.8, 53.6, 55.6, 90.1, 118.8, 127.2, 128.9, 132.5, 133.9, 156.7, 157.3, 163.3, 166.4. TLC-MS (ESI) *m/z*: 365.2 $[M + H]^+$ *m/z*: 362.9 $[M - H]^-$. HPLC (A): t_R = 3.38 min, purity: 98.3 % (*254 nm*).

tert-Butyl 3-(methyl(6-(3-phenylureido)pyrimidin-4-yl)amino)piperidine-1-carboxylate (19)

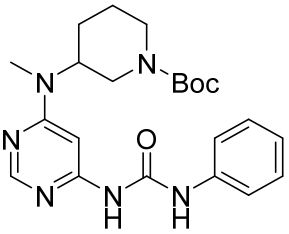

Molecular formula: $C_{22}H_{30}N_6O_3$

Molecular weight: 426.52

Compound **16** (95 mg, 0.30 mmol) and phenyl isocyanate (40 µL, 0.46 mmol) were dissolved in anhydrous toluene (7 mL) under an atmosphere of argon. The reaction mixture was stirred at 90 °C for 16 h. Afterwards the precipitate was filtered off, washed with toluene and dried in vacuo to afford 79 mg (61.7 %) as a white solid. ^{1}H NMR (300 MHz, $CDCl_3$) δ 1.48 (s, 9H), 1.59 - 1.73 (m, 2H), 1.74 - 1.84 (m, 1H), 1.86 (br. s., 1H), 2.64 (t, *J* = 11.4 Hz, 1H), 2.79 (t, *J* = 11.7 Hz, 1H), 2.92 (s, 3H), 4.10 (br. s., 2H), 4.58 (br. s., 1H), 6.01 (s, 1H), 7.01 - 7.16 (m, 1H), 7.28 - 7.37 (m, 2H), 7.60 (d, *J* = 7.7 Hz, 2H), 8.36 (s, 1H), 9.06 (br. s., 1H), 11.55 (br. s., 1H). TLC-MS (ESI) *m/z*: 449.1 $[M + Na]^+$ *m/z*: 425.0 $[M - H]^-$. HPLC (A): t_R = 9.68 min.

1-(6-(Methyl(piperidin-3-yl)amino)pyrimidin-4-yl)-3-phenylurea (19a)

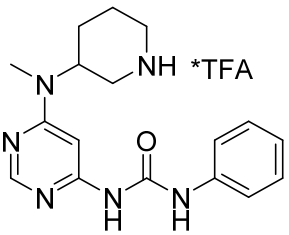

Molecular formula: $C_{17}H_{22}N_6O$ * TFA

Molecular weight: 440.43 (326.40)

The title compound was synthesized according to **General Procedure B** from compound **19** (79 mg, 0.19 mmol) but instead of a basic aqueous work-up, the solvents were evaporated in vacuo to afford 79 mg (96.8 %) of the white trifluoroacetate salt. ^{1}H NMR

(300 MHz, DMSO-d_6) δ 1.40 - 1.56 (m, 1H), 1.60 - 1.74 (m, 3H), 2.36 (t, *J* = 11.4 Hz, 1H), 2.54 - 2.66 (m, 1H), 2.75 - 2.83 (m, 2H), 2.85 (s, 3H), 4.41 (br. s., 1H), 6.69 (s, 1H), 6.97 - 7.07 (m, 1H), 7.30 (t, *J* = 7.9 Hz, 2H), 7.44 - 7.52 (m, 2H), 8.26 (s, 1H), 9.24 (s, 1H), 10.27 (s, 1H). TLC-MS (ESI) *m/z*: 327.4 $[M + H]^+$ *m/z*: 325.2 $[M - H]^-$. HPLC (A): t_R = 3.75 min.

1-(6-((1-(2-Cyanoethyl)piperidin-3-yl)(methyl)amino)pyrimidin-4-yl)-3-phenylurea (20)

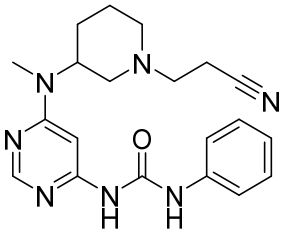

Molecular formula: $C_{20}H_{25}N_7O$

Molecular weight: 379.47

Compound **19a** (64 mg, 0.19 mmol) was dissolved in anhydrous MeOH (5 mL) before Et_3N (54 µL, 0.38 mmol) and acrylonitrile (15 µL, 0.23 mmol) were added. The reaction mixture was stirred for 16 h at room temperature before the solvent was removed under reduced pressure. The product was purified by flash chromatography (SiO_2, DCM:EtOH 98:2 → 95:5) to afford 37 mg (52.6 %) as a white solid. ^{1}H NMR (300 MHz, $CDCl_3$) δ 1.44 - 1.62 (m, 1H), 1.68 - 1.87 (m, 3H), 1.99 - 2.11 (m, 1H), 2.16 (t, *J* = 10.5 Hz, 1H), 2.45 - 2.56 (m, 2H), 2.68 - 2.77 (m, 2H), 2.81 - 2.99 (m, 5H), 4.69 (br. s., 1H), 6.09 (br. s., 1H), 7.04 - 7.13 (m, 1H), 7.28 - 7.36 (m, 2H), 7.61 (d, *J* = 7.6 Hz, 2H), 8.36 (s, 1H), 9.61 (br. s., 1H), 11.53 (br. s., 1H). ^{13}C NMR (75 MHz, $CDCl_3$) δ 16.0, 24.6, 27.7, 30.0, 51.6, 52.8, 53.6, 55.7, 86.5, 118.9, 120.1, 123.4, 128.8, 138.5, 153.9, 155.9, 158.3, 162.5. TLC-MS (ESI) *m/z*: 380.2 $[M + H]^+$ *m/z*: 378.2 $[M - H]^-$. HPLC (A): t_R = 5.23 min, purity: 100.0 % (*254 nm*).

tert-Butyl 3-((6-(cyclopropanecarboxamido)pyrimidin-4-yl)(methyl)amino)piperidine-1-carboxylate (21)

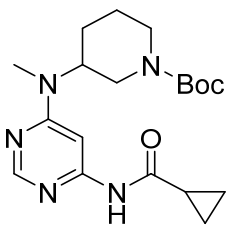

Molecular formula: $C_{19}H_{29}N_5O_3$

Molecular weight: 375.47

Compound **5** (186 mg, 0.57 mmol), cyclopropanecarboxamide (73 mg, 0.85 mmol), XantPhos (33 mg, 0.057 mmol), $Pd_2(dba)_3$ (26 mg, 0.029 mmol) and Cs_2CO_3 (556 mg, 1.70 mmol) were dissolved in anhydrous DMF (5 mL) under an atmosphere of argon. The reaction mixture was stirred at 110 °C for 18 h. After cooling to room temperature, the reaction was quenched with saturated NH_4Cl solution. It was extracted with EtOAc (3x) and the combined organic phases were washed with saturated NH_4Cl solution (2x) and brine (1x). After drying over anhydrous Na_2SO_4 the solvent was removed under reduced pressure. Finally, the product was purified by flash chromatography (SiO_2, *n*-hexane:EtOAc 100:0 → 20:80) to afford 167 mg (78.0 %) of an off-white solid. ^{1}H NMR (300 MHz, $CDCl_3$) δ 0.87 - 0.94 (m, 2H), 1.09 (dd, *J* = 4.4, 3.1 Hz, 2H), 1.46 (s, 9H), 1.53 - 1.72 (m, 3H), 1.73 - 1.82 (m, 1H), 1.86 (br. s., 1H), 2.61 (t, *J* = 11.2 Hz, 1H), 2.78 (t, *J* = 11.8 Hz, 1H), 2.94 (s, 3H), 4.08 (br. s., 2H), 4.57 (br. s., 1H), 7.41 (s, 1H), 8.30 (d, *J* = 0.8 Hz, 1H), 9.37 (br. s., 1H). TLC-MS (ESI) *m/z*: 376.0 $[M + H]^+$ *m/z*: 373.8 $[M - H]^-$. HPLC (A): t_R = 6.18 min.

N-(6-((1-(2-Cyanoacetyl)piperidin-3-yl)(methyl)amino)pyrimidin-4-yl)cyclopropanecarboxamide (22)

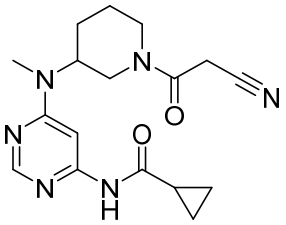

Molecular formula: $C_{17}H_{22}N_6O_2$

Molecular weight: 342.40

Compound **21** (72 mg, 0.19 mmol) was treated according to **General Procedure B**. With the deprotected intermediate, the title compound was synthesized according to **General Procedure D** using cyanoacetic acid (20 mg, 0.23 mmol), PyBOP (120 mg, 0.23 mmol) and DIPEA (98 µL, 0.58 mmol). The product was purified by flash chromatography (SiO_2, DCM:EtOH 98:2 → 95:5) to afford 38 mg (57.7 %) of a yellow solid. ^{1}H NMR (300 MHz, DMSO-d_6) δ 0.73 - 0.94 (m, 4H), 1.39 - 1.64 (m, 1H), 1.65 - 1.90 (m, 3H), 1.95 - 2.08 (m, 1H), 2.75 - 3.26 (m, 5H), 3.53 - 3.73 (m, 1H), 3.93 - 4.13 (m, 2H), 4.18 - 4.68 (m, 2H), 7.20 - 7.34 (m, 1H), 8.25 - 8.38 (m, 1H), 10.92 (br. s., 1H). ^{13}C NMR (101 MHz, DMSO-*d*$_6$) δ 8.6, 14.9, 24.5, 25.2, 27.4, 30.2, 45.0, 51.9, 55.3, 89.5, 116.5, 156.8, 162.0, 162.9, 174.2, 174.3. TLC-MS (ESI) *m/z*: 340.9 $[M - H]^-$. HPLC (A): t_R = 1.67 min, purity: 95.6 % (*254 nm*).

N-(6-((1-(3-Hydroxy-4-methoxybenzoyl)piperidin-3-yl)(methyl)-amino)pyrimidin-4-yl)cyclopropanecarboxamide (23)

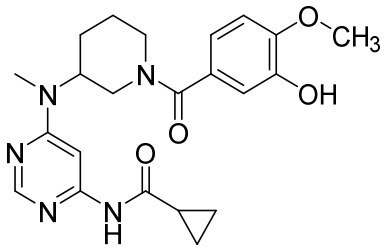

Molecular formula: $C_{23}H_{28}N_4O_4$

Molecular weight: 425.49

Compound **21** (72 mg, 0.19 mmol) was treated according to **General Procedure B**. With the deprotected intermediate, the title compound was synthesized according to **General Procedure D** using isovanillic acid (39 mg, 0.23 mmol), PyBOP (120 mg, 0.23 mmol) and DIPEA (98 µL, 0.58 mmol). The product was purified by flash chromatography (SiO_2, DCM:EtOH 98:2 → 95:5) to afford 35 mg (42.7 %) of a beige solid. ^{1}H NMR (300 MHz, $CDCl_3$) δ 0.75 - 0.99 (m, 3H), 0.99 - 1.15 (m, 2H), 1.52 - 2.02 (m, 6H), 2.67 (br. s., 1H), 2.76 - 2.99 (m, 4H), 3.85 (s, 3H), 4.72 (br. s., 2H), 6.81 (d, *J* = 8.3 Hz, 1H), 6.98 (d, *J* = 8.2 Hz, 1H), 7.08 (br. s., 1H), 7.38 (s, 1H), 8.36 (s, 1H), 9.64 (br. s., 1H). ^{13}C NMR (75 MHz, $CDCl_3$) δ 8.7, 15.9, 24.8, 28.3, 30.0, 46.2, 51.7, 54.3, 55.9, 90.0, 110.6, 113.9, 119.7, 128.7, 145.4, 148.0, 156.5, 156.9, 163.1, 170.6, 173.9. TLC-MS (ESI) *m/z*: 426.2 $[M + H]^+$ *m/z*: 424.0 $[M - H]^-$. HPLC (A): t_R = 2.77 min, purity: 98.5 % (*254 nm*).

tert-Butyl 3-(methyl(6-(phenylamino)pyrimidin-4-yl)amino)piperidine-1-carboxylate (24a)

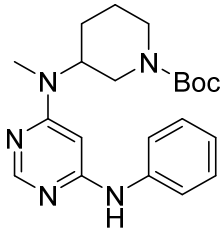

Molecular formula: $C_{21}H_{29}N_5O_2$

Molecular weight: 383.50

Compound **5** (0.64 g, 1.97 mmol), aniline (1.29 g, 2.96 mmol), $Pd_2(dba)_3$ (144 mg, 0.065 mmol), XPhos (127 mg, 0.111 mmol) and NaO*t*Bu (0.59 g, 5.91 mmol) were dissolved in anhydrous DMF (15 mL) and processed according to **General Procedure A**. Purification by flash chromatography (SiO_2, *n*-hexane/EtOAc 100:0 → 20:80) afforded 673 mg (82.7%) of a white solid. ^{1}H NMR (300 MHz, $CDCl_3$) δ 1.40 - 1.49 (m, 9H), 1.59 - 1.71 (m, 2H), 1.72 - 1.81 (m, 1H), 1.85 (d, *J* = 1.8 Hz, 1H), 2.61 (t, *J* = 11.6 Hz, 1H),

2.74 (t, *J* = 11.8 Hz, 1H), 2.85 (s, 3H), 4.08 (br. s., 2H), 4.46 (br. s., 1H), 5.87 (s, 1H), 7.07 - 7.22 (m, 2H), 7.28 - 7.41 (m, 4H), 8.25 (s, 1H). TLC-MS (ESI) *m/z*: 384.2 $[M + H]^+$ *m/z*: 382.1 $[M - H]^-$. HPLC (A): t_R = 6.17 min.

tert-Butyl 3-((6-((3-fluorophenyl)amino)pyrimidin-4-yl)(methyl)amino)-piperidine-1-carboxylate (24b)

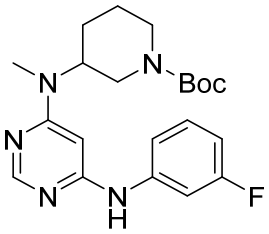

Molecular formula: $C_{21}H_{28}FN_5O_2$

Molecular weight: 401.49

Compound **5** (660 mg, 2.02 mmol), 3-fluoroaniline (336 mg, 3.03 mmol), $Pd_2(dba)_3$ (92 mg, 0.10 mmol), XPhos (96 mg. 0.20 mmol) and NaO*t*Bu (582 mg, 6.06 mmol) were dissolved in anhydrous DMF (15 mL) and processed according to **General Procedure A**. Purification was achieved by flash chromatography (SiO_2, *n*-hexane:EtOAc 100:0 → 20:80) to afford 683 mg (83.7 %) of an off-white solid. ^{1}H NMR (300 MHz, $CDCl_3$) δ 1.44 (s, 9H), 1.57 - 1.71 (m, 2H), 1.72 - 1.82 (m, 1H), 1.83 - 1.91 (m, 1H), 2.53 - 2.67 (m, 1H), 2.74 (t, *J* = 11.8 Hz, 1H), 2.87 (s, 3H), 4.08 (br. s., 2H), 4.46 (br. s., 1H), 5.89 (d, *J* = 0.6 Hz, 1H), 6.77 (td, *J* = 8.3, 1.9 Hz, 1H), 7.06 (dd, *J* = 8.0, 1.2 Hz, 1H), 7.16 (dt, *J* = 10.7, 2.2 Hz, 1H), 7.23 - 7.33 (m, 1H), 7.63 (br. s., 1H), 8.28 (d, *J* = 0.5 Hz, 1H). ^{13}C NMR (75 MHz, $CDCl_3$) δ 24.7, 28.1, 28.3, 29.8, 43.7, 46.2, 51.2, 79.7, 82.5, 108.3 (d, $^2J_{CF}$ = 24.9 Hz), 110.1 (d, $^2J_{CF}$ = 22.7 Hz), 116.7 (d, $^4J_{CF}$ = 2.8 Hz), 130.4 (d, $^3J_{CF}$ = 9.4 Hz), 141.3 (d, $^3J_{CF}$ = 10.5 Hz), 154.8, 157.5, 160.5, 162.7, 163.2 (d, $^1J_{CF}$ = 245.5 Hz). TLC-MS (ESI) *m/z*: 402.0 $[M + H]^+$ *m/z*: 399.9 $[M - H]^-$. HPLC (A): t_R = 7.43 min.

tert-Butyl 3-((6-((3-hydroxyphenyl)amino)pyrimidin-4-yl)-(methyl)amino)-piperidine-1-carboxylate (24c)

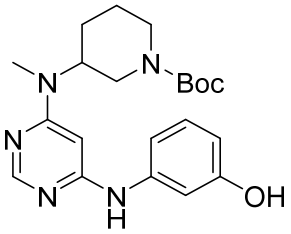

Molecular formula: $C_{21}H_{29}N_5O_3$

Molecular weight: 399.50

Compound **5 (**320 mg, 0.98 mmol), 3-aminophenole (330 mg, 3.03 mmol), $Pd_2(dba)_3$ (92 mg, 0.10 mmol), XPhos (96 mg, 0.20 mmol) and NaO*t*Bu (582 mg, 6.06 mmol) were dissolved in anhydrous DMF (15 mL) and processed according to **General Procedure A**. Purification was achieved by flash chromatography (SiO_2, *n*-hexane:EtOAc 100:0 → 20:80) to afford 265 mg (67.9 %) of a brownish solid. ^{1}H NMR (300 MHz, $CDCl_3$) δ 1.43 (s, 9H), 1.49 - 1.80 (m, 3H), 1.85 (br. s., 1H), 2.52 - 2.75 (m, 2H), 2.86 (s, 3H), 4.03 (br. s., 2H), 4.22 (br. s., 1H), 6.06 (s, 1H), 6.59 (dd, *J* = 8.1, 1.5 Hz, 1H), 6.66 (dd, *J* = 8.1, 1.5 Hz, 1H), 6.92 (br. s., 1H), 7.12 (t, *J* = 8.0 Hz, 1H), 7.66 (br. s., 1H), 7.98 (s, 1H), 8.20 (s, 1H). TLC-MS (ESI) *m/z*: 400.1 $[M + H]^+$ *m/z*: 397.9 $[M - H]^-$. HPLC (A): t_R = 5.04 min.

N^4-Methyl-N^6-phenyl-N^4-(piperidin-3-yl)pyrimidine-4,6-diamine (25a)

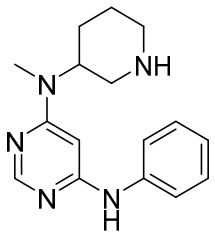

Molecular formula: $C_{16}H_{21}N_5$

Molecular weight: 283.38

The title compound was synthesized according to **General Procedure B** starting from Compound **24a** (650 mg, 1.70 mmol) to afford 497 mg (103.2 %) of a solid. ^{1}H NMR (400 MHz, $CDCl_3$) δ 1.64 - 1.80 (m, 2H), 1.87 (d, *J* = 10.2 Hz, 2H), 2.53 - 2.66 (m, 1H), 2.75 (t, *J* = 11.7 Hz, 1H), 2.82 (s, 3H), 3.15 (d, *J* = 11.9 Hz, 2H), 4.58 (br. s., 1H), 5.09 (br. s., 1H), 5.88 (s, 1H), 7.10 (quin, *J* = 4.3 Hz, 1H), 7.35 (d, *J* = 4.3 Hz, 4H), 8.24 (d, *J* = 0.9 Hz, 1H). TLC-MS (ESI) *m/z*: 284.2 $[M + H]^+$ *m/z*: 282.0 $[M - H]^-$. HPLC (A): t_R = 1.40 min.

N^4-(3-Fluorophenyl)-N^6-methyl-N^6-(piperidin-3-yl)pyrimidine-4,6-diamine (25b)

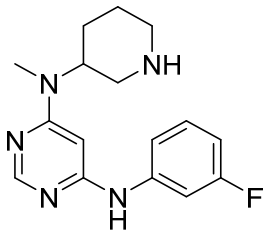

Molecular formula: $C_{16}H_{20}FN_5$

Molecular weight: 301.17

The title compound was synthesized according to **General Procedure B** starting from **24b** (200 mg, 0.50 mmol) to afford 144 mg (96.14 %) of a yellow solid. ^{1}H NMR (300 MHz, $CDCl_3$) δ 1.54 - 1.70 (m, 2H), 1.74 - 1.89 (m, 2H), 2.37 (br. s., 1H), 2.43 - 2.54 (m, 1H), 2.66 (t, *J* = 11.5 Hz, 1H), 2.83 (s, 3H), 3.02 (d, *J* = 12.4 Hz, 2H), 4.49 (br. s., 1H), 5.86 (s, 1H), 6.75 (tdd, *J* = 8.3, 2.4, 0.6 Hz, 1H), 7.04 (dd, *J* = 8.1, 1.3 Hz, 1H), 7.15 (dt, *J* = 10.8, 2.2 Hz, 1H), 7.21 - 7.31 (m, 1H), 8.00 (br. s., 1H), 8.25 (s, 1H). ^{13}C NMR (75 MHz, $CDCl_3$) δ 23.7, 27.2, 29.8, 44.3, 46.3, 50.7, 83.6, 107.8 (d, *J* = 24.9 Hz), 109.6 (d, *J* = 21.6 Hz), 116.2 (d, *J* = 2.8 Hz), 130.2 (d, *J* = 9.4 Hz), 141.4 (d, *J* = 10.5 Hz), 157.4, 160.7, 162.2, 163.1 (d, *J* = 244.9 Hz). TLC-MS (ESI) *m/z*: 302.0 $[M + H]^+$ *m/z*: 300.1 $[M - H]^-$. HPLC (A): t_R = 2.24 min.

3-((6-(Methyl(piperidin-3-yl)amino)pyrimidin-4-yl)amino)phenol (25c)

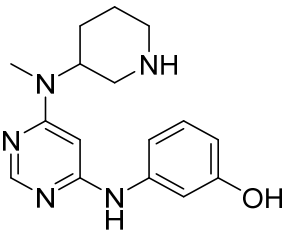

Molecular formula: $C_{16}H_{21}N_5O$

Molecular weight: 299.38

The title compound was synthesized according to **General Procedure B** starting from **24c** (265 mg, 0.66 mmol) to afford 182 mg (91.5 %) of a brown solid. ^{1}H NMR (300 MHz, DMSO-*d*$_6$) δ 1.41 - 1.75 (m, 4H), 2.35 - 2.46 (m, 1H), 2.58 - 2.68 (m, 1H), 2.80 (s, 3H), 2.82 - 2.92 (m, 2H), 4.45 (br. s., 1H), 5.84 (s, 1H), 6.30 - 6.36 (m, 1H), 6.89 - 7.06 (m, 2H), 7.16 (t, *J* = 2.1 Hz, 1H), 8.15 (s, 1H), 8.92 (s, 1H), 9.27 (br. s., 1H). TLC-MS (ESI) *m/z*: 300.2 $[M + H]^+$ *m/z*: 298.1 $[M - H]^-$. HPLC (A): t_R = 1.45 min.

Furan-3-yl(3-(methyl(6-(phenylamino)pyrimidin-4-yl)amino)piperidin-1-yl)methanone (26)

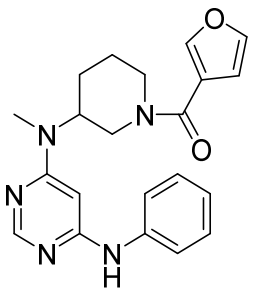

Molecular formula: $C_{21}H_{23}N_5O_2$

Molecular weight: 377.45

The title compound was synthesized according to **General Procedure C** starting from Compound **25a** (97 mg, 0.34 mmol), furan-3-carboxylic acid (42 mg, 0.37 mmol) and 0.5 M DCC in DCM solution (755 µL, 0.37 mmol). The product was purified thrice by flash chromatography (SiO_2, DCM:EtOH 95:5 & SiO_2, DCM:EtOH 98:2 → 97:3 & SiO_2, DCM:EtOH 100:0 → 94:6) to afford 42 mg (32.4 %) of a white solid. ^{1}H NMR (300 MHz, $CDCl_3$) δ 1.62 - 2.00 (m, 4H), 2.58 - 2.98 (m, 5H), 4.19 (br. s., 1H), 4.77 (br. s., 2H), 5.85 (s, 1H), 6.68 (br. s., 1H), 7.08 - 7.18 (m, 1H), 7.28 - 7.43 (m, 5H), 7.59 (s, 1H), 7.91 (br. s., 1H), 8.27 (s, 1H). ^{13}C NMR (75 MHz, $CDCl_3$) δ 24.9, 28.5, 29.9, *(C^2-Pip. missing)*, *(C^6-Pip. missing)*, 51.3, 81.8, 110.3, 120.9, 122.1, 124.0, 129.4, 139.1, 142.7, 143.8, 157.6, 161.2, 162.6, 163.9. TLC-MS (ESI) *m/z*: 378.0 $[M + H]^+$ *m/z*: 375.8 $[M - H]^-$. HPLC (A): t_R = 3.05 min, purity: 100.0 % (*254 nm*).

5-(3-(Methyl(6-(phenylamino)pyrimidin-4-yl)amino)piperidine-1-carbonyl)pyrrolidin-2-one (27)

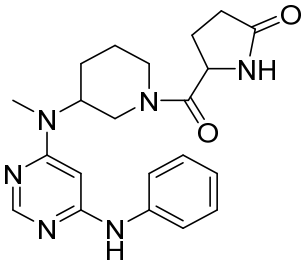

Molecular formula: $C_{21}H_{26}N_6O_2$

Molecular weight: 394.48

The title compound was synthesized according to **General Procedure C** starting from compound **25a** (100 mg, 0.35 mmol), 2-pyrrolidone-5-carboxylic acid (50 mg, 0.39 mmol) and 0.5 M DCC in DCM solution (780 µL, 0.39 mmol). The product was purified twice by flash chromatography (SiO_2, DCM:EtOH 98:2 → 90:10 & SiO_2, DCM:EtOH:Et_3N 95:4:1) to afford 96 mg (67.0 %) of an off-white solid. ^{1}H NMR (300 MHz, $CDCl_3$) δ 1.51 - 1.69 (m, 1H), 1.75 - 2.01 (m, 3H), 2.09 - 2.24 (m, 1H), 2.25 - 2.34 (m, 1H), 2.41 - 2.56 (m, 2H), 2.56 - 2.72 (m, 1H), 2.82 (s, 3H), 2.90 (dd, *J* = 13.0, 11.5 Hz, 1H), 3.86 (d, *J* = 13.0 Hz, 1H), 4.34 - 4.52 (m, 2H), 4.63 (d, *J* = 11.9 Hz, 1H), 5.86 (s, 1H), 7.12 (t, *J* = 7.0 Hz, 1H), 7.27 - 7.40 (m, 4H), 7.82 (br. s., 1H), 8.50 (s, 1H), 8.78 (s, 1H). ^{13}C NMR (75 MHz, $CDCl_3$) δ 23.3, 24.7, 29.0, 29.8, 30.1, 42.9, 48.2, 52.8, 53.8, 81.9, 122.2, 124.2, 129.5, 139.0, 158.0, 161.4, 162.2, 168.9, 178.6. TLC-MS (ESI) *m/z*: 395.0 $[M + H]^+$ *m/z*: 392.8 $[M - H]^-$. HPLC (A): t_R = 1.64 min, purity: 99.9 % (*254 nm*).

Ethyl 3-(3-(methyl(6-(phenylamino)pyrimidin-4-yl)amino)piperidin-1-yl)-3-oxopropanoate (28)

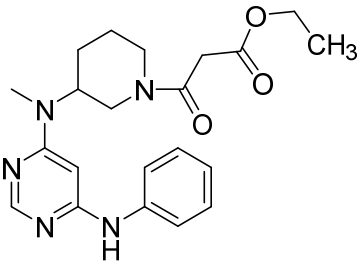

Molecular formula: $C_{21}H_{27}N_5O_3$

Molecular weight: 397.48

The title compound was synthesized according to **General Procedure C** starting from compound **25a** (100 mg, 0.35 mmol), ethyl potassium malonate (66 mg, 0.39 mmol) and 0.5 M DCC in DCM solution (780 µL, 0.39 mmol). Because reaction control did not show full conversion after 5 h, another 400 µL (0.2 mmol) of 0.5 M DCC in DCM solution were added and the reaction was further stirred overnight. The product was purified by flash chromatography (SiO_2, DCM:EtOH 100:0 → 90:10) to afford 28 mg (20.0 %) of a white solid. ^{1}H NMR (300 MHz, $CDCl_3$) δ 1.13 - 1.25 (m, 3H), 1.31 - 1.90 (m, 4H), 2.65 - 2.79 (m, 1H), 2.84 (s, 3H), 2.90 - 3.24 (m, 1H), 3.53 (d, *J* = 12.2 Hz, 2H), 3.58 - 3.78 (m, 1H), 4.03 - 4.16 (m, 2H), 4.20 - 4.56 (m, 2H), 5.86 (d, *J* = 8.4 Hz, 1H), 6.88 - 6.98 (m, 1H), 7.21 - 7.32 (m, 2H), 7.58 (dd, *J* = 8.5, 1.0 Hz, 2H), 8.17 (d, *J* = 3.9 Hz, 1H), 9.06 (s, 1H). TLC-MS (ESI) *m/z*: 398.0 $[M + H]^+$ *m/z*: 395.8 $[M - H]^-$. HPLC (A): t_R = 2.71 min, purity: 98.9 % (*254 nm*).

Cyclopropyl(3-(methyl(6-(phenylamino)pyrimidin-4-yl)amino)piperidin-1-yl)methanone (29)

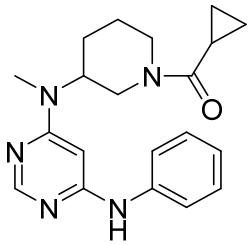

Molecular formula: $C_{20}H_{25}N_5O$

Molecular weight: 351.45

The title compound was synthesized according to **General Procedure C** starting from compound **25a** (100 mg, 0.35 mmol), cyclopropane carboxylic acid (42 mg, 0.39 mmol) and 0.5 M DCC in DCM solution (780 µL, 0.39 mmol). The product was purified by flash chromatography (SiO_2, DCM:EtOH 97:3) to afford 101 mg (81.4 %) of a white solid. ^{1}H NMR (300 MHz, $CDCl_3$) δ 0.74 (br. s., 2H), 0.85 - 0.96 (m, 1H), 0.96 - 1.09 (m, 1H),

1.53 - 1.68 (m, 1H), 1.68 - 1.88 (m, 3H), 1.88 - 2.00 (m, 1H), 2.37 - 2.81 (m, 1H), 2.87 (s, 3H), 3.02 (d, *J* = 10.6 Hz, 1H), 4.20 (br. s., 1H), 4.40 - 4.80 (m, 2H), 5.88 (s, 1H), 7.07 - 7.20 (m, 1H), 7.28 - 7.41 (m, 4H), 8.24 (d, *J* = 0.8 Hz, 1H). ^{13}C NMR (75 MHz, $CDCl_3$) δ 7.3, 11.2, 24.5, 28.3, 29.8, 45.7, 48.1, 51.7, 81.7, 122.0, 124.0, 129.3, 139.2, 157.5, 161.2, 162.7, 172.2. TLC-MS (ESI) *m/z*: 352.1 $[M + H]^+$ *m/z*: 350.0 $[M - H]^-$. HPLC (A): t_R = 2.99 min, purity: 98.8 % (*254 nm*).

3-(3-((6-((3-Fluorophenyl)amino)pyrimidin-4-yl)(methyl)amino)piperidin-1-yl)propanenitrile (30)

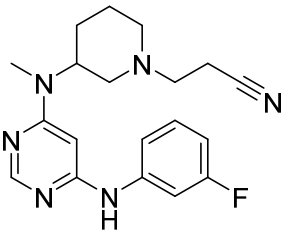

Molecular formula: $C_{19}H_{23}FN_6$

Molecular weight: 354.43

Compound **25b** (75 mg, 0.25 mmol) was dissolved in anhydrous MeOH (10 mL) before acrylonitrile (20 µL, 0.30 mmol) was added. The reaction mixture was stirred at room temperature for 18 h. As the reaction was incomplete, another 15 µL acrylonitrile were added and the reaction mixture was stirred for another 5 h before the solvent was removed under reduced pressure. The product was purified by flash chromatography (SiO_2, DCM:EtOH 98:2 → 95:5) to afford 29 mg (32.9 %) as a green-greyish solid. ^{1}H NMR (300 MHz, $CDCl_3$) δ 1.41 - 1.61 (m, 1H), 1.62 - 1.87 (m, 3H), 1.96 - 2.20 (m, 2H), 2.45 - 2.55 (m, 2H), 2.63 - 2.79 (m, 2H), 2.80 - 2.92 (m, 5H), 4.55 (br. s., 1H), 5.79 - 5.97 (m, 1H), 6.76 (tdd, *J* = 8.3, 2.5, 0.8 Hz, 1H), 7.02 - 7.08 (m, 1H), 7.18 (dt, *J* = 10.8, 2.2 Hz, 1H), 7.23 - 7.32 (m, 1H), 7.82 (s, 1H), 8.27 (d, *J* = 0.7 Hz, 1H). ^{13}C NMR (75 MHz, $CDCl_3$) δ 16.0, 24.5, 27.7, 29.9, 51.7, 52.8, 53.4, 55.6, 82.6, 108.1 (d, $^2J_{CF}$ = 24.8 Hz), 110.0 (d, $^2J_{CF}$ = 21.6 Hz), 116.5 (d, $^4J_{CF}$ = 2.7 Hz), 118.8, 130.4 (d, $^3J_{CF}$ = 9.4 Hz), 141.3 (d, $^3J_{CF}$ = 11.6 Hz) 157.6, 160.5, 162.6, 163.2 (d, $^1J_{CF}$ = 245.6 Hz). TLC-MS (ESI) *m/z*: 355.0 $[M + H]^+$ *m/z*: 352.9 $[M - H]^-$. HPLC (A): t_R = 2.80 min, purity: 99.9 % (*254 nm*).

3-(3-((6-((3-Hydroxyphenyl)amino)pyrimidin-4-yl)(methyl)amino)piperidin-1-yl)propanenitrile (31)

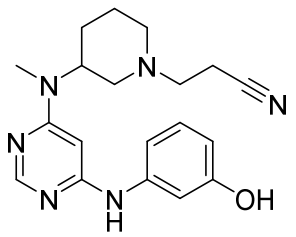

Molecular formula: $C_{19}H_{24}N_6O$

Molecular weight: 352.44

Compound **25c** (69 mg, 0.23 mmol) was dissolved in anhydrous MeOH (5 mL) and acrylonitrile (22 µL, 0.34 mmol) was added. The reaction mixture was stirred at room temperature for 18 h. Then the solvent was removed under reduced pressure and the product was purified by flash chromatography (SiO_2, DCM:EtOH 97:3 → 92:8) to afford 41 mg (50.8 %) of a white solid. ^{1}H NMR (300 MHz, DMSO-*d*$_6$) δ 1.43 - 1.65 (m, 3H), 1.68 - 1.78 (m, 1H), 1.83 - 1.98 (m, 1H), 2.12 (t, *J* = 10.6 Hz, 1H), 2.53 - 2.70 (m, 4H), 2.71 - 2.89 (m, 5H), 4.54 (br. s., 1H), 5.83 (s, 1H), 6.32 (ddd, *J* = 7.9, 2.3, 1.0 Hz, 1H), 6.88 - 6.96 (m, 1H), 6.97 - 7.06 (m, 1H), 7.16 (t, *J* = 2.1 Hz, 1H), 8.16 (s, 1H), 8.90 (s, 1H), 9.23 (s, 1H). ^{13}C NMR (101 MHz, DMSO-*d*$_6$) δ 14.9, 24.3, 27.0, 29.4, 50.7, 51.9, 52.9, 55.2, 83.6, 106.3, 108.5, 110.1, 119.9, 129.1, 141.8, 156.9, 157.5, 160.8, 161.7. TLC-MS (ESI) *m/z*: 353.0 $[M + H]^+$ *m/z*: 350.9 $[M - H]^-$. HPLC (A): t_R = 1.36 min, purity: 100.0 % (*254 nm*).

6-Chloro-*N*-(3-chlorophenyl)pyrimidin-4-amine * HCl (4)

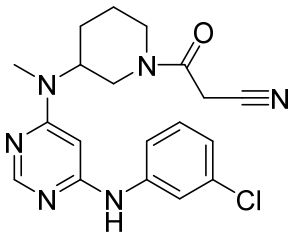

Molecular formula: $C_{10}H_7Cl_2N_3$ * HCl

Molecular weight: 276.55 (240.09)

4,6-Dichloropyrimidine (750 mg, 5.04 mmol), 3-chloroaniline (530 mg, 4.12 mmol) and conc. HCl (750 µL) were dissolved in iPrOH (7.5 mL). The mixture was heated to 85 °C in a pressure tube for 2.5 h, cooled to room temperature and stored at 4 °C overnight. The formed precipitate was collected by filtration, washed with small amounts of ice-cold iPrOH and dried in vacuo to afford 950 mg (83.3 %) of a white solid. ^{1}H NMR (250 MHz, DMSO-*d*$_6$) δ 7.00 (d, *J* = 0.7 Hz, 1H), 7.08 (ddd, *J* = 7.9, 2.1, 1.0 Hz, 1H), 7.34 (t, *J* = 8.1 Hz, 1H), 7.57 (ddd, *J* = 8.2, 2.0, 1.0 Hz, 1H), 7.96 (t, *J* = 2.1 Hz, 1H), 8.53 (d, *J* = 0.7 Hz,

1H), 10.53 (s, 1H). ^{13}C NMR (75 MHz, DMSO-d_6) δ 106.0, 118.4, 119.4, 122.6, 130.4, 133.2, 140.8, 157.7, 158.3, 161.1. TLC-MS (ESI) *m/z*: 238.1 $[M - H]^-$. HPLC (A): t_R = 7.94 min.

3-(3-((6-((3-Chlorophenyl)amino)pyrimidin-4-yl)(methyl)amino)piperidin-1-yl)-3-oxopropanenitrile (1)

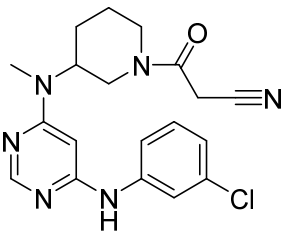

Molecular formula: $C_{19}H_{21}ClN_5O$

Molecular weight: 384.87

Compound **4** (200 mg, 0.72 mmol) and *N*-Boc-3-(methylamino)piperidine (170 mg, 0.79 mmol) were put together in a flask and heated neat at 150 °C for 4 h.[217] The black melt was cooled down to room temperature and dissolved in MeOH. The solution was filtered and purification by flash chromatography was attempted (SiO_2, DCM:EtOH 95:5). However, 215 mg (94.0 %) of an only partially purified compound could be isolated as the separation proved to be inadequate under these conditions. Tests with SiO_2 and different solvent mixtures, addition of Et_3N or NH_3 to the solvent mix as well as purification via C18-reversed phase silica gel did also not give satisfactory results. Therefore, the compound was used in the next step without further purification. [Identity was confirmed using TLC-MS (ESI) *m/z*: 318.1 $[M + H]^+$ *m/z*: 315.9 $[M - H]^-$. HPLC (A): t_R = 1.54 min.] The crude product was treated according to **General Procedure D** using cyanoacetic acid (69 mg, 0.81 mmol), PyBOP (422 mg, 0.81 mmol) and DIPEA (355 µL, 2.03 mmol). Purification by flash chromatography (SiO_2, DCM:EtOH 99:1 → 95:5 & SiO_2, *n*-hexane:EtOAc 30:70) afforded 39 mg (15.0 % *over 2 steps*) of a yellowish solid. ^{1}H NMR (300 MHz, $CDCl_3$) δ 1.57 - 2.06 (m, 4H), 2.67 - 3.03 (m, 5H), 3.44 - 3.78 (m, 2H), 3.95 - 4.63 (m, 3H), 5.96 (d, *J* = 4.8 Hz, 1H), 7.03 - 7.13 (m, 1H), 7.18 - 7.33 (m, 3H), 7.42 (s, 1H), 8.28 (d, *J* = 6.2 Hz, 1H). ^{13}C NMR (75 MHz, $CDCl_3$) δ 24.1, 25.6, 28.7, 31.4, 44.7, 47.1, 52.6, 83.5, 114.0, 119.5, 121.4, 123.8, 130.4, 134.8, 140.4, 157.8, 160.8, 161.9, 162.5. TLC-MS (ESI) *m/z*: 385.0 $[M + H]^+$ *m/z*: 382.9 $[M - H]^-$. HPLC (A): t_R = 3.21 min, purity: 99.4 % (*254 nm*).

6-Chloro-*N*-(3-fluorophenyl)pyrimidin-4-amine (32)

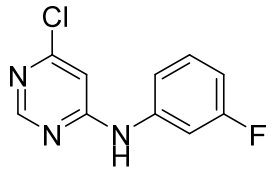

Molecular formula: $C_{10}H_7ClFN_3$

Molecular weight: 223.64

4,6-Dichloropyrimidine (300 mg, 2.01 mmol), 3-fluoroaniline (250 mg, 2.22 mmol) and DIPEA (525 µL, 3.00 mmol) were dissolved in *n*-BuOH (4 mL). The mixture was stirred at 120 °C for 5 h. The solvent was removed under reduced pressure and the title compound was purified by flash chromatography (SiO_2, *n*-hexane/EtOAc 80:20) to afford 280 mg (61.6 %) of an off-white solid. ^{1}H NMR (300 MHz, DMSO-d_6) δ 6.80 - 6.95 (m, 2H), 7.26 - 7.42 (m, 2H), 7.68 - 7.76 (m, 1H), 8.53 (s, 1H), 10.05 (s, 1H). TLC-MS (ESI) *m/z*: 221.8 $[M - H]^-$. HPLC (A): t_R = 6.19 min.

tert-Butyl 3-((6-((3-fluorophenyl)amino)pyrimidin-4-yl)amino)piperidine-1-carboxylate (33)

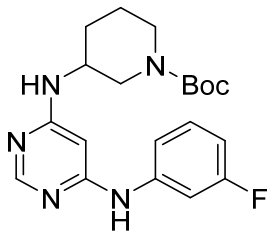

Molecular formula: $C_{20}H_{26}FN_5O_2$

Molecular weight: 387.46

The title compound was synthesized according to **General Procedure A** starting from compound **32** (200 mg, 0.73 mmol), *N*-Boc-3-aminopiperidine (220 mg, 1.08 mmol), XPhos (35 mg, 0.073 mmol), $Pd_2(dba)_3$ (33 mg, 0.036 mmol) and NaO*t*Bu (211 mg, 2.19 mmol). The product was purified by flash chromatography (SiO_2, *n*-hexane:EtOAc 100:0 → 30:70) to yield 118 mg (41.7 %) of a solid. ^{1}H NMR (300 MHz, $CDCl_3$) δ 1.33 - 1.48 (m, 9H), 1.51 - 1.64 (m, 2H), 1.67 - 1.81 (m, 1H), 1.90 - 2.04 (m, 1H), 2.82 - 3.31 (m, 2H), 3.61 (br. s., 2H), 3.85 (br. s., 1H), 5.12 (br. s., 1H), 5.84 (s, 1H), 6.73 - 6.84 (m, 1H), 7.00 - 7.17 (m, 2H), 7.28 - 7.36 (m, 1H), 7.57 (br. s., 1H), 8.21 (s, 1H). TLC-MS (ESI) *m/z*: 388.2 $[M + H]^+$ *m/z*: 386.0 $[M - H]^-$. HPLC (A): t_R = 4.25-8.00 min (extremely broad peak).

3-(3-((6-((3-Fluorophenyl)amino)pyrimidin-4-yl)amino)piperidin-1-yl)propanenitrile (34)

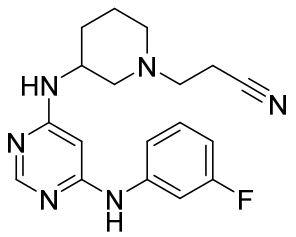

Molecular formula: $C_{18}H_{21}FN_6$

Molecular weight: 340.41

Compound **33** (73 mg, 0.19 mmol) was treated according to **General Procedure B**. The dried product was dissolved in anhydrous MeOH (5 mL) and acrylonitrile (14 µL, 0.21 mmol) was added. The reaction mixture was stirred for 14 h at room temperature before the solvent was removed under reduced pressure. The product was purified by flash chromatography (SiO_2, DCM:EtOH 97:3) to yield 38 mg (58.8 %) of a yellow solid. ^{1}H NMR (300 MHz, $CDCl_3$) δ 1.43 - 1.78 (m, 4H), 2.25 - 2.53 (m, 5H), 2.54 - 2.69 (m, 3H), 3.80 (br. s., 1H), 5.46 (d, *J* = 3.5 Hz, 1H), 5.74 (s, 1H), 6.63 - 6.78 (m, 1H), 6.95 (dd, *J* = 8.1, 1.2 Hz, 1H), 7.05 (dt, *J* = 10.7, 2.2 Hz, 1H), 7.15 - 7.26 (m, 1H), 7.89 (s, 1H), 8.14 (s, 1H). ^{13}C NMR (75 MHz, $CDCl_3$) δ 16.0, 22.1, 28.7, 46.5, 53.1, 53.2, 57.9, 108.4 (d, $^2J_{CF}$ = 24.4 Hz), 110.2 (d, $^2J_{CF}$ = 21.3 Hz), 116.8 (d, $^4J_{CF}$ = 3.3 Hz), 118.7, 130.4 (d, $^3J_{CF}$ = 10.0 Hz), 130.5, 141.1 (d, $^3J_{CF}$ = 10.5 Hz), 158.3, 160.4, 162.1, 163.2 (d, $^1J_{CF}$ = 244.9 Hz). TLC-MS (ESI) *m/z*: 341.2 $[M + H]^+$ *m/z*: 339.1 $[M - H]^-$. HPLC (A): t_R = 1.73 min, purity: 98.6 % (*254 nm*).

tert-Butyl 3-((2-chloropyrimidin-4-yl)(methyl)amino)piperidine-1-carboxylate (36)

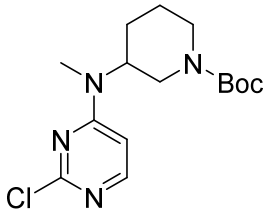

Molecular formula: $C_{15}H_{23}ClN_4O_2$

Molecular weight: 326.83

2,4-Dichloropyrimidine (500 mg, 3.36 mmol), *N*-Boc-3-(methylamino)piperidine (863 mg, 4.03 mmol) and DIPEA (1.76 mL, 10.07 mmol) were dissolved in iPrOH (7.5 mL). The mixture was stirred at 85 °C for 16 h before the solvent was removed under reduced pressure. Purification by flash chromatography (SiO_2, *n*-hexane:EtOAc 70:30) afforded 885 mg (80.6 %) of a clear oil. ^{1}H NMR (300 MHz, $CDCl_3$) δ 1.48 (s, 9H), 1.60 - 1.86

(m, 3H), 1.87 - 1.97 (m, 1H), 2.64 (t, *J* = 12.0 Hz, 1H), 2.78 (dd, *J* = 12.5, 11.1 Hz, 1H), 2.98 (s, 3H), 3.79 - 4.36 (m, 3H), 6.39 (d, *J* = 6.0 Hz, 1H), 8.06 (d, *J* = 6.1 Hz, 1H). TLC-MS (ESI) *m/z*: 349.2 $[M + Na]^+$. HPLC (A): t_R = 7.03 min, purity: 100.0 % (*254 nm*). Small amounts of the corresponding *tert*-butyl 3-((4-chloropyrimidin-2-yl)(methyl)amino)piperidine-1-carboxylate regioisomer were also isolated and analyzed: ^{1}H NMR (300 MHz, $CDCl_3$) δ 1.46 (s, 9H), 1.58 - 1.82 (m, 3H), 1.83 - 1.97 (m, 1H), 2.61 (t, *J* = 11.8 Hz, 1H), 2.79 (dd, *J* = 12.1, 11.5 Hz, 1H), 3.05 (s, 3H), 4.08 (br. s., 2H), 4.50 - 4.65 (m, 1H), 6.50 (d, *J* = 5.1 Hz, 1H), 8.16 (d, *J* = 5.1 Hz, 1H). HPLC (A): t_R = 9.58 min.

tert-Butyl 3-(methyl(2-(phenylamino)pyrimidin-4-yl)amino)piperidine-1-carboxylate (37)

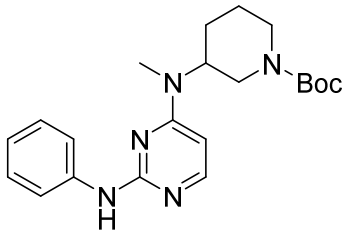

Molecular formula: $C_{21}H_{29}N_5O_2$

Molecular weight: 383.50

Compound **36** (159 mg, 0.49 mmol), aniline (68 mg, 0.73 mmol), $Pd_2(dba)_3$ (22 mg,0.049 mmol), XPhos (23 mg, 0.024 mmol) and NaO*t*Bu (140 mg, 1.46 mmol) were dissolved in anhydrous DMF (2.5 mL) and processed according to **General Procedure A**. Purification by flash chromatography (SiO_2, DCM:EtOH 97:3) afforded 102 mg (50.8 %) of a white solid. ^{1}H NMR (300 MHz, $CDCl_3$) δ 1.41 - 1.51 (m, 9H), 1.58 - 1.98 (m, 4H), 2.64 (t, *J* = 12.5 Hz, 1H), 2.79 (t, *J* = 11.9 Hz, 1H), 2.97 (s, 3H), 4.13 (br. s., 2H), 4.35 (br. s., 1H), 6.02 (d, *J* = 6.1 Hz, 1H), 6.94 - 7.02 (m, 1H), 7.04 (s, 1H), 7.27 - 7.36 (m, 2H), 7.59 (dd, *J* = 8.6, 1.0 Hz, 2H), 7.99 (d, *J* = 6.1 Hz, 1H). TLC-MS (ESI) *m/z*: 384.5 $[M + H]^+$. HPLC (A): t_R = 6.58 min.

3-(3-(Methyl(2-(phenylamino)pyrimidin-4-yl)amino)piperidin-1-yl)propanenitrile (38)

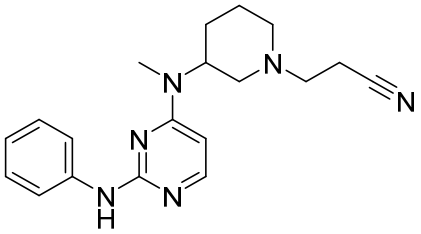

Molecular formula: $C_{24}H_{24}N_6$

Molecular weight: 336.44

Compound **37** (92 mg, 0.24 mmol) was treated according to **General Procedure B**. After drying in vacuo, the product was dissolved in in anhydrous MeOH (5 mL) and acrylonitrile (20 µL, 0.30 mmol) was added. The reaction mixture was stirred for 16 h at room temperature before the solvent was removed under reduced pressure. Purification by flash chromatography (SiO_2, DCM:EtOH 96:4) afforded 55 mg (68.1 %) of a yellow solid. ^{1}H NMR (300 MHz, $CDCl_3$) δ 1.47 - 1.62 (m, 1H), 1.65 - 1.87 (m, 3H), 2.05 (td, *J* = 11.3, 2.5 Hz, 1H), 2.14 (t, *J* = 10.5 Hz, 1H), 2.44 - 2.53 (m, 2H), 2.66 - 2.78 (m, 2H), 2.84 - 2.91 (m, 2H), 2.92 - 2.97 (m, 3H), 4.57 (br. s, 1H), 5.98 (d, *J* = 6.1 Hz, 1H), 6.93 - 7.02 (m, 1H), 7.27 - 7.34 (m, 2H), 7.45 (s, 1H), 7.62 (dd, *J* = 8.6, 1.0 Hz, 2H), 7.99 (d, *J* = 6.1 Hz, 1H). ^{13}C NMR (75 MHz, $CDCl_3$) δ 15.9, 24.7, 27.7, 29.9, 51.9, 52.9, 53.4, 55.5, 95.0, 118.7, 118.9, 121.5, 128.7, 140.3, 156.2, 159.4, 162.3. TLC-MS (ESI) *m/z*: 337.4 $[M + H]^+$. HPLC (A): t_R = 2.24 min, purity: 100.0 % (*254 nm*).

4-Chloro-6-phenoxypyrimidine (39a)

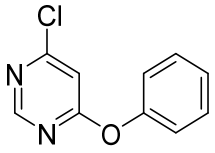

Molecular formula: $C_{10}H_7ClN_2O$

Molecular weight: 206.63

4,6-Dichloropyrimidine (0.97 g, 6.51 mmol), phenol (0.56 g, 5.95 mmol) and K_2CO_3 (2.07 g, 14.98 mmol) were dissolved in DMF (15 mL). The mixture was stirred at room temperature for 3 h before saturated $NaHCO_3$ solution (50 mL) was added and the mixture was extracted with EtOAc (3x). The combined organic phases were washed with brine, dried over Na_2SO_4 and removed under reduced pressure to afford 0.80 g (64.7 %) of an orange solid. ^{1}H NMR (300 MHz, $CDCl_3$) δ 6.92 (d, *J* = 0.7 Hz, 1H), 7.12 - 7.20 (m, 2H), 7.29 - 7.36 (m, 1H), 7.42 - 7.51 (m, 2H), 8.60 (s, 1H). ^{13}C NMR (75 MHz, $CDCl_3$) δ

107.8, 121.4, 126.3, 130.0, 151.9, 158.5, 161.9, 170.3. TLC-MS (ESI) *m/z*: 205.2 [M - H]$^-$. HPLC (A): t_R = 5.76 min.

4-Chloro-6-(3-chlorophenoxy)pyrimidine (39b)

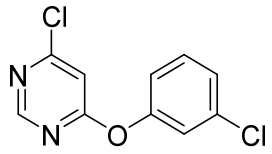

Molecular formula: $C_{10}H_6Cl_2N_2O$

Molecular weight: 241.07

4,6-Dichloropyrimidine (1.43 g, 9.60 mmol), 3-chlorophenol (1.03 g, 8.01 mmol), K_2CO_3 (1.66 g, 12.00 mmol) and NaI (20 mg, 0.13 mmol) were dissolved in MeCN (20 mL). The mixture was stirred at room temperature for 24 h. Then the reaction was poured onto 1 N aqueous sodium hydroxide solution (25 mL) and the mixture was extracted with Et_2O (3x). The collected organic phases were washed with brine, dried over Na_2SO_4 and removed under reduced pressure to afford 1.89 g (97.4 %) of an orange solid. ^{1}H NMR (250 MHz, DMSO-*d*$_6$) δ 7.25 (ddd, *J* = 8.1, 2.3, 1.1 Hz, 1H), 7.36 - 7.42 (m, 1H), 7.43 - 7.46 (m, 2H), 7.51 (t, *J* = 8.1 Hz, 1H), 8.67 (d, *J* = 0.7 Hz, 1H). TLC-MS (ESI) *m/z*: 239.1 [M - H]$^-$. HPLC (A): t_R = 7.93 min.

tert-Butyl 3-(methyl(6-phenoxypyrimidin-4-yl)amino)piperidine-1-carboxylate (40a)

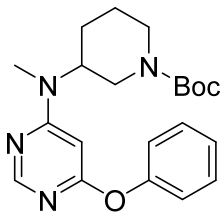

Molecular formula: $C_{21}H_{28}N_4O_3$

Molecular weight: 384.48

Compound **39a** (300 mg, 1.45 mmol), *N*-Boc-3-(methylamino)piperidine (465 mg, 2.17 mmol) and DIPEA (760 µL, 4.35 mmol) were dissolved in DMF (10 mL). The reaction mixture was stirred for 96 h at 80 °C. Saturated aqueous $NaHCO_3$ (15 mL) was added and the product was extracted with EtOAc (3x). The combined organic phases were washed with brine and after drying over anhydrous Na_2SO_4, the solvent was removed under reduced pressure. The product was purified by flash chromatography (SiO_2, *n*-hexane:EtOAc 85:15) to afford 311 mg (55.7 %) of the title compound. ^{1}H NMR (300 MHz, $CDCl_3$) δ 1.46 (s, 9H), 1.56 - 1.73 (m, 2H), 1.74 - 1.83 (m, 1H), 1.84 - 1.94 (m, 1H), 2.62 (t, *J* = 12.0 Hz, 1H), 2.77 (t, *J* = 11.8 Hz, 1H), 2.91 (s, 3H), 4.09 (br. s., 2H),

4.43 (br. s., 1H), 5.90 (s, 1H), 7.10 - 7.16 (m, 2H), 7.17 - 7.25 (m, 1H), 7.36 - 7.43 (m, 2H), 8.31 (s, 1H). ^{13}C NMR (75 MHz, $CDCl_3$) δ 24.7, 28.1, 28.3, 29.9, 43.6, 46.3, 51.6, 79.8, 86.2, 121.4, 125.1, 129.6, 153.0, 154.7, 157.6, 164.1, 170.1. TLC-MS (ESI) *m/z*: 385.1 $[M + H]^+$. HPLC (A): t_R = 8.91 min.

tert-Butyl 3-((6-(3-chlorophenoxy)pyrimidin-4-yl)(methyl)amino)-piperidine-1-carboxylate (40b)

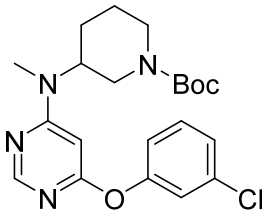

Molecular formula: $C_{21}H_{27}ClN_4O_3$

Molecular weight: 418.92

Compound **39b** (370 mg, 1.53 mmol), *N*-Boc-3-(methylamino)piperidine (395 mg, 1.84 mmol) and DIPEA (805 µL, 4.60 mmol) were dissolved in DMF (10 mL). The reaction mixture was stirred for 144 h at 80 °C. Saturated aqueous $NaHCO_3$ solution (15 mL) was added and the product was extracted with EtOAc (3x). The combined organic phases were washed with brine and after drying over anhydrous Na_2SO_4, the solvent was removed under reduced pressure. The product was purified by flash chromatography (SiO_2, *n*-hexane:EtOAc 85:15) to afford 454 mg (70.8 %) of an orange semi-solid. ^{1}H NMR (300 MHz, $CDCl_3$) δ 1.38 - 1.51 (m, 9H), 1.52 - 1.82 (m, 3H), 1.82 - 1.94 (m, 1H), 2.61 (t, *J* = 12.0 Hz, 1H), 2.76 (t, *J* = 11.8 Hz, 1H), 2.91 (s, 3H), 4.08 (br. s., 2H), 4.40 (br. s., 1H), 5.93 (s, 1H), 6.97 - 7.05 (m, 1H), 7.10 - 7.21 (m, 2H), 7.25 - 7.34 (m, 1H), 8.28 (s, 1H). ^{13}C NMR (75 MHz, $CDCl_3$) δ 24.6, 28.0, 28.3, 29.9, 43.6, 46.1, 51.7, 79.8, 86.5, 119.7, 121.9, 125.2, 130.2, 134.7, 153.6, 154.7, 157.5, 164.1, 169.5. TLC-MS (ESI) *m/z*: 441.2 $[M + Na]^+$. HPLC (A): t_R = 10.27 min.

N-Methyl-6-phenoxy-*N*-(piperidin-3-yl)pyrimidin-4-amine (41a)

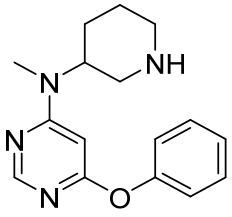

Molecular formula: $C_{16}H_{20}N_4O$

Molecular weight: 284.36

The title compound was synthesized according to **General Procedure B** starting from compound **40a** (300 mg, 0.78 mmol) to afford 180 mg (81.1 %) of the product. ^{1}H NMR (300 MHz, $CDCl_3$) δ 1.56 - 1.73 (m, 2H), 1.77 - 1.91 (m, 2H), 2.25 (br. s., 1H), 2.50 (td, *J* = 12.2, 2.5 Hz, 1H), 2.63 - 2.75 (m, 1H), 2.87 (s, 3H), 2.98 - 3.11 (m, 2H), 4.50 (br. s., 1H), 5.85 (s, 1H), 7.09 - 7.15 (m, 2H), 7.17 - 7.25 (m, 1H), 7.35 - 7.44 (m, 2H), 8.29 (s, 1H). ^{13}C NMR (75 MHz, $CDCl_3$) δ 26.8, 28.4, 29.9, 45.9, 48.8, 53.1, 86.0, 121.3, 125.0, 129.6, 153.1, 157.6, 164.0, 170.1. TLC-MS (ESI) *m/z*: 285.2 $[M + H]^+$. HPLC (A): t_R = 2.94 min.

6-(3-Chlorophenoxy)-*N*-methyl-*N*-(piperidin-3-yl)pyrimidin-4-amine (41b)

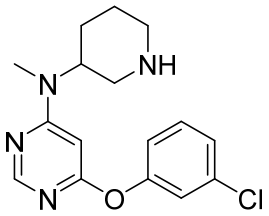

Molecular formula: $C_{16}H_{19}ClN_4O$

Molecular weight: 318.81

The title compound was synthesized according to **General Procedure B** starting from compound **40b** (430 mg, 1.03 mmol) to afford 272 mg (82.7 %) of the product. ^{1}H NMR (300 MHz, $CDCl_3$) δ 1.60 - 1.74 (m, 2H), 1.77 - 1.93 (m, 2H), 2.53 (td, *J* = 12.3, 2.7 Hz, 1H), 2.67 - 2.78 (m, 1H), 2.87 (s, 3H), 3.01 - 3.13 (m, 2H), 3.30 (br. s., 1H), 4.53 (br. s., 1H), 5.90 (s, 1H), 6.98 - 7.05 (m, 1H), 7.10 - 7.20 (m, 2H), 7.28 - 7.33 (m, 1H), 8.27 (s, 1H). ^{13}C NMR (75 MHz, $CDCl_3$) δ 26.3, 28.2, 29.9, 45.7, 48.4, 52.9, 86.4, 119.6, 121.8, 125.2, 130.2, 134.7, 153.7, 157.5, 164.0, 169.4. TLC-MS (ESI) *m/z*: 319.2 $[M + H]^+$. HPLC (A): t_R = 4.74 min.

3-(3-(Methyl(6-phenoxypyrimidin-4-yl)amino)piperidin-1-yl)-3-oxopropanenitrile (42)

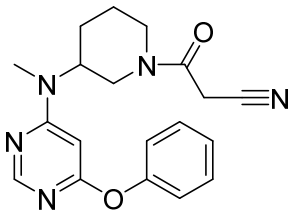

Molecular formula: $C_{19}H_{21}N_5O_2$

Molecular weight: 351.41

The title compound was synthesized according to **General Procedure D** starting from compound **41a** (32 mg, 0.11 mmol), cyanoacetic acid (12 mg, 0.14 mmol), PyBOP (71

mg, 0.14 mmol) and DIPEA (58 µL, 0.34 mmol). The product was purified by flash chromatography (SiO_2, DCM:EtOH 97:3) to afford 29 mg (72.5 %) of a white solid. ^{1}H NMR (300 MHz, $CDCl_3$) δ 1.63 - 1.95 (m, 4H), 2.37 - 2.75 (m, 1H), 2.78 - 2.86 (m, 3H), 2.90 - 3.10 (m, 1H), 3.39 - 3.70 (m, 3H), 4.53 (d, *J* = 9.1 Hz, 2H), 5.77 - 5.86 (m, 1H), 7.06 (d, *J* = 8.2 Hz, 2H), 7.14 - 7.21 (m, 1H), 7.28 - 7.42 (m, 2H), 8.23 (s, 1H). ^{13}C NMR (75 MHz, $CDCl_3$) δ 24.4, 25.1, 28.0, 30.2, 43.9, 47.8, 51.9, 86.5, 114.0, 121.4, 125.3, 129.7, 152.9, 157.6, 160.6, 164.0, 170.3. TLC-MS (ESI) *m/z*: 374.1 $[M + Na]^+$ *m/z*: 350.2 $[M - H]^-$. HPLC (A): t_R = 4.29 min, purity: 99.7 % (*254 nm*).

3-(3-((6-(3-Chlorophenoxy)pyrimidin-4-yl)(methyl)amino)piperidin-1-yl)-3-oxopropanenitrile (43)

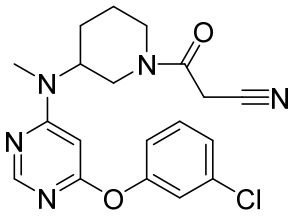

Molecular formula: $C_{19}H_{20}ClN_5O_2$

Molecular weight: 385.85

The title compound was synthesized according to **General Procedure D** starting from compound **41b** (70 mg, 0.22 mmol), cyanoacetic acid (22 mg, 0.26 mmol), PyBOP (137 mg, 0.26 mmol) and DIPEA (115 µL, 0.66 mmol). The product was purified by flash chromatography (SiO_2, DCM:EtOH 97:3) to afford 22 mg (26.0 %) of a yellow solid. ^{1}H NMR (300 MHz, $CDCl_3$) δ 1.58 - 2.05 (m, 4H), 2.50 - 2.83 (m, 1H), 2.92 (s, 3H), 3.03 - 3.18 (m, 1H), 3.44 - 3.78 (m, 3H), 4.52 - 4.69 (m, 2H), 5.92 - 5.97 (m, 1H), 7.04 (dt, *J* = 8.1, 1.0 Hz, 1H), 7.16 (t, *J* = 2.0 Hz, 1H), 7.19 - 7.25 (m, 1H), 7.30 - 7.38 (m, 1H), 8.31 (d, *J* = 0.6 Hz, 1H). ^{13}C NMR (75 MHz, $CDCl_3$) δ 24.4, 25.1, 28.0, 30.3, 43.9, 47.8, 51.2, 86.9, 113.9, 119.8, 122.0, 125.5, 130.3, 134.9, 153.5, 157.5, 160.4, 164.1, 169.8. TLC-MS (ESI) *m/z*: 408.1 $[M + Na]^+$ *m/z*: 384.0 $[M - H]^-$. HPLC (A): t_R = 6.26 min, purity: 98.7 % (*254 nm*).

3-(3-((6-(3-Chlorophenoxy)pyrimidin-4-yl)(methyl)amino)piperidin-1-yl)propanenitrile (44)

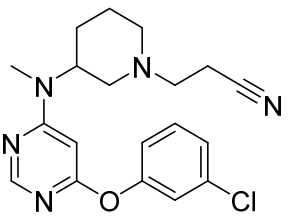

Molecular formula: $C_{19}H_{22}ClN_5O$

Molecular weight: 371.87

Compound **41b** (69 mg, 0.21 mmol) was dissolved in anhydrous MeOH (5 mL) before acrylonitrile (150 µL, 2.09 mmol) was added. The reaction mixture was stirred for 5 h at room temperature. Then the solvent was removed under reduced pressure and purification by flash chromatography (SiO_2, *n*-hexane:EtOAc 70:30 → 30:70) afforded 64 mg (93.7 %) of an orange wax. ^{1}H NMR (300 MHz, $CDCl_3$) δ 1.44 - 1.63 (m, 1H), 1.65 - 1.87 (m, 3H), 2.04 (td, *J* = 11.2, 2.6 Hz, 1H), 2.19 (t, *J* = 10.6 Hz, 1H), 2.45 - 2.57 (m, 2H), 2.67 - 2.78 (m, 2H), 2.79 - 3.01 (m, 5H), 4.62 (br. s., 1H), 5.91 (s, 1H), 7.02 (ddd, *J* = 8.1, 2.2, 1.0 Hz, 1H), 7.14 (t, *J* = 2.0 Hz, 1H), 7.16 - 7.21 (m, 1H), 7.28 - 7.35 (m, 1H), 8.27 - 8.32 (m, 1H). ^{13}C NMR (75 MHz, $CDCl_3$) δ 15.8, 24.4, 27.5, 30.1, 51.9, 52.6, 53.4, 55.5, 86.4, 118.7, 119.7, 121.9, 125.2, 130.2, 134.7, 153.7, 157.6, 164.1, 169.5. TLC-MS (ESI) *m/z*: 372.0 $[M + H]^+$. HPLC (A): t_R = 4.63 min, purity: 95.5 % (*254 nm*).

(3-(Methyl(6-phenoxypyrimidin-4-yl)amino)piperidin-1-yl)(thiophen-3-yl)methanone (45)

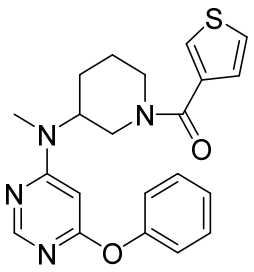

Molecular formula: $C_{21}H_{22}N_4O_2S$

Molecular weight: 394.49

The title compound was synthesized according to **General Procedure D** starting from compound **41a** (55 mg, 0.19 mmol), 3-thiophenecarboxylic acid (37 mg, 0.29 mmol), PyBOP (149 mg, 0.29 mmol) and DIPEA (125 µL, 0.72 mmol). The product was purified by flash chromatography (SiO_2, DCM:EtOH 97:3) to afford 70 mg (74.2 %) of a yellow solid. ^{1}H NMR (300 MHz, $CDCl_3$) δ 1.59 - 2.10 (m, 4H), 2.50 - 3.08 (m, 5H), 4.09 (br. s., 1H), 4.76 (br. s., 2H), 5.85 (br. s., 1H), 7.09 - 7.17 (m, 2H), 7.19 - 7.33 (m, 3H), 7.36

- 7.46 (m, 2H), 7.61 - 7.77 (m, 1H), 8.32 (d, *J* = 0.6 Hz, 1H). ^{13}C NMR (75 MHz, $CDCl_3$) δ 24.9, 28.3, 30.0, *(C^2-Pip. missing)*, *(C^6-Pip. missing)*, 51.7, 86.3, 121.4, 125.2, 125.7, 126.7, 127.2, 129.6, 136.1, 152.9, 157.4, 163.9, 166.0, 170.1. TLC-MS (ESI) *m/z*: 394.9 $[M + Na]^+$. HPLC (A): t_R = 6.73 min, purity: 99.2 % (*254 nm*).

(3-Hydroxy-4-methoxyphenyl)(3-(methyl(6-phenoxypyrimidin-4-yl)amino)piperidin-1-yl)methanone (46)

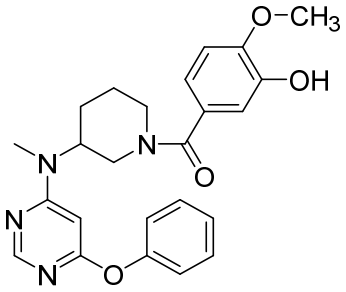

Molecular formula: $C_{24}H_{26}N_4O_4$

Molecular weight: 434.50

The title compound was synthesized according to **General Procedure D** starting from compound **41a** (55 mg, 0.19 mmol), isovanillic acid (39 mg, 0.23 mmol), PyBOP (121 mg, 0.23 mmol) and DIPEA (100 µL, 0.58 mmol). The product was purified by flash chromatography (SiO_2, DCM:EtOH 97:3) to afford 25 mg (29.8 %) of a white solid. ^{1}H NMR (300 MHz, $CDCl_3$) δ 1.12 - 1.35 (m, 1H), 1.35 - 1.62 (m, 1H), 1.62 - 1.93 (m, 4H), 1.94 - 2.05 (m, 1H), 2.82 - 2.97 (m, 4H), 3.89 (s, 3H), 4.72 (br. s., 2H), 5.83 (br. s., 1H), 6.84 (d, *J* = 8.3 Hz, 1H), 7.04 (d, *J* = 8.2 Hz, 1H), 7.07 - 7.17 (m, 3H), 7.20 - 7.26 (m, 1H), 7.35 - 7.50 (m, 2H), 8.37 (s, 1H). ^{13}C NMR (75 MHz, $CDCl_3$) δ 25.1, 28.4, 30.1, *(C^2-Pip. missing)*, *(C^6-Pip. missing)*, 51.9, 56.0, 86.2, 110.3, 113.9, 119.8, 121.4, 125.3, 129.7, 145.3, 147.8, 152.9, 157.4, 164.0, 167.4, 169.9, 170.6. TLC-MS (ESI) *m/z*: 457.1 $[M + Na]^+$ *m/z*: 433.0 $[M - H]^-$. HPLC (A): t_R = 5.96 min, purity: 96.0 % (*254 nm*).

Ethyl 3-(3-(methyl(6-phenoxypyrimidin-4-yl)amino)piperidin-1-yl)-3-oxopropanoate (47)

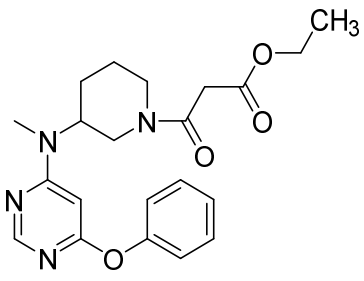

Molecular formula: $C_{21}H_{26}N_4O_4$

Molecular weight: 398.46

The title compound was synthesized according to **General Procedure D** starting from compound **41a** (55 mg, 0.19 mmol), ethyl potassium malonate (49 mg, 0.29 mmol), PyBOP (149 mg, 0.29 mmol) and DIPEA (125 µL, 0.72 mmol). The product was purified by flash chromatography (SiO_2, DCM:EtOH 97:3) to afford 22 mg (23.1 %) of an orange sticky oil. ^{1}H NMR (300 MHz, $CDCl_3$) δ 1.15 - 1.24 (m, 3H), 1.53 - 1.92 (m, 4H), 2.35 - 2.73 (m, 1H), 2.79 - 2.88 (m, 3H), 2.90 - 3.05 (m, 1H), 3.37 - 3.50 (m, 2H), 3.60 - 3.75 (m, 1H), 4.08 - 4.19 (m, 2H), 4.34 - 4.68 (m, 2H), 5.82 (d, *J* = 3.2 Hz, 1H), 7.01 - 7.10 (m, 2H), 7.11 - 7.19 (m, 1H), 7.27 - 7.41 (m, 2H), 8.23 (s, 1H). ^{13}C NMR (75 MHz, $CDCl_3$) δ 14.0, 24.6, 27.9, 30.1, 41.3, 42.0, 45.3, 51.7, 61.4, 86.3, 121.3, 125.2, 129.6, 152.9, 157.4, 163.9, 164.7, 167.5, 170.0. TLC-MS (ESI) *m/z*: 396.9 $[M - H]^-$. HPLC (A): t_R = 5.81 min, purity: 97.3 % (*254 nm*).

Cyclopropyl(3-(methyl(6-phenoxypyrimidin-4-yl)amino)piperidin-1-yl)methanone (48)

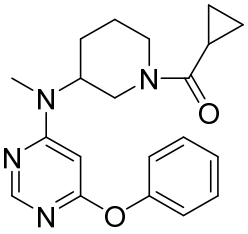

Molecular formula: $C_{20}H_{24}N_4O_2$

Molecular weight: 352.44

The title compound was synthesized according to **General Procedure D** starting from compound **41a** (32 mg, 0.11 mmol), cyclopropanecarboxylic acid (20 mg, 0.23 mmol), PyBOP (121 mg, 0.23 mmol) and DIPEA (100 µL, 0.58 mmol). The product was purified by flash chromatography (SiO_2, DCM:EtOH 97:3 → 95:5) to afford 50 mg (80.7 %) of an orange solid. ^{1}H NMR (300 MHz, $CDCl_3$) δ 0.66 - 0.83 (m, 2H), 0.85 - 1.10 (m, 2H), 1.60 - 2.00 (m, 5H), 2.41 - 2.88 (m, 1H), 2.92 (s, 3H), 3.07 (br. s., 1H), 4.04 - 4.42 (m, 1H), 4.61 (br. s., 2H), 5.89 (s, 1H), 7.10 - 7.16 (m, 2H), 7.18 - 7.26 (m, 1H), 7.35 - 7.47 (m, 2H), 8.30 (s, 1H). ^{13}C NMR (101 MHz, DMSO-d_6) δ 6.7, 10.5, 24.7, 27.3, 29.6, 42.7, 46.0, 51.4, 86.3, 121.3, 124.8, 129.5, 152.9, 157.1, 163.7, 169.4, 171.1. TLC-MS (ESI) *m/z*: 375.1 $[M + Na]^+$ *m/z*: 351.1 $[M - H]^-$. HPLC (A): t_R = 6.10 min, purity: 97.4 % (*254 nm*).

tert-Butyl 3-((6-(3-fluorobenzoyl)pyrimidin-4-yl)(methyl)amino)-piperidine-1-carboxylate (49)

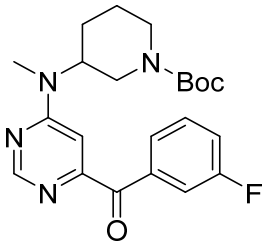

Molecular formula: $C_{22}H_{27}FN_4O_3$

Molecular weight: 414.48

Compound **5** (100 mg, 0.31 mmol) was dissolved in anhydrous DMF (10 mL) under an atmosphere of argon and cooled to -20 °C. Then sodium hydride 60% in mineral oil (25 mg, 0.61 mmol) was added and the reaction mixture was stirred for 30 minutes before 3-fluorophenylacetonitrile (62 mg, 0.46 mmol) was added dropwise. The solution was slowly brought to room temperature and was stirred for 48 h in the absence of oxygen. Then the reaction vessel was opened to let air enter the system and it was stirred for another 48 h before H_2O (60 mL) was added to the reaction and it was extracted with EtOAc (3x20mL). The crude product was used without further purification (yield calculated see compound **50**). ^{1}H NMR (300 MHz, $CDCl_3$) δ 1.46 (s, 9H), 1.57 - 1.87 (m, 3H), 1.87 - 1.98 (m, 1H), 2.65 (t, *J* = 11.8 Hz, 1H), 2.83 (t, *J* = 11.8 Hz, 1H), 3.03 (s, 3H), 4.11 (br. s., 2H), 4.56 (br. s., 1H), 7.05 (s, 1H), 7.25 - 7.33 (m, 1H), 7.41 - 7.51 (m, 1H), 7.81 (d, *J* = 9.4 Hz, 1H), 7.89 (d, *J* = 7.8 Hz, 1H), 8.71 (s, 1H). TLC-MS (ESI) *m/z*: 438.5 $[M + Na]^+$. HPLC (A): t_R = 9.01 min.

3-(3-((6-(3-Fluorobenzoyl)pyrimidin-4-yl)(methyl)amino)piperidin-1-yl)propanenitrile (50)

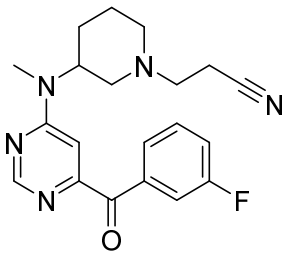

Molecular formula: $C_{20}H_{22}FN_5O$

Molecular weight: 367.43

The crude product **49** was treated according to **General Procedure B**. The deprotected compound was dissolved in anhydrous MeOH (5 mL) and acrylonitrile (100 µL, 1.88 mmol) was added. After 4 h stirring at room temperature, the solvent was removed under reduced pressure and the product was purified by flash chromatography (SiO_2,

DCM:EtOH 97:3) to yield 86 mg (75.5 % over 4 steps starting from **5**) of a yellow oil. ^{1}H NMR (300 MHz, $CDCl_3$) δ 1.41 - 1.81 (m, 4H), 1.98 (td, *J* = 11.2, 2.6 Hz, 1H), 2.15 (t, *J* = 10.5 Hz, 1H), 2.39 - 2.49 (m, 2H), 2.61 - 2.71 (m, 2H), 2.76 - 2.85 (m, 2H), 2.86 - 3.05 (m, 3H), 4.30 - 5.19 (m, 1H), 6.96 (s, 1H), 7.22 (tdd, *J* = 8.38, 2.7, 1.0 Hz, 1H), 7.38 (td, *J* = 8.0, 5.5 Hz, 1H), 7.73 (ddd, *J* = 9.5, 2.5, 1.5 Hz, 1H), 7.81 (dt, *J* = 7.8, 1.2 Hz, 1H), 8.62 (d, *J* = 1.1 Hz, 1H). ^{13}C NMR (75 MHz, $CDCl_3$) δ 15.8, 24.3, 27.4, 30.0, 51.8, 52.5, 53.4, 55.4, 102.3, 117.4 (d, $^{2}J_{CF}$ = 22.7 Hz), 118.6, 120.3 (d, $^{2}J_{CF}$ = 21.6 Hz), 126.6 (d, $^{4}J_{CF}$ = 2.8 Hz), 129.8 (d, $^{3}J_{CF}$ = 7.7 Hz), 137.3 (d, $^{3}J_{CF}$ = 6.6 Hz), 157.4, 159.9, 162.2 (d, $^{1}J_{CF}$ = 247.1 Hz), 162.4, 192.3. TLC-MS (ESI) *m/z*: 390.0 $[M + Na]^+$. HPLC (A): t_R = 2.74 min, purity: 98.3 % (*254 nm*).

4-Chloro-7-tosyl-7*H*-pyrrolo[2,3-*d*]pyrimidine (52)

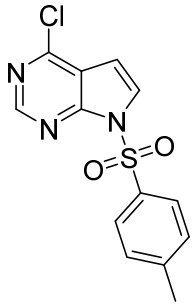

Molecular formula: $C_{13}H_{10}ClN_3O_2S$

Molecular weight: 307.75

4-Chloro-7*H*-pyrrolo[2,3-*d*]pyrimidine (250 mg, 1.63 mmol) and sodium hydride 60% in mineral oil (98 mg, 2.45 mmol) were suspended in ice-cooled, anhydrous THF under an atmosphere of argon. After stirring at 0 °C for 30 minutes, tosyl chloride (372 mg, 1.95 mmol) was added and the mixture was allowed to warm to room temperature and stirred for 5 more h. Then the reaction mixture was stored at -20 °C for 48 h before being poured into ice-cold H_2O (25 mL). After the addition of brine (100 mL), the precipitate was filtered off and dried in vacuo to afford 459 mg (91.5 %) of a yellow solid. ^{1}H NMR (300 MHz, DMSO-*d*$_6$) δ 2.37 (s, 3H), 6.96 (d, *J* = 4.1 Hz, 1H), 7.43 - 7.52 (m, *J* = 8.1 Hz, 2H), 8.01 - 8.09 (m, 2H), 8.12 (d, *J* = 4.0 Hz, 1H), 8.82 (s, 1H). ^{13}C NMR (75 MHz, DMSO-*d*$_6$) δ 21.1, 103.2, 119.2, 127.8, 128.6, 130.3, 133.7, 146.5, 150.5, 152.0, 152.5. TLC-MS (ESI) *m/z*: 305.8 $[M - H]^-$. HPLC (A): t_R = 7.14 min.

tert-Butyl 3-(methyl(7-tosyl-7*H*-pyrrolo[2,3-*d*]pyrimidin-4-yl)amino)-piperidine-1-carboxylate (53)

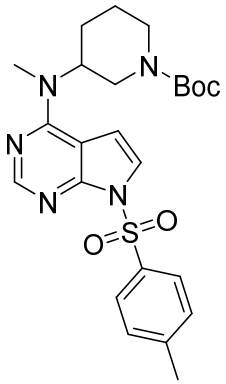

Molecular formula: $C_{24}H_{31}N_5O_4S$

Molecular weight: 485.6

Compound **52 (**200 mg, 0.65 mmol), *N*-Boc-3-(methylamino)piperidine (167 mg, 0.78 mmol) and DIPEA (340 µL, 1.95 mmol) were dissolved in anhydrous DMF (5 mL) and stirred at 70 °C overnight. Then the reaction mixture was stored at -20 °C for 16 h before being poured into ice-cooled H_2O. After the addition of saturated aqueous NH_4Cl solution (100 mL), the precipitate was filtered off and dried in vacuo to afford 207 mg (65.4 %) of product. ^{1}H NMR (300 MHz, DMSO-*d*$_6$) δ 1.19 (d, *J* = 6.2 Hz, 4H), 1.38 (s, 9H), 1.67 - 1.81 (m, 2H), 2.35 (s, 3H), 3.16 (s, 3H), 3.90 (d, *J* = 11.0 Hz, 2H), 4.58 (br. s., 1H), 6.90 (d, *J* = 3.7 Hz, 1H), 7.42 (d, *J* = 8.2 Hz, 2H), 7.62 (d, *J* = 4.0 Hz, 1H), 7.97 (d, *J* = 8.3 Hz, 2H), 8.25 (s, 1H). TLC-MS (ESI) *m/z*: 484.1 $[M - H]^-$. HPLC (A): t_R = 9.28 min.

3-(3-(Methyl(7*H*-pyrrolo[2,3-*d*]pyrimidin-4-yl)amino)piperidin-1-yl)propanenitrile (54)

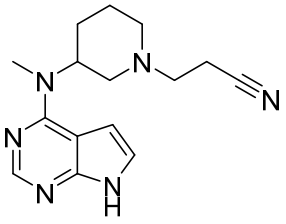

Molecular formula: $C_{15}H_{20}N_6$

Molecular weight: 284.37

Compound **53** (185 mg, 0.38 mmol) was dissolved in anhydrous THF (7.5 mL) before the addition of NaO*t*Bu (274 mg, 2.85 mmol). The reaction was stirred at room temperature overnight. Complete conversion was seen in HPLC (*Method A*; ret. time. 4.22 min). The reaction was mixed with diluted aqueous NH_4Cl solution and then extracted with EtOAc (3x). Purification was achieved by flash chromatography (SiO_2, DCM:EtOH 96:4). The purified product was redissolved in DCM (4 mL). After the addition of TFA (1 mL), the mixture was stirred at room temperature for 3 more h. Work-

up was performed according to **General Procedure B**. The resulting *N*-methyl-*N*-(piperidin-3-yl)-7*H*-pyrrolo[2,3-*d*]pyrimidin-4-amine was dissolved in anhydrous MeOH (5 mL) and acrylonitrile (10 µL, 0.15 mmol) was added. After 18 h, the solvents were evaporated and the compound was dried in vacuo to afford 38 mg (35.1 % *over 3 steps*) of a yellow solid. ^{1}H NMR (300 MHz, $CDCl_3$) δ 1.67 (td, *J* = 11.3, 4.6 Hz, 1H), 1.73 - 1.88 (m, 2H), 1.93 (d, *J* = 11.6 Hz, 1H), 2.07 (td, *J* = 11.0, 3.3 Hz, 1H), 2.23 (t, *J* = 10.5 Hz, 1H), 2.47 - 2.57 (m, 2H), 2.64 - 2.83 (m, 2H), 2.92 (d, *J* = 11.0 Hz, 1H), 3.00 - 3.09 (m, 1H), 3.27 (s, 3H), 4.83 (br. s., 1H), 6.60 (d, *J* = 3.6 Hz, 1H), 7.11 (d, *J* = 3.6 Hz, 1H), 8.34 (s, 1H), 12.04 (br. s., 1H). ^{13}C NMR (75 MHz, $CDCl_3$) δ 15.9, 24.7, 28.0, 31.3, 53.0, 53.3, 53.5, 55.9, 101.9, 102.8, 118.8, 120.5, 150.5, 151.5, 157.4. TLC-MS (ESI) *m/z*: 285.2 $[M + H]^+$ *m/z*: 283.0 $[M - H]^-$. HPLC (A): t_R = 1.24 min, purity: 100.0 % (*254 nm*).

1-Ethyl-3-(4-(4-(4-fluorophenyl)-2-(methylthio)-1*H*-imidazol-5-yl)pyridin-2-yl)urea (69)

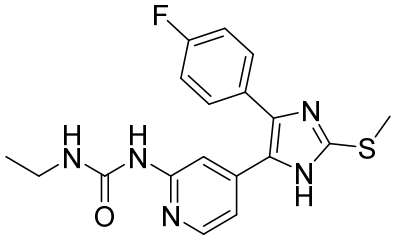

Molecular formula: $C_{18}H_{18}FN_5OS$

Molecular weight: 371.43

4-(4-(4-Fluorophenyl)-2-(methylthio)-1*H*-imidazol-5-yl)pyridin-2-amine[271] (143 mg, 0.48 mmol) was dissolved in anhydrous THF (5 mL) under an atmosphere of argon. Ethyl isocyanate (55 µL, 0.77 mmol) was added in one portion and the reaction was stirred at 55 °C. The solvents were removed under reduced pressure and purification by flash chromatography (SiO_2, DCM:EtOH 95:5) afforded 68 mg (38.5%) of a beige solid. ^{1}H NMR (300 MHz, DMSO-*d*$_6$) δ 1.08 (t, *J* = 7.2 Hz, 3H), 2.61 (s, 3H), 3.12 - 3.23 (m, 2H), 6.84 (dd, *J* = 5.4, 1.4 Hz, 1H), 7.12 - 7.33 (m, 2H), 7.36 - 7.54 (m, 3H), 8.00 (d, *J* = 5.4 Hz, 1H), 8.44 (br. s., 1H), 9.17 (s, 1H), 12.72 (s, 1H). ^{13}C NMR (75 MHz, DMSO-*d*$_6$) δ 15.1, 15.4, 33.8, 108.5, 114.2, 115.8 (d, $^{2}J_{CF}$ = 21.6 Hz), 126.6 (d, $^{4}J_{CF}$ = 2.8 Hz), 130.1, 130.7 (d, $^{3}J_{CF}$ = 8.3 Hz), 134.3, 138.5, 142.2, 143.9, 146.3, 154.0, 154.7, 162.0 (d, $^{1}J_{CF}$ = 247.1 Hz). TLC-MS (ESI) *m/z* = 394.2 $[M + Na]^+$ *m/z* = 370.2 $[M - H]^-$. HPLC (A): t_R = 5.04 min, purity: 96.1 % (*254 nm*).

2-(4-Fluorophenyl)-1-(2-((4-methoxybenzyl)amino)pyridin-4-yl)-2-oxoethyl acetate (124)

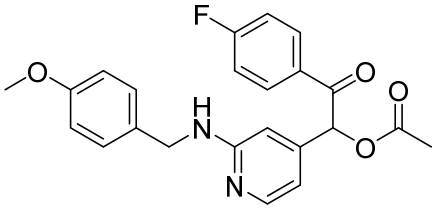

Molecular formula: $C_{23}H_{21}FN_2O_4$

Molecular weight: 408.43

tert-Butyl (4-(2-(4-fluorophenyl)-2-oxoethyl)pyridin-2-yl)(4-methoxybenzyl)-carbamate[271] (1.00 g, 2.22 mmol) was dissolved in glacial acetic acid (10 mL) before lead tetraacetate (1.13 g, 2.55 mmol) was added. The reaction mixture was heated to 120 °C for 16 h. After cooling to room temperature, the solvent was evaporated in vacuo before saturated aqueous $NaHCO_3$ was added and it was extracted with DCM (3x). The combined organic layers were dried over anhydrous Na_2SO_4 and the solvent was removed under reduced pressure. Purification by flash chromatography (SiO_2, *n*-hexane/EtOAc 50:50) afforded 476 mg (52.5%) of a yellow solid. ^{1}H NMR (300 MHz, $CDCl_3$) δ 2.20 (s, 3H), 3.80 (s, 3H), 4.40 (d, J = 5.5 Hz, 2H), 5.08 (t, J = 5.3 Hz, 1H), 6.40 (s, 1H), 6.59 (s, 1H), 6.63 (dd, J = 5.2, 1.4 Hz, 1H), 6.82 - 6.88 (m, 2H), 7.03 - 7.11 (m, 2H), 7.20 - 7.26 (m, 2H), 7.86 - 7.94 (m, 2H), 8.08 (d, J = 5.2 Hz, 1H). ^{13}C NMR (75 MHz, $CDCl_3$) δ 20.6, 45.7, 55.2, 76.4, 105.8, 111.8, 114.0, 115.9 (d, $^2J_{CF}$ = 22.1 Hz), 128.7, 130.5, 130.6 (d, $^4J_{CF}$ = 2.8 Hz), 131.4 (d, $^3J_{CF}$ = 9.4 Hz), 143.3, 149.0, 158.9, 165.9 (d, $^1J_{CF}$ = 256.0 Hz), 170.1, 191.6. TLC-MS (ESI) m/z = 408.9 $[M + H]^+$ m/z = 406.8 $[M - H]^-$. HPLC (A): t_R = 3.80 min.

4-(4-(4-Fluorophenyl)-2-methyloxazol-5-yl)-*N*-(4-methoxybenzyl)pyridin-2-amine (125)

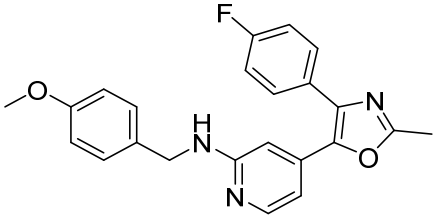

Molecular formula: $C_{23}H_{20}FN_3O_2$

Molecular weight: 389.43

Compound **124** (440 mg, 1.08 mmol) and NH_4OAc (830 mg, 10.80 mmol) were dissolved in glacial acetic acid (12 mL) and heated to 120 °C for 18 h. After cooling to room

temperature, the solvent was removed under reduced pressure and saturated aqueous $NaHCO_3$ solution was added. It was extracted with DCM (3x), before the combined organic layers were dried over anhydrous Na_2SO_4 and the solvent was again removed under reduced pressure. Purification by flash chromatography (SiO_2, DCM:EtOH 97:3) afforded 245 mg (58.3%) of an orange solid. ^{1}H NMR (300 MHz, $CDCl_3$) δ 2.53 (s, 3H), 3.79 (s, 3H), 4.36 (d, *J* = 5.7 Hz, 2H), 5.09 (t, *J* = 5.6 Hz, 1H), 6.54 (s, 1H), 6.73 (dd, *J* = 5.4, 1.4 Hz, 1H), 6.85 (d, *J* = 8.7 Hz, 2H), 7.05 (t, *J* = 8.8 Hz, 2H), 7.20 (d, *J* = 8.8 Hz, 2H), 7.57 (dd, *J* = 8.9, 5.4 Hz, 2H), 8.05 (dd, *J* = 5.4, 0.6 Hz, 1H). ^{13}C NMR (75 MHz, $CDCl_3$) δ 13.9, 45.7, 55.2, 102.3, 109.5, 114.0, 115.6 (d, $^2J_{CF}$ = 22.1 Hz), 128.1 (d, $^4J_{CF}$ = 3.3 Hz), 128.5, 130.1 (d, $^3J_{CF}$ = 8.3 Hz), 130.7, 137.0, 137.2, 143.3, 148.7, 158.8, 158.9, 160.9, 162.7 (d, $^1J_{CF}$ = 248.2 Hz). TLC-MS (ESI) *m*/*z* = 389.9 $[M + H]^+$.

4-(4-(4-Fluorophenyl)-2-methyloxazol-5-yl)pyridin-2-amine (126)

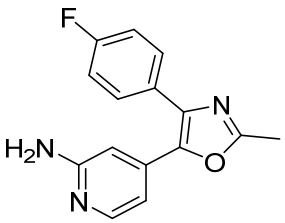

Molecular formula: $C_{15}H_{12}FN_3O$

Molecular weight: 269.28

Compound **125** (120 mg, 0.31 mmol) was dissolved in DCM (3 mL) and trifluoroacetic acid (3 mL). The solution was heated to 50 °C for 8 h before the reaction was quenched with saturated aqueous $NaHCO_3$ and it was extracted with DCM (3x). The combined organic layers were dried over anhydrous Na_2SO_4 and the solvent was removed under reduced pressure. Purification by flash chromatography (SiO_2, DCM:2M NH_3 in MeOH 97:3) afforded 65 mg (78.3%) of a beige solid. ^{1}H NMR (300 MHz, $CDCl_3$) δ 2.53 (s, 3H), 4.50 (br. s., 2H), 6.65 (dd, *J* = 1.4, 0.7 Hz, 1H), 6.75 (dd, *J* = 5.5, 1.5 Hz, 1H), 7.08 (t, *J* = 8.8 Hz, 2H), 7.58 (dd, *J* = 8.9, 5.4 Hz, 2H), 8.00 (dd, *J* = 5.5, 0.7 Hz, 1H). ^{13}C NMR (75 MHz, $CDCl_3$) δ 13.9, 104.1, 110.3, 115.7 (d, $^2J_{CF}$ = 22.1 Hz), 128.0 (d, $^4J_{CF}$ = 3.3 Hz), 130.1 (d, $^3J_{CF}$ = 8.3 Hz), 137.2, 137.5, 143.0, 148.6, 158.8, 161.1, 162.8 (d, $^1J_{CF}$ = 248.8 Hz). TLC-MS (ESI) *m*/*z* = 270.2 $[M + H]^+$.

N-(4-(4-(4-Fluorophenyl)-2-methyloxazol-5-yl)pyridin-2-yl)-cyclopropanecarboxamide (123)

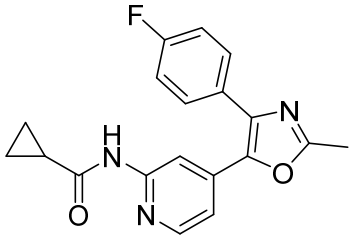

Molecular formula: $C_{19}H_{16}FN_3O_2$

Molecular weight: 337.35

Compound **126** (59 mg, 0.22 mmol) was dissolved in anhydrous pyridine (4 mL) and cooled to 0 °C. Cyclopropanecarbonyl chloride (46 mg, 0.44 mmol) was added and the mixture was stirred at room temperature for 18 h. The solvent was removed in vacuo and purification by flash chromatography (SiO_2, *n*-hexane/EtOAc 55:45) afforded 54 mg (73.0%) of a yellow solid. ^{1}H NMR (300 MHz, $CDCl_3$) δ 0.89 (s, 2H), 1.08 - 1.16 (m, 2H), 1.54 - 1.65 (m, 1H), 2.55 (s, 3H), 7.05 - 7.15 (m, 3H), 7.53 - 7.65 (m, 2H), 8.16 (dd, J = 5.4, 0.6 Hz, 1H), 8.50 (d, J = 0.5 Hz, 1H), 9.19 (s, 1H). ^{13}C NMR (75 MHz, $CDCl_3$) δ 8.4, 14.0, 15.7, 110.1, 115.2, 115.8 (d, $^2J_{CF}$ = 22.1 Hz), 127.8 (d, $^4J_{CF}$ = 3.3 Hz), 130.2 (d, $^3J_{CF}$ = 8.3 Hz), 138.1, 138.3, 142.7, 147.6, 152.5, 162.9, 161.7 (d, $^1J_{CF}$ = 248.8 Hz), 172.6. TLC-MS (ESI) m/z = 270.2 $[M + H]^+$. HPLC (A): t_R = 6.79 min, purity: 99.2 % (*254 nm*).

N-(4-Bromopyridin-2-yl)cyclopropanecarboxamide (136)

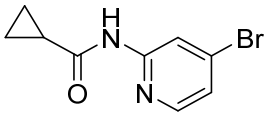

Molecular formula: $C_9H_9BrN_2O$

Molecular weight: 241.09

4-Bromopyridine-2-amine (3.00 g, 17.34 mmol) was dissolved in DCM (40 mL) and pyridine (1.82 mL, 22.54 mmol) was added at 0 °C. Cyclopropylcarbonyl chloride (1.73 mL, 19.07 mmol) was then added dropwise and the solution was stirred at room temperature for 6 h. Saturated aqueous $NaHCO_3$ solution (15 mL) and H_2O (30 mL) were added and the organic phase was separated and dried over anhydrous Na_2SO_4. The solvent was removed under reduced pressure and dried in vacuo to afford 3.50 g (83.7%) of a white crystalline solid. ^{1}H NMR (300 MHz, DMSO-d_6) δ 0.79 - 0.88 (m, 4H), 1.89 - 2.12 (m, 1H), 7.34 (dd, J = 5.3, 1.8 Hz, 1H), 8.22 (dd, J = 5.3, 0.4 Hz, 1H), 8.33 (dd, J = 1.7,

0.4 Hz, 1H), 11.03 (s, 1H). TLC-MS (ESI) m/z = 239.0/241.0 $[M - H]^-$. HPLC (A): t_R = 4.94 min.

N-(4-(4,4,5,5-Tetramethyl-1,3,2-dioxaborolan-2-yl)pyridin-2-yl)cyclopropanecarboxamide (131)

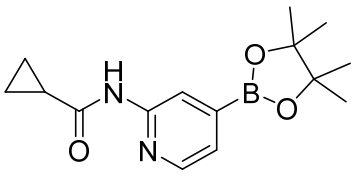

Molecular formula: $C_{15}H_{21}BN_2O_3$

Molecular weight: 288.15

Compound **136** (1.00 g, 4.15 mmol), bis(pinacolato)diboron (1.26 g, 4.98 mmol), potassium acetate (1.43 g, 14.52 mmol) and Pd(dppf)Cl_2·DCM (136 mg, 0.166 mmol) were dissolved in anhydrous, degassed 1,4-dioxane (10 mL) under an atmosphere of argon. The reaction mixture was stirred at 85 °C for 18 h and after cooling to room temperature, EtOAc (30 mL) was added. The solution was filtered over celite and the filtrate was removed under reduced pressure and redissolved in EtOAc (50 mL). A spoon of activated charcoal was added to the solution and the resulting suspension was stirred at 85 °C for 30 min. The hot reaction mixture was filtered again over celite and the filtrate was removed under reduced pressure. The crude product was suspended in *n*-heptane and agitated for 30 min using an ultrasonic bath. The title compound was collected by filtration to yield 1.05 g (88.1%) of a beige solid. ^{1}H NMR (300 MHz, DMSO-*d*$_6$) δ 0.74 - 0.86 (m, 4H), 1.30 (s, 12H), 1.94 - 2.05 (m, 1H), 7.24 (dd, *J* = 4.8, 0.9 Hz, 1H), 8.33 (dd, *J* = 4.7, 0.9 Hz, 1H), 8.35 (s, 1H), 10.77 (s, 1H). ^{13}C NMR (101 MHz, DMSO-*d*$_6$) δ 7.7, 14.2, 24.6, 84.3, 118.4, 123.5, 138.6, 147.5, 151.9, 172.6. HPLC (A): t_R = 1.36 min.

2-Bromo-1-(3-(trifluoromethyl)phenyl)ethan-1-one (128a)

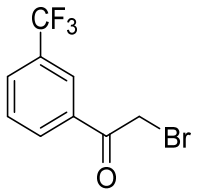

Molecular formula: $C_9H_6BrF_3O$

Molecular weight: 267.05

1-(3-(trifluoromethyl)phenyl)ethan-1-one (2.00 g, 10.63 mmol) was dissolved in DCM (20 mL) and the solution was stirred at room temperature, while bromine (1.70 g, 10.63

mmol) in DCM (10 mL) was added dropwise.[272] The reaction was quenched with saturated aqueous $NaHCO_3$ solution (20 mL) and the phases were separated. The organic phase was dried over anhydrous Na_2SO_4 and purified by flash chromatography (SiO_2, *n*-hexane/EtOAc 90:10) to afford 2.33 g (82.0%) of the title compound. ^{1}H NMR (300 MHz, $CDCl_3$) δ 4.47 (s, 2H), 7.63 - 7.70 (m, 1H), 7.88 (d, *J* = 7.8 Hz, 1H), 8.18 (d, *J* = 7.9 Hz, 1H), 8.25 (s, 1H).

2-Bromo-1-(3-trifluoromethoxy)phenyl)ethan-1-one (128b)

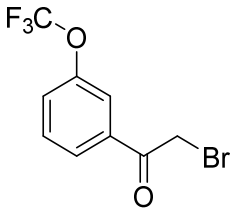

Molecular formula: $C_9H_6BrF_3O_2$

Molecular weight: 283.04

1-(3-(trifluoromethoxy)phenyl)ethan-1-one (2.00 g, 9.80 mmol) was dissolved in DCM (20 mL) and the solution was stirred at room temperature, while bromine (1.57 g, 9.80 mmol) in DCM (10 mL) was added dropwise.[272] The reaction was quenched with saturated aqueous $NaHCO_3$ solution (20 mL) and the phases were separated. The organic phase was dried over anhydrous Na_2SO_4 and purified by flash chromatography (SiO_2, *n*-hexane/EtOAc 90:10) to afford 2.37 g (85.3%) of the title compound. ^{1}H NMR (300 MHz, $CDCl_3$) δ 4.44 (s, 2H), 7.44 - 7.51 (m, 1H), 7.53 - 7.61 (m, 1H), 7.85 (s, 1H), 7.93 (dt, *J* = 7.6, 1.4 Hz, 1H).

2-Methyl-4-(3-(trifluoromethyl)phenyl)oxazole (129a)

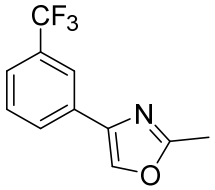

Molecular formula: $C_{11}H_8F_3NO$

Molecular weight: 227.19

Compound **128a** (1.28 g, 4.79 mmol) and acetamide (1.30 g, 22.00 mmol) were heated to 140 °C in a microwave reaction vial for 3 h. After cooling to room temperature, saturated aqueous $NaHCO_3$ solution (20 mL) was added and it was extracted with EtOAc (3x). The combined organic layers were dried over anhydrous Na_2SO_4 and the solvent was removed

under reduced pressure. Purification by flash chromatography (SiO_2, *n*-hexane/EtOAc 90:10) afforded 614 mg (56.4%) of a yellow liquid. ^{1}H NMR (300 MHz, $CDCl_3$) δ 2.53 (s, 3H), 7.46 - 7.58 (m, 2H), 7.84 - 7.91 (m, 2H), 7.98 (s, 1H). ^{13}C NMR (75 MHz, $CDCl_3$) δ 13.9, 122.2 (q, $^3J_{CF3}$ = 3.9 Hz), 124.4 (q, $^3J_{CF3}$ = 3.9 Hz), 128.5, 129.2, 131.2 (q, $^2J_{CF3}$ = 32.6 Hz), 132.0, 133.9, 139.5, 162.2. TLC-MS (ESI) *m/z* = 227.9 $[M + H]^+$. HPLC (A): t_R = 7.04 min.

2-Methyl-4-(3-(trifluoromethoxy)phenyl)oxazole (129b)

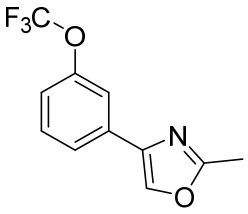

Molecular formula: $C_{11}H_8F_3NO_2$

Molecular weight: 243.19

The title compound was prepared following the procedure as described for compound **129a** starting from **128b** (800 mg, 2.82 mmol) and acetamide (1.30 g, 22.00 mmol). Purification by flash chromatography (SiO_2, *n*-hexane/EtOAc 90:10) afforded 382 mg (55.7%) of an orange solid. ^{1}H NMR (300 MHz, $CDCl_3$) δ 2.52 (s, 3H), 7.15 (ddt, *J* = 8.2, 2.3, 1.1 Hz, 1H), 7.41 (t, *J* = 8.0 Hz, 1H), 7.59 (br. s, 1H), 7.62 (dt, *J* = 7.8, 1.2 Hz, 1H), 7.84 (s, 1H). ^{13}C NMR (75 MHz, $CDCl_3$) δ 13.9, 118.0, 120.1, 120.5 (d, $^1J_{OCF3}$ = 257.6 Hz), 123.6, 130.1, 133.3, 133.8, 139.5, 149.7, 162.1. TLC-MS (ESI) *m/z* = 243.9 $[M + H]^+$. HPLC (A): t_R = 8.46 min.

5-Bromo-2-methyl-4-(3-(trifluoromethyl)phenyl)oxazole (130a)

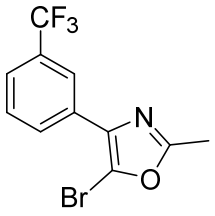

Molecular formula: $C_{11}H_7BrF_3NO$

Molecular weight: 306.08

Compound **129a** (400 mg, 1.76 mmol) was dissolved in glacial acetic acid (6 mL) and *N*-bromosuccinimide (329 mg, 1.85 mmol) was added in one portion. The mixture was stirred at room temperature for 4 h before an ice-water mix was added and it was extracted

with EtOAc (3x). The combined organic layers were dried over anhydrous Na_2SO_4 and the solvent was removed under reduced pressure. Purification by flash chromatography (SiO_2, *n*-hexane/EtOAc 90:10 → 70:30) afforded 360 mg (53.1%) of the title compound. ^{1}H NMR (300 MHz, $CDCl_3$) δ 2.53 (s, 3H), 7.50 - 7.63 (m, 2H), 8.14 (d, J = 7.5 Hz, 1H), 8.23 (s, 1H). ^{13}C NMR (75 MHz, $CDCl_3$) δ 14.1, 116.6, 123.1 (q, $^3J_{CF3}$ = 3.9 Hz), 124.0 (q, $^1J_{CF3}$ = 272.6 Hz), 124.7 (q, $^3J_{CF3}$ = 3.9 Hz), 129.0, 129.2, 130.9, 131.0 (q, $^2J_{CF3}$ = 32.6 Hz), 135.6, 162.5. HPLC (A): t_R = 9.91 min.

5-Bromo-2-methyl-4-(3-(trifluoromethyl)phenyl)oxazole (130b)

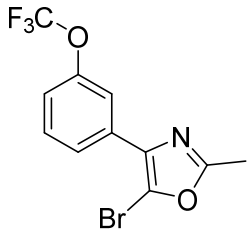

Molecular formula: $C_{11}H_8F_3NO_2$

Molecular weight: 243.19

The title compound was prepared following the procedure as described for compound **130a** starting from **129b** (370 mg, 1.52 mmol) and *N*-bromosuccinimide (284 mg, 1.60 mmol). Purification by flash chromatography (SiO_2, *n*-hexane/EtOAc 90:10) afforded 301 mg (61.5%) of the title compound. ^{1}H NMR (300 MHz, $CDCl_3$) δ 2.52 (s, 3H), 7.20 (ddt, J = 8.3, 2.3, 1.1 Hz, 1H), 7.45 (t, J = 8.0 Hz, 1H), 7.84 (s, 1H), 7.89 (dt, J = 7.9, 1.2 Hz, 1H). ^{13}C NMR (75 MHz, $CDCl_3$) δ 14.1, 116.6, 118.9, 120.4, 120.5 (d, $^1J_{OCF3}$ = 257.1 Hz), 124.5, 129.9, 132.1, 135.6, 149.5, 162.4. HPLC (A): t_R = 10.77 min.

N-(4-(2-Methyl-4-(3-(trifluoromethyl)phenyl)oxazol-5-yl)pyridin-2-yl)cyclopropanecarboxamide (132)

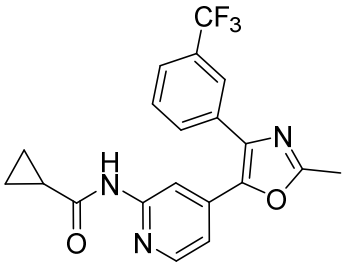

Molecular formula: $C_{20}H_{16}F_3N_3O_2$

Molecular weight: 387.36

Compound **130a** (250 mg, 0.82 mmol), **131** (353 mg, 1.23 mmol), K_2CO_3 (339 mg, 2.45 mmol) and $PdCl_2(PPh_3)_2$ (57 mg, 0.082 mmol) were dissolved in a mix of degassed DMF

(4.8 mL) and degassed H_2O (1.2 mL) under an atmosphere of argon. The reaction mix was heated to 85 °C for 18 h and after cooling to room temperature, saturated aqueous NH_4Cl solution (15 mL) and H_2O (25 mL) were added. It was extracted with EtOAc (3x) and the combined organic layers were dried over anhydrous Na_2SO_4 and the solvent was removed under reduced pressure. Purification by flash chromatography (SiO_2, DCM:EtOH 99:1) afforded 261 mg (82.5%) of a crystalline white solid. ^{1}H NMR (300 MHz, $CDCl_3$) δ 0.82 - 0.93 (m, 2H), 1.05 - 1.15 (m, 2H), 1.54 - 1.66 (m, 1H), 2.57 (s, 3H), 7.08 (dd, *J* = 5.3, 1.6 Hz, 1H), 7.48 - 7.56 (m, 1H), 7.61 - 7.66 (m, 1H), 7.81 (d, *J* = 7.7 Hz, 1H), 7.91 (s, 1H), 8.18 (dd, *J* = 5.3, 0.6 Hz, 1H), 8.53 (d, *J* = 0.6 Hz, 1H), 9.23 (s, 1H). ^{13}C NMR (75 MHz, $CDCl_3$) δ 8.5, 14.0, 15.7, 110.3, 115.4, 123.8 (q, $^1J_{CF3}$ = 272.6 Hz), 125.1 q, ($^3J_{CF3}$ = 3.9 Hz), 125.4 (q, $^3J_{CF3}$ = 3.5 Hz), 129.2, 131.2 q (q, $^2J_{CF3}$ = 32.6 Hz), 131.4, 132.6, 137.5, 138.0, 143.4, 147.8, 152.5, 162.0, 172.6. TLC-MS (ESI) *m/z* = 387.9 $[M + H]^+$ *m/z* = 386.0 $[M - H]^-$. HPLC (A): t_R = 8.74 min, purity: 99.0 % (*254 nm*).

5-Bromo-2-methyl-4-(3-(trifluoromethyl)phenyl)oxazole (133)

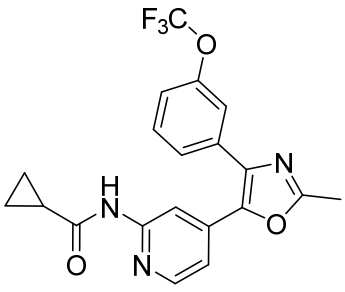

Molecular formula: $C_{20}H_{16}F_3N_3O_3$

Molecular weight: 403.36

The title compound was prepared following the procedure as described for compound **132** starting from **130b** (150 mg, 0.47 mmol), **131** (201 mg, 0.70 mmol), K_2CO_3 (193 mg, 1.40 mmol) and $PdCl_2(PPh_3)_2$ (33 mg, 0.047 mmol). Purification by flash chromatography (SiO_2, *n*-hexane/EtOAc 60:40 → 40:60) afforded 166 mg (88.3%) of a yellow solid. ^{1}H NMR (300 MHz, $CDCl_3$) δ 0.84 - 0.93 (m, 2H), 1.07 - 1.17 (m, 2H), 1.54 - 1.67 (m, 1H), 2.56 (s, 3H), 7.11 (dd, *J* = 5.4, 1.6 Hz, 1H), 7.23 (dt, *J* = 8.2, 1.1 Hz, 1H), 7.44 (t, *J* = 8.0 Hz, 1H), 7.48 (br. s., 1H), 7.59 (dt, *J* = 7.7, 1.2 Hz, 1H), 8.19 (d, *J* = 5.4 Hz, 1H), 8.53 (s, 1H), 9.25 (s, 1H). ^{13}C NMR (75 MHz, $CDCl_3$) δ 8.4, 14.0, 15.7, 110.4, 115.5, 120.4 (d, $^1J_{OCF3}$ = 257.6 Hz)., 120.8, 121.2, 126.6, 130.2, 133.7, 137.3, 138.0, 143.4, 147.7, 149.3, 152.6, 161.9, 172.6. TLC-MS (ESI) *m/z* = 403.9 $[M + H]^+$ *m/z* = 401.9 $[M - H]^-$. HPLC (A): t_R = 8.92 min, purity: 99.5 % (*254 nm*).

N-(4-(1-(tetrahydro-2*H*-pyran-2-yl)-1*H*-pyrazol-4-yl)pyridin-2-yl)cyclopropanecarboxamide (137)

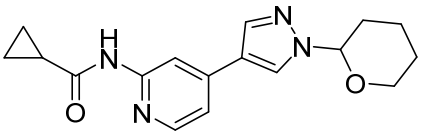

Molecular formula: $C_{17}H_{20}N_4O_2$

Molecular weight: 312.37

Compound **136** (350 mg, 1.45 mmol), 1-(tetrahydro-2*H*-pyran-2-yl)-1*H*-pyrazole-4-boronic acid pinacol ester (565 mg, 2.03 mmol), K_2CO_3 (401 mg, 2.90 mmol) and Pd(dppf)Cl_2·DCM (118 mg, 0.145 mmol) were dissolved in degassed 1,4-dioxane (6 mL)/H_2O (1 mL) under an atmosphere of argon. The mixture was stirred at 95 °C for 18 h. The reaction mixture was allowed to cool to room temperature and more H_2O was added. It was extracted with EtOAc (3x) and the combined organic layers were dried over anhydrous Na_2SO_4. The solvent was removed under reduced pressure and purification by flash chromatography (SiO_2, DCM:EtOH 97:3) afforded 137 mg (30.2%) of an off-white solid. ^{1}H NMR (300 MHz, $CDCl_3$) δ 0.87 - 0.96 (m, 2H), 1.09 - 1.17 (m, 2H), 1.53 - 1.61 (m, 1H), 1.62 - 1.78 (m, 3H), 1.99 - 2.16 (m, 3H), 3.66 - 3.79 (m, 1H), 4.03 - 4.14 (m, 1H), 5.37 - 5.45 (m, 1H), 7.14 (dd, *J* = 5.3, 1.6 Hz, 1H), 7.92 (d, *J* = 0.6 Hz, 1H), 8.06 (d, *J* = 0.5 Hz, 1H), 8.22 (dd, *J* = 5.2, 0.6 Hz, 1H), 8.38 (d, *J* = 0.7 Hz, 1H), 8.50 (br. s., 1H). TLC-MS (ESI) *m/z* = 313.0 $[M + H]^+$ *m/z* = 311.0 $[M - H]^-$. HPLC (A): t_R = 2.83 min.

N-(4-(1*H*-Pyrazol-4-yl)pyridin-2-yl)cyclopropanecarboxamide (138)

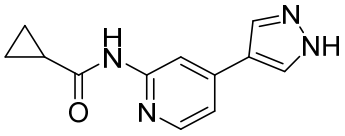

Molecular formula: $C_{12}H_{12}N_4O$

Molecular weight: 228.26

Compound **137** (260 mg, 0.83 mmol) was dissolved in MeOH (7 mL) and 4 M HCl in dioxane (2 mL) was added. The resulting solution was stirred at room temperature for 18 h and the solvent was then removed under reduced pressure. Saturated aqueous $NaHCO_3$ (15 mL) was added and after the addition of DCM (10 mL) a white solid precipitated between the two layers. Collection of the white solid by suction filtration afforded 122 mg (64.2%) of the title compound. ^{1}H NMR (300 MHz, $CDCl_3$) δ 0.70 - 0.80 (m, 4H), 1.90 - 2.01 (m, 1H), 7.25 (dd, *J* = 5.2, 1.6 Hz, 1H), 7.89 (s, 1H),

8.16 (d, *J* = 5.2 Hz, 1H), 8.19 (d, *J* = 0.7 Hz, 1H), 8.26 (s, 1H), 10.67 (s, 1H), 13.12 (br. s., 1H). TLC-MS (ESI) *m*/*z* = 226.9 $[M - H]^-$. HPLC (A): t_R = 1.30 min.

4-(2-(Cyclopropanecarboxamido)pyridin-4-yl)-1*H*-pyrazole-1-carboxamide (134)

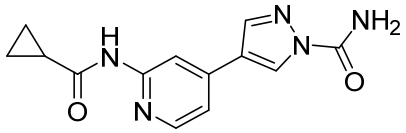

Molecular formula: $C_{13}H_{13}N_5O_2$

Molecular weight: 271.28

Compound **138** (110 mg, 0.48 mmol) was dissolved in 90% aq. acetic acid (5 mL) and a solution of NaOCN (47 mg, 0.72 mmol) in H_2O (5 mL) was added. The reaction was stirred at room temperature for 16 h before more H_2O (15 mL) was added. The product precipitated as a white solid and was collected by suction filtration. Further purification by flash chromatography (SiO_2, DCM:EtOH 96:4) afforded 63 mg (48.2%) of a white solid. ^{1}H NMR (300 MHz, DMSO-*d*$_6$) δ 0.72 - 0.92 (m, 4H), 1.92 - 2.12 (m, 1H), 7.47 (dd, *J* = 5.2, 1.5 Hz, 1H), 7.96 (br. s., 1H), 8.05 (s, 1H), 8.26 (d, *J* = 0.6 Hz, 1H), 8.30 (d, *J* = 5.2 Hz, 1H), 8.33 (d, *J* = 0.6 Hz, 1H), 8.84 (d, *J* = 0.6 Hz, 1H), 10.83 (s, 1H). ^{13}C NMR (75 MHz, DMSO-*d*$_6$) δ 7.7, 14.2, 109.4, 116.1, 122.4, 126.8, 140.0, 140.4, 148.6, 150.0, 152.8, 172.8. TLC-MS (ESI) *m*/*z* = 293.9 $[M + Na]^+$ *m*/*z* = 270.0 $[M - H]^-$. HPLC (A): t_R = 1.54 min, purity: 100.0 % (*254 nm*).

References

(1) Hippius, H.; Neundörfer, G. The discovery of Alzheimer's disease. *Dialogues in Clinical Neuroscience* **2003**, *5*, 101–108.
(2) Kalaria, R. N.; Maestre, G. E.; Arizaga, R.; Friedland, R. P.; Galasko, D.; Hall, K.; Luchsinger, J. A.; Ogunniyi, A.; Perry, E. K.; Potocnik, F. *et al.* Alzheimer's disease and vascular dementia in developing countries: prevalence, management, and risk factors. *Lancet Neurol.* **2008**, *7*, 812–826.
(3) Alzheimer's Disease International. *World Alzheimer Report 2018: The state of the art of dementia research: New frontiers*, 2018.
(4) Wilkinson, D. A review of the effects of memantine on clinical progression in Alzheimer's disease. *Int. J. Geriatr. Psychiatry* **2012**, *27*, 769–776.
(5) Johnson, J. W.; Kotermanski, S. E. Mechanism of action of memantine. *Curr. Opin. Pharmacol.* **2006**, *6*, 61–67.
(6) Glenner, G. G.; Wong, C. W. Alzheimer's disease: initial report of the purification and characterization of a novel cerebrovascular amyloid protein. *Biochem. Biophys. Res. Commun.* **1984**, *120*, 885–890.
(7) Grundke-Iqbal, I.; Iqbal, K.; Tung, Y. C.; Quinlan, M.; Wisniewski, H. M.; Binder, L. I. Abnormal phosphorylation of the microtubule-associated protein tau (tau) in Alzheimer cytoskeletal pathology. *Proc. Natl. Acad. Sci. U. S. A.* **1986**, *83*, 4913–4917.
(8) Hardy, J.; Higgins, G. Alzheimer's disease: the amyloid cascade hypothesis. *Science* **1992**, *256*, 184–185.
(9) Canter, R. G.; Penney, J.; Tsai, L.-H. The road to restoring neural circuits for the treatment of Alzheimer's disease. *Nature* **2016**, *539*, 187–196.
(10) Walsh, D. M.; Selkoe, D. J. A beta oligomers - a decade of discovery. *J. Neurochem.* **2007**, *101*, 1172–1184.
(11) Selkoe, D. J.; Hardy, J. The amyloid hypothesis of Alzheimer's disease at 25 years. *EMBO Mol. Med.* **2016**, *8*, 595–608.
(12) Götz, J.; Chen, F.; van Dorpe, J.; Nitsch, R. M. Formation of neurofibrillary tangles in P301l tau transgenic mice induced by Abeta 42 fibrils. *Science* **2001**, *293*, 1491–1495.
(13) Oddo, S.; Caccamo, A.; Shepherd, J. D.; Murphy, M.P.; Golde, T. E.; Kayed, R.; Metherate, R.; Mattson, M. P.; Akbari, Y.; LaFerla, F. M. Triple-Transgenic Model of Alzheimer's Disease with Plaques and Tangles. *Neuron* **2003**, *39*, 409–421.
(14) Murray, M. E.; Kouri, N.; Lin, W.-L.; Jack, C. R.; Dickson, D. W.; Vemuri, P. Clinicopathologic assessment and imaging of tauopathies in neurodegenerative dementias. *Alzheimer's Research & Therapy* **2014**, *6*, 1.
(15) Alonso, A. d. C.; Zaidi, T.; Novak, M.; Grundke-Iqbal, I.; Iqbal, K. Hyperphosphorylation induces self-assembly of τ into tangles of paired helical filaments/straight filaments. *Proc. Natl. Acad. Sci. U. S. A.* **2001**, *98*, 6923–6928.
(16) Bretteville, A.; Planel, E. Tau Aggregates: Toxic, Inert, or Protective Species? *J. Alzheimer's Dis.* **2008**, *14*, 431–436.
(17) Querfurth, H. W.; LaFerla, F. M. Alzheimer's disease. *N. Engl. J. Med.* **2010**, *362*, 329–344.
(18) Citron, M. Alzheimer's disease: strategies for disease modification. *Nat. Rev. Drug Discov.* **2010**, *9*, 387–398.

(19) Aisen, P. S.; Cummings, J.; Jack, C. R.; Morris, J. C.; Sperling, R.; Frölich, L.; Jones, R. W.; Dowsett, S. A.; Matthews, B. R.; Raskin, J. *et al.* On the path to 2025: understanding the Alzheimer's disease continuum. *Alzheimer's Research & Therapy* **2017**, *9*, 60.
(20) Khoury, G. A.; Baliban, R. C.; Floudas, C. A. Proteome-wide post-translational modification statistics: frequency analysis and curation of the swiss-prot database. *Sci. Rep.* **2011**, *1*.
(21) Fabbro, D.; Cowan-Jacob, S. W.; Moebitz, H. Ten things you should know about protein kinases: IUPHAR Review 14. *Br. J. Pharmacol.* **2015**, *172*, 2675–2700.
(22) Hunter, T. Protein kinases and phosphatases: the yin and yang of protein phosphorylation and signaling. *Cell* **1995**, *80*, 225–236.
(23) Druker, B. J.; Talpaz, M.; Resta, D. J.; Peng, B.; Buchdunger, E.; Ford, J. M.; Lydon, N. B.; Kantarjian, H.; Capdeville, R.; Ohno-Jones, S. *et al.* Efficacy and safety of a specific inhibitor of the BCR-ABL tyrosine kinase in chronic myeloid leukemia. *N. Engl. J. Med.* **2001**, *344*, 1031–1037.
(24) David, S.; Shoemaker, M.; Haley, B. E. Abnormal properties of creatine kinase in Alzheimer's disease brain: Correlation of reduced enzyme activity and active site photolabeling with aberrant cytosol-membrane partitioning. *Mol. Brain Res.* **1998**, *54*, 276–287.
(25) Waetzig, G. H.; Seegert, D.; Rosenstiel, P.; Nikolaus, S.; Schreiber, S. p38 Mitogen-Activated Protein Kinase Is Activated and Linked to TNF- Signaling in Inflammatory Bowel Disease. *J. Immunol.* **2002**, *168*, 5342–5351.
(26) Anamika, K.; Garnier, N.; Srinivasan, N. Functional diversity of human protein kinase splice variants marks significant expansion of human kinome. *BMC Genomics* **2009**, *10*, 622.
(27) Manning, G.; Whyte, D. B.; Martinez, R.; Hunter, T.; Sudarsanam, S. The protein kinase complement of the human genome. *Science* **2002**, *298*, 1912–1934.
(28) Eid, S.; Turk, S.; Volkamer, A.; Rippmann, F.; Fulle, S. KinMap: a web-based tool for interactive navigation through human kinome data. *BMC Bioinf.* **2017**, *18*, 16.
(29) Taylor, S. S.; Kornev, A. P. Protein kinases: evolution of dynamic regulatory proteins. *Trends Biochem. Sci.* **2011**, *36*, 65–77.
(30) Hanks, S. K.; Hunter, T. Protein kinases 6. The eukaryotic protein kinase superfamily: kinase (catalytic) domain structure and classification. *FASEB J.* **1995**, *9*, 576–596.
(31) Nolen, B.; Taylor, S.; Ghosh, G. Regulation of protein kinases; controlling activity through activation segment conformation. *Mol. Cell* **2004**, *15*, 661–675.
(32) Taylor, S. S.; Radzio-Andzelm, E. Three protein kinase structures define a common motif. *Structure* **1994**, *2*, 345–355.
(33) Romano, P. R.; Garcia-Barrio, M. T.; Zhang, X.; Wang, Q.; Taylor, D. R.; Zhang, F.; Herring, C.; Mathews, M. B.; Qin, J.; Hinnebusch, A. G. Autophosphorylation in the Activation Loop Is Required for Full Kinase Activity In Vivo of Human and Yeast Eukaryotic Initiation Factor 2α Kinases PKR and GCN2. *Mol. Cell. Biol.* **1998**, *18*, 2282–2297.
(34) Kornev, A. P.; Taylor, S. S.; Eyck, L. F. ten. A helix scaffold for the assembly of active protein kinases. *Proc. Natl. Acad. Sci. U. S. A.* **2008**, *105*, 14377–14382.
(35) Traxler, P.; Furet, P. Strategies toward the design of novel and selective protein tyrosine kinase inhibitors. *Pharmacol. Ther.* **1999**, *82*, 195–206.
(36) Roskoski, R. Classification of small molecule protein kinase inhibitors based upon the structures of their drug-enzyme complexes. *Pharmacol. Res.* **2016**, *103*, 26–48.

(37) Davis, M. I.; Hunt, J. P.; Herrgard, S.; Ciceri, P.; Wodicka, L. M.; Pallares, G.; Hocker, M.; Treiber, D. K.; Zarrinkar, P. P. Comprehensive analysis of kinase inhibitor selectivity. *Nat. Biotechnol.* **2011**, *29*, 1046–1051.
(38) Schindler, T. Structural Mechanism for STI-571 Inhibition of Abelson Tyrosine Kinase. *Science* **2000**, *289*, 1938–1942.
(39) Wu, P.; Nielsen, T. E.; Clausen, M. H. Small-molecule kinase inhibitors: an analysis of FDA-approved drugs. *Drug Discovery Today* **2016**, *21*, 5–10.
(40) Pemovska, T.; Johnson, E.; Kontro, M.; Repasky, G. A.; Chen, J.; Wells, P.; Cronin, C. N.; McTigue, M.; Kallioniemi, O.; Porkka, K. *et al.* Axitinib effectively inhibits BCR-ABL1(T315I) with a distinct binding conformation. *Nature* **2015**, *519*, 102–105.
(41) Kumar, R.; Crouthamel, M.-C.; Rominger, D. H.; Gontarek, R. R.; Tummino, P. J.; Levin, R. A.; King, A. G. Myelosuppression and kinase selectivity of multikinase angiogenesis inhibitors. *Br. J. Cancer* **2009**, *101*, 1717–1723.
(42) Wentsch, H. K.; Walter, N. M.; Bührmann, M.; Mayer-Wrangowski, S.; Rauh, D.; Zaman, G. J. R.; Willemsen-Seegers, N.; Buijsman, R. C.; Henning, M.; Dauch, D. *et al.* Optimized Target Residence Time: Type I1/2 Inhibitors for p38α MAP Kinase with Improved Binding Kinetics through Direct Interaction with the R-Spine. *Angew. Chem., Int. Ed.* **2017**, *56*, 5363–5367.
(43) Simard, J. R.; Klüter, S.; Grütter, C.; Getlik, M.; Rabiller, M.; Rode, H. B.; Rauh, D. A new screening assay for allosteric inhibitors of cSrc. *Nat. Chem. Biol.* **2009**, *5*, 394–396.
(44) Müller, S.; Chaikuad, A.; Gray, N. S.; Knapp, S. The ins and outs of selective kinase inhibitor development. *Nat. Chem. Biol.* **2015**, *11*, 818–821.
(45) Rice, K. D.; Aay, N.; Anand, N. K.; Blazey, C. M.; Bowles, O. J.; Bussenius, J.; Costanzo, S.; Curtis, J. K.; Defina, S. C.; Dubenko, L. *et al.* Novel Carboxamide-Based Allosteric MEK Inhibitors: Discovery and Optimization Efforts toward XL518 (GDC-0973). *ACS Med. Chem. Lett.* **2012**, *3*, 416–421.
(46) Abe, H.; Kikuchi, S.; Hayakawa, K.; Iida, T.; Nagahashi, N.; Maeda, K.; Sakamoto, J.; Matsumoto, N.; Miura, T.; Matsumura, K. *et al.* Discovery of a Highly Potent and Selective MEK Inhibitor: GSK1120212 (JTP-74057 DMSO Solvate). *ACS Med. Chem. Lett.* **2011**, *2*, 320–324.
(47) Adrián, F. J.; Ding, Q.; Sim, T.; Velentza, A.; Sloan, C.; Liu, Y.; Zhang, G.; Hur, W.; Ding, S.; Manley, P. *et al.* Allosteric inhibitors of Bcr-abl-dependent cell proliferation. *Nat. Chem. Biol.* **2006**, *2*, 95–102.
(48) Cox, K. J.; Shomin, C. D.; Ghosh, I. Tinkering outside the kinase ATP box: allosteric (type IV) and bivalent (type V) inhibitors of protein kinases. *Future Med. Chem.* **2011**, *3*, 29–43.
(49) Lechtenberg, B. C.; Mace, P. D.; Sessions, E. H.; Williamson, R.; Stalder, R.; Wallez, Y.; Roth, G. P.; Riedl, S. J.; Pasquale, E. B. Structure-Guided Strategy for the Development of Potent Bivalent ERK Inhibitors. *ACS Med. Chem. Lett.* **2017**, *8*, 726–731.
(50) Zhao, Z.; Bourne, P. E. Progress with covalent small-molecule kinase inhibitors. *Drug Discovery Today* **2018**, *23*, 727–735.
(51) Ferguson, F. M.; Gray, N. S. Kinase inhibitors: the road ahead. *Nat. Rev. Drug Discov.* **2018**, *17*, 353–377.
(52) Chaikuad, A.; Koch, P.; Laufer, S. A.; Knapp, S. The Cysteinome of Protein Kinases as a Target in Drug Development. *Angew. Chem., Int. Ed.* **2018**, *57*, 4372–4385.
(53) Dalton, S. E.; Dittus, L.; Thomas, D. A.; Convery, M. A.; Nunes, J.; Bush, J. T.; Evans, J. P.; Werner, T.; Bantscheff, M.; Murphy, J. A. *et al.* Selectively Targeting the

Kinome-Conserved Lysine of PI3Kδ as a General Approach to Covalent Kinase Inhibition. *J. Am. Chem. Soc.* **2018**, *140*, 932–939.
(54) Lin, S.; Yang, X.; Jia, S.; Weeks, A. M.; Hornsby, M.; Lee, P. S.; Nichiporuk, R. V.; Iavarone, A. T.; Wells, J. A.; Toste, F. D. *et al.* Redox-based reagents for chemoselective methionine bioconjugation. *Science* **2017**, *355*, 597–602.
(55) Niessen, S.; Dix, M. M.; Barbas, S.; Potter, Z. E.; Lu, S.; Brodsky, O.; Planken, S.; Behenna, D.; Almaden, C.; Gajiwala, K. S. *et al.* Proteome-wide Map of Targets of T790M-EGFR-Directed Covalent Inhibitors. *Cell Chem. Biol.* **2017**, *24*, 1388-1400.e7.
(56) Bauer, R. A. Covalent inhibitors in drug discovery: from accidental discoveries to avoided liabilities and designed therapies. *Drug Discovery Today* **2015**, *20*, 1061–1073.
(57) Finlay, M. R. V.; Anderton, M.; Ashton, S.; Ballard, P.; Bethel, P. A.; Box, M. R.; Bradbury, R. H.; Brown, S. J.; Butterworth, S.; Campbell, A. *et al.* Discovery of a potent and selective EGFR inhibitor (AZD9291) of both sensitizing and T790M resistance mutations that spares the wild type form of the receptor. *J. Med. Chem.* **2014**, *57*, 8249–8267.
(58) Woyach, J. A.; Furman, R. R.; Liu, T.-M.; Ozer, H. G.; Zapatka, M.; Ruppert, A. S.; Xue, L.; Li, D. H.-H.; Steggerda, S. M.; Versele, M. *et al.* Resistance mechanisms for the Bruton's tyrosine kinase inhibitor ibrutinib. *N. Engl. J. Med.* **2014**, *370*, 2286–2294.
(59) Pao, W.; Miller, V.; Zakowski, M.; Doherty, J.; Politi, K.; Sarkaria, I.; Singh, B.; Heelan, R.; Rusch, V.; Fulton, L. *et al.* EGF receptor gene mutations are common in lung cancers from "never smokers" and are associated with sensitivity of tumors to gefitinib and erlotinib. *Proc. Natl. Acad. Sci. U. S. A.* **2004**, *101*, 13306–13311.
(60) Karaman, M. W.; Herrgard, S.; Treiber, D. K.; Gallant, P.; Atteridge, C. E.; Campbell, B. T.; Chan, K. W.; Ciceri, P.; Davis, M. I.; Edeen, P. T. *et al.* A quantitative analysis of kinase inhibitor selectivity. *Nat. Biotechnol.* **2008**, *26*, 127–132.
(61) Wager, T. T.; Hou, X.; Verhoest, P. R.; Villalobos, A. Moving beyond rules: the development of a central nervous system multiparameter optimization (CNS MPO) approach to enable alignment of druglike properties. *ACS Chem. Neurosci.* **2010**, *1*, 435–449.
(62) Gunosewoyo, H.; Yu, L.; Munoz, L.; Kassiou, M. Kinase targets in CNS drug discovery. *Future Med. Chem.* **2017**, *9*, 303–314.
(63) Shi, Y.; Mader, M. Brain penetrant kinase inhibitors: Learning from kinase neuroscience discovery. *Bioorg. Med. Chem. Lett.* **2018**, *28*, 1981–1991.
(64) Embi, N.; Rylatt, D. B.; Cohen, P. Glycogen Synthase Kinase-3 from Rabbit Skeletal Muscle. *Eur. J. Biochem.* **1980**, *107*, 519–527.
(65) Ali, A.; Hoeflich, K. P.; Woodgett, J. R. Glycogen Synthase Kinase-3: Properties, Functions, and Regulation. *Chem. Rev.* **2001**, *101*, 2527–2540.
(66) Mukai, F.; Ishiguro, K.; Sano, Y.; Fujita, S. C. Alternative splicing isoform of tau protein kinase I/glycogen synthase kinase 3β. *J. Neurochem.* **2002**, *81*, 1073–1083.
(67) Wood-Kaczmar, A.; Kraus, M.; Ishiguro, K.; Philpott, K. L.; Gordon-Weeks, P. R. An alternatively spliced form of glycogen synthase kinase-3beta is targeted to growing neurites and growth cones. *Mol. Cell. Neurosci.* **2009**, *42*, 184–194.
(68) Soutar, M. P. M.; Kim, W.-Y.; Williamson, R.; Peggie, M.; Hastie, C. J.; McLauchlan, H.; Snider, W. D.; Gordon-Weeks, P. R.; Sutherland, C. Evidence that glycogen synthase kinase-3 isoforms have distinct substrate preference in the brain. *J. Neurochem.* **2010**, *115*, 974–983.
(69) Castaño, Z.; Gordon-Weeks, P. R.; Kypta, R. M. The neuron-specific isoform of glycogen synthase kinase-3beta is required for axon growth. *J. Neurochem.* **2010**, *113*, 117–130.

(70) Berman, H. M.; Westbrook, J.; Feng, Z.; Gilliland, G.; Bhat, T. N.; Weissig, H.; Shindyalov, I. N.; Bourne, P. E. The Protein Data Bank. *Nucleic Acids Research* **2000**, *28*, 235–242.
(71) Doble, B. W. GSK-3: tricks of the trade for a multi-tasking kinase. *J. Cell Sci.* **2003**, *116*, 1175–1186.
(72) Saito, Y.; Vandenheede, J. R.; Cohen, P. The mechanism by which epidermal growth factor inhibits glycogen synthase kinase 3 in A431 cells. *Biochemical Journal* **1994**, *303*, 27–31.
(73) Hughes, K.; Nikolakaki, E.; Plyte, S. E.; Totty, N. F.; Woodgett, J. R. Modulation of the glycogen synthase kinase-3 family by tyrosine phosphorylation. *EMBO J.* **1993**, *12*, 803–808.
(74) Thornton, T. M.; Pedraza-Alva, G.; Deng, B.; Wood, C. D.; Aronshtam, A.; Clements, J. L.; Sabio, G.; Davis, R. J.; Matthews, D. E.; Doble, B. *et al.* Phosphorylation by p38 MAPK as an alternative pathway for GSK3beta inactivation. *Science* **2008**, *320*, 667–670.
(75) Kerkela, R.; Kockeritz, L.; Macaulay, K.; Zhou, J.; Doble, B. W.; Beahm, C.; Greytak, S.; Woulfe, K.; Trivedi, C. M.; Woodgett, J. R. *et al.* Deletion of GSK-3beta in mice leads to hypertrophic cardiomyopathy secondary to cardiomyoblast hyperproliferation. *J. Clin. Invest.* **2008**, *118*, 3609–3618.
(76) Liu, K. J.; Arron, J. R.; Stankunas, K.; Crabtree, G. R.; Longaker, M. T. Chemical rescue of cleft palate and midline defects in conditional GSK-3beta mice. *Nature* **2007**, *446*, 79–82.
(77) Doble, B. W.; Patel, S.; Wood, G. A.; Kockeritz, L. K.; Woodgett, J. R. Functional Redundancy of GSK-3α and GSK-3β in Wnt/β-Catenin Signaling Shown by Using an Allelic Series of Embryonic Stem Cell Lines. *Dev. Cell* **2007**, *12*, 957–971.
(78) Cole, A.; Frame, S.; Cohen, P. Further evidence that the tyrosine phosphorylation of glycogen synthase kinase-3 (GSK3) in mammalian cells is an autophosphorylation event. *Biochemical Journal* **2004**, *377*, 249–255.
(79) Bax, B.; Carter, P. S.; Lewis, C.; Guy, A. R.; Bridges, A.; Tanner, R.; Pettman, G.; Mannix, C.; Culbert, A. A.; Brown, M. J.B. *et al.* The Structure of Phosphorylated GSK-3β Complexed with a Peptide, FRATtide, that Inhibits β-Catenin Phosphorylation. *Structure* **2001**, *9*, 1143–1152.
(80) Dajani, R.; Fraser, E.; Roe, S.M.; Young, N.; Good, V.; Dale, T. C.; Pearl, L. H. Crystal Structure of Glycogen Synthase Kinase 3β. *Cell* **2001**, *105*, 721–732.
(81) ter Haar, E.; Coll, J. T.; Austen, D. A.; Hsiao, H. M.; Swenson, L.; Jain, J. Structure of GSK3beta reveals a primed phosphorylation mechanism. *Nat. Struct. Biol.* **2001**, *8*, 593–596.
(82) Wang, Y.; Roach, P. J. Inactivation of rabbit muscle glycogen synthase by glycogen synthase kinase-3. Dominant role of the phosphorylation of Ser-640 (site-3a). *J. Biol. Chem.* **1993**, *268*, 23876–23880.
(83) Cohen, P.; Frame, S. The renaissance of GSK3. *Nat. Rev. Mol. Cell Biol.* **2001**, *2*, 769–776.
(84) Frame, S.; Cohen, P.; Biondi, R. M. A common phosphate binding site explains the unique substrate specificity of GSK3 and its inactivation by phosphorylation. *Mol. Cell* **2001**, *7*, 1321–1327.
(85) Cross, D. A.; Alessi, D. R.; Cohen, P.; Andjelkovich, M.; Hemmings, B. A. Inhibition of glycogen synthase kinase-3 by insulin mediated by protein kinase B. *Nature* **1995**, *378*, 785–789.
(86) Beurel, E.; Grieco, S. F.; Jope, R. S. Glycogen synthase kinase-3 (GSK3): regulation, actions, and diseases. *Pharmacol. Ther.* **2014**, *0*, 114–131.

(87) Sutherland, C. What Are the bona fide GSK3 Substrates? *Int. J. Alzheimer's Dis.* **2011**.
(88) Ikeda, S.; Kishida, M.; Matsuura, Y.; Usui, H.; Kikuchi, A. GSK-3beta-dependent phosphorylation of adenomatous polyposis coli gene product can be modulated by beta-catenin and protein phosphatase 2A complexed with Axin. *Oncogene* **2000**, *19*, 537–545.
(89) Wittmann, T.; Waterman-Storer, C. M. Spatial regulation of CLASP affinity for microtubules by Rac1 and GSK3β in migrating epithelial cells. *J. Cell Biol.* **2005**, *169*, 929–939.
(90) Hagen, T.; Vidal-Puig, A. Characterisation of the phosphorylation of β-catenin at the GSK-3 priming site Ser45. *Biochem. Biophys. Res. Commun.* **2002**, *294*, 324–328.
(91) Aplin, A. E.; Gibb, G. M.; Jacobsen, J. S.; Gallo, J. M.; Anderton, B. H. In vitro phosphorylation of the cytoplasmic domain of the amyloid precursor protein by glycogen synthase kinase-3beta. *J. Neurochem.* **1996**, *67*, 699–707.
(92) Scales, T. M. E.; Lin, S.; Kraus, M.; Goold, R. G.; Gordon-Weeks, P. R. Nonprimed and DYRK1A-primed GSK3 beta-phosphorylation sites on MAP1B regulate microtubule dynamics in growing axons. *J. Cell Sci.* **2009**, *122*, 2424–2435.
(93) Wei, W.; Jin, J.; Schlisio, S.; Harper, J. W.; Kaelin, W. G. The v-Jun point mutation allows c-Jun to escape GSK3-dependent recognition and destruction by the Fbw7 ubiquitin ligase. *Cancer Cell* **2005**, *8*, 25–33.
(94) Hughes, K.; Ramakrishna, S.; Benjamin, W. B.; Woodgett, J. R. Identification of multifunctional ATP-citrate lyase kinase as the alpha-isoform of glycogen synthase kinase-3. *Biochemical Journal* **1992**, *288 (Pt 1)*, 309–314.
(95) Sánchez, C.; Pérez, M.; Avila, J. GSK3β-mediated phosphorylation of the microtubule-associated protein 2C (MAP2C) prevents microtubule bundling. *Eur. J. Cell Biol.* **2000**, *79*, 252–260.
(96) Gregory, M. A.; Qi, Y.; Hann, S. R. Phosphorylation by glycogen synthase kinase-3 controls c-myc proteolysis and subnuclear localization. *J. Biol. Chem.* **2003**, *278*, 51606–51612.
(97) Yamamoto, H.; Kishida, S.; Kishida, M.; Ikeda, S.; Takada, S.; Kikuchi, A. Phosphorylation of axin, a Wnt signal negative regulator, by glycogen synthase kinase-3beta regulates its stability. *J. Biol. Chem.* **1999**, *274*, 10681–10684.
(98) Hanger, D. P.; Hughes, K.; Woodgett, J. R.; Brion, J. P.; Anderton, B. H. Glycogen synthase kinase-3 induces Alzheimer's disease-like phosphorylation of tau: generation of paired helical filament epitopes and neuronal localisation of the kinase. *Neurosci. Lett.* **1992**, *147*, 58–62.
(99) Bullock, B. P.; Habener, J. F. Phosphorylation of the cAMP response element binding protein CREB by cAMP-dependent protein kinase A and glycogen synthase kinase-3 alters DNA-binding affinity, conformation, and increases net charge. *Biochemistry* **1998**, *37*, 3795–3809.
(100) Welsh, G. I.; Miller, C. M.; Loughlin, A. J.; Price, N. T.; Proud, C. G. Regulation of eukaryotic initiation factor eIF2B: glycogen synthase kinase-3 phosphorylates a conserved serine which undergoes dephosphorylation in response to insulin. *FEBS Letters* **1998**, *421*, 125–130.
(101) Krymsky, M. A.; Kudryashov, D. S.; Shirinsky, V. P.; Lukas, T. J.; Watterson, D. M.; Vorotnikov, A. V. Phosphorylation of kinase-related protein (telokin) in tonic and phasic smooth muscles. *J. Muscle Res. Cell Motil.* **2001**, *22*, 425–437.
(102) Beals, C. R.; Sheridan, C. M.; Turck, C. W.; Gardner, P.; Crabtree, G. R. Nuclear export of NF-ATc enhanced by glycogen synthase kinase-3. *Science* **1997**, *275*, 1930–1934.

(103) Rylatt, D. B.; Aitken, A.; Bilham, T.; Condon, G. D.; Embi, N.; Cohen, P. Glycogen synthase from rabbit skeletal muscle. Amino acid sequence at the sites phosphorylated by glycogen synthase kinase-3, and extension of the N-terminal sequence containing the site phosphorylated by phosphorylase kinase. *Eur. J. Biochem.* **1980**, *107*, 529–537.
(104) Hoeflich, K. P.; Luo, J.; Rubie, E. A.; Tsao, M. S.; Jin, O.; Woodgett, J. R. Requirement for glycogen synthase kinase-3beta in cell survival and NF-kappaB activation. *Nature* **2000**, *406*, 86–90.
(105) Sharfi, H.; Eldar-Finkelman, H. Sequential phosphorylation of insulin receptor substrate-2 by glycogen synthase kinase-3 and c-Jun NH2-terminal kinase plays a role in hepatic insulin signaling. *Am. J. Physiol.: Endocrinol. Metab.* **2008**, *294*, E307-15.
(106) Foltz, D. R.; Santiago, M. C.; Berechid, B. E.; Nye, J. S. Glycogen synthase kinase-3beta modulates notch signaling and stability. *Curr. Biol.* **2002**, *12*, 1006–1011.
(107) Kirschenbaum, F.; Hsu, S. C.; Cordell, B.; McCarthy, J. V. Glycogen synthase kinase-3beta regulates presenilin 1 C-terminal fragment levels. *J. Biol. Chem.* **2001**, *276*, 30701–30707.
(108) Turenne, G. A.; Price, B. D. Glycogen synthase kinase3 beta phosphorylates serine 33 of p53 and activates p53's transcriptional activity. *BMC Cell Biol.* **2001**, *2*, 12.
(109) Qu, L.; Huang, S.; Baltzis, D.; Rivas-Estilla, A.-M.; Pluquet, O.; Hatzoglou, M.; Koumenis, C.; Taya, Y.; Yoshimura, A.; Koromilas, A. E. Endoplasmic reticulum stress induces p53 cytoplasmic localization and prevents p53-dependent apoptosis by a pathway involving glycogen synthase kinase-3beta. *Genes Dev.* **2004**, *18*, 261–277.
(110) Beurel, E.; Jope, R. S. Differential Regulation of STAT Family Members by Glycogen Synthase Kinase-3*. *J. Biol. Chem.* **2008**, *283*, 21934–21944.
(111) Logan, C. Y.; Nusse, R. The Wnt signaling pathway in development and disease. *Annu. Rev. Cell Dev. Biol.* **2004**, *20*, 781–810.
(112) Nusse, R.; Clevers, H. Wnt/β-Catenin Signaling, Disease, and Emerging Therapeutic Modalities. *Cell* **2017**, *169*, 985–999.
(113) Willert, K.; Nusse, R. Wnt Proteins. *Cold Spring Harbor Perspectives in Biology* **2012**, *4*.
(114) Stamos, J. L.; Weis, W. I. The β-catenin destruction complex. *Cold Spring Harbor Perspectives in Biology* **2013**, *5*, a007898.
(115) *Post-genomic cardiology;* Marín-García, J., Ed., 2. Aufl.; Academic Press; Elsevier Reference Monographs: London, UK, s.l., 2014.
(116) Komiya, Y.; Habas, R. Wnt signal transduction pathways. *Organogenesis* **2008**, *4*, 68–75.
(117) Polakis, P. The oncogenic activation of beta-catenin. *Curr. Opin. Genet. Dev.* **1999**, *9*, 15–21.
(118) Deng, J.; Miller, S. A.; Wang, H.-Y.; Xia, W.; Wen, Y.; Zhou, B. P.; Li, Y.; Lin, S.-Y.; Hung, M.-C. β-catenin interacts with and inhibits NF-κB in human colon and breast cancer. *Cancer Cell* **2002**, *2*, 323–334.
(119) Cohen, Y.; Chetrit, A.; Sirota, P.; Modan, B. Cancer morbidity in psychiatric patients: influence of lithium carbonate treatment. *Med. Oncol.* **1998**, *15*, 32–36.
(120) Bhat, R. V.; Andersson, U.; Andersson, S.; Knerr, L.; Bauer, U.; Sundgren-Andersson, A. K. The Conundrum of GSK3 Inhibitors: Is it the Dawn of a New Beginning? *J. Alzheimer's Dis.* **2018**, *64*, S547-S554.
(121) Cohen, P. The Croonian Lecture 1998. Identification of a protein kinase cascade of major importance in insulin signal transduction. *Phil. Trans. R. Soc. B* **1999**, *354*, 485–495.
(122) Boucher, J.; Kleinridders, A.; Kahn, C. R. Insulin Receptor Signaling in Normal and Insulin-Resistant States. *Cold Spring Harbor Perspectives in Biology* **2014**, *6*.

(123) Beffert, U.; Morfini, G.; Bock, H. H.; Reyna, H.; Brady, S. T.; Herz, J. Reelin-mediated signaling locally regulates protein kinase B/Akt and glycogen synthase kinase 3beta. *J. Biol. Chem.* **2002**, *277*, 49958–49964.
(124) McCubrey, J. A.; Rakus, D.; Gizak, A.; Steelman, L. S.; Abrams, S. L.; Lertpiriyapong, K.; Fitzgerald, T. L.; Yang, L. V.; Montalto, G.; Cervello, M. *et al.* Effects of mutations in Wnt/β-catenin, hedgehog, Notch and PI3K pathways on GSK-3 activity-Diverse effects on cell growth, metabolism and cancer. *Biochim. Biophys. Acta* **2016**, *1863*, 2942–2976.
(125) Guha, S.; Cullen, J. P.; Morrow, D.; Colombo, A.; Lally, C.; Walls, D.; Redmond, E. M.; Cahill, P. A. Glycogen synthase kinase 3 beta positively regulates Notch signaling in vascular smooth muscle cells: role in cell proliferation and survival. *Basic Res. Cardiol.* **2011**, *106*, 773–785.
(126) Beaulieu, J.-M.; Gainetdinov, R. R.; Caron, M. G. The Akt-GSK-3 signaling cascade in the actions of dopamine. *Trends Pharmacol. Sci.* **2007**, *28*, 166–172.
(127) Patel, P.; Woodgett, J. R. Glycogen Synthase Kinase 3: A Kinase for All Pathways? *Curr. Top. Dev. Biol.* **2017**, *123*, 277–302.
(128) Klein, P. S.; Melton, D. A. A molecular mechanism for the effect of lithium on development. *Proc. Natl. Acad. Sci. U. S. A.* **1996**, *93*, 8455–8459.
(129) Kirshenboim, N.; Plotkin, B.; Shlomo, S. B.; Kaidanovich-Beilin, O.; Eldar-Finkelman, H. Lithium-Mediated Phosphorylation of Glycogen Synthase Kinase-3b Involves PI3 Kinase-Dependent Activation of Protein Kinase C-α. *J. Mol. Neurosci.* **2004**, *24*, 237–246.
(130) Li, X.; Liu, M.; Cai, Z.; Wang, G.; Li, X. Regulation of glycogen synthase kinase-3 during bipolar mania treatment. *Bipolar Disord.* **2010**, *12*, 741–752.
(131) Khan, I.; Tantray, M. A.; Alam, M. S.; Hamid, H. Natural and synthetic bioactive inhibitors of glycogen synthase kinase. *Eur. J. Med. Chem.* **2017**, *125*, 464–477.
(132) Meijer, L.; Skaltsounis, A.-L.; Magiatis, P.; Polychronopoulos, P.; Knockaert, M.; Leost, M.; Ryan, X. P.; Vonica, C. A.; Brivanlou, A.; Dajani, R. *et al.* GSK-3-Selective Inhibitors Derived from Tyrian Purple Indirubins. *Chem. Biol.* **2003**, *10*, 1255–1266.
(133) https://www.chemicalprobes.org/.
(134) Wang, Y.; Cornett, A.; King, F. J.; Mao, Y.; Nigsch, F.; Paris, C. G.; McAllister, G.; Jenkins, J. L. Evidence-Based and Quantitative Prioritization of Tool Compounds in Phenotypic Drug Discovery. *Cell Chem. Biol.* **2016**, *23*, 862–874.
(135) Ring, D. B.; Johnson, K. W.; Henriksen, E. J.; Nuss, J. M.; Goff, D.; Kinnick, T. R.; Ma, S. T.; Reeder, J. W.; Samuels, I.; Slabiak, T. *et al.* Selective glycogen synthase kinase 3 inhibitors potentiate insulin activation of glucose transport and utilization in vitro and in vivo. *Diabetes* **2003**, *52*, 588–595.
(136) Wagman, A. S.; Boyce, R. S.; Brown, S. P.; Fang, E.; Goff, D.; Jansen, J. M.; Le, V. P.; Levine, B. H.; Ng, S. C.; Ni, Z.-J. *et al.* Synthesis, Binding Mode, and Antihyperglycemic Activity of Potent and Selective (5-Imidazol-2-yl-4-phenylpyrimidin-2-yl)2-(2-pyridylamino)ethylamine Inhibitors of Glycogen Synthase Kinase 3. *J. Med. Chem.* **2017**, *60*, 8482–8514.
(137) Hall, A. P.; Escott, K. J.; Sanganee, H.; Hickling, K. C. Preclinical toxicity of AZD7969: Effects of GSK3β inhibition in adult stem cells. *Toxicol. Pathol.* **2015**, *43*, 384–399.
(138) Domínguez, J. M.; Fuertes, A.; Orozco, L.; del Monte-Millán, M.; Delgado, E.; Medina, M. Evidence for Irreversible Inhibition of Glycogen Synthase Kinase-3β by Tideglusib*. *J. Biol. Chem.* **2011**, *287*, 893–904.

(139) Lovestone, S.; Boada, M.; Dubois, B.; Hüll, M.; Rinne, J. O.; Huppertz, H.-J.; Calero, M.; Andrés, M. V.; Gómez-Carrillo, B.; León, T. *et al.* A phase II trial of tideglusib in Alzheimer's disease. *J. Alzheimer's Dis.* **2015**, *45*, 75–88.
(140) Tolosa, E.; Litvan, I.; Höglinger, G. U.; Burn, D.; Lees, A.; Andrés, M. V.; Gómez-Carrillo, B.; León, T.; del Ser, T. A phase 2 trial of the GSK-3 inhibitor tideglusib in progressive supranuclear palsy. *Mov. Disord.* **2014**, *29*, 470–478.
(141) NCT03692312. *Efficacy and Safety of Tideglusib in Congenital Myotonic Dystrophy*.
(142) NCT02858908. *Study of Tideglusib in Adolescent and Adult Patients With Myotonic Dystrophy*.
(143) Engler, T. A.; Henry, J. R.; Malhotra, S.; Cunningham, B.; Furness, K.; Brozinick, J.; Burkholder, T. P.; Clay, M. P.; Clayton, J.; Diefenbacher, C. *et al.* Substituted 3-imidazo1,2-apyridin-3-yl- 4-(1,2,3,4-tetrahydro-1,4diazepino-6,7,1-hiindol-7-yl)pyrrole-2,5-diones as highly selective and potent inhibitors of glycogen synthase kinase-3. *J. Med. Chem.* **2004**, *47*, 3934–3937.
(144) Gray, J. E.; Infante, J. R.; Brail, L. H.; Simon, G. R.; Cooksey, J. F.; Jones, S. F.; Farrington, D. L.; Yeo, A.; Jackson, K. A.; Chow, K. H. *et al.* A first-in-human phase I dose-escalation, pharmacokinetic, and pharmacodynamic evaluation of intravenous LY2090314, a glycogen synthase kinase 3 inhibitor, administered in combination with pemetrexed and carboplatin. *Invest. New Drugs* **2015**, *33*, 1187–1196.
(145) Rizzieri, D. A.; Cooley, S.; Odenike, O.; Moonan, L.; Chow, K. H.; Jackson, K.; Wang, X.; Brail, L.; Borthakur, G. An open-label phase 2 study of glycogen synthase kinase-3 inhibitor LY2090314 in patients with acute leukemia. *Leuk. Lymphoma* **2016**, *57*, 1800–1806.
(146) Lo Monte, F.; Kramer, T.; Gu, J.; Anumala, U. R.; Marinelli, L.; La Pietra, V.; Novellino, E.; Franco, B.; Demedts, D.; van Leuven, F. *et al.* Identification of glycogen synthase kinase-3 inhibitors with a selective sting for glycogen synthase kinase-3α. *J. Med. Chem.* **2012**, *55*, 4407–4424.
(147) Wagner, F. F.; Benajiba, L.; Campbell, A. J.; Weïwer, M.; Sacher, J. R.; Gale, J. P.; Ross, L.; Puissant, A.; Alexe, G.; Conway, A. *et al.* Exploiting an Asp-Glu "switch" in glycogen synthase kinase 3 to design paralog-selective inhibitors for use in acute myeloid leukemia. *Sci. Transl. Med.* **2018**, *10*, eaam8460.
(148) A Paralog-Selective Inhibitor May Allow for Targeting of GSK3α in AML. *Cancer Discovery* **2018**, *8*, 528.
(149) Lovestone, S.; Killick, R.; Di Forti, M.; Murray, R. Schizophrenia as a GSK-3 dysregulation disorder. *Trends Neurosci.* **2007**, *30*, 142–149.
(150) Marsell, R.; Sisask, G.; Nilsson, Y.; Sundgren-Andersson, A. K.; Andersson, U.; Larsson, S.; Nilsson, O.; Ljunggren, O.; Jonsson, K. B. GSK-3 inhibition by an orally active small molecule increases bone mass in rats. *Bone* **2012**, *50*, 619–627.
(151) Dugo, L.; Collin, M.; Allen, D. A.; Patel, N. S. A.; Bauer, I.; Mervaala, E. M. A.; Louhelainen, M.; Foster, S. J.; Yaqoob, M. M.; Thiemermann, C. GSK-3beta inhibitors attenuate the organ injury/dysfunction caused by endotoxemia in the rat. *Crit. Care Med.* **2005**, *33*, 1903–1912.
(152) Hirotani, S.; Zhai, P.; Tomita, H.; Galeotti, J.; Marquez, J. P.; Gao, S.; Hong, C.; Yatani, A.; Avila, J.; Sadoshima, J. Inhibition of glycogen synthase kinase 3beta during heart failure is protective. *Circ. Res.* **2007**, *101*, 1164–1174.
(153) van der Vaart, A.; Meng, X.; Bowers, M. S.; Batman, A. M.; Aliev, F.; Farris, S. P.; Hill, J. S.; Green, T. A.; Dick, D.; Wolstenholme, J. T. *et al.* Glycogen synthase kinase 3 beta regulates ethanol consumption and is a risk factor for alcohol dependence. *Neuropsychopharmacology* **2018**, *43*, 2521–2531.

(154) Neves, V. C. M.; Babb, R.; Chandrasekaran, D.; Sharpe, P. T. Promotion of natural tooth repair by small molecule GSK3 antagonists. *Sci. Rep.* **2017**, *7*, 39654.
(155) Sato, N.; Meijer, L.; Skaltsounis, L.; Greengard, P.; Brivanlou, A. H. Maintenance of pluripotency in human and mouse embryonic stem cells through activation of Wnt signaling by a pharmacological GSK-3-specific inhibitor. *Nat. Med.* **2004**, *10*, 55–63.
(156) Ying, Q.-L.; Wray, J.; Nichols, J.; Batlle-Morera, L.; Doble, B.; Woodgett, J.; Cohen, P.; Smith, A. The ground state of embryonic stem cell self-renewal. *Nature* **2008**, *453*, 519–523.
(157) Huang, J.; Guo, X.; Li, W.; Zhang, H. Activation of Wnt/β-catenin signalling via GSK3 inhibitors direct differentiation of human adipose stem cells into functional hepatocytes. *Sci. Rep.* **2017**, *7*, 40716.
(158) Hooper, C.; Killick, R.; Lovestone, S. The GSK3 hypothesis of Alzheimer's disease. *J. Neurochem.* **2008**, *104*, 1433–1439.
(159) Pei, J. J.; Tanaka, T.; Tung, Y. C.; Braak, E.; Iqbal, K.; Grundke-Iqbal, I. Distribution, levels, and activity of glycogen synthase kinase-3 in the Alzheimer disease brain. *J. Neuropathol. Exp. Neurol.* **1997**, *56*, 70–78.
(160) Blalock, E. M.; Geddes, J. W.; Chen, K. C.; Porter, N. M.; Markesbery, W. R.; Landfield, P. W. Incipient Alzheimer's disease: microarray correlation analyses reveal major transcriptional and tumor suppressor responses. *Proc. Natl. Acad. Sci. U. S. A.* **2004**, *101*, 2173–2178.
(161) Sherrington, R.; Rogaev, E. I.; Liang, Y.; Rogaeva, E. A.; Levesque, G.; Ikeda, M.; Chi, H.; Lin, C.; Li, G.; Holman, K. *et al.* Cloning of a gene bearing missense mutations in early-onset familial Alzheimer's disease. *Nature* **1995**, *375*, 754–760.
(162) Hardy, J. Amyloid, the presenilins and Alzheimer's disease. *Trends Neurosci.* **1997**, *20*, 154–159.
(163) Maesako, M.; Uemura, K.; Kubota, M.; Hiyoshi, K.; Ando, K.; Kuzuya, A.; Kihara, T.; Asada, M.; Akiyama, H.; Kinoshita, A. Effect of glycogen synthase kinase 3 β-mediated presenilin 1 phosphorylation on amyloid β production is negatively regulated by insulin receptor cleavage. *Neurosci.* **2011**, *177*, 298–307.
(164) Uemura, K.; Kuzuya, A.; Shimozono, Y.; Aoyagi, N.; Ando, K.; Shimohama, S.; Kinoshita, A. GSK3beta activity modifies the localization and function of presenilin 1. *J. Biol. Chem.* **2007**, *282*, 15823–15832.
(165) Takashima, A.; Noguchi, K.; Michel, G.; Mercken, M.; Hoshi, M.; Ishiguro, K.; Imahori, K. Exposure of rat hippocampal neurons to amyloid beta peptide (25-35) induces the inactivation of phosphatidyl inositol-3 kinase and the activation of tau protein kinase I/glycogen synthase kinase-3 beta. *Neurosci. Lett.* **1996**, *203*, 33–36.
(166) Bedse, G.; Di Domenico, F.; Serviddio, G.; Cassano, T. Aberrant insulin signaling in Alzheimer's disease: current knowledge. *Front. Neurosci.* **2015**, *9*.
(167) Rana, A. K.; Singh, D. Targeting glycogen synthase kinase-3 for oxidative stress and neuroinflammation: Opportunities, challenges and future directions for cerebral stroke management. *Neuropharmacology* **2018**, *139*, 124–136.
(168) Llorens-Martín, M.; Fuster-Matanzo, A.; Teixeira, C. M.; Jurado-Arjona, J.; Ulloa, F.; Defelipe, J.; Rábano, A.; Hernández, F.; Soriano, E.; Avila, J. GSK-3β overexpression causes reversible alterations on postsynaptic densities and dendritic morphology of hippocampal granule neurons in vivo. *Mol. Psychiatry* **2013**, *18*, 451–460.
(169) Phiel, C. J.; Wilson, C. A.; Lee, V. M.-Y.; Klein, P. S. GSK-3alpha regulates production of Alzheimer's disease amyloid-beta peptides. *Nature* **2003**, *423*, 435–439.

(170) Ly, P. T. T.; Wu, Y.; Zou, H.; Wang, R.; Zhou, W.; Kinoshita, A.; Zhang, M.; Yang, Y.; Cai, F.; Woodgett, J. *et al.* Inhibition of GSK3β-mediated BACE1 expression reduces Alzheimer-associated phenotypes. *J. Clin. Invest.* **2013**, *123*, 224–235.
(171) Ma, T. GSK3 in Alzheimer's disease: mind the isoforms. *J. Alzheimer's Dis.* **2014**, *39*, 707–710.
(172) Ishiguro, K.; Shiratsuchi, A.; Sato, S.; Omori, A.; Arioka, M.; Kobayashi, S.; Uchida, T.; Imahori, K. Glycogen synthase kinase 3β is identical to tau protein kinase I generating several epitopes of paired helical filaments. *FEBS Letters* **1993**, *325*, 167–172.
(173) Lucas, J. J.; Hernández, F.; Gómez-Ramos, P.; Morán, M. A.; Hen, R.; Avila, J. Decreased nuclear β-catenin, tau hyperphosphorylation and neurodegeneration in GSK-3β conditional transgenic mice. *EMBO J.* **2001**, *20*, 27–39.
(174) Caricasole, A.; Copani, A.; Caraci, F.; Aronica, E.; Rozemuller, A. J.; Caruso, A.; Storto, M.; Gaviraghi, G.; Terstappen, G. C.; Nicoletti, F. Induction of Dickkopf-1, a negative modulator of the Wnt pathway, is associated with neuronal degeneration in Alzheimer's brain. *J. Neurosci.* **2004**, *24*, 6021–6027.
(175) Pei, J.-J.; Braak, E.; Braak, H.; Grundke-Iqbal, I.; Iqbal, K.; Winblad, B.; Cowburn, R. F. Distribution of Active Glycogen Synthase Kinase 3β (GSK-3β) in Brains Staged for Alzheimer Disease Neurofibrillary Changes. *J. Neuropathol. Exp. Neurol.* **1999**, *58*, 1010–1019.
(176) Tang, Q.-L.; Xie, X.-B.; Wang, J.; Chen, Q.; Han, A.-J.; Zou, C.-Y.; Yin, J.-Q.; Liu, D.-W.; Liang, Y.; Zhao, Z.-Q. *et al.* Glycogen synthase kinase-3β, NF-κB signaling, and tumorigenesis of human osteosarcoma. *J. Natl. Cancer Inst.* **2012**, *104*, 749–763.
(177) Maixner, D. W.; Weng, H.-R. The Role of Glycogen Synthase Kinase 3 Beta in Neuroinflammation and Pain. *J. Pharm. Pharmacol.* **2013**, *1*.
(178) Beurel, E. Regulation by Glycogen Synthase Kinase-3 of Inflammation and T Cells in CNS Diseases. *Front. Mol. Neurosci.* **2011**, *4*.
(179) Lee, J. C.; Laydon, J. T.; McDonnell, P. C.; Gallagher, T. F.; Kumar, S.; Green, D.; McNulty, D.; Blumenthal, M. J.; Heys, J. R.; Landvatter, S. W. *et al.* A protein kinase involved in the regulation of inflammatory cytokine biosynthesis. *Nature* **1994**, *372*, 739–746.
(180) Schett, G.; Zwerina, J.; Firestein, G. The p38 mitogen-activated protein kinase (MAPK) pathway in rheumatoid arthritis. *Ann. Rheum. Dis.* **2008**, *67*, 909–916.
(181) Goldstein, D. M.; Gabriel, T. Pathway to the clinic: inhibition of P38 MAP kinase. A review of ten chemotypes selected for development. *Curr. Top. Med. Chem.* **2005**, *5*, 1017–1029.
(182) Sweeney, S. E. The as-yet unfulfilled promise of p38 MAPK inhibitors. *Nat. Rev. Rheumatol.* **2009**, *5*, 475–477.
(183) Zarubin, T.; Han, J. Activation and signaling of the p38 MAP kinase pathway. *Cell Res.* **2005**, *15*, 11–18.
(184) Mittelstadt, P. R.; Salvador, J. M.; Fornace, A. J.; Ashwell, J. D. Activating p38 MAPK: new tricks for an old kinase. *Cell Cycle* **2005**, *4*, 1189–1192.
(185) Hensley, K.; Floyd, R. A.; Zheng, N.-Y.; Nael, R.; Robinson, K. A.; Nguyen, X.; Pye, Q. N.; Stewart, C. A.; Geddes, J.; Markesbery, W. R. *et al.* p38 Kinase Is Activated in the Alzheimer's Disease Brain. *J. Neurochem.* **1999**, *72*, 2053–2058.
(186) Tian, L.; Ma, L.; Kaarela, T.; Li, Z. Neuroimmune crosstalk in the central nervous system and its significance for neurological diseases. *J. Neuroinflammation* **2012**, *9*, 155.
(187) DiSabato, D.; Quan, N.; Godbout, J. P. Neuroinflammation: The Devil is in the Details. *J. Neurochem.* **2016**, *139*, 136–153.

(188) Bachstetter, A. D.; Xing, B.; Almeida, L. de; Dimayuga, E. R.; Watterson, D. M.; van Eldik, L. J. Microglial p38α MAPK is a key regulator of proinflammatory cytokine up-regulation induced by toll-like receptor (TLR) ligands or beta-amyloid (Aβ). *J. Neuroinflammation* **2011**, *8*, 79.
(189) Colié, S.; Sarroca, S.; Palenzuela, R.; Garcia, I.; Matheu, A.; Corpas, R.; Dotti, C. G.; Esteban, J. A.; Sanfeliu, C.; Nebreda, A. R. Neuronal p38α mediates synaptic and cognitive dysfunction in an Alzheimer's mouse model by controlling β-amyloid production. *Sci. Rep.* **2017**, *7*, 45306.
(190) Reynolds, C. H.; Nebreda, A. R.; Gibb, G. M.; Utton, M. A.; Anderton, B. H. Reactivating Kinase/p38 Phosphorylates τ Protein In Vitro. *J. Neurochem.* **1997**, *69*, 191–198.
(191) Goedert, M.; Hasegawa, M.; Jakes, R.; Lawler, S.; Cuenda, A.; Cohen, P. Phosphorylation of microtubule-associated protein tau by stress-activated protein kinases. *FEBS Letters* **1997**, *409*, 57–62.
(192) Zhu, X.; Rottkamp, C. A.; Boux, H.; Takeda, A.; Perry, G.; Smith, M. A. Activation of p38 kinase links tau phosphorylation, oxidative stress, and cell cycle-related events in Alzheimer disease. *J. Neuropathol. Exp. Neurol.* **2000**, *59*, 880–888.
(193) Andorfer, C.; Kress, Y.; Espinoza, M.; Silva, R. de; Tucker, K. L.; Barde, Y.-A.; Duff, K.; Davies, P. Hyperphosphorylation and aggregation of tau in mice expressing normal human tau isoforms. *J. Neurochem.* **2003**, *86*, 582–590.
(194) Maphis, N.; Jiang, S.; Xu, G.; Kokiko-Cochran, O. N.; Roy, S. M.; van Eldik, L. J.; Watterson, D. M.; Lamb, B. T.; Bhaskar, K. Selective suppression of the α isoform of p38 MAPK rescues late-stage tau pathology. *Alzheimer's Research & Therapy* **2016**, *8*, 54.
(195) Duffy, J. P.; Harrington, E. M.; Salituro, F. G.; Cochran, J. E.; Green, J.; Gao, H.; Bemis, G. W.; Evindar, G.; Galullo, V. P.; Ford, P. J. *et al.* The Discovery of VX-745: A Novel and Selective p38α Kinase Inhibitor. *ACS Med. Chem. Lett.* **2011**, *2*, 758–763.
(196) Alam, J.; Blackburn, K.; Patrick, D. Neflamapimod: Clinical Phase 2b-Ready Oral Small Molecule Inhibitor of p38α to Reverse Synaptic Dysfunction in Early Alzheimer's Disease. *J. Prev. Alzheimer's Dis.* **2017**, *4*, 273–278.
(197) Scheltens, P.; Prins, N.; Lammertsma, A.; Yaqub, M.; Gouw, A.; Wink, A. M.; Chu, H.-M.; van Berckel, B. N. M.; Alam, J. An exploratory clinical study of p38α kinase inhibition in Alzheimer's disease. *Ann. Clin. Transl. Neurol.* **2018**, *5*, 464–473.
(198) Kim, W. S.; Kågedal, K.; Halliday, G. M. Alpha-synuclein biology in Lewy body diseases. *Alzheimer's Research & Therapy* **2014**, *6*, 73.
(199) Li, D.-W.; Liu, Z.-Q.; Chen, W.; Yao, M.; Li, G.-R. Association of glycogen synthase kinase-3β with Parkinson's disease (review). *Mol. Med. Rep.* **2014**, *9*, 2043–2050.
(200) Wang, W.; Yang, Y.; Ying, C.; Li, W.; Ruan, H.; Zhu, X.; You, Y.; Han, Y.; Chen, R.; Wang, Y. *et al.* Inhibition of glycogen synthase kinase-3beta protects dopaminergic neurons from MPTP toxicity. *Neuropharmacology* **2007**, *52*, 1678–1684.
(201) Koh, S.-H.; Kim, Y.; Kim, H. Y.; Hwang, S.; Lee, C. H.; Kim, S. H. Inhibition of glycogen synthase kinase-3 suppresses the onset of symptoms and disease progression of G93A-SOD1 mouse model of ALS. *Exp. Neurol.* **2007**, *205*, 336–346.
(202) Palomo, V.; I. Perez, D.; Gil, C.; Martinez, A. The Potential Role of Glycogen Synthase Kinase 3 Inhibitors as Amyotrophic Lateral Sclerosis Pharmacological Therapy. *Curr. Med. Chem.* **2011**, *18*, 3028–3034.
(203) L'Episcopo, F.; Drouin-Ouellet, J.; Tirolo, C.; Pulvirenti, A.; Giugno, R.; Testa, N.; Caniglia, S.; Serapide, M. F.; Cisbani, G.; Barker, R. A. *et al.* GSK-3β-induced Tau pathology drives hippocampal neuronal cell death in Huntington's disease: involvement of astrocyte-neuron interactions. *Cell Death Dis.* **2016**, *7*, e2206.

(204) Fan, J.; Gladding, C. M.; Wang, L.; Zhang, L. Y. J.; Kaufman, A. M.; Milnerwood, A. J.; Raymond, L. A. P38 MAPK is involved in enhanced NMDA receptor-dependent excitotoxicity in YAC transgenic mouse model of Huntington disease. *Neurobiol. Dis.* **2012**, *45*, 999–1009.
(205) Dewil, M.; dela Cruz, V. F.; van den Bosch, L.; Robberecht, W. Inhibition of p38 mitogen activated protein kinase activation and mutant SOD1(G93A)-induced motor neuron death. *Neurobiol. Dis.* **2007**, *26*, 332–341.
(206) Corrêa, S. A. L.; Eales, K. L. The Role of p38 MAPK and Its Substrates in Neuronal Plasticity and Neurodegenerative Disease. *J. Signal Transduction* **2012**, *2012*, 649079.
(207) Cummings, J.; Lee, G.; Ritter, A.; Zhong, K. Alzheimer's disease drug development pipeline: 2018. *Alzheimer's Dementia* **2018**, *4*, 195–214.
(208) Stanislav Andreev. Master thesis: "From JAK to GSK-3: Hit-optimization of 9H-pyrimido[4,5-b]indole-based inhibitors", Eberhard Karls Universität, Tübingen, 2014.
(209) Halekotte, J.; Witt, L.; Ianes, C.; Krüger, M.; Bührmann, M.; Rauh, D.; Pichlo, C.; Brunstein, E.; Luxenburger, A.; Baumann, U. *et al.* Optimized 4,5-Diarylimidazoles as Potent/Selective Inhibitors of Protein Kinase CK1δ and Their Structural Relation to p38α MAPK. *Molecules* **2017**, *22*.
(210) Hann, M. M. Molecular obesity, potency and other addictions in drug discovery. *MedChemComm* **2011**, *2*, 349.
(211) Flanagan, M. E.; Blumenkopf, T. A.; Brissette, W. H.; Brown, M. F.; Casavant, J. M.; Shang-Poa, C.; Doty, J. L.; Elliott, E. A.; Fisher, M. B.; Hines, M. *et al.* Discovery of CP-690,550: A potent and selective Janus kinase (JAK) inhibitor for the treatment of autoimmune diseases and organ transplant rejection. *J. Med. Chem.* **2010**, *53*, 8468–8484.
(212) Pattison, M. J.; Mackenzie, K. F.; Arthur, J. S. C. Inhibition of JAKs in macrophages increases lipopolysaccharide-induced cytokine production by blocking IL-10-mediated feedback. *J. Immunol.* **2012**, *189*, 2784–2792.
(213) Michael Forster. Diploma thesis: "Synthese neuer JAK3-Inhibitoren durch SNAr-Substitution an elektronenarmen Heterocyclen", Eberhard Karls Universität, Tübingen, 2012.
(214) Zhang, Q.; Liu, Y.; Gao, F.; Ding, Q.; Cho, C.; Hur, W.; Jin, Y.; Uno, T.; Joazeiro, C. A. P.; Gray, N. Discovery of EGFR selective 4,6-disubstituted pyrimidines from a combinatorial kinase-directed heterocycle library. *J. Am. Chem. Soc.* **2006**, *128*, 2182–2183.
(215) Guagnano, V.; Furet, P.; Spanka, C.; Bordas, V.; Le Douget, M.; Stamm, C.; Brueggen, J.; Jensen, M. R.; Schnell, C.; Schmid, H. *et al.* Discovery of 3-(2,6-dichloro-3,5-dimethoxy-phenyl)-1-{6-4-(4-ethyl-piperazin-1-yl)-phenylamino-pyrimidin-4-yl}-1-methyl-urea (NVP-BGJ398), a potent and selective inhibitor of the fibroblast growth factor receptor family of receptor tyrosine kinase. *J. Med. Chem.* **2011**, *54*, 7066–7083.
(216) Norman, P. The use of salt-inducible kinase inhibitors to treat autoimmune and inflammatory diseases: evaluation of WO2013136070. *Expert Opin. Ther. Pat.* **2014**, *24*, 943–946.
(217) Ling, J.; Liu, J. VEGFR Tyrosine Kinase Inhibitors, Nov 20, 2014.
(218) Louie, J.; Hartwig, J. F. Palladium-catalyzed synthesis of arylamines from aryl halides. Mechanistic studies lead to coupling in the absence of tin reagents. *Tetrahedron Lett.* **1995**, *36*, 3609–3612.
(219) Guram, A. S.; Rennels, R. A.; Buchwald, S. L. A Simple Catalytic Method for the Conversion of Aryl Bromides to Arylamines. *Angew. Chem., Int. Ed.* **1995**, *34*, 1348–1350.

(220) Brown, D. G.; Boström, J. Analysis of Past and Present Synthetic Methodologies on Medicinal Chemistry: Where Have All the New Reactions Gone? *J. Med. Chem.* **2016**, *59*, 4443–4458.
(221) Hartwig, J. F.; Richards, S.; Barañano, D.; Paul, F. Influences on the Relative Rates for C−N Bond-Forming Reductive Elimination and β-Hydrogen Elimination of Amides. A Case Study on the Origins of Competing Reduction in the Palladium-Catalyzed Amination of Aryl Halides. *J. Am. Chem. Soc.* **1996**, *118*, 3626–3633.
(222) Hamann, B. C.; Hartwig, J. F. Systematic Variation of Bidentate Ligands Used in Aryl Halide Amination. Unexpected Effects of Steric, Electronic, and Geometric Perturbations. *J. Am. Chem. Soc.* **1998**, *120*, 3694–3703.
(223) Stanislav Andreev. *Unpublished data*.
(224) Gehringer, M.; Forster, M.; Pfaffenrot, E.; Bauer, S. M.; Laufer, S. A. Novel hinge-binding motifs for Janus kinase 3 inhibitors: A comprehensive structure-activity relationship study on tofacitinib bioisosteres. *ChemMedChem* **2014**, *9*, 2516–2527.
(225) Zegzouti, H.; Zdanovskaia, M.; Hsiao, K.; Goueli, S. A. ADP-Glo: A Bioluminescent and homogeneous ADP monitoring assay for kinases. *Assay Drug Dev. Technol.* **2009**, *7*, 560–572.
(226) Goettert, M.; Graeser, R.; Laufer, S. A. Optimization of a nonradioactive immunosorbent assay for p38alpha mitogen-activated protein kinase activity. *Anal. Biochem.* **2010**, *406*, 233–234.
(227) Goettert, M.; Luik, S.; Graeser, R.; Laufer, S. A. A direct ELISA assay for quantitative determination of the inhibitory potency of small molecules inhibitors for JNK3. *J. Pharm. Biomed. Anal.* **2011**, *55*, 236–240.
(228) Bauer, S. M.; Gehringer, M.; Laufer, S. A. A direct enzyme-linked immunosorbent assay (ELISA) for the quantitative evaluation of Janus Kinase 3 (JAK3) inhibitors. *Anal. Methods* **2014**, *6*, 8817–8822.
(229) DiMartino, M. J.; Griswold, D. E.; Berkowitz, B. A.; Poste, G.; Hanna, N. Pharmacologic characterization of the antiinflammatory properties of a new dual inhibitor of lipoxygenase and cyclooxygenase. *Agents Actions* **1987**, *20*, 113–123.
(230) SB 203580 is a specific inhibitor of a MAP kinase homologue which is stimulated by cellular stresses and interleukin-1. *FEBS Letters* **1995**, *364*, 229–233.
(231) Ansideri, F.; Macedo, J. T.; Eitel, M.; El-Gokha, A.; Zinad, D. S.; Scarpellini, C.; Kudolo, M.; Schollmeyer, D.; Boeckler, F. M.; Blaum, B. S. *et al.* Structural Optimization of a Pyridinylimidazole Scaffold: Shifting the Selectivity from p38α Mitogen-Activated Protein Kinase to c-Jun N-Terminal Kinase 3. *ACS Omega* **2018**, *3*, 7809–7831.
(232) Günther, M.; Lategahn, J.; Juchum, M.; Döring, E.; Keul, M.; Engel, J.; Tumbrink, H. L.; Rauh, D.; Laufer, S. Trisubstituted Pyridinylimidazoles as Potent Inhibitors of the Clinically Resistant L858R/T790M/C797S EGFR Mutant: Targeting of Both Hydrophobic Regions and the Phosphate Binding Site. *J. Med. Chem.* **2017**, *60*, 5613–5637.
(233) Takle, A. K.; Brown, M. J. B.; Davies, S.; Dean, D. K.; Francis, G.; Gaiba, A.; Hird, A. W.; King, F. D.; Lovell, P. J.; Naylor, A. *et al.* The identification of potent and selective imidazole-based inhibitors of B-Raf kinase. *Bioorg. Med. Chem. Lett.* **2006**, *16*, 378–381.
(234) Callahan, J. F.; Burgess, J. L.; Fornwald, J. A.; Gaster, L. M.; Harling, J. D.; Harrington, F. P.; Heer, J.; Kwon, C.; Lehr, R.; Mathur, A. *et al.* Identification of novel inhibitors of the transforming growth factor beta1 (TGF-beta1) type 1 receptor (ALK5). *J. Med. Chem.* **2002**, *45*, 999–1001.

(235) Semones, M.; Feng, Y.; Johnson, N.; Adams, J. L.; Winkler, J.; Hansbury, M. Pyridinylimidazole inhibitors of Tie2 kinase. *Bioorg. Med. Chem. Lett.* **2007**, *17*, 4756–4760.
(236) Koch, P.; Ansideri, F. 2-Alkylsulfanyl-4(5)-aryl-5(4)-heteroarylimidazoles: An Overview on Synthetic Strategies and Biological Activity. *Arch. Pharm.* **2017**, *350*.
(237) Williams, J. A.; Hyland, R.; Jones, B. C.; Smith, D. A.; Hurst, S.; Goosen, T. C.; Peterkin, V.; Koup, J. R.; Ball, S. E. Drug-drug interactions for UDP-glucuronosyltransferase substrates: a pharmacokinetic explanation for typically observed low exposure (AUCi/AUC) ratios. *Drug Metab. Dispos.* **2004**, *32*, 1201–1208.
(238) Zhang, L.; Peng, X.-M.; Damu, G. L. V.; Geng, R.-X.; Zhou, C.-H. Comprehensive review in current developments of imidazole-based medicinal chemistry. *Med. Res. Rev.* **2014**, *34*, 340–437.
(239) Gleeson, M. P. Generation of a set of simple, interpretable ADMET rules of thumb. *J. Med. Chem.* **2008**, *51*, 817–834.
(240) Laufer, S. A.; Wagner, G. K.; Kotschenreuther, D. A.; Albrecht, W. Novel substituted pyridinyl imidazoles as potent anticytokine agents with low activity against hepatic cytochrome P450 enzymes. *J. Med. Chem.* **2003**, *46*, 3230–3244.
(241) Kammerer, B.; Scheible, H.; Zurek, G.; Godejohann, M.; Zeller, K. P.; Gleiter, C. H.; Albrecht, W.; Laufer, S. In vitro metabolite identification of ML3403, a 4-pyridinylimidazole-type p38 MAP kinase inhibitor by LC-Qq-TOF-MS and LC-SPE-cryo-NMR/MS. *Xenobiotica* **2007**, *37*, 280–297.
(242) Kammerer, B.; Scheible, H.; Albrecht, W.; Gleiter, C. H.; Laufer, S. Pharmacokinetics of ML3403 ({4-5-(4-fluorophenyl)-2-methylsulfanyl-3H-imidazol-4-yl-pyridin-2-yl}-(1-phenylethyl)-amine), a 4-Pyridinylimidazole-type p38 mitogen-activated protein kinase inhibitor. *Drug Metab. Dispos.* **2007**, *35*, 875–883.
(243) Bühler, S.; Goettert, M.; Schollmeyer, D.; Albrecht, W.; Laufer, S. A. Chiral sulfoxides as metabolites of 2-thioimidazole-based p38α mitogen-activated protein kinase inhibitors: enantioselective synthesis and biological evaluation. *J. Med. Chem.* **2011**, *54*, 3283–3297.
(244) Pierre, K.; Christiane, B.; Hartmut, J.; Stefan, L. Targeting the ribose and phosphate binding site of p38 mitogen-activated protein (MAP) kinase: synthesis and biological testing of 2-alkylsulfanyl-, 4(5)-aryl-, 5(4)-heteroaryl-substituted imidazoles. *J. Med. Chem.* **2008**, *51*, 5630–5640.
(245) Laufer, S. A.; Hauser, D. R. J.; Domeyer, D. M.; Kinkel, K.; Liedtke, A. J. Design, synthesis, and biological evaluation of novel Tri- and tetrasubstituted imidazoles as highly potent and specific ATP-mimetic inhibitors of p38 MAP kinase: focus on optimized interactions with the enzyme's surface-exposed front region. *J. Med. Chem.* **2008**, *51*, 4122–4149.
(246) Laufer, S.; Hauser, D.; Stegmiller, T.; Bracht, C.; Ruff, K.; Schattel, V.; Albrecht, W.; Koch, P. Tri- and tetrasubstituted imidazoles as p38α mitogen-activated protein kinase inhibitors. *Bioorg. Med. Chem. Lett.* **2010**, *20*, 6671–6675.
(247) Griffen, E.; Leach, A. G.; Robb, G. R.; Warner, D. J. Matched molecular pairs as a medicinal chemistry tool. *J. Med. Chem.* **2011**, *54*, 7739–7750.
(248) Laufer, S. A.; Liedtke, A. J. A concise and optimized four-step approach toward 2-(aryl-)alkylsulfanyl-, 4(5)-aryl-, 5(4)-heteroaryl-substituted imidazoles using alkyl- or arylalkyl thiocyanates. *Tetrahedron Lett.* **2006**, *47*, 7199–7203.
(249) Urs Haun. Master thesis: "Von 2-Alkylsulfanylimidazolen zu 2-Alkylimidazolen - Synthese von 2-Alkyl-4(5)-aryl-5(4)-heteroarylimidazolen als Kinasehemmstoffe", Eberhard Karls Universität, Tübingen, 2017.
(250) Fehr, S.; Unger, A.; Schaeffeler, E.; Herrmann, S.; Laufer, S.; Schwab, M.; Albrecht, W. Impact of p38 MAP Kinase Inhibitors on LPS-Induced Release of TNF-α

in Whole Blood and Primary Cells from Different Species. *Cell. Physiol. Biochem.* **2015**, *36*, 2237–2249.
(251) Yao, X.; Anderson, D. L.; Ross, S. A.; Lang, D. G.; Desai, B. Z.; Cooper, D. C.; Wheelan, P.; McIntyre, M. S.; Bergquist, M. L.; MacKenzie, K. I. *et al.* Predicting QT prolongation in humans during early drug development using hERG inhibition and an anaesthetized guinea-pig model. *Br. J. Pharmacol.* **2008**, *154*, 1446–1456.
(252) Hopkins, A. L.; Keserü, G. M.; Leeson, P. D.; Rees, D. C.; Reynolds, C. H. The role of ligand efficiency metrics in drug discovery. *Nat. Rev. Drug Discov.* **2014**, *13*, 105–121.
(253) Arnott, J. A.; Planey, S. L. The influence of lipophilicity in drug discovery and design. *Expert opinion on drug discovery* **2012**, *7*, 863–875.
(254) Wager, T. T.; Hou, X.; Verhoest, P. R.; Villalobos, A. Central Nervous System Multiparameter Optimization Desirability: Application in Drug Discovery. *ACS Chem. Neurosci.* **2016**, *7*, 767–775.
(255) Juchum, M.; Günther, M.; Döring, E.; Sievers-Engler, A.; Lämmerhofer, M.; Laufer, S. Trisubstituted Imidazoles with a Rigidized Hinge Binding Motif Act As Single Digit nM Inhibitors of Clinically Relevant EGFR L858R/T790M and L858R/T790M/C797S Mutants: An Example of Target Hopping. *J. Med. Chem.* **2017**, *60*, 4636–4656.
(256) Selig, R.; Schollmeyer, D.; Albrecht, W.; Laufer, S. The application of Stille cross-coupling reactions with multiple nitrogen containing heterocycles. *Tetrahedron* **2011**, *67*, 9204–9213.
(257) Revesz, L.; Bonne, F.; Makavou, P. Vicinal bromostannanes as novel building blocks for the preparation of di- and trisubstituted imidazoles. *Tetrahedron Lett.* **1998**, *39*, 5171–5174.
(258) Bellina, F.; Cauteruccio, S.; Rossi, R. Efficient and practical synthesis of 4(5)-aryl-1H-imidazoles and 2,4(5)-diaryl-1H-imidazoles via highly selective palladium-catalyzed arylation reactions. *J. Org. Chem.* **2007**, *72*, 8543–8546.
(259) Joo, J. M.; Touré, B. B.; Sames, D. C-H bonds as ubiquitous functionality: a general approach to complex arylated imidazoles via regioselective sequential arylation of all three C-H bonds and regioselective N-alkylation enabled by SEM-group transposition. *J. Org. Chem.* **2010**, *75*, 4911–4920.
(260) Sämann, C.; Coya, E.; Knochel, P. Full functionalization of the imidazole scaffold by selective metalation and sulfoxide/magnesium exchange. *Angew. Chem., Int. Ed.* **2014**, *53*, 1430–1434.
(261) Niculescu-Duvaz, D.; Niculescu-Duvaz, I.; Suijkerbuijk, B. M. J. M.; Ménard, D.; Zambon, A.; Davies, L.; Pons, J.-F.; Whittaker, S.; Marais, R.; Springer, C. J. Potent BRAF kinase inhibitors based on 2,4,5-trisubstituted imidazole with naphthyl and benzothiophene 4-substituents. *Bioorg. Med. Chem.* **2013**, *21*, 1284–1304.
(262) Carrera, A. C.; Alexandrov, K.; Roberts, T. M. The conserved lysine of the catalytic domain of protein kinases is actively involved in the phosphotransfer reaction and not required for anchoring ATP. *Proc. Natl. Acad. Sci. U. S. A.* **1993**, *90*, 442–446.
(263) Ziegler, K.; Hauser, D. R. J.; Unger, A.; Albrecht, W.; Laufer, S. A. 2-Acylaminopyridin-4-ylimidazoles as p38 MAP kinase inhibitors: Design, synthesis, and biological and metabolic evaluations. *ChemMedChem* **2009**, *4*, 1939–1948.
(264) Muth, F.; El-Gokha, A.; Ansideri, F.; Eitel, M.; Döring, E.; Sievers-Engler, A.; Lange, A.; Boeckler, F. M.; Lämmerhofer, M.; Koch, P. *et al.* Tri- and Tetrasubstituted Pyridinylimidazoles as Covalent Inhibitors of c-Jun N-Terminal Kinase 3. *J. Med. Chem.* **2017**, *60*, 594–607.
(265) Langmuir, I. ISOMORPHISM, ISOSTERISM AND COVALENCE. *J. Am. Chem. Soc.* **1919**, *41*, 1543–1559.

(266) Burger, A. Isosterism and bioisosterism in drug design. *Jucker E. (eds) Progress in Drug Research / Fortschritte der Arzneimittelforschung / Progrès des recherches pharmaceutiques. Vol 37. Birkhäuser Basel*; pp 287–371.
(267) Ritchie, T. J.; Macdonald, S. J. F.; Peace, S.; Pickett, S. D.; Luscombe, C. N. The developability of heteroaromatic and heteroaliphatic rings – do some have a better pedigree as potential drug molecules than others? *MedChemComm* **2012**, *3*, 1062.
(268) McClure, K. F.; Letavic, M. A.; Kalgutkar, A. S.; Gabel, C. A.; Audoly, L.; Barberia, J. T.; Braganza, J. F.; Carter, D.; Carty, T. J.; Cortina, S. R. *et al.* Structure-activity relationships of triazolopyridine oxazole p38 inhibitors: identification of candidates for clinical development. *Bioorg. Med. Chem. Lett.* **2006**, *16*, 4339–4344.
(269) Liang, S. H.; Chen, J. M.; Normandin, M. D.; Chang, J. S.; Chang, G. C.; Taylor, C. K.; Trapa, P.; Plummer, M. S.; Para, K. S.; Conn, E. L. *et al.* Discovery of a Highly Selective Glycogen Synthase Kinase-3 Inhibitor (PF-04802367) That Modulates Tau Phosphorylation in the Brain: Translation for PET Neuroimaging. *Angew. Chem., Int. Ed.* **2016**, *55*, 9601–9605.
(270) Kim, K. S.; Kimball, S. D.; Misra, R. N.; Rawlins, D. B.; Hunt, J. T.; Xiao, H.-Y.; Lu, S.; Qian, L.; Han, W.-C.; Shan, W. *et al.* Discovery of Aminothiazole Inhibitors of Cyclin-Dependent Kinase 2: Synthesis, X-ray Crystallographic Analysis, and Biological Activities. *J. Med. Chem.* **2002**, *45*, 3905–3927.
(271) Heider, F.; Ansideri, F.; Tesch, R.; Pantsar, T.; Haun, U.; Döring, E.; Kudolo, M.; Poso, A.; Albrecht, W.; Laufer, S. *et al.* Pyridinylimidazoles as dual Glycogen Synthase Kinase 3β/p38α Mitogen-activated Protein Kinase Inhibitors. *Eur. J. Med. Chem.* **2019**.
(272) May, S. A.; Johnson, M. D.; Braden, T. M.; Calvin, J. R.; Haeberle, B. D.; Jines, A. R.; Miller, R. D.; Plocharczyk, E. F.; Rener, G. A.; Richey, R. N. *et al.* Rapid Development and Scale-Up of a 1 H -4-Substituted Imidazole Intermediate Enabled by Chemistry in Continuous Plug Flow Reactors. *Org. Process Res. Dev.* **2012**, *16*, 982–1002.

Appendix

Publication I

Heider, F.; Haun, U.; Döring, E.; Kudolo, M.; Sessler, C.; Albrecht, W.; Laufer, S.; Koch, P. – From 2-Alkylsulfanylimidazoles to 2-Alkylimidazoles: An Approach towards Metabolically More Stable p38α MAP Kinase Inhibitors. *Molecules* **2017**, *22* (10), 1729.

molecules

MDPI

Article

From 2-Alkylsulfanylimidazoles to 2-Alkylimidazoles: An Approach towards Metabolically More Stable p38α MAP Kinase Inhibitors

Fabian Heider [1], Urs Haun [1], Eva Döring [1], Mark Kudolo [1], Catharina Sessler [1], Wolfgang Albrecht [2], Stefan Laufer [1] and Pierre Koch [1,*]

[1] Department of Pharmaceutical and Medicinal Chemistry, Institute of Pharmaceutical Sciences, Eberhard Karls Universität Tübingen, Auf der Morgenstelle 8, 72076 Tübingen, Germany; fabian.heider@uni-tuebingen.de (F.H.); urs.haun@student.uni-tuebingen.de (U.H.); eva.doering@uni-tuebingen.de (E.D.); mark.kudolo@uni-tuebingen.de (M.K.); catharina.sessler@uni-tuebingen.de (C.S.); stefan.laufer@uni-tuebingen.de (S.L.)

[2] Teva-ratiopharm, Graf-Arco-Str. 3, 89079 Ulm, Germany; wolfgang.albrecht@ratiopharm.de

* Correspondence: pierre.koch@uni-tuebingen.de; Tel.: +49-7071-29-74579

Received: 13 September 2017; Accepted: 10 October 2017; Published: 14 October 2017

Abstract: In vitro and in vivo metabolism studies revealed that 2-alkylsulfanylimidazole **ML3403** (4-(5-(4-fluorophenyl)-2-(methylthio)-1*H*-imidazol-4-yl)-*N*-(1-phenylethyl)pyridin-2-amine) undergoes rapid oxidation to the sulfoxide. Replacing the sulfur atom present in the two potent p38α mitogen-activated protein (MAP) kinase inhibitors **ML3403** and **LN950** (2-((5-(4-fluorophenyl)-4-(2-((3-methylbutan-2-yl)amino)pyridin-4-yl)-1*H*-imidazol-2-yl)thio)ethan-1-ol) by a methylene group resulted in 2-alkylimidazole derivatives **1** and **2**, respectively, having a remarkably improved metabolic stability. The 2-alkylimidazole analogs **1** and **2** showed 20% and 10% biotransformation after 4 h of incubation with human liver microsomes, respectively. They display a 4-fold increased binding affinity towards the target kinase as well as similar in vitro potency and ex vivo efficacy relative to their 2-alkylsulfanylimidazole counterparts **ML3403** and **LN950**. For example, 2-alkylimidazole **2**, the analog of **LN950**, inhibits both the p38α MAP kinase as well as the LPS-stimulated tumor necrosis factor-α release from human whole blood in the low double-digit nanomolar range.

Keywords: kinase inhibitors; p38α MAP kinase; trisubstituted imidazoles; metabolic stability; Alzheimer's disease; neurodegenerative diseases; cancer

1. Introduction

The p38α mitogen-activated protein (MAP) kinase is a ubiquitously expressed serine/threonine kinase, which is implicated in various cellular processes such as cell survival, proliferation and differentiation. Because it promotes the expression of pro-inflammatory cytokines such as tumor necrosis factor-α (TNF-α) and interleukin-1β (IL-1β), the p38α MAP kinase has received a lot of attention as a target for drug discovery programs since the mid-1990s. Several p38α MAP kinase inhibitors were tested in clinical trials against cancer and chronic inflammatory diseases like rheumatoid arthritis or chronic obstructive pulmonary disease. Despite these major efforts, up to date there is still no p38α MAP kinase inhibitor on the market, as most of the trials were terminated due to adverse events or lack of efficacy. However, recent studies suggest an important role of the kinase in the pathogenesis of neurodegenerative diseases like multiple sclerosis and Alzheimer's

disease [1–3]. Recently, two phase II studies of selective p38α MAP kinase inhibitor **VX-745** (Figure S1, supplementary materials) to treat Alzheimer's disease have been completed [4,5].

Developed by SmithKline Beecham Pharmaceuticals, **SB203580** is a trisubstituted imidazole representing one of the first prototypical p38α MAP kinase inhibitors (Figure 1).

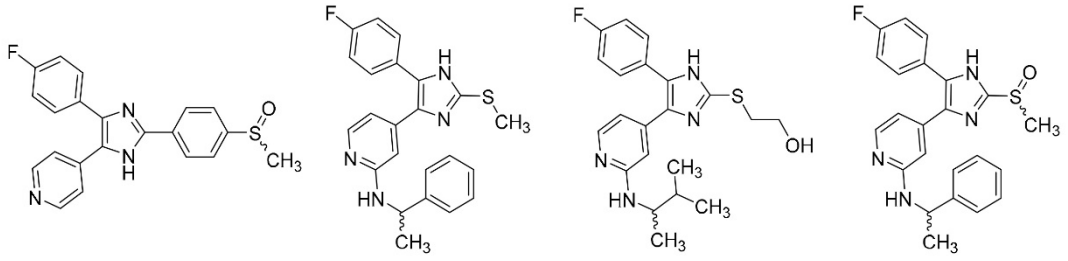

Figure 1. Pyridinylimidazoles as p38α MAP kinase inhibitors.

In collaboration with the University of Tübingen, Merckle GmbH disclosed a structural analog **ML3403**, which has been widely investigated in a variety of studies [6–10]. A further optimization study resulted in 2-(2-hydroxyethylsulfanyl)-4-(4-fluorophenyl)-5-(2-aminopyridin-4-yl)imidazole (**LN950**) [11]. Compared to **ML3403**, **LN950** displays an improved p38α MAP kinase inhibitory activity as well as a two orders of magnitude higher inhibition of lipopolysaccharide (LPS)-stimulated TNF-α release from human whole blood (HWB) (Figure 1).

Both inhibitors, **ML3403** and **LN950**, possess an alkylsulfanyl moiety in the imidazole-C2 position, which is prone to oxidation by metabolic enzymes such as cytochrome p450 (CYP). The metabolic stability of **ML3403** was extensively investigated in in vitro (animal and human liver microsomes) as well as in vivo (Wistar rats) studies [12,13]. Sulfoxide **ML3603** (Figure 1) was identified as the main metabolite in all studies and acts as an active metabolite. The conversion of **ML3403** to **ML3603** is mainly driven by the four CYP isoenzymes CYP1A2, CYP2C19, CYP2D6, and CYP3A4. The sulfoxide is then to a certain extent further metabolized to the corresponding sulfone; in addition *N*-dealkylation of the phenylethyl moiety as well as *N*-oxidation of the pyridine have also been observed. In phase II metabolism, *N*-conjugation of the dealkylated product by *N*-methyltransferase was predominantly registered. Kammerer et al. [13] showed the in vitro half-life of **ML3403** in male and female human liver microsomes (HLM) to be 32.7 min. In vitro experiments using mouse and rat liver microsomes also showed short half-lives of 5.9 and 11.4 min, respectively.

While the metabolite **ML3603** itself is active on p38α MAP kinase, it would be favorable to have a metabolically stable compound as a pharmacological tool compound since active metabolites can affect e.g., dosing calculations, dose-response relations and off-target effects.

In order to develop metabolically more stable p38α MAP kinase inhibitors, we removed the metabolic hot spot in **ML3403** and **LN950** and synthesized analogs of both inhibitors (compounds **1** and **2**), wherein the sulfur atom was replaced by a methylene group (Figure 2).

We evaluated the binding affinity as well as the inhibitory activity of the novel compounds toward the target kinase and their ability to inhibit the LPS-stimulated TNF-α release in human whole blood. The obtained biological data of **1** and **2** were compared to those of the parent compounds in order to estimate the influence of the sulfur atom present in **ML3403** and **LN950**. Moreover, the metabolic stability in human liver microsomes (HLM) of all four inhibitors was investigated. To rule out any interference and possible side-effects due to CYP inhibition, we subjected the compounds to a CYP inhibition assay.

Molecules **2017**, *22*, 1729 3 of 11

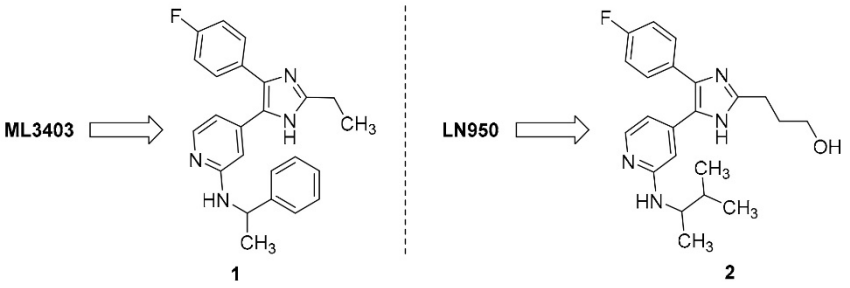

Figure 2. Modifications of **ML3403** and **LN950**.

2. Results and Discussion

2.1. Chemistry

The synthesis of the **ML3403** analog **1** was performed in a concise three-step synthetic route, as depicted in Scheme 1. Ethanone **3** was oxidized to the corresponding α-diketone **4** in a Riley oxidation using selenium dioxide. The imidazole ring formation was achieved in a Radziszewski imidazole synthesis by reacting dione **4** in the presence of 7 M ammonia in methanol and propanal. In the last step, the amino moiety at the pyridine-C2 position was introduced via a nucleophilic aromatic substitution reaction.

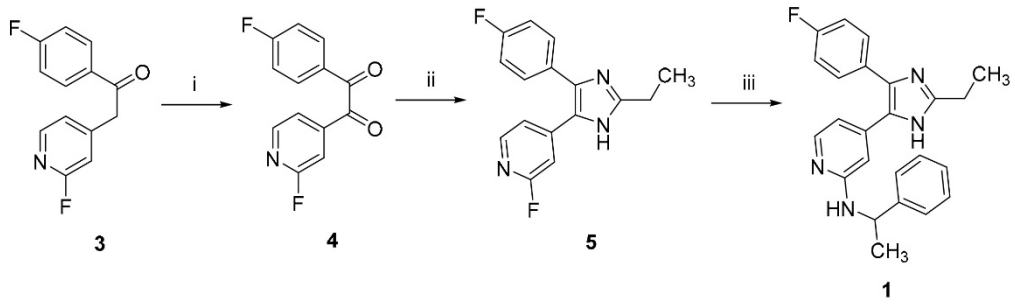

Scheme 1. Synthesis of 2-ethylimidazole **1**. (i) SeO_2, acetic acid, 50 °C, 3 h, 62%; (ii) propanal, 7 M ammonia in methanol, reflux temperature, 4 h, 43%; (iii) 1-phenylethylamine (excess), 160 °C, 72 h, 68%.

For the synthesis of the **LN950** analog **2**, a similar strategy consisting of Riley oxidation of an ethanone followed by Radziszewski imidazole synthesis was pursued (Scheme 2). Ethanone **6** [11] already bears the 3-methylbut-2-ylamine moiety at the pyridine-C2 position as well as a Boc-protecting group. Riley oxidation of ethanone **6** under acidic conditions resulted in the α-diketone **7**, wherein the Boc-protecting group was cleaved, too.

Triisopropylsilyl (TIPS)-protected aldehyde **9** was synthesized by the oxidation of primary alcohol **8** using a copper(I)/(2,2,6,6-tetramethylpiperidin-1-yl)oxyl (TEMPO) catalyst system according to Hoover and Stahl [14]. The ring closing reaction of dione **7** and aldehyde **9** in the presence of ammonium acetate in methanol afforded imidazole **10**. Finally, the TIPS-protecting group was removed under acidic conditions to yield the trisubstituted imidazole **2**.

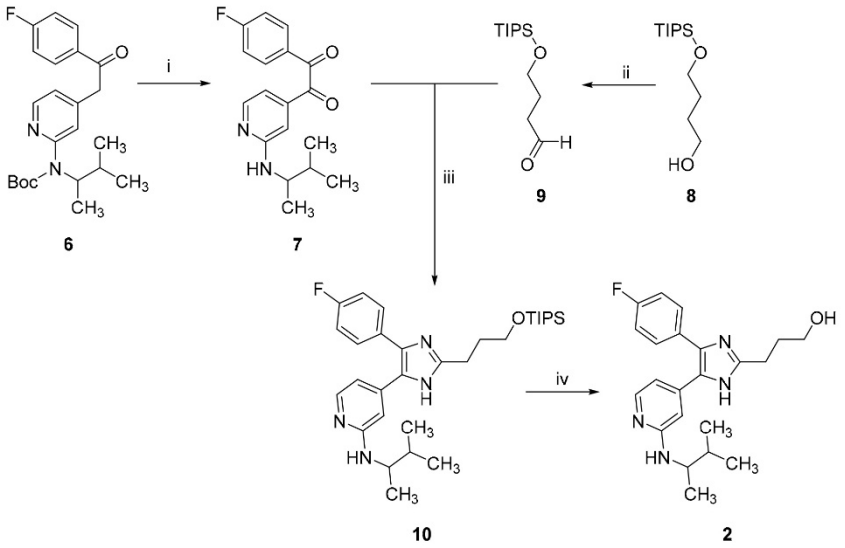

Scheme 2. Synthesis of 2-(3-hydroxypropyl)imidazole **2**. (i) SeO_2, acetic acid, reflux temperature, 1.5 h, 39%; (ii) *N*-methylimidazole, 2,2′-bipyridinyl, $Cu(MeCN)_4CF_3SO_3$, (2,2,6,6-tetramethylpiperidin-1-yl)oxyl, MeCN, room temperature (rt), 1.5 h, 20%; (iii) NH_4OAc, methanol, reflux temperature, 4 h, 20%; (iv) HCl, methanol, rt, 1 h, 73%.

2.2. Biological Evaluation

2-Alkylsulfanyl imidazoles **1** and **2** were evaluated in an enzyme-linked immunosorbent assay (ELISA) [15] as well as in a fluorescence polarization (FP)-based assay [16] for their ability to inhibit and bind to the p38α MAP kinase. Moreover, the ability of the novel compounds to inhibit the LPS-stimulated TNF-α release in HWB was tested [17]. In this ex vivo assay, the efficacy of the inhibitors is determined more specifically with regard to pharmacokinetic characteristics such as cellular permeability and plasma protein binding. The obtained data of **1** and **2** were compared to those of their parent compounds **ML3403** and **LN950**, respectively. The results are listed in Table 1.

2-Alkylimidazoles **1** and **2** are both potent inhibitors and potent binders of the target kinase, displaying IC_{50} and K_i values down to the low single-digit nanomolar range.

Table 1. Evaluation of trisubstituted imidazoles for their inhibition of p38α MAP kinase (ELISA assay), their binding affinity to p38α MAP kinase (FP assay) as well as for their inhibition of TNF-α release in LPS-stimulated human whole blood (HWB assay).

Cpd	ELISA Assay p38α IC_{50} [nM] [a]	FP Assay p38α K_i [nM] [a]	HWB Assay TNF-α IC_{50} [nM] [b]
ML3403	40 ± 5 [c]	38 ± 1 [e]	2979 ± 874
1	25 ± 2	11 ± 3	2539 ± 20
LN950	11 ± 0.9 [d]	4 ± 1 [e]	37 ± 4 [d]
2	11 ± 5	1 ± 0.2	32 ± 1

[a] n = 3; [b] n = 2; [c] value taken from Laufer and coworkers [7]; [d] value taken from Koch and coworkers [11]; [e] value taken from Ansideri et al. [16].

Comparison of the biological data of the 2-alkylsulfanylimidazole derivatives **ML3403** and **LN950** with their 2-alkylimidazole counterparts **1** and **2** reveals the replacement of the sulfur atom by a methylene group not to have any influence on the biological activity of these inhibitors. However, the 2-alkylimidazole derivatives display a 4-fold stronger binding affinity toward p38α MAP kinase compared to their corresponding 2-alkylsulfanylimidazoles. The most potent 2-alkylimidazole derived inhibitor **2** is 3.6-fold more active than the p38α MAP kinase reference compound **ML3403**.

2.3. Microsomal Stability Studies

Inhibitors **ML3403**, **LN950**, **1** and **2** were further tested for their metabolic stability in pooled adult male & female HLM.

ML3403 is rapidly metabolized in our study displaying an in vitro half-life of 0.86 h (Figure 3). After an incubation time of 4 h, less than 20% of **ML3403** were present (Figure 3 and Table S1, supplementary materials). Analysis of the metabolites by LC-MS (Tables S2-S5, supplementary materials) confirmed the aforementioned sulfoxide **ML3603** (m/z 421.5) to represent the main metabolite (almost 75% of all metabolites after 4 h). Up to 6% of the corresponding sulfone (m/z 437.4) was observed. Other low abundance metabolites were detected having an m/z ratio of 301.4 (*N*-dealkylation) and 317.5 (*N*-dealkylation + sulfoxidation). These findings are in agreement with the previously reported study by Kammerer et al. [13].

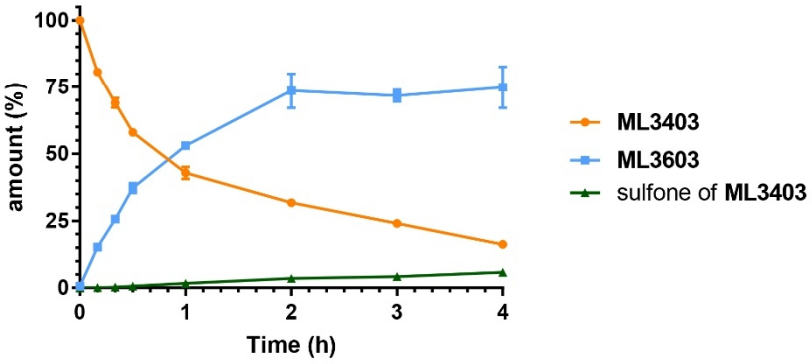

Figure 3. Metabolic stability of **ML3403** and the formation of main metabolites (sulfoxide **ML3603** and sulfone).

In contrast, 2-alkylimidazole **1** displays excellent metabolic stability remaining unmetabolized at up to 80% after the incubation time of 4 h (Figure 4 and Table S6, supplementary materials). Among the identified metabolites (Tables S7–S10, supplementary materials), m/z 283.6 was present, representing the *N*-dealkylated metabolite. Additionally, the LC-MS analysis shows two peaks in close proximity, both having an m/z ratio of 403.3. It is conceivable that both peaks correspond to the diastereomers resulting from the hydroxylation of the methylene group present in the ethyl moiety. The most prominent metabolite after the final sampling is seen at m/z 299.5 and is a combination of both *N*-dealkylation and possible hydroxylation, accounting for almost 50% of all arising metabolites.

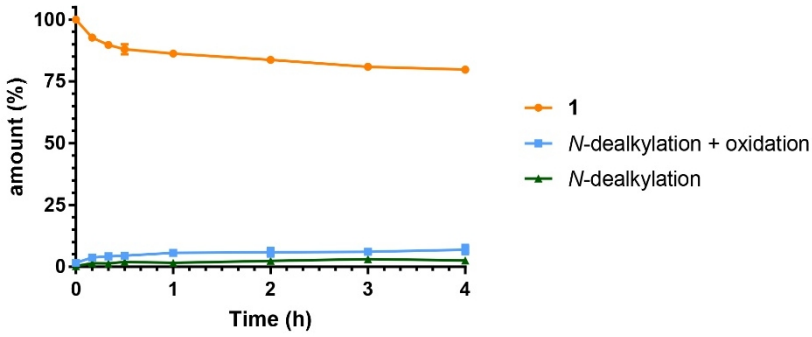

Figure 4. Metabolic stability of **1** and the formation of main metabolites (*N*-dealkylation as well as oxidation and *N*-dealkylation of **1**).

LN950 undergoes a similar but slightly slower biotransformation like **ML3403**. Over a time span of 4 h, **LN950** exhibits >70% degradation, most likely leading to the oxidation of the sulfur atom at the imidazole-C2 position (Figure 5 and Table S11, supplementary materials). Examination of the metabolites showed an almost identical pattern in comparison with **ML3403**, giving the corresponding sulfoxide as the main metabolite, as well as the sulfone and some *N*-dealkylated product (Tables S12–S14, supplementary materials).

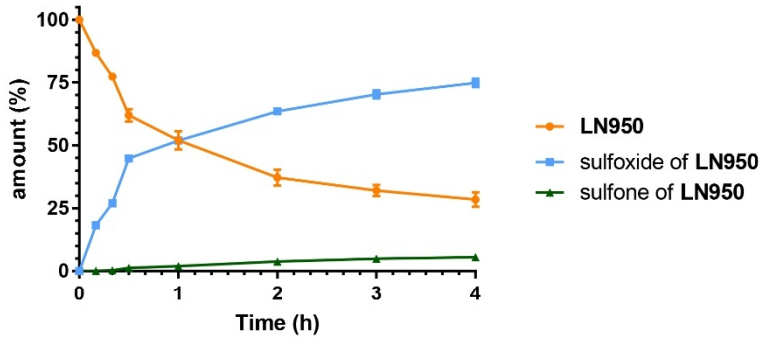

Figure 5. Metabolic stability of **LN950** and the formation of main metabolites (sulfoxide and sulfone of **LN950**).

The **LN950** analog, imidazole **2**, wherein the sulfur atom was replaced by a methylene group, shows under same conditions an exquisite metabolic profile. After 4 h, a degradation of only 10% could be observed (Figure 6 and Table S15, supplementary materials). Several metabolites were detected, all in low quantities (Tables S16 and S17, supplementary materials). Overall, a similar metabolite pattern as that for compound **1** was observed. In detail, CYP-mediated oxidation (hydroxylation or *N*-oxide) and to a small extent *N*-dealkylation occured. Comparison of the substituents at the imidazole-C2 position of 2-alkylimidazoles **1** and **2** leads to the assumption that the more polar 2-hydroxyethyl moiety of **2** is less susceptible for hydroxylation by CYP than the ethyl moiety present in **1** when incubated with HLM.

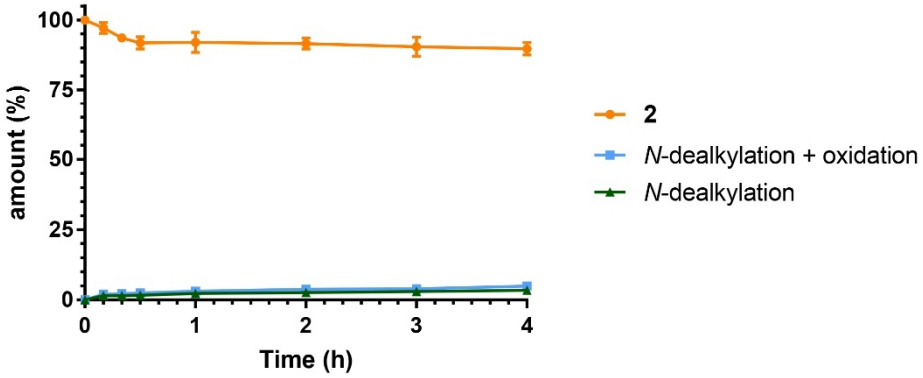

Figure 6. Metabolic stability of **2** and the formation of main metabolites (*N*-dealkylation as well as oxidation and *N*-dealkylation of **2**).

2.4. CYP Inhibition

Pyridinylimidazoles, like **SB203580**, are known to inhibit CYP isoenzymes due to the capability of the heterocyclic rings' nitrogen atoms to coordinate with the iron present in these proteins [18]. High CYP inhibition is associated with side-effects such as hepatotoxicity and is also responsible for many clinically relevant drug-drug interactions [19].

In an initial screening, **ML3403** and **LN950** as well as imidazoles **1** and **2** were studied for the purpose of assessing their inhibitory activity on the CYP isoforms 1A2, 2C9, 2C19, 2D6 and 3A4 (Table 2). At a test concentration of 10 μM, **ML3403** displays more than 50% inhibition of four out of the five major drug metabolizing CYP isoforms. Compared to **ML3403**, **LN950** shows a reduced CYP inhibition profile. **LN950** is a low inhibitor of CYP isoenzymes 1A2 and 2D6 and exhibits moderate to high affinity for the other three tested CYP isoforms. The 2-alkylimidazoles **1** and **2** display a higher affinity toward the tested CYP isoforms compared to their corresponding 2-alkylsulfanylimidazole counterparts. 2-Alkylimidazoles **1** and **2** inhibit all five CYP isoforms by more than 70% and 60%, respectively. The most potent inhibitor, 2-alkylimidazole **2**, shows a similar inhibition of CYP isoforms 1A2 and 2C19 as well as a reduced 2C9 CYP inhibition in comparison to the p38α MAP kinase reference compound **ML3403**. However, the CYP isoforms 2D6 and 3A4 are inhibited more strongly by 2-alkylimidazole **2** than by **ML3403**. Since the tested concentration of 10 μM in the CYP inhibition assay represents almost 1000-fold the IC_{50} value of imidazole **2** in the kinase activity assay, a certain margin of safety might be given concerning CYP inhibition-associated side effects.

Table 2. (%) inhibition of the most important CYP isoenzymes at 10 μM.

CYP	1A2	2C9	2C19	2D6	3A4
ML3403 [a]	66.7	79.0	83.5	31.1	79.2
1	85.6	85.1	71.0	90.2	97.6
LN950	28.0	91.5	63.0	41.5	61.0
2	69.4	61.9	83.6	78.8	92.1

[a] values taken from Laufer and coworkers [6].

3. Materials and Methods

3.1. Chemistry

Reagents and solvents were obtained from commercial sources and used without further purification. Thin layer chromatography (TLC) reaction controls were performed for all reactions using fluorescent silica gel 60 F_{254} plates (Merck, Darmstadt, Germany) and visualized under natural light and UV illumination at 254 and 366 nm. The purity of tested compounds **1** and **2** were determined by reverse phase high performance liquid chromatography (HPLC) (Agilent Technologies, Santa Clara, CA, USA). HPLC was carried out on an Agilent 1100 Series HPLC system, equipped with an UV DAD (detection at 218 nm, 254 nm and 280 nm). The chromatographic separation was performed on an XBridge^{TM} C18 column (Waters, Milford, MA, USA) (150 mm × 4.6 mm, 5 μm) at 30 °C oven temperature. The injection volume was 10 μL and the flow rate was 1.5 mL/min using the following gradient: 0.01 M KH_2PO_4, pH 2.3 (solvent A), methanol (solvent B), 45% B to 85% B in 9 min; 85% B for 6 min; stop time 16 min. Flash column chromatography was performed using an Interchim PuriFlash 430 automated flash chromatography system (Interchim, Montluçon, France) with Davisil LC60A 20–45 μm silica from Grace Davison or PuriFlash SIHP 30 μm columns. Nuclear magnetic resonance (NMR) spectra were measured on a Bruker Avance III HD NMR spectrometer (Bruker Daltonik GmbH, Bremen, Germany) at 300 MHz in the Organic Chemistry Institute, Eberhard Karls Universität Tübingen. The chemical shifts δ are reported in parts per million (ppm) relative to tetramethylsilane. All spectra were calibrated against the (residual proton) peak of the deuterated solvent used. Mass spectra were performed on an Advion Expression S electrospray ionization mass spectrometer (ESI-MS) with an Advion Plate Express (TLC interface) (Advion, Ithaka, NY, USA).

3.1.1. Synthesis of 2-Alkylimidzole **1**

1-(4-Fluorophenyl)-2-(2-fluoropyridin-4-yl)ethane-1,2-dione (**4**) [20]. 1-(4-Fluorophenyl)-2-(2-fluoropyridin-4-yl)ethan-1-one (**3**) (1500 mg, 6.43 mmol) was dissolved in glacial acetic acid (10 mL) and selenium dioxide (928 mg, 8.36 mmol) was added. The reaction mixture was heated to

50 °C for 3 h. After cooling to rt, the reaction was filtered and the solvent was removed under reduced pressure. The crude product was taken up in ethyl acetate and washed with saturated $NaHCO_3$ solution. The aqueous layer was adjusted to pH 10 with 1 M aq. NaOH solution and extracted twice with ethyl acetate. The combined organic layers were dried over anhydrous Na_2SO_4, the solvent was removed under reduced pressure and the residue was purified by flash chromatography (SiO_2, *n*-hexane/EtOAc 9:1 to 7:3) to give an orange solid (987 mg, 62%). ^{1}H-NMR (300 MHz, DMSO-d_6) δ 7.43–7.53 (m, 2H), 7.69 (d, *J* = 0.8 Hz, 1H), 7.83 (dt, *J* = 5.0, 1.7 Hz, 1H), 8.09–8.18 (m, 2H), 8.55 (d, *J* = 5.1 Hz, 1H); MS-ESI (*m*/*z*) 301.9 $[M + Na + MeOH]^+$; HPLC: t_R = 5.73 min.

4-(2-Ethyl-4-(4-fluorophenyl)-1H-imidazol-5-yl)-2-fluoropyridine (**5**). Compound **4** (250 mg, 1.01 mmol) was dissolved in methanol (5 mL). Subsequently, 7 M ammonia in methanol solution (2.89 mL, 20.23 mmol) and propionaldehyde (88.11 mg, 1.52 mmol) were added successively. The reaction mixture was heated to 80 °C for 4 h. After removing the solvent under reduced pressure, the crude product was directly purified by flash chromatography (SiO_2, DCM/EtOH 97:3) to give a white solid (125 mg, 43%). ^{1}H-NMR (300 MHz, DMSO-d_6) δ 1.28 (t, *J* = 7.6 Hz, 3H), 2.64–2.77 (m, 2H), 7.09 (s, 1H), 7.17–7.40 (m, 3H), 7.47–7.56 (m, 2H), 8.06 (d, *J* − 5.4 Hz, 1H), 12.41 (br. s, 1H); MS-ESI (*m*/*z*) 286.0 $[M + H]^+$, 284.0 $[M - H]^-$; HPLC: t_R = 3.68 min.

4-(2-Ethyl-4-(4-fluorophenyl)-1H-imidazol-5-yl)-N-(1-phenylethyl)pyridin-2-amine (**1**). Compound **5** (60 mg, 0.21 mmol) was dissolved in α-methylbenzylamine (1 mL) and heated for 72 h to 160 °C. After cooling to rt, the crude mixture was purified by flash chromatography (SiO_2, DCM/EtOH 97:3) to give a white solid (57 mg, 68%). ^{1}H-NMR (300 MHz, $CDCl_3$) δ 1.18–1.25 (m, 3H), 1.38–1.44 (m, 3H), 2.63 (q, *J* = 7.6 Hz, 2H), 4.44 (quin, *J* = 6.5 Hz, 1H), 5.03 (d, *J* = 5.7 Hz, 1H), 6.3 (br. s, 1H), 6.65 (d, *J* = 4.7 Hz, 1H), 6.91–6.99 (m, 2H), 7.10–7.25 (m, 5H), 7.33 (dd, *J* = 8.0, 5.6 Hz, 2H), 7.90 (d, *J* = 5.4 Hz, 1H); ^{13}C-NMR (75 MHz, $CDCl_3$) δ 12.6, 21.7, 24.3, 51.8, 104.0, 111.4, 115.5 (d, *J* = 21.6 Hz), 125.6, 126.9, 128.5, 130.0 (d, *J* = 8.3 Hz), 144.3, 147.8, 150.2, 158.1, 162.3 (d, *J* = 247.7 Hz); MS-ESI (*m*/*z*) 387.1 $[M + H]^+$; 385.1 $[M - H]^-$; HPLC: t_R = 7.23 min (100% purity).

3.1.2. Synthesis of 2-Alkylimidzole **2**

4-(Triisopropylsilyl)oxy)butanal (**9**). 4-(Triisopropylsilyl)oxy)butan-1-ol (**8**) [21] (4,600 mg, 18.68 mmol) was dissolved in MeCN (50 mL) before $Cu(MeCN)_4CF_3SO_3$ (352 mg, 0.93 mmol), 2,2′-bipyridyl (149 mg, 0.93 mmol), TEMPO (146 mg, 0.93 mmol) and *N*-methylimidazole (154 mg, 1.87 mmol) were added successively. The mixture was stirred at rt for 16 h. *n*-Hexane and water were added and the organic layer was separated. The aqueous layer was extracted three times with diethyl ether. The combined organic layers were washed with brine and dried over anhydrous Na_2SO_4. The solvent was removed under reduced pressure and the residue was purified by flash chromatography (SiO_2, *n*-hexane/EtOAc 90:10) to yield a yellowish oil (2580 mg, 56%). ^{1}H-NMR (300 MHz, $CDCl_3$) δ 0.99–1.13 (m, 21H), 1.67–1.79 (m, 2H), 2.55 (m, 2H), 3.72 (dt, *J* = 16.6, 6.5 Hz, 2H), 9.39 (s, 1H).

1-(4-Fluorophenyl)-2-(2-((3-methylbutan-2-yl)amino)pyridin-4-yl)ethane-1,2-dione (**7**). *tert*-Butyl-(4-(2-(4-fluorophenyl)-2-oxoethyl)pyridin-2-yl)(3-methylbutan-2-yl)carbamate (**6**) (395 mg, 0.99 mmol) was dissolved in glacial acetic acid (8 mL). Selenium dioxide (142 mg, 1.28 mmol) was added and the reaction was heated to reflux temperature for 1.5 h. After cooling to rt, the reaction was filtered and the solvent was removed under reduced pressure. The crude product was taken up in ethyl acetate and washed with saturated $NaHCO_3$ solution. The aqueous layer was adjusted to pH 10 with 1 M aq. NaOH and extracted twice with ethyl acetate. The combined organic layers were dried over anhydrous Na_2SO_4, the solvent was removed under reduced pressure and the residue was purified by flash chromatography (SiO_2, *n*-hexane/EtOAc 80:20 to 60:40) to give a white solid (121 mg, 39%). ^{1}H-NMR (300 MHz, $CDCl_3$) δ 0.95 (dd, *J* = 10.0, 6.8 Hz, 6H), 1.15 (d, *J* = 6.5 Hz, 3H), 1.82 (dq, *J* = 12.3, 6.8 Hz, 1H), 3.69–3.78 (m, 1H), 6.82 (s, 1H), 6.91 (dd, *J* = 5.2, 1.4 Hz, 1H), 7.18–7.25 (m, 2H), 7.94–8.09 (m, 2H), 8.25 (dd, *J* = 5.2, 0.5 Hz, 1H); MS-ESI (*m*/*z*) 315.1 $[M + H]^+$; 313.1 $[M - H]^-$; HPLC: t_R = 5.07 min.

4-(4-(4-Fluorophenyl)-2-(3-((triisopropylsilyl)oxy)propyl)-1H-imidazol-5-yl)-N-(3-methylbutan-2-yl)pyridin-2-amine (**10**). Compound **7** (125 mg, 0.40 mmol) was dissolved in methanol (10 mL). Ammonium acetate (613 mg, 7.95 mmol) and aldehyde **9** (147 mg, 0.60 mmol) were added. The reaction was heated to 80 °C for 4 h. After cooling to rt, saturated $NaHCO_3$ solution was added. The aqueous phase was adjusted to pH 10 with 1 M aq. NaOH and extracted thrice with ethyl acetate. The combined organic layers were dried over anhydrous Na_2SO_4, the solvent was removed under reduced pressure and the residue was purified by flash chromatography (SiO_2, *n*-hexane/EtOAc 50:50 to 0:100) to give a colorless oil (43 mg, 20%). ^{1}H-NMR (300 MHz, $CDCl_3$) δ 0.87 (dd, *J* = 6.8, 1.6 Hz, 6H), 1.03–1.05 (m, 24H), 1.71 (td, *J* = 6.7, 5.4 Hz, 1H), 1.93–2.06 (m, 2H), 2.96 (d, *J* = 6.1 Hz, 2H), 3.34–3.51 (m, 1H), 3.84 (d, *J* = 4.5 Hz, 2H), 4.39 (d, *J* = 8.2 Hz, 1H), 6.19–6.54 (m, 1H), 6.57–6.70 (m, 1H), 6.94–7.15 (m, 2H), 7.31–7.44 (m, 1H), 7.57 (br. s, 1H), 7.89 (d, *J* = 4.9 Hz, 1H), 9.96–10.24 (m, 1H); MS-ESI (*m*/*z*) 539.2 $[M + H]^+$, 537.1 $[M - H]^-$; HPLC: t_R = 5.12 min.

3-(4-(4-Fluorophenyl)-5-(2-((3-methylbutan-2-yl)amino)pyridin-4-yl)-1H-imidazol-2-yl)propan-1-ol (**2**). Compound **10** (125 mg, 0.40 mmol) was dissolved in methanol (10 mL) and 2 M aq. HCl solution was added. The reaction was stirred at rt for 1 h. The organic solvent was removed under reduced pressure and the aqueous residue was treated with saturated $NaHCO_3$ solution. A white precipitate was formed, collected by filtration and taken up in ethyl acetate. The organic solution was dried over anhydrous Na_2SO_4 and the compound was purified by flash chromatography (SiO_2, DCM/EtOH 92:08 to 85:15) to give an off-white solid (22 mg, 73%). ^{1}H-NMR (300 MHz, $CDCl_3$) δ 0.85 (d, *J* = 6.5 Hz, 6H), 1.02 (d, *J* = 6.6 Hz, 3H), 1.63–1.75 (m, 1H), 1.98 (dt, *J* = 11.5, 5.8 Hz, 2H), 2.86–2.96 (m, 2H), 3.32–3.43 (m, 1H), 3.79 (t, *J* = 5.3 Hz, 2H), 4.53 (d, *J* = 8.5 Hz, 1H), 6.45 (s, 1H), 6.57 (d, *J* = 4.5 Hz, 1H), 7.03 (t, *J* = 8.6 Hz, 2H), 7.46 (dd, *J* = 8.6, 5.4 Hz, 2H), 7.90 (d, *J* = 5.4 Hz, 1H); ^{13}C-NMR (75 MHz, DMSO-d_6) δ 16.9, 17.7, 18.8, 26.5, 29.8, 32.5, 52.2, 62.3, 103.8, 110.5, 115.6 (d, *J* = 21.6 Hz), 130.1 (d, *J* = 7.7 Hz), 147.8, 148.9, 158.5, 162.4 (d, *J* = 247.7 Hz); MS-ESI (*m*/*z*) 383.1 $[M + H]^+$, 381.1 $[M - H]^-$; HPLC: t_R = 6.53 min (100% purity).

3.2. HLM Stability Test

Pooled human liver microsomes (adult male & female) were purchased from Merck (Schnelldorf, Germany). These microsomes were characterized in protein and CYP content. All incubations (final total volume 1050 µL) were made in the presence of an NADPH-regenerating system, consisting of 5 mM Glucose-6-phosphate, 5 U/mL Glucose-6-phosphate dehydrogenase and 1 mM $NADP^+$. The substrate (100 µM), the NADPH regenerating system and 4 mM $MgCl_2 \times 6\ H_2O$ in 0.1 M Tris buffer (pH 7.4 at 37 °C) were preincubated for 5 min in an incubator at 37 °C and 750 rpm. The incubation mix was split into 50 µL aliquots and the reaction was started by addition of the HLM. Thereby the microsomal protein content was standardized to 1 mg/mL. To follow the course of metabolism, the reaction tubes were quenched at selected time points (0, 10, 20, 30, 60, 120, 180 and 240 min) by adding 100 µL internal standard at a concentration of 22.5 µM in MeCN. The samples were vortexed for 30 s and centrifuged (19,800 relative centrifugal force/4 °C/10 min). The supernatant was directly used for LC-MS analysis (for detailed LC-MS conditions, see supplementary materials). All incubations were conducted in triplicates and incubations with heat-inactivated HLM were used to prove that analyte reduction results from metabolic degradation only. In all incubations, a limit of 1% organic solvent was not exceeded.

3.3. CYP Inhibition Test

CYP inhibition (fluorimetric detection) assay was performed by Eurofins Panlabs Inc. (St. Charles, MO, USA) with human recombinant CYP enzyme and the appropriate CYP substrate.

4. Conclusions

Replacement of the sulfur atom present in both known p38α MAP kinase inhibitors **ML3403** and **LN950** by a methylene group results in 2-alkylimidazole derivatives **1** and **2**, showing remarkably improved microsomal stability. Both compounds undergo minimal hydroxylation and *N*-dealkylation upon incubation with HLM. Trisubstituted imidazoles **1** and **2** display a 4-fold increase in binding affinity toward the kinase and possess a similar inhibition profile of p38α MAP kinase and the LPS-stimulated TNF-α release from HWB like their 2-alkylsulfanylimidazole counterparts **ML3403** and **LN950**. However, the exchange of the sulfur atom present in **ML3403** and **LN950** by a methylene group is accompanied with a slightly higher CYP inhibition profile of **1** and **2**. The most potent inhibitor, 2-alkylimidazole **2**, inhibits both the p38α MAP kinase as well as the LPS-stimulated TNF-α release from human whole blood in the low double-digit nanomolar range. Moreover, the excellent metabolic profile of **2** gives advantage over the mixed pharmacokinetics of the p38α MAP kinase reference inhibitor **ML3403** and its active metabolite. Therefore, 2-alkylimidazole **2** is a good alternative to evaluate the role of this kinase in in vitro and in vivo studies.

Supplementary Materials: The following are available online, Figure S1 (Structure of **VX-745**) and Tables S1–S17 (metabolic stability of the title compounds in HLM and metabolite formation).

Acknowledgments: We thank Katharina Bauer and Jens Strobach for their assistance in the p38α MAP kinase ELISA assay. Luiza Oprezka is gratefully acknowledged for her assistance in the metabolism study. This study was supported by the Federal Ministry of Education and Research (BMBF) within the BioPharma—Neuroallianz consortium.

Author Contributions: F.H., U.H., E.D., M.K., C.S., W.A., S.L. and P.K. conceived and designed the experiments; F.H. and U.H. performed synthesis; E.D. performed the metabolism experiments; C.S. and M.K. performed the biological evaluation in vitro; F.H., W.A., S.L. and P.K. analyzed the data; F.H. and P.K. wrote the paper.

Conflicts of Interest: The authors declare no conflict of interest.

References

1. Bachstetter, A.D.; Xing, B.; de Almeida, L.; Dimayuga, E.R.; Watterson, D.M.; van Eldik, L.J. Microglial p38α MAPK is a key regulator of proinflammatory cytokine up-regulation induced by toll-like receptor (TLR) ligands or beta-amyloid (Aβ). *J. Neuroinflamm.* **2011**, *8*, 79. [CrossRef] [PubMed]
2. Hensley, K.; Floyd, R.A.; Zheng, N.-Y.; Nael, R.; Robinson, K.A.; Nguyen, X.; Pye, Q.N.; Stewart, C.A.; Geddes, J.; Markesbery, W.R.; et al. p38 Kinase is activated in the Alzheimer's disease brain. *J. Neurochem.* **1999**, *72*, 2053–2058. [CrossRef] [PubMed]
3. Lee, J.K.; Kim, N.-J. Recent advances in the inhibition of p38 MAPK as a potential strategy for the treatment of Alzheimer's disease. *Molecules* **2017**, *22*. [CrossRef] [PubMed]
4. ClinicalTrials. Gov Registration Number: NCT02423122. Available online: https://clinicaltrials.gov/ct2/show/NCT02423122 (accessed on 17 August 2017).
5. ClinicalTrials. Gov Registration Number: NCT02423200. Available online: https://clinicaltrials.gov/ct2/show/NCT02423200 (accessed on 17 August 2017).
6. Laufer, S.A.; Wagner, G.K.; Kotschenreuther, D.A.; Albrecht, W. Novel substituted pyridinyl imidazoles as potent anticytokine agents with low activity against hepatic cytochrome P450 enzymes. *J. Med. Chem.* **2003**, *46*, 3230–3244. [CrossRef] [PubMed]
7. Laufer, S.A.; Hauser, D.R.J.; Domeyer, D.M.; Kinkel, K.; Liedtke, A.J. Design, synthesis, and biological evaluation of novel Tri- and tetrasubstituted imidazoles as highly potent and specific ATP-mimetic inhibitors of p38 MAP kinase: Focus on optimized interactions with the enzyme's surface-exposed front region. *J. Med. Chem.* **2008**, *51*, 4122–4149. [CrossRef] [PubMed]
8. Munoz, L.; Ramsay, E.E.; Manetsch, M.; Ge, Q.; Peifer, C.; Laufer, S.; Ammit, A.J. Novel p38 MAPK inhibitor ML3403 has potent anti-inflammatory activity in airway smooth muscle. *Eur. J. Pharmacol.* **2010**, *635*, 212–218. [CrossRef] [PubMed]
9. Graziosi, L.; Mencarelli, A.; Santorelli, C.; Renga, B.; Cipriani, S.; Cavazzoni, E.; Palladino, G.; Laufer, S.; Burnet, M.; Donini, A.; et al. Mechanistic role of p38 MAPK in gastric cancer dissemination in a rodent model peritoneal metastasis. *Eur. J. Pharmacol.* **2012**, *674*, 143–152. [CrossRef] [PubMed]

10. Koch, D.A.; Silva, R.B.M.; de Souza, A.H.; Leite, C.E.; Nicoletti, N.F.; Campos, M.M.; Laufer, S.; Morrone, F.B. Efficacy and gastrointestinal tolerability of ML3403, a selective inhibitor of p38 MAP kinase and CBS-3595, a dual inhibitor of p38 MAP kinase and phosphodiesterase 4 in CFA-induced arthritis in rats. *Rheumatology* **2014**, *53*, 425–432. [CrossRef] [PubMed]
11. Koch, P.; Bäuerlein, C.; Jank, H.; Laufer, S. Targeting the ribose and phosphate binding site of p38 mitoge*N*-activated protein (MAP) kinase: Synthesis and biological testing of 2-alkylsulfanyl-, 4(5)-aryl-, 5(4)-heteroaryl-substituted imidazoles. *J. Med. Chem.* **2008**, *51*, 5630–5640. [CrossRef] [PubMed]
12. Kammerer, B.; Scheible, H.; Zurek, G.; Godejohann, M.; Zeller, K.P.; Gleiter, C.H.; Albrecht, W.; Laufer, S. In vitro metabolite identification of ML3403, a 4-pyridinylimidazole-type p38 MAP kinase inhibitor by LC-Qq-TOF-MS and LC-SPE-cryo-NMR/MS. *Xenobiotica* **2007**, *37*, 280–297. [CrossRef] [PubMed]
13. Kammerer, B.; Scheible, H.; Albrecht, W.; Gleiter, C.H.; Laufer, S. Pharmacokinetics of ML3403 ({4–5-(4-fluorophenyl)-2-methylsulfanyl-3*H*-imidazol-4-yl-pyridin-2-yl}-(1-phenylethyl)-amine), a 4-Pyridinylimidazole-type p38 mitoge-activated protein kinase inhibitor. *Drug Metab. Dispos.* **2007**, *35*, 875–883. [CrossRef] [PubMed]
14. Hoover, J.M.; Stahl, S.S. Highly practical copper(I)/TEMPO catalyst system for chemoselective aerobic oxidation of primary alcohols. *J. Am. Chem. Soc.* **2011**, *133*, 16901–16910. [CrossRef] [PubMed]
15. Goettert, M.; Graeser, R.; Laufer, S.A. Optimization of a nonradioactive immunosorbent assay for p38alpha mitogen-activated protein kinase activity. *Anal. Biochem.* **2010**, *406*, 233–234. [CrossRef] [PubMed]
16. Ansideri, F.; Lange, A.; El-Gokha, A.; Boeckler, F.M.; Koch, P. Fluorescence polarization-based assays for detecting compounds binding to inactive c-Jun *N*-terminal kinase 3 and p38α mitogen-activated protein kinase. *Anal. Biochem.* **2016**, *503*, 28–40. [CrossRef] [PubMed]
17. Zegzouti, H.; Goueli, S.A. (Eds.) *Kinase Screening and Profiling: Methods and Protocols*; Humana Press: New York, NY, USA, 2016.
18. Adams, J.L.; Boehm, J.C.; Kassis, S.; Gorycki, P.D.; Webb, E.F.; Hall, R.; Sorenson, M.; Lee, J.C.; Ayrton, A.; Griswold, D.E.; et al. Pyrimidinylimidazole inhibitors of CSBP/P38 kinase demonstrating decreased inhibition of hepatic cytochrome P450 enzymes. *Bioorg. Med. Chem. Lett.* **1998**, *8*, 3111–3116. [CrossRef]
19. Lynch, T.; Price, A.L. The Effect of Cytochrome P450 metabolism on drug response, interactions, and adverse effects. *Am. Fam. Phys.* **2007**, *76*, 391–396.
20. Koch, P.; Jahns, H.; Schattel, V.; Goettert, M.; Laufer, S. Pyridinylquinoxalines and pyridinylpyridopyrazines as lead compounds for novel p38 alpha mitogen-activated protein kinase inhibitors. *J. Med. Chem.* **2010**, *53*, 1128–1137. [CrossRef] [PubMed]
21. Günther, M.; Juchum, M.; Kelter, G.; Fiebig, H.; Laufer, S. Lung Cancer: EGFR Inhibitors with low Nanomolar activity against a therapy-resistant L858R/T790M/C797S mutant. *Angew. Chem. Int. Ed. Engl.* **2016**, *55*, 10890–10894. [CrossRef] [PubMed]

Sample Availability: Samples of the compounds **1** and **2** are available from the authors.

Supplementary Materials

From 2-alkylsulfanylimidazoles to 2-alkylimidazoles: An approach towards metabolically more stable p38α MAP kinase inhibitors

Fabian Heider[1], Urs Haun[1], Eva Döring[1], Mark Kudolo[1], Catharina Sessler[1], Wolfgang Albrecht[2], Stefan Laufer[1] and Pierre Koch[1,*]

[1]Department of Pharmaceutical and Medicinal Chemistry, Institute of Pharmaceutical Sciences, Eberhard Karls Universität Tübingen, Auf der Morgenstelle 8, 72076 Tübingen, Germany; pierre.koch@uni-tuebingen.de
[2]Teva-ratiopharm, Graf-Arco-Str. 3, 89079 Ulm, Germany

Table of Contents

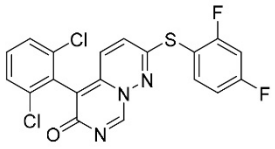

VX-745

Figure S1. Structure of selective p38α MAP kinase inhibitor **VX-745**.

Screening of Metabolites by LC-MS Analysis

Metabolite formation was analyzed with an Alliance 2695 Separations Module (Waters GmbH, Eschborn). Samples maintained at 4°C, the column temperature was set to 40°C and injection volume was 10 µL. The chromatographic separation for analytes **1** and **ML3404** was performed on a Phenomenex Synergi Max-RP column (150 x 4.6 mm; 5 µm); **LN950** and **2** on a Phenomenex Synergi Polar-RP column (150 x 4.6 mm; 5 µm) with a precolumn of the same material, respectively. An isocratic gradient of 8.5 min with 30% solvent A (90% H_2O, 10% ACN, 0.1% formic acid) and 70% solvent B (ACN, 0.1% formic acid) at a flow rate of 400 µL/min was used for **LN950**. **1** and **ML3404** were chromatographically separated by a binary gradient of 11.25 min with the equal solvents as mentioned before at a flow rate of 400 µL/min. The initial composition of 10% B was held for 20 sec, followed by a linear gradient up to 85% B in 5.8 min, holding for 30 sec, immediately changing to 10% B and reequilibrating at the end. The detection was performed on a Micromass Quattro micro triple quadrupole mass spectrometer (Waters GmbH, Eschborn) using the electrospray-ionization in the positive-mode. Correspondent to the analyte the spray voltage was set to 3.0-4.0 kV. The heated capillary operated at 250°C and the desolvation gas flow worked at 500 L/h.

Metabolic stability of ML3403 in HLM

Table S1. Degradation of **ML3404**

ML3403 [min]	#1 %	#2 %	#3 %	AVERAGE %	standard deviation
0	100.00	100.00	100.00	100.00	0.00
10	79.36	81.21	81.21	80.59	1.07
20	68.53	70.91	67.46	68.97	1.77
30	56.67	57.76	59.38	57.93	1.36
60	40.42	43.10	44.89	42.80	2.25
120	32.28	31.22	31.66	31.72	0.53
180	24.12	24.00	--*	24.06	0.08
240	15.55	15.71	17.47	16.25	1.07

Table S2. Formation of Metabolite **ML3603**: Sulfoxide of **ML3403** (*m*/*z* 421.5)

421.5 [min]	#1 %	#2 %	#3 %	AVERAGE %	standard deviation
0	0.60	0.67	0.62	0.63	0.04
10	15.61	14.30	15.67	15.19	0.78
20	25.79	26.25	24.86	25.63	0.71
30	38.75	37.61	35.26	37.21	1.78
60	52.92	52.65	53.40	52.99	0.38
120	74.60	79.32	66.69	73.54	6.38
180	73.27	70.16	--*	71.71	2.20
240	83.78	71.29	69.59	74.88	7.75

Table S3. Formation of Metabolite: Sulfone of **ML3403** (*m*/*z* 437.4)

437.4 [min]	#1 %	#2 %	#3 %	AVERAGE %	standard deviation
0	0.00	0.00	0.00	0.00	0.00
10	0.09	0.11	0.08	0.10	0.01
20	0.22	0.33	0.37	0.31	0.08
30	0.70	0.68	0.52	0.63	0.10
60	1.91	1.65	1.63	1.73	0.16
120	2.94	4.27	3.40	3.54	0.67
180	4.31	4.22	--*	4.27	0.06
240	6.80	4.89	5.65	5.78	0.96

Table S4. Formation of Metabolite: *N*-dealkylation of **ML3403** (*m/z* 301.4)

301.4 [min]	#1 %	#2 %	#3 %	AVERAGE %	standard deviation
0	0.00	0.01	0.00	0.00	0.01
10	0.93	0.87	0.80	0.87	0.06
20	1.00	1.50	1.27	1.26	0.25
30	1.95	1.90	1.87	1.91	0.04
60	2.85	2.66	2.60	2.70	0.13
120	3.09	3.15	2.90	3.05	0.13
180	2.75	2.58	--*	2.67	0.13
240	2.71	1.97	2.09	2.26	0.40

Table S5. Formation of Metabolite: *N*-dealkylation + sulfoxidation of **ML3403** (*m/z* 317.5)

317.5 [min]	#1 %	#2 %	#3 %	AVERAGE %	standard deviation
0	0.00	0.00	0.00	0.00	0.00
10	0.05	0.07	0.04	0.05	0.01
20	0.18	0.26	0.24	0.23	0.04
30	0.26	0.36	0.31	0.31	0.05
60	0.81	0.81	0.89	0.84	0.05
120	2.52	3.23	1.88	2.54	0.67
180	3.09	2.96	--*	3.03	0.09
240	5.74	2.97	3.15	3.95	1.55

*sample was unanalyzable

Metabolic stability of 2-alkylimidazole 1 in HLM

Table S6. Degradation of **1**

1 [min]	#1 %	#2 %	#3 %	AVERAGE %	standard deviation
0	100.00	100.00	100.00	100.00	0.00
10	92.49	92.16	93.50	92.72	0.70
20	89.74	90.56	88.96	89.75	0.80
30	87.23	90.22	86.43	87.96	2.00
60	85.50	86.45	86.86	86.27	0.70
120	84.04	83.16	83.76	83.65	0.45
180	81.61	80.46	80.62	80.90	0.62
240	80.88	78.33	80.04	79.75	1.30

Table S7. Formation of Metabolite: *N*-dealkylation of **1** (*m*/*z* 283.6)

283.6 [min]	#1 %	#2 %	#3 %	AVERAGE %	standard deviation
0	0.15	0.36	0.45	0.32	0.15
10	2.03	1.44	0.88	1.45	0.57
20	1.81	0.92	1.45	1.40	0.45
30	2.02	1.67	2.19	1.96	0.26
60	2.22	1.33	1.27	1.61	0.53
120	2.37	1.99	2.97	2.44	0.49
180	4.32	2.41	2.61	3.11	1.05
240	3.48	1.68	2.61	2.59	0.90

Table S8. Formation of Metabolite: oxidation (hydroxylation or *N*-oxide) of **1** [peak 1] (*m*/*z* 403.3)

403.3 #1 [min]	#1 %	#2 %	#3 %	AVERAGE %	standard deviation
0	0.19	0.20	0.31	0.23	0.06
10	0.73	0.93	0.79	0.82	0.10
20	0.91	0.91	0.78	0.87	0.07
30	0.91	1.01	0.93	0.95	0.05
60	1.48	1.62	0.98	1.36	0.34
120	1.41	1.25	1.15	1.27	0.13
180	1.26	1.70	1.39	1.45	0.23
240	1.63	2.03	1.40	1.69	0.32

Table S9. Formation of Metabolite: oxidation (hydroxylation or *N*-oxide) of **1** [peak 2] (*m*/*z* 403.3)

403.3 #2 [min]	#1 %	#2 %	#3 %	AVERAGE %	standard deviation
0	0.66	0.67	0.57	0.63	0.06
10	1.66	2.06	2.06	1.93	0.23
20	1.79	2.80	1.67	2.08	0.62
30	2.07	2.47	1.85	2.13	0.32
60	2.07	2.90	1.81	2.26	0.57
120	2.40	3.84	2.14	2.80	0.92
180	2.89	2.96	2.26	2.70	0.38
240	2.67	3.92	2.53	3.04	0.77

Table S10. Formation of Metabolite: oxidation (hydroxylation or *N*-oxide) + *N*-dealkylation of **1** (*m*/*z* 299.5)

299.5 [min]	#1 %	#2 %	#3 %	AVERAGE %	standard deviation
0	1.53	1.55	1.67	1.58	0.08
10	3.66	4.22	3.66	3.85	0.32
20	4.07	4.86	3.91	4.28	0.51
30	3.82	5.28	4.48	4.53	0.73
60	5.28	7.05	4.53	5.62	1.30
120	5.37	7.77	4.59	5.91	1.66
180	6.13	6.54	5.66	6.11	0.44
240	6.11	9.20	5.66	6.99	1.93

Metabolic stability of LN950 in HLM

Table S11. Degradation of **LN950**

LN950 [min]	#1 %	#2 %	#3 %	AVERAGE %	standard deviation
0	100.00	100.00	100.00	100.00	0.00
10	87.14	86.54	86.92	86.86	0.31
20	78.90	77.41	75.93	77.42	1.48
30	63.72	63.03	59.15	61.96	2.47
60	54.65	53.40	47.91	51.99	3.59
120	40.46	37.14	34.09	37.23	3.19
180	32.27	34.26	29.76	32.10	2.25
240	30.74	29.49	25.25	28.49	2.88

Table S12. Formation of Metabolite: Sulfoxide of **LN950** (*m/z* 417.2)

417.2 [min]	#1 %	#2 %	#3 %	AVERAGE %	standard deviation
0	0.00	0.00	0.00	0.00	0.00
10	17.81	17.98	19.04	18.28	0.67
20	26.33	26.44	28.11	26.96	0.99
30	43.59	44.48	46.49	44.85	1.49
60	51.15	52.58	52.16	51.97	0.73
120	64.39	63.22	63.12	63.58	0.70
180	68.65	70.55	71.79	70.33	1.58
240	76.67	73.48	74.41	74.85	1.64

Table S13. Formation of Metabolite: Sulfone of **LN950** (*m/z* 433.2)

433.2 [min]	#1 %	#2 %	#3 %	AVERAGE %	standard deviation
0	0.00	0.00	0.00	0.00	0.00
10	0.00	0.16	0.16	0.11	0.09
20	0.00	0.43	0.45	0.29	0.25
30	1.09	1.16	1.45	1.24	0.19
60	1.77	1.97	2.27	2.00	0.25
120	3.27	4.09	3.96	3.77	0.44
180	4.33	4.91	5.65	4.96	0.67
240	5.33	5.19	6.27	5.59	0.59

Table S14. Formation of Metabolite: *N*-dealkylation of **LN950** (*m*/*z* 331.1)

331.1 [min]	#1 %	#2 %	#3 %	AVERAGE %	standard deviation
0	0.00	0.00	0.00	0.00	0.00
10	2.11	2.30	2.26	2.23	0.10
20	3.27	3.35	3.35	3.32	0.04
30	5.42	5.38	5.33	5.38	0.05
60	5.95	6.09	5.83	5.96	0.13
120	6.31	6.23	5.56	6.03	0.41
180	6.21	6.20	6.03	6.15	0.10
240	6.11	6.11	5.58	5.93	0.30

Metabolic stability of 2-alkylimidazole 2 in HLM

Table S15. Degradation of **2**

2 [min]	#1 %	#2 %	#3 %	AVERAGE %	standard deviation
0	100.00	100.00	100.00	100.00	0.00
10	95.05	97.48	98.92	97.15	1.96
20	91.81	94.65	94.25	93.57	1.54
30	91.71	89.70	94.12	91.84	2.21
60	91.28	88.75	95.94	91.99	3.65
120	91.51	89.68	93.50	91.57	1.91
180	90.53	86.95	93.80	90.42	3.43
240	89.68	87.61	91.90	89.73	2.15

Table S16. Formation of Metabolite: *N*-dealkylation of **2** (*m*/*z* 313.3)

313.1 [min]	#1 %	#2 %	#3 %	AVERAGE %	standard deviation
0	0.00	0.00	0.00	0.00	0.00
10	1.36	1.84	1.51	1.57	0.25
20	1.46	1.51	1.68	1.55	0.12
30	1.68	1.64	1.89	1.73	0.13
60	2.46	2.01	2.38	2.28	0.24
120	3.00	2.34	2.59	2.65	0.33
180	3.17	2.74	3.18	3.03	0.25
240	3.73	3.03	3.50	3.42	0.36

Table S17. Formation of Metabolite: oxidation (hydroxylation or *N*-oxide) + *N*-dealkylation of **2** (*m*/*z* 399.2)

399.2 [min]	#1 %	#2 %	#3 %	AVERAGE %	standard deviation
0	0.00	0.00	0.00	0.00	0.00
10	1.81	2.39	1.91	2.04	0.31
20	2.25	2.20	2.27	2.24	0.04
30	2.50	2.41	2.47	2.46	0.04
60	3.12	2.91	3.36	3.13	0.22
120	3.93	3.76	3.76	3.81	0.10
180	4.11	3.73	4.17	4.00	0.24
240	5.47	4.42	4.92	4.94	0.53

Publication II

Heider, F.; Ansideri, F.; Tesch, R.; Pantsar, T.; Haun, U.; Döring, E.; Kudolo, M.; Poso, A.; Albrecht, W.; Laufer, S. A.; Koch, P. – Pyridinylimidazoles as dual glycogen synthase kinase 3β/p38α mitogen-activated protein kinase inhibitors. *European Journal of Medicinal Chemistry* **2019**, *175*, 309-329.

European Journal of Medicinal Chemistry 175 (2019) 309–329

Contents lists available at ScienceDirect

European Journal of Medicinal Chemistry

journal homepage: http://www.elsevier.com/locate/ejmech

Research paper

Pyridinylimidazoles as dual glycogen synthase kinase 3β/p38α mitogen-activated protein kinase inhibitors

Fabian Heider [a], Francesco Ansideri [a], Roberta Tesch [a], Tatu Pantsar [b, c], Urs Haun [a], Eva Döring [a], Mark Kudolo [a], Antti Poso [b, c], Wolfgang Albrecht [d], Stefan A. Laufer [a], Pierre Koch [a, e, *]

[a] Department of Pharmaceutical and Medicinal Chemistry, Institute of Pharmaceutical Sciences, Eberhard Karls Universität Tübingen, Auf der Morgenstelle 8, 72076, Tübingen, Germany
[b] School of Pharmacy, University of Eastern Finland, P.O. BOX 1627, 70211, Kuopio, Finland
[c] Department of Internal Medicine VIII, University Hospital Tübingen, Otfried-Müller-Strasse 14, 72076, Tübingen, Germany
[d] Teva-ratiopharm, Graf-Arco-Str. 3, 89079, Ulm, Germany
[e] Department of Pharmaceutical/Medicinal Chemistry II, Institute of Pharmacy, University of Regensburg, Universitätsstraße 31, 93053, Regensburg, Germany

ARTICLE INFO

Article history:
Received 27 January 2019
Received in revised form
29 March 2019
Accepted 13 April 2019
Available online 24 April 2019

Keywords:
Kinase inhibitors
Pyridinylimidazoles
Glycogen synthase kinase 3β
p38α MAP kinase
Dual inhibitors
Alzheimer's disease

ABSTRACT

Compounds simultaneously inhibiting two targets that are involved in the progression of the same complex disease may exhibit additive or even synergistic therapeutic effects. Here we unveil 2,4,5-trisubstituted imidazoles as dual inhibitors of p38α mitogen-activated protein kinase and glycogen synthase kinase 3β (GSK3β). Both enzymes are potential therapeutic targets for neurodegenerative disorders, like Alzheimer's disease. A set of 39 compounds was synthesized and evaluated in kinase activity assays for their ability to inhibit both target kinases. Among the synthesized compounds, potent dual-target-directed inhibitors showing IC_{50} values down to the low double-digit nanomolar range, were identified. One of the best balanced dual inhibitors presented in here is *N*-(4-(2-ethyl-4-(4-fluorophenyl)-1*H*-imidazol-5-yl)pyridin-2-yl)cyclopropanecarboxamide (**20c**) (p38α, IC_{50} = 16 nM; GSK3β, IC_{50} = 35 nM) featuring an excellent metabolic stability and an appreciable isoform selectivity over the closely related GSK3α. Our findings were rationalized by computational docking studies based on previously published X-ray structures.

1. Introduction

Neurodegenerative disorders, like Alzheimer's disease (AD), present one of the major medical challenges of the 21st century. It was estimated that in 2015 more than 46 million people worldwide were affected by AD [1]. With globally increasing life expectancy, the prevalence of AD is going to rise constantly. Currently, there are four active pharmaceutical ingredients approved by the FDA for the treatment of AD. However, none of them is able to stop or cure the disease. Therefore, there is a high unmet medical need for the development of new treatment options and strategies.

In the last decade, much effort has been put into the development of new therapeutic concepts – with little success. One of the reasons for the low clinical success rate of new therapies is undoubtedly the still poor understanding of the pathophysiology of AD. As AD is a complex disease with a multicausal pathogenesis, a multi-target approach might be a promising and required strategy for the treatment of this devastating condition.

Several kinases have been implicated in the pathology of AD. Glycogen synthase kinase3β (GSK3β) is a serine/threonine kinase for which significant evidence has been collected for its involvement in AD pathology over the years [2–5]. GSK3β is responsible for the hyperphosphorylation of the microtubule-associated protein tau, and is often referred to as a tau-kinase [6,7]. Overactivity of GSK3β has also been connected to an increased production of β-amyloids (Aβ) [8], memory deficits [9], oxidative stress and neuroinflammation [10]. Thus, the kinase plays a crucial role in almost every pathway leading to the hallmarks of AD [11]. The p38α mitogen-activated protein (MAP) kinase [12] is a serine/threonine kinase, which has been identified as a drug target for chronic

* Corresponding author. Department of Pharmaceutical and Medicinal Chemistry, Institute of Pharmaceutical Sciences, Eberhard Karls Universität Tübingen, Auf der Morgenstelle 8, 72076, Tübingen, Germany.
E-mail address: pierre.koch@uni-tuebingen.de (P. Koch).

https://doi.org/10.1016/j.ejmech.2019.04.035
0223-5234/

inflammatory diseases since the mid-1990s [13]. This enzyme plays a central role in the biosynthesis of proinflammatory cytokines, like the tumor necrosis factor (TNF)-α, both at translational and transcriptional levels. The connection between the kinase and AD was drawn by Hensley et al., who found increased activity of p38α MAP kinase in human postmortem brain tissue from AD patients [14]. Since then, an increasing amount of evidence has been piling up to establish a link between cytokine overproduction in the central nervous system (CNS) modulated by p38α MAP kinase and neuroinflammation [15–18]. Furthermore, the kinase has also been suspected to be involved in the hyperphosphorylation of tau proteins. A study with a brain-penetrant, selective p38α inhibitor significantly diminished tau phosphorylation and signs of insoluble tau aggregates on top of the expected reduction of proinflammatory cytokine released in a tauopathy mouse model [19]. Recently, two phase II studies on the selective p38α MAP kinase inhibitor Neflamapimod for the treatment of AD were completed successfully [20,21]. Two follow-up phase II studies were launched in early 2018 (NCT03435861 & NCT03402659).

GSK3β and p38α MAP kinase both belong to the CMGC group and share an overall sequence similarity of 42%. A closer analysis of their ATP binding pockets reveals several distinctions between the two enzymes (Fig. 1). Most importantly the gatekeeper residue in p38α MAP kinase is Thr106, whereas a slightly bulkier Leu132 occupies this position in GSK3β. Moreover, the hinge region is composed of fairly different amino acids.

Pyridinylimidazoles are versatile scaffolds in kinase drug discovery and have been used to target several kinases such as p38α MAP kinase [22–26], CK1δ [27], TEK [28], (triple mutant) EGFR and the JNK family [29,30]. Recently, synthetic strategies towards 2-alkylsulfanyl-4-aryl-5-(pyridin-4-yl)imidazoles as well as their biological activities were reviewed by our group [31].

A screening of pyridinylimidazole-type p38α MAP kinase inhibitors from our in-house library (TüKIC, Tübingen Kinase Inhibitor Collection) versus GSK3β led to the identification of compound **1a**, serving as a lead compound for this study to design potent dual GSK3β/p38α MAP kinase inhibitors (Fig. 2). Independently from us, compound **1a** has recently been disclosed by Halekotte et al. in an effort to synthesize CK1δ inhibitors [27].

Based on the initial screening data, first structure-activity relationships (SARs) were generated. An amide at the pyridine-C2 position seemed to be crucial for GSK3β activity. It was also assumed that 2,4,5-trisubstituted imidazoles, in general, show a higher affinity towards GSK3β than 1,2,4,5-tetrasubstituted imidazole derivatives. Previous SAR studies on the p38α MAP kinase revealed that a tri- and tetrasubstitution pattern on the central imidazole core as well as a wide variety of substituents at the pyridine-C2 position (including amides) are well tolerated by the kinase [31].

The aim of the present study was to design brain penetrant and metabolically stable dual inhibitors of GSK3β and p38α MAP kinase, which might serve as potential drugs for the treatment of neurodegenerative diseases. A series of 39 pyridinylimidazoles was synthesized and variations at the pyridine-C2 position, the imidazole-C2 and C4 positions as well as on both imidazole-N atoms were performed to further improve the GSK3β inhibitory activity while maintaining the excellent potency on p38α MAP kinase.

2. Results and discussion

2.1. Chemistry

The 2-methylsulfanylimidazoles **1a-u** and 2-benzylsulfanylimidazoles **2a-e** were synthesized by a linear approach. Diversity at the pyridine-C2 position was introduced in the last step of the synthetic sequences (Schemes 1 and 2). The key intermediates 5-(2-aminopyridin-4-yl)imidazoles (**10a**, **10b**) were synthesized by a novel synthetic approach derived from a strategy published by our group in 2008 (Scheme 1) [24]. Starting from *N*-Boc protected 2-amino-4-methylpyridine **3**, a *p*-methoxybenzyl (pMB) moiety was introduced as second protecting group of the amino function. The fully protected 4-picoline **4** was reacted with sodium hexamethyldisilazide (NaHMDS) in THF and ethyl 4-fluorobenzoate to obtain ethanone **5**. An excess of sodium nitrite dissolved in water was added dropwise to an acidic solution of **5** to give α-oximino ketone **6**. Subsequent treatment with Pd/C using hydrogen at atmospheric pressure in methanolic HCl resulted in both, reduction of the oximino group into a primary amino group as well as cleavage of the Boc group. Conveniently, the acid labile pMB was stable under these conditions. Cyclization of aminoketone **7** with potassium thiocyanate followed by the reaction with methyl iodide or benzyl bromide resulted in *S*-substituted intermediates **9a** and **9b**, respectively. Finally, the pMB group was removed in neat trifluoroacetic acid (TFA) with gentle heating to yield the key intermediates **10a** and **10b**.

The acylamino function at the pyridine-C2 position of imidazoles **1b**, **1c**, **1s**, **2b,** and **2c** was introduced via Buchwald-Hartwig arylamidation by reacting known 2-chloropyridine derivatives **11a-b** [26,32] with the corresponding amides in the presence of a Pd catalyst (Scheme 2). In case of imidazoles **1a**,**d-r**,**t-u** and **2a**,**d-e**, the amide moiety was installed depending on the commercial availability of the starting material either by direct acylation of 2-aminopridine derivates **10a** and **10b** with acid chlorides or by reacting **10a** and **10b** with the corresponding carboxylic acids in the presence of a coupling reagent. The sulfoxides **12a** and **12b** were obtained by oxidation of 2-methylsulfanylimidazoles **1c** and **1m** with hydrogen peroxide, respectively. (Scheme 2).

The synthesis of tetrasubstituted imidazoles **14** and **16** started from known 4-(4-(4-fluorophenyl)-1-methyl-2-(methylthio)-1*H*-imidazol-5-yl)pyridin-2-amine **13** [25] and 2-chloro-4-(5-(4-fluorophenyl)-1-methyl-2-(methylthio)-1*H*-imidazol-4-yl)pyridine **15** [22], respectively (Scheme 3). The cyclopropylamide moiety at the pyridine-C2 position was introduced either by reaction of pyridine-2-amine compound **13** and cyclopropanecarbonyl chloride or by Buchwald-Hartwig arylamidation of 2-chloropyridine derivative **15** and cyclopropanecarboxamide.

4,5-Disubstituted imidazole **20a** and 2,4,5-trisubstituted imidazoles **20b-g** were prepared in analogy to our recently reported protocol [33] based on the Radziszewski imidazole synthesis in four steps starting from ethanone **5** (Scheme 4). Treatment of **5** under Riley-Oxidation conditions yielded the corresponding α-diketone **17**. Under these acidic conditions, the Boc protecting group was already cleaved and in the next step, the pMB protecting group was removed using neat TFA. Then, the primary aromatic amine **18** was acylated with cyclopropanecarbonyl chloride. Interestingly, even using only one equivalent of acyl chloride, beside the expected monoacylated main product **19a** a substantial amount of double acylation (compound **19b**) was observed. Since the monoacylated product **19a**, however, could not be isolated, we used cyclopropanecarbonyl chloride in excess and continued our synthetic sequence with the double-acylated intermediate **19b**. Ring closing reaction to the imidazoles **20a-g** was achieved by reacting the α-diketone **19b** with ammonium acetate and different (hetero)aromatic, aliphatic aldehydes as well as formaldehyde. Conveniently, the second acyl was cleaved during this step. The yields in this reaction fluctuated between 5% and 65%. The reaction of non-enolizable aldehydes gave generally significantly higher yields than aldehydes with an enolizable system. In case of latter ones, an acid catalyzed aldol-reaction took place before the ring closing

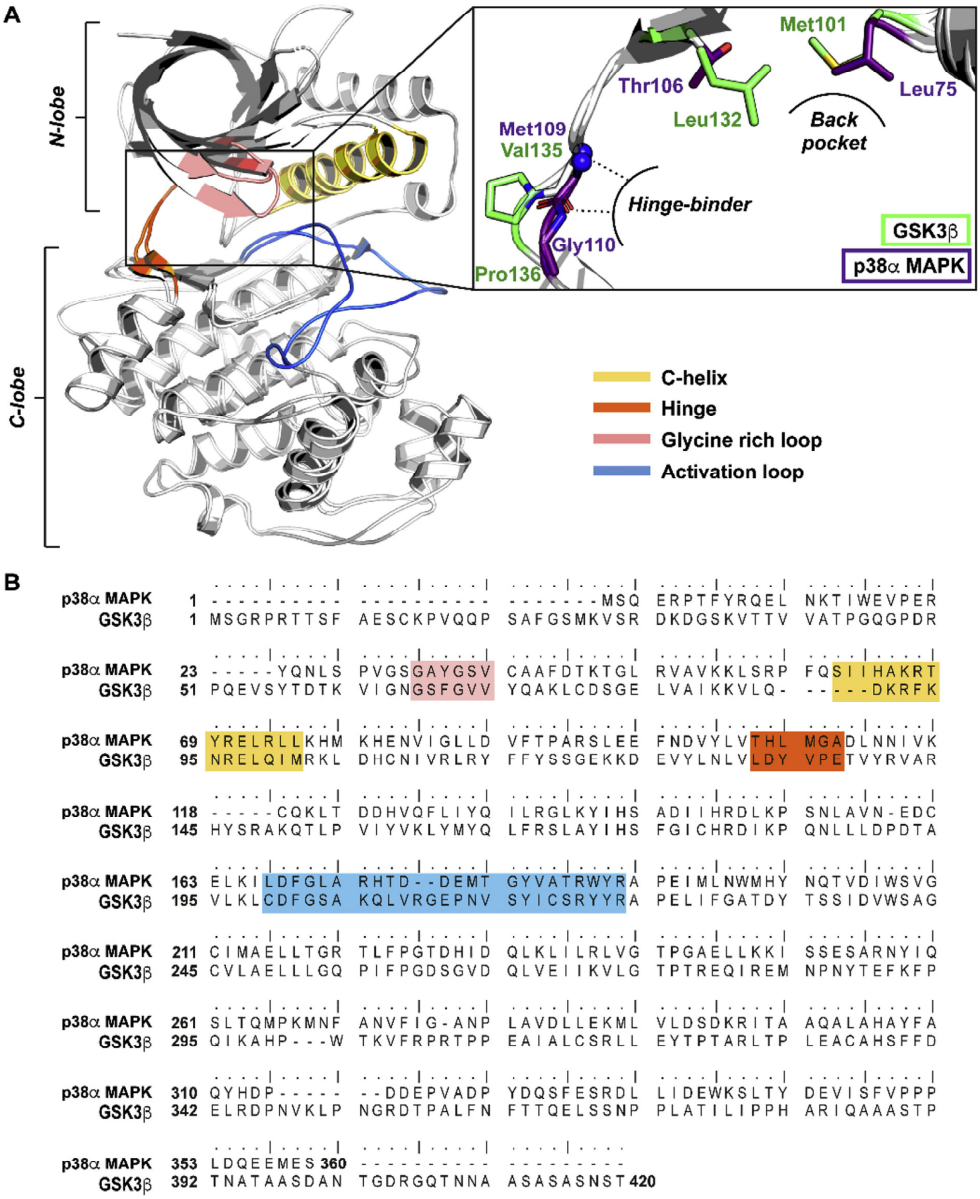

Fig. 1. (A) Structural overlay of GSK3β and p38α MAP kinase. The most crucial differences in the amino acids of the ATP binding site are highlighted in green (GSK3β) and purple (p38α MAP kinase). (B) Sequence alignment of GSK3β (UniProt code P49841) and p38α MAP kinase (UniProt code Q16539). The amino acids belonging to each region are highlighted as depicted in (A).

reaction. For these compounds, we observed a second relatively distinct spot on the TLC and the mass of this spot corresponded to a molecule formed by ring closing reaction with the aldol product.

The disubstituted imidazole **25** was prepared starting from commercially available 2-methylimidazole (**21**), which was protected in the first step using 2-(trimethylsilyl)ethoxymethyl (SEM) chloride (Scheme 5). A procedure previously described by Markey and Kelly was used [34], employing a directed *ortho*-metalation using *n*-butyllithium followed by the addition of tributyltin chloride, to obtain imidazole-5-stannane **23**. Intermediate **23** was reacted via a Stille coupling with *N*-(4-bromopyridin-2-yl)cyclopropanecarboxamide to yield imidazole **24**. Final product **25** was

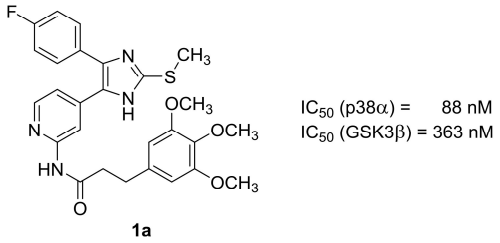

Fig. 2. Structure and biological data of in-house library screening hit **1a**.

obtained after removal of the SEM protecting group under acidic conditions.

2.2. Biological evaluation

2.2.1. Kinase activity assays and molecular modeling

The synthesized compounds were tested for their ability to inhibit p38α MAP kinase and GSK3β using an enzyme-linked immunosorbent assay (ELISA) [35] and the Promega ADP-Glo™ platform [36], respectively. As reference compounds, we selected SB203580 ($IC_{50} = 41$ nM) for the p38α MAP kinase activity assay and SB216763 ($IC_{50} = 89$ nM) for the GSK3β assay. To estimate the GSK3 isoform selectivity, selected compounds were further evaluated for their inhibitory potency toward GSK3α using again the ADP-Glo™ activity assay. Specific inhibitors were further investigated for their metabolic stability in human liver microsomes (HLM) as well as in an *ex vivo* experiment for their ability to inhibit the lipopolysaccharide (LPS)-stimulated TNF-α release from human whole blood (HWB) [37]. In latter assay, SB203580 was used as reference compound ($IC_{50} = 3202$ nM). Moreover, the two most promising inhibitors (**1c** and **20c**) were evaluated for their brain penetration, their cytochrome P450 (CYP450) inhibition as well as for their affinity to the human Ether-a-go-go-related gene (hERG) channel.

A possible binding mode for lead compound **1a** (Table 1) within the ATP binding site of p38α MAP kinase is depicted in Fig. 3. The pyridine nitrogen atom as well as the NH at the pyridine-C2 position act as a classical donor-acceptor hinge-binding motif engaging in two H-bond interactions to the backbone of Met109 of the hinge region. A charge-assisted H-bond interaction occurs between the side chain of the Lys53 and the imidazole-N3 nitrogen. Moreover, the imidazole ring lays on top of the Phe169 forming an aromatic π–π stacking interaction. The 4-fluorophenyl ring occupies the hydrophobic region I (HR I). Access to this region is controlled by the gatekeeper residue Thr106. Targeting of HR I might be an important factor for selectivity over other protein kinases since bulkier gatekeepers often do not tolerate large substituents [38].

Since different regions within the ATP binding site are highly conserved among all protein kinases, a similar binding mode of the lead compound **1a** was expected for GSK3β. Because of the gatekeeper on GSK3β being a bulkier amino acid (Leu132, in contrast to Thr106 in p38α MAP kinase), a simple rigid docking could lead to a misguided evaluation. Thus, we utilized an Induced Fit docking (IFD) [39–41] approach to study the binding to GSK3β. The IFD revealed a comparative binding mode of compound **1a** with GSK3β as in p38α MAP kinase. As depicted in Fig. 4, the hinge-binding motif (pyridine-2-amine) is, as expected, able to act as a donor-acceptor to both, the carbonyl and NH group of Val135. Similar to the pose for p38α MAP kinase, the 4-fluorophenyl ring is located in the HR I of GSK3β. The proposed binding mode suggested a possible cation-π interaction between the 2,3,4-trimethoxyphenyl ring and Arg141. However, as the Lys85 in GSK3β is in a fixed conformation between two negatively charged residues (Asp200 and Glu97) and it is located farther away compared to the corresponding Lys53 in p38α MAP kinase, we did not observe the charge-assisted H-bond between the imidazole ring and the Lys85. Instead, one of the imidazole tautomers is capable to form a H-bond with the Asp200 of the activation loop (part of the DFG motif). Since an equilibrium of the two possible tautomeric forms is expected, we suggest that the other imidazole tautomer (H-bond acceptor) may interact via a water-mediated H-bond with the Lys85. This interaction is observed in several X-ray structures of other protein kinases (e.g.

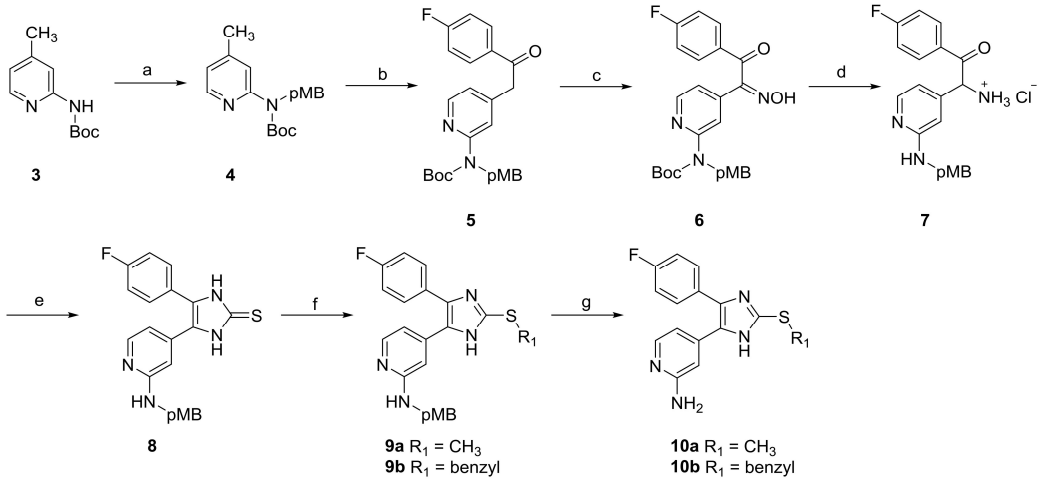

Scheme 1. Synthesis of key intermediates **10a** and **10b**. Reagents and conditions: (a) NaH, 4-methoxybenzyl chloride, DMF, 0 °C then rt, 18 h; (b) NaHMDS, ethyl 4-fluorobenzoate, THF, 0 °C then rt, 2 h, 67% (over 2 steps); (c) $NaNO_2$, acetic acid, rt, 1 h, 100%; (d) H_2, Pd/C 10%, methanolic HCl, 45 °C, 6 h; (e) KSCN, DMF, 160 °C, 2 h, 62% (over 2 steps); (f) CH_3I, NaO*t*Bu, MeOH, 55 °C, 2 h, 84% (in case of preparation of **11a**) or benzyl bromide, Cs_2CO_3, DMF, rt, 36 h, 35% (in case of preparation of **11b**); (g) TFA, 45 °C, 96–97%.

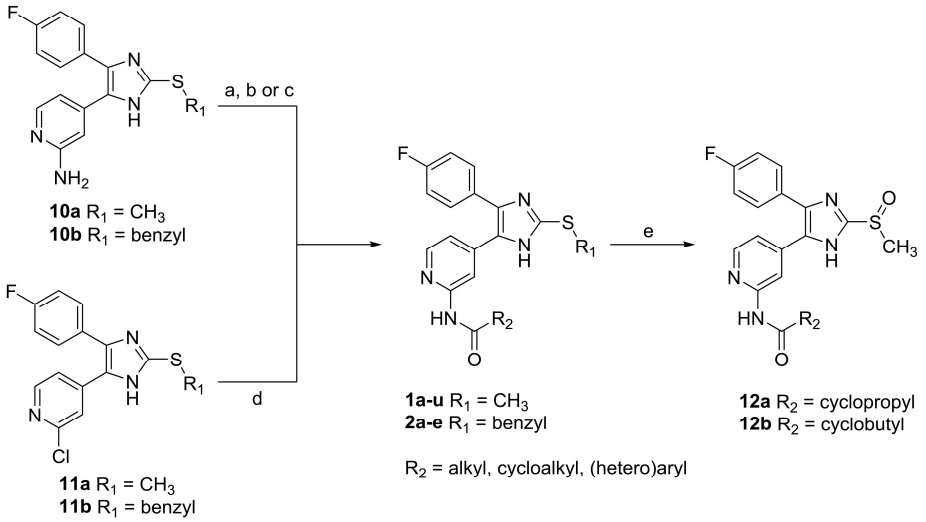

Scheme 2. Synthesis of compounds **1a-u**, **2a-e** and sulfoxides **12a-b**. Reagents and conditions: (a) carboxylic acid, PyBOP, DIPEA, DCM, rt, 40–93%; (b) carboxylic acid, HATU, DIPEA, DCM, rt, 21–85%; (c) acyl chloride, pyridine, 0 °C then rt; (d) amide, $Pd_2(dba)_3$, XantPhos, Cs_2CO_3, DMF, 100 °C, 16 h, 19–78%; (e) H_2O_2, MeCN, rt, 72–96 h, 42–51%. For R_2, see Tables 1–2.

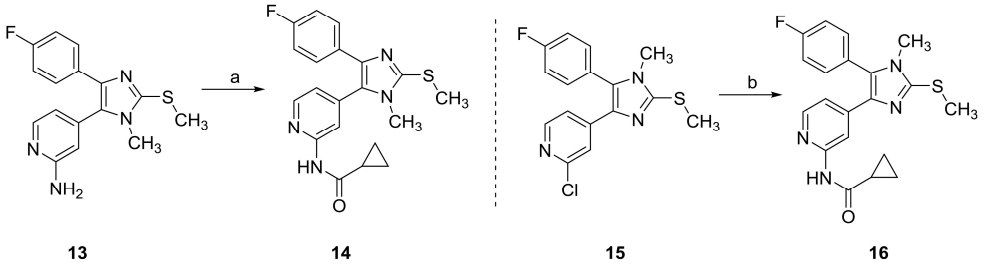

Scheme 3. Synthesis of tetrasubstituted 2-acylaminopyridinylimidazole. Reagents and conditions: (a) cyclopropanecarbonyl chloride, pyridine, 0 °C then rt, 2 h, 31%; (b) cyclopropanecarboxamide, $Pd_2(dba)_3$, XantPhos, Cs_2CO_3, DMF, 100 °C, 16 h, 63%.

JNK3) complexed with similar pyridinylimidazole-type inhibitors [42].

Based on our initial HTS data analysis, we concluded that GSK3β inhibition was strongly enhanced when *N*-(pyridin-2-yl)amides instead of *N*-(pyridin-2-yl)amines were present at the pyridine-C2 position. From previous studies, we also knew that p38α MAP kinase tolerates both amines and amides in this position equally well [25]. Therefore, a set of compounds bearing different amides at the pyridine-C2 position was planned to collect first SAR, especially in regards to GSK3β. Our first synthetic efforts led to the series of compounds presented in Table 1 (**1b-u**).

Compared to the lead structure **1a**, the close analogs **1f** and **1g** bearing only one methoxy group at the phenyl ring are less active against GSK3β. This indicates that the electronic properties of the phenyl ring play an important role in the binding, probably, via contributing to the cation–π interaction with the Arg141 residue. The decreased electron density in the phenyl ring could lead to a weakened cation–π interaction as electron-withdrawing substituents are known to attenuate these types of interactions. Consequently, inhibitor **1i** (GSK3β, IC_{50} = 995 nM) bearing an 3-(4-(trifluoromethyl)phenyl)propanamide moiety showed a 3-fold reduced GSK3β inhibition than the lead compound. These findings support our proposed orientation of our inhibitor molecule within the ATP bindings site. Meanwhile, these inhibitors (**1f**, **1g** and **1i)** retained their high inhibitory activity against p38α MAP kinase while displaying a substantial loss of activity versus GSK3β. Shortening of the C-linker of **1a** and **1i** by one methylene group resulted in compounds **1e** and **1h**, respectively. These compounds exhibited decreased GSK3β inhibition, while p38α MAP kinase inhibition of **1e** was increased almost by 7-fold compared to **1a**. To rationalize the data at hand, we decided to use already published crystal structures of p38α MAP kinase (PDB ID: 5ML5) and GSK3β (PDB ID: 4PTC) for the molecular modeling experiments. According to the computational approach, on GSK3β our compounds bind to the hinge region with two H-bonds to Val135, which is followed by Pro136, Glu137 and Thr138. Interestingly, Glu137 participates in a salt bridge interaction with Arg141 (Fig. 5A). In the case of p38α MAP kinase, the corresponding amino acids are Met109, Gly110, Ala111 and Asp112, while the corresponding residue to the Arg141 on p38α MAP kinase is Asn115, which is unable to interact with the

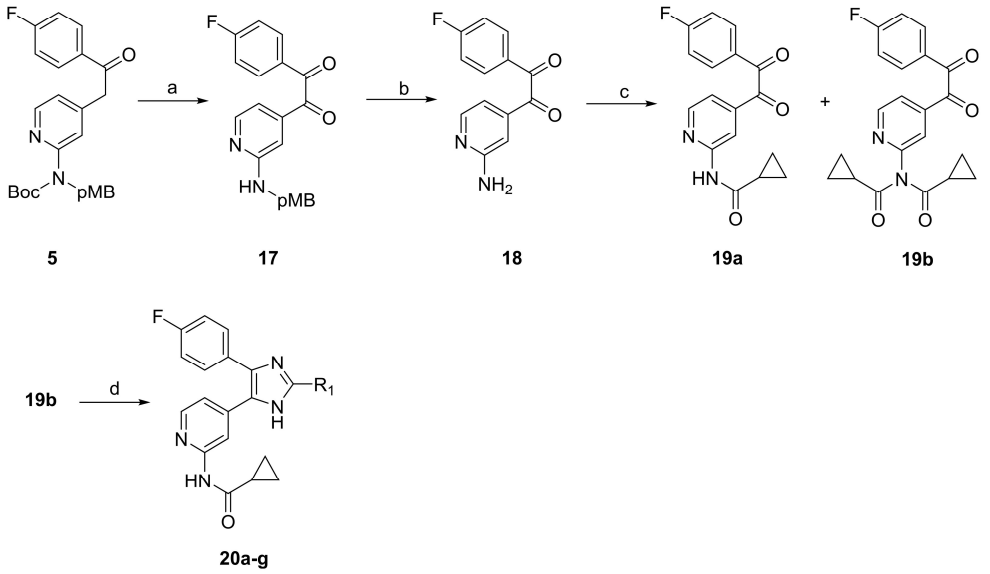

Scheme 4. Synthesis of 4-aryl-5-heteroaryl-substituted imidazole **20a** and 2-alkyl/aryl-4-aryl-5-heteroaryl-substituted Imidazole **20b-g**. Reagents and conditions: (a) SeO_2, acetic acid, 130 °C, 1.5 h, 44%; (b) TFA, rt, 97%; (c) cyclopropanecarbonyl chloride, DIPEA, DCM, rt, 18 h, 21%; (d) R_1-CHO, NH_4OAc, acetic acid, 130 °C, 3–4 h, 5–65%. For R_1, see Table 4.

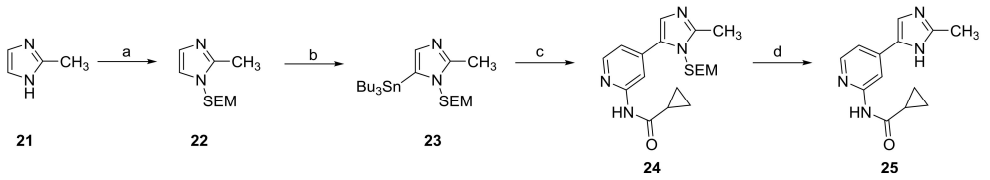

Scheme 5. Synthesis of 2-methyl-5-heteroaryl-substituted imidazole **25**. Reagents and conditions: (a) NaH, SEMCl, THF, 0 °C then rt, 18 h, 96%; (b) *n*-butyllithium, tributyltin chloride, Et_2O, 0 °C then rt, 2 h, 25%; (c) *N*-(4-bromopyridin-2-yl)cyclopropanecarboxamide, $Pd(PPh_3)_4$, 1,4-dioxane, 105 °C, 18 h, 77%; (d) TFA, DCM, rt, 6 h, 89%.

hinge region. Another important structural feature on p38α MAP kinase is the "glycine flip". The peptide bond of Met109 and Gly110 can flip 180°, which has already been reported in the literature to explain the selectivity of another class of compounds [43]. Instead of the flexible glycine residue, GSK3β has a rigid Pro136 in this position. Finally, GSK3β has a bulky Tyr134 residue, which is stabilized on top of the hinge-region and forms a H-bond to the fixed Pro136 (Fig. 5B). This Tyr134 occupies more space in the hinge region compared to the Leu108 in this position on p38α MAP kinase. Based on these three aspects, the flexibility of the residues in the hinge region, the stabilizing salt-bridge Glu137–Arg141 and the bulky Tyr134, we hypothesize that the hinge region of GSK3β is clearly more constrained and crowded (in the vicinity of the hinge) than in p38α MAP kinase. This would explain the hindered binding of the shortened C-linker chain compounds **1e** and **1h** to GSK3β. The importance of these three aspects was further exemplified by the dramatical loss of activity towards GSK3β with the bulky and/or planar structural properties containing compounds **1j**, **1t** and **1u**.

With a molecular weight of >500 Da, the inhibitors discussed so far are fairly heavy when considering the desired properties needed for CNS penetration [44]. Additionally, our insights from the IFD urged us to abandon any bulky residues that may clash with the rigid hinge region of GSK3β. Therefore, analogs of lead structure **1a** bearing smaller moieties at the pyridine-C2 position were synthesized. Compound **1b** with an *N*-acetyl moiety at the pyridine-C2 amino function displays improved GSK3β inhibition (GSK3β, IC_{50} = 152 nM) and a promising p38α MAP kinase/GSK3β inhibition ratio of 3.3. Following this observation, a series of inhibitors (**1b-d, 1j, 1l-u**) were synthesized bearing small cycloalkanecarboxamide moieties at the pyridine-C2 position. Introduction of a cyclopropanecarboxamide resulted in the potent and balanced dual inhibitor **1c**, showing IC_{50} values down to the low double-digit nanomolar range for both target kinases (p38α, IC_{50} = 24 nM; GSK3β, IC_{50} = 40 nM). The proposed binding mode of **1c** is depicted in Fig. 6.

Modifications on the cyclopropyl ring resulted in a loss of GSK3β activity. The introduction of a phenyl ring in position 2 of the cyclopropyl ring (**1k**) resulted in a slight improvement of p38α MAP kinase inhibition but also in a substantial drop of GSK3β activity. The change of the spacer length between the amide function and the cyclopropyl ring (**1l**) as well as replacement of the small cyclopropyl ring by bigger cyclobutyl (**1m**) or cyclopentyl (**1d**) rings decreased the GSK3β inhibitory potency slightly. The introduction of a trifluoromethyl group in position 1 of the cyclopropyl ring (**1j**) led to a complete loss of GSK3β activity, which is in good agreement with our hinge flexibility hypothesis (see Fig. 5B). Interestingly,

Table 1
Structures and kinase activity of 2-methylsulfanylimidazoles **1a-u**, **14**, **16** and **26**.

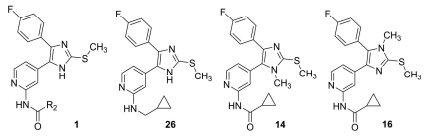

Cpd	R_2	IC_{50} [nM] ± SEM	
		p38α MAP kinase[a]	GSK3β[b]
1a	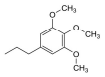	88 ± 8	363 ± 16
1b		45 ± 1	152 ± 9
1c		24 ± 0	40 ± 5
1d		40 ± 0.4	136 ± 45
1e		13 ± 1	510 ± 43
1f	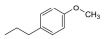	55 ± 6	542 ± 34
1g		36 ± 2	471 ± 15
1h		29 ± 1	3242 ± 592
1i		27 ± 2	956 ± 56
1j		184 ± 53	>10,000
1k		15 ± 0.1	808 ± 31
1l		15 ± 0	215 ± 49
1m		27 ± 0	132 ± 9
1n		20 ± 1	183 ± 7
1o		38 ± 0	395 ± 69
1p		18 ± 0	170 ± 7
1q		21 ± 1	73 ± 7
1r		28 ± 2	527 ± 44
1s		23 ± 0.4	126 ± 23
1t		22 ± 1	3654 ± 115
1u		42 ± 8	>10,000
26	–	14 ± 0	>10,000
14	–	222 ± 4	638 ± 19
16	–	1603 ± 733	1780 ± 16

[a] n = 3.
[b] n = 2.

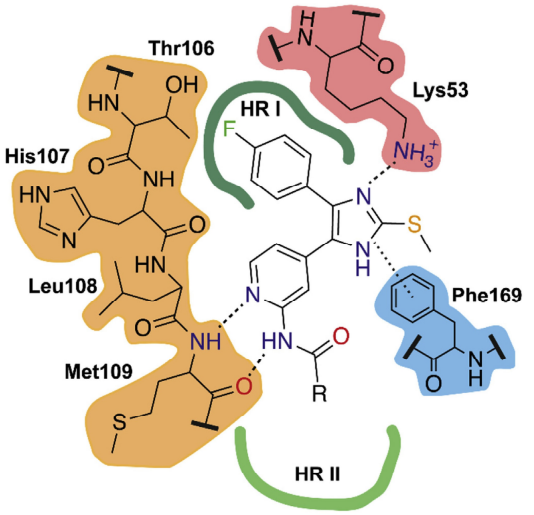

Fig. 3. Two-dimensional schematic binding mode of pyridinylimidazoles in p38α MAP kinase. The binding mode is derived from published crystallographic data (PDB ID: 5ML5). The 4-fluorophenyl ring occupies HR I, while the HR II is rather large and solvent exposed. H-bonds and the π–π stacking interaction between the imidazole ring and Phe169 are indicated with a black dashed line.

compound **1j** had also one order of magnitude reduced inhibitory potency on p38α MAP kinase, which indicates that the trifluoromethyl group attached to the cyclopropyl is already too close to the hinge region and may distort the H-bond interactions with Met109 (see Fig. 3). Nevertheless, the flexibility of the hinge region on p38α MAP kinase still enables the binding of this compound much better than GSK3β does.

Attempts to address the solvent interface (Fig. 7) with more polar groups attached to small cycloalkyl groups in order to gain binding affinity through enthalpically favourable, stabilized water networks, resulted in compounds **1n** and **1q**. Compared to the cyclobutane analog **1m**, imidazole **1n** bearing a 3-oxocyclobutyl substituent at the amide function displayed no improvement in GSK3β inhibition. In comparison to the parent cyclopentyl compound **1d**, pyridinylimidazole **1q** having a 3-oxocyclopentyl substituent showed a 2-fold increased GSK3β inhibitory activity. The two *cis*/*trans* 3-chlorocyclobutyl isomers (**1o** and **1p**) showed a roughly 2-fold difference in inhibition for both kinases with the *cis*-isomer being the more potent one.

Compound **1s** bearing a 2-oxopyrrolidin-1-acetamide at the pyridine-C2 position displayed a similar p38α MAP kinase/GSK3β inhibition profile as **1d** bearing a cyclopentylamide at the same position. Imidazole **1r** having 2-tetrahydrofuranyl at the amide function showed a decreased GSK3β activity (factor 4) compared to **1d**. The introduction of aromatic heterocyclic rings directly at the amide function (**1t** and **1u**) resulted in a tremendous loss of GSK3β inhibitory activity as a consequence of the aforementioned rigidity of the GSK3β hinge region (Fig. 5B). In contrast, none of the modifications at the pyridine-C2 position had any meaningful impact on p38α MAP kinase inhibition. All pyridinylimidazoles reported in Table 1 except **1j**, **14** and **16** are potent p38α MAP kinase inhibitors displaying IC_{50} values in the double-digit nanomolar range. Replacement of the carbonyl part of the amide group by a methylene group resulted in a complete loss of GSK3β affinity (compare **26** vs **1c**), whereas this modification slightly increased p38α MAP

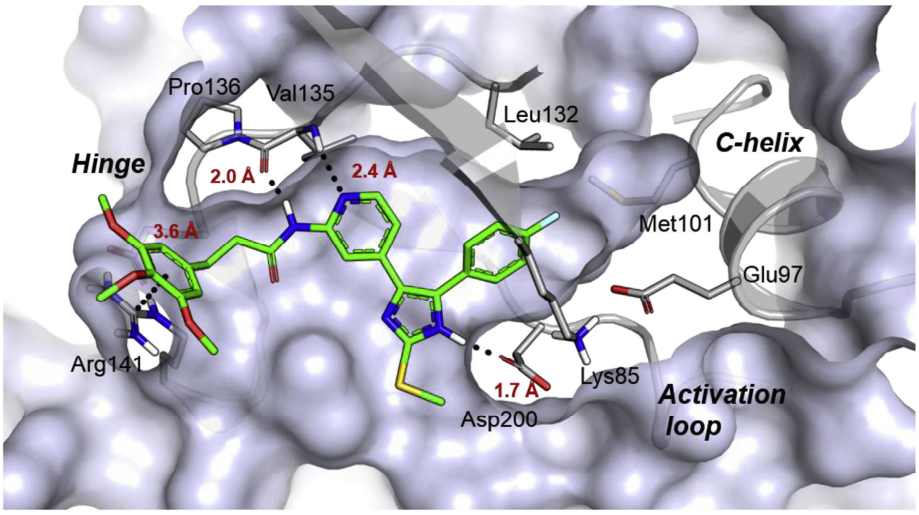

Fig. 4. Proposed binding mode of **1a** on GSK3β obtained by IFD (PDB ID: 4PTC). H-bonds between the inhibitor and the kinase as well as the cation–π interaction between the trimethoxyphenyl ring and Arg141 are shown with black dashed lines.

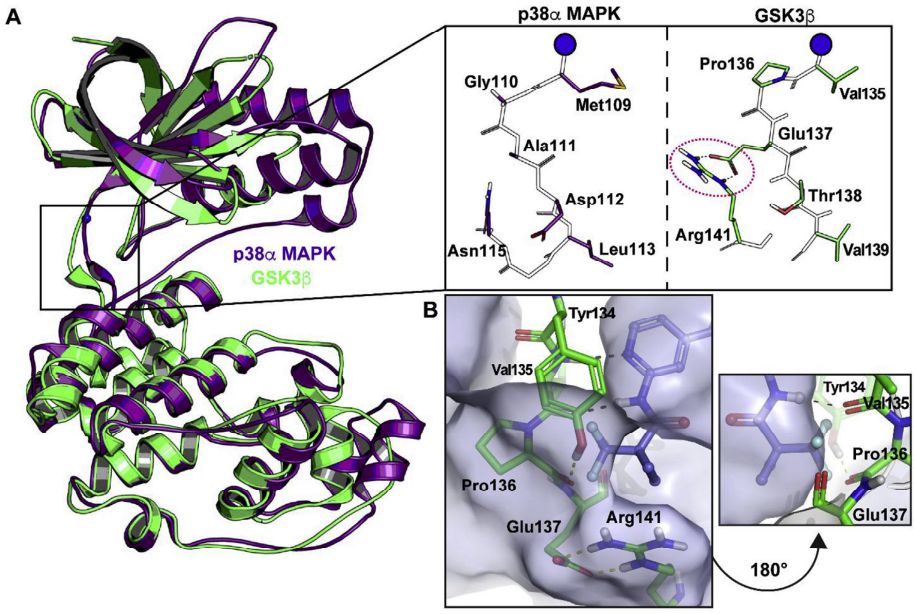

Fig. 5. **(A)** Differences in the hinge region of p38α MAP kinase (purple) and GSK3β (green). The activation loops of both structures are omitted for clarity. The blue sphere represents the NH group of Met109 and Val135 in each kinase that forms a H-bond with the pyridine. The stabilizing salt bridge between Glu137 and Arg141 in GSK3β is highlighted by a red circle. **(B)** The rigid environment of the GSK3β hinge region prevents the accommodation of compounds with bulkier moieties in close proximity to the hinge binding motif. Compound **1j** is unable to fit into the GSK3β while maintaining H-bonding to the hinge. The (trifluoromethyl)cyclopropyl moiety clash with the protein is illustrated here by crossing the cavity surface (PDB ID: 4PTC). (For interpretation of the references to color in this figure legend, the reader is referred to the Web version of this article.)

kinase inhibitory activity. Those findings exemplify the importance of the amide group at the pyridine-C2 for the binding to GSK3β. This arises most likely from solvent interactions that have been observed to play a crucial role for the compound affinity, as demonstrated in other studies [45]. Indeed, we noticed important solvent interactions with the amide in our molecular dynamics

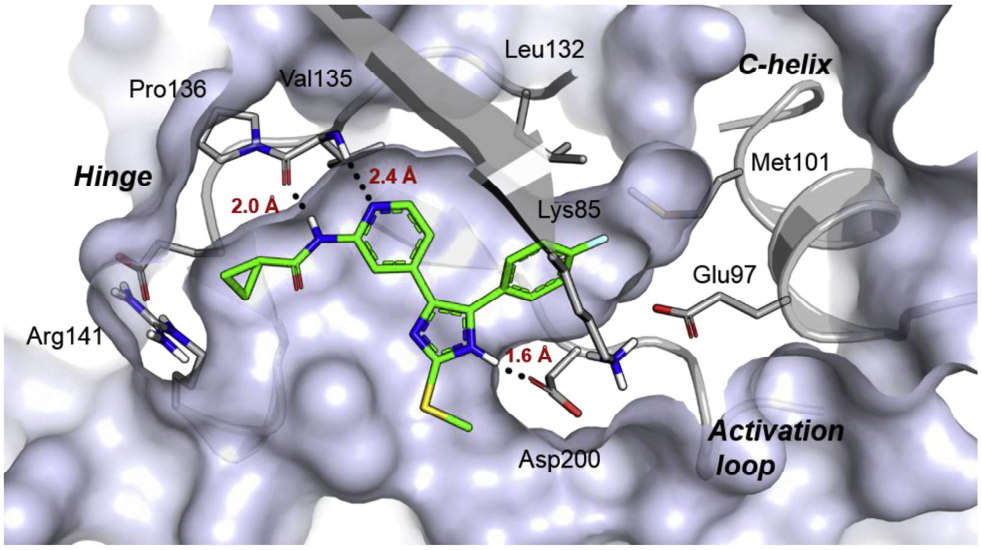

Fig. 6. Proposed binding mode of **1c** on GSK3β obtained by IFD (PDB ID: 4PTC). The cyclopropyl moiety occupies ideally the small and rigid front pocket (HR II) area. H-bonds between the inhibitor and the kinase are shown as black dashed line.

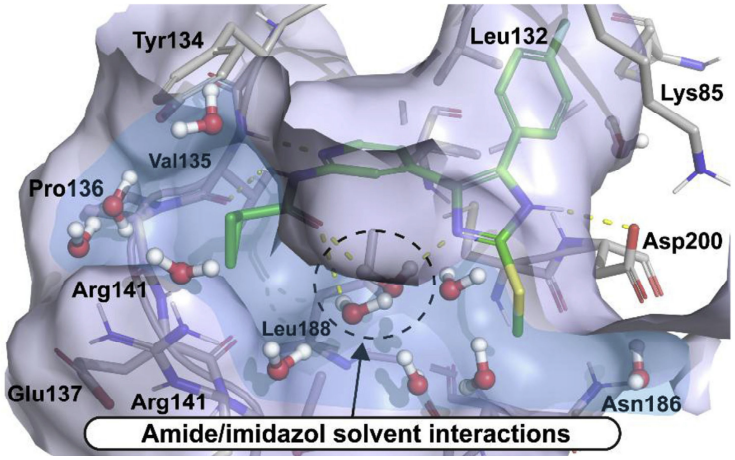

Fig. 7. The output conformation of the compound **1c** after 200 ns MD simulation (PDB ID: 4PTC). The carbonyl group of the amide and the imidazole-N3 participate in the solvent interactions. The protein surface is illustrated with light purple color and the solvent access to the binding site is highlighted in blue. The water molecules are displayed within 4 Å from the ligand. (For interpretation of the references to color in this figure legend, the reader is referred to the Web version of this article.)

(MD) simulation (Fig. 7). Moreover, there seems to be a possibility for solvent mediated, bridged interactions between the amide carbonyl and the imidazole-N3. This may help to stabilize the active conformation of the molecule, ultimately enhancing the overall binding affinity. Interestingly, this effect was only dramatic with GSK3β. The bulky and charged Arg141 residue in GSK3β clearly shields the solvent access to the binding site and influences to the water network organization. In case of the more flexible and open p38α MAP kinase, the water network reorganization within the pocket is tolerated thus enabling the binding of **26**.

The introduction of substituents on the imidazole-N1 or -N3 atom of potent dual p38α MAP kinase/GSK3β inhibitor **1c** resulted in a drop of both GSK3β and p38α MAP kinase inhibitory activity (compounds **14** and **16**). This effect was more pronounced in the case of **16**. The methylation of the nitrogen atom adjacent to the 4-fluorophenyl ring resulted in two orders of magnitude reduced p38α MAP kinase inhibitory activity, compromising the charge-assisted H-bond to the Lys53 (see Fig. 3). In addition, in the case of GSK3β, **16** would also disrupt either the H-bond to Asp200 or the potential water-mediated interaction to Lys85 depending on the

NH tautomerism (see Fig. 4).

In previous studies, our group showed that bigger moieties at the imidazole-C2 position were well tolerated by p38α MAP kinase [24]. Therefore, the inhibitory potency of a small series of five compounds, wherein the *S*-methyl group at this position was replaced by a *S*-benzyl group, was evaluated (Table 2). In case of GSK3β, imidazoles **2a-d** displayed a decreased affinity (3- to 6-fold) in comparison to their *S*-methyl counterparts **1a-d**.

Computational studies of **2c** with GSK3β revealed that the *S*-benzyl substituent is oriented towards the solvent accessible region and displays contacts with the lipophilic glycine rich loop residues, mainly with Phe67, Val70, and Ile62. In agreement with previous observations, imidazoles **2a-e** bearing *S*-benzyl moiety at the imidazole-C2 position displayed similar p38α MAP kinase inhibitory activity as their *S*-methyl counterparts. Compound **2e** with a 4-fluorophenylacetamide at the pyridine-C2 position represents the most potent p38α MAP kinase inhibitor in this series having an IC_{50} value in the low single-digit nanomolar range and displaying a greater than 500-fold selectivity over GSK3β.

Previous studies on *in vitro* metabolic stability of similar p38α MAP kinase inhibitors revealed that the alkylsulfanyl moiety at the imidazole-C2 position is susceptible to oxidation, resulting in the corresponding 2-alkylsulfinylimidazoles as main metabolites [33,46]. To estimate the impact of the metabolism on the inhibition profile, the corresponding sulfoxides of **1c** and **1m** were additionally evaluated for their ability to inhibit both target kinases (Table 3). Sulfoxides **12a** and **12b** showed a 3- and 6-fold reduced GSK3β inhibition compared to **1c** and **1m**, respectively, while the two compounds displayed a similar p38α MAP kinase inhibition profile like their *S*-methyl counterparts.

In order to remove the metabolic hotspot of the 2-methylsulfanylimidazoles, another series of pyridinylimidazoles were synthesized wherein the imidazole-C2 position was modified. To this end, alkyl (**20b**,**c**), aryl (**20d**), arylalkyl (**20e**,**f**) and heteroaryl (**20g**) substituents were introduced to this position (Table 4). In case of p38α MAP kinase, substitution of the imidazole-C2 position had no influence on the inhibitory activity and compounds **20b-g** displayed IC_{50} values in the same range as the simple disubstituted imidazole **20a**. Looking at GSK3β, introduction of a phenyl residue (**20d**) led to a distinctly reduced inhibitory potency. Compared to **20a**, imidazole **20c** with a small ethyl moiety at the imidazole C2-position is the only example in this series displaying a significantly improved inhibition as well as a p38α MAP kinase/GSK3β inhibition profile similar to the most potent compound out of the *S*-methyl series (**1c**).

As observed in previous studies [29,42], the removal of the 4-fluorophenyl ring (**25**) led to a complete loss of p38α MAP kinase inhibitory activity (Table 5). Moreover, this structural modification resulted in a 32-fold reduced inhibitory activity of GSK3β (**25** vs. **20b**), demonstrating the importance of this residue also for GSK3β inhibition.

Table 2
Structures and kinase activity of 2-benzylsulfanylimidazole **2a-e**.

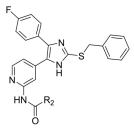

Cpd	R_2	IC_{50} [nM] ± SEM	
		p38α MAP kinase[a]	GSK3β[b]
2a	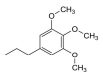	61 ± 4	1149 ± 167
2b		51 ± 5	560 ± 23
2c		41 ± 3	229 ± 3
2d		20 ± 2	663 ± 45
2e		3 ± 0	1499 ± 51

[a] n = 3.
[b] n = 2.

Table 3
Structures and kinase activity of 2-methylsulfinylimidazoles **12a** and **12b**.

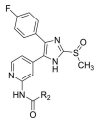

Cpd	R_2	IC_{50} [nM] ± SEM	
		p38α MAP kinase[a]	GSK3β[b]
12a		44 ± 0	236 ± 45
12b		29 ± 6	428 ± 19

[a] n = 3.
[b] n = 2.

Table 4
Structures and kinase activity of 4,5-disubstituted imidazole **20a**, 2,4,5-trisubstituted imidazoles **20b-g** and 1,5-disubstituted imidazole **25**.

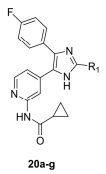

20a-g

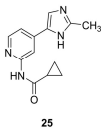

25

Cpd		IC_{50} [nM] ± SEM	
	R_1	p38α MAP kinase[a]	GSK3β[b]
20a		19 ± 1	64 ± 4
20b		19 ± 1	53 ± 12
20c		16 ± 1	35 ± 6
20d		27 ± 1	570 ± 98
20e		18 ± 0	59 ± 11
20f		20 ± 0.5	133 ± 7
20g		18 ± 1	156 ± 14
25	–	>10,000 (1%)[c]	1684 ± 120

[a] n = 3.
[b] n = 2.
[c] Percent inhibition at indicated concentration, tested in a LANCE assay at Eurofins Cerep SA, France (reference compound in this assay: SB203580, IC_{50} = 65 nM).

Table 5
GSK3α/β isoform selectivity.

Cpd	IC_{50} [nM] ± SEM[a]	
	GSK3β	GSK3α
1c	40 ± 5	300 ± 31
2c	229 ± 3	853 ± 268
1a	363 ± 16	2046 ± 220
12a	236 ± 45	1337 ± 25
20c	35 ± 6	301 ± 22
20e	59 ± 11	428 ± 96

[a] n = 2.

2.2.2. GSK3β ATP-competitiveness

Compounds **1c** and **20c** were tested at three different ATP concentrations (25 μM, 100 μM and 500 μM) to confirm their ATP-competitiveness. As expected from our postulated binding mode, higher concentrations of ATP led to significantly increased IC_{50} values from 18 nM to 46 nM at 25 μM of ATP to 423 nM and 492 nM at 500 μM of ATP in case of **1c** and **20c**, respectively (Figs. S3 and S4, supplementary data). This ATP-dependent behavior of both compounds is a strong indicator for ATP-competitive binding of this inhibitor class.

2.2.3. GSK3 isoform selectivity

The sequences of GSK3α and GSK3β are highly conserved, showing 98% identity in the kinase domain [47]. The few existing variations in their amino acid composition are mostly minor changes and occur in areas that display no direct interactions with the ATP binding site. In the hinge region, the only difference is that the Asp133 of GSK3β is replaced by the Glu196 in GSK3α. The side-chain of Asp133/Glu196 is pointing outwards from the ATP pocket towards the solvent and is putatively interacting with the positively charged residues (*e.g.* Arg113 in GSK3β) in the solvent interface. To evaluate the structural influence of this difference among the isoforms is tedious as there is no publicly available crystal structure of GSK3α. During the preparation of this manuscript, however, Wagner and co-workers demonstrated that the switch between these two amino acids may have an influence on the topology of the ATP binding site and the HR I [48]. These changes in the binding site dynamics might explain the slight selectivity of the selected 2-methylsulfanyl (**1a**,**c**), 2-benzylsulfanyl (**2c**) and 2-alkylimidazole (**20c**,**e**) derivatives for GSK3β versus GSK3α (Table 5). The closely related analogs **1c** and **20c** proved to be the most selective compounds with a 7.5- and 8.6-fold selectivity towards GSK3β, respectively.

2.2.4. Metabolism

The two potent dual GSK3β/p38α MAP kinase inhibitors **1c** and **20c**, as well as the highly active and p38α MAP kinase selective compound **2e**, were further evaluated for their metabolic stability in mixed male&female HLM (Tables S1–S3, supplementary data). The 2-methylsulfanylimidazole **1c** was oxidized to the corresponding sulfoxide **12a** with a reasonable half-life of 190 min. After 4 h of incubation time, about 44% of **1c** remained unmetabolized. Sulfoxide **12a** was detected as sole metabolite (65% after 4 h). The cyclopropylamide moiety was not affected by the microsomes. In contrast, 2-ethlysulfanylimidazole **20c** showed excellent metabolic stability in the HLM experiment, leaving more than 90% of the inhibitor unmetabolized after 4 h. Benzylsulfanylimidazole **2e** exhibited better metabolic stability than **1c** although more metabolites were formed during the incubation (66% of **2e** remained untouched after 4 h). Similar to the experiment with **1c**, the corresponding sulfoxide of **2e** was detected as the main metabolite (11%). In addition, other biotransformation reactions took place on **2e** as well as on its sulfoxide, *e.g.* oxidation to the corresponding sulfone.

2.2.5. Pharmacokinetic and CNS penetration study

To further assess the plasma stability and evaluate brain penetration, the most potent dual p38α MAP kinase/GSK3β inhibitors **1c** and **20c** were tested in adult male RjOrl:Swiss CD-1 mice. The mice were treated with a single dose intravenous injection (10 mg/kg) and plasma samples were collected 10, 30 and 120 min after the dosing. After the last sample was obtained, the mice were sacrificed for dissection of the brains. Blood and brain samples were analyzed via LC-MS after preparation (see supplementary data).

In contrast to the *in vitro* HLM experiments, 2-methylsulfanylimidazole **1c** showed an even faster biotransformation rate to the corresponding sulfoxide **12a** *in vivo*. After 10 min, the ratio between *S*-methyl (**1c**) and sulfoxide (**12a**) was already 1:2. After 2 h, inhibitor **1c** was almost completely metabolized. The active metabolite **12a** showed a slight blood-brain barrier penetration (brain concentration: 65.8 ng/g after 2 h), whereas the concentration of 2-methylsulfanylimidazole **1c** in the brain was one-order of magnitude lower. The *in vitro* metabolically stable inhibitor **20c** showed relatively fast plasma clearance from 850 ng/mL after 10 min to 95 ng/mL after 2 h. The brain concentration of **20c** 2 h after dosing was 13.3 ng/g, which estimates a brain concentration of **20c** exceeding its IC_{50} values on GSK3β and p38α MAP kinase of 1.1-fold and 2.5-fold, respectively.

The HWB assay presents a possibility to evaluate the effectiveness of p38α MAP kinase inhibitors in regard to their modulation of proinflammatory cytokine secretion in a cell-based system [37]. In this *ex vivo* assay, the amount of TNF-α release from HWB after LPS-stimulation is quantified and the efficacy of the inhibitors is evaluated more specifically with respect to *in vivo* parameters like plasma protein binding and cellular permeability. The release of LPS-stimulated TNF-α from HWB was inhibited by the compounds **1c** and **20c** at concentrations in the submicromolar range (Table 6). The 2-alkylimidazole derivative **20c** displayed slightly increased inhibition compared to the 2-methylsulfanyl derivative **1c**. This observation correlates well with the data from the p38α MAP kinase activity assay.

Further pharmacological profiling of the dual p38α MAP kinase/GSK3β inhibitors **1c** and **20c** included the evaluation of their ability to inhibit hERG and relevant CYP isoforms (Table 6). At a test concentration of 10 μM, imidazole **1c** displays a 30% inhibition of hERG and inhibits three of the tested CYP isoform higher than 70%. Low inhibition of CYP2D6 and moderate inhibition of CYP2C19 was observed. At the same concentration, 2-ethylimidazole **20c** shows both a higher inhibition of hERG (43%) and an elevated CYP inhibition profile than the 2-methylsulfanylimidazole counterpart **1c**. This finding is in good agreement with recently reported results of a study with similar imidazole derivatives [49].

The water solubility of dual GSK3β/p38α MAP kinase inhibitors **1c** and **20c** was measured in PBS buffer at a pH value of 7.8 (Figs. S1 and S2, supplementary data). While 2-methylsulfanylimidazole **1c** showed moderate solubility (0.051 mg/mL), the 2-ethylimidazole **20c** displayed a 3-fold improved solubility (0.155 mg/mL).

Finally, compound **20c** was further screened against a panel of 45 diverse kinases in order to achieve a preliminary evaluation of its selectivity within the kinome. Ten additional kinases were inhibited more than 60% at a testing concentration of 1 μM apart from GSK3β and p38α MAPK (Table 7 and Table S4, supplementary data). Among these, the tyrosine kinase receptors VEGFR2, EGFR, FGRF2 and FGFR3 were found as targets. Also, the p38α MAPK-related kinase JNK1 was identified as an off-target.

Table 6
Inhibition of LPS-stimulated TNF-α release from HWB as well as *in vitro* CYP and hERG Inhibition Data.

Cpd	IC_{50} [nM] ± SEM[a]	% inhibition @ 10 μM					
	TNF-α release	hERG	CYP1A2	CYP2C9	CYP2C19	CYP2D6	CYP3A4
1c	541 ± 217	30.1	88.4	77.7	56.1	14.6	75.6
20c	317 ± 4	43.3	83.6	83.6	81.7	58.3	75.1

[a] n = 2.

Table 7
Off target activity of **20c** (test concentration: 1 μM).

90–100% inhibition	75–90% inhibition	60–75% inhibition
Abl	EPHA2	EPHA3
EGFR	JNK1	FGFR2
EphB4		
FGFR3		
HGK (MAP4K4)		
KDR (VEGFR2)		

3. Conclusion

A comprehensive series of 2,4,5-trisubstituted imidazoles was synthesized and biologically evaluated, providing for the first-time valuable insights into the SARs of this class of compounds with respect to their p38α MAP kinase and GSK3β inhibitory potencies. Structural modifications led to promising inhibitors targeting simultaneously both kinases relevant for the pathophysiology of AD. The most promising balanced dual inhibitor *N*-(4-(2-ethyl-4-(4-fluorophenyl)-1*H*-imidazol-5-yl)pyridin-2-yl)cyclopropanecarboxamide (**20c**) displayed IC_{50} values in the low double-digit nanomolar range and shows excellent metabolic stability. In addition to this, compound **20c** demonstrated an 8.5-fold isoform selectivity over GSK3α and seems to possess favourable pharmacokinetic properties, like the ability to cross the blood-brain barrier in mice.

4. Experimental section

4.1. Chemistry

4.1.1. General

All reagents and solvents were obtained from commercial sources and used without further purification. Thin layer chromatography (TLC) reaction controls were performed for all reactions using fluorescent silica gel 60 F_{254} plates (Merck) and visualized under natural light and UV illumination at 254 and 366 nm. All tested compounds were determined to be ≥ 95% purity by reverse phase high-performance liquid chromatography (HPLC) (254 nm). HPLC were carried out on an Agilent 1100 Series HPLC system, equipped with an UV DAD (detection at 218 nm, 254 nm, and 280 nm). The chromatographic separation was performed on a XBridge™ C18 column (150 mm × 4.6 mm, 5 μm) at 30 °C oven temperature. The injection volume was 10 μL and the flow 1.5 mL/min using the following gradient: 0.01 M KH_2PO_4, pH 2.3 (solvent A), methanol (solvent B), 45% B to 85% B in 9 min; 85% B for 6 min; stop time 16 min. Flash column chromatography was performed using an Interchim PuriFlash 430 automated flash chromatography system with Davisil LC60A 20–45 μm silica from Grace Davison or PuriFlash SIHP 30 μm columns. Nuclear magnetic resonance (NMR) spectra were measured on a Bruker Avance III HD NMR spectrometer at 300 MHz in the Organic Chemistry Institute, Eberhard Karls Universität Tübingen. The chemical shifts δ are reported in parts per million (ppm) relative to TMS. All spectra were calibrated against the (residual proton) peak of the deuterated solvent used. Mass spectra were performed on an Advion Expression S electrospray ionization mass spectrometer (ESI-MS) with an Advion Plate Express (TLC interface).

4.2. Experimental procedures

4.2.1. General procedure for the Buchwald-Hartwig coupling (General procedure A)

The amide (1.5–3 equiv), $Pd_2(dba)_3$ (5 mol %), XantPhos (10 mol %), cesium carbonate (3 equiv) and the 2-chloropyridinylimidazole derivative (**11a** or **11b**) were dissolved under an atmosphere of argon in DMF (6.5 mL/mmol). The reaction mixture was then stirred at 100 °C for 16 h. The reaction mixture was allowed to cool to rt and sat. ammonium chloride solution was added. It was extracted with ethyl acetate (3x) and the combined organic layers were washed with sat. ammonium chloride solution (2x) and brine. After drying over anhydrous Na_2SO_4 the solvent was evaporated under reduced pressure.

4.2.2. General procedure for the amide coupling with PyBOP (General procedure B)

The carboxylic acid (1–2.5 equiv) and (benzotriazol-1-yloxy) tripyrrolidinophosphonium hexafluorophosphate (PyBOP) (1–2.5 equiv) were dissolved in DCM (25 mL/mmol). The resulting mixture was stirred for 10 min at rt before the amine (1 equiv) and diisopropylethylamine (3 equiv) were added. The reaction was stirred overnight at rt. The solvent was evaporated under reduced pressure and the residue was dissolved in DCM and washed with brine and sat. sodium bicarbonate solution. The organic layer was dried over anhydrous Na_2SO_4 before the solvent was again evaporated under reduced pressure.

4.2.3. General procedure for the amide coupling with HATU (General procedure C)

The carboxylic acid (1–3 equiv) and 1-[bis(dimethylamino) methylene]-1*H*-1,2,3-triazolo[4,5-*b*]pyridinium 3-oxide hexafluorophosphate (HATU) (1–1.4 equiv) were dissolved in DCM (25 mL/mmol). The resulting mixture was stirred for 10 min at rt before the amine (1 equiv) was added and the mixture was stirred for 20 more min. Then diisopropylethylamine (3 equiv) was added and the reaction was stirred overnight at rt. The solvent was evaporated under reduced pressure and the residue was dissolved in DCM and washed with brine and sat. sodium bicarbonate solution. The organic layer was dried over anhydrous Na_2SO_4 before the solvent was again evaporated under reduced pressure.

4.2.4. General procedure for the Radziszewski imidazole synthesis (General procedure D)

The diketone **19a** was dissolved in acetic acid (20 mL/mmol) and ammonium acetate (20 equiv) and the aldehyde (1.5 equiv) were added. The reaction mixture was heated to 130 °C for 4 h. After cooling to rt, the reaction was diluted with DCM and sat. sodium bicarbonate solution was added until gas evolution ceased. The phases were separated and the aqueous layer was adjusted to pH 10–11 with 1 M NaOH and extracted thrice with DCM.

*4.2.4.1. tert-Butyl (4-methoxybenzyl)(4-methylpyridin-2-yl)carbamate (**4**).* A solution of *tert*-butyl (4-methylpyridin-2-yl)carbamate (2.00 g, 9.60 mmol) in DMF (20 mL) was cooled to 0 °C and sodium hydride 60% in mineral oil (576 mg, 14.40 mmol) was added portionwise over 5 min. The resultant mixture was stirred for 30 min at 0 °C before 4-methoxybenzyl chloride (1.56 mL, 11.52 mmol) was added in one portion and the reaction was stirred at rt for 18 h. Water (200 mL) was added and it was extracted with ethyl acetate (3x). The combined organic layers were dried over anhydrous Na_2SO_4 and concentrated in vacuo to afford a brown solid (3.27 g), which was used in the next step without further purification. ^{1}H NMR (300 MHz, $CDCl_3$) δ 1.43 (s, 9H), 2.33 (s, 3H), 3.77 (s, 3H), 5.11 (s, 2H), 6.76–6.87 (m, 3H), 7.17–7.25 (m, 2H), 7.45 (s, 1H), 8.25 (d, J = 5.0 Hz, 1H). ^{13}C NMR (75 MHz, $CDCl_3$) δ 21.1, 28.2, 49.4, 55.7, 81.1, 113.5, 120.3, 120.8, 128.6, 131.6, 147.2, 148.1, 154.3, 154.5, 158.4. TLC-MS (ESI) m/z = 350.8 $[M + Na]^+$.

*4.2.4.2. tert-Butyl (4-(2-(4-fluorophenyl)-2-oxoethyl)pyridin-2-yl)(4-methoxybenzyl)carbamate (**5**).* Under an atmosphere of argon, compound **4** (1.41 g, 4.29 mmol) was dissolved in THF (35 mL) and the solution was cooled to 0 °C. Sodium bis(-trimethylsilyl)amide(4.30 mL, 8.60 mmol, 2 M in THF) was added via syringe over 10 min and the resulting mixture was stirred for 45 min while still being cooled to 0 °C. Then ethyl 4-fluorobenzoate (867 mg, 5.16 mmol) dissolved in THF (5 mL) was added in one portion and the reaction was further stirred for 2 h at rt. H_2O (150 mL) was added and the solution was carefully adjusted to pH = 7 using 0.5 M aqueous HCl. The organic layer was separated and the aqueous layer was extracted with ethyl acetate (2x). The combined organic layers were dried over anhydrous Na_2SO_4 and concentrated in vacuo to afford a brown solid (1.24 g, 67% over 2 steps). ^{1}H NMR (300 MHz, DMSO-d_6) δ 1.36 (s, 9H), 3.70 (s, 3H), 4.47 (s, 2H), 5.02 (s, 2H), 6.79–6.86 (m, 2H), 7.04 (dd, J = 5.1, 1.3 Hz, 1H), 7.13–7.19 (m, 2H), 7.30–7.41 (m, 2H), 7.50 (s, 1H), 8.08–8.16 (m, 2H), 8.30 (dd, J = 5.1, 0.4 Hz, 1H). ^{13}C NMR (75 MHz, $CDCl_3$) δ 27.7, 43.9, 48.8, 54.9, 80.6, 113.5, 115.8 (d, $^2J_{CF}$ = 22.1 Hz), 120.7, 121.6, 128.3, 130.9, 131.3 (d, $^3J_{CF}$ = 9.4 Hz), 133.0 (d, $^4J_{CF}$ = 2.8 Hz), 145.4, 147.1, 153.4, 154.0, 158.1, 165.2 (d, $^1J_{CF}$ = 252.1 Hz), 195.1. TLC-MS (ESI) m/z = 473.2 $[M + Na]^+$.

*4.2.4.3. tert-Butyl-(4-(2-(4-fluorophenyl)-1-(hydroxyimino)-2-oxoethyl)pyridin-2-yl)(4-methoxybenzyl)carbamate (**6**).* Sodium nitrite (483 mg, 7.00 mmol) was dissolved in H_2O (5 mL) and added dropwise to a solution of **5** (1.05 g, 2.33 mmol) in glacial acetic acid (15 mL) at 10 °C. The resulting mixture was stirred for 60 min before H_2O (50 mL) was added and the aqueous phase was extracted with ethyl acetate (3x). The combined organic layers were dried over anhydrous Na_2SO_4 and concentrated in vacuo to afford an orange-brown solid (1.12 g, 100%). ^{1}H NMR (300 MHz, $CDCl_3$) δ 1.36 (s, 9H), 3.75 (s, 3H), 5.08 (s, 2H), 6.73–6.79 (m, 2H), 7.08–7.13 (m, 2H), 7.14–7.17 (m, 2H), 7.18 (d, J = 2.7 Hz, 1H), 7.76 (s, 1H), 7.89–7.97 (m, 2H), 8.35 (d, J = 5.3 Hz, 1H). ^{13}C NMR (75 MHz, $CDCl_3$) δ 28.0, 49.7, 55.1, 81.9, 113.5, 116.3, 116.4 (d, $^2J_{CF}$ = 22.7 Hz), 116.8, 128.6, 130.6, 131.0 (d, $^4J_{CF}$ = 2.8 Hz), 132.2 (d, $^3J_{CF}$ = 9.4 Hz), 140.3, 148.0, 153.8, 154.1, 154.9, 158.4, 166.6 (d, $^1J_{CF}$ = 257.6 Hz), 192.1 TLC-MS (ESI) m/z = 502.0 $[M + Na]^+$ m/z = 478.1 $[M - H]^-$.

*4.2.4.4. 2-Amino-1-(4-fluorophenyl)-2-(2-((4-methoxybenzyl)amino)pyridin-4-yl)ethan-1-one-hydrochloride (**7**).* In a three-neck round-bottom flask, compound **6** (1.12 g, 2.33 mmol) was dissolved in a 1:1 mixture of methanol (15 mL) and hydrochloric acid in methanol (15 mL). Palladium on carbon 10 wt % (250 mg) was added and the flask was evacuated and backfilled with hydrogen gas. The reaction was carefully heated to 45 °C and vigorously stirred for 6 h under an atmosphere of hydrogen. The reaction mixture was filtered through Celite and the solvent was evaporated to give **7** as a yellow solid (904 mg), which was used in the next step without further purification. TLC-MS (ESI) m/z = 366.3 $[M+H]^+$ m/z = 364.3 $[M-H]-$.

*4.2.4.5. 4-(4-Fluorophenyl)-5-(2-((4-methoxybenzyl)amino)pyridin-4-yl)-1,3-dihydro-2H-imidazole-2-thione (**8**).* Compound **7** (1.00 g, 2.49 mmol) and potassium thiocyanate (532 mg, 5.47 mmol) were dissolved in DMF (7 mL) under an atmosphere of argon and stirred at 160 °C for 2 h. After cooling to rt, H_2O (75 mL) was added and the precipitate was filtered off and dried in vacuo to afford **8** as a yellow solid (644 mg, 62% over 2 steps). ^{1}H NMR (300 MHz, DMSO-d_6) δ 3.73 (s, 3H), 4.35 (d, J = 5.2 Hz, 2H), 6.45 (d, J = 5.0 Hz, 1H), 6.60 (s, 1H), 6.89 (d, J = 8.5 Hz, 2H), 7.16–7.33 (m, 5H), 7.46 (dd, J = 8.6, 5.4 Hz, 2H), 7.88 (d, J = 5.6 Hz, 1H), 12.70 (d, J = 5.2 Hz, 2H). TLC-MS (ESI) m/z = 407.6 $[M + H]^+$ m/z = 405.3 $[M - H]^-$.

*4.2.4.6. 4-(5-(4-Fluorophenyl)-2-(methylthio)-1H-imidazol-4-yl)-N-(4-methoxybenzyl)pyridin-2-amine (**9a**).* Compound **8** (644 mg, 1.58 mmol) was dissolved in methanol (12 mL) and cooled to 0 °C before sodium *tert*-butoxide (305 mg, 3.17 mmol) and methyl iodide (100 μL, 1.60 mmol) were added. The reaction was stirred at 55 °C for 2 h. Afterwards the solvent was evaporated and the crude product was purified by flash column chromatography (SiO_2, DCM/EtOH 97:03 to 85:15) to afford a brown solid (560 mg, 84%). ^{1}H NMR (300 MHz, DMSO-d_6) δ 2.60 (s, 3H), 3.72 (s, 3H), 4.33 (d, J = 5.5 Hz, 2H), 6.47 (d, J – 4.7 Hz, 1H), 6.70 (br. s., 1H), 6.81–6.89 (m, 2H), 6.96–7.08 (m, 1H), 7.19 (d, J = 8.5 Hz, 3H), 7.28 (t, J = 8.6 Hz, 1H), 7.40–7.56 (m, 2H), 7.73–8.00 (m, 1H), 12.60 (br. s., 1H). TLC-MS (ESI) m/z = 421.2 $[M + H]^+$ m/z = 419.0 $[M - H]^-$.

*4.2.4.7. 4-(2-(Benzylthio)-5-(4-fluorophenyl)-1H-imidazol-4-yl)-N-(4-methoxybenzyl)pyridin-2-amine (**9b**).* Compound **8** (1.00 g, 2.46 mmol) was dissolved in DMF (6 mL) before cesium carbonate (425 mg, 3.08 mmol) and benzyl bromide (290 μL, 2.46 mmol) were added. The reaction was stirred at rt for 36 h, before water (50 mL) was added and it was extracted with ethyl acetate (3x). The combined organic layers were dried over anhydrous Na_2SO_4, concentrated in vacuo and purified by flash column chromatography (SiO_2, DCM/EtOH 97:03 to 85:15) to yield **9b** as a brown oil (435 mg, 35%). ^{1}H NMR (300 MHz, DMSO-d_6) δ 3.71 (s, 3H), 4.25–4.49 (m, 4H), 6.49 (br. s., 1H), 6.73 (br. s., 1H), 6.86 (d, J = 8.1 Hz, 2H), 7.02 (d, J = 15.9 Hz, 1H), 7.11–7.60 (m, 11H), 7.74–8.01 (m, 1H), 12.69 (br. s., 1H). TLC-MS (ESI) m/z = 497.3 $[M + H]^+$ m/z = 495.4 $[M - H]^-$.

*4.2.4.8. 4-(5-(4-Fluorophenyl)-2-(methylthio)-1H-imidazol-4-yl) pyridin-2-amine (**10a**).* Compound **9a** (650 mg, 1.55 mmol) was dissolved in TFA (6 mL) and heated to 55 °C until reaction control by TLC showed complete conversion. The solvent was evaporated and the product was redissolved in ethyl acetate and then washed with sat. sodium bicarbonate solution (2x). Purification by flash column chromatography (SiO_2, DCM/EtOH 95:05 to 90:10) afforded a golden solid (451 mg, 97%). ^{1}H NMR (300 MHz, DMSO-d_6) δ 2.61 (s, 3H), 5.98 (br. s., 2H), 6.45 (dd, J = 5.4, 1.5 Hz, 1H), 6.72 (br. s., 1H), 7.10–7.36 (m, 2H), 7.48 (br. s., 2H), 7.69–7.92 (m, 1H), 12.62 (br. s., 1H). TLC-MS (ESI) m/z = 301.4 $[M + H]^+$ m/z = 299.2 $[M - H]^-$.

*4.2.4.9. 4-(2-(Benzylthio)-5-(4-fluorophenyl)-1H-imidazol-4-yl)pyridin-2-amine (**10b**).* Compound **9b** (398 mg, 0.80 mmol) was dissolved in TFA (6 mL) and heated to 55 °C until reaction control by TLC showed complete conversion. The solvent was evaporated and the product was redissolved in ethyl acetate and then washed with sat. sodium bicarbonate solution (2x). Purification by flash column chromatography (SiO_2, DCM/EtOH 95:05 to 90:10) afforded a brown solid (289 mg, 96%). ^{1}H NMR (300 MHz, DMSO-d_6) δ 4.38 (s,

2H), 5.94 (br. s., 2H), 6.44 (d, $J = 4.6$ Hz, 1H), 7.11–7.56 (m, 10H), 7.68–7.91 (m, 1H), 12.71 (br. s., 1H); TLC-MS (ESI) $m/z = 377.2$ $[M + H]^+$ $m/z = 375.3$ $[M - H]^-$.

*4.2.4.10. N-(4-(5-(4-Fluorophenyl)-2-(methylthio)-1H-imidazol-4-yl)pyridin-2-yl)-3-(3,4,5-trimethoxyphenyl)propanamide (**1a**) [27].*. The title compound was prepared according to **general procedure B** starting from **10a** (50 mg, 0.17 mmol) and 3-(3,4,5-trimethoxyphenyl)propionic acid (52 mg, 0.22 mmol). Purification by flash column chromatography (SiO_2, DCM/EtOH 97:03) afforded **1a** as a yellow solid (35 mg, 40%). ^{1}H NMR (300 MHz, $CDCl_3$) δ 2.63 (s, 3H), 2.64–2.70 (m, 2H), 2.88–2.97 (m, 2H), 3.77 (s, 6H), 3.79 (s, 3H), 6.38 (s, 2H), 6.92–7.10 (m, 3H), 7.32–7.46 (m, 2H), 8.00 (d, $J = 5.4$ Hz, 1H), 8.31 (br. s., 1H), 8.71 (br. s., 1H). ^{13}C NMR (75 MHz, $CDCl_3$) δ 16.1, 31.7, 39.4, 56.1, 60.8, 105.3, 111.4, 115.8 (d, $^2J_{CF} = 22.1$ Hz), 117.7, 130.2 (d, $^3J_{CF} = 7.7$ Hz), 136.2, 136.4, 147.5, 151.6, 153.2, 162.6 (d, $^1J_{CF} = 248.0$ Hz); TLC-MS (ESI) $m/z = 545.7$ $[M + Na]^+$ $m/z = 521.4$ $[M - H]^-$. HPLC: $t_R = 7.55$ min (96.3% purity).

*4.2.4.11. N-(4-(5-(4-Fluorophenyl)-2-(methylthio)-1H-imidazol-4-yl) pyridin-2-yl)acetamide (**1b**) [50].*. The title compound was prepared according to **general procedure A** starting from **11a** (200 mg, 0.63 mmol) and acetamide (111 mg, 1.89 mmol). Purification by flash column chromatography (SiO_2, DCM/EtOH 96:04) afforded **1b** as a yellow solid (118 mg, 55%). ^{1}H NMR (300 MHz, DMSO-d_6) δ 2.03–2.09 (m, 3H), 2.62 (s, 3H), 6.98–7.09 (m, 1H), 7.17 (s, 1H), 7.29 (t, $J = 8.9$ Hz, 1H), 7.43–7.55 (m, 2H), 8.13 (d, $J = 5.4$ Hz, 1H), 8.29 (s, 1H), 10.33 (s, 1H), 12.71 (br. s., 1H). ^{13}C NMR (75 MHz, DMSO-d_6) δ 15.2, 23.9, 110.4, 115.9 (d, $^2J_{CF} = 21.5$ Hz), 116.5, 126.6 (d, $^4J_{CF} = 3.3$ Hz), 130.1, 130.7 (d, $^3J_{CF} = 8.3$ Hz), 134.5, 142.2, 143.8, 147.7, 152.5, 162.0 (d, $^1J_{CF} = 245.5$ Hz), 169.0. TLC-MS (ESI) $m/z = 343.3$ $[M + H]^+$ $m/z = 341.1$ $[M - H]^-$. HPLC: $t_R = 3.60$ min (96.7% purity).

*4.2.4.12. N-(4-(4-(4-Fluorophenyl)-2-(methylthio)-1H-imidazol-5-yl)pyridin-2-yl)cyclopropanecarboxamide (**1c**).* The title compound was prepared according to **general procedure A** starting from **11a** (200 mg, 0.63 mmol) and cyclopropanecarboxamide (40 mg, 0.47 mmol). Purification by flash column chromatography (SiO_2, *n*-hexane/EtOAc 70:30 to 20:80) afforded **1c** as a yellow solid (43 mg, 42%). ^{1}H NMR (300 MHz, DMSO-d_6) δ 0.78 (d, $J = 5.9$ Hz, 4H), 1.93–2.04 (m, 1H), 2.62 (s, 3H), 6.97 (dd, $J = 5.3$, 1.6 Hz, 1H), 7.12–7.33 (m, 2H), 7.43–7.54 (m, 2H), 8.11 (d, $J = 5.2$ Hz, 1H), 8.34 (s, 1H), 10.60–10.84 (m, 1H), 12.66–12.82 (m, 1H). ^{13}C NMR (75 MHz, DMSO-d_6) δ 7.5, 14.2, 15.1, 110.6, 115.8 (d, $^2J_{CF} = 21.5$ Hz), 116.3, 126.6 (d, $^4J_{CF} = 3.3$ Hz), 130.0, 130.7 (d, $^3J_{CF} = 8.3$ Hz), 134.5, 142.2, 143.8, 147.6, 152.5, 161.9 (d, $^1J_{CF} = 247.1$ Hz), 172.3. TLC-MS (ESI) $m/z = 369.1$ $[M + H]^+$ $m/z = 366.9$ $[M - H]^-$. HPLC: $t_R = 5.16$ min (97.4% purity).

*4.2.4.13. N-(4-(5-(4-Fluorophenyl)-2-(methylthio)-1H-imidazol-4-yl)pyridin-2-yl)cyclopentanecarboxamide (**1d**).* The title compound was prepared according to **general procedure B** starting from **10a** (93 mg, 0.31 mmol) and cyclopentanecarboxylic acid (46 mg, 0.40 mmol). Purification by flash column chromatography (SiO_2, DCM/EtOH 97:03) afforded **1d** as a yellow solid (60 mg, 49%). ^{1}H NMR (300 MHz, DMSO-d_6) δ 1.46–1.58 (m, 2H), 1.60–1.73 (m, 4H), 1.75–1.90 (m, 2H), 2.62 (s, 3H), 2.83–2.99 (m, 1H), 6.97 (dd, $J = 5.3$, 1.6 Hz, 1H), 7.25 (br. s., 2H), 7.42–7.56 (m, 2H), 8.15 (br. s., 1H), 8.31 (br. s., 1H), 10.34 (br. s., 1H), 12.74 (br. s, 1H). ^{13}C NMR (75 MHz, $CDCl_3$) δ 16.0, 25.9, 30.2, 45.3, 111.1, 115.7 (d, $^2J_{CF} = 22.1$ Hz), 117.2, 130.2 (d, $^3J_{CF} = 7.7$ Hz), 146.2, 152.0, 162.6 (d, $^1J_{CF} = 248.2$ Hz), 181.7. TLC-MS (ESI) $m/z = 397.2$ $[M + H]^+$ $m/z = 395.2$ $[M - H]^-$. HPLC: $t_R = 7.12$ min (97.0% purity).

*4.2.4.14. N-(4-(5-(4-Fluorophenyl)-2-(methylthio)-1H-imidazol-4-yl)pyridin-2-yl)-2-(3,4,5-trimethoxyphenyl)acetamide (**1e**).* The title compound was prepared according to **general procedure B** starting from **10a** (72 mg, 0.24 mmol) and 2-(3,4,5-trimethoxyphenyl) acetic acid (136 mg, 0.6 mmol). Purification by flash column chromatography (SiO_2, DCM/EtOH 97:03) afforded **1e** as a yellow solid (88 mg, 77%). ^{1}H NMR (300 MHz, $CDCl_3$) δ 2.59 (s, 3H), 3.61 (s, 2H), 3.77 (s, 6H), 3.80 (s, 3H), 6.45 (s, 2H), 6.96 (t, $J = 8.7$ Hz, 2H), 7.05 (d, $J = 4.9$ Hz, 1H), 7.35 (dd, $J = 8.5$, 5.5 Hz, 2H), 8.02 (d, $J = 5.4$ Hz, 1H), 8.33 (s, 1H), 8.48 (br. s., 1H). ^{13}C NMR (75 MHz, $CDCl_3$) δ 16.1, 45.0, 56.1, 60.8, 106.4, 111.3, 115.7 (d, $^2J_{CF} = 21.6$ Hz), 117.9, 129.4, 130.2 (d, $^3J_{CF} = 7.7$ Hz), 137.3, 143.5, 147.5, 151.5, 153.6, 162.5 (d, $^1J_{CF} = 248.2$ Hz), 169.8. TLC-MS (ESI) $m/z = 508.9$ $[M + H]^+$ $m/z = 507.1$ $[M - H]^-$. HPLC: $t_R = 6.20$ min (100.0% purity).

*4.2.4.15. N-(4-(5-(4-Fluorophenyl)-2-(methylthio)-1H-imidazol-4-yl)pyridin-2-yl)-3-(4-methoxyphenyl)propanamide (**1f**).* The title compound was prepared according to **general procedure B** starting from **10a** (72 mg, 0.24 mmol) and 3-(4-methoxyphenyl)propionic acid (108 mg, 0.60 mmol). Purification by flash column chromatography (SiO_2, DCM/EtOH 97:03) afforded **1f** as a yellow solid (50 mg, 45%). ^{1}H NMR (300 MHz, $CDCl_3$) δ 2.55–2.71 (m, 5 H), 2.91 (t, $J = 7.7$ Hz, 2H), 3.75 (s, 3H), 6.75–6.82 (m, 2H), 6.95–7.11 (m, 5 H), 7.40 (dd, $J = 8.1$, 5.5 Hz, 2H), 7.97 (d, $J = 5.5$ Hz, 1H), 8.33 (s, 1H), 9.00 (br. s., 1H). ^{13}C NMR (75 MHz, $CDCl_3$) δ 16.1, 30.3, 39.4, 55.2, 111.3, 113.9, 115.7 (d, $^2J_{CF} = 21.6$ Hz), 117.5, 129.2, 130.2 (d, $^3J_{CF} = 8.3$ Hz), 132.3, 147.0, 151.6, 158.0, 162.6 (d, $^1J_{CF} = 248.2$ Hz), 171.4; TLC-MS (ESI) $m/z = 462.8$ $[M + H]^+$ $m/z = 461.0$ $[M - H]^-$. HPLC: $t_R = 7.56$ min (99.5% purity).

*4.2.4.16. N-(4-(5-(4-Fluorophenyl)-2-(methylthio)-1H-imidazol-4-yl)pyridin-2-yl)-3-(3-methoxyphenyl)propanamide (**1g**).* The title compound was prepared according to **general procedure B** starting from **10a** (72 mg, 0.24 mmol) and 3-(3-methoxyphenyl)propionic acid (108 mg, 0.60 mmol). Purification by flash column chromatography (SiO_2, DCM/EtOH 97:03) afforded **1f** as a yellow solid (73 mg, 66%). ^{1}H NMR (300 MHz, $CDCl_3$) δ 2.61 (s, 3H), 2.65 (d, $J = 8.0$ Hz, 2H), 2.93 (t, $J = 7.3$ Hz, 2H), 3.73 (s, 3H), 6.67–6.75 (m, 3H), 6.94–7.05 (m, 3H), 7.11–7.18 (m, 1H), 7.38 (dd, $J = 8.2$, 5.6 Hz, 2H). 7.97 (d, $J = 5.3$ Hz, 1H). 8.32 (br. s., 1H). 9.12 (br. s., 1H). ^{13}C NMR (75 MHz, $CDCl_3$) δ 16.1, 45.0, 56.1, 60.8, 106.4, 111.3, 115.7 (d, $^2J_{CF} = 21.6$ Hz), 117.9, 129.4, 130.2 (d, $^3J_{CF} = 7.7$ Hz), 137.3, 143.5, 147.5, 151.5, 153.6, 162.5 (d, $^1J_{CF} = 248.2$ Hz), 170.6; TLC-MS (ESI) $m/z = 462.9$ $[M + H]^+$ $m/z = 461.1$ $[M - H]^-$. HPLC: $t_R = 7.74$ min (100.0% purity).

*4.2.4.17. N-(4-(5-(4-Fluorophenyl)-2-(methylthio)-1H-imidazol-4-yl)pyridin-2-yl)-2-(4-(trifluoromethyl)phenyl)acetamide (**1h**).* The title compound was prepared according to **general procedure C** starting from **10a** (36 mg, 0.12 mmol) and 4-(trifluoromethyl) phenylacetic acid (31 mg, 0.15 mmol). Purification by flash column chromatography (SiO_2, *n*-hexane/EtOAc 50:50) afforded **1h** as a yellow solid (43 mg, 73%). ^{1}H NMR (300 MHz, DMSO-d_6) δ 2.61 (s, 3H), 3.18 (s, 2H), 7.02 (dd, $J = 5.3$, 1.6 Hz, 1H), 7.23 (t, $J = 8.8$ Hz, 2H), 7.43–7.51 (m, 2H), 7.56 (d, $J = 8.1$ Hz, 2H), 7.69 (d, $J = 8.1$ Hz, 2H), 8.18 (d, $J = 5.2$ Hz, 1H), 8.26 (s, 1H), 10.75 (s, 1H), 12.72 (br. s., 1H). ^{13}C NMR (101 MHz, DMSO-d_6) δ 15.0, 42.6, 110.6, 115.6 (d, $^2J_{CF} = 22.0$ Hz), 116.8, 124.3 (q, $^1J_{CF3} = 272.2$ Hz), 125.0 (q, $^3J_{CF3} = 3.7$ Hz), 127.3 (q, $^2J_{CF3} = 31.5$ Hz), 129.9, 130.3 (d, $^3J_{CF} = 8.3$ Hz), 140.6, 142.6, 147.7, 152.3, 161.8 (d, $^1J_{CF} = 245.2$ Hz), 169.0. TLC-MS (ESI) $m/z = 487.3$ $[M + H]^+$ $m/z = 485.2$ $[M - H]^-$. HPLC: $t_R = 8.85$ min (100.0% purity).

*4.2.4.18. N-(4-(5-(4-Fluorophenyl)-2-(methylthio)-1H-imidazol-4-yl)pyridin-2-yl)-3-(4-(trifluoromethyl)phenyl)propanamide (**1i**).*

The title compound was prepared according to **general procedure B** starting from **10a** (72 mg, 0.24 mmol) and 3-[4-(trifluoromethyl) phenyl]propionic acid (78 mg, 0.36 mmol). Purification by flash column chromatography (SiO_2, *n*-hexane/EtOAc 50:50) afforded **1i** as a yellow solid (49 mg, 41%). ^{1}H NMR (300 MHz, $CDCl_3$) δ 2.63 (s, 3H), 2.70 (t, J = 7.4 Hz, 2H), 2.98–3.06 (m, 2H), 7.00 (t, J = 8.6 Hz, 2H), 7.09 (d, J = 4.9 Hz, 1H), 7.27 (d, J = 8.0 Hz, 2H), 7.38 (dd, J = 8.3, 5.4 Hz, 2H), 7.50 (d, J = 8.0 Hz, 2H), 7.97 (d, J = 5.3 Hz, 1H), 8.29 (br. s., 1H), 9.09 (br. s., 1H). ^{13}C NMR (75 MHz, $CDCl_3$) δ 16.1, 30.6, 38.3, 111.2, 115.8 (d, $^2J_{CF}$ = 22.1 Hz), 117.5, 124.2 (q, $^1J_{CF3}$ = 271.4 Hz), 125.4 (q, $^3J_{CF3}$ = 3.9 Hz), 128.6 (q, $^2J_{CF3}$ = 32.6 Hz), 128.7, 130.2 (d, $^3J_{CF}$ = 8.3 Hz), 143.8, 144.4, 146.2, 151.2, 162.7 (d, $^1J_{CF}$ = 248.8 Hz), 170.8. TLC-MS (ESI) m/z = 501.0 $[M + H]^+$ m/z = 499.1 $[M - H]^-$. HPLC: t_R = 9.32 min (97.1% purity).

*4.2.4.19. N-(4-(5-(4-Fluorophenyl)-2-(methylthio)-1H-imidazol-4-yl)pyridin-2-yl)-1-(trifluoromethyl)cyclopropane-1-carboxamide (**1j**).* The title compound was prepared according to **general procedure C** starting from **10a** (72 mg, 0.24 mmol) and 1-(trifluoromethyl)cyclopropane-1-carboxylic acid (51 mg, 0.33 mmol). Purification by flash column chromatography (SiO_2, *n*-hexane/EtOAc 50:50) afforded **1j** as a yellow solid (43 mg, 41%). ^{1}H NMR (300 MHz, $CDCl_3$) δ 1.30–1.37 (m, 2H), 1.45–1.53 (m, 2H), 2.64 (d, J = 3.9 Hz, 3H), 6.97–7.10 (m, 3H), 7.33–7.43 (m, 2H), 8.10 (d, J = 5.3 Hz, 1H), 8.22 (s, 1H), 8.40 (br. s., 1H). ^{13}C NMR (75 MHz, $CDCl_3$) δ 12.6, 16.2, 28.6 (q, $^2J_{CF3}$ = 33.7 Hz), 111.4, 115.9 (d, $^2J_{CF}$ = 21.6 Hz), 118.1, 125.4 (q, $^1J_{CF3}$ = 273.1 Hz), 130.2 (d, $^3J_{CF}$ = 8.3 Hz), 143.4, 147.8, 151.1, 162.7 (d, $^1J_{CF}$ = 248.8 Hz), 164.6. TLC-MS (ESI) m/z = 437.2 $[M + H]^+$ m/z = 435.3 $[M - H]^-$. HPLC: t_R = 8.04 min (97.6% purity).

*4.2.4.20. trans-N-(4-(5-(4-Fluorophenyl)-2-(methylthio)-1H-imidazol-4-yl)pyridin-2-yl)-2-phenylcyclopropane-1-carboxamide (**1k**).* The title compound was prepared according to **general procedure C** starting from **10a** (53 mg, 0.18 mmol) and *trans*-2-phenylcyclopropane-1-carboxylic acid [51] (43 mg, 0.27 mmol). Purification by flash column chromatography (SiO_2, DCM/EtOH 97:03) afforded **1k** as a semi-white solid (30 mg, 38%). ^{1}H NMR (300 MHz, $CDCl_3$) δ 1.35 (ddd, J = 8.0, 6.6, 4.6 Hz, 1H), 1.67 (dt, J = 9.4, 4.7 Hz, 1H), 1.78–1.88 (m, 1H), 2.49–2.59 (m, 1H), 2.64 (s, 3H), 6.89–6.96 (m, 1H), 6.98–7.10 (m, 4H), 7.14–7.29 (m, 3H), 7.34–7.50 (m, 2H), 7.90 (d, J = 5.4 Hz, 1H), 8.34 (s, 1H), 9.29 (br. s., 1H). ^{13}C NMR (75 MHz, $CDCl_3$) δ 16.1, 16.6, 26.5, 27.5, 111.1, 115.8 (d, $^2J_{CF}$ = 21.6 Hz), 117.4, 126.0, 126.5, 128.5, 130.1 (d, $^3J_{CF}$ = 8.3 Hz), 140.0, 143.7, 147.4, 151.9, 162.6 (d, $^1J_{CF}$ = 248.2 Hz), 171.0. TLC-MS (ESI) m/z 444.9 $[M + H]^+$ m/z = 443.0 $[M - H]^-$. HPLC: t_R = 8.67 min (100.0% purity).

*4.2.4.21. 2-Cyclopropyl-N-(4-(5-(4-fluorophenyl)-2-(methylthio)-1H-imidazol-4-yl)pyridin-2-yl)acetamide (**1l**).* The title compound was prepared according to **general procedure B** starting from **10a** (72 mg, 0.24 mmol) and cyclopropylacetic acid (36 mg, 0.36 mmol). Purification by flash column chromatography (SiO_2, DCM/EtOH 96:04) afforded **1l** as a yellow solid (53 mg, 58%). ^{1}H NMR (300 MHz, DMSO-d_6) δ 0.11–0.23 (m, 2H), 0.40–0.51 (m, 2H), 0.93–1.13 (m, 1H), 2.26 (d, J = 7.1 Hz, 2H), 2.63 (s, 3H), 7.03 (dd, J = 5.4, 1.6 Hz, 1H), 7.26 (t, J = 8.9 Hz, 2H), 7.50 (dd, J = 8.9, 5.5 Hz, 2H), 8.16 (d, J = 5.4 Hz, 1H), 8.23 (d, J = 0.64 Hz, 1H), 10.44 (s, 1H). ^{13}C NMR (75 MHz, DMSO-d_6) δ 4.0, 7.6, 15.0, 41.0, 110.6, 115.7 (d, $^2J_{CF}$ = 21.6 Hz), 116.6, 130.5 (d, $^3J_{CF}$ = 7.8 Hz), 142.9, 146.8, 152.0, 161.9 (d, $^1J_{CF}$ = 245.4 Hz), 171.8. TLC-MS (ESI) m/z = 383.0 $[M + H]^+$ m/z = 381.0 $[M - H]^-$. HPLC: t_R = 6.04 min (100.0% purity).

*4.2.4.22. N-(4-(5-(4-Fluorophenyl)-2-(methylthio)-1H-imidazol-4-yl)pyridin-2-yl)cyclobutanecarboxamide (**1m**).* Compound **10a** (125 mg, 0.30 mmol) was dissolved in pyridine (5 mL) and cooled to 0 °C. Cyclobutanecarbonyl chloride (102 μL, 0.89 mmol) was added dropwise with a syringe and the mixture was stirred overnight at rt. Purification by flash column chromatography (SiO_2, *n*-hexane/EtOAc 70:30) afforded **1m** as a yellow solid (24 mg, 21%). ^{1}H NMR (300 MHz, $CDCl_3$) δ 1.80–2.04 (m, 2H), 2.12–2.25 (m, 2H), 2.25–2.40 (m, 2H), 2.65 (s, 3H), 3.18 (quin, J = 8.5 Hz, 1H), 6.97–7.07 (m, 3H), 7.43 (dd, J = 8.1, 5.6 Hz, 2H), 8.04 (dd, J = 5.4, 0.4 Hz, 1H), 8.16 (br. s., 1H), 8.36 (s, 1H); ^{13}C NMR (75 MHz, $CDCl_3$) δ 16.1, 17.9, 25.1, 40.7, 111.0, 115.7 (d, $^2J_{CF}$ = 21.6 Hz), 117.6, 130.1 (d, $^3J_{CF}$ = 8.3 Hz), 147.4, 151.7, 162.6 (d, $^1J_{CF}$ = 248.2 Hz), 173.9; TLC-MS (ESI) m/z = 383.2 $[M + H]^+$ m/z = 381.2 $[M - H]^-$. HPLC: t_R = 6.30 min (99.1% purity).

*4.2.4.23. N-(4-(5-(4-Fluorophenyl)-2-(methylthio)-1H-imidazol-4-yl)pyridin-2-yl)-3-oxocyclobutane-1-carboxamide (**1n**).* The title compound was prepared according to **general procedure B** starting from **10a** (72 mg, 0.24 mmol) and 3-oxocyclobutanecarboxylic acid (41 mg, 0.36 mmol). Purification by flash column chromatography (SiO_2, *n*-hexane/EtOAc 50:50) afforded **1n** as a yellow solid (88 mg, 93%). ^{1}H NMR (300 MHz, DMSO-d_6) δ 2.62 (s, 3H), 3.25 (td, J = 4.8, 2.3 Hz, 4H), 3.40–3.55 (m, 1H), 7.01 (dd, J = 5.3, 1.6 Hz, 1H), 7.25 (t, J = 8.9 Hz, 2H), 7.44–7.54 (m, 2H), 8.17 (d, J = 5.2 Hz, 1H), 8.36 (s, 1H), 10.71 (s, 1H). ^{13}C NMR (75 MHz, DMSO-d_6) δ 15.1, 28.1, 51.0, 110.8, 115.7 (d, $^2J_{CF}$ = 21.6 Hz), 116.8, 130.4 (d, $^3J_{CF}$ = 8.3 Hz), 142.7, 147.8, 152.4, 161.8 (d, $^1J_{CF}$ = 244.9 Hz), 172.9, 205.1. TLC-MS (ESI) m/z = 397.0 $[M + H]^+$ m/z = 395.0 $[M - H]^-$. HPLC: t_R = 4.09 min (97.2% purity).

*4.2.4.24. trans-3-Chloro-N-(4-(5-(4-fluorophenyl)-2-(methylthio)-1H-imidazol-4-yl)pyridin-2-yl)cyclobutane-1-carboxamide (**1o**) and cis-3-hloro-N-(4-(5-(4-fluorophenyl)-2-(methylthio)-1H-imidazol-4-yl)pyridin-2-yl)cyclobutane-1-carboxamide (**1p**).* The title compounds were prepared according to **general procedure C** starting from **10a** (72 mg, 0.24 mmol) and 3-chlorocyclobutanecarboxylic acid (48 mg, 0.36 mmol). Purification by flash column chromatography (SiO_2, DCM/EtOH 97:03) afforded the separated cis and trans isomers each as a yellow solid (total yield 85 mg, 85% in a ratio of trans/cis 2.5:1). The *cis* and *trans* geometry was confirmed by 2D NOESY experiments.

*4.2.4.25. trans-3-Chloro-N-(4-(5-(4-fluorophenyl)-2-(methylthio)-1H-imidazol-4-yl)pyridin-2-yl)cyclobutane-1-carboxamide (**1o**).* ^{1}H NMR (300 MHz, DMSO-d_6) δ 2.37–2.48 (m, 2H), 2.62 (s, 3H), 2.75 (ddd, J = 13.07, 7.75, 4.9 Hz, 2H), 3.56 (tt, J = 9.5, 4.8 Hz, 1H), 4.65 (quin, J = 6.8 Hz, 1H), 6.99 (dd, J = 5.3, 1.5 Hz, 1H), 7.27 (br. s., 2H), 7.48 (dd, J = 8.6, 5.6 Hz, 2H), 8.13 (br. s., 1H), 8.36 (br. s., 1H), 10.39 (br. s., 1H), 12.72 (br. s., 1H). ^{13}C NMR (75 MHz, MeOD) δ 16.8, 37.6, 38.3, 52.5, 113.4, 116.9 (d, $^2J_{CF}$ = 21.6 Hz), 119.0, 131.8 (d, $^3J_{CF}$ = 8.3 Hz), 145.2, 149.2, 153.6, 164.3 (d, $^1J_{CF}$ = 247.1 Hz), 175.4. TLC-MS (ESI) m/z = 417.1 $[M + H]^+$ m/z = 415.2 $[M - H]^-$.HPLC: t_R = 6.87 min (98.2% purity).

*4.2.4.26. cis-3-Chloro-N-(4-(5-(4-fluorophenyl)-2-(methylthio)-1H-imidazol-4-yl)pyridin-2-yl)cyclobutane-1-carboxamide (**1p**).* ^{1}H NMR (300 MHz, MeOD) δ 2.44–2.58 (m, 2H), 2.64 (s, 3H), 2.67–2.80 (m, 2H), 2.99–3.13 (m, 1H), 4.34–4.46 (m, 1H), 7.07 (dd, J = 5.3, 1.4 Hz, 1H), 7.13 (t, J = 8.8 Hz, 2H), 7.40–7.48 (m, 2H), 8.13 (d, J = 5.3 Hz, 1H), 8.17 (s, 1H). ^{13}C NMR (75 MHz, MeOD) δ 16.8, 35.9, 38.7, 49.3, 113.4, 116.9 (d, $^2J_{CF}$ = 22.1 Hz), 119.1, 131.8 (d, $^3J_{CF}$ = 8.3 Hz), 145.3, 149.2, 153.4, 164.3 (d, $^1J_{CF}$ = 246.6 Hz), 173.8. TLC-MS (ESI) m/z = 417.1 $[M + H]^+$ m/z = 415.2 $[M - H]^-$. HPLC: t_R = 6.64 min (99.1% purity).

*4.2.4.27. N-(4-(5-(4-Fluorophenyl)-2-(methylthio)-1H-imidazol-4-yl)pyridin-2-yl)-3-oxocyclopentane-1-carboxamide (**1q**).* The title compound was prepared according to **general procedure C** starting from **10a** (72 mg, 0.24 mmol) and 3-oxocyclopentanecarboxylic acid (53 mg, 0.42 mmol). Purification by flash column chromatography (SiO_2, DCM/EtOH 97:03) afforded **1q** as a yellow solid (53 mg, 54%). ^{1}H NMR (300 MHz, $CDCl_3$) δ 2.09–2.30 (m, 3H), 2.33–2.38 (m, 1H), 2.40–2.46 (m, 1H), 2.49–2.57 (m, 1H), 2.61 (s, 3H), 2.97–3.13 (m, 1H), 6.94–7.06 (m, 3H), 7.37 (dd, J = 8.7, 5.3 Hz, 2H), 7.99 (d, J = 5.4 Hz, 1H), 8.24 (br. s., 1H), 8.52 (br. s., 1H). ^{13}C NMR (75 MHz, DMSO-d_6) δ 16.1, 25.3, 27.1, 37.4, 41.4, 111.3, 115.8 (d, $^2J_{CF}$ = 22.1 Hz), 117.6, 130.2 (d, $^3J_{CF}$ = 7.8 Hz), 143.9, 146.7, 151.5, 162.6 (d, $^1J_{CF}$ = 248.2 Hz), 172.9, 217.2. TLC-MS (ESI) m/z = 433.2 $[M + Na]^+$ m/z = 409.3 $[M - H]^-$. HPLC: t_R = 4.31 min (98.3% purity).

*4.2.4.28. N-(4-(5-(4-Fluorophenyl)-2-(methylthio)-1H-imidazol-4-yl)pyridin-2-yl)tetrahydrofuran-2-carboxamide (**1r**).* The title compound was prepared according to **general procedure B** starting from **10a** (93 mg, 0.30 mmol) and tetrahydro-2-furoic acid (46 mg, 0.40 mmol). Purification by flash column chromatography (SiO_2, DCM/EtOH 97:03) afforded **1r** as a yellow solid (60 mg, 50%). ^{1}H NMR (300 MHz, $CDCl_3$) δ 1.79–1.97 (m, 2H), 1.99–2.11 (m, 1H), 2.19–2.34 (m, 1H), 2.60 (s, 3H), 3.85–3.95 (m, 1H), 4.01 (dt, J = 8.2, 6.5 Hz, 1H), 4.39 (dd, J = 8.5, 5.8 Hz, 1H), 6.92–7.00 (m, 2H), 7.03 (dd, J = 5.4, 1.5 Hz, 1H), 7.33–7.41 (m, 2H), 8.07 (dd, J = 5.3, 0.6 Hz, 1H), 8.28–8.34 (m, 1H), 9.00 (s, 1H). ^{13}C NMR (75 MHz, $CDCl_3$) δ 16.1, 25.5, 30.2, 69.7, 78.3, 110.9, 115.6 (d, $^2J_{CF}$ – 21.6 Hz), 117.9, 130.1 (d, $^3J_{CF}$ = 8.3 Hz), 143.6, 147.8, 150.8, 162.4 (d, $^1J_{CF}$ = 248.1 Hz), 172.3. TLC-MS (ESI) m/z = 399.2 $[M + H]^+$ m/z = 397.2 $[M - H]^-$. HPLC: t_R = 5.98 min (97.6% purity).

*4.2.4.29. N-(4-(5-(4-Fluorophenyl)-2-(methylthio)-1H-imidazol-4-yl)pyridin-2-yl)furan-3-carboxamide (**1t**).* The title compound was prepared according to **general procedure C** starting from **10a** (72 mg, 0.24 mmol) and 3-furoic acid (37 mg, 0.33 mmol). Purification by flash column chromatography (SiO_2, *n*-hexane/EtOAc 50:50) afforded **1t** as a yellow solid (26 mg, 27%). ^{1}H NMR (300 MHz, DMSO-d_6) δ 2.68 (s, 3H), 7.10 (dd, J = 1.9, 0.7 Hz, 1H), 7.13 (dd, J = 5.3, 1.5 Hz, 1H), 7.32 (t, J = 8.6 Hz, 2H), 7.52–7.61 (m, 2H), 7.82 (t, J = 1.7 Hz, 1H), 8.28 (d, J = 5.2 Hz, 1H), 8.41 (s, 1H), 8.57 (dd, J = 1.4, 0.7 Hz, 1H), 10.61 (s, 1H), 12.76 (br. s., 1H). ^{13}C NMR (75 MHz, DMSO-d_6) δ 15.0, 109.4, 111.6, 115.7 (d, $^2J_{CF}$ = 22.1 Hz), 117.0, 122.5, 130.4 (d, $^3J_{CF}$ = 8.3 Hz), 142.8, 144.3, 146.6, 147.6, 152.3, 160.7, 161.8 (d, $^1J_{CF}$ = 244.9 Hz). TLC-MS (ESI) m/z = 395.3 $[M + H]^+$ m/z = 393.2 $[M - H]^-$. HPLC: t_R = 5.90 min (99.3% purity).

*4.2.4.30. N-(4-(5-(4-Fluorophenyl)-2-(methylthio)-1H-imidazol-4-yl)pyridin-2-yl)picolinamide (**1u**).* The title compound was prepared according to **general procedure B** starting from **10a** (72 mg, 0.24 mmol) and 3-picolinic acid (44 mg, 0.36 mmol). Purification by flash column chromatography (SiO_2, *n*-hexane/EtOAc 50:50) afforded **1u** as a yellow solid (58 mg, 64%). ^{1}H NMR (300 MHz, DMSO-d_6) δ 2.65 (s, 3H), 7.15 (dd, J = 5.2, 1.6 Hz, 1H), 7.21–7.38 (m, 2H), 7.49–7.59 (m, 2H), 7.72 (ddd, J = 7.5, 4.8, 1.3 Hz, 1H), 8.06–8.14 (m, 1H), 8.16–8.21 (m, 1H), 8.23 (br. s., 1H), 8.54 (br. s., 1H), 8.75 (dd, J = 4.7, 0.5 Hz, 1H), 10.37 (br. s., 1H), 12.77 (br. s., 1H). ^{13}C NMR (75 MHz, DMSO-d_6) δ 15.1, 110.0, 115.9 (d, $^2J_{CF}$ = 21.6 Hz), 117.2, 122.2, 126.6 (d, $^4J_{CF}$ = 3.3 Hz), 127.5, 130.5, 130.8 (d, $^3J_{CF}$ = 8.3 Hz), 134.1, 138.5, 142.4, 144.3, 148.2, 148.5, 148.7, 151.0, 162.1, 161.7 (d, $^1J_{CF}$ = 246.6 Hz). TLC-MS (ESI) m/z = 406.0 $[M + H]^+$ m/z = 404.0 $[M - H]^-$. HPLC: t_R = 7.71 min (97.5% purity).

*4.2.4.31. N-(4-(5-(4-Fluorophenyl)-2-(methylthio)-1H-imidazol-4-yl)pyridin-2-yl)-2-(2-oxopyrrolidin-1-yl)acetamide (**1s**).* The title compound was prepared according to **general procedure A** starting from **11a** (130 mg, 0.41 mmol) and 2-oxopyrrolidin-1-acetamid (87 mg, 0.61 mmol). Purification by flash column chromatography (SiO_2, *n*-hexane/EtOAc 70:30 to 20:80) afforded **1c** as a yellow solid (33 mg, 19%). ^{1}H NMR (300 MHz, $CDCl_3$) δ 2.01–2.17 (m, 2H), 2.42–2.53 (m, 2H), 2.64 (s, 3H), 3.51 (t, J = 7.0 Hz, 2H), 4.12 (s, 2H), 6.87–7.02 (m, 3H), 7.35 (dd, J = 8.6, 5.4 Hz, 2H), 7.96 (d, J = 5.3 Hz, 1H), 8.12 (br. s., 1H), 9.38 (br. s., 1H). ^{13}C NMR (75 MHz, $CDCl_3$) δ 16.1, 18.0, 30.4, 47.1, 48.5, 111.4, 115.5 (d, $^2J_{CF}$ = 21.6 Hz), 117.9, 130.1 (d, $^3J_{CF}$ = 8.3 Hz), 143.9, 147.3, 151.3, 162.4 (d, $^1J_{CF}$ = 248.7 Hz), 166.6, 176.8. TLC-MS (ESI) m/z = 447.2 $[M + Na]^+$ m/z = 423.9 $[M - H]^-$. HPLC: t_R = 3.96 min (100.0% purity).

4.2.5.36. trans-N-(4-(5-(4-Fluorophenyl)-2-(methylthio)-1H-imidazol-4-yl)pyridin-2-yl)-2-

*4.2.4.32. N-(4-(2-(Benzylthio)-5-(4-fluorophenyl)-1H-imidazol-4-yl)pyridin-2-yl)-3-(3,4,5-trimethoxyphenyl)propanamide (**2a**).* The title compound was prepared according to **general procedure B** starting from **10b** (78 mg, 0.21 mmol) and 3-(3,4,5-trimethoxyphenyl)propionic acid (65 mg, 0.27 mmol). Purification by flash column chromatography (SiO_2, DCM/EtOH 97:03) afforded **2a** as a yellow solid (56 mg, 45%). ^{1}H NMR (300 MHz, $CDCl_3$) δ 2.58–2.70 (m, 2H), 2.86–2.98 (m, 2H), 3.76 (s, 6H), 3.79 (s, 3H), 4.30 (s, 2H), 6.38 (s, 2H), 7.00 (t, J = 8.7 Hz, 3H), 7.17–7.30 (m, 5H), 7.31–7.45 (m, 2H), 7.98 (d, J = 5.2 Hz, 1H), 8.32 (br. s., 1H), 8.66 (br. s., 1H). ^{13}C NMR (75 MHz, $CDCl_3$) δ 31.7, 39.0, 39.4, 56.1, 60.8, 105.3, 111.4, 115.7 (d, $^2J_{CF}$ = 21.0 Hz), 117.7, 127.6, 128.7, 129.0, 130.2 (d, $^3J_{CF}$ – 8.3 Hz), 136.2, 136.4, 137.4, 141.1, 147.5, 151.7, 153.2, 162.6 (d, $^1J_{CF}$ = 248.7 Hz), 170.9. TLC-MS (ESI) m/z = 597.1 $[M - H]^-$. HPLC: t_R = 8.57 min (97.2% purity).

*4.2.4.33. N-(4-(2-(Benzylthio)-5-(4-fluorophenyl)-1H-imidazol-4-yl)pyridin-2-yl)acetamide (**2b**).* The title compound was prepared according to **general procedure A** starting from **11b** (100 mg, 0.25 mmol) and acetamide (44 mg, 0.75 mmol). Purification by flash column chromatography (SiO_2, DCM/EtOH 97:03 to 95:05) afforded **2b** as a yellow solid (82 mg, 78%). ^{1}H NMR (300 MHz, $CDCl_3$) δ 2.08 (s, 3H), 4.28 (s, 2H), 6.93–7.03 (m, 2H), 7.08 (br. s., 1H), 7.18–7.28 (m, 5 H), 7.35 (br. s., 2H), 8.01 (d, J = 5.3 Hz, 1H), 8.30 (br. s., 1H), 9.11 (br. s., 1H), 10.67 (br. s., 1H). ^{13}C NMR (75 MHz, $CDCl_3$) δ 24.4, 38.9, 111.4, 115.7 (d, J = 21.7 Hz), 117.7, 127.5, 128.5, 128.9, 130.1 (d, J = 8.3 Hz), 137.3, 141.3, 147.3, 151.8, 162.5 (d, J = 248.3 Hz), 169.2. TLC-MS (ESI) m/z = 419.2 $[M + H]^+$ m/z = 417.0 $[M - H]^-$. HPLC: t_R = 6.42 min (98.2% purity).

*4.2.4.34. N-(4-(2-(Benzylthio)-5-(4-fluorophenyl)-1H-imidazol-4-yl)pyridin-2-yl)cyclopropanecarboxamide (**2c**).* The title compound was prepared according to **general procedure A** starting from **11b** (125 mg, 0.32 mmol) and cyclopropanecarboxamide (40 mg, 0.47 mmol). Purification by flash column chromatography (SiO_2, DCM/EtOH 97:03 to 95:05) afforded **2c** as a yellow solid (90 mg, 64%). ^{1}H NMR (300 MHz, $CDCl_3$) δ 0.77–0.89 (m, 2H), 0.98–1.07 (m, 2H), 1.47–1.62 (m, 1H), 4.28 (s, 2H), 6.99 (t, J = 8.6 Hz, 3H), 7.15–7.29 (m, 5 H), 7.35 (br. s., 2H), 8.02 (d, J = 5.3 Hz, 1H), 8.26 (br. s., 1H), 9.10 (br. s., 1H). ^{13}C NMR (75 MHz, $CDCl_3$) δ 8.4, 15.7, 39.0, 111.4, 115.7 (d, $^2J_{CF}$ = 22.2 Hz), 117.4, 127.5, 128.6, 129.0, 130.1 (d, $^3J_{CF}$ = 8.3 Hz), 137.3, 141.0, 147.3, 151.9, 162.5 (d, $^1J_{CF}$ = 247.9 Hz), 172.6. TLC-MS (ESI) m/z = 445.6 $[M + H]^+$ m/z = 443.3 $[M - H]^-$. HPLC: t_R = 7.62 min (98.9% purity).

*4.2.4.35. N-(4-(2-(Benzylthio)-5-(4-fluorophenyl)-1H-imidazol-4-yl)pyridin-2-yl)cyclopentanecarboxamide (**2d**).* The title compound was prepared according to **general procedure B** starting from **10b** (78 mg, 0.21 mmol) and cyclopentanecarboxylic acid (31 mg, 0.27 mmol). Purification by flash column chromatography (SiO_2, *n*-hexane/EtOAc 70:30 to 0:100) afforded **2d** as a yellow solid (40 mg,

41%). ^{1}H NMR (300 MHz, $CDCl_3$) δ 1.52–1.98 (m, 8H), 2.71 (quin, J = 7.9 Hz, 1H), 4.29 (s, 2H), 6.93–7.06 (m, 3H), 7.19–7.30 (m, 5H), 7.31–7.45 (m, 2H), 8.00 (d, J = 5.4 Hz, 1H), 8.34 (br. s., 1H), 8.66 (br. s., 1H). ^{13}C NMR (75 MHz, $CDCl_3$) δ 26.0, 30.4, 39.0, 46.7, 111.4, 115.8 (d, $^2J_{CF}$ = 21.5 Hz), 117.5, 127.6, 128.6, 129.0, 130.2 (d, $^3J_{CF}$ = 8.3 Hz), 137.4, 141.0,147.1, 152.0, 162.6 (d, $^1J_{CF}$ = 248.4 Hz), 175.4. TLC-MS (ESI) m/z = 472.9 $[M + H]^+$ m/z = 471.1 $[M - H]^-$. HPLC: t_R = 9.14 min (95.4% purity).

*4.2.4.36. N-(4-(2-(Benzylthio)-5-(4-fluorophenyl)-1H-imidazol-4-yl) pyridin-2-yl)-2-(4-fluorophenyl)acetamide (**2e**).* The title compound was prepared according to **general procedure B** starting from **10b** (78 mg, 0.21 mmol) and 4-fluorophenylacetic acid (42 mg, 0.27 mmol). Purification by flash column chromatography (SiO_2, DCM/EtOH 97:03 to 95:05) afforded **2e** as a yellow solid (73 mg, 69%). ^{1}H NMR (300 MHz, $CDCl_3$) δ 3.67 (s, 2H), 4.30 (s, 2H), 6.96–7.11 (m, 5H), 7.18–7.32 (m, 7H), 7.37 (br. s., 2H), 8.02 (d, J = 5.4 Hz, 1H), 8.17 (br. s., 1H), 8.28 (br. s., 1H). ^{13}C NMR (75 MHz, $CDCl_3$) δ 38.8, 43.7, 111.1, 115.8 (d, $^2J_{CF}$ = 21.6 Hz), 115.9 (d, $^2J_{CF}$ = 21.0 Hz), 117.8, 127.5, 128.6, 129.0, 129.5 (d, $^4J_{CF}$ = 3.3 Hz), 130.1 (d, $^3J_{CF}$ = 7.7 Hz), 130.9 (d, $^3J_{CF}$ = 8.3 Hz), 137.4, 141.3, 147.4, 151.4, 162.1 (d, $^1J_{CF}$ = 246.6 Hz), 162.6 (d, $^1J_{CF}$ = 248.2 Hz), 169.6. TLC-MS (ESI) m/z = 534.9 $[M + Na]^+$ m/z = 511.2 $[M - H]^-$. HPLC: t_R = 10.54 min (95.0% purity).

*4.2.4.37. N-(4-(4-(4-Fluorophenyl)-2-(methylsulfinyl)-1H-imidazol-5-yl)pyridin-2-yl)cyclopropanecarboxamide (**12a**).* Compound **1c** (73 mg, 0.19 mmol) was dissolved in acetontrile (10 mL) and a 28–31 % wt. aqueous solution of H_2O_2 (20 µL, 0.195 mmol) was added before the solution was stirred for 24 h at rt. An additional 60 µL (0.585 mmol) of aqueous H_2O_2 solution (0.39 mmol) was added and the mixture was further stirred until reaction control by TLC showed complete conversion of the starting material (48 h). Purification by flash column chromatography (SiO_2, DCM/EtOH 97:3) afforded **12a** as a yellow solid (37 mg, 51%). ^{1}H NMR (300 MHz, $CDCl_3$) δ 0.82–0.92 (m, 2H), 1.02–1.12 (m, 2H), 1.61–1.74 (m, 1H), 3.12 (s, 3H), 6.94 (d, J = 4.8 Hz, 1H), 7.08 (t, J = 8.6 Hz, 2H), 7.39–7.49 (m, 2H), 7.88 (d, J = 5.3 Hz, 1H), 8.50 (s, 1H), 9.30 (br. s., 1H), 13.08 (br. s, 1H). ^{13}C NMR (75 MHz, $CDCl_3$) δ 8.5, 15.6, 40.9, 112.1, 116.0 (d, $^2J_{CF}$ = 21.0 Hz), 117.4, 130.7 (d, $^3J_{CF}$ = 8.3 Hz), 146.9, 147.9, 152.2, 163.0 (d, $^1J_{CF}$ = 247.1 Hz), 172.7; TLC-MS (ESI) m/z = 407.2 $[M + Na]^+$ m/z = 383.2 $[M - H]^-$. HPLC: t_R = 3.47 min (100.0% purity).

*4.2.4.38. N-(4-(4-(4-Fluorophenyl)-2-(methylsulfinyl)-1H-imidazol-5-yl)pyridin-2-yl)cyclobutanecarboxamide (**12b**).* Compound **1m** (60 mg, 0.16 mmol) was dissolved in acetonitrile (10 mL) and a 28–31 % wt. aqueous solution of H_2O_2 (30 µL, 0.293 mmol) was added before the solution was stirred for 24 h at rt. An additional 60 µL (0.585 mmol) of aqueous H_2O_2 solution (0.39 mmol) was added and the mixture was further stirred until reaction control by TLC showed complete conversion of the starting material (72 h). Purification by flash column chromatography (SiO2, *n*-hexane/EtOAc 70:30 to 20:80) afforded **12b** as a yellow solid (26 mg, 42%). ^{1}H NMR (300 MHz, DMSO-d_6) δ 1.72–1.85 (m, 1H), 1.85–2.00 (m, 1H), 2.01–2.26 (m, 4H), 3.09 (s, 3H), 3.35 (quin, J = 8.2 Hz, 1H), 6.99 (dd, J = 5.2, 1.5 Hz, 1H), 7.29 (t, J = 8.9 Hz, 2H), 7.47–7.58 (m, 2H), 8.18 (d, J = 5.2 Hz, 1H), 8.38 (s, 1H), 10.27 (s, 1H), 13.89 (br. s., 1H). ^{13}C NMR (75 MHz, DMSO-d_6) δ 17.7, 24.4, 39.1, 111.2, 115.8 (d, $^2J_{CF}$ = 21.6 Hz), 116.9, 130.8 (d, $^3J_{CF}$ = 8.3 Hz), 147.9, 148.8, 152.7, 162.1 (d, $^1J_{CF}$ = 244.9 Hz), 173.6. TLC-MS (ESI) m/z = 421.1 $[M + Na]^+$ m/z = 397.2 $[M - H]^-$. HPLC: t_R = 4.81 min (99.8% purity).

*4.2.4.39. N-(4-(4-(4-Fluorophenyl)-1-methyl-2-(methylthio)-1H-imidazol-5-yl)pyridin-2-yl)cyclopropanecarboxamide (**14**) [25].* 4-(4-(4-Fluorophenyl)-1-methyl-2-(methylthio)-1*H*-imidazol-5-yl)pyridin-2-amine (**13**) [25] (150 mg, 0.48 mmol) was dissolved in pyridine (5 mL) and cooled to 0 °C. Cyclopropanecarbonyl chloride (87 µL, 0.95 mmol) was added dropwise via syringe. The reaction was stirred for 2 h before H_2O (40 mL) was added and it was extracted with ethyl acetate (3x). The combined organic layers were dried over anhydrous Na_2SO_4, concentrated in vacuo and purified by flash column chromatography (SiO_2, n-hexane/EtOAc 50:50) to give **14** as a yellow solid (57 mg, 31%). ^{1}H NMR (300 MHz, DMSO-d_6) δ 0.79–0.90 (m, 4H), 2.01–2.12 (m, 1H), 2.69 (s, 3H), 3.44 (s, 3H), 7.06–7.22 (m, 3H), 7.39–7.53 (m, 2H), 8.10 (d, J = 0.5 Hz, 1H), 8.46 (dd, J = 5.0, = 0.6 Hz, 1H), 11.02 (s, 1H). ^{13}C NMR (75 MHz, DMSO-d_6) δ 7.7, 14.2, 15.3, 31.6, 114.3, 115.2 (d, $^2J_{CF}$ = 21.0 Hz), 120.3, 127.9, 128.2 (d, $^3J_{CF}$ = 7.7 Hz), 130.4 (d, $^4J_{CF}$ = 3.3 Hz), 137.0, 139.9, 143.9, 148.8, 152.8, 161.0 (d, $^1J_{CF}$ = 245.5 Hz), 172.8; TLC-MS (ESI) m/z = 383.1 $[M + H]^+$ m/z = 383.1 $[M - H]^-$. HPLC: t_R = 6.39 min (100.0% purity).

*4.2.4.40. N-(4-(5-(4-Fluorophenyl)-1-methyl-2-(methylthio)-1H-imidazol-4-yl)pyridin-2-yl)cyclopropanecarboxamide (**16**).* The title compound was prepared according to **general procedure A** starting from 2-chloro-4-(5-(4-fluorophenyl)-1-methyl-2-(methylthio)-1*H*-imidazol-4-yl)pyridine (**15**) [22] (100 mg, 0.30 mmol) and cyclopropanecarboxamide (38.3 mg, 0.45 mmol). Purification by flash column chromatography (SiO_2, *n*-hexane/EtOAc 70:30 to 50:50) afforded **16** as a yellow solid (72 mg, 63%). ^{1}H NMR (300 MHz, $CDCl_3$) δ 0.77–0.86 (m, 2H), 1.01–1.09 (m, 2H), 1.46–1.58 (m, 1H), 2.73 (s, 3H), 3.35 (s, 3H), 6.96 (dd, J = 5.3, 1.6 Hz, 1H), 7.15–7.23 (m, 2H), 7.27–7.34 (m, 2H), 8.01 (dd, J = 5.4, 0.6 Hz, 1H), 8.33 (s, 1H), 8.85 (br. s, 1H). ^{13}C NMR (75 MHz, $CDCl_3$) 8.1, 15.5, 15.7, 31.2, 111.0, 116.5 (d, $^2J_{CF}$ = 21.6 Hz), 119.2, 125.9 (d, $^4J_{CF}$ = 3.3 Hz), 132.0 (d, $^3J_{CF}$ = 8.3 Hz), 132.4, 135.8, 144.3, 144.3, 147.0, 151.9, 163.2 (d, $^1J_{CF}$ = 249.9 Hz), 171.9; TLC-MS (ESI) m/z = 383.4 $[M + H]^+$ m/z = 381.4 $[M - H]^-$. HPLC: t_R = 5.50 min (98.9% purity).

*4.2.4.41. 1-(4-Fluorophenyl)-2-(2-((4-methoxybenzyl)amino)pyridin-4-yl)ethane-1,2-dione (**17**).* Compound **7** (4.00 g, 8.88 mmol) was dissolved in acetic acid and selenium dioxide (1.17 g, 10.66 mmol) was added. The reaction mixture was stirred at 130 °C for 1.5 h. After cooling to rt, the mixture was filtered and the solvent was removed under reduced pressure. The residue was dissolved in DCM (20 mL) and washed with sat. sodium bicarbonate solution (3x). The aqueous layer was adjusted to pH 10–11 with 1 M NaOH and extracted twice with DCM. The combined organic layers were dried over anhydrous Na_2SO_4 and the compound was purified by flash chromatography (SiO_2, *n*-hexane/EtOAc 85:15 to 70:30) to give **17** as a yellow solid (1.41 g, 44%). ^{1}H NMR (300 MHz, $CDCl_3$) δ 3.80 (s, 3H), 4.47 (d, J = 4.3 Hz, 2H), 5.20 (br. s., 1H), 6.81–6.89 (m, 3H), 7.00 (dd, J = 5.3, 1.4 Hz, 1H), 7.14–7.27 (m, 4H), 7.93–8.01 (m, 2H), 8.29 (dd, J = 5.2, 0.7 Hz, 1H). TLC-MS (ESI) m/z = 397.1 $[M + MeOH]^+$ m/z = 363.0 $[M - H]^-$. HPLC: t_R = 5.40 min.

*4.2.4.42. 1-(2-Aminopyridin-4-yl)-2-(4-fluorophenyl)ethane-1,2-dione (**18**).* Compound **17** (1.18 g, 3.25 mmol) was dissolved in TFA (15 mL) and stirred at rt until reaction control by TLC showed complete conversion. The solvent was removed under reduced pressure and the residue was dissolved in DCM (20 mL) and washed with sat. sodium bicarbonate solution (3x). The aqueous layer was adjusted to pH 10–11 with 1 M NaOH and extracted twice with DCM. The combined organic layers were dried over anhydrous Na_2SO_4 and purified by flash chromatography (SiO_2, *n*-hexane/EtOAc 70:30 to 50:50) to give **18** as an orange-yellow solid (769 mg, 97%). ^{1}H NMR (300 MHz, $CDCl_3$) δ 6.46 (s, 2H), 6.84–6.87 (m, 2H), 7.47 (t, J = 8.9 Hz, 2H), 8.03 (dd, J = 9.0, 5.4 Hz, 2H), 8.17 (d, J = 6.1 Hz, 1H). ^{13}C NMR (75 MHz, DMSO-d_6) δ 107.8, 108.7, 116.9 (d,

$^2J_{CF}$ = 22.1 Hz), 128.7 (d, $^4J_{CF}$ = 2.8 Hz), 133.0 (d, $^3J_{CF}$ = 10.5 Hz), 139.3, 149.8, 160.7, 166.4 (d, $^1J_{CF}$ = 256.5 Hz), 192.4, 194.6. TLC-MS (ESI) *m/z* = 276.9 [M + MeOH]$^+$ *m/z* = 242.9 [M − H]$^-$. HPLC: t_R = 2.18 min.

*4.2.4.43. N-(Cyclopropanecarbonyl)-N-(4-(2-(4-fluorophenyl)-2-oxoacetyl)pyridin-2-yl)cyclopropanecarboxamide (**19b**).* Compound **18** (1.06 g, 4.35 mmol) was dissolved in DCM (15 mL), cooled to 0 °C and *N,N*-diisopropylethylamine (2.50 mL, 15.22 mmol) was added. Subsequently a solution of cyclopropanecarbonyl chloride (1.82 g, 17.39 mmol) in DCM (10 mL) was added dropwise to the cooled solution. After 1 h, the cooling bath was removed and the mixture was stirred at rt for 17 h. Water (50 mL) was added and the organic layer was collected, washed with sat. sodium bicarbonate solution (2x) and dried over anhydrous Na_2SO_4. Purification by flash chromatography (SiO_2, *n*-hexane/EtOAc 90:10 to 50:50) afforded **19b** as an orange solid (350 mg, 21%). ^{1}H NMR (300 MHz, $CDCl_3$) δ 0.91–0.99 (m, 4H), 1.17–1.24 (m, 4H), 1.99 (tt, *J* = 7.9, 4.6 Hz, 2H), 7.19–7.26 (m, 2H), 7.79–7.86 (m, 2H), 8.01–8.14 (m, 2H), 8.85 (dd, *J* = 5.0, 0.9 Hz, 1H). TLC-MS (ESI) *m/z* = 435.0 [M + MeOH + Na]$^+$. HPLC: t_R = 6.89 min.

*4.2.4.44. N-(4-(4-(4-Fluorophenyl)-1H-imidazol-5-yl)pyridin-2-yl) cyclopropanecarboxamide (**20a**).* The title compound was prepared according to **general procedure D** starting from **19b** (200 mg, 0.53 mmol) using ammonium acetate (811 mg, 10.52 mmol) and paraformaldehyde (24 mg, 0.79 mmol). Purification by flash chromatography (SiO_2, DCM/EtOH 95:05) afforded **20a** as a white solid (110 mg, 65%). ^{1}H NMR (300 MHz, DMSO-d_6) δ 0.78 (d, *J* = 5.9 Hz, 4H), 1.95–2.04 (m, 1H), 7.01 (dd, *J* = 5.2, 1.5 Hz, 1H), 7.26 (t, *J* = 8.9 Hz, 2H), 7.45–7.54 (m, 2H), 7.87 (s, 1H), 8.17 (d, *J* = 5.2 Hz, 1H), 8.33 (s, 1H), 10.73 (s, 1H), 12.79 (br. s., 1H). ^{13}C NMR (75 MHz, DMSO-d_6) δ 7.6, 14.2, 110.9, 115.7 (d, $^2J_{CF}$ = 22.1 Hz), 116.7, 130.3 (d, $^3J_{CF}$ = 8.3 Hz), 136.4, 147.8, 152.6, 161.7 (d, $^1J_{CF}$ = 244.4 Hz), 172.4.TLC-MS (ESI) *m/z* = 322.9 [M + H]$^+$ *m/z* = 321.0 [M − H]$^-$. HPLC: t_R = 2.98 min (98.3% purity).

*4.2.4.45. N-(4-(4-(4-Fluorophenyl)-2-methyl-1H-imidazol-5-yl)pyridin-2-yl)cyclopropanecarboxamide (**20b**).* The title compound was prepared according to **general procedure D** starting from **19b** (100 mg, 0.26 mmol) using ammonium acetate (405 mg, 5.26 mmol) and acetaldehyde (17 mg, 0.39 mmol). Purification by flash chromatography (SiO_2, DCM/EtOH 95:05 to 90:10) afforded **20b** as a white solid (10 mg, 11%). ^{1}H NMR (300 MHz, DMSO-d_6) δ 0.78 (d, *J* = 6.1 Hz, 4H), 1.94–2.03 (m, 1H), 2.34 (s, 3H), 6.96 (dd, *J* = 5.2, 1.6 Hz, 1H), 7.23 (t, *J* = 8.8 Hz, 2H), 7.42–7.50 (m, 2H), 8.12 (d, *J* = 5.1 Hz, 1H), 8.29 (br. s., 1H), 10.66 (br. s., 1H), 12.33 (br. s., 1H). ^{13}C NMR (75 MHz, $CDCl_3$) δ 8.4, 13.9, 25.6, 111.0, 115.6 (d, $^2J_{CF}$ = 21.6), 117.4, 130.0 (d, $^3J_{CF}$ = 8.3 Hz), 145.6, 147.6, 151.9, 162.4 (d, $^1J_{CF}$ = 247.7 Hz), 172.7. TLC-MS (ESI) *m/z* = 337.1 [M + H]$^+$ *m/z* = 335.1 [M − H]$^-$. HPLC: t_R = 3.43 min (95.7%)

*4.2.4.46. N-(4-(2-Ethyl-4-(4-fluorophenyl)-1H-imidazol-5-yl)pyridin-2-yl)cyclopropanecarboxamide (**20c**).* The title compound was prepared according to **general procedure D** starting from **19b** (150 mg, 0.39 mmol) using ammonium acetate (608 mg, 7.89 mmol) and propionaldehyde (34 mg, 0.59 mmol). Purification by flash chromatography (SiO_2, DCM/EtOH 97:03 to 94:06) afforded **20c** as a white solid (47 mg, 34%). ^{1}H NMR (300 MHz, $CDCl_3$) δ 0.81–0.89 (m, 2H), 0.99–1.05 (m, 2H), 1.29 (t, *J* = 7.7 Hz, 3H), 1.53–1.63 (m, 1H), 2.71 (q, *J* = 7.6 Hz, 2H), 6.94–7.03 (m, 3H), 7.39 (dd, *J* = 8.6, 5.4 Hz, 2H), 8.05 (d, *J* = 5.4 Hz, 1H), 8.26 (s, 1H), 9.19 (br. s., 1H). ^{13}C NMR (75 MHz, $CDCl_3$) δ 8.4, 12.6, 15.7, 21.7, 111.2, 115.6 (d, $^2J_{CF}$ = 21.6 Hz), 117.5, 130.1 (d, $^3J_{CF}$ = 8.3 Hz), 147.4, 150.8, 152.0, 162.4 (d, $^1J_{CF}$ = 247.1 Hz), 172.7. TLC-MS (ESI) *m/z* = 351.0 [M + H]$^+$ *m/z* = 349.1 [M − H]$^-$. HPLC: t_R = 3.84 min (95.1% purity).

*4.2.4.47. N-(4-(4-(4-Fluorophenyl)-2-phenyl-1H-imidazol-5-yl)pyridin-2-yl)cyclopropanecarboxamide (**20d**).* The title compound was prepared according to **general procedure D** starting from **19b** (100 mg, 0.26 mmol) using ammonium acetate (405 mg, 5.26 mmol) and benzaldehyde (42 mg, 0.39 mmol). Purification by flash chromatography (SiO_2, *n*-hexane/EtOAc 50:50) afforded **20d** as a white solid (25 mg, 24%). ^{1}H NMR (300 MHz, DMSO-d_6) δ 0.75–0.84 (m, 4H), 1.96–2.05 (m, 1H), 7.06 (dd, *J* = 5.3, 1.4 Hz, 1H), 7.29 (t, *J* = 8.5 Hz, 2H), 7.36–7.44 (m, 1H), 7.44–7.53 (m, 2H), 7.53–7.62 (m, 2H), 8.04–8.11 (m, 2H), 8.18 (d, *J* = 4.6 Hz, 1H), 8.40 (br. s., 1H), 10.73 (br. s., 1H). ^{13}C NMR (75 MHz, DMSO-d_6) δ 7.6, 14.2, 111.1, 115.7 (d, $^2J_{CF}$ = 21.6 Hz), 116.5, 125.4, 128.7, 128.8, 129.9, 130.9 (d, $^3J_{CF}$ = 8.9 Hz), 146.2, 147.7, 152.5, 161.9 (d, $^1J_{CF}$ = 242.1 Hz), 172.4. TLC-MS (ESI) *m/z* = 421.0 [M + Na]$^+$ *m/z* = 397.0 [M − H]$^-$. HPLC: t_R = 6.74 min (98.9% purity).

*4.2.4.48. N-(4-(2-Benzyl-4-(4-fluorophenyl)-1H-imidazol-5-yl)pyridin-2-yl)cyclopropanecarboxamide (**20e**).* The title compound was prepared according to **general procedure D** starting from **19b** (150 mg, 0.39 mmol) using ammonium acetate (608 mg, 7.89 mmol) and phenylacetaldehyde (61 mg, 0.59 mmol). Purification by flash chromatography (SiO_2, *n*-hexane/EtOAc 70:30 to 30:70) afforded **20e** as a tan white solid (8 mg, 5%). ^{1}H NMR (300 MHz, DMSO-d_6) δ 0.82 (d, *J* = 5.96 Hz, 4H), 2.01–2.06 (m, 1H), 4.03–4.13 (m, 2H), 7.01 (dd, *J* = 5.27, 1.51 Hz, 1H), 7.27 (td, *J* = 5.91, 2.48 Hz, 3H), 7.32–7.41 (m, 4H), 7.51 (dd, *J* = 8.62, 5.59 Hz, 2H), 8.16 (br. s., 1H), 8.34 (br. s., 1H), 10.72 (br. s., 1H), 12.21–12.99 (m, 1H). ^{13}C NMR (75 MHz, DMSO-d_6) δ 7.6, 14.2, 34.0, 110.7, 115.6 (d, $^2J_{CF}$ = 22.1 Hz), 116.6, 126.4, 128.4, 128.5, 130.3 (d, $^3J_{CF}$ = 7.7 Hz), 138.2, 147.7, 152.6, 161.8 (d, $^1J_{CF}$ = 244.9 Hz), 172.4. TLC-MS (ESI) *m/z* = 413.1 [M + H]$^+$ *m/z* = 411.1 [M − H]$^-$. HPLC: t_R = 6.65 min (95.9% purity).

*4.2.4.49. N-(4-(4-(4-Fluorophenyl)-2-phenethyl-1H-imidazol-5-yl) pyridin-2-yl)cyclopropanecarboxamide (**20f**).* Compound **19b** (150 mg, 0.39 mmol) was dissolved in methanol (8 mL) before 7 M ammonia in methanol (1.12 mL, 7.89 mmol) and 3-phenylpropionaldehyde (79 mg, 0.59 mmol) were added. The reaction was heated to 80 °C for 3 h. Evaporation of the solvent and subsequent purification by flash chromatography (SiO_2, *n*-hexane/EtOAc 90:10 to 15:85) afforded **20f** as a brown solid (25 mg, 15%). ^{1}H NMR (300 MHz, DMSO-d_6) δ 0.79 (d, *J* = 6.1 Hz, 4H), 2.00 (quin, *J* = 6.2 Hz, 1H), 2.91–3.10 (m, 4H), 6.98 (dd, *J* = 5.2, 1.6 Hz, 1H), 7.15–7.37 (m, 7H), 7.48 (dd, *J* = 8.7, 5.6 Hz, 2H), 8.08–8.41 (m, 2H), 10.68 (br. s., 1H), 12.42 (br. s., 1H). ^{13}C NMR (75 MHz, $CDCl_3$) δ 8.5, 15.8, 30.5, 34.7, 111.2, 115.7 (d, $^2J_{CF}$ = 21.6 Hz), 117.5, 126.4, 128.4, 128.6, 130.1 (d, $^3J_{CF}$ = 8.3 Hz), 140.7, 147.5, 148.8, 152.0, 162.5 (d, $^1J_{CF}$ = 247.7 Hz), 172.7. TLC-MS (ESI) *m/z* = 427.1 [M + H]$^+$ *m/z* = 425.2 [M − H]$^-$. HPLC: t_R = 6.89 min (97.5% purity).

*4.2.4.50. N-(4-(4-(4-Fluorophenyl)-2-(furan-2-yl)-1H-imidazol-5-yl) pyridin-2-yl)cyclopropanecarboxamide (**20g**).* The title compound was prepared according to **general procedure D** starting from **19b** (150 mg, 0.39 mmol) using ammonium acetate (608 mg, 7.89 mmol) and 2-furaldehyde (57 mg, 0.59 mmol). Purification by flash chromatography (SiO_2, DCM/EtOH 97:03 to 95:05) afforded **20g** as a brown solid (79 mg, 52%). ^{1}H NMR (300 MHz, DMSO-d_6) δ 0.80 (d, *J* = 5.9 Hz, 4H), 1.13–1.24 (m, 1H), 6.66 (dd, *J* = 3.2, 1.7 Hz, 1H), 7.02 (d, *J* = 3.4 Hz, 2H), 7.29 (br. s., 2H), 7.55 (dd, *J* = 8.6, 5.6 Hz, 2H), 7.84 (s, 1H), 8.12–8.44 (m, 2H), 10.76 (br. s., 1H), 13.10 (br. s., 1H). ^{13}C NMR (75 MHz, DMSO-d_6) δ 7.6, 14.2, 108.1, 111.1, 111.9, 115.7 (d, $^2J_{CF}$ = 21.6 Hz), 116.9, 130.7 (d, $^3J_{CF}$ = 8.3 Hz), 139.2, 143.4, 145.2, 147.7, 152.5, 161.9 (d, $^1J_{CF}$ = 245.5 Hz), 172.4. TLC-MS (ESI) *m/*

z = 389.0 $[M + H]^+$ m/z = 387.0 $[M - H]^-$. HPLC: t_R = 5.70 min (100.0% purity).

*4.2.4.51. 2-Methyl-1-((2-(trimethylsilyl)ethoxy)methyl)-1H-imidazole (**22**).* 2-Methylimidazole (**21**) (925 mg, 11.27 mmol) was dissolved in THF (40 mL), cooled to 0 °C and sodium hydride 60% in mineral oil (500 mg, 12.50 mmol) was added portionwise over 5 min. After 30 min of stirring at 0 °C, 2-(trimethylsilyl)ethoxymethyl chloride (2.00 mL, 11.30 mmol) was added dropwise and the mixture was stirred at rt for 18 h. Purification by flash chromatography (SiO_2, *n*-hexane/EtOAc 90:10 to 60:40) afforded **22** as a clear oil (2.30 g, 96%). ^{1}H NMR (300 MHz, $CDCl_3$) δ −0.02 (s, 9H), 0.82–0.95 (m, 2H), 2.43 (s, 3H), 3.39–3.53 (m, 2H), 5.18 (s, 2H), 6.90 (s, 2H).

*4.2.4.52. 2-Methyl-5-(tributylstannyl)-1-((2-(trimethylsilyl)ethoxy)methyl)-1H-imidazole (**23**).* The title compound was synthesized according to a previously reported method [34] to give **23** as a clear oil (1.41 g, 25%). ^{1}H NMR (300 MHz, $CDCl_3$) δ 0.00 (s, 9H), 0.85–0.96 (m, 12H), 1.02–1.11 (m, 5H), 1.25–1.40 (m, 7H), 1.46–1.56 (m, 5H), 2.48 (s, 3H), 3.37–3.47 (m, 2H), 5.14 (s, 2H), 6.90 (s, 1H). TLC-MS (ESI) m/z = 373.0 $[M + H]^+$.

*4.2.4.53. N-(4-(2-Methyl-1-((2-(trimethylsilyl)ethoxy)methyl)-1H-imidazol-5-yl)pyridin-2-yl)cyclopropanecarboxamide (**24**).* Compound **23** (462 mg, 0.92 mmol), *N*-(4-bromopyridin-2-yl) cyclopropanecarboxamide (222 mg, 0.92 mmol) and $Pd(PPh_3)_4$ (77 mg, 0.069 mmol) were dissolved in degassed 1,4-dioxane (9 mL) under an atmosphere of argon. The reaction mixture was heated to 105 °C for 18 h before the solution was filtered through a pad of Celite. The pad was washed with DCM (30 mL) and the solvents were removed under reduced pressure. Purification by flash chromatography (SiO_2, DCM/EtOH 95:05) afforded **24** as an off-white solid (265 mg, 77%). ^{1}H NMR (300 MHz, $CDCl_3$) δ −0.04 (s, 9H), 0.84–0.92 (m, 4H), 1.06–1.15 (m, 2H), 1.55–1.67 (m, 1H), 2.53 (s, 3H), 3.45–3.55 (m, 2H), 5.28 (s, 2H), 7.16 (dd, J = 5.3, 1.6 Hz, 1H), 7.18 (s, 1H), 8.27 (dd, J = 5.2, 0.6 Hz, 1H), 8.30 (d, J = 0.6 Hz, 1H), 9.17 (s, 1H). ^{13}C NMR (75 MHz, $CDCl_3$) δ −1.5, 8.3, 13.7, 15.7, 17.7, 66.0, 72.7, 112.2, 118.0, 128.6, 131.3, 140.0, 148.0, 148.8, 152.2, 172.5. TLC-MS (ESI) m/z = 394.9 $[M + Na]^+$ m/z = 371.0 $[M - H]^-$. HPLC: t_R = 5.99 min (100.0% purity).

*4.2.4.54. N-(4-(2-Methyl-1H-imidazol-5-yl)pyridin-2-yl)cyclopropanecarboxamide (**25**).* Compound **24** (69 mg, 0.19 mmol) was dissolved in DCM (2 mL) before TFA (2 mL) was added and the solution was stirred for 6 h at rt. Sat. sodium bicarbonate solution (15 mL) was added and the organic layer was separated. The aqueous phase was extracted with DCM (4x) and the combined organic layers were dried over anhydrous Na_2SO_4 before the solvent was removed under reduced pressure. Purification by flash chromatography (SiO_2, DCM/EtOH 95:05 to 90:10) afforded **25** as a tan white solid (40 mg, 89%). ^{1}H NMR (300 MHz, DMSO-d_6) δ 0.74–0.86 (m, 4H), 1.96–2.06 (m, 1H), 2.32 (s, 3H), 7.35 (dd, J = 5.2, 1.6 Hz, 1H), 7.61 (s, 1H), 8.18 (d, J = 5.2 Hz, 1H), 8.40 (d, J = 0.4 Hz, 1H), 10.64 (s, 1H), 12.07 (br. s., 1H). ^{13}C NMR (75 MHz, DMSO-d_6) δ 7.6, 13.8, 14.3, 108.1, 114.5, 116.6, 136.5, 143.5, 145.4, 147.9, 152.7, 172.5. TLC-MS (ESI) m/z = 243.0 $[M + H]^+$ m/z = 241.0 $[M - H]^-$. HPLC: t_R = 1.35 min (99.1% purity).

*4.2.4.55. N-(Cyclopropylmethyl)-4-(4-(4-fluorophenyl)-2-(methylthio)-1H-imidazol-5-yl)pyridin-2-amine (**26**).* Compound **11a** (100 mg, 0.31 mmol) and cyclopropanemethylamine (545 µL, 6.29 mmol) were combined in a small reaction vessel. The reaction was heated to 160 °C for 48 h. The reaction mixture was allowed to cool to rt and H_2O (15 mL) was added. It was extracted with ethyl acetate (3x) and the combined organic layers were washed with brine. After drying over anhydrous Na_2SO_4 the solvent was removed under reduced pressure and purified by flash chromatography (SiO_2, DCM/EtOH 97:03) afforded **26** as a yellow solid (23 mg, 21%). ^{1}H NMR (300 MHz, MeOD) δ 0.15–0.22 (m, 2H), 0.43–0.52 (m, 2H), 0.91–1.08 (m, 1H), 2.61 (s, 3H), 3.02 (d, J = 6.8 Hz, 2H), 6.52 (dd, J = 5.5, 1.4 Hz, 1H), 6.57 (s, 1H), 7.05–7.17 (m, 2H), 7.38–7.49 (m, 2H), 7.79 (dd, J = 5.5, 0.4 Hz, 1H). ^{13}C NMR (75 MHz, MeOD) δ 4.0, 11.7, 17.0, 47.8, 107.0, 111.8, 116.7 (d, $^2J_{CF}$ = 21.6 Hz), 131.8 (d, $^3J_{CF}$ = 8.3 Hz), 144.6, 148.3, 160.7, 164.1 (d, $^1J_{CF}$ = 246.6 Hz). TLC-MS (ESI) m/z = 355.5 $[M + H]^+$ m/z = 353.4 $[M - H]^-$. HPLC: t_R = 5.08 min (100.0% purity).

4.3. GSK3 assay

Inhibitory activity on GSK3α and GSK3β was evaluated by using the ADP-Glo™ Kinase Assay kit from Promega (Promega Corporation, Madison, WI 53711, USA) [36]. The assay was performed in white, non-treated 384-well plates (Corning) using a concentration of 0.50 ng/µL of recombinant human GSK3α or 0.58 ng/µL of recombinant human GSK3β, 25 µM ATP, and 0.2 µg/µL GSK3 substrate G50-58 (sequence: YRRAAVPPSPSLSRHSSPHQ(pS)EDEEE) in presence of serial dilutions of test compounds. A control consisting of uninhibited kinase and one presenting ATP/substrate solution were also included in the plate. Kinase was pre-incubated with the test compounds for 10 min at rt and the reaction was then started with the addition of substrate/ATP and run for 60 min at rt. After the addition of ADP-Glo™ reagent (5 µL, 60 min incubation) and kinase detection reagent (10 µL, 30 min incubation), the luminescence was measured using a FilterMax F5 microplate reader (Molecular Devices) with an integration time of 500 ms. Raw data were normalized to the values of control wells and analyzed using the software GraphPad Prism v.7.03. Each experiment was performed two times in quadruplicate.

4.4. Molecular modeling

All the modeling was conducted with Maestro Small-Molecule Drug Discovery Suite 2017-4 (Schrödinger, LLC) with OPLS3 force field [52]. Prior to docking, the small-molecules were prepared with LipPrep (default settings) using Epik [53,54] to generate the potential tautomers and ionization states. The Induced Fit docking [39–41] was performed with the GSK3β crystal structure (PDB ID: 4PTC), which was prepared using Protein Preparation Wizard (default settings) [55]. The box center was defined by the co-crystalized ligand. H-bond constrains were applied to the hinge region Val135 (backbone NH and O). The default settings were used in the IFD, except the Glide redocking was conducted with XP precision [56]. The MD simulation was conducted with Desmond [57]. The system was solvated in a cubic box (edges 13 Å from the protein) and neutralized with counterions (Cl^-). The water was described with TIP3P water model [58]. The final system consisted of 58,185 atoms. The default relaxation protocol was used before the 200 ns production simulation, which was conducted in NPT ensemble (300 K; 1.01325 bar). The figures were prepared with PyMOL 2.2.3 (Schrödinger, LLC).

Notes

The authors declare no competing financial interest.

Acknowledgments

We thank Jens Strobach and Katharina Bauer for their assistance in the p38α MAP kinase ELISA activity assay. We appreciate the

helpful comments of Johannes Heidrich on the use of PyMOL and Schrödinger Maestro. This study was supported by the Federal Ministry of Education and Research (BMBF) within the BioPharma-Neuroallianz consortium (Neuro-T8B project).

Appendix A. Supplementary data

Supplementary data to this article can be found online at https://doi.org/10.1016/j.ejmech.2019.04.035.

Abbreviations

AD	Alzheimer's disease
GSK3	glycogen synthase kinase 3
MAP	mitogen-activated protein
PyBOP	(benzotriazol-1-yloxy)tripyrrolidinophosphonium hexafluorophosphate
HATU	1-[bis(dimethylamino)methylene]-1*H*-1,2,3-triazolo [4,5-*b*]pyridinium 3-oxide hexafluorophosphate
HWB	human whole blood
LPS	lipopolysaccharide
NaHMDS	sodium hexamethyldisilazide
SEM	2-(trimethylsilyl)ethoxymethyl
TFA	trifluoroacetic acid
TNF-α	tumor necrosis factor-α.

References

[1] M. Prince, A. Comas-Herrera, M. Knapp, M. Guerchet, M. Karagiannidou, World Alzheimer Report 2016: Improving Healthcare for People Living with Dementia: Coverage, Quality and Costs Now and in the Future, Alzheimer's Disease International (ADI), London, UK., 2016.
[2] C. Hooper, R. Killick, S. Lovestone, The GSK3 hypothesis of Alzheimer's disease, J. Neurochem. 104 (2008) 1433–1439.
[3] A. Kremer, J.V. Louis, T. Jaworski, F. van Leuven, GSK3 and Alzheimer's disease: facts and fiction, Front. Mol. Neurosci. 4 (2011) 17.
[4] M. Llorens-Martin, J. Jurado, F. Hernandez, J. Avila, GSK-3beta, a pivotal kinase in Alzheimer disease, Front. Mol. Neurosci. 7 (2014) 46.
[5] A. Takashima, GSK-3 is essential in the pathogenesis of Alzheimer's disease, J. Alzheimer's Dis. 9 (2006) 309–317.
[6] A. Cavallini, S. Brewerton, A. Bell, S. Sargent, S. Glover, C. Hardy, R. Moore, J. Calley, D. Ramachandran, M. Poidinger, E. Karran, P. Davies, M. Hutton, P. Szekeres, S. Bose, An unbiased approach to identifying tau kinases that phosphorylate tau at sites associated with Alzheimer disease, J. Biol. Chem. 288 (2013) 23331–23347.
[7] J.-Z. Wang, I. Grundke-Iqbal, K. Iqbal, Kinases and phosphatases and tau sites involved in Alzheimer neurofibrillary degeneration, Eur. J. Neurosci. 25 (2007) 59–68.
[8] B. DaRocha-Souto, M. Coma, B.G. Perez-Nievas, T.C. Scotton, M. Siao, P. Sanchez-Ferrer, T. Hashimoto, Z. Fan, E. Hudry, I. Barroeta, L. Sereno, M. Rodriguez, M.B. Sanchez, B.T. Hyman, T. Gomez-Isla, Activation of glycogen synthase kinase-3 beta mediates beta-amyloid induced neuritic damage in Alzheimer's disease, Neurobiol. Dis. 45 (2012) 425–437.
[9] P.T. Ly, Y. Wu, H. Zou, R. Wang, W. Zhou, A. Kinoshita, M. Zhang, Y. Yang, F. Cai, J. Woodgett, W. Song, Inhibition of GSK3beta-mediated BACE1 expression reduces Alzheimer-associated phenotypes, J. Clin. Investig. 123 (2013) 224–235.
[10] A.K. Rana, D. Singh, Targeting glycogen synthase kinase-3 for oxidative stress and neuroinflammation: opportunities, challenges and future directions for cerebral stroke management, Neuropharmacology 139 (2018) 124–136.
[11] R.G. Canter, J. Penney, L.-H. Tsai, The road to restoring neural circuits for the treatment of Alzheimer's disease, Nature 539 (2016) 187–196.
[12] E. Herlaar, Z. Brown, p38 MAPK signalling cascades in inflammatory disease, Mol. Med. Today 5 (1999) 439–447.
[13] J.C. Lee, J.T. Laydon, P.C. McDonnell, T.F. Gallagher, S. Kumar, D. Green, D. McNulty, M.J. Blumenthal, J.R. Heys, S.W. Landvatter, A protein kinase involved in the regulation of inflammatory cytokine biosynthesis, Nature 372 (1994) 739–746.
[14] K. Hensley, R.A. Floyd, N.-Y. Zheng, R. Nael, K.A. Robinson, X. Nguyen, Q.N. Pye, C.A. Stewart, J. Geddes, W.R. Markesbery, E. Patel, G.V.W. Johnson, G. Bing, p38 kinase is activated in the Alzheimer's disease brain, J. Neurochem. 72 (1999) 2053–2058.
[15] A.D. Bachstetter, B. Xing, L. Almeida, E.R. Dimayuga, D.M. Watterson, L.J. van Eldik, Microglial p38alpha MAPK is a key regulator of proinflammatory cytokine up-regulation induced by toll-like receptor (TLR) ligands or beta-amyloid (Abeta), J. Neuroinflammation 8 (2011) 79.
[16] L. Munoz, A.J. Ammit, Targeting p38 MAPK pathway for the treatment of Alzheimer's disease, Neuropharmacology 58 (2010) 561–568.
[17] L. Munoz, H. Ralay Ranaivo, S.M. Roy, W. Hu, J.M. Craft, L.K. McNamara, L.W. Chico, L.J. van Eldik, D.M. Watterson, A novel p38 alpha MAPK inhibitor suppresses brain proinflammatory cytokine up-regulation and attenuates synaptic dysfunction and behavioral deficits in an Alzheimer's disease mouse model, J. Neuroinflammation 4 (2007) 21.
[18] A. Sun, M. Liu, X.V. Nguyen, G. Bing, P38 MAP kinase is activated at early stages in Alzheimer's disease brain, Exp. Neurol. 183 (2003) 394–405.
[19] N. Maphis, S. Jiang, G. Xu, O.N. Kokiko-Cochran, S.M. Roy, L.J. Van Eldik, D.M. Watterson, B.T. Lamb, K. Bhaskar, Selective suppression of the alpha isoform of p38 MAPK rescues late-stage tau pathology, Alzheimer's Res. Ther. 8 (2016) 54.
[20] J. Alam, K. Blackburn, D. Patrick, Neflamapimod: clinical phase 2b-ready oral small molecule inhibitor of p38alpha to reverse synaptic dysfunction in early Alzheimer's disease, J. Prev. Alzheimer's Dis. 4 (2017) 273–278.
[21] P. Scheltens, N. Prins, A. Lammertsma, M. Yaqub, A. Gouw, A.M. Wink, H.M. Chu, B.N.M. van Berckel, J. Alam, An exploratory clinical study of p38alpha kinase inhibition in Alzheimer's disease, Ann. Clin. Transl. Neurol. 5 (2018) 464–473.
[22] F. Ansideri, S. Andreev, A. Kuhn, W. Albrecht, S. Laufer, P. Koch, A diverse and versatile regiospecific synthesis of tetrasubstituted alkylsulfanylimidazoles as p38α mitogen-activated protein kinase inhibitors, Molecules 23 (2018) 221.
[23] A. Cuenda, J. Rouse, Y.N. Doza, R. Meier, P. Cohen, T.F. Gallagher, P.R. Young, J.C. Lee, SB 203580 is a specific inhibitor of a MAP kinase homologue which is stimulated by cellular stresses and interleukin-1, FEBS Lett. 364 (1995) 229–233.
[24] P. Koch, C. Bäuerlein, H. Jank, S. Laufer, Targeting the ribose and phosphate binding site of p38 mitogen-activated protein (MAP) kinase: synthesis and biological testing of 2-alkylsulfanyl-, 4(5)-aryl-, 5(4)-heteroaryl-substituted imidazoles, J. Med. Chem. 51 (2008) 5630–5640.
[25] S. Laufer, D. Hauser, T. Stegmiller, C. Bracht, K. Ruff, V. Schattel, W. Albrecht, P. Koch, Tri- and tetrasubstituted imidazoles as p38alpha mitogen-activated protein kinase inhibitors, Bioorg, Med. Chem. Lett. 20 (2010) 6671–6675.
[26] S.A. Laufer, G.K. Wagner, D.A. Kotschenreuther, W. Albrecht, Novel substituted pyridinyl imidazoles as potent anticytokine agents with low activity against hepatic cytochrome P450 enzymes, J. Med. Chem. 46 (2003) 3230–3244.
[27] J. Halekotte, L. Witt, C. Ianes, M. Kruger, M. Buhrmann, D. Rauh, C. Pichlo, E. Brunstein, A. Luxenburger, U. Baumann, U. Knippschild, J. Bischof, C. Peifer, Optimized 4,5-diarylimidazoles as potent/selective inhibitors of protein kinase CK1delta and their structural relation to p38alpha MAPK, Molecules 22 (2017) 522.
[28] M. Semones, Y. Feng, N. Johnson, J.L. Adams, J. Winkler, M. Hansbury, Pyridinylimidazole inhibitors of Tie2 kinase, Bioorg. Med. Chem. Lett. 17 (2007) 4756–4760.
[29] F. Muth, A. El-Gokha, F. Ansideri, M. Eitel, E. Döring, A. Sievers-Engler, A. Lange, F.M. Boeckler, M. Lämmerhofer, P. Koch, S.A. Laufer, Tri- and tetra-substituted pyridinylimidazoles as covalent inhibitors of c-Jun N-terminal kinase 3, J. Med. Chem. 60 (2017) 594–607.
[30] F. Muth, M. Günther, S.M. Bauer, E. Döring, S. Fischer, J. Maier, P. Drückes, J. Köppler, J. Trappe, U. Rothbauer, P. Koch, S.A. Laufer, Tetra-substituted pyridinylimidazoles as dual inhibitors of p38 alpha mitogen-activated protein kinase and c-Jun N-terminal kinase 3 for potential treatment of neurodegenerative diseases, J. Med. Chem. 58 (2015) 443–456.
[31] P. Koch, F. Ansideri, 2-Alkylsulfanyl-4(5)-aryl-5(4)-heteroarylimidazoles: an overview on synthetic strategies and biological activity, Arch. Pharm. 350 (2017), e1700258.
[32] S.A. Laufer, A.J. Liedtke, A concise and optimized four-step approach toward 2-(aryl-)alkylsulfanyl-, 4(5)-aryl-, 5(4)-heteroaryl-substituted imidazoles using alkyl- or arylalkyl thiocyanates, Tetrahedron Lett. 47 (2006) 7199–7203.
[33] F. Heider, U. Haun, E. Döring, M. Kudolo, C. Sessler, W. Albrecht, S. Laufer, P. Koch, From 2-alkylsulfanylimidazoles to 2-alkylimidazoles: an approach towards metabolically more stable p38α MAP kinase inhibitors, Molecules 22 (2017) 1729.
[34] M.D. Markey, T.R. Kelly, Synthesis of cribrostatin 6, J. Org. Chem. 73 (2008) 7441–7443.
[35] M. Goettert, R. Graeser, S.A. Laufer, Optimization of a nonradioactive immunosorbent assay for p38alpha mitogen-activated protein kinase activity, Anal. Biochem. 406 (2010) 233–234.
[36] H. Zegzouti, M. Zdanovskaia, K. Hsiao, S.A. Goueli, ADP-Glo, A Bioluminescent and homogeneous ADP monitoring assay for kinases, Assay Drug Dev. Technol. 7 (2009) 560–572.
[37] S.M. Bauer, J.M. Kubiak, U. Rothbauer, S. Laufer, From enzyme to whole blood: sequential screening procedure for identification and evaluation of p38 MAPK inhibitors, in: H. Zegzouti, S. Goueli (Eds.), Kinase Screening and Profiling, Humana Press, New York, NY, 2016, pp. 123–148.
[38] S. Blencke, B. Zech, O. Engkvist, Z. Greff, L. Orfi, Z. Horváth, G. Kéri, A. Ullrich, H. Daub, Characterization of a conserved structural determinant controlling protein kinase sensitivity to selective inhibitors, Chem. Biol. 11 (2004) 691–701.
[39] R. Farid, T. Day, R.A. Friesner, R.A. Pearlstein, New insights about HERG blockade obtained from protein modeling, potential energy mapping, and docking studies, Bioorg. Med. Chem. 14 (2006) 3160–3173.
[40] W. Sherman, T. Day, M.P. Jacobson, R.A. Friesner, R. Farid, Novel procedure for modeling ligand/receptor induced fit effects, J. Med. Chem. 49 (2006)

534–553.
[41] W. Sherman, H.S. Beard, R. Farid, Use of an induced fit receptor structure in virtual screening, Chem. Biol. Drug Des. 67 (2006) 83–84.
[42] F. Ansideri, J.T. Macedo, M. Eitel, A. El-Gokha, D.S. Zinad, C. Scarpellini, M. Kudolo, D. Schollmeyer, F.M. Boeckler, B.S. Blaum, S.A. Laufer, P. Koch, Structural optimization of a pyridinylimidazole scaffold: shifting the selectivity from p38α mitogen-activated protein kinase to c-Jun N-terminal kinase 3, ACS Omega 3 (2018) 7809–7831.
[43] C.E. Fitzgerald, S.B. Patel, J.W. Becker, P.M. Cameron, D. Zaller, V.B. Pikounis, S.J. O'Keefe, G. Scapin, Structural basis for p38 alpha MAP kinase quinazolinone and pyridol-pyrimidine inhibitor specificity, Nat. Struct. Biol. 10 (2003) 764–769.
[44] H. Pajouhesh, G.R. Lenz, Medicinal chemical properties of successful central nervous system drugs, NeuroRx 2 (2005) 541–553.
[45] S.G. Krimmer, J. Cramer, M. Betz, V. Fridh, R. Karlsson, A. Heine, G. Klebe, Rational design of thermodynamic and kinetic binding profiles by optimizing surface water networks coating protein-bound ligands, J. Med. Chem. 59 (2016) 10530–10548.
[46] B. Kammerer, H. Scheible, G. Zurek, M. Godejohann, K.P. Zeller, C.H. Gleiter, W. Albrecht, S. Laufer, In vitro metabolite identification of ML3403, a 4-pyridinylimidazole-type p38 MAP kinase inhibitor by LC-Qq-TOF-MS and LC-SPE-cryo-NMR/MS, Xenobiotica 37 (2007) 280–297.
[47] J.R. Woodgett, Molecular cloning and expression of glycogen synthase kinase-3/factor A, EMBO J. 9 (1990) 2431–2438.
[48] F.F. Wagner, L. Benajiba, A.J. Campbell, M. Weiwer, J.R. Sacher, J.P. Gale, L. Ross, A. Puissant, G. Alexe, A. Conway, M. Back, Y. Pikman, I. Galinsky, D.J. DeAngelo, R.M. Stone, T. Kaya, X. Shi, M.B. Robers, T. Machleidt, J. Wilkinson, O. Hermine, A. Kung, A.J. Stein, D. Lakshminarasimhan, M.T. Hemann, E. Scolnick, Y.L. Zhang, J.Q. Pan, K. Stegmaier, E.B. Holson, Exploiting an Asp-Glu "switch" in glycogen synthase kinase 3 to design paralog-selective inhibitors for use in acute myeloid leukemia, Sci. Transl. Med. 10 (2018), eaam8460.
[49] F. Heider, U. Haun, E. Döring, M. Kudolo, C. Sessler, W. Albrecht, S. Laufer, P. Koch, From 2-alkylsulfanylimidazoles to 2-alkylimidazoles: an approach towards metabolically more stable p38α MAP kinase inhibitors, Molecules 22 (2017).
[50] S. Bühler, M. Goettert, D. Schollmeyer, W. Albrecht, S.A. Laufer, Chiral sulfoxides as metabolites of 2-thioimidazole-based p38 alpha mitogen-activated protein kinase inhibitors: enantioselective synthesis and biological evaluation, J. Med. Chem. 54 (2011) 3283–3297.
[51] S.J. Cho, N.H. Jensen, T. Kurome, S. Kadari, M.L. Manzano, J.E. Malberg, B. Caldarone, B.L. Roth, A.P. Kozikowski, Selective 5-hydroxytryptamine 2C receptor agonists derived from the lead compound tranylcypromine: identification of drugs with antidepressant-like action, J. Med. Chem. 52 (2009) 1885–1902.
[52] E. Harder, W. Damm, J. Maple, C. Wu, M. Reboul, J.Y. Xiang, L. Wang, D. Lupyan, M.K. Dahlgren, J.L. Knight, J.W. Kaus, D.S. Cerutti, G. Krilov, W.L. Jorgensen, R. Abel, R.A. Friesner, OPLS3: a force field providing broad coverage of drug-like small molecules and proteins, J. Chem. Theory Comput. 12 (2016) 281–296.
[53] J.R. Greenwood, D. Calkins, A.P. Sullivan, J.C. Shelley, Towards the comprehensive, rapid, and accurate prediction of the favorable tautomeric states of drug-like molecules in aqueous solution, J. Comput. Aided Mol. Des. 24 (2010) 591–604.
[54] J.C. Shelley, A. Cholleti, L.L. Frye, J.R. Greenwood, M.R. Timlin, M. Uchimaya, Epik: a software program for pK(a) prediction and protonation state generation for drug-like molecules, J. Comput. Aided Mol. Des. 21 (2007) 681–691.
[55] G.M. Sastry, M. Adzhigirey, T. Day, R. Annabhimoju, W. Sherman, Protein and ligand preparation: parameters, protocols, and influence on virtual screening enrichments, J. Comput. Aided Mol. Des. 27 (2013) 221–234.
[56] R.A. Friesner, R.B. Murphy, M.P. Repasky, L.L. Frye, J.R. Greenwood, T.A. Halgren, P.C. Sanschagrin, D.T. Mainz, Extra precision glide: docking and scoring incorporating a model of hydrophobic enclosure for protein-ligand complexes, J. Med. Chem. 49 (2006) 6177–6196.
[57] K.J. Bowers, C. Edmond, H. Xu, R.O. Dror, M.P. Eastwood, B.A. Gregerson, J.L. Klepeis, I. Kolossvary, M.A. Moraes, F.D. Sacerdoti, J.K. Salmon, Y. Shan, D.E. Shaw, Scalable Algorithms for molecular dynamics simulations on commodity clusters, in: Proceedings of the ACM/IEEE Conference on Supercomputing (SC06), Tampa, Florida, November 11–17, 2006.
[58] W.L. Jorgensen, J. Chandrasekhar, J.D. Madura, R.W. Impey, M.L. Klein, Comparison of simple potential functions for simulating liquid water, J. Chem. Phys. 79 (1983) 926–935.

Supporting Information

Pyridinylimidazoles as dual Glycogen Synthase Kinase 3β/p38α Mitogen-activated Protein Kinase Inhibitors

Fabian Heider,[1] Francesco Ansideri,[1] Roberta Tesch,[1] Tatu Pantsar,[2,3] Urs Haun,[1] Eva Döring,[1] Mark Kudolo[1], Antti Poso,[2,3] Wolfgang Albrecht,[4] Stefan A. Laufer[1] and Pierre Koch[1,5]*

[1]Department of Pharmaceutical and Medicinal Chemistry, Institute of Pharmaceutical Sciences, Eberhard Karls Universität Tübingen, Auf der Morgenstelle 8, 72076 Tübingen, Germany
[2]School of Pharmacy, University of Eastern Finland, P.O.BOX 1627, 70211 Kuopio, Finland
[3]Department of Internal Medicine VIII, University Hospital Tübingen, Otfried-Müller-Strasse 14, 72076 Tübingen, Germany
[4]Teva-ratiopharm, Graf-Arco-Str. 3, 89079 Ulm, Germany
[5]Department of Pharmaceutical/Medicinal Chemistry II, Institute of Pharmacy, University of Regensburg, Universitätsstraße 31, 93053 Regensburg, Germany

Table of Contents

Screening of Metabolites by LC-MS Analysis

The metabolite formation was analyzed with an Alliance 2695 Separations Module (Waters GmbH, Eschborn). Samples were maintained at 4 °C, the column temperature was set to 40 °C and injection volume was 10 µL. The chromatographic separation for all analytes was performed on a Phenomenex Synergi Polar-RP column (150 x 4.6 mm; 5 µm) with a precolumn of the same material. An isocratic gradient of 9 min with 30 % solvent A (90 % H_2O, 10 % ACN, 0.1 % formic acid) and 70 % solvent B (ACN, 0.1 % formic acid) at a flow rate of 370 µL/min was used for **1c**. For **20c**, an isocratic gradient of 10 min with 31.5 % solvent A (90 % H_2O, 10 % ACN, 0.1 % formic acid) and 68.5 % solvent B (ACN, 0.1 % formic acid) at a flow rate of 350 µL/min was used. For **2e**, an isocratic gradient of 9.5 min with 30 % solvent A (90 % H_2O, 10 % ACN, 0.1 % formic acid) and 70 % solvent B (ACN, 0.1 % formic acid) at a flow rate of 400 µL/min was employed. The detection was performed on a Micromass Quattro micro triple quadrupole mass spectrometer (Waters GmbH, Eschborn) using the electrospray-ionization in the positive-mode.
Spray voltage was set to 4.0 kV. The heated capillary operated at 250 °C and the desolvation gas flow worked at 500 L/h.

Metabolic stability in human liver microsomes

Table S1. Degradation of **1c**

time [min]	#1 [%]	#2 [%]	#3 [%]	AVERAGE [%]	SD
0	100.00	100.00	100.00	100.00	0.00
10	98.94	98.19	99.40	98.84	0.50
20	99.25	95.28	99.25	97.93	1.87
30	90.27	89.61	89.04	89.64	0.50
60	82.49	81.95	80.91	81.78	0.65
120	65.71	64.55	67.32	65.86	1.14
180	52.46	52.54	51.17	52.06	0.63
240	43.81	44.68	43.52	44.00	0.49

Table S2. Degradation of **20c**

time [min]	#1 [%]	#2 [%]	#3 [%]	AVERAGE [%]	SD
0	100.00	100.00	100.00	100.00	0.00
10	95.36	94.97	95.90	95.41	0.38
20	90.94	96.85	92.31	93.36	2.53
30	91.62	95.88	93.96	93.82	1.74
60	95.32	97.07	93.05	95.15	1.64
120	93.82	96.08	99.39	96.43	2.29
180	97.38	100.08	---	98.73	1.35
240	96.83	99.73	---	98.28	1.45

Table S3. Degradation of **20e**

time [min]	#1 [%]	#2 [%]	AVERAGE [%]	SD
0	100.00	100.00	100.00	0.00
10	94.27	90.52	92.40	1.88
20	85.12	82.12	83.62	1.50
30	78.34	77.88	78.11	0.23
60	68.87	69.99	69.43	0.56
120	67.42	72.27	69.85	2.43
180	67.25	70.19	68.72	1.47
240	66.81	65.30	66.06	0.76

Solubility testing

To investigate the solubility of the compounds, a dilution series of the corresponding compounds was prepared in methanol (1, 0.5, 0.1, 0.05, 0.01 mg/mL) and measured by HPLC (detection at 254 nm). Plotting the area underneath the curve to the mass concentration of the solutions gave a calibration line, which was used to calculate the solubility afterwards. A saturated solution of the corresponding compound in PBS buffer (pH 7.8) was prepared and sonicated for 1 h. The same samples were then filtered, measured by HPLC and the peak area was used to estimate the solubility using the previously gathered equation.

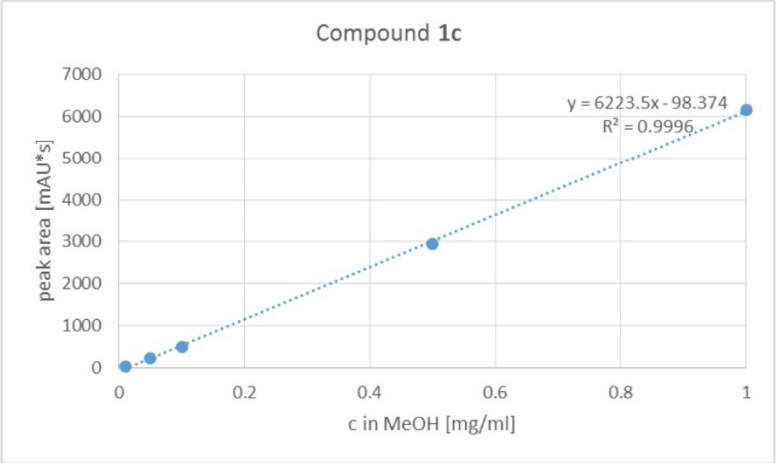

Figure S1. Calibration line with concentrations ranging from 0.01 mg/mL to 1 mg/mL of **1c**.

➔ Solubility of compound **1c**: 0.051 mg/mL

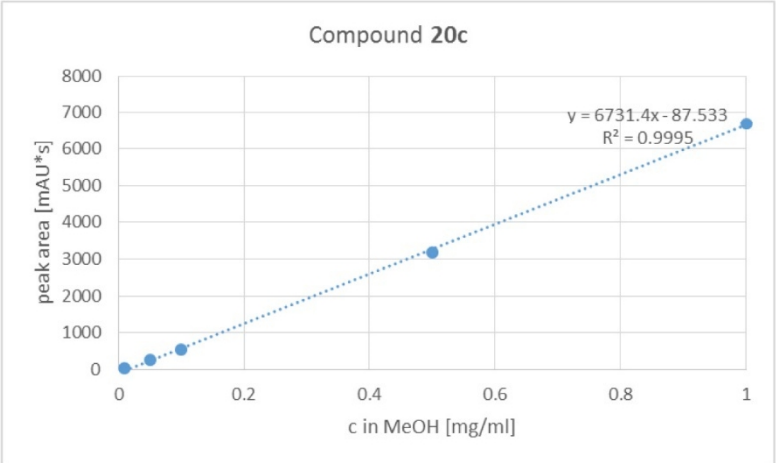

Figure S2. Calibration line with concentrations ranging from 0.01 mg/mL to 1 mg/mL of **20c**.

➔ Solubility of compound **20c**: 0.155 mg/mL

Kinase selectivity screening of 20c.

Compound **20c** was tested at Cerep, Eurofins (Celle L'Evescault, France) in the ExpresS Diversity Kinase Panel against 45 selected human kinases at a concentration of 1 µM.

Table S4. Inhibition of selected kinases (n=2).

#	kinase name	kinase family[a]	mean inhibition [%]
1	Abl	TK	91.47
2	Akt1 (PKBalpha)	AGC	2.06
3	Aurora-A	other	2.76
4	CaMK2alpha	CAMK	-2.55
5	CDK1	CAMGC	-11.56
6	CDK2	CAMGC	11.15
7	CHK1	CAMK	9.05
8	CHK2	CAMK	-9.70
9	c-Raf (Raf-1)	TKL	59.75
10	EGFR	TK	93.35
11	EPHA2	TK	95.53
12	EPHA3	TK	76.63
13	EphB4	TK	94.67
14	ERK2 (MAPK1)	CMGC	10.94
15	FGFR	TK	47.03
16	FGFR2	TK	74.38
17	FGFR3	TK	64.45
18	GSK3beta	CMGC	96.97
19	HGK (MAP4K4)	STE	97.87
20	IKKalpha	Other	-2.16
21	IR	RTK	4.24
22	IRAK4	TKL	2.96
23	JAK3	TK	24.83
24	JNK1	CMGC	78.26
25	KDR (VEGFR2)	TK	98.73
26	LCK	TK	56.43
27	MAPKAPK2	CAMK	-4.86
28	MARK1	CAMK	-5.30
29	Met	TK	54.87
30	MNK2	CAMK	1.16
31	NEK2	Other	-1.98
32	PAK2	STE	5.58
33	PAK4	STE	4.82
34	PDK1	AGC	-5.07
35	PIM2	CAMK	-0.24
36	PKA	AGC	-7.30
37	PKCbeta	AGC	10.68
38	PLK1	Other	2.78
39	ROCK1	AGC	-8.13
40	SAPK2A (p38alpha)	CMGC	93.63

Table S4. continued.

#	kinase name	kinase family[a]	mean inhibition [%]
41	SGK1	AGC	8.36
42	SIK	CAMK	8.06
43	SRC	TK	51.61
44	TAO2	STE	54.43
45	TRKA	TK	10.60

[a]AGC: containing PKA, PKG and PKC families; CAMK: calcium/calmoduline-dependent protein kinases; CK1: casein kinase 1-like; CMGC: containing CDK, MAPK, GSK3 and CLK families; TK: tyrosine kinase; TKL: tyrosine kinase-like; STE: homologs of yeast sterile 7, sterile 11, sterile 20 kinases.

Characterization as ATP-competitive GSK3β inhibitors

Compounds **1c** (Figure S3) and **20c** (Figure S4) were tested at three different ATP concentrations (25 µM, 100 µM and 500 µM) to prove their ATP-competitiveness.

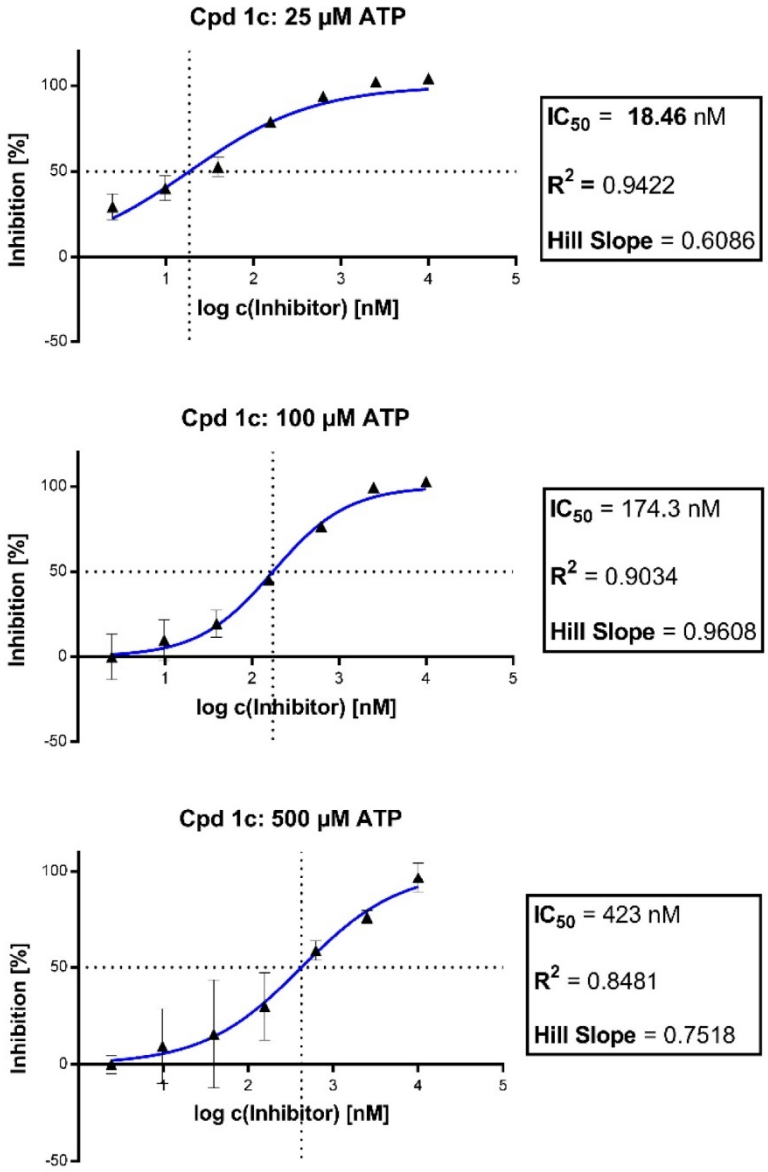

Figure S3. ADP-Glo assay results of **1c** at different ATP concentrations.

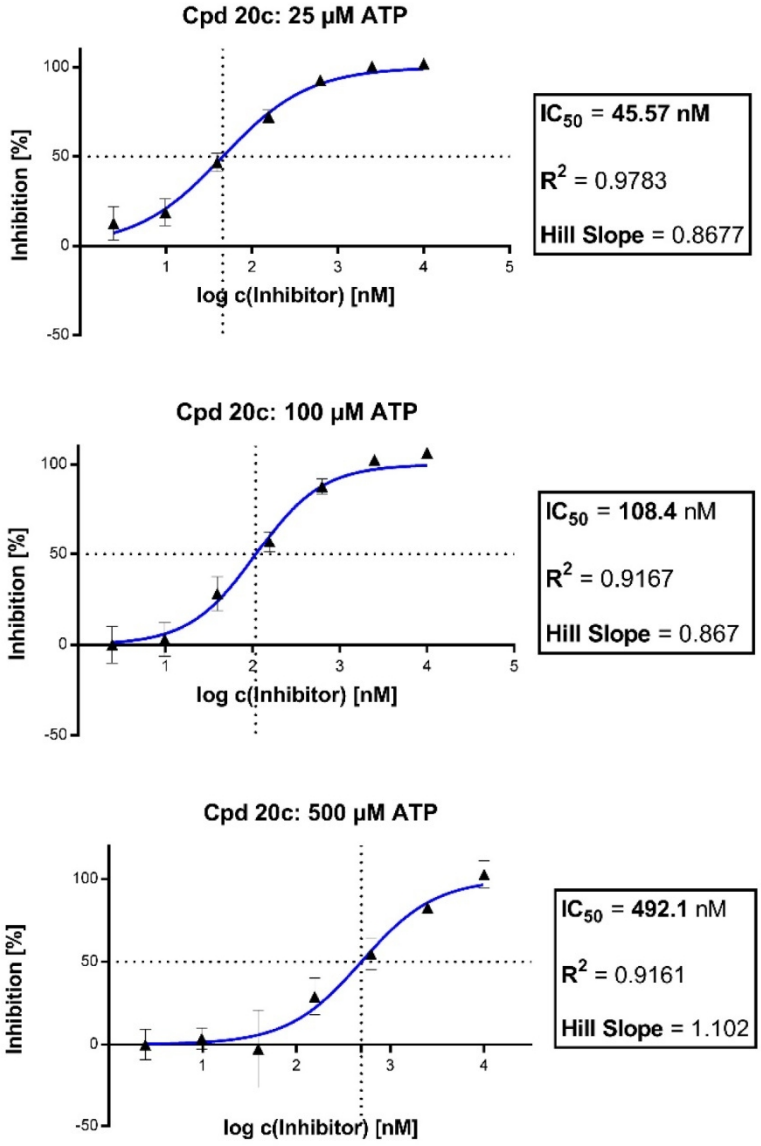

Figure S4. ADP-Glo assay results of **20c** at different ATP concentrations.

CYP and hERG inhibition

CYP and hERG inhibition assays were performed by Reaction Biology Corp. (Devault, PA, USA).

CYP inhibition assay (fluorimetric detection) was performed at 10 µM inhibitor concentration in single dose duplicate mode with human recombinant CYP enzyme and the appropriate CYP substrates:

CYP1A2: 3-Cyano-7-ethoxycoumarin
CYP2C9: Vivid® OOMR Substrate
CYP2C19: Vivid® EOMCC Substrate
CYP2D6: Vivid® EOMCC Substrate (*sic!*)
CYP3A4 Vivid® BOMR Substrate: Cyp3A4

Furafylline was used as a positive control compound for CYP1A2, while Ketoconazole was used as a positive control compound for all other tested CYP enzymes.

The hERG assay is based on the competition of a fluorescently labeled tracer (Predictor™ hERG Tracer Red) binding to the membrane preparation containing hERG (Predictor™ hERG Membrane).

Compounds and tracer were mixed with the membrane preparation (in the dark) and the FP was measured after 4 h incubation at rt.

PK evaluation/CNS penetration in male CD1 mice

Compounds **1c** and **20c** were evaluated in regard to their basic pharmacokinetic parameters including brain penetration after intravenous administration to male RjOrl:Swiss CD-1 mice.

The experiments were performed by a CRO (Pharmacelsus GmbH, Saarbrücken, Germany) in accordance with the regulations of the local Animal Welfare authorities. The animals were checked for clinical signs throughout the study. They showed a normal behavior throughout the duration of the experiment and no adverse effects were observed.

The compounds were formulated (10 % DMA, 40 % PEG, 30 % PEG, 20 % H_2O) and administered by intravenous injection into the tail vein (2 mL/kg → 10 mg/kg). Three serial samples were obtained from each mouse 10 min, 30 min and 120 min after dosing. A volume of 80 µL Li-heparin plasma was obtained from the retrobulbar venous plexus under isoflurane anesthesia. Whole blood was stored on ice until centrifugation (10 minutes at 3000 g, 4 °C). Plasma was prepared within 45 min after collection. Subsequently, the mice were sacrificed for dissection of the brains. All samples were frozen and stored at -20 °C until the LC-MS analysis.

LC-MS settings:

The LC-MS system consisted of an Accela U-HPLC pump and an Accela Open Autosampler (Thermo Fisher Scientific, USA) combined with a Q-Exactive mass spectrometer (Orbitrap™ technology with accurate mass) equipped with a H-ESI (heated electrospray interface) (Thermo Fisher Scientific, USA). The generated data was evaluated using the standard software Xcalibur 2.2. The LC flow rate was set to 600 µl/min and the compounds were separated on an analytical column (Kinetex Phenyl-Hexyl, 2.6 µm, 50x2,1 mm, Phenomenex, Germany) with pre-column (Gemini C6-Phenyl Security Guard Cartridge 4x2mm, Phenomenex, Germany). Gradient elution with water/0.2% HFBA as aqueous phase (A) and acetonitrile/0.2% HFBA as organic phase (B).

% B: 15 (0-0.1 min) to 97(0.4-1.7 min) to 15(1.8–2.5 min).

Stock solutions of **1c**, **20c** and **12a** (= metabolite of **1c**) (2 mg/mL in DMSO) were diluted with DMSO to a final concentration of 100 µg/mL (start solution). Working solutions were prepared by further dilution of the start solution in DMSO.

For quantification, the ISTD method was applied and the system calibrated using logarithmic regression as mathematical model for an accurate best-fit calibration. The concentration levels for calibration were chosen in the range of actual sample concentrations. The selectivity expressed as signal to noise ratio was ≥ 5. Method variability was assessed evaluating the within-run accuracy and precision.

Preparation of the blood samples:

Calibration standards and QCs were prepared by spiking 20 µL of drug free blank plasma with 2.4 µL working solution. The calibration standards and quality controls were prepared in duplicates. A volume of 20 µL of unknown samples, zero samples and blanks were spiked with 2.4 µL DMSO.

After 10 min of equilibration, a volume of 40 µL acetonitrile containing the internal standard (Diazepam, 300 ng/mL) was added to each calibration standard, QC, zero sample and unknown sample, while a volume of 40 µL plain acetonitrile was added to all blanks. Samples were vigorously shaken and centrifuged for 10 min at 6000 g at 20 °C. The particle free supernatant was diluted 1+1 with water. An aliquot was transferred to 200 µL sampler vials and subsequently subjected to LC-MS with an injection volume of 15 µL. An aliquot was transferred to 200 µL sampler vials and subsequently subjected to LC-MS with an injection volume of 15 µL.

Preparation of the brain samples:

Brains were homogenized in 1 volume of PBS using a Tissue Homogenizer (2x 10 sec, 5000 rpm Precellys® 24/Dual (Peqlab Biotechnologie GmbH) combined with Precellys Kit ceramic beads, 2.8 mm).

Calibration standards and QCs were prepared by spiking 50 µL of drug free blank brain homogenate with 6 µL working solution. The calibration standards and quality controls were prepared in duplicates. A volume of 50 µL of unknown samples, zero samples and blanks were spiked with 6 µL DMSO. After

10 min of equilibration, a volume of 100 µL acetonitrile containing the internal standard (Diazepam, 300 ng/mL) was added to each calibration standard, QC, zero sample and unknown sample, while a volume of 100 µL plain acetonitrile was added to all blanks. Samples were vigorously shaken and centrifuged for 10 min at 6000 g at 20°C. The particle free supernatant was diluted 1+1 with water. An aliquot was transferred to 200 µL sampler vials and subsequently subjected to LC-MS with an injection volume of 15 µL.

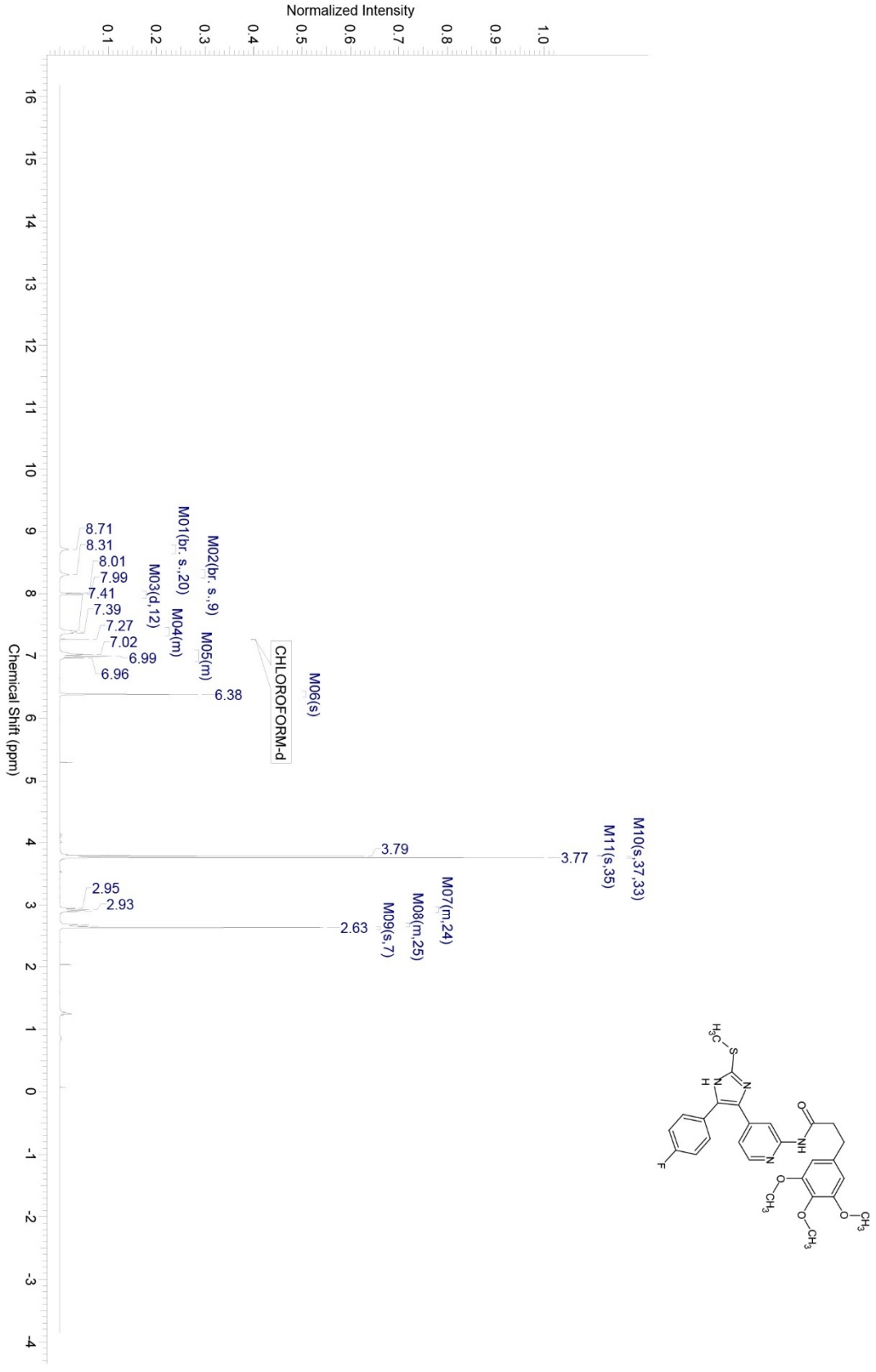
Normalized Intensity
Chemical Shift (ppm)
8.71
8.31
8.01
7.99
7.41
7.39
7.27
7.02
6.99
6.96
6.38
3.79
3.77
2.95
2.93
2.63
M01(br. s.,20)
M02(br. s.,9)
M03(d,12)
M04(m)
M05(m)
M06(s)
M07(m,24)
M08(m,25)
M09(s,7)
M10(s,37,33)
M11(s,35)
CHLOROFORM-d
Cpd 1a

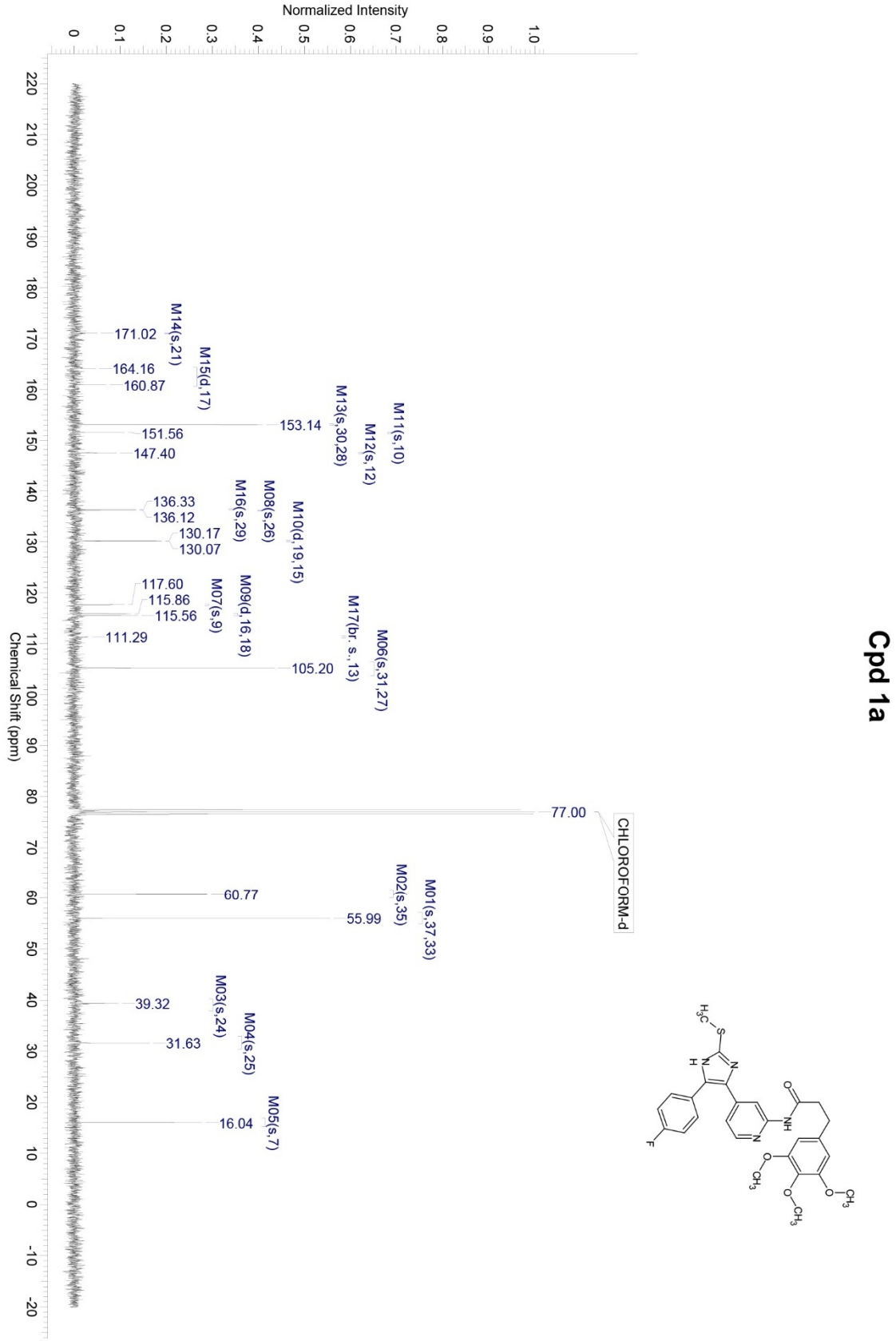
Cpd 1a
Normalized Intensity
Chemical Shift (ppm)
171.02
164.16
160.87
153.14
151.56
147.40
136.33
136.12
130.17
130.07
117.60
115.86
115.56
111.29
105.20
77.00
60.77
55.99
39.32
31.63
16.04
M14(s,21)
M15(d,17)
M13(s,30,28)
M11(s,10)
M12(s,12)
M16(s,29)
M08(s,26)
M10(d,19,15)
M07(s,9)
M09(d,16,18)
M17(br. s.,13)
M06(s,31,27)
CHLOROFORM-d
M02(s,35)
M01(s,37,33)
M03(s,24)
M04(s,25)
M05(s,7)

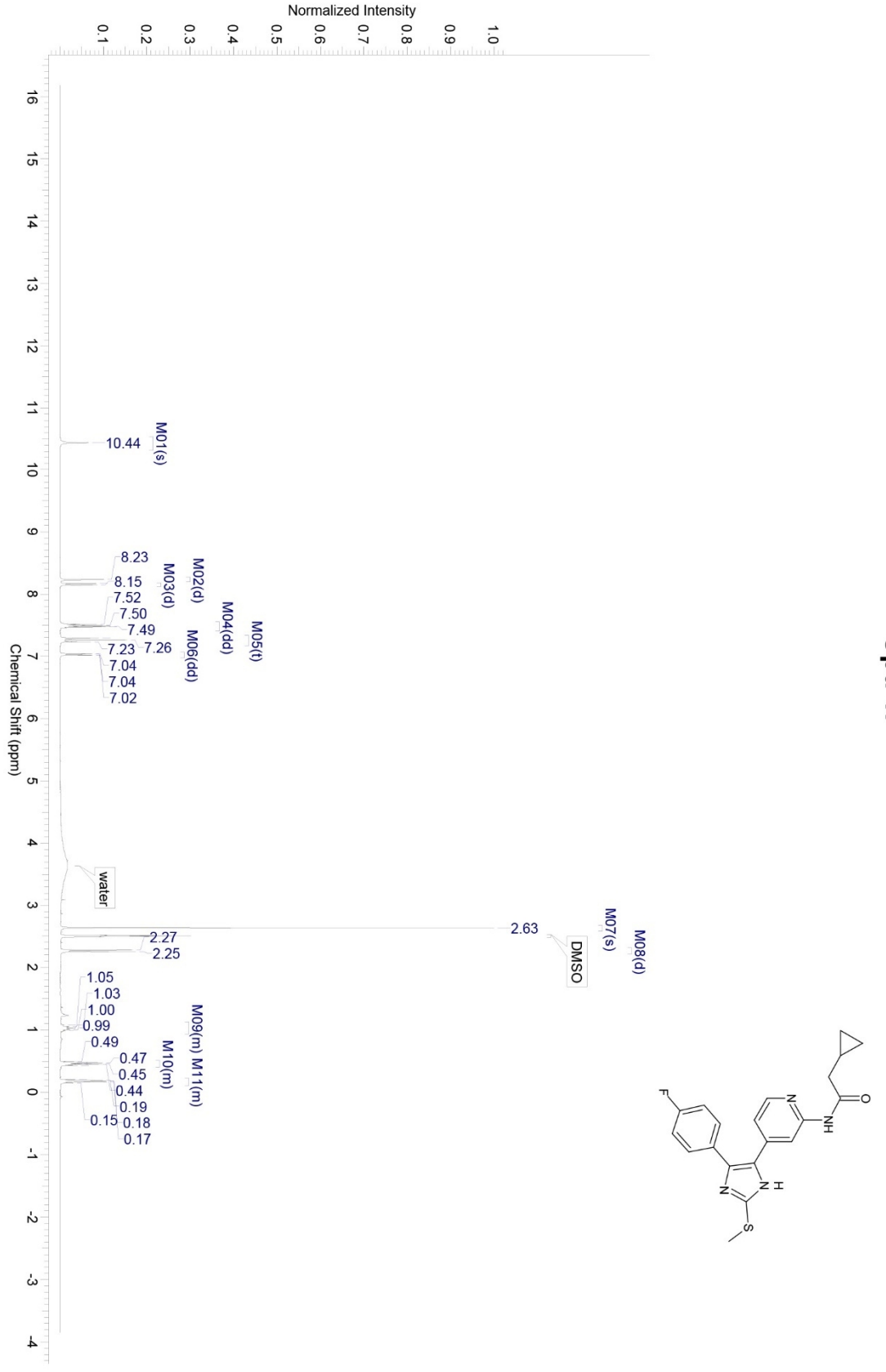
Normalized Intensity
Chemical Shift (ppm)
10.44
M01(s)
8.23
8.15
M03(d)
7.52
7.50
7.49
M02(d)
M04(dd)
M05(t)
7.23
7.26
M06(dd)
7.04
7.04
7.02
water
2.63
M07(s)
DMSO
M08(d)
2.27
2.25
1.05
1.03
1.00
0.99
0.49
0.47
0.45
0.44
0.19
0.15
0.18
0.17
M10(m)
M09(m) M11(m)
Cpd 1l

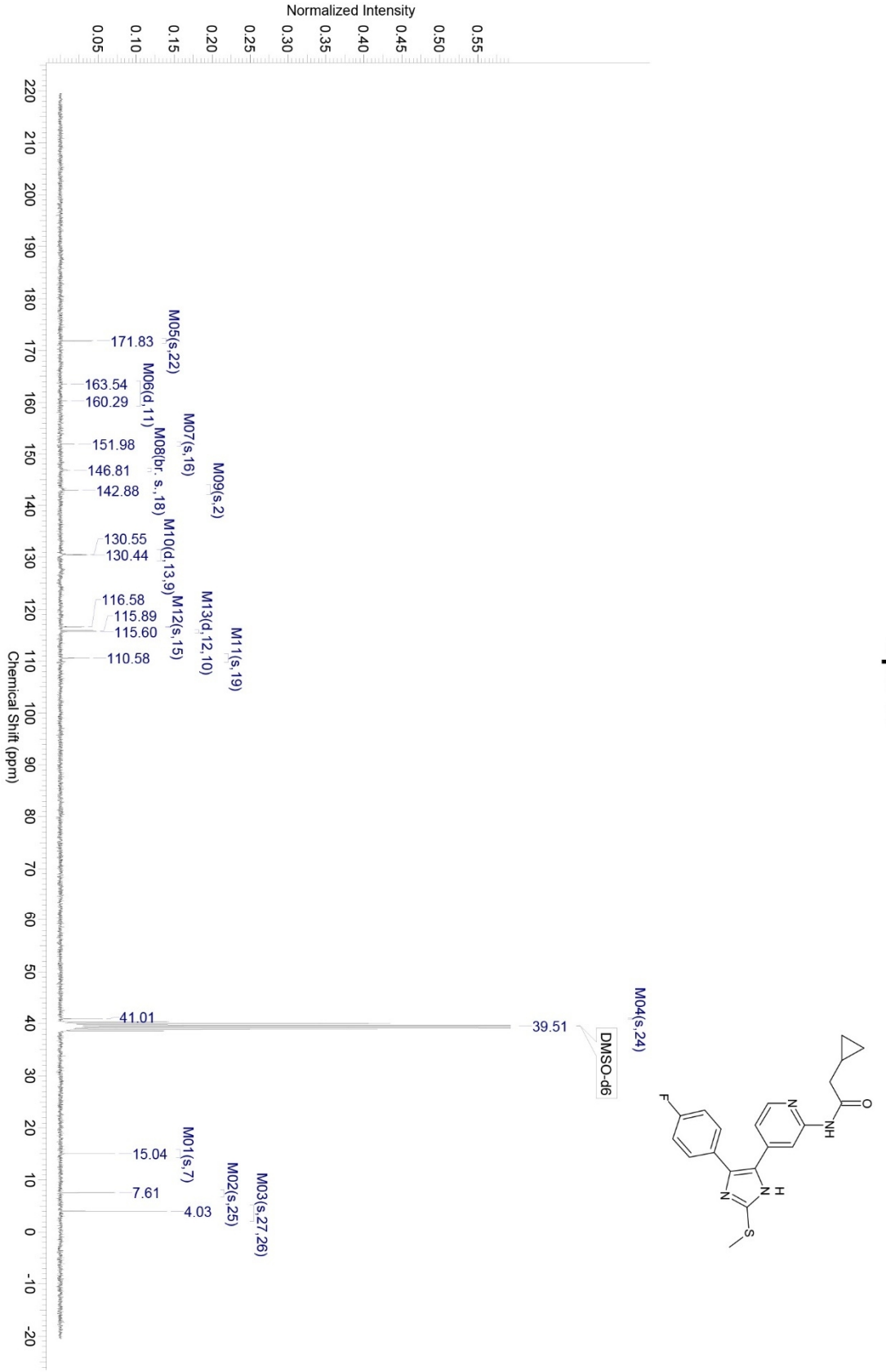
Normalized Intensity
0.05
0.10
0.15
0.20
0.25
0.30
0.35
0.40
0.45
0.50
0.55
Chemical Shift (ppm)
220
210
200
190
180
170
160
150
140
130
120
110
100
90
80
70
60
50
40
30
20
10
0
-10
-20
171.83
163.54
160.29
151.98
146.81
142.88
130.55
130.44
116.58
115.89
115.60
110.58
41.01
39.51
15.04
7.61
4.03
M05(s,22)
M06(d,11)
M07(s,16)
M08(br. s,18)
M09(s,2)
M10(d,13,9)
M12(s,15)
M13(d,12,10)
M11(s,19)
M04(s,24)
DMSO-d6
M01(s,7)
M02(s,25)
M03(s,27,26)
F
N
NH
O
N
H
N
S

Cpd 1l

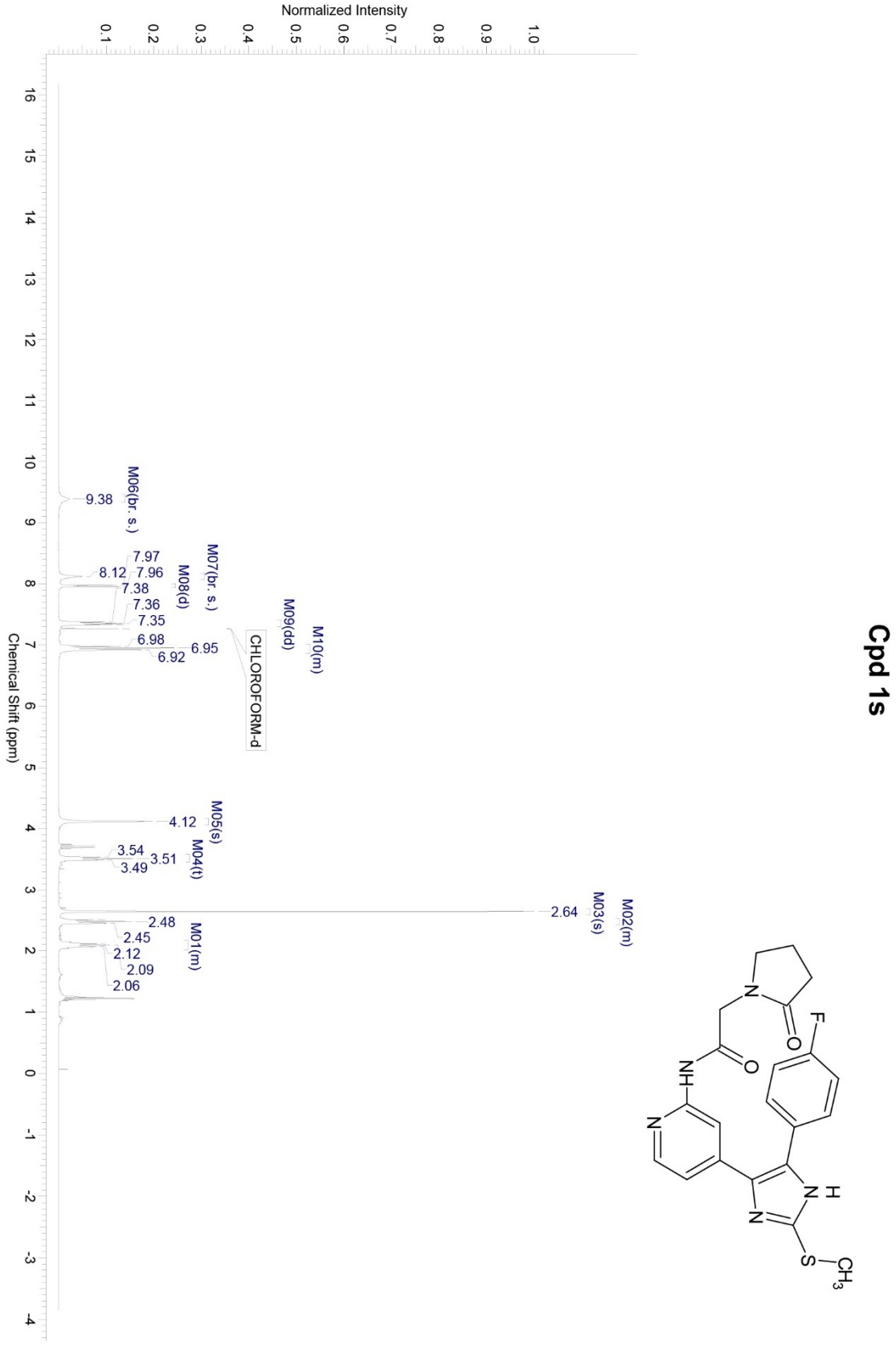
Cpd 1s
Normalized Intensity
Chemical Shift (ppm)
9.38
M06(br. s.)
8.12
7.97
7.96
M08(d)
7.38
7.36
7.35
M07(br. s.)
6.98
6.95
6.92
CHLOROFORM-d
M09(dd)
M10(m)
4.12
M05(s)
3.54
3.51
3.49
M04(t)
2.64
M02(m)
M03(s)
2.48
2.45
2.12
2.09
2.06
M01(m)
F
O
O
NH
N
N
H
N
S
CH3

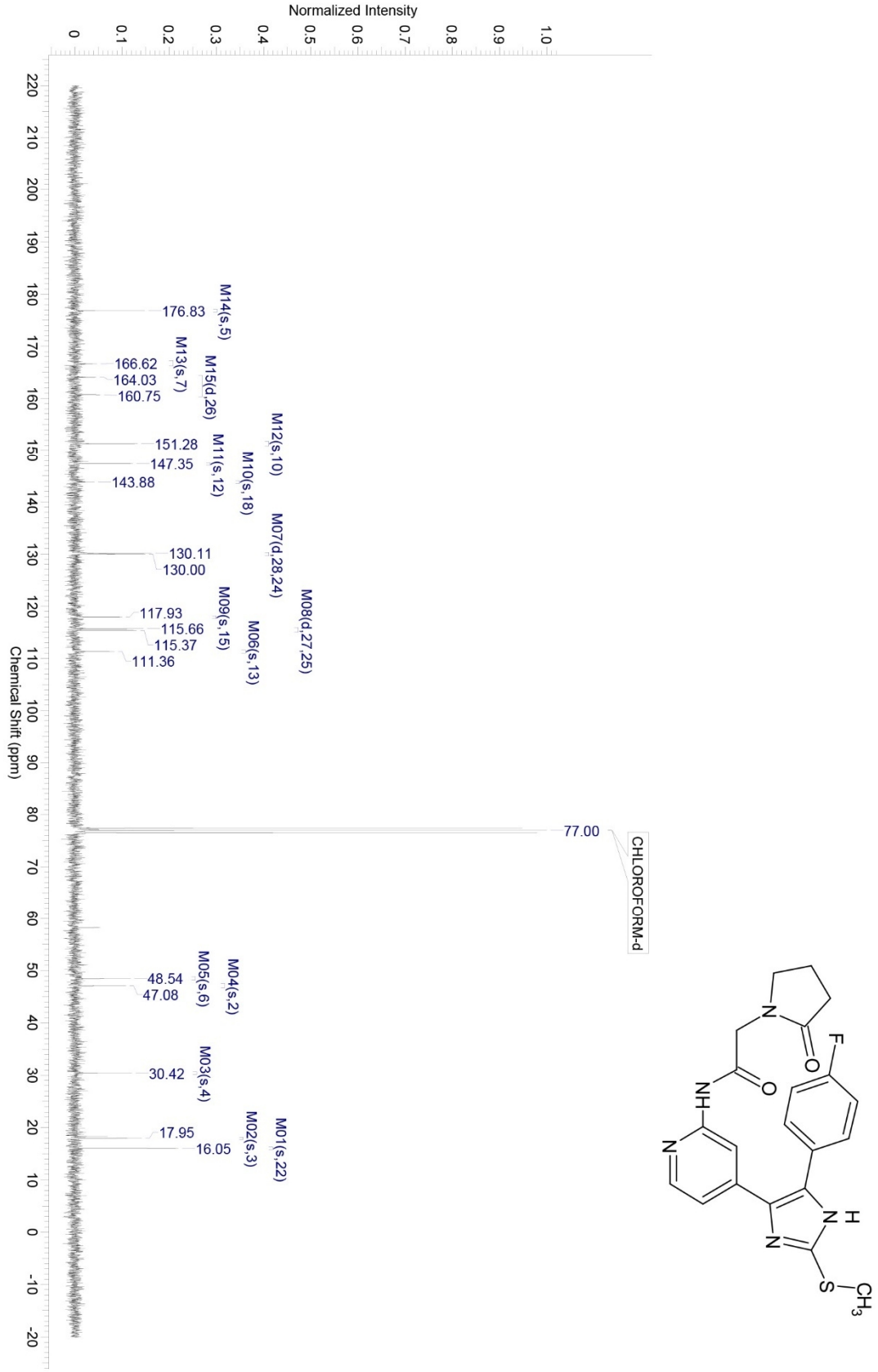
Cpd 1s
Normalized Intensity
Chemical Shift (ppm)
176.83
166.62
164.03
160.75
151.28
147.35
143.88
130.11
130.00
117.93
115.66
115.37
111.36
77.00
48.54
47.08
30.42
17.95
16.05
M14(s,5)
M13(s,7)
M15(d,26)
M12(s,10)
M11(s,12)
M10(s,18)
M07(d,28,24)
M08(d,27,25)
M09(s,15)
M06(s,13)
CHLOROFORM-d
M05(s,6)
M04(s,2)
M03(s,4)
M02(s,3)
M01(s,22)
F
O
O
NH
N
N
H
N
S
CH3

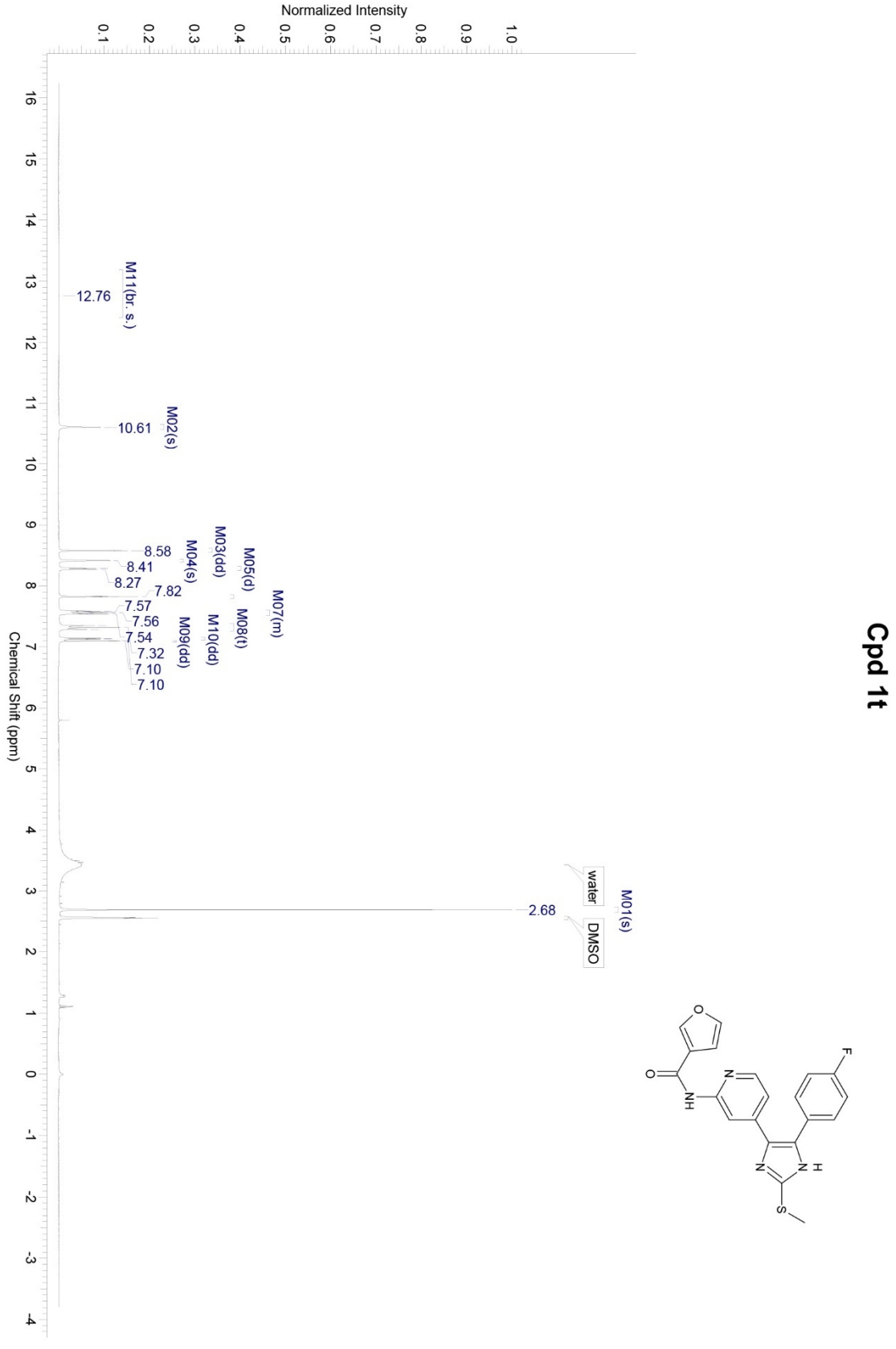
Normalized Intensity
Chemical Shift (ppm)
12.76
M11(br. s.)
10.61
M02(s)
8.58
8.41
8.27
7.82
7.57
7.56
7.54
7.32
7.10
7.10
M04(s)
M03(dd)
M05(d)
M08(t)
M07(m)
M10(dd)
M09(dd)
2.68
water
DMSO
M01(s)
Cpd 1t

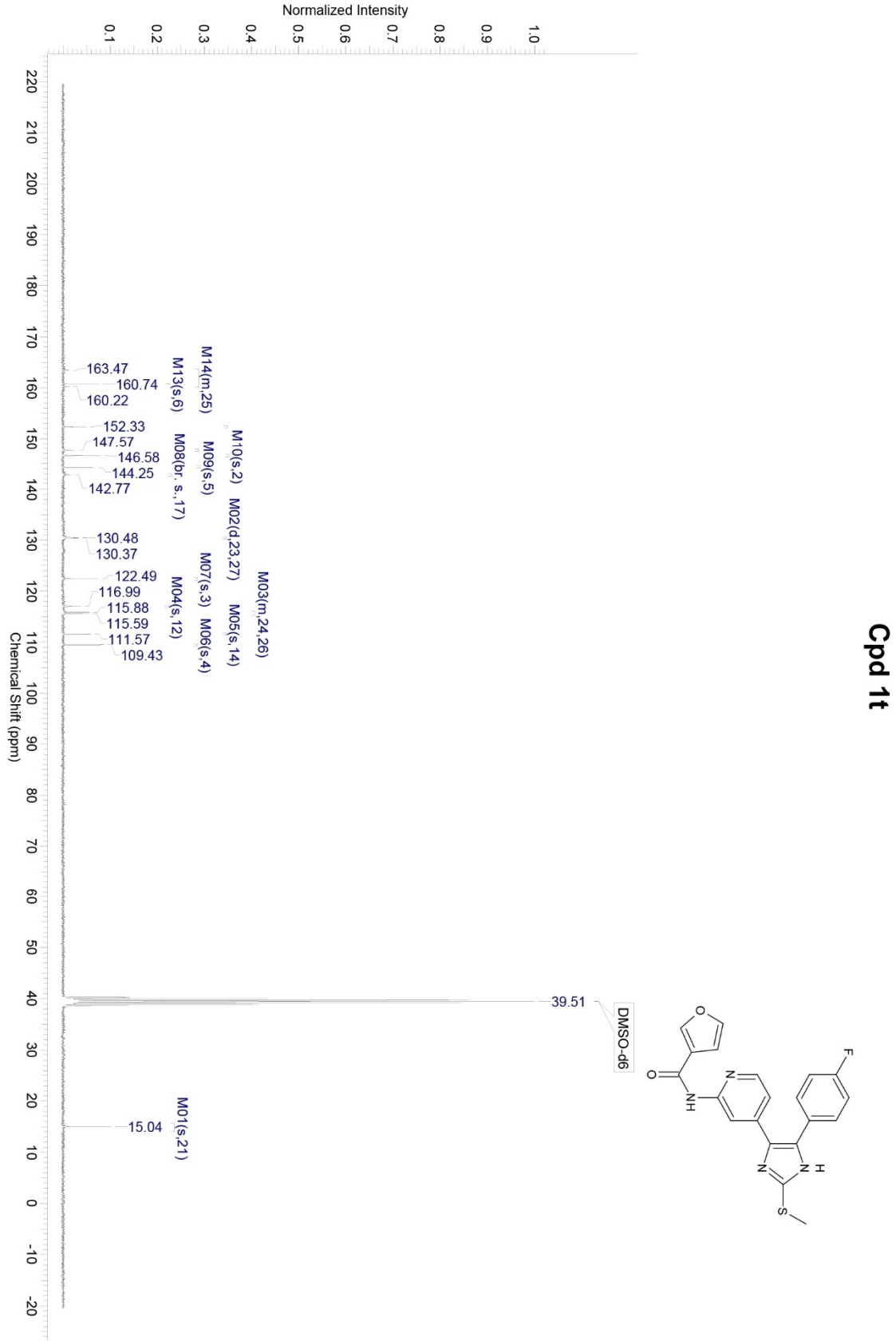
Normalized Intensity
Chemical Shift (ppm)
163.47
160.74
160.22
152.33
147.57
146.58
144.25
142.77
130.48
130.37
122.49
116.99
115.88
115.59
111.57
109.43
39.51
15.04
M14(m,25)
M13(s,6)
M10(s,2)
M08(br. s.,17)
M02(d,23.27)
M09(s,5)
M03(m,24.26)
M07(s,3)
M05(s,14)
M06(s,4)
M04(s,12)
M01(s,21)
DMSO-d6
Cpd 1t

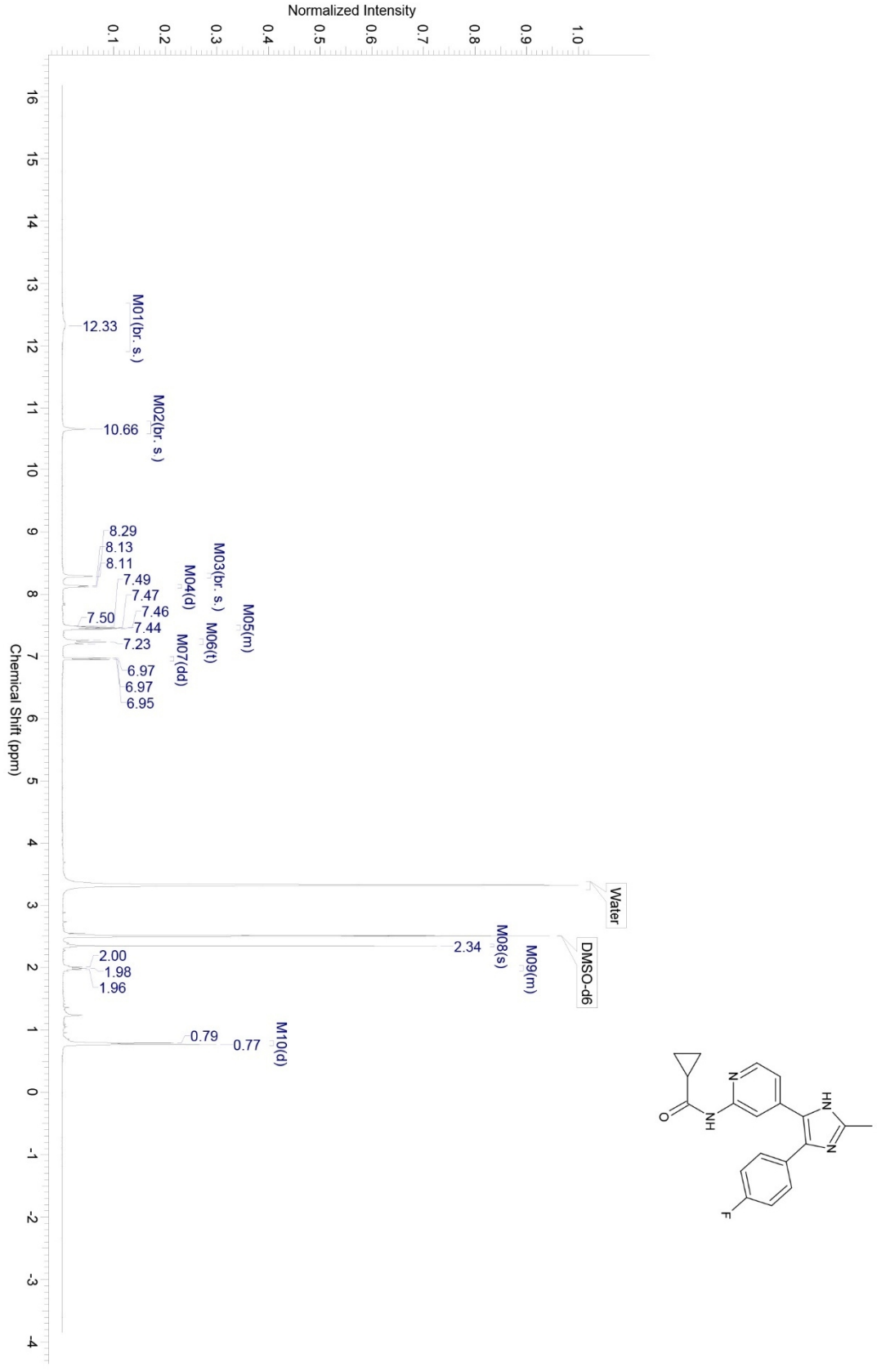
Normalized Intensity
Chemical Shift (ppm)
12.33
M01(br. s.)
10.66
M02(br. s.)
8.29
8.13
8.11
7.49
7.47
7.46
7.50
7.44
7.23
6.97
6.97
6.95
M03(br. s.)
M04(d)
M05(m)
M06(t)
M07(dd)
Water
2.34
M08(s)
M09(m)
DMSO-d6
2.00
1.98
1.96
0.79
0.77
M10(d)
Cpd 20b

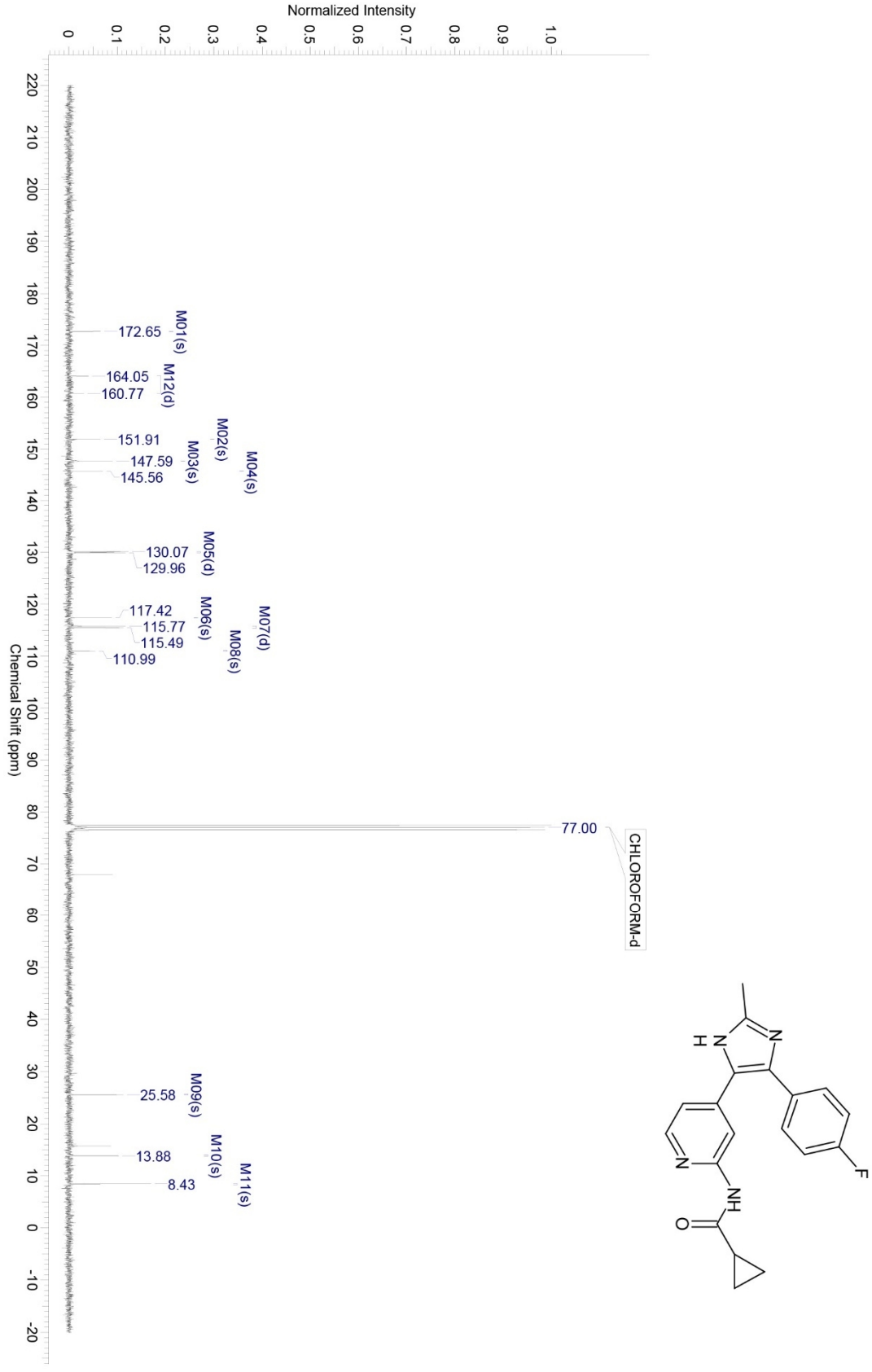
Normalized Intensity
0
0.1
0.2
0.3
0.4
0.5
0.6
0.7
0.8
0.9
1.0
Chemical Shift (ppm)
220
210
200
190
180
170
160
150
140
130
120
110
100
90
80
70
60
50
40
30
20
10
0
-10
-20
172.65
M01(s)
164.05
160.77
M12(d)
151.91
M02(s)
147.59
M03(s)
145.56
M04(s)
130.07
129.96
M05(d)
117.42
115.77
115.49
M06(s)
M07(d)
M08(s)
110.99
77.00
CHLOROFORM-d
25.58
M09(s)
13.88
M10(s)
8.43
M11(s)
Cpd 20b
N
H
N
N
NH
O
F

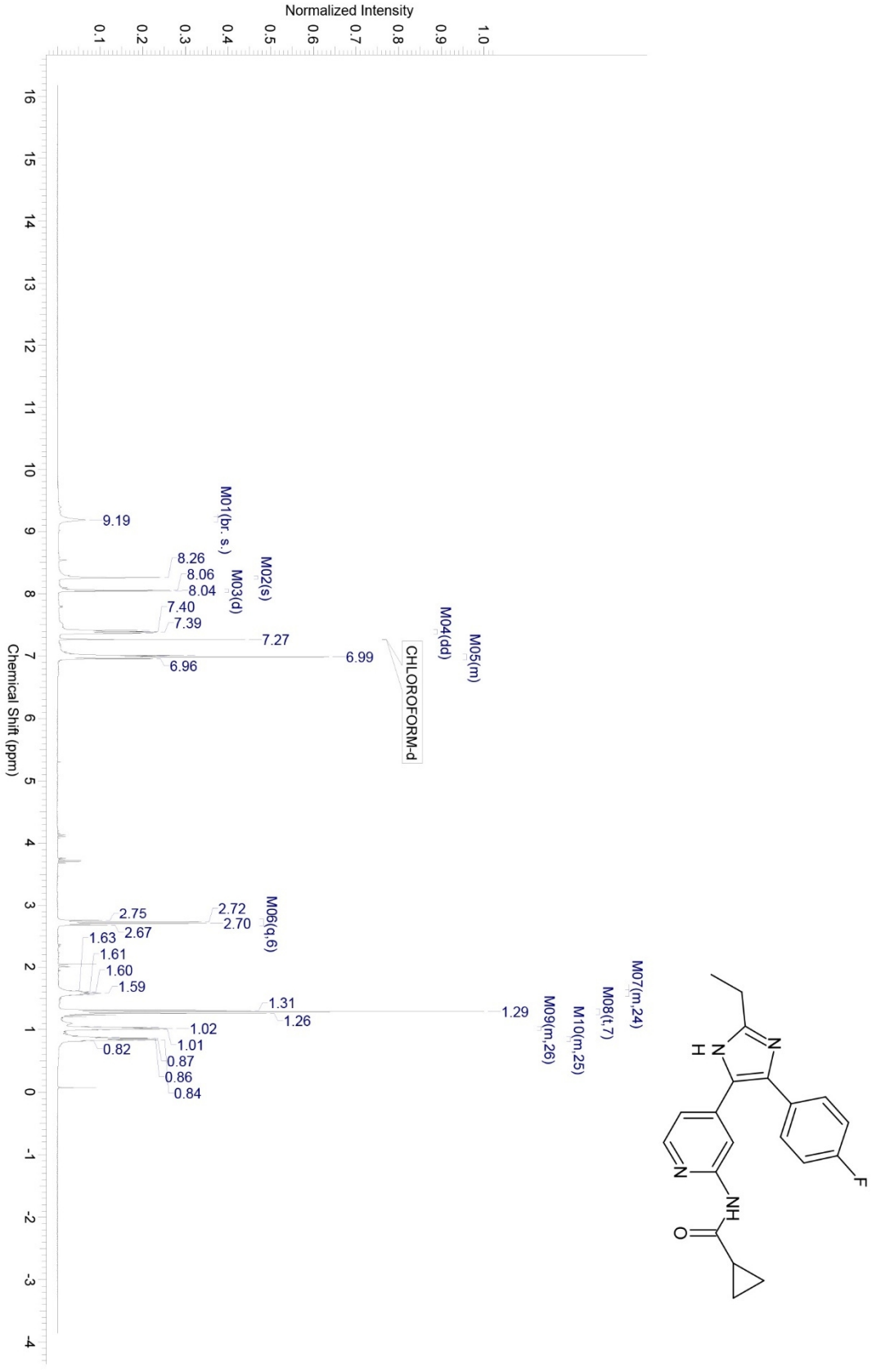
Normalized Intensity
Chemical Shift (ppm)
9.19
8.26
8.06
8.04
7.40
7.39
7.27
6.99
6.96
2.75
2.72
2.70
2.67
1.63
1.61
1.60
1.59
1.31
1.29
1.26
1.02
1.01
0.87
0.86
0.84
0.82
M01(br. s.)
M02(s)
M03(d)
M04(dd)
M05(m)
M06(q,6)
M07(m,24)
M08(t,7)
M09(m,26)
M10(m,25)
CHLOROFORM-d
Cpd 20c

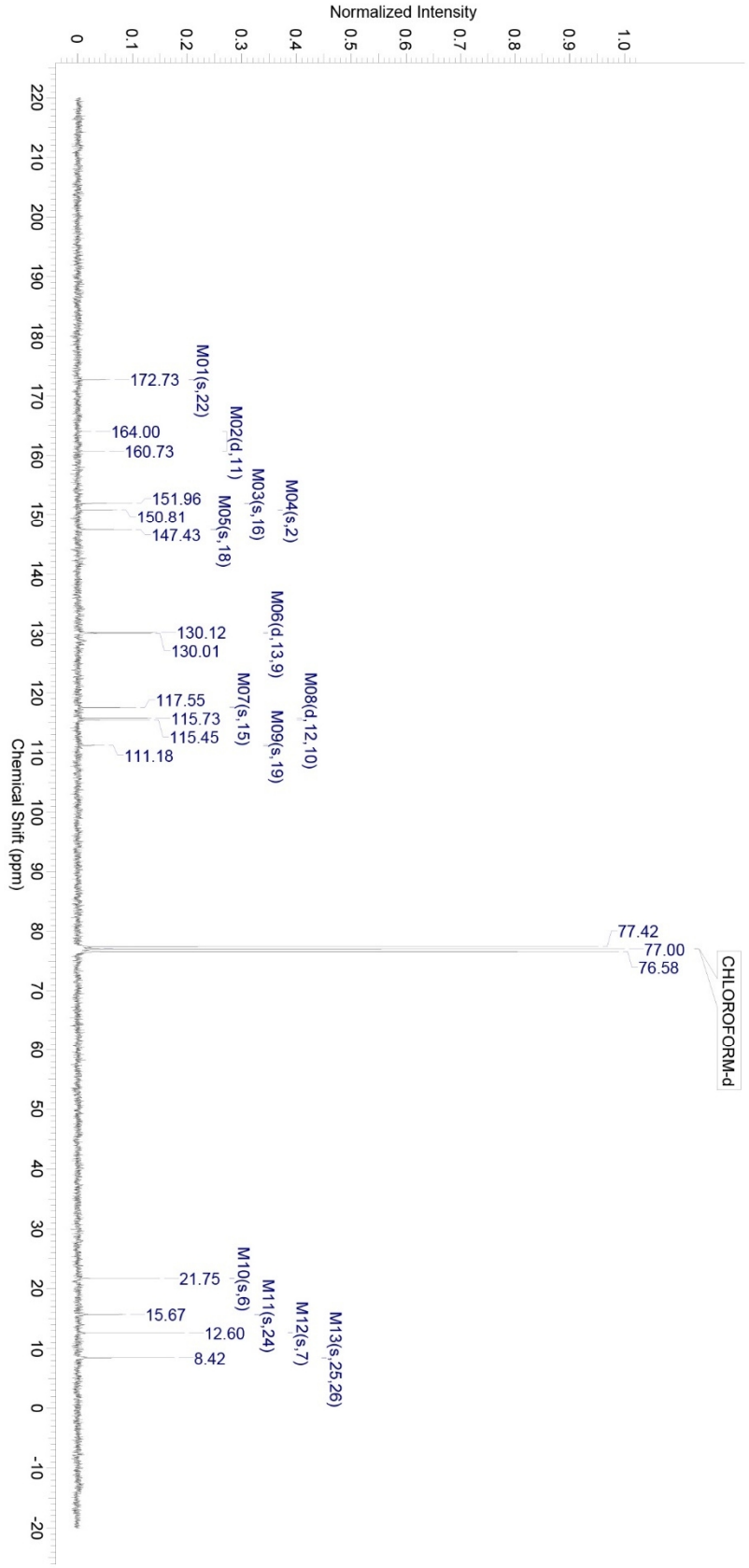
Normalized Intensity
0
0.1
0.2
0.3
0.4
0.5
0.6
0.7
0.8
0.9
1.0
Chemical Shift (ppm)
220
210
200
190
180
170
160
150
140
130
120
110
100
90
80
70
60
50
40
30
20
10
0
-10
-20
172.73
M01(s,22)
164.00
160.73
M02(d,11)
151.96
150.81
147.43
M03(s,16)
M04(s,2)
M05(s,18)
130.12
130.01
M06(d,13.9)
117.55
115.73
115.45
111.18
M07(s,15)
M08(d,12.10)
M09(s,19)
77.42
77.00
76.58
CHLOROFORM-d
21.75
15.67
12.60
8.42
M10(s,6)
M11(s,24)
M12(s,7)
M13(s,25.26)

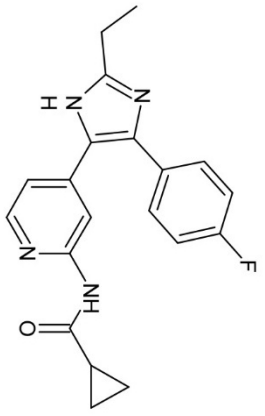
H
N
N
N
NH
O
F

Cpd 20c

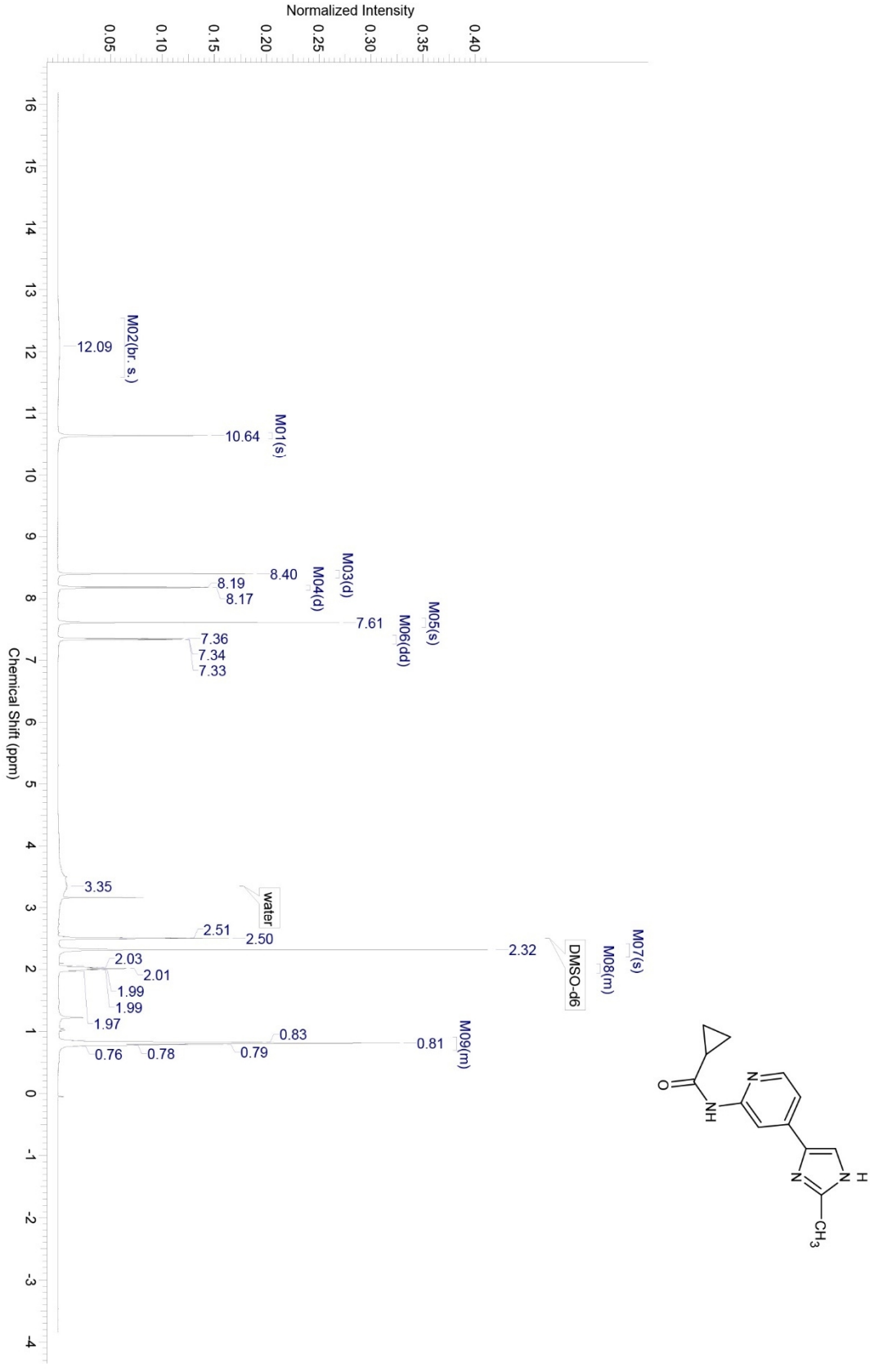
Normalized Intensity
0.05
0.10
0.15
0.20
0.25
0.30
0.35
0.40
Chemical Shift (ppm)
16
15
14
13
12
11
10
9
8
7
6
5
4
3
2
1
0
-1
-2
-3
-4
12.09
M02(br. s.)
10.64
M01(s)
8.40
8.19
8.17
M03(d)
M04(d)
7.61
M05(s)
7.36
7.34
7.33
M06(dd)
3.35
water
2.51
2.50
2.32
DMSO-d6
M07(s)
M08(m)
2.03
2.01
1.99
1.99
1.97
0.83
0.81
0.76
0.78
0.79
M09(m)
Cpd 25
O
NH
N
N
N
H
CH3

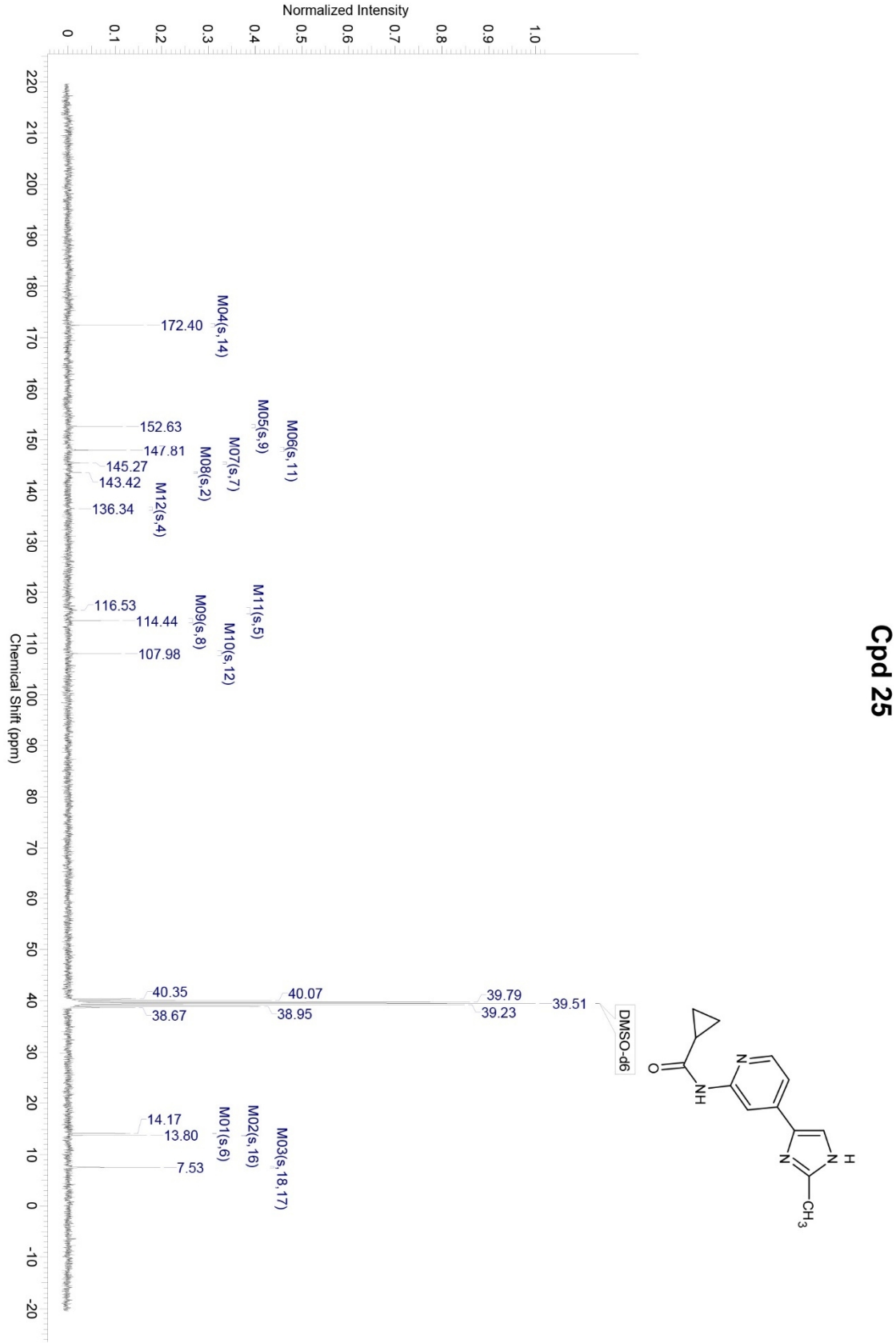
Normalized Intensity
0
0.1
0.2
0.3
0.4
0.5
0.6
0.7
0.8
0.9
1.0
Chemical Shift (ppm)
220
210
200
190
180
170
160
150
140
130
120
110
100
90
80
70
60
50
40
30
20
10
0
-10
-20
172.40
M04(s,14)
152.63
147.81
145.27
143.42
136.34
M12(s,4)
M08(s,2)
M07(s,7)
M05(s,9)
M06(s,11)
116.53
114.44
107.98
M09(s,8)
M10(s,12)
M11(s,5)
40.35
40.07
39.79
39.51
38.67
38.95
39.23
DMSO-d6
14.17
13.80
7.53
M01(s,6)
M02(s,16)
M03(s,18,17)
O
NH
N
N
H
CH3

Cpd 25

Publication III

Heider, F.; Pantsar, T.; Kudolo M.; Ansideri, F.; De Simone, A.; Andrisano, V.; Pruccoli, L.; Schneider, T.; Goettert, M.; Tarozzi, A.; Laufer, S.; Koch, P. – Pyridinylimidazoles as GSK3β Inhibitors: The Impact of Tautomerism on Compound Activity via Water Networks. *ACS Medicinal Chemistry Letters*, **2019**, *10*, 1407-1414.

* Heider and Pantsar contributed equally to this work.

ACS Medicinal Chemistry Letters
Cite This: ACS Med. Chem. Lett. 2019, 10, 1407−1414
Letter
pubs.acs.org/acsmedchemlett

Pyridinylimidazoles as GSK3β Inhibitors: The Impact of Tautomerism on Compound Activity via Water Networks

Fabian Heider,[†,#] Tatu Pantsar,[‡,§,#] Mark Kudolo,[†] Francesco Ansideri,[†] Angela De Simone,[∥] Letizia Pruccoli,[∥] Taiane Schneider,[⊥] Marcia Inês Goettert,[⊥] Andrea Tarozzi,[∥] Vincenza Andrisano,[∥] Stefan A. Laufer,[†] and Pierre Koch*[,†,▽]

[†]Department of Pharmaceutical and Medicinal Chemistry, Institute of Pharmaceutical Sciences, Eberhard Karls Universität Tübingen, Auf der Morgenstelle 8, 72076 Tübingen, Germany

[‡]School of Pharmacy, University of Eastern Finland, P.O. BOX 1627, 70211 Kuopio, Finland

[§]Department of Internal Medicine VIII, University Hospital Tübingen, Otfried-Müller-Straße 14, 72076 Tübingen, Germany

[∥]Department for Life Quality Studies, Alma Mater Studiorum-University of Bologna, Corso D'Augusto, 237, 47921 Rimini, Italy

[⊥]Cell Culture Laboratory, Postgraduate Program in Biotechnology, University of Vale do Taquari (Univates), Lajeado, RS 95900-00, Brazil

[▽]Department of Pharmaceutical/Medicinal Chemistry II, Institute of Pharmacy, University of Regensburg, Universitätsstraße 31, 93053 Regensburg, Germany

Supporting Information

ABSTRACT: Glycogen synthase kinase-3β (GSK3β) is involved in many pathological conditions and represents an attractive drug target. We previously reported dual GSK3β/p38α mitogen-activated protein kinase inhibitors and identified *N*-(4-(4-(4-fluorophenyl)-2-methyl-1*H*-imidazol-5-yl)pyridin-2-yl)cyclopropanecarboxamide (**1**) as a potent dual inhibitor of both target kinases. In this study, we aimed to design selective GSK3β inhibitors based on our pyridinylimidazole scaffold. Our efforts resulted in several novel and potent GSK3β inhibitors with IC_{50} values in the low nanomolar range. 5-(2-(Cyclopropanecarboxamido)pyridin-4-yl)-4-cyclopropyl-1*H*-imidazole-2-carboxamide (**6g**) displayed very good kinase selectivity as well as metabolical stability and inhibited GSK3β activity in neuronal SH-SY5Y cells. Interestingly, we observed the importance of the 2-methylimidazole's tautomeric state for the compound activity. Finally, we reveal how this crucial tautomerism effect is surmounted by imidazole-2-carboxamides, which are able to stabilize the binding via enhanced water network interactions, regardless of their tautomeric state.

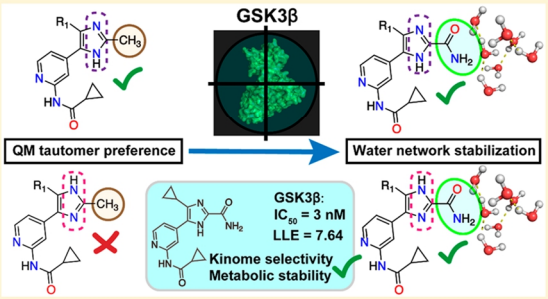

KEYWORDS: *Protein kinase inhibitors, glycogen synthase kinase-3β, pyridinylimidazoles, tautomerism, molecular dynamics simulation, quantum mechanics*

Glycogen synthase kinase-3β (GSK3β) is a ubiquitously expressed serine/threonine kinase, which plays an important role in a variety of different cell signaling pathways. GSK3β plays a crucial role in almost every pathway leading to the hallmarks of Alzheimer's disease[1,2] and is often referred to as a tau-kinase due to its capacity to modulate tau hyperphosphorylation. Overactivity of GSK3β has also been connected to an increased production of β-amyloids,[3] neuroinflammation, and oxidative stress.[4]

GSK3β has also been associated with a plethora of other pathological conditions such as diabetes,[5] cancer,[6−8] schizophrenia,[9] bipolar disorders,[10] and osteoporosis.[11] Thus, GSK3β is considered to be an attractive drug target.

We recently reported a series of pyridinylimidazoles as dual GSK3β/p38α MAP kinase (MAPK) inhibitors and identified trisubstituted imidazole **1** as a potent balanced inhibitor of both target enzymes (Figure 1).[12] Furthermore, we observed that the removal of the *para*-fluorophenyl ring (**2**), which might be located in the hydrophobic region (HR) I of the ATP binding site, resulted in a significantly reduced GSK3β inhibition with a complete loss of activity against p38α MAPK. In this study, our aim was to further improve the

Received: April 17, 2019
Accepted: August 26, 2019
Published: August 26, 2019

DOI: 10.1021/acsmedchemlett.9b00177
ACS Med. Chem. Lett. 2019, 10, 1407−1414

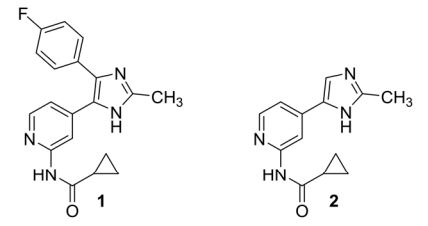

Figure 1. Pyridinylimidazole-based lead compounds **1** and **2**.

activity of our pyridinylimidazole scaffold while shifting the selectivity toward GSK3β.

Recently, employing quantum mechanics (QM) in drug design and development has become increasingly popular. For instance, QM can be utilized to improve docking and scoring, determining protonation states and optimizing structures as well as ligand binding energies.[13,14] Also, the importance of water in drug design is gaining more and more emphasis.[15] The effect of water network stabilization for ligand binding has been demonstrated e.g. by Klebe and co-workers.[16] In addition, molecular dynamics (MD) simulations offer valuable insights into ligand binding interactions.[17] By utilizing QM calculations with MD simulations, we disclosed the importance of tautomerism and water networks for the activity of our pyridinylimidazole compounds. In this case, the observed SAR could not have been clarified by simplified computational tools, such as docking, which has major caveats especially related to the solvent effects and dynamics of the system[18] that were found determining for the activity differences among imidazoles.

■ RESULTS AND DISCUSSION

Detailed descriptions of the synthetic sequences are reported in Schemes S1−S14 (Supporting Information, SI).

To address the alarming diffuse trend of increasing the inhibitor logP value in the lead optimization,[19] we monitored the lipophilic ligand efficacy (LLE) of the synthesized compounds.[20] The LLE of our lead compounds **1** and **2** was already high with values of 5.10 and 4.40, respectively (Table 1).

Initially, we examined the influence of different substituents reaching into the HR I of GSK3β. To this end, we synthesized a series of 2-methylpyridinylimidazoles with different cycloaliphatic and aromatic moieties attached to the imidazole-C4 position.

Replacing the aromatic ring with cycloalkyl moieties at the imidazole-C4 position (**3j−m**) resulted in a substantial loss of activity, leading to modest inhibitors of GSK3β in the micromolar range displaying complete inactivity against p38α MAPK.

Compounds with bulky moieties, such as 2-naphtyl (**3h**), were inactive, probably because of a steric clash in the HR I.

Replacement of the *para*-fluorophenyl ring with the 5-membered heteroaromatic rings thiophene (**3d**) or furan (**3e**) as well as other minor changes on the *para*-fluorophenyl ring, such as addition of a methyl (**3o**) or a second fluorine atom (**3i**), led to inhibitors with slightly increased IC_{50} values compared to **1**. Introduction of a pyrimidine (**3g**) at the imidazole-C4 led to a completely inactive derivative. The less lipophilic *ortho*- and *meta*-hydroxyphenyl derivatives (**3a** and **3b**, respectively) turned out to be potent GSK3β inhibitors with sound LLE values, while the *para*-hydroxyphenyl compound (**3c**) displayed substantially diminished inhibition against both kinases. All potent GSK3β inhibitors bearing an aromatic ring in the HR I, however, remained potent inhibitors of p38α MAPK, except for **3e** with 10-fold selectivity for GSK3β.

To elucidate the observed dramatic loss of activity of certain compounds, we investigated the influence of the R_1-substituent on the imidazole ring's tautomeric state. To this end, we conducted QM calculations to assess the probability of different tautomeric states and conformations for the compounds (Figure 2, *see* SI *for details*). Indeed, QM results indicated that the active compounds generally prefer tautomer A or at least represent a reasonable population of this tautomeric state (Table S3, Supporting Information). For instance, the low nanomolar inhibitors **3a**, **3b**, **3d**, and **3e** display a clear preference for tautomer A (>71.5%). In turn, the less active compounds **3c** and **3j−m** display a clearly diminished population of tautomer A (<17%).

Obviously, the preference of a specific tautomeric state does not fully determine the compound activity. For example, the inactive compound **3g** clearly prefers tautomer A (85.9%), but the pyrimidine group is suboptimal for the hydrophobic region (solvent preference). On the contrary, the highly lipophilic *para*-fluorophenyl substituent in compound **1** clearly increases potency, despite its preference for tautomer B. Interestingly, the inactive 2-methoxyphenyl derivative **3f** appears only in a specific conformation as tautomer A, wherein the methoxy-group folds on top of the pyridinyl ring (Table S3, Supporting Information), which most likely impedes the binding. Overall, the tautomeric state preference partially, but not solely, determines the 2-methylimidazole activity.

Next, we attempted to improve the binding affinity of **1** via enhancing interactions at the solvent interface in the HR II. To this end, MD simulations (200 ns) demonstrated the potential suitability of compounds bearing *N*-(pyridin-2-yl)tri- or tetrazolepropanamide moieties (**4a**,**b**; Figures S2−S4, Supporting Information). Both displayed cation−π interactions with the Arg141 and improved solvent interactions combined with significantly lower log P values (Table 2). The simulation of **4a** highlighted an identical binding mode for the triazole ring as observed in a crystal structure (PDB ID: 5K5N).[21]

Compounds **4a** and **4b** show a similar potency as the lead compound **1** but with enhanced LLE values. Removal of the *para*-fluorophenyl anchor resulted in compounds **4c** and **4d**, both displaying substantially reduced inhibitory potency. This clearly results from the negative log P values of these compounds, which seems to compromise their binding affinity (entropic penalty). Nevertheless, these compounds still exhibit mediocre target inhibition and fit nicely into the SAR of the series.

To overcome the highlighted tautomerism-related issues observed with the 2-methylimidazoles, we designed and synthesized a series of imidazole-2-carboxamides. Instead of the acceptor nitrogen of tautomer A, the 2-carboxamides could neglect the tautomeric state of the imidazole by presenting the amide oxygen toward the Lys85 region. This amino acid side chain has been successfully targeted by carbonyl groups; for example, Pfizer disclosed 6-amino-4-(pyrimidin-4-yl)pyridones interacting with Lys85,[24] while Bristol-Myers Squibb reported potent pyrrolopyridinones.[25] Moreover, we investigated ethyl

DOI: 10.1021/acsmedchemlett.9b00177
ACS Med. Chem. Lett. 2019, 10, 1407−1414

Table 1. Activity and Physicochemical Parameters of 2-Methylimidazoles 3a−o

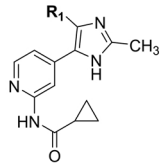

Cpd	R_1	IC_{50} ± SEM [μM] GSK3β[a]	IC_{50} [μM] p38α MAPK	Alog P[b]	LLE	Tautomer A population (%)[c]
1	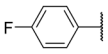	0.053 ± 0.012[d]	0.019[d,e]	2.88	4.40	29.386
2		1.68 ± 0.12[d]	>10[d,e]	0.72	5.10	n.d.[f]
3a		0.011 ± 0.001	0.050	2.40	5.56	85.508
3b	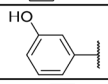	0.043 ± 0.005	0.024	2.40	4.97	2.834 (93.885[g])
3c	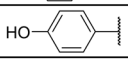	0.893 ± 0.001	1.851	2.40	3.65	12.687
3d		0.069 ± 0.000	0.048	2.40	4.77	81.318
3e		0.099 ± 0.033	0.987	1.84	5.17	71.467
3f	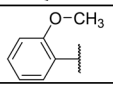	>10	0.504	2.65	-	31.19
3g		>10	>10	0.89	-	85.892
3h	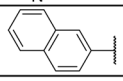	>10	0.081	3.58	-	20.289
3i	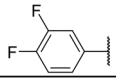	0.059 ± 0.007	0.019	3.08	4.15	n.d.
3j		3.09 ± 0.30	>10	1.76	3.75	6.014
3k		4.11 ± 0.19	>10	2.22	3.17	10.229
3l		5.46 ± 0.01	>10	2.68	2.59	16.734
3m		4.64 ± 1.16	>10	3.13	2.20	16.552
3n	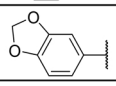	0.467 ± 0.006	0.030	2.44	3.89	n.d.
3o	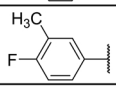	0.117 ± 0.015	0.007	3.36	3.57	n.d.

[a] $n = 2$. [b] Calculated with Canvas (Schrödinger LLC).[22] [c] According to QM Conformer & Tautomer Predictor of Maestro (Schrödinger, LLC, New York, NY, 2018) (*see* SI and Table S3 *for details*). [d] Values taken from Heider et al.[12] [e] Determined by ELISA activity assay.[23] [f] n.d. = not determined. [g] The intramolecular H-bond to amide conformation excluded (*see* Table S3, SI).

esters as well as a hydroxyl moiety for their suitability to address the Lys85 residue.

In contrast to methylimidazole **2**, imidazole-2-carboxamide **6a** showed a >35-fold improvement in potency (LLE 7.49) (Table 3). In the case of compound **1**, the introduction of a carboxamide moiety at the imidazole-C2 position (**6h**) did not substantially improve the inhibitory activity. Installation of an ethyl ester (**5a** and **5c**) yielded mediocre inhibitors high-

DOI: 10.1021/acsmedchemlett.9b00177
ACS Med. Chem. Lett. 2019, 10, 1407−1414

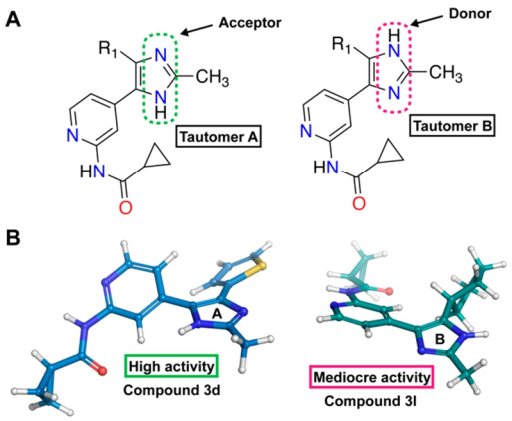

Figure 2. (**A**) The imidazole ring has two potential tautomeric forms: in tautomer A, the nitrogen next to the R_1-group is unprotonated and can act as a H-bond acceptor, whereas in tautomer B it is protonated and can act as a H-bond donor. (**B**) The R_1-group influences the preferred tautomeric state and conformation. As an example, the lowest energy conformations (in solution) of the highly active compound **3d** and of the poorly active compound **3l** are shown here. Compound **3d** prefers the active conformation with tautomer A, and **3l** exists in the inactive conformation with tautomer B.

lighting the importance of the amide function. Introduction of a hydroxy moiety at the imidazole-C2 methyl group resulted in **6i**, showing a 2-fold reduction in GSK3β inhibition and no shift in the IC_{50} value of p38α MAPK. In most cases, imidazole-2-carboxamides were better inhibitors of GSK3β than their corresponding 2-methylimidazole counterparts (e.g., **6c** vs **3f**, **6e** vs **3o**). Only the already potent 2-hydroxyphenyl **3a** (vs **6b**) displayed no improvement in activity.

The most striking differences existed in cycloalkyl substituted compounds **6f** and **6g**, exhibiting dramatically improved potency against GSK3β along with higher LLE values compared to the corresponding 2-methylimidazole derivatives **3m** and **3j**, which displayed only mediocre activities and preferred tautomer B. Moreover, all three compounds showed significant selectivity over p38α MAPK, and compound **6g** was among the best from this series (GSK3β, IC_{50}: 0.003 μM; p38α MAPK, IC_{50} >10 μM; LLE 7.64).

To further investigate these dramatic activity differences, we first confirmed that the amide group replacing the methyl group on the imidazole-C2 position had no influence on the tautomeric state preference (Table S3). As an example, the cyclopropyl-substituted compounds **3j** and **6g** display an analogous population of the tautomeric state A, namely 6.0% and 6.7% for **3j** and **6g**, respectively. Nevertheless, the potency of these two inhibitors is dramatically different, with the imidazole-2-carboxamide derivative **6g** showing a 3 orders of magnitude higher activity than its methyl counterpart (**3j**).

To gain a deeper insight into the compound binding and the activity differences between 2-methylimidazoles and imidazole-2-carboxamides, we conducted a total of 8 μs MD simulations for the selected compounds bound to GSK3β in their preferred tautomeric state: **3j** and **6g** in tautomeric state B and **3a** and **6b** in tautomeric state A. The initial 1 μs MD simulations suggested unstable binding only for **3j**, where its lipophilic cyclopropyl group is exposed to water in the HR I (Figure 3 and Figures S5 and S9, Supporting Information). Whereas with **6g** the amide stabilizes a water network near Asp200 and the cyclopropyl group is shielded from the solvent, allowing the stable binding of tautomer B (Figure 3 *and* Figures S5 and S9, Supporting Information). With tautomer A preferring **3a** and **6b**, the 2-hydroxyphenyl was shielded from solvent regardless of the methyl or amide group substituent on the imidazole ring (Figure 3 and Figures S7 and S9, Supporting Information). These observations were confirmed in unbiased simulations, conducted using another crystal structure as the starting configuration (Figures S6, S8 and S10, Supporting Information). Based on these data, the energetically favorable tautomer B of **3j** does not support the suggested stabilizing interactions with the dynamic water network, which leads to water exposed HR I, whereas the preferred tautomer A of **3a** is capable to shield the HR I from water via direct or water mediated

Table 2. Activity and Physicochemical Parameters of *N*-(Pyridin-2-yl)tri- or tetrazolepropanamide Bearing 2-Methylimidazoles 4a–d

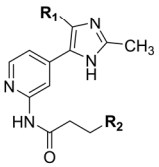

Cpd	R_1	R_2	IC_{50} ± SEM [μM] GSK3β[a]	IC_{50} [μM] p38α MAPK	Alog P[b]	LLE
4a			0.082 ± 0.007	0.041	1.16	5.92
4b	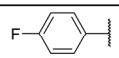		0.072 ± 0.008	0.038	1.83	5.32
4c	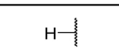		5.18 ± 0.10	>10	-0.99	6.27
4d	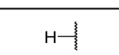		4.42 ± 0.29	>10	-0.32	5.65

[a] n = 2. [b] Calculated with Canvas (Schrödinger LLC).[22]

DOI: 10.1021/acsmedchemlett.9b00177
ACS Med. Chem. Lett. 2019, 10, 1407–1414

Table 3. Inhibition Data and Physicochemical Parameters of Ethyl Imidazole-2-carboxylates 5 and Imidazole-2-carboxamides 6−8

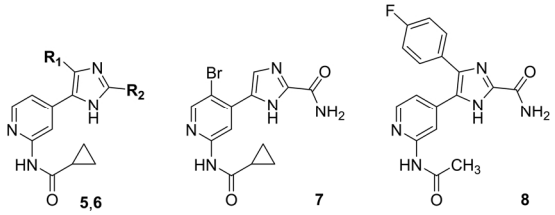

Cpd	R_1	R_2	IC_{50} ± SEM [μM] GSK3β[a]	IC_{50} [μM] p38α MAPK	Alog P[b]	LLE
5a	H	CH_3	0.739 ± 0.186	>10	1.07	5.06
6a	H	NH_2	0.047 ± 0.020	>10[c]	-0.16	7.49
5c	F	CH_3	0.899 ± 0.010	0.089	3.23	2.82
6h	F	NH_2	0.039 ± 0.017	0.019[c]	1.99	5.52
6i	F	OH	0.091 ± 0.006	0.016	2.20	4.84
6j	H_3C	NH_2	0.013 ± 0.001	>10	0.12	7.76
6g	cyclopropyl	NH_2	0.003 ± 0.000	>10	0.88	7.64
6f	cyclohexyl	NH_2	0.003 ± 0.000	>10	2.25	6.27
6b	2-OH-phenyl	NH_2	0.023 ± 0.001	0.158	1.52	6.12
6c	2-$O-CH_3$-phenyl	NH_2	0.265 ± 0.017	2.35	1.77	4.81
6e	2-H_3C-4-F-phenyl	NH_2	0.079 ± 0.003	0.016	2.48	4.62
6d	2-F_3C-O-phenyl	NH_2	0.352 ± 0.002	2.04	3.91	2.54
7	-	-	0.354[d]	>10	0.59	5.86
8	-	-	0.047 ± 0.004	0.117	1.24	6.09

[a] $n = 2$. [b] Calculated with Canvas (Schrödinger LLC).[22] [c] Determined by ELISA activity assay.[23] [d] $n = 1$.

interactions to Lys85 and maintain a stable binding (Figures S5−S8, Supporting Information). Thus, QM calculations with the MD simulations provide a potential explanation for the observed activity differences.

Selected compounds (**1**, **3a**, **3i**, **6a**, and **6h**) were further tested for their GSK3β affinity in a previously reported ESI-QTOF assay (Tables S1 and S2, Supporting Information).[26] Using this completely different assay system, the potency trend of these GSK3β inhibitors obtained in the ADP-Glo activity assay was confirmed.

Moreover, inhibitors **3a** and **6g** were tested for their metabolic stability by incubation with human liver microsomes (HLM) over a period of 4 h (Tables S4 and S5, Supporting Information). Both compounds displayed excellent metabolic stability in this assay.

DOI: 10.1021/acsmedchemlett.9b00177
ACS Med. Chem. Lett. 2019, 10, 1407−1414

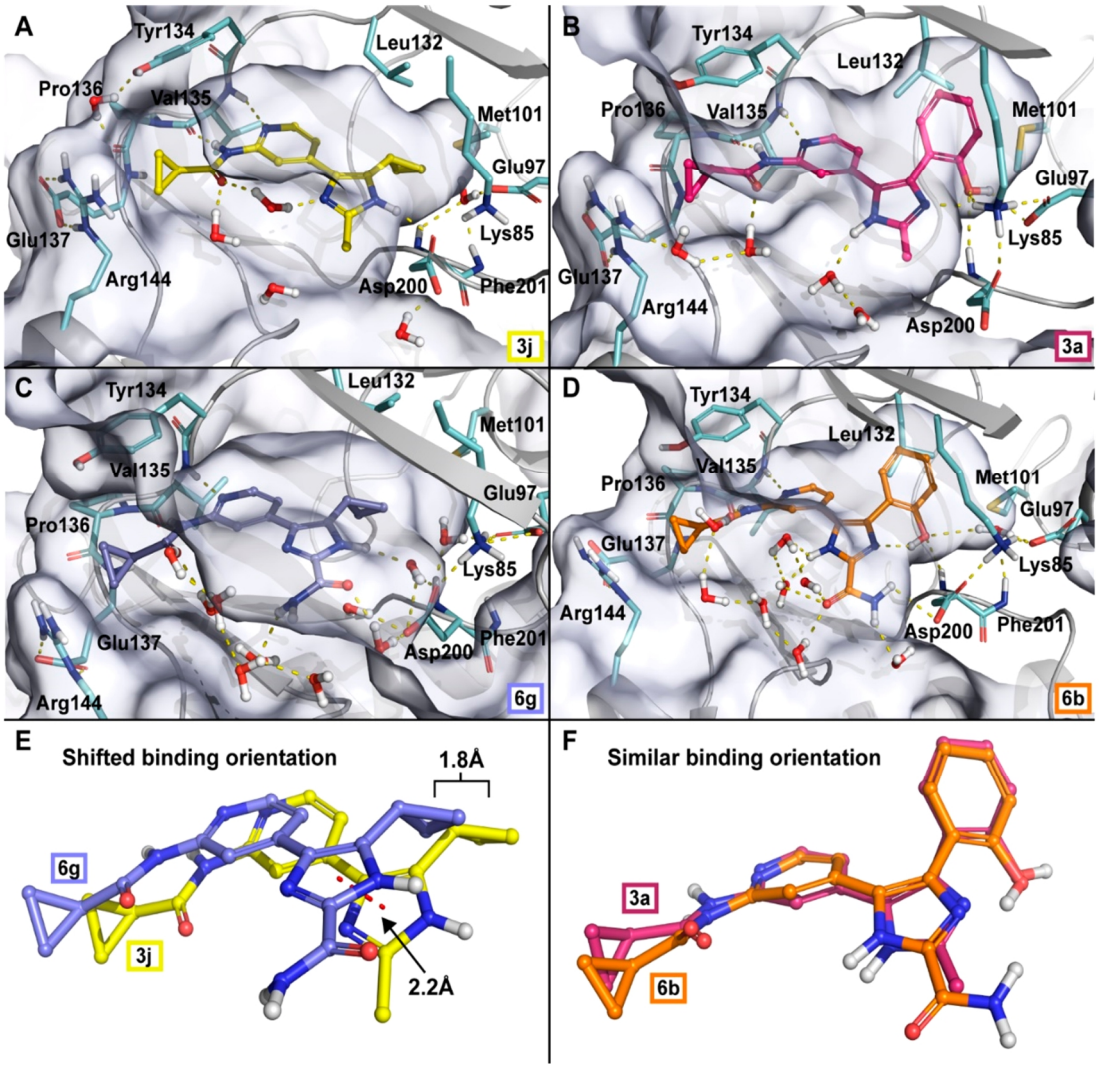

Figure 3. Representative snapshots from MD simulations of compounds **3j** (**A**), **3a** (**B**), **6g** (**C**), and **6b** (**D**). (**E**) Compound **3j** appears in a shifted binding orientation compared to **6g**, whereas both 2-hydroxyphenyl derivatives (**F**) **3a** and **6b** display similar binding orientation in the simulations. The shift in the binding orientation of compound **3j** occurs due to direct H-bond interaction from the imidazole to Asp200. This interaction, with the increased solvent exposure of the lipophilic cyclopropyl group (*see* Figures S5–S6, Supporting Information), explains the 3 orders of magnitude difference in activity between **3j** and **6g**. The protein surface is illustrated in transparent light blue color and hydrogen bonds with yellow dashed lines in **A**–**D**.

Further pharmacological profiling of the potent GSK3β inhibitor **6g** included the evaluation of its ability to inhibit relevant CYP isoforms (Table 4). At a test concentration of 10 μM, imidazole-2-carboxamide **6g** shows a clean CYP inhibition profile. Only low inhibition of CYP1A2 was observed.

Table 4. Inhibition of CYP450 Isoenzymes

	% inhibition of CYP isoform @ 10 μM				
Cpd	1A2	2C9	2C19	2D6	3A4
6g	25.5	0.8	−2.0	−2.8	−2.3

To assess the overall kinome selectivity, the most promising inhibitor **6g** was screened against a representative panel of 68 diverse kinases (Table S6, Supporting Information), including the target kinase GSK3β and all members of the MAP kinases. At a concentration of 0.5 μM (>160-fold its IC_{50} value on the target kinase) only CDK2, CDK9, JNK3, MLK2, and VEGFR2 were substantially inhibited by **6g**, suggesting an acceptable kinome selectivity for this compound.

To confirm the biological activity of imidazole-2-carboxamide **6g**, we tested it in a cell-based GSK3β assay. At the tested concentration of 1 μM, **6g** inhibits GSK3β activity, in terms of inactive phospho-GSK3α/β (Ser21/9) increase, after 1 h of treatment in neuronal SH-SY5Y cells (Figure 4).

DOI: 10.1021/acsmedchemlett.9b00177
ACS Med. Chem. Lett. 2019, 10, 1407–1414

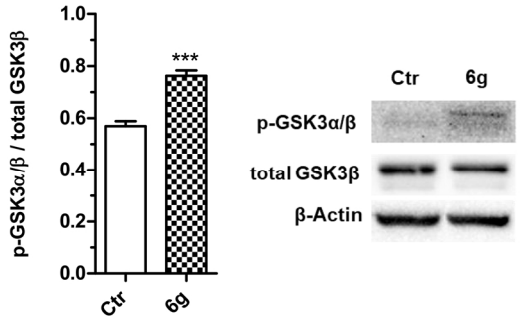

Figure 4. Inhibition of GSK3β activity in neuronal SH-SY5Y cells. Cells were incubated with compound **6g** [1 μM] for 1 h. At the end of incubation, the phosphorylation of GSK3α/β (Ser21/9) (inactive GSK3α/β form) was determined by Western blotting. Data are expressed as the ratio between phospho-GSK3α/β and total GSK3β levels normalized against β-actin and reported as mean ± SD of at least three independent experiments (***p < 0.001 versus untreated cells; t test).

Since CDK2, CDK9, and VEGFR2 are off-targets of **6g**, we also determined its cytotoxic profile on different cell lines after 48 h of incubation. A margin of safety is given concerning cytotoxic side effects. In the case of tested nontumorigenic cells, the concentration to cause a 50% decrease in cell viability is in the low micromolar range, which corresponds to >1000-fold the IC_{50} value of the GSK3β kinase activity assay (Figure S11, Supporting Information).

In the case of the selected tumorigenic cells (Figure S12, Supporting Information), compound **6g** shows antiproliferative activity in a human breast cancer cell line (Figure S12B, Supporting Information), at 0.1 μM and less at 0.01 μM. This may be a relevant result, as GSK3β is a target in the treatment of human breast cancer.[27] Breast cancer patients with overexpression of GSK3β presented poor prognosis, and GSK3β inhibition suppressed the viability and proliferation of breast cancer cells in vitro.[28]

In summary, we synthesized a diverse set of 33 novel di- and trisubstituted pyridinylimidazoles. The most potent GSK3β inhibitors **6f**, **6g**, and **6j** were selective over p38α MAPK and had reasonable (CNS) druglike log P values. Imidazole **6g** was metabolically stable in HLM, displayed a very good selectivity profile, and showed no affinity toward pharmacologically relevant CYP isoenzymes. Importantly, the LLE values of the series illustrate that the series' potency is not driven by molecular obesity.[29]

The SAR of the synthesized compounds was explained with QM calculations and MD simulations. The series represent an interesting example of the influence of the 2-methylimidazole tautomerism on the compound activity. The effect of tautomerism was indirectly surmounted by introducing the water-network stabilizing 2-carboxamide, thus exemplifying the importance to consider that subtle molecular differences may have significant influence on the dynamics of the system.

■ ASSOCIATED CONTENT

Supporting Information

The Supporting Information is available free of charge on the ACS Publications website at DOI: 10.1021/acsmedchemlett.9b00177.

Experimental details for preparation of the compounds; ESI-QTOF assay; cell-based GSK3β assay; molecular modeling, QM calculations and MD simulations; metabolic stability in HLM; kinome selectivity screening; inhibition of CYP450 isoenzymes; cell toxicity data (PDF)

■ AUTHOR INFORMATION

Corresponding Author

*E-mail: pierre.koch@uni-tuebingen.de (Pierre Koch).

ORCID

Fabian Heider: 0000-0003-2472-2457
Tatu Pantsar: 0000-0002-0369-2909
Letizia Pruccoli: 0000-0002-0739-2102
Andrea Tarozzi: 0000-0001-7983-8575
Vincenza Andrisano: 0000-0003-4396-1904
Stefan A. Laufer: 0000-0001-6952-1486
Pierre Koch: 0000-0003-4620-4650

Author Contributions

#F.H. and T.P. contributed equally to this work.

Notes

The authors declare no competing financial interest.

QM output conformations and MD movies and full raw trajectories are freely available at http://dx.doi.org/10.5281/zenodo.3362889.

■ ACKNOWLEDGMENTS

We thank Jens Strobach for his assistance with the p38α MAPK ADP Glo assay. The authors wish to acknowledge CSC-IT Center for Science, Finland, for computational resources. T.P. acknowledges the Orion Research Foundation sr for financial support.

■ ABBREVIATIONS

GSK, glycogen synthase kinase; HR, hydrophobic region; MAPK, MAP kinase; LLE, lipophilic ligand efficacy; MD, molecular dynamics; QM, quantum mechanics

■ REFERENCES

(1) Hooper, C.; Killick, R.; Lovestone, S. The GSK3 hypothesis of Alzheimer's disease. *J. Neurochem.* **2008**, *104*, 1433−1439.

(2) Canter, R. G.; Penney, J.; Tsai, L.-H. The road to restoring neural circuits for the treatment of Alzheimer's disease. *Nature* **2016**, *539*, 187−196.

(3) DaRocha-Souto, B.; Coma, M.; Perez-Nievas, B. G.; Scotton, T. C.; Siao, M.; Sanchez-Ferrer, P.; Hashimoto, T.; Fan, Z.; Hudry, E.; Barroeta, I.; Sereno, L.; Rodriguez, M.; Sanchez, M. B.; Hyman, B. T.; Gomez-Isla, T. Activation of glycogen synthase kinase-3 beta mediates β-amyloid induced neuritic damage in Alzheimer's disease. *Neurobiol. Dis.* **2012**, *45*, 425−37.

(4) Rana, A. K.; Singh, D. Targeting glycogen synthase kinase-3 for oxidative stress and neuroinflammation: Opportunities, challenges and future directions for cerebral stroke management. *Neuropharmacology* **2018**, *139*, 124−136.

(5) Eldar-Finkelman, H.; Schreyer, S. A.; Shinohara, M. M.; LeBoeuf, R. C.; Krebs, E. G. Increased glycogen synthase kinase-3 activity in diabetes- and obesity-prone C57BL/6J mice. *Diabetes* **1999**, *48*, 1662−1666.

(6) Kitano, A.; Shimasaki, T.; Chikano, Y.; Nakada, M.; Hirose, M.; Higashi, T.; Ishigaki, Y.; Endo, Y.; Takino, T.; Sato, H.; Sai, Y.; Miyamoto, K.-I.; Motoo, Y.; Kawakami, K.; Minamoto, T. Aberrant glycogen synthase kinase 3β is involved in pancreatic cancer cell invasion and resistance to therapy. *PLoS One* **2013**, *8*, No. e55289.

DOI: 10.1021/acsmedchemlett.9b00177
ACS Med. Chem. Lett. 2019, 10, 1407−1414

(7) Ugolkov, A. V.; Bondarenko, G. I.; Dubrovskyi, O.; Berbegall, A. P.; Navarro, S.; Noguera, R.; O'Halloran, T. V.; Hendrix, M. J.; Giles, F. J.; Mazar, A. P. 9-ING-41, a small-molecule glycogen synthase kinase-3 inhibitor, is active in neuroblastoma. *Anti-Cancer Drugs* **2018**, *29*, 717−724.
(8) Yoshino, Y.; Ishioka, C. Inhibition of glycogen synthase kinase-3 beta induces apoptosis and mitotic catastrophe by disrupting centrosome regulation in cancer cells. *Sci. Rep.* **2015**, *5*, 13249.
(9) Lovestone, S.; Killick, R.; Di Forti, M.; Murray, R. Schizophrenia as a GSK-3 dysregulation disorder. *Trends Neurosci.* **2007**, *30*, 142−149.
(10) Jope, R. S.; Roh, M.-S. Glycogen Synthase Kinase-3 (GSK3) in Psychiatric Diseases and Therapeutic Interventions. *Curr. Drug Targets* **2006**, *7*, 1421−1434.
(11) Marsell, R.; Sisask, G.; Nilsson, Y.; Sundgren-Andersson, A. K.; Andersson, U.; Larsson, S.; Nilsson, O.; Ljunggren, O.; Jonsson, K. B. GSK-3 inhibition by an orally active small molecule increases bone mass in rats. *Bone* **2012**, *50*, 619−627.
(12) Heider, F.; Ansideri, F.; Tesch, R.; Pantsar, T.; Haun, U.; Döring, E.; Kudolo, M.; Poso, A.; Albrecht, W.; Laufer, S. A.; Koch, P. Pyridinylimidazoles as dual glycogen synthase kinase 3β/p38α mitogen-activated protein kinase inhibitors. *Eur. J. Med. Chem.* **2019**, *175*, 309−329.
(13) Crespo, A.; Rodriguez-Granillo, A.; Lim, V. T. Quantum-Mechanics Methodologies in Drug Discovery: Applications of Docking and Scoring in Lead Optimization. *Curr. Top. Med. Chem.* **2017**, *17*, 2663−2680.
(14) Zhou, T.; Huang, D.; Caflisch, A. Quantum Mechanical Methods for Drug Design. *Curr. Top. Med. Chem.* **2010**, *10*, 33−45.
(15) Spyrakis, F.; Ahmed, M. H.; Bayden, A. S.; Cozzini, P.; Mozzarelli, A.; Kellogg, G. E. The Roles of Water in the Protein Matrix: A Largely Untapped Resource for Drug Discovery. *J. Med. Chem.* **2017**, *60*, 6781−6827.
(16) Krimmer, S. G.; Cramer, J.; Betz, M.; Fridh, V.; Karlsson, R.; Heine, A.; Klebe, G. Rational Design of Thermodynamic and Kinetic Binding Profiles by Optimizing Surface Water Networks Coating Protein-Bound Ligands. *J. Med. Chem.* **2016**, *59*, 10530−10548.
(17) Ganesan, A.; Coote, M. L.; Barakat, K. Molecular dynamics-driven drug discovery: leaping forward with confidence. *Drug Discovery Today* **2017**, *22*, 249−269.
(18) Pantsar, T.; Poso, A. Binding Affinity via Docking: Fact and Fiction. *Molecules* **2018**, *23*, 1899.
(19) Leeson, P. D.; Young, R. J. Molecular Property Design: Does Everyone Get It? *ACS Med. Chem. Lett.* **2015**, *6*, 722−725.
(20) Hopkins, A. L.; Keserü, G. M.; Leeson, P. D.; Rees, D. C.; Reynolds, C. H. The role of ligand efficiency metrics in drug discovery. *Nat. Rev. Drug Discovery* **2014**, *13*, 105−121.
(21) Liang, S. H.; Chen, J. M.; Normandin, M. D.; Chang, J. S.; Chang, G. C.; Taylor, C. K.; Trapa, P.; Plummer, M. S.; Para, K. S.; Conn, E. L.; Lopresti-Morrow, L.; Lanyon, L. F.; Cook, J. M.; Richter, K. E. G.; Nolan, C. E.; Schachter, J. B.; Janat, F.; Che, Y.; Shanmugasundaram, V.; Lefker, B. A.; Enerson, B. E.; Livni, E.; Wang, L.; Guehl, N. J.; Patnaik, D.; Wagner, F. F.; Perlis, R.; Holson, E. B.; Haggarty, S. J.; El Fakhri, G.; Kurumbail, R. G.; Vasdev, N. Discovery of a Highly Selective Glycogen Synthase Kinase-3 Inhibitor (PF-04802367) That Modulates Tau Phosphorylation in the Brain: Translation for PET Neuroimaging. *Angew. Chem., Int. Ed.* **2016**, *55*, 9601−9605.
(22) Ghose, A. K.; Viswanadhan, V. N.; Wendoloski, J. J. Prediction of Hydrophobic (Lipophilic) Properties of Small Organic Molecules Using Fragmental Methods: An Analysis of ALOGP and CLOGP Methods. *J. Phys. Chem. A* **1998**, *102*, 3762−3772.
(23) Goettert, M.; Graeser, R.; Laufer, S. A. Optimization of a nonradioactive immunosorbent assay for p38α mitogen-activated protein kinase activity. *Anal. Biochem.* **2010**, *406*, 233−234.
(24) Coffman, K.; Brodney, M.; Cook, J.; Lanyon, L.; Pandit, J.; Sakya, S.; Schachter, J.; Tseng-Lovering, E.; Wessel, M. 6-amino-4-(pyrimidin-4-yl)pyridones: novel glycogen synthase kinase-3β inhibitors. *Bioorg. Med. Chem. Lett.* **2011**, *21*, 1429−1433.
(25) Sivaprakasam, P.; Han, X.; Civiello, R. L.; Jacutin-Porte, S.; Kish, K.; Pokross, M.; Lewis, H. A.; Ahmed, N.; Szapiel, N.; Newitt, J. A.; Baldwin, E. T.; Xiao, H.; Krause, C. M.; Park, H.; Nophsker, M.; Lippy, J. S.; Burton, C. R.; Langley, D. R.; Macor, J. E.; Dubowchik, G. M. Discovery of new acylaminopyridines as GSK-3 inhibitors by a structure guided in-depth exploration of chemical space around a pyrrolopyridinone core. *Bioorg. Med. Chem. Lett.* **2015**, *25*, 1856−1863.
(26) De Simone, A.; Fiori, J.; Naldi, M.; D'Urzo, A.; Tumiatti, V.; Milelli, A.; Andrisano, V. Application of an ESI-QTOF method for the detailed characterization of GSK-3β inhibitors. *J. Pharm. Biomed. Anal.* **2017**, *144*, 159−166.
(27) Ugolkov, A.; Gaisina, I.; Zhang, J. S.; Billadeau, D. D.; White, K.; Kozikowski, A.; Jain, S.; Cristofanilli, M.; Giles, F.; O'Halloran, T.; Cryns, V. L.; Mazar, A. P. GSK-3 inhibition overcomes chemoresistance in human breast cancer. *Cancer Lett.* **2016**, *380*, 384−392.
(28) Walz, A.; Ugolkov, A.; Chandra, S.; Kozikowski, A.; Carneiro, B. A.; O'Halloran, T. V.; Giles, F. J.; Billadeau, D. D.; Mazar, A. P. Molecular Pathways: Revisiting Glycogen Synthase Kinase-3β as a Target for the Treatment of Cancer. *Clin. Cancer Res.* **2017**, *23*, 1891−1897.
(29) Hann, M. M. Molecular obesity, potency and other addictions in drug discovery. *MedChemComm* **2011**, *2*, 349−355.

DOI: 10.1021/acsmedchemlett.9b00177
ACS Med. Chem. Lett. 2019, 10, 1407−1414

SUPPORTING INFORMATION

Pyridinylimidazoles as GSK3β inhibitors: the impact of tautomerism on compound activity via water networks

Fabian Heider[†#], Tatu Pantsar[‡§#], Mark Kudolo[†], Francesco Ansideri[†], Angela De Simone[‖], Letizia Pruccoli[‖], Taiane Schneider[▽], Marcia Inês Goettert[▽], Andrea Tarozzi[‖], Vincenza Andrisano[‖], Stefan A. Laufer[†], Pierre Koch[†⊥*]

[†]Department of Pharmaceutical and Medicinal Chemistry, Institute of Pharmaceutical Sciences, Eberhard Karls Universität Tübingen, Auf der Morgenstelle 8, 72076 Tübingen, Germany.

[‡]School of Pharmacy, University of Eastern Finland, P.O.BOX 1627, 70211 Kuopio, Finland.

[§] Department of Internal Medicine VIII, University Hospital Tübingen, Otfried-Müller-Straße 14, 72076 Tübingen, Germany.

[‖]Department for Life Quality Studies, Alma Mater Studiorum-University of Bologna, Corso D'Augusto, 237, 47921 Rimini, Italy.

[▽]Cell Culture Laboratory, Postgraduate Program in Biotechnology, University of Vale do Taquari (Univates), Lajeado, RS 95900-00, Brazil

[⊥]Department of Pharmaceutical/Medicinal Chemistry II, Institute of Pharmacy, University of Regensburg, Universitätsstraße 31, 93053 Regensburg, Germany.

Table of Contents:

1. Synthetic procedures

General

All reagents and solvents were obtained from commercial sources (Merck, abcr, ChemPur, Acros, AlfaAesar or Activate Scientific) and used without further purification. Thin layer chromatography (TLC) reaction controls were performed for all reactions using fluorescent silica gel 60 F254 plates (Merck) and visualized under natural light and UV illumination at 254 and 366 nm. All tested compounds were determined to be ≥95% purity by reverse phase high-performance liquid chromatography (HPLC) (254 nm). HPLC were carried out on an Agilent 1100 series HPLC system, equipped with an UV DAD (detection at 218 nm, 254 nm, and 280 nm). The chromatographic separation was performed on a XBridge™ C18 column (150 mm x 4.6 mm, 5 µm) at 30 °C oven temperature. For Method A, the injection volume was 5 µL and the flow 1.5 mL / min using the following gradient:
0.01 M KH_2PO_4, pH 2.3 (solvent A), methanol (solvent B), 45% B to 85% B in 9 min; 85% B for 6 min; stop time 15 min. For Method B, the injection volume was 5 µL and the flow 1.5 mL / min using the following gradient: 0.01 M KH_2PO_4, pH 2.3 (solvent A), methanol (solvent B), 5% B to 95% B in 15 min; 95% B for 3 min; stop time 18 min. Flash column chromatography was performed using an Interchim PuriFlash 430 automated flash chromatography system with Davisil LC60A 20 - 45 µm silica from Grace Davison or PuriFlash SIHP 30 µm columns. Reverse-phase flash column chromatography was performed using the same system with a PuriFlash C18-HP, 15 µM 35g column. Nuclear magnetic resonance (NMR) spectra were measured on a Bruker Avance III HD NMR spectrometer at 300 MHz or a Bruker Bruker Avance III HDX at 400 MHz. The chemical shifts δ are reported in parts per million (ppm) relative to TMS. All spectra were calibrated against the (residual proton) peak of the deuterated solvent used. If a mixture of deuterated solvent was used the spectrum was calibrated against $CDCl_3$ unless otherwise stated. Mass spectra were recorded on an Advion Expression S electrospray ionization mass spectrometer (ESI-MS) with an Advion Plate Express (TLC interface).

General Procedures

General Procedure A (Radziszewski synthesis):

The corresponding diketone (1 eq.), acetaldehyde (2 eq.) and NH_4OAc (10 eq.), were dissolved in MeOH (0.2 M) and heated to reflux for 3 h. After cooling to rt, the solvent was evaporated and the crude product was taken up in a mix of EtOAc and H_2O. The organic phase was collected and the aqueous layer was extracted twice more with EtOAc. The combined organic layers were dried over anhydrous Na_2SO_4 before the solvent was removed under reduced pressure and the compound was purified by flash chromatography.

General Procedure B (Buchwald-Hartwig amidation):

The amide (1.5 eq.), $Pd_2(dba)_3$ (5 mol%), XantPhos (10 mol%), cesium carbonate (3 eq.) and the 2-chloropyridinylimidazole derivative (1 eq.) were dissolved under an atmosphere of argon in DMF (0.3 M). The reaction mixture was then stirred at 100 °C for 16 h. The reaction mixture was allowed to cool to rt and sat. aq. NH_4Cl solution was added. It was extracted with EtOAc (3x) and the combined organic layers were washed with sat. aq. NH_4Cl solution (2x) and brine. After drying over anhydrous Na_2SO_4 the solvent was removed under reduced pressure and the compound was purified by flash chromatography.

General Procedure C

The acetophenone (1 eq.) was dissolved in DMSO (0.6 M) and aq. HBr solution 48% (3 eq.) was added. The solution was stirred in an open flask at 55 °C for 18 h.[1] After cooling to rt, H_2O was added and it was extracted with EtOAc (3x). The combined organic layers were dried over anhydrous Na_2SO_4 and the solvent was removed under reduced pressure. The crude product was immediately dissolved in MeOH (0.2 M). In a second flask, NH_4OAc (5 eq.) was also dissolved in MeOH (5 M) before ethyl glyoxylate (polymer form ~50% in toluene; 3 eq.) was added in one portion. The previously prepared solution of 2,2-dihydroxyethan-1-one derivative in MeCN was then added dropwise over 15 min. After 1.5 h, the solvent was evaporated, H_2O was added and it was extracted with EtOAc (5x). The combined organic layers were dried over anhydrous Na_2SO_4 before the solvent was removed under reduced pressure and the compound was purified by flash chromatography.

General Procedure D (Suzuki coupling Method A)

The bromoimidazole derivative, (aryl)boronic acid (1.3 – 1.6 eq.), cesium fluoride (3 eq.), benzyltriethylammonium chloride (0.06 eq.) and $Pd(dppf)Cl_2$·DCM (0.06 eq.) were dissolved in a degassed 1:1 mixture of toluene/H_2O (4 mL). The mixture was heated to 100 °C under an atmosphere of argon for 18 h. The reaction mixture was allowed to cool to rt and more H_2O was added. It was extracted with EtOAc (3x) and the combined organic layers were dried over anhydrous Na_2SO_4. The solvent was removed under reduced pressure and the compound was purified by flash chromatography.

General Procedure E (SEM deprotection)

The compound was dissolved in a 1:5 mixture of trifluoroacetic acid in DCM and stirred at rt until reaction control showed full conversion (5 – 72 h). Sat. aq. $NaHCO_3$ solution was carefully added until the aqueous layer was adjusted to pH 7. The organic layer was collected and depending on the estimated polarity of the compound it was extracted with either DCM (3x) or EtOAc (3x). The combined organic layers were dried over anhydrous Na_2SO_4 before the solvent was removed under reduced pressure.

General Procedure F (Suzuki coupling Method B)

The bromoimidazole (1 eq.), (aryl)boronic acid (1.3 – 1.6 eq.), potassium carbonate (3 eq.) and $Pd(dppf)Cl_2$·DCM (0.06 eq.) were dissolved in degassed DMF (2.5 mL). The mixture was heated to 80 °C under an atmosphere of argon for 18 h. The reaction mixture was allowed to cool to rt and sat. aq. NH_4Cl solution was added. It was extracted with EtOAc (3x) and the combined organic layers were dried

over anhydrous Na_2SO_4. The solvent was removed under reduced pressure and the compound was purified by flash chromatography.

General Procedure G (HATU coupling)

The carboxylic acid (1 eq.), 1-[bis(dimethylamino)methylene]-1*H*-1,2,3-triazolo[4,5-*b*]pyridinium 3-oxid hexafluorophosphate (1 eq.) and *N*,*N*-diisopropylethylamine (3 eq.) were dissolved in DCM under an atmosphere of argon. The mixture was stirred at rt for 10 min before the amine (0.7 eq.) was added and the solution was stirred for 18 h. H_2O was added to the reaction and the organic layer was collected. It was then extracted with EtOAc (3x) and the combined organic layers were dried over anhydrous Na_2SO_4. The solvent was removed under reduced pressure and the compound was purified by flash chromatography.

Synthesis of 3a-g

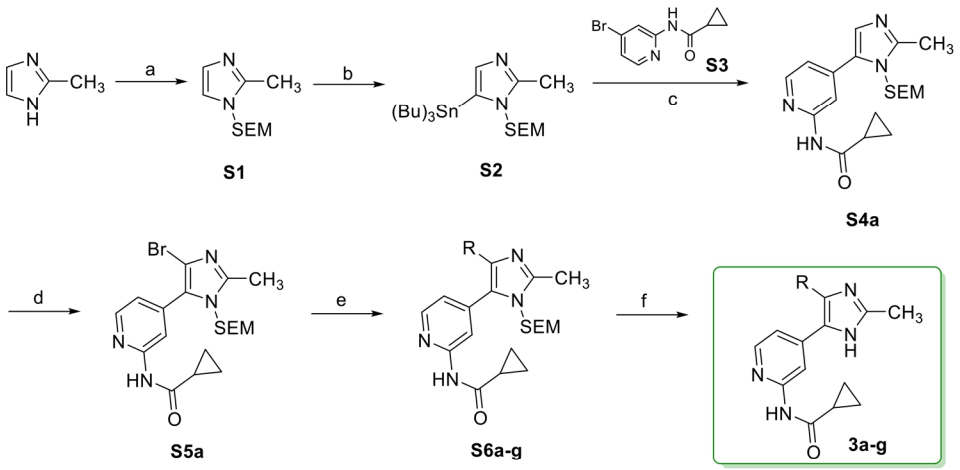

Scheme S1. *Reagents and conditions:* (a) NaH, SEM-Cl, THF, 0 °C then rt, 18 h, 96%; (b) *n*-BuLi, tributyltin chloride, Et_2O, 0 °C then rt, 2 h, 26%; (c) $Pd(PPh_3)_4$, 1,4-dioxane, 105 °C, 77%; (d) NBS, MeCN, -20 °C, 20 min, 77-88%; (e) arylboronic acid, CsF, benzyltriethylammonium chloride, $Pd(dppf)Cl_2 \cdot DCM$, toluene/H_2O, 100 °C, 16 h, 53-89%; (f) trifluoroacetic acid, DCM, rt, 6 h, 25-85%.

2-Methyl-1-((2-(trimethylsilyl)ethoxy)methyl)-1*H*-imidazole (S1)[2]

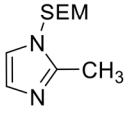

2-Methylimidazole (925 mg, 11.27 mmol) was dissolved in THF (40 mL), cooled to 0 °C and sodium hydride 60% in mineral oil (500 mg, 12.50 mmol) was added portionwise over 5 min. After 30 min of stirring at 0 °C, 2-(trimethylsilyl)ethoxymethyl chloride (2.00 mL, 11.30 mmol) was added dropwise and

the mixture was stirred at rt for 18 h. Purification by flash chromatography (SiO_2, n-hexane/EtOAc 90:10 to 60:40) afforded **3** as a clear oil (2.30 g, 96%). ^{1}H NMR (300 MHz, $CDCl_3$) δ -0.02 (s, 9H), 0.82 - 0.95 (m, 2H), 2.43 (s, 3H), 3.39 - 3.53 (m, 2H), 5.18 (s, 2H), 6.90 (s, 2H).

2-Methyl-5-(tributylstannyl)-1-((2-(trimethylsilyl)ethoxy)methyl)-1*H*-imidazole (S2)[2]

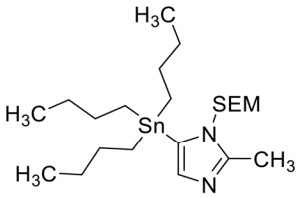

The title compound was synthesized according to the method reported by Markey and Kelly[3] to give **S2** as a clear oil (1.41 g, 25%). ^{1}H NMR (300 MHz, $CDCl_3$) δ 0.00 (s, 9H), 0.86 - 0.93 (m, 11H), 1.03 - 1.11 (m, 5H), 1.22 - 1.40 (m, 9H), 1.48 - 1.55 (m, 4H), 2.47 (s, 3H), 3.36 - 3.47 (m, 2H), 5.14 (s, 2H), 6.90 (s, 1H). TLC-MS (ESI) *m*/*z*: calculated for $C_{22}H_{45}N_2OSiSn$ $[M\text{-}SEM+2H]^+$ 373.2, found 373.0.

***N*-(4-Bromopyridin-2-yl)cyclopropanecarboxamide (S3)[4]**

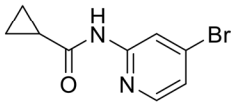

4-Bromopyridine-2-amine (3.00 g, 17.34 mmol) was dissolved in DCM (40 mL) and pyridine (1.82 mL, 22.54 mmol) was added at 0 °C. Cyclopropylcarbonyl chloride (1.73 mL, 19.07 mmol) was added dropwise and the solution was stirred at rt for 6 h. Sat. aq. $NaHCO_3$ solution (15 mL) and H_2O (30 mL) were added and the organic phase was separated and dried over anhydrous Na_2SO_4. The solvent was removed under reduced pressure and dried in vacuo to afford 3.50 g (83.7%) of a white crystalline solid. ^{1}H NMR (300 MHz, DMSO-d_6) δ 0.79 - 0.88 (m, 4 H), 1.89 - 2.12 (m, 1 H), 7.34 (dd, *J* = 5.3, 1.8 Hz, 1 H), 8.22 (dd, *J* = 5.3, 0.4 Hz, 1 H), 8.33 (dd, *J* = 1.7, 0.4 Hz, 1 H), 11.03 (s, 1 H). TLC-MS (ESI) *m*/*z*: calculated for $C_9H_9BrN_2O$ $[M\text{-}H]^-$ 239.0/241.0, found 239.0/241.0. HPLC: t_R = 4.94 min (99.3% purity).

***N*-(4-(2-Methyl-1-((2-(trimethylsilyl)ethoxy)methyl)-1*H*-imidazol-5-yl)pyridin-2-yl)cyclopropanecarboxamide (S4a)[2]**

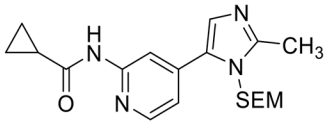

Compound **S2** (462 mg, 0.92 mmol), *N*-(4-bromopyridin-2-yl)cyclopropanecarboxamide (**S3**) (222 mg, 0.92 mmol) and $Pd(PPh_3)_4$ (77 mg, 0.069 mmol) were dissolved in degassed 1,4-dioxane (9 mL) under an atmosphere of argon. The reaction mixture was heated to 105 °C for 18 h before the solution was filtered through a pad of Celite. The pad was washed with DCM (30 mL) and the solvents were removed under reduced pressure. Purification by flash chromatography (SiO_2, DCM/EtOH 95:05) afforded 24 as an off-white solid (265 mg, 77%). ^{1}H NMR (300 MHz, $CDCl_3$) δ -0.04 (s, 9H), 0.84 - 0.92 (m, 4H), 1.06 -

1.15 (m, 2H), 1.55 - 1.67 (m, 1H), 2.53 (s, 3H), 3.45 - 3.55 (m, 2H), 5.28 (s, 2H), 7.16 (dd, *J* = 5.3, 1.6 Hz, 1H), 7.18 (s, 1H), 8.27 (dd, *J* = 5.2, 0.6 Hz, 1H), 8.30 (d, *J* = 0.6 Hz, 1H), 9.17 (s, 1H). ^{13}C NMR (75 MHz, $CDCl_3$) δ -1.5, 8.3, 13.7, 15.7, 17.7, 66.0, 72.7, 112.2, 118.0, 128.6, 131.3, 140.0, 148.0, 148.8, 152.2, 172.5. TLC-MS (ESI) *m*/*z*: calculated for $C_{19}H_{28}N_4O_2Si$ [M-H]$^-$ 371.2, found 371.0. HPLC: t_R = 5.99 min.

_N_-(4-(4-Bromo-2-methyl-1-((2-(trimethylsilyl)ethoxy)methyl)-1H-imidazol-5-yl)pyridin-2-yl)cyclopropanecarboxamide (S5a)

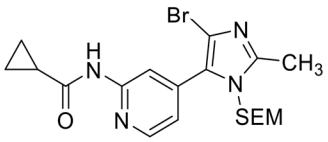

Compound **S4a** (150 mg, 0.40 mmol) was dissolved in MeCN (10 mL) under an atmosphere of argon and the solution was cooled to -20 °C. *N*-Bromosuccinimide (79 mg, 0.44 mmol) was added in one portion and the mixture was stirred at -20 °C for 5 h min before it was quenched with sat. aq. Na_2SO_3 solution. The aqueous phase was extracted with EtOAc (3x) and the combined organic layers were dried over anhydrous Na_2SO_4 and the solvent was removed under reduced pressure. Purification by flash chromatography (SiO_2, DCM:EtOH 97:3) afforded 160 mg (88.2%) of a light yellow solid. ^{1}H NMR (300 MHz, $CDCl_3$) δ -0.06 (s, 9H), 0.80 - 0.93 (m, 4H), 1.07 - 1.14 (m, 2H), 1.58 - 1.68 (m, 1H), 2.49 (s, 3H), 3.32 - 3.43 (m, 2H), 5.20 (s, 2H), 7.21 (dd, *J* = 5.2, 1.6 Hz, 1H), 8.28 (d, *J* = 0.6 Hz, 1H), 8.34 (dd, *J* = 5.2, 0.6 Hz, 1H), 9.31 (s, 1H). ^{13}C NMR (75 MHz, $CDCl_3$) δ -1.6, 8.4, 13.5, 15.7, 17.6, 66.2, 73.2, 114.4, 115.2, 120.0, 127.5, 138.9, 147.5, 147.7, 152.0, 172.5. TLC-MS (ESI) *m*/*z*: calculated for $C_{19}H_{27}BrN_4O_2Si$ [M-H]$^-$ 449.1/451.1, found 449.2/451.1. HPLC: t_R = 8.02 min.

_N_-(4-(4-(2-Hydroxyphenyl)-2-methyl-1-((2-(trimethylsilyl)ethoxy)methyl)-1*H*-imidazol-5-yl)pyridin-2-yl)cyclopropanecarboxamide (S6a)

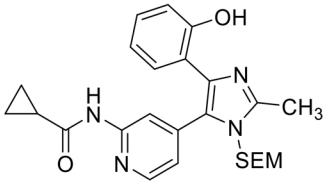

The title compound was synthesized according to **General Procedure D** starting from compound **S5a** (140 mg, 0.31 mmol), 2-hydroxyphenylboronic acid (68 mg, 0.50 mmol), cesium fluoride (141 mg, 0.93 mmol), benzyltriethylammonium chloride (4.2 mg, 0.019 mmol) and Pd(dppf)Cl_2·DCM (15 mg, 0.019 mmol). Purification by flash chromatography (SiO_2, DCM:EtOH 97:3) afforded 115 mg (79.8%) of a solid. ^{1}H NMR (300 MHz, $CDCl_3$) δ -0.04 (s, 9H), 0.74 - 0.86 (m, 2H), 0.88 - 0.96 (m, 2H), 1.06 - 1.15 (m, 2H), 1.57 - 1.68 (m, 1H), 2.55 (s, 3H), 3.34 (dd, *J* = 9.0, 7.7 Hz, 2H), 5.12 (s, 2H), 6.49 - 6.56 (m, 1H), 6.90 (dd, *J* = 7.9, 1.6 Hz, 1H), 6.93 - 6.99 (m, 1H), 7.04 - 7.11 (m, 2H), 8.30 (s, 1H), 8.35 (d, *J* = 5.1 Hz, 1H), 9.03 (br. s., 1H). ^{13}C NMR (75 MHz, $CDCl_3$) δ -1.5, 8.5, 13.2, 15.7, 17.7, 66.2, 72.6, 115.9, 116.6, 117.5,

118.4, 121.9, 124.9, 126.2, 128.4, 135.8, 141.5, 144.5, 148.3, 152.4, 156.8, 172.4. TLC-MS (ESI) *m*/*z*: calculated for $C_{25}H_{32}N_4O_3Si$ $[M+H]^+$ 465.2, found 465.2. HPLC: t_R = 6.95 min.

_N_-(4-(4-(3-Hydroxyphenyl)-2-methyl-1-((2-(trimethylsilyl)ethoxy)methyl)-1_H_-imidazol-5-yl)pyridin-2-yl)cyclopropanecarboxamide (S6b)

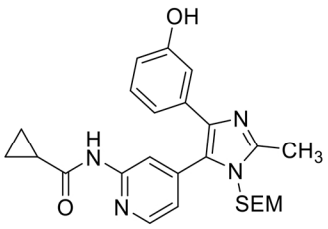

The title compound was synthesized according to **General Procedure D** starting from compound **S5a** (120 mg, 0.27 mmol), 3-hydroxyphenylboronic acid (75 mg, 0.54 mmol), cesium fluoride (171 mg, 1.12 mmol), benzyltriethylammonium chloride (5.1 mg, 0.023 mmol) and Pd(dppf)Cl_2·DCM (18.4 mg, 0.023 mmol). Purification by flash chromatography (SiO_2, DCM:EtOH 97:3) afforded 110 mg (89.1%) of a solid. ^{1}H NMR (300 MHz, $CDCl_3$) δ -0.05 (s, 9H), 0.77 - 0.89 (m, 4H), 1.02 - 1.09 (m, 2H), 1.58 - 1.66 (m, 1H), 2.48 (s, 3H), 3.22 - 3.36 (m, 2H), 5.09 (s, 2H), 6.70 (d, *J* = 8.0 Hz, 1H), 6.90 - 6.99 (m, 2H), 7.01 - 7.11 (m, 2H), 8.12 (d, *J* = 5.1 Hz, 1H), 8.30 (s, 1H), 9.24 (s, 1H). ^{13}C NMR (75 MHz, $CDCl_3$) δ -1.5, 8.5, 13.6, 15.5, 17.7, 66.1, 72.5, 114.5, 114.9, 115.6, 119.0, 121.6, 125.8, 129.5, 134.2, 137.5, 141.1, 147.0, 147.8, 151.9, 156.9, 173.0. TLC-MS (ESI) *m*/*z*: calculated for $C_{25}H_{32}N_4O_3Si$ $[M+H]^+$ 465.2, found 465.5. HPLC: t_R = 6.94 min.

_N_-(4-(4-(4-Hydroxyphenyl)-2-methyl-1-((2-(trimethylsilyl)ethoxy)methyl)-1_H_-imidazol-5-yl)pyridin-2-yl)cyclopropanecarboxamide (S6c)

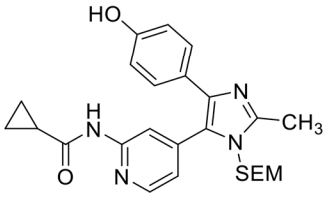

The title compound was synthesized according to **General Procedure D** (heated for 36 h) starting from compound **S5a** (160 mg, 0.35 mmol), 4-hydroxyphenylboronic acid pinacol ester (125 mg, 0.57 mmol), cesium fluoride (162 mg, 1.06 mmol), benzyltriethylammonium chloride (4.8 mg, 0.021 mmol) and Pd(dppf)Cl_2·DCM (17.0 mg, 0.021 mmol). Purification by flash chromatography (SiO_2, DCM:EtOH 97:3 to 95:5) afforded 110 mg (67.6%) of a solid. ^{1}H NMR (300 MHz, $CDCl_3$) δ -0.06 (s, 9H), 0.81 - 0.93 (m, 4H), 1.08 (br. s., 2H), 1.51 - 1.70 (m, 1H), 2.54 (s, 3H), 3.30 - 3.45 (m, 2H), 5.18 (s, 2H), 6.60 (d, *J* = 5.5 Hz, 2H), 6.95 (d, *J* = 4.1 Hz, 1H), 7.14 (d, *J* = 6.6 Hz, 2H), 8.23 (br. s., 2H), 9.29 (br. s., 1H). ^{13}C NMR (75 MHz, $CDCl_3$) δ -1.5, 8.4, 13.0, 15.7, 17.7, 66.1, 72.7, 115.4, 115.6, 121.6, 123.9, 124.8, 129.1, 138.2, 141.2, 146.9, 147.8, 152.1, 156.7, 172.6. TLC-MS (ESI) *m*/*z*: calculated for $C_{25}H_{32}N_4O_3Si$ $[M+H]^+$ 465.2, found 465.5. HPLC: t_R = 6.50 min.

_N_-(4-(2-Methyl-4-(thiophen-2-yl)-1-((2-(trimethylsilyl)ethoxy)methyl)-1_H_-imidazol-5-yl)pyridin-2-yl)cyclopropanecarboxamide (S6d)

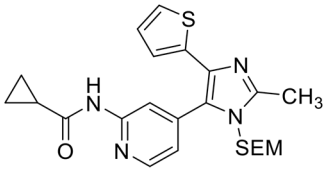

The title compound was synthesized according to **General Procedure D** starting from compound **S5a** (120 mg, 0.27 mmol), 2-thienylboronic acid (54 mg, 0.43 mmol), cesium fluoride (121 mg, 0.80 mmol), benzyltriethylammonium chloride (3.6 mg, 0.016 mmol) and Pd(dppf)Cl_2·DCM (13 mg, 0.016 mmol). Purification by flash chromatography (SiO_2, DCM:EtOH 97:3) afforded 108 mg (89.3%) of a solid. ^{1}H NMR (300 MHz, $CDCl_3$) δ -0.06 (s, 9H), 0.79 - 0.94 (m, 4H), 1.06 - 1.14 (m, 2H), 1.61 (s, 1H), 2.55 (s, 3H), 3.28 - 3.42 (m, 2H), 5.12 (s, 2H), 6.88 (dd, *J* = 5.0, 3.7 Hz, 1H), 6.97 (dd, *J* = 3.6, 1.0 Hz, 1H), 7.13 (dt, *J* = 5.0, 1.7 Hz, 2H), 8.28 (s, 1H), 8.34 (d, *J* = 5.0 Hz, 1H), 8.93 (s, 1H). ^{13}C NMR (75 MHz, $CDCl_3$) δ -1.5, 8.4, 13.4, 15.7, 17.7, 66.0, 72.8, 115.7, 121.6, 123.3, 124.0, 125.0, 127.2, 133.0, 137.0, 140.8, 146.8, 148.0, 152.2, 172.3. TLC-MS (ESI) *m*/*z*: calculated for $C_{23}H_{30}N_4O_2SSi$ $[M+H]^+$ 455.2, found 455.2. HPLC: t_R = 8.13 min.

_N_-(4-(4-(Furan-2-yl)-2-methyl-1-((2-(trimethylsilyl)ethoxy)methyl)-1_H_-imidazol-5-yl)pyridin-2-yl)cyclopropanecarboxamide (S6e)

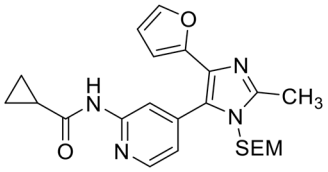

The title compound was synthesized according to **General Procedure D** starting from compound **S5a** (150 mg, 0.33 mmol), 2-furanylboronic acid (59 mg, 0.53 mmol), cesium fluoride (151 mg, 1.00 mmol), benzyltriethylammonium chloride (4.5 mg, 0.020 mmol) and Pd(dppf)Cl_2·DCM (13 mg, 0.016 mmol). Purification by flash chromatography (SiO_2, DCM:EtOH 97:3) afforded 118 mg (81.0%) of a solid. ^{1}H NMR (300 MHz, $CDCl_3$) δ -0.04 (s, 9H), 0.81 - 0.94 (m, 4H), 1.04 - 1.12 (m, 2H), 1.55 - 1.66 (m, 1H), 2.55 (s, 3H), 3.33 (dd, *J* = 8.9, 7.7 Hz, 2H), 5.16 (s, 2H), 6.34 (dd, *J* = 3.3, 1.8 Hz, 1H), 6.44 (dd, *J* = 3.3, 0.6 Hz, 1H), 7.14 (dd, *J* = 5.1, 1.3 Hz, 1H), 7.28 - 7.30 (m, 1H), 8.26 (s, 1H), 8.33 (d, *J* = 5.1 Hz, 1H), 8.75 (br. s., 1H). ^{13}C NMR (75 MHz, $CDCl_3$) δ -1.6, 8.3, 13.3, 15.4, 17.6, 66.0, 72.6, 106.1, 110.9, 115.6, 121.3, 125.5, 130.3, 140.5, 141.3, 147.3, 147.4, 148.8, 152.0, 172.6. TLC-MS (ESI) *m*/*z*: calculated for $C_{23}H_{30}N_4O_3Si$ $[M+Na]^+$ 461.2, found 461.5. HPLC: t_R = 7.75 min.

***N*-(4-(4-(2-Methoxyphenyl)-2-methyl-1-((2-(trimethylsilyl)ethoxy)methyl)-1*H*-imidazol-5-yl)pyridin-2-yl)cyclopropanecarboxamide (S6f)**

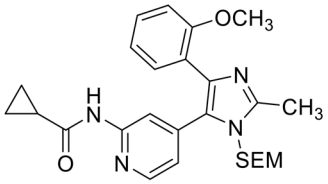

The title compound was synthesized according to **General Procedure D** starting from compound **S5a** (200 mg, 0.44 mmol), 2-methoxyphenylboronic acid (101 mg, 0.67 mmol), cesium fluoride (202 mg, 1.33 mmol), benzyltriethylammonium chloride (6 mg, 0.027 mmol) and $Pd(dppf)Cl_2$·DCM (22 mg, 0.027 mmol). Purification by flash chromatography (SiO_2, DCM:EtOH 97:3) afforded 113 mg (53.3%) of the title compound. ^{1}H NMR (300 MHz, $CDCl_3$) δ 0.00 (s, 9H), 0.82 - 0.99 (m, 4H), 1.06 - 1.15 (m, 2H), 1.60 - 1.72 (m, 1H), 2.61 (s, 3H), 3.43 - 3.52 (m, 2H), 3.47 (s, 3H), 5.31 (s, 2H), 6.78 - 6.86 (m, 2H), 6.96 (td, *J* = 7.5, 0.9 Hz, 1H), 7.23 - 7.31 (m, 1H), 7.46 (dd, *J* = 7.5, 1.7 Hz, 1H), 8.15 (d, *J* = 5.1 Hz, 1H), 8.27 (s, 1H), 9.64 (s, 1H). ^{13}C NMR (75 MHz, $CDCl_3$) δ -1.6, 8.1, 13.4, 15.3, 17.6, 54.5, 65.8, 72.8, 110.7, 113.8, 119.9, 120.4, 123.2, 127.6, 128.8, 131.4, 135.9, 141.8, 146.9, 147.0, 151.9, 156.4, 172.3. TLC-MS (ESI) *m*/*z*: calculated for $C_{26}H_{34}N_4O_3Si$ $[M+H]^+$ 479.2, found 479.3. HPLC: t_R = 7.03 min.

***N*-(4-(2-Methyl-4-(pyrimidin-5-yl)-1-((2-(trimethylsilyl)ethoxy)methyl)-1*H*-imidazol-5-yl)pyridin-2-yl)cyclopropanecarboxamide (S6g)**

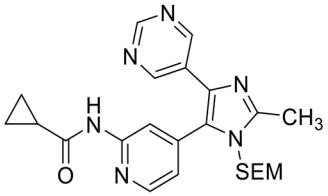

Compound **S5a** (90 mg, 0.20 mmol), pyrimidine-5-boronic acid (37 mg, 0.30 mmol), K_2CO_3 (83 mg, 0.60 mmol) and $Pd(PPh_3)_4$ (23 mg, 0.020 mmol) were dissolved in a degassed 3:1 mixture of DME/H_2O (4 mL) under an atmosphere of argon. The mixture was heated to 105 °C under an atmosphere of argon for 18 h. The reaction mixture was allowed to cool to rt and more H_2O was added. It was extracted with EtOAc (3x) and the combined organic layers were dried over anhydrous Na_2SO_4. The solvent was removed under reduced pressure and the compound was purified by flash chromatography (SiO_2, DCM:EtOH 97:3 to 95:5) to yield 60 mg (66.7%) of the title compound. ^{1}H NMR (300 MHz, $CDCl_3$) δ -0.04 (s, 9H), 0.81 - 0.88 (m, 2H), 0.89 - 0.95 (m, 2H), 1.03 - 1.12 (m, 2H), 1.54 - 1.66 (m, 1H), 2.58 (s, 3H), 3.32 - 3.45 (m, 2H), 5.14 (s, 2H), 6.97 (dd, *J* = 5.1, 1.3 Hz, 1H), 8.28 (s, 1H), 8.33 (d, *J* = 5.0 Hz, 1H), 8.72 (s, 1H), 8.81 (s, 2H), 9.03 (s, 1H). ^{13}C NMR (75 MHz, $CDCl_3$) δ -1.6, 8.4, 13.3, 15.5, 17.6, 66.2, 72.7, 115.2, 120.5, 128.0, 128.0, 131.6, 139.9, 147.8, 148.5, 152.7, 154.6, 156.4, 172.6. TLC-MS (ESI) *m*/*z*: calculated for $C_{23}H_{30}N_6O_2Si$ $[M+Na]^+$ 473.2, found 473.5. HPLC: t_R = 7.69 min.

***N*-(4-(4-(2-Hydroxyphenyl)-2-methyl-1*H*-imidazol-5-yl)pyridin-2-yl)cyclopropanecarboxamide (3a)**

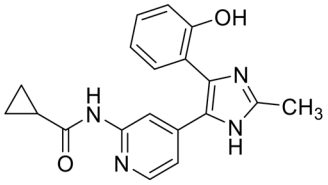

The compound was synthesized according to **General Procedure E** starting from compound **S6a** (115 mg, 0.25 mmol). Purification by flash chromatography (SiO_2, DCM:EtOH 95:5) afforded 70 mg (84.6%) of an off-white solid. ^{1}H NMR (300 MHz, $CDCl_3$) δ 0.90 - 0.99 (m, 2H), 1.05 - 1.13 (m, 2H), 1.56 - 1.67 (m, 1H), 2.47 (s, 3H), 6.70 (td, *J* = 7.5, 1.2 Hz, 1H), 7.01 (dd, *J* = 8.2, 1.1 Hz, 1H), 7.13 - 7.20 (m, 1H), 7.27 - 7.30 (m, 1H), 7.37 (dd, *J* = 7.8, 1.6 Hz, 1H), 8.18 (s, 1H), 8.18 - 8.20 (m, 1H), 8.57 (br. s., 1H). ^{13}C NMR (75 MHz, $CDCl_3$/MeOD [2:1 v/v]) δ 7.3, 12.3, 14.2, 111.4, 115.7, 117.1, 117.5, 118.8, 128.9, 129.1, 142.7, 144.6, 146.7, 151.2, 154.5, 173.2. TLC-MS (ESI) *m*/*z*: calculated for $C_{19}H_{18}N_4O_2$ $[M+H]^+$ 335.2, found 335.2. HPLC: t_R = 2.14 min (99.7% purity).

***N*-(4-(4-(3-Hydroxyphenyl)-2-methyl-1*H*-imidazol-5-yl)pyridin-2-yl)cyclopropanecarboxamide (3b)**

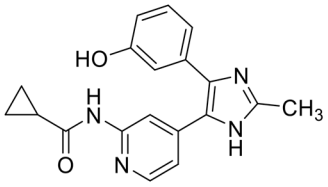

The title compound was synthesized according to **General Procedure E** starting from compound **S6b** (110 mg, 0.24 mmol). Purification by flash chromatography (SiO_2, DCM:EtOH 95:5 to 90:10) afforded 33 mg (41.7%) of a solid. ^{1}H NMR (400 MHz, DMSO-d_6) δ 0.75 - 0.82 (m, 4H), 1.95 - 2.03 (m, 1H), 2.33 (s, 3H), 6.71 - 6.90 (m, 3H), 6.98 (dd, *J* = 5.2, 1.2 Hz, 1H), 7.17 - 7.26 (m, 1H), 8.07 (d, *J* = 4.2 Hz, 1H), 8.40 (s, 1H), 9.56 (s, 1H), 10.61 (s, 1H), 12.19 (br. s., 1H). ^{13}C NMR (101 MHz, DMSO-d_6) δ 7.5, 13.7, 14.2, 110.9, 114.9, 115.0, 116.4, 118.9, 128.9, 129.8, 132.1, 132.8, 144.4, 144.7, 147.2, 152.5, 157.5, 172.2. TLC-MS (ESI) *m*/*z*: calculated for $C_{19}H_{18}N_4O_2$ $[M+H]^+$ 335.2, found 335.3. HPLC: t_R = 1.88 min (99.4% purity).

***N*-(4-(4-(4-Hydroxyphenyl)-2-methyl-1*H*-imidazol-5-yl)pyridin-2-yl)cyclopropanecarboxamide (3c)**

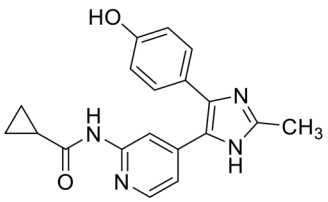

The compound was synthesized according to **General Procedure E** starting from compound **S6c** (110 mg, 0.24 mmol). Purification by flash chromatography (SiO_2, DCM:EtOH 95:5) afforded 41 mg (51.8%) of a green-yellowish solid. ^{1}H NMR (300 MHz, DMSO-d_6) δ 0.66 - 0.88 (m, 4H), 1.93 - 2.04 (m, 1H), 2.32 (s, 3H), 6.80 (d, *J* = 8.5 Hz, 2H), 6.96 (dd, *J* = 5.3, 1.5 Hz, 1H), 7.24 (d, *J* = 8.6 Hz, 2H), 8.06 (d, *J* = 5.3 Hz, 1H), 8.36 (s, 1H), 9.64 (s, 1H), 10.60 (s, 1H), 12.09 (br. s., 1H). ^{13}C NMR (75 MHz, DMSO-d_6) δ 7.5, 13.7, 14.2, 110.5, 115.5, 116.1, 129.6, 144.2, 147.3, 152.5, 157.2, 172.3. TLC-MS (ESI) *m*/*z*: calculated for $C_{19}H_{18}N_4O_2$ $[M+H]^+$ 335.2, found 335.5. HPLC: t_R = 1.80 min (99.7% purity).

***N*-(4-(2-Methyl-4-(thiophen-2-yl)-1*H*-imidazol-5-yl)pyridin-2-yl)cyclopropanecarboxamide (3d)**

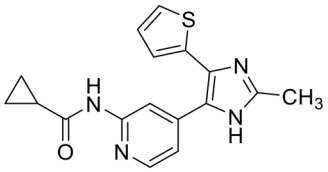

The compound was synthesized according to **General Procedure E** starting from compound **S6d** (98 mg, 0.22 mmol). Purification by flash chromatography (SiO_2, DCM:EtOH 95:5) afforded 39 mg (55.9%) of a beige solid. ^{1}H NMR (300 MHz, DMSO-d_6) δ 0.71 - 0.85 (m, 4H), 2.01 (quin, *J* = 6.1 Hz, 1H), 2.33 (s, 3H), 7.02 - 7.09 (m, 1H), 7.12 (dd, *J* = 5.2, 1.2 Hz, 1H), 7.20 (d, *J* = 2.7 Hz, 1H), 7.51 (d, *J* = 4.9 Hz, 1H), 8.21 (d, *J* = 5.2 Hz, 1H), 8.35 (s, 1H), 10.74 (s, 1H), 12.37 (br. s., 1H). ^{13}C NMR (75 MHz, DMSO-d_6) δ 7.6, 13.6, 14.2, 111.0, 116.8, 125.4, 126.0, 127.6, 145.4, 147.8, 152.6, 172.5. TLC-MS (ESI) *m*/*z*: calculated for $C_{17}H_{16}N_4OS$ $[M+H]^+$ 325.1, found 325.3. HPLC: t_R = 2.33 min (99.8% purity).

***N*-(4-(4-(Furan-2-yl)-2-methyl-1*H*-imidazol-5-yl)pyridin-2-yl)cyclopropanecarboxamide (3e)**

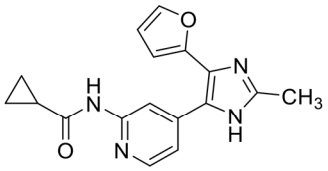

The compound was synthesized according to **General Procedure E** starting from compound **S6e** (115 mg, 0.26 mmol). Purification by flash chromatography (SiO_2, DCM:EtOH 95:5) afforded 24 mg (24.7%) of a light yellow solid. ^{1}H NMR (300 MHz, $CDCl_3$) δ 0.84 - 0.93 (m, 2H), 1.00 - 1.13 (m, 2H), 1.58 - 1.68 (m, 1H), 2.40 (s, 3H), 6.42 (dd, *J* = 3.4, 1.8 Hz, 1H), 6.71 (d, *J* = 3.3 Hz, 1H), 7.34 - 7.43 (m, 2H), 8.20 (d, *J* = 5.4 Hz, 1H), 8.41 (s, 1H), 9.04 (br. s., 1H). ^{13}C NMR (75 MHz, $CDCl_3$/MeOD [2:1 v/v]) δ 8.0, 12.8, 14.9, 107.7, 111.1, 111.6, 117.8, 141.6, 146.2, 147.0, 151.2, 173.5. TLC-MS (ESI) *m*/*z*: calculated for $C_{17}H_{16}N_4O_2$ $[M+H]^+$ 309.1, found 309.2. HPLC: t_R = 2.20 min (99.2% purity).

***N*-(4-(4-(2-Methoxyphenyl)-2-methyl-1*H*-imidazol-5-yl)pyridin-2-yl)cyclopropanecarboxamide (3f)**

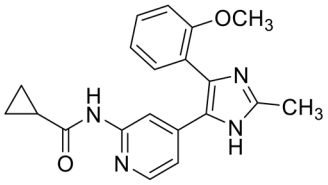

The compound was synthesized according to **General Procedure E** starting from compound **S6f** (110 mg, 0.23 mmol). Purification by flash chromatography (SiO_2, DCM:EtOH 95:5 to 90:10) afforded 49 mg (61.2%) of a beige solid. ^{1}H NMR (400 MHz, DMSO-d_6) δ 0.71 - 0.84 (m, 4H), 1.93 - 2.02 (m, 1H), 2.33 (s, 3H), 3.64 (s, 3H), 6.79 (dd, *J* = 5.3, 1.4 Hz, 1H), 7.00 (td, *J* = 7.4, 0.7 Hz, 1H), 7.11 (d, *J* = 8.2 Hz, 1H), 7.25 (dd, *J* = 7.5, 1.6 Hz, 1H), 7.37 - 7.45 (m, 1H), 7.99 (d, *J* = 5.4 Hz, 1H), 8.33 (s, 1H), 10.54 (s, 1H), 12.10 (br. s., 1H). ^{13}C NMR (101 MHz, DMSO-d_6) δ 7.5, 13.7, 14.2, 55.2, 109.9, 111.7, 115.3, 120.5, 130.1, 131.2, 144.2, 147.0, 152.3, 156.8, 172.1. TLC-MS (ESI) *m*/*z*: calculated for $C_{20}H_{20}N_4O_4$ $[M+H]^+$ 349.2, found 349.3. HPLC: t_R = 2.57 min (100.0% purity).

***N*-(4-(2-Methyl-4-(pyrimidin-5-yl)-1*H*-imidazol-5-yl)pyridin-2-yl)cyclopropanecarboxamide (3g)**

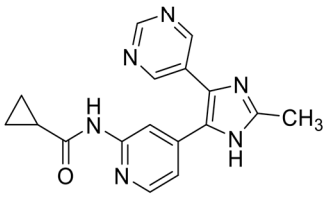

The compound was synthesized according to **General Procedure E** starting from compound **S6g** (60 mg, 0.13 mmol). Purification by flash chromatography (SiO_2, DCM:EtOH 98:2 to 90:10) afforded 26 mg (61.0%) of a yellow solid. ^{1}H NMR (400 MHz, DMSO-d_6) δ 0.71 - 0.84 (m, 4H), 1.90 - 2.07 (m, 1H), 2.39 (s, 3H), 7.05 (dd, *J* = 5.2, 1.6 Hz, 1H), 8.16 - 8.29 (m, 2H), 8.83 (s, 2H), 9.10 (s, 1H), 10.79 (s, 1H), 12.40 (br. s., 1H). ^{13}C NMR (101 MHz, DMSO-d_6) δ 7.7, 13.6, 14.2, 110.6, 116.6, 146.7, 148.4, 152.7, 155.2, 156.9, 172.6. TLC-MS (ESI) *m*/*z*: calculated for $C_{17}H_{16}N_6O$ $[M+H]^+$ 321.1, found 321.3. HPLC: t_R = 1.37 min (96.9% purity).

Synthesis of 3h and 3i

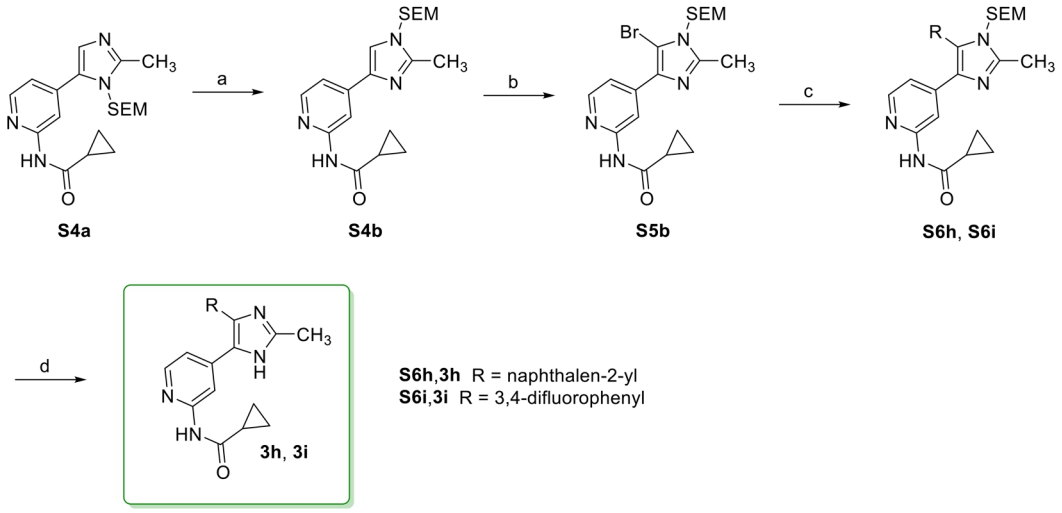

Scheme S2. *Reagents and conditions:* (a) SEM-Cl (5 mol%), MeCN, 85 °C, 18 h, 88%; (b) NBS, MeCN, -20 °C, 20 min, 77-88%; (c) arylboronic acid, CsF, benzyltriethylammonium chloride, Pd(dppf)Cl_2·DCM, toluene/H_2O, 100 °C, 16 h, 53-89%; (d) trifluoroacetic acid, DCM, rt, 6 h, 25-85%.

_N_-(4-(2-Methyl-1-((2-(trimethylsilyl)ethoxy)methyl)-1_H_-imidazol-4-yl)pyridin-2-yl)cyclopropanecarboxamide (S4b)

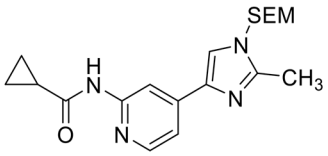

Compound **S4a** (349 mg, 0.94 mmol) was dissolved in MeCN (10 mL) and catalytic amounts of 2-(trimethylsilyl)ethoxymethyl chloride (8.31 µL, 0.047 mmol) were added. The mixture was stirred at 80 °C for 18 h to perform a "SEM switch" according to Sames an coworkers.[5] Purification by flash chromatography (SiO_2, DCM:EtOH 95:05) afforded 307 mg (88.0%) of the title compound. ^{1}H NMR (300 MHz, $CDCl_3$) δ -0.06 (s, 9H), 0.78 - 0.89 (m, 4H), 0.99 - 1.12 (m, 2H), 1.68 (dq, *J* = 8.1, 3.9 Hz, 1H), 2.44 (s, 3H), 3.39 - 3.52 (m, 2H), 5.16 (s, 2H), 7.45 (s, 1H), 7.53 (dd, *J* = 5.4, 1.5 Hz, 1H), 8.18 (d, *J* = 5.4 Hz, 1H), 8.45 (s, 1H), 10.20 (br. s., 1H). ^{13}C NMR (75 MHz, $CDCl_3$) δ -1.6, 8.3, 12.8, 15.4, 17.6, 66.4, 75.4, 109.2, 115.2, 119.0, 136.9, 144.4, 146.4, 146.5, 151.8, 173.2. TLC-MS (ESI) *m*/*z*: calculated for $C_{19}H_{28}N_4O_2Si$ $[M-H]^-$ 371.2, found 371.0. HPLC: t_R = 7.11 min.

***N*-(4-(5-Bromo-2-methyl-1-((2-(trimethylsilyl)ethoxy)methyl)-1*H*-imidazol-4-yl)pyridin-2-yl)cyclopropanecarboxamide (S5b)**

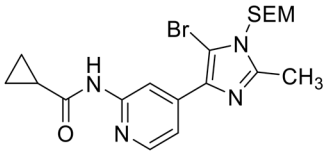

Compound **S4b** (670 mg, 1.80 mmol) was dissolved in MeCN (15 mL) under an atmosphere of argon and the solution was cooled to -20 °C. *N*-Bromosuccinimide (336 mg, 1.88 mmol) was added in one portion and the mixture was stirred at -20 °C for 20 min before it was quenched with sat. aq. Na_2SO_3 solution. The aqueous phase was extracted with EtOAc (3x) and the combined organic layers were dried over anhydrous Na_2SO_4 and the solvent was removed under reduced pressure. Purification by flash chromatography (SiO_2, DCM:EtOAc 80:20 to 10:90) afforded 622 mg (76.6%) of a pale yellow solid. ^{1}H NMR (300 MHz, $CDCl_3$) δ -0.01 (s, 9H), 0.82 - 0.96 (m, 4H), 1.09 - 1.17 (m, 2H), 1.58 - 1.69 (m, 1H), 2.52 (s, 3H), 3.55 - 3.63 (m, 2H), 5.32 (s, 2H), 7.66 (dd, *J* = 5.4, 1.7 Hz, 1H), 8.27 (dd, *J* = 5.4, 0.7 Hz, 1H), 8.95 (s, 1H), 9.28 (br. s, 1H). ^{13}C NMR (75 MHz, $CDCl_3$) δ -1.6, 8.1, 13.8, 15.4, 17.6, 66.3, 73.2, 102.2, 110.6, 116.5, 134.0, 143.0, 146.7, 147.2, 152.0, 172.8. TLC-MS (ESI) *m*/*z*: calculated for $C_{19}H_{27}BrN_4O_2Si$ $[M-H]^-$ 449.1/451.1, found 449.0/450.9. HPLC: t_R = 9.13 min.

***N*-(4-(2-Methyl-5-(naphthalen-2-yl)-1-((2-(trimethylsilyl)ethoxy)methyl)-1*H*-imidazol-4-yl)pyridin-2-yl)cyclopropanecarboxamide (S6h)**

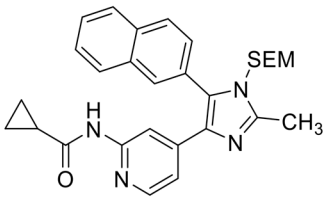

The title compound was synthesized according to **General Procedure D** starting from compound **S5b** (85 mg, 0.19 mmol), 2-napthylboronic acid (85 mg, 0.30 mmol), cesium fluoride (86 mg, 0.57 mmol), benzyltriethylammonium chloride (2.6 mg, 0.011 mmol) and $Pd(dppf)Cl_2$·DCM (9.2 mg, 0.011 mmol). Purification by flash chromatography (SiO_2, DCM:EtOH 97:3 to 95:5) afforded 79 mg (86.6%) of a solid. ^{1}H NMR (300 MHz, $CDCl_3$) δ 0.00 (s, 9H), 0.79 (dd, *J* = 7.7, 3.3 Hz, 2H), 0.83 - 0.92 (m, 2H), 0.98 - 1.06 (m, 2H), 1.51 - 1.62 (m, 1H), 2.65 (s, 3H), 3.35 - 3.45 (m, 2H), 5.14 (s, 2H), 6.94 (dd, *J* = 5.4, 1.5 Hz, 1H), 7.49 (dd, *J* = 8.4, 1.7 Hz, 1H), 7.58 - 7.68 (m, 2H), 7.88 - 8.05 (m, 5H), 8.57 (s, 1H), 9.50 (s, 1H). ^{13}C NMR (75 MHz, $CDCl_3$) δ -1.6, 7.9, 13.4, 15.3, 17.7, 65.9, 72.4, 111.8, 116.7, 126.5, 126.9, 127.2, 127.7, 128.1, 128.2, 128.8, 130.6, 131.2, 133.2, 133.2, 134.3, 144.6, 146.1, 146.8, 152.1, 172.0. TLC-MS (ESI) *m*/*z*: calculated for $C_{29}H_{34}N_4O_2Si$ $[M+Na]^+$ 521.2, found 521.3. HPLC: t_R = 10.34 min.

***N*-(4-(5-(3,4-Difluorophenyl)-2-methyl-1-((2-(trimethylsilyl)ethoxy)methyl)-1*H*-imidazol-4-yl)pyridin-2-yl)cyclopropanecarboxamide (S6i)**

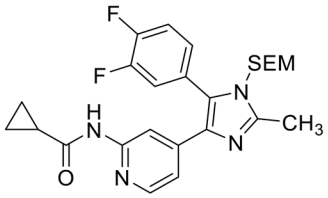

The title compound was synthesized according to **General Procedure D** starting from compound **S5b** (200 mg, 0.44 mmol), 3,4-difluorophenylboronic acid (92 mg, 0.58 mmol), cesium fluoride (202 mg, 1.33 mmol), benzyltriethylammonium chloride (6.0 mg, 0.027 mmol) and Pd(dppf)Cl_2·DCM (21.7 mg, 0.027 mmol). Purification by flash chromatography (SiO_2, *n*-hexane:EtOAc 80:20 to 20:80) afforded 172 mg (80.1%) of a solid. ^{1}H NMR (300 MHz, $CDCl_3$) δ 0.00 (s, 9H), 0.79 (dd, *J* = 7.3, 2.9 Hz, 2H), 0.84 - 0.93 (m, 2H), 0.97 - 1.11 (m, 2H), 1.56 (d, *J* = 3.9 Hz, 1H), 2.55 (s, 3H), 3.42 (t, *J* = 8.3 Hz, 2H), 5.03 (s, 2H), 7.08 (d, *J* = 5.0 Hz, 1H), 7.17 - 7.75 (m, 3H), 8.11 (d, *J* = 5.1 Hz, 1H), 8.30 (s, 1H), 9.71 (br. s., 1H). ^{13}C NMR (75 MHz, $CDCl_3$) δ -1.6, 8.1, 13.2, 15.4, 17.7, 66.1, 72.4, 111.6, 116.7 (d, $^2J_{CF}$ = 17.1 Hz), 118.1 (d, $^2J_{CF}$ = 17.7 Hz), 120.1, 126.4 (dd, $^3J_{CF}$ = 6.1, 4.4 Hz), 127.5 (dd, $^3J_{CF}$ = 6.4, 3.6 Hz), 129.2, 134.5, 144.1, 146.3, 146.7, 150.4, 150.9 (dd, $^1J_{CF}$ = 253.2, 15.5 Hz, 151.9 (dd, $^1J_{CF}$ = 256.0, 17.1 Hz), 172.2. TLC-MS (ESI) *m*/*z*: calculated for $C_{25}H_{30}F_2N_4O_2Si$ $[M+H]^+$ 485.2, found 485.3. HPLC: t_R = 10.05 min (100.0% purity).

***N*-(4-(2-Methyl-4-(naphthalen-2-yl)-1*H*-imidazol-5-yl)pyridin-2-yl)cyclopropanecarboxamide (3h)**

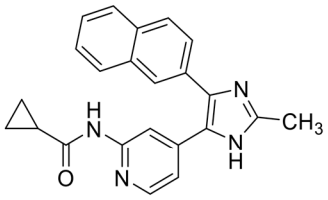

The compound was synthesized according to **General Procedure E** starting from compound **S6h** (138 mg, 0.28 mmol). Purification by flash chromatography (SiO_2, DCM:EtOH 95:5) afforded 86 mg (84.4%) of a yellowish solid. ^{1}H NMR (300 MHz, DMSO-d_6) δ 0.69 - 0.83 (m, 4H), 1.93 - 2.04 (m, 1H), 2.39 (s, 3H), 6.98 (dd, *J* = 5.3, 1.6 Hz, 1H), 7.47 - 7.58 (m, 3H), 7.84 - 7.96 (m, 3H), 8.02 (s, 1H), 8.09 (d, *J* = 5.1 Hz, 1H), 8.40 (s, 1H), 10.68 (s, 1H), 12.42 (br. s., 1H). ^{13}C NMR (75 MHz, $CDCl_3$/MeOD [2:1 v/v]) δ 7.7, 12.6, 14.5, 111.5, 117.4, 125.7, 125.8, 125.8, 126.6, 127.2, 127.5, 127.8, 129.3, 132.4, 133.0, 134.2, 142.7, 145.8, 146.9, 151.4, 173.3. TLC-MS (ESI) *m*/*z*: calculated for $C_{23}H_{20}N_4O$ $[M+H]^+$ 369.2, found 369.2. HPLC: t_R = 5.07 min (100.0% purity).

***N*-(4-(4-(3,4-Difluorophenyl)-2-methyl-1*H*-imidazol-5-yl)pyridin-2-yl)cyclopropanecarboxamide (3i)**

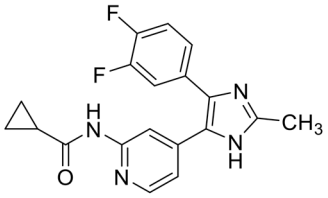

The compound was synthesized according to **General Procedure E** starting from compound **S6i** (165 mg, 0.34 mmol). Purification by flash chromatography (SiO_2, DCM:EtOH 95:5) afforded 102 mg (84.6%) of a yellowish solid. ^{1}H NMR (300 MHz, $CDCl_3$) δ 0.85 - 0.95 (m, 2H), 1.02 - 1.10 (m, 2H), 1.55 - 1.69 (m, 1H), 2.44 (s, 3H), 7.02 (dd, *J* = 5.4, 1.6 Hz, 1H), 7.07 - 7.16 (m, 1H), 7.18 - 7.25 (m, 1H), 7.27 - 7.36 (m, 1H), 8.10 (dd, *J* = 5.4, 0.5 Hz, 1H), 8.21 (d, *J* = 0.8 Hz, 1H), 8.90 (br. s., 1H). TLC-MS (ESI) *m*/*z*: calculated for $C_{19}H_{16}F_2N_4O$ $[M+H]^+$ 355.1, found 355.2. HPLC: t_R = 3.63 min (100.0% purity).

Synthesis of 3j-m

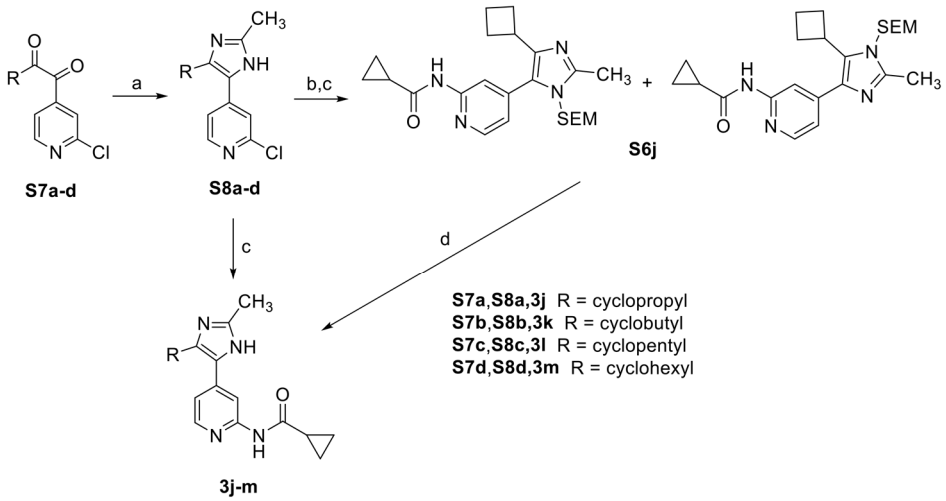

Scheme S3. *Reagents and conditions:* (a) CH_3CHO, NH_4OAc, MeOH, 65 °C, 3 h, 38-54%; (b) NaH, SEM-Cl, THF, 0 °C to rt, 18 h, 100%; (c) cyclopropanecarboxamide, Cs_2CO_3, $Pd_2(dba)_3$, XantPhos, DMF, 100 °C, 16 h, 8-77%; (d) trifluoroacetic acid, DCM, rt, 24 h, 52%.

2-Chloro-4-(4-cyclopropyl-2-methyl-1*H*-imidazol-5-yl)pyridine (S8a)

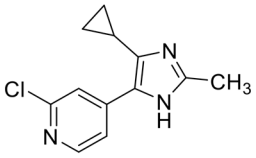

The title compound was prepared according to **General Procedure A** starting from 1-(2-chloropyridin-4-yl)-2-cyclopropylethane-1,2-dione[1] (**S7a**) (2.50 g, 11.93 mmol). Purification by flash chromatography (SiO_2, DCM:EtOH 99:1 to 90:10) afforded 1.22 g (43.59%) of a brown-orange wax. ^{1}H NMR (300 MHz, $CDCl_3$) δ 0.69 - 0.81 (m, 2H), 0.96 - 1.07 (m, 2H), 1.90 - 2.03 (m, 1H), 2.35 (s, 3H), 7.67 (dd, *J* = 5.4, 1.4 Hz, 1H), 7.77 (d, *J* = 0.9 Hz, 1H), 8.28 (d, *J* = 5.4 Hz, 1H), 10.17 (br. s., 1H). ^{13}C NMR (75 MHz, $CDCl_3$) δ 7.1, 7.5, 18.3, 119.1, 120.4, 130.9, 134.1, 144.3, 144.8, 149.0, 151.5. TLC-MS (ESI) *m*/*z*: calculated for $C_{12}H_{12}ClN_3$ $[M+H]^+$ 234.1, found 233.8. HPLC: t_R = 1.57 min.

2-Chloro-4-(4-cyclobutyl-2-methyl-1*H*-imidazol-5-yl)pyridine (S8b)

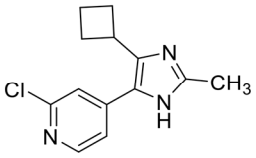

The title compound was prepared according to **General Procedure A** starting from 1-(2-chloropyridin-4-yl)-2-cyclobutylethane-1,2-dione[1] (**S7b**) (782 mg, 3.49 mmol). Purification by flash chromatography (SiO_2, DCM:EtOH 95:05 to 90:10) afforded 337 mg (39.0%) of a red oil. ^{1}H NMR (300 MHz, $CDCl_3$) δ 1.76 - 1.90 (m, 1H), 1.97 - 2.11 (m, 1H), 2.22 (quind, *J* = 9.3, 2.1 Hz, 2H), 2.31 - 2.44 (m, 2H), 2.38 (s, 3H), 3.75 - 3.84 (m, 1H), 7.38 (dd, *J* = 5.3, 1.5 Hz, 1H), 7.48 (d, *J* = 0.9 Hz, 1H), 8.27 (d, *J* = 5.3 Hz, 1H). ^{13}C NMR (75 MHz, $CDCl_3$) δ 18.2, 18.3, 29.0, 31.5, 119.6, 120.9, 129.4, 135.7, 144.7, 145.2, 149.1, 151.6. TLC-MS (ESI) *m*/*z*: calculated for $C_{13}H_{14}ClN_3$ $[M+H]^+$ 248.1, found 248.0. HPLC: t_R = 2.49 min.

2-Chloro-4-(4-cyclopentyl-2-methyl-1*H*-imidazol-5-yl)pyridine (S8c)

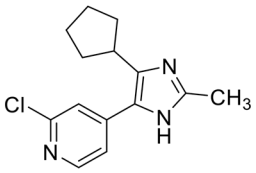

The title compound was prepared according to **General Procedure A** starting from 1-(2-chloropyridin-4-yl)-2-cyclopentylethane-1,2-dione[1] (**S7c**) (946 mg, 3.98 mmol). Purification by flash chromatography (SiO_2, DCM:EtOH 95:05 to 90:10) afforded 565 mg (54.2%) of a beige solid. ^{1}H NMR (300 MHz, $CDCl_3$) δ 1.56 - 1.88 (m, 6H), 2.02 - 2.18 (m, 2H), 2.41 (s, 3H), 3.28 - 3.42 (m, 1H), 7.44 (dd, *J* = 5.3, 1.3 Hz, 1H), 7.56 (s, 1H), 8.30 (dd, *J* = 4.9, 3.0 Hz, 1H). ^{13}C NMR (75 MHz, $CDCl_3$) δ 13.8, 25.4, 33.3, 36.5, 119.9, 121.2, 130.3, 135.8, 144.7, 145.8, 149.1, 151.6. TLC-MS (ESI) *m*/*z*: calculated for $C_{14}H_{16}ClN_3$ $[M+H]^+$ 262.1, found 261.8. HPLC: t_R = 3.24 min (100.0% purity).

2-Chloro-4-(4-cyclohexyl-2-methyl-1*H*-imidazol-5-yl)pyridine (S7d)

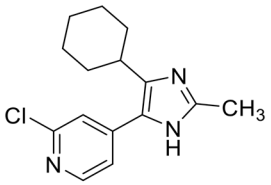

The title compound was prepared according to **General Procedure A** starting from 1-(2-chloropyridin-4-yl)-2-cyclohexylethane-1,2-dione[1] (**S7d**) (781 mg, 3.10 mmol). Purification by flash chromatography (SiO_2, DCM:EtOH 95:05 to 90:10) afforded 326 mg (38.1%) of a yellow solid. ^{1}H NMR (300 MHz, $CDCl_3$) δ 1.09 - 1.28 (m, 1H), 1.29 - 1.56 (m, 4H), 1.69 - 1.99 (m, 5H), 2.38 (s, 3H), 2.83 - 3.01 (m, 1H), 7.41 (dd, *J* = 5.3, 1.4 Hz, 1H), 7.55 (s, 1H), 8.29 (d, *J* = 5.3 Hz, 1H). ^{13}C NMR (75 MHz, $CDCl_3$) δ 13.9, 25.8, 26.4, 33.0, 35.4, 119.7, 121.2, 129.7, 137.1, 144.4, 145.8, 149.3, 151.8. TLC-MS (ESI) *m*/*z*: calculated for $C_{15}H_{18}ClN_3$ $[M+H]^+$ 276.1, found 275.8. HPLC: t_R = 4.39 min (100.0% purity).

***N*-(4-(4(5)-Cyclobutyl-2-methyl-1-((2-(trimethylsilyl)ethoxy)methyl)-1*H*-imidazol-5(4)-yl)pyridin-2-yl)cyclopropanecarboxamide (S6j)**

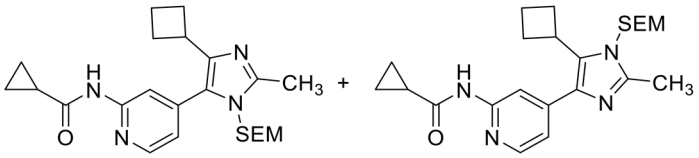

Compound **S8b** (282 mg, 1.14 mmol) was dissolved in THF (15 mL) and the solution was cooled to 0 °C. NaH 60% dispersion in mineral oil (64 mg, 1.60 mmol) was added in one portion and the resulting suspension was stirred for 30 min. Then 2-(trimethylsilyl)ethoxymethyl chloride (212 µL, 1.20 mmol) was added, the ice-bath was removed and the solution was stirred for 18 h. H_2O (25 mL) was added and it was extracted with EtOAc (3x). The combined organic layers were dried over anhydrous Na_2SO_4 and the solvent was removed under reduced pressure. The crude product was dried in vacuo before it was processed according to **General Procedure B**. Purification by flash chromatography (SiO_2, DCM:EtOH 95:05 to 90:10) afforded 216 mg (76.6%) of a mix of two regioisomers (ratio 2.5:1) over 2 steps. *isomer 1:* ^{1}H NMR (300 MHz, $CDCl_3$) δ -0.07 (s, 9H), 0.77 - 0.92 (m, 4H), 1.04 - 1.13 (m, 2H), 1.56 - 1.68 (m, 1H), 1.77 - 2.02 (m, 2H), 2.16 (qt, *J* = 8.3, 2.6 Hz, 2H), 2.32 - 2.48 (m, 2H), 2.51 (s, 3H), 3.29 - 3.40 (m, 2H), 3.46 (quin, *J* = 8.8 Hz, 1H), 5.13 (s, 2H), 6.97 (dd, *J* = 5.2, 1.5 Hz, 1H), 8.13 (s, 1H), 8.29 (d, *J* = 5.2 Hz, 1H), 9.14 (s, 1H). ^{13}C NMR (75 MHz, $CDCl_3$) -1.6, 8.3, 13.5, 15.7, 17.6, 18.4, 28.7, 32.6, 65.8, 72.6, 114.4, 120.0, 125.3, 140.7, 142.9, 146.7, 147.6, 152.0, 172.3. *isomer 2:* ^{1}H NMR (300 MHz, $CDCl_3$) δ 0.00 (s, 9H), 0.75 (dd, *J* = 7.9, 3.0 Hz, 2H), 0.84 (dd, *J* = 7.7, 3.2 Hz, 2H), 1.02 - 1.12 (m, 2H), 1.42 (s, 1H), 1.59 - 2.18 (m, 4H), 2.32 - 2.48 (m, 5H), 3.44 - 3.57 (m, 2H), 3.75 - 3.93 (m, 1H), 5.13 (s, 2H), 7.27 (s, 1H), 8.05 - 8.30 (m, 2H), 9.46 (s, 1H). ^{13}C NMR (75 MHz, $CDCl_3$) δ -1.5, 8.1, 13.3, 15.5, 17.8, 18.6, 28.9, 31.3, 65.8, 73.0, 114.2, 119.3, 133.1, 134.0, 145.1, 146.0, 146.6, 151.3, 172.5 TLC-MS (ESI) *m*/*z*: calculated for $C_{23}H_{34}N_4O_2Si$ $[M+H]^+$ 427.2, found 427.3. HPLC: t_R = 7.24 min & 8.74 min.

***N*-(4-(4-Cyclopropyl-2-methyl-1*H*-imidazol-5-yl)pyridin-2-yl)cyclopropanecarboxamide (3j)**

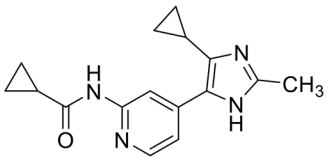

The title compound was prepared according to **General Procedure B** starting from **S8a** (238 mg, 1.02 mmol). Purification by flash chromatography (SiO_2, DCM:EtOH 95:05 to 90:10) afforded 51 mg (17.7%) of an off-white solid. ^{1}H NMR (300 MHz, $CDCl_3$) δ 0.70 - 0.77 (m, 2H), 0.83 - 0.91 (m, 2H), 0.97 - 1.05 (m, 2H), 1.05 - 1.12 (m, 2H), 1.57 - 1.68 (m, 1H), 2.01 (tt, *J* = 8.3, 5.2 Hz, 1H), 2.32 (s, 3H), 7.49 (dd, *J* = 5.4, 1.4 Hz, 1H), 8.22 (d, *J* = 5.4 Hz, 1H), 8.58 (s, 1H), 9.26 (br. s., 1H). ^{13}C NMR (75 MHz, $CDCl_3$) δ 7.4, 7.6, 8.3, 13.9, 15.8, 110.4, 116.5, 130.9, 135.0, 143.4, 143.6, 147.5, 151.9, 172.7. TLC-MS (ESI) *m*/*z*: calculated for $C_{15}H_{18}N_4O$ $[M+H]^+$ 283.1, found 282.8. HPLC: t_R = 1.93 min (99.4% purity).

***N*-(4-(4-Cyclobutyl-2-methyl-1*H*-imidazol-5-yl)pyridin-2-yl)cyclopropanecarboxamide (3k)**

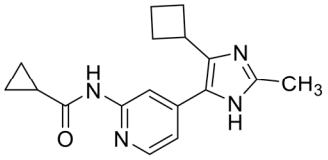

The mix of regioisomers from **S6j** (210 mg, 0.49 mmol) was dissolved in DCM (5 mL) and trifluoroacetic acid (1 mL). The solution was stirred at rt for 24 h before additional DCM and sat. aq. $NaHCO_3$ solution was added until the aqueous phase was adjusted to pH 7. The organic layer was separated and the solvent was removed under reduced pressure. Purification by flash chromatography (SiO_2, DCM:EtOH 95:05 to 90:10) afforded 76 mg (52.2%) of an off-white solid. ^{1}H NMR (300 MHz, $CDCl_3$) δ 0.86 - 0.94 (m, 2H), 1.08 - 1.15 (m, 2H), 1.52 - 1.63 (m, 1H), 1.83 - 1.97 (m, 1H), 2.00 - 2.33 (m, 4H), 2.40 - 2.49 (m, 4H), 3.86 (quin, *J* = 8.7 Hz, 1H), 7.30 (d, *J* = 4.4 Hz, 1H), 8.14 (s, 1H), 8.18 (d, *J* = 5.2 Hz, 1H), 8.34 (br. s., 1H). ^{13}C NMR (75 MHz, $CDCl_3$) δ 8.4, 13.6, 15.7, 18.2, 28.7, 32.0, 110.5, 116.9, 127.8, 138.1, 143.0, 144.5, 147.5, 151.6, 172.9. TLC-MS (ESI) *m*/*z*: calculated for $C_{17}H_{20}N_4O$ $[M+H]^+$ 297.2, found 297.3. HPLC: t_R = 2.76 min (100.0% purity).

***N*-(4-(4-Cyclopentyl-2-methyl-1*H*-imidazol-5-yl)pyridin-2-yl)cyclopropanecarboxamide (3l)**

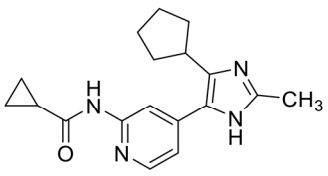

The title compound was prepared according to **General Procedure B** starting from **S8c** (300 mg, 1.15 mmol). Purification by flash chromatography (SiO_2, DCM:EtOH 95:05 to 90:10) afforded 33 mg (9.3%) of an off-white solid. ^{1}H NMR (300 MHz, $CDCl_3$/MeOD [1:1 v/v]) δ 0.81 - 0.94 (m, 2H), 1.05 - 1.14 (m, 2H), 1.56 - 1.64 (m, 1H), 1.66 - 1.86 (m, 6H), 2.05 - 2.19 (m, 2H), 2.47 (s, 3H), 3.32 - 3.44 (m, 1H), 7.31

(d, *J* = 4.4 Hz, 1H), 8.22 (d, *J* = 5.2 Hz, 1H), 8.32 (s, 1H), 8.52 (br. s., 1H). ^{13}C NMR (75 MHz, $CDCl_3$/MeOD [1:1 v/v]) δ 7.2, 12.1, 14.3, 24.8, 32.5, 35.9, 111.2, 116.9, 129.5, 135.8, 143.6, 144.2, 146.8, 151.1, 173.3. TLC-MS (ESI) *m*/*z*: calculated for $C_{18}H_{22}N_4O$ $[M+H]^+$ 311.2, found 311.0. HPLC: t_R = 3.49 min (98.5% purity).

***N*-(4-(4-Cyclohexyl-2-methyl-1*H*-imidazol-5-yl)pyridin-2-yl)cyclopropanecarboxamide (3m)**

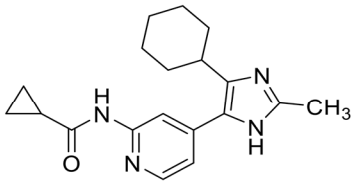

The title compound was prepared according to **General Procedure B** starting from **S8d** (250 mg, 0.91 mmol). Purification by flash chromatography (SiO_2, DCM:EtOH 95:05 to 90:10) afforded 22 mg (7.5%) of a yellow solid. ^{1}H NMR (300 MHz, $CDCl_3$) δ 0.82 - 0.89 (m, 2H), 1.04 - 1.12 (m, 2H), 1.25 - 1.52 (m, 5H), 1.56 - 1.65 (m, 1H), 1.66 - 1.83 (m, 3H), 1.89 (d, *J* = 9.7 Hz, 2H), 2.34 (br. s., 3H), 2.89 - 3.05 (m, 1H), 7.27 (d, *J* = 5.1 Hz, 1H), 8.21 (d, *J* = 5.3 Hz, 1H), 8.34 (s, 1H), 9.30 (br. s., 1H). ^{13}C NMR (75 MHz, $CDCl_3$) δ 8.2, 13.8, 15.7, 25.8, 26.3, 32.9, 35.4, 111.1, 114.3, 117.1, 129.2, 138.2, 144.0, 147.5, 152.0, 172.6. TLC-MS (ESI) *m*/*z*: calculated for $C_{19}H_{24}N_4O$ $[M+H]^+$ 325.2, found 325.1. HPLC: t_R = 4.73 min (100.0% purity).

Synthesis of 3n

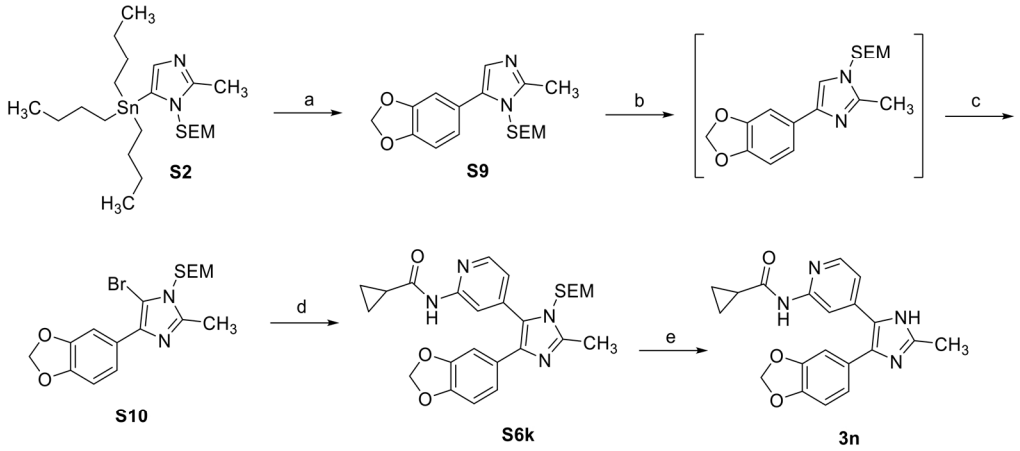

Scheme S4. *Reagents and conditions:* (a) 5-bromo-1,3-benzodioxole, $Pd(PPh_3)_4$, 1,4-dioxane, 105 °C, 18 h, 83%; (b) SEM-Cl, MeCN, 80 °C, 18 h; (c) NBS, MeCN, 0 °C, 30 min, 46% (*over 2 steps*); (d) **S11**, CsF, benzyltriethylammonium chloride, $Pd(dppf)Cl_2$·DCM, toluene/H_2O, 100 °C, 16 h, 32%; (e) trifluoroacetic acid, DCM, rt, 24 h, 50%.

5-(Benzo[*d*][1,3]dioxol-5-yl)-2-methyl-1-((2-(trimethylsilyl)ethoxy)methyl)-1*H*-imidazole (S9)

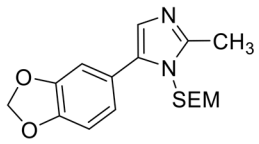

Compound **S2** (563 mg, 1.12 mmol), 5-bromo-1,3-benzodioxole (338 mg, 1.68 mmol) and $Pd(PPh_3)_4$ (97 mg, 0.084 mmol) were dissolved in degassed 1,4-dioxane (8 mL) under an atmosphere of argon. The reaction mixture was heated to 105 °C for 18 h before the solution was filtered through a pad of celite. The pad was washed with DCM (30 mL) and the solvents were removed under reduced pressure. Purification by flash chromatography (SiO_2, *n*-hexane:EtOAc 60:40 to 30:70) afforded 310 mg (83.1%) of a clear oil. ^{1}H NMR (300 MHz, $CDCl_3$) δ -0.03 (s, 9H), 0.84 - 0.91 (m, 2H), 2.50 (s, 3H), 3.38 - 3.47 (m, 2H), 5.14 (s, 2H), 6.00 (s, 2H), 6.81 - 6.95 (m, 4H). ^{13}C NMR (75 MHz, $CDCl_3$) δ -1.5, 13.6, 17.7, 65.8, 72.3, 101.2, 108.5, 109.5, 122.8, 123.9, 125.7, 133.5, 146.3, 147.4, 147.8. TLC-MS (ESI) *m*/*z*: calculated for $C_{17}H_{24}N_2O_3Si$ $[M+H]^+$ 333.2, found 333.3. HPLC: t_R = 6.44 min.

4-(Benzo[*d*][1,3]dioxol-5-yl)-5-bromo-2-methyl-1-((2-(trimethylsilyl)ethoxy)methyl)-1*H*-imidazole (S10)

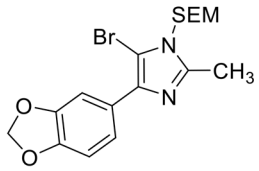

Compound **S9** (300 mg, 0.90 mmol) was dissolved in MeCN (10 mL) and catalytic amounts of 2-(trimethylsilyl)ethoxymethyl chloride (7.96 µL, 0.045 mmol) were added. The mixture was stirred at 80 °C for 18 h to perform a "SEM switch"[4]. The solvent was removed under reduced pressure and the crude product was redissolved in MeCN (15 mL). The solution was cooled to 0 °C and *N*-bromosuccinimide (160 mg, 0.90 mmol) was added in one portion. The reaction was further stirred at 0 °C for 30 min before sat. aq. Na_2SO_3 solution was added and it was extracted with EtOAc (3x). Purification by flash chromatography (SiO_2, *n*-hexane:EtOAc 60:40) afforded 170 mg (45.8%) of a tangerine oil. ^{1}H NMR (300 MHz, $CDCl_3$) δ 0.01 (s, 9H), 0.90 - 0.99 (m, 2H), 2.53 (s, 3H), 3.57 - 3.66 (m, 2H), 5.30 (s, 2H), 5.98 (s, 2H), 6.86 (d, *J* = 8.5 Hz, 1H), 7.40 - 7.48 (m, 2H). ^{13}C NMR (75 MHz, $CDCl_3$) δ -1.6, 13.9, 17.7, 66.1, 73.1, 98.2, 100.8, 107.3, 108.0, 120.4, 127.1, 136.7, 146.4, 146.6, 147.4. TLC-MS (ESI) *m*/*z*: calculated for $C_{17}H_{23}BrN_2O_3Si$ $[M+H]^+$ 411.1/413.1, found 411.4/413.4. HPLC: t_R = 10.39 min.

***N*-(4-(4,4,5,5-Tetramethyl-1,3,2-dioxaborolan-2-yl)pyridin-2-yl)cyclopropanecarboxamide (S11)[4]**

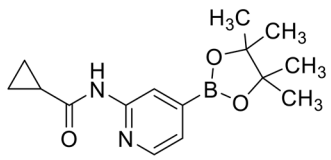

Compound **S3** (1.00 g, 4.15 mmol), Bis(pinacolato)diboron (1.26 g, 4.98 mmol), KOAc (1.43 g, 14.52 mmol) and Pd(dppf)Cl_2·DCM (136 mg, 0.166 mmol) were dissolved in degassed 1,4-dioxane (10 mL) under an atmosphere of argon. The reaction mixture was stirred at 85 °C for 18 h and after cooling to rt, EtOAc (30 mL) was added. The solution was filtered over celite and the filtrate was removed under reduced pressure and redissolved in EtOAc (50 mL). A spoon of activated charcoal was added to the solution and the resulting suspension was stirred at 85 °C for 30 min. The hot reaction mixture was filtered again over celite and the filtrate was removed under reduced pressure. The crude product was suspended in *n*-heptane and agitated for 30 min using an ultrasonic bath. The title compound was collected by filtration to yield 1.05 g (88.1%) of a beige solid. ^{1}H NMR (300 MHz, DMSO-d_6) δ 0.74 - 0.86 (m, 4H), 1.30 (s, 12H), 1.94 - 2.05 (m, 1H), 7.24 (dd, *J* = 4.8, 0.9 Hz, 1H), 8.33 (dd, *J* = 4.7, 0.9 Hz, 1H), 8.35 (s, 1H), 10.77 (s, 1H). ^{13}C NMR (101 MHz, DMSO-d_6) δ 7.7, 14.2, 24.6, 84.3, 118.4, 123.5, 138.6, 147.5, 151.9, 172.6. HPLC: t_R = 1.36 min.

_N_-(4-(4-(Benzo[_d_][1,3]dioxol-5-yl)-2-methyl-1-((2-(trimethylsilyl)ethoxy)methyl)-1_H_-imidazol-5-yl)pyridin-2-yl)cyclopropanecarboxamide (S6k)

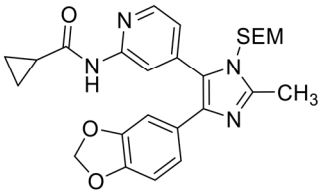

The title compound was synthesized according to **General Procedure D** starting from compound **S10** (165 mg, 0.40 mmol), **S11** (173 mg, 0.60 mmol), cesium fluoride (183 mg, 1.20 mmol), benzyltriethylammonium chloride (5.5 mg, 0.024 mmol) and Pd(dppf)Cl_2·DCM (19.7 mg, 0.024 mmol). Purification by flash chromatography (SiO_2, DCM:EtOH 97:3) afforded 64 mg (32.4%) of the title compound. ^{1}H NMR (300 MHz, $CDCl_3$) δ -0.06 (s, 9H), 0.80 - 0.95 (m, 4H), 1.05 - 1.12 (m, 2H), 1.56 - 1.66 (m, 1H), 2.54 (s, 3H), 3.31 - 3.40 (m, 2H), 5.14 (s, 2H), 5.90 (s, 2H), 6.64 - 7.25 (m, 4H), 8.21 - 8.29 (m, 2H), 9.04 (br. s., 1H). TLC-MS (ESI) *m*/*z*: calculated for $C_{26}H_{32}N_4O_4Si$ $[M+H]^+$ 493.2, found 493.8. HPLC: t_R = 7.60 min.

_N_-(4-(5-(Benzo[_d_][1,3]dioxol-5-yl)-2-methyl-1_H_-imidazol-4-yl)pyridin-2-yl)cyclopropanecarboxamide (3n)

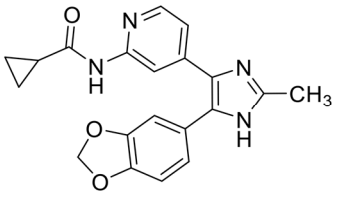

The title compound was synthesized according to **General Procedure E** starting from **S6k** (60 mg, 0.12 mmol). Purification by flash chromatography (SiO_2, DCM:EtOH 95:5) afforded 22 mg (49.8%) of an off-white solid. ^{1}H NMR (300 MHz, DMSO-d_6) δ 0.78 (d, *J* = 6.1 Hz, 4H), 1.89 - 2.04 (m, 1H), 2.33 (s, 3H),

6.05 (s, 2H), 6.82 - 7.03 (m, 4H), 8.11 (d, *J* = 5.2 Hz, 1H), 8.32 (s, 1H), 10.65 (s, 1H), 12.37 (br. s., 1H). ^{13}C NMR (101 MHz, DMSO-d_6) δ 7.6, 13.6, 14.2, 101.2, 108.5, 108.6, 110.6, 116.4, 122.0, 144.5, 146.9, 147.4, 147.5, 152.5, 172.3. TLC-MS (ESI) *m*/*z*: calculated for $C_{20}H_{18}N_4O_3$ $[M+H]^+$ 363.1, found 363.4. HPLC: t_R = 2.70 min (98.0% purity).

Synthesis of 3o

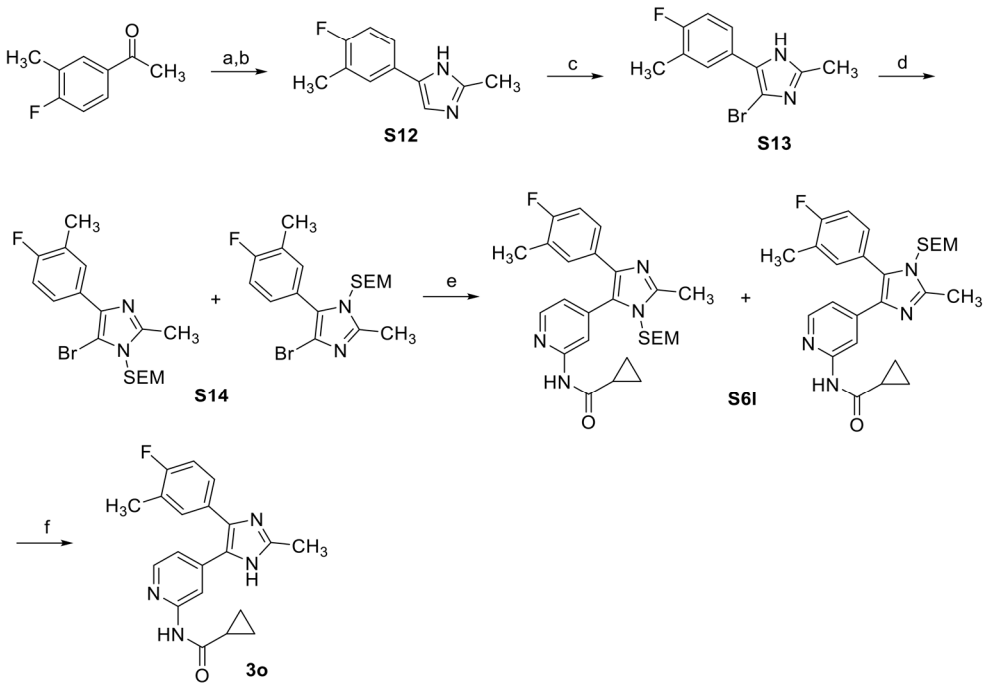

Scheme S5. *Reagents and conditions:* (a) 48% aq. HBr/DMSO, 55 °C, 18 h; (b) ethyl glyoxylate (polymer form ~50% in toluene), NH_4OAc, MeOH/MeCN, rt, 1.5 h, 28% (*over 2 steps*); (c) NBS, MeCN, 0 °C, 1 h, 70%; (d) SEM-Cl, NaH, THF, 0 °C to rt, 18 h, 76%; (e) **S11**, CsF, benzyltriethylammonium chloride, Pd(dppf)Cl_2·DCM, toluene/H_2O, 100 °C, 18 h, 14%; (f) trifluoroacetic acid, DCM, rt, 88%.

5-(4-Fluoro-3-methylphenyl)-2-methyl-1*H*-imidazole (S12)

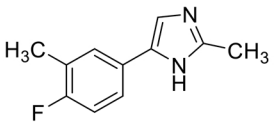

4'-Fluoro-3'-methylacetophenone (500 mg, 3.29 mmol) was treated according to a modified **General Procedure C**. After the oxidation, the 1-(4-fluoro-3-methylphenyl)-2,2-dihydroxyethan-1-one was dissolved in MeOH (20 mL) and added dropwise to a previously prepared solution of NH_4OAc (1.27 g, 16.43 mmol) and acetaldehyde (550 µL, 9.86 mmol) in MeOH (10 mL). After 1.5 h, the solvent was

evaporated, H_2O was added and it was extracted with EtOAc (5x). The combined organic layers were dried over anhydrous Na_2SO_4 before the solvent was removed under reduced pressure and the compound was purified by flash chromatography (SiO_2, DCM:EtOH 97:3 to 90:10) to afford 172 mg (27.5%) of a brown-red oil. ^{1}H NMR (300 MHz, $CDCl_3$) δ 2.19 (s, 3H), 2.38 (s, 3H), 6.91 (t, *J* = 8.8 Hz, 1H), 7.05 (s, 1H), 7.31 - 7.48 (m, 2H). ^{13}C NMR (75 MHz, $CDCl_3$) δ 12.9, 14.4 (d, $^3J_{CF}$ = 3.3 Hz), 114.4, 115.2 (d, $^2J_{CF}$ = 22.7 Hz), 123.7 (d, $^3J_{CF}$ = 8.3 Hz), 125.2 (d, $^2J_{CF}$ = 17.7 Hz), 127.2 (d, $^4J_{CF}$ = 3.3 Hz), 128.0 (d, $^3J_{CF}$ = 5.0 Hz), 135.8, 145.0, 160.6 (d, $^1J_{CF}$ = 245.5 Hz). TLC-MS (ESI) *m*/*z*: calculated for $C_{11}H_{11}FN_2$ $[M+H]^+$ 191.1, found 191.1. HPLC: t_R = 2.52 min.

4-Bromo-5-(4-fluoro-3-methylphenyl)-2-methyl-1*H*-imidazole (S13)

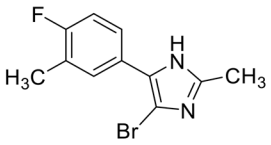

Compound **S12** (172 mg, 0.90 mmol) was dissolved in MeCN (5 mL), cooled to 0 °C and *N*-bromosuccinimide (161 mg, 0.90 mmol) was added in one portion. The mixture was stirred for 1 h at 0 °C before the reaction was quenched with sat. aq. Na_2SO_3 solution. The aqueous phase was extracted with EtOAc (3x) and the combined organic layers were dried over anhydrous Na_2SO_4 and the solvent was removed under reduced pressure. Purification by flash chromatography (SiO_2, *n*-hexane:EtOAc 90:10 to 30:70) afforded 170 mg (69.8%) of a white solid. ^{1}H NMR (300 MHz, DMSO-d_6) δ 2.27 (d, *J* = 1.7 Hz, 3H), 2.29 (s, 3H), 7.16 - 7.29 (m, 1H), 7.47 - 7.64 (m, 2H), 12.44 (br. s., 1H). TLC-MS (ESI) *m*/*z*: calculated for $C_{11}H_{10}BrFN_2$ $[M+H]^+$ 269.1/271.1, found 269.1/271.1. HPLC: t_R = 5.93 min.

4(5)-Bromo-5(4)-(4-fluoro-3-methylphenyl)-2-methyl-1-((2-(trimethylsilyl)ethoxy)methyl)-1*H*-imidazole (S14)

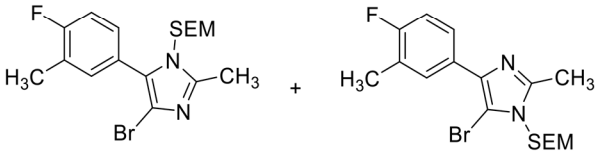

The title compound was prepared following the procedure as described for compound **S6j** starting from compound **S13** (130 mg, 0.48 mmol). Purification by flash chromatography (SiO_2, *n*-hexane:EtOAc 65:35) afforded 118 mg (76.2%) of a solid as a mixture of both regioisomers. TLC-MS (ESI) *m*/*z*: calculated for $C_{17}H_{24}BrFN_2OSi$ $[M+H]^+$ 399.1/401.1, found 399.1/401.1. HPLC: t_R = 11.29 min & 11.69 min.

***N*-(4-(5(4)-(4-Fluoro-3-methylphenyl)-2-methyl-1-((2-(trimethylsilyl)ethoxy)methyl)-1*H*-imidazol-4(5)-yl)pyridin-2-yl)cyclopropanecarboxamide (S6l)**

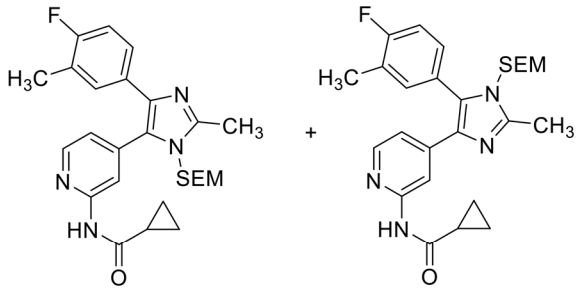

The title compound was synthesized according to **General Procedure D** starting from compound **S14** (100 mg, 0.25 mmol), **S11** (123 mg, 0.43 mmol), cesium fluoride (114 mg, 0.75 mmol), benzyltriethylammonium chloride (3.4 mg, 0.015 mmol) and $Pd(dppf)Cl_2$·DCM (12 mg, 0.015 mmol). Purification by flash chromatography (SiO_2, *n*-hexane:EtOAc 65:35) afforded 17 mg (14.3%) of only one pure regioisomer. ^{1}H NMR (300 MHz, $CDCl_3$) δ -0.05 (s, 9H), 0.80 - 0.93 (m, 4H), 1.04 - 1.13 (m, 2H), 1.57 - 1.65 (m, 1H), 2.20 (d, *J* = 1.7 Hz, 3H), 2.55 (s, 3H), 3.27 - 3.43 (m, 2H), 5.16 (s, 2H), 6.75 - 6.86 (m, 1H), 6.94 (dd, *J* = 5.2, 1.5 Hz, 1H), 7.02 - 7.11 (m, 1H), 7.41 (dd, *J* = 7.6, 1.7 Hz, 1H), 8.23 (dd, *J* = 5.2, 0.6 Hz, 1H), 8.27 (s, 1H), 8.98 (s, 1H). ^{13}C NMR (75 MHz, $CDCl_3$) δ -1.5, 8.4, 13.4, 14.4, 15.7, 17.7, 66.0, 72.7, 114.6, 115.2 , 121.4, 124.6, 125.6, 126.4, 129.6, 130.6, 137.6, 141.4, 146.9, 147.8, 152.3, 160.5 (d, $^1J_{CF}$ = 246.0 Hz), 172.4. TLC-MS (ESI) *m*/*z*: calculated for $C_{26}H_{33}N_4O_2Si$ $[M+H]^+$ 481.7, found 481.7. HPLC: t_R = 9.02 min.

***N*-(4-(4-(4-Fluoro-3-methylphenyl)-2-methyl-1*H*-imidazol-5-yl)pyridin-2-yl)cyclopropanecarboxamide (30)**

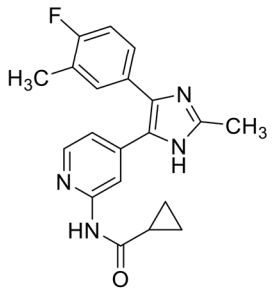

The title compound was synthesized according to **General Procedure E** starting from one pure isomer of **S6l** (17 mg, 0.049 mmol). Purification by flash chromatography (SiO_2, DCM:EtOH 95:5) afforded 11 mg (88.4%) of an off-white solid. ^{1}H NMR (300 MHz, $CDCl_3$) δ 0.88 - 0.91 (m, 2H), 1.02 - 1.09 (m, 2H), 1.59 - 1.68 (m, 1H), 2.24 (d, *J* = 1.7 Hz, 3H), 2.43 (s, 3H), 6.95 (t, *J* = 9.0 Hz, 1H), 7.05 (dd, *J* = 5.4, 1.6 Hz, 1H), 7.17 - 7.24 (m, 1H), 7.32 (dd, *J* = 7.4, 1.7 Hz, 1H), 8.03 (d, *J* = 5.3 Hz, 1H), 8.29 (s, 1H), 9.09 (br. s., 1H). ^{13}C NMR (75 MHz, $CDCl_3$) δ 8.5, 14.0, 14.4 (d, $^3J_{CF}$ = 3.3 Hz), 15.7, 110.7, 115.2 (d, $^2J_{CF}$ = 22.7 Hz), 117.2, 125.3 (d, $^2J_{CF}$ = 17.7 Hz), 127.4 (d, $^3J_{CF}$ = 8.3 Hz), 131.5 (d, $^3J_{CF}$ = 5.0 Hz), 145.6,

147.0, 151.8, 161.1 (d, $^{1}J_{CF}$ = 246.0 Hz), 172.9. TLC-MS (ESI) *m/z*: calculated for $C_{20}H_{17}FN_4O$ $[M+H]^+$ 351.2, found 351.5. HPLC: t_R = 4.31 min.

Synthesis of 4a and 4b

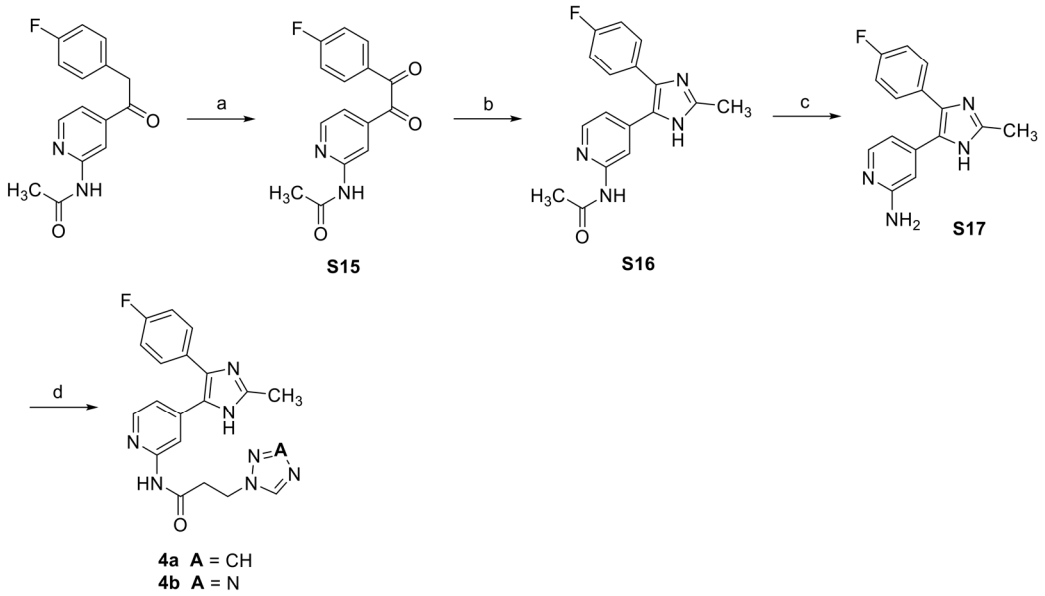

Scheme S6. *Reagents and conditions:* (a) SeO_2, acetic acid, 70 °C, 3 h, 84%; (b) acetaldehyde, NH_4OAc, MeOH, 65 °C, 3 h, 53%; (c) 10% aq. HCl, 110 °C, 18 h, 47%; (d) carboxylic acid, HATU, DIPEA, rt, 18 h, 42-56%.

N-(4-(2-(4-Fluorophenyl)-2-oxoacetyl)pyridin-2-yl)acetamide (S15)

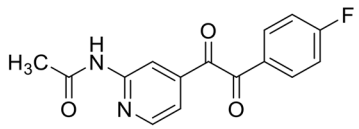

N-(4-(2-(4-fluorophenyl)acetyl)pyridin-2-yl)acetamide[6] (8.20 g, 30.12 mmol) was dissolved in glacial acetic acid (150 mL) and selenium dioxide (5.01 g, 45.17 mmol) was added before the mixture was heated to 70 °C for 3 h. After cooling to rt, the solution was filtered over celite and the solvent was removed in vacuo. Purification by flash chromatography (SiO_2, *n*-hexane:EtOAc 60:40) afforded 7.26 g (84.2%) of a bright yellow solid. ^{1}H NMR (300 MHz, DMSO-d_6) δ 2.11 (s, 3H), 7.36 - 7.57 (m, 3H), 7.95 - 8.17 (m, 2H), 8.47 - 8.69 (m, 2H), 10.87 (s, 1H). ^{13}C NMR (75 MHz, DMSO-d_6) δ 23.9, 112.0, 116.8 (d, $^{2}J_{CF}$ = 22.7 Hz), 117.7, 128.6 (d, $^{4}J_{CF}$ = 2.8 Hz), 133.3 (d, $^{3}J_{CF}$ = 10.5 Hz), 140.1, 149.7, 153.3, 166.4 (d,

$^1J_{CF}$ = 256.6 Hz), 169.8, 191.4, 193.1. TLC-MS (ESI) *m*/*z*: calculated for $C_{15}H_{11}FN_2O_3$ $[M+H]^+$ 287.1, found 287.1. HPLC: t_R = 4.44 min.

_N_-(4-(5-(4-Fluorophenyl)-2-methyl-1_H_-imidazol-4-yl)pyridin-2-yl)acetamide (S16)

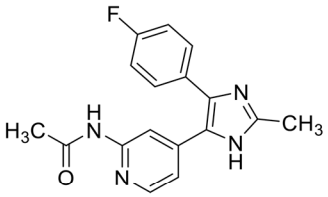

The title compound was synthesized according to **General Procedure A** starting from **S15** (7.26 g, 25.36 mmol). Purification by flash chromatography (SiO_2, DCM:EtOH 97:03 to 95:05) afforded 4.18 g (53.1%) of a yellow solid. ^{1}H NMR (300 MHz, DMSO-d_6) δ 2.04 (s, 3H), 2.34 (s, 3H), 6.97 - 7.20 (m, 2H), 7.27 (t, *J* = 8.7 Hz, 1H), 7.39 - 7.53 (m, 2H), 8.01 - 8.38 (m, 2H), 10.29 (s, 1H), 12.28 (br. s., 1H). ^{13}C NMR (75 MHz, $CDCl_3$/MeOD [2:1 v/v]) δ 13.0, 23.6, 111.2, 115.3 (d, $^2J_{CF}$ = 21.6 Hz), 117.4, 129.9 (d, $^3J_{CF}$ = 8.3 Hz), 145.8, 147.2, 151.3, 162.2 (d, $^1J_{CF}$ = 245.5 Hz), 169.9. TLC-MS (ESI) *m*/*z*: calculated for $C_{17}H_{15}FN_4O$ $[M+H]^+$ 311.1, found 311.2. HPLC: t_R = 1.91 min.

4-(4-(4-Fluorophenyl)-2-methyl-1_H_-imidazol-5-yl)pyridin-2-amine (S17)

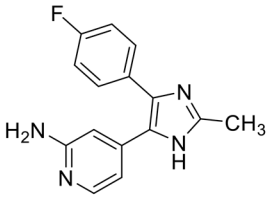

Compound **S16** (570 mg, 1.84 mmol) was dissolved in 10% aq. HCl (15 mL) and refluxed for 18 h. After cooling to rt, the solution is neutralized with 20% aq. NaOH and the forming precipitate is filtered off and dried in vacuo to give 233 mg (47.3%) of a beige-brown solid. ^{1}H NMR (300 MHz, DMSO-d_6) δ 2.32 (s, 3H), 5.72 (s, 1H), 5.92 (s, 1H), 6.37 - 6.70 (m, 2H), 7.14 (t, *J* = 8.9 Hz, 1H), 7.23 - 7.31 (m, 1H), 7.40 - 7.55 (m, 2H), 7.68 - 7.89 (m, 1H), 12.15 (br. s., 1H). ^{13}C NMR (75 MHz, $CDCl_3$/MeOD [2:1 v/v]) δ 12.6, 105.9, 111.4, 115.1 (d, $^2J_{CF}$ = 21.6 Hz), 129.8 (d, $^3J_{CF}$ = 7.7 Hz), 145.2, 146.2, 158.7, 162.1 (d, $^1J_{CF}$ = 247.1 Hz). TLC-MS (ESI) *m*/*z*: calculated for $C_{15}H_{13}FN_4$ $[M+H]^+$ 269.1, found 269.2. HPLC: t_R = 1.29 min HPLC: t_R = 4.39 min (method B).

_N_-(4-(5-(4-Fluorophenyl)-2-methyl-1_H_-imidazol-4-yl)pyridin-2-yl)-3-(1_H_-1,2,4-triazol-1-yl)propanamide TFA salt (4a)

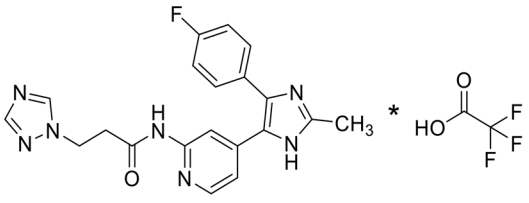

The title compound was synthesized according to **General Procedure G** (in 5 mL DMF) starting from compound **S17** (100 mg, 0.37 mmol) and 3-(1*H*-1,2,4-triazol-1-yl)propanoic acid (75 mg, 0.53 mmol). Purification by flash chromatography (SiO_2, DCM/2M ammonia in MeOH 90:10) and subsequent purification by RP-18 flash chromatography (MeCN:H_2O [8:2]/H_2O + 0.1% TFA) afforded 82 mg (56.3%) of the TFA salt. ^{1}H NMR (300 MHz, DMSO-d_6) δ 2.64 (s, 3H), 3.00 (t, *J* = 6.4 Hz, 2H), 4.45 (t, *J* = 6.3 Hz, 2H), 7.08 (dd, *J* = 5.2, 1.2 Hz, 1H), 7.29 - 7.42 (m, 2H), 7.49 - 7.61 (m, 2H), 8.20 (s, 1H), 8.34 (d, *J* = 5.2 Hz, 1H), 8.47 (br. s., 1H), 10.78 (s, 1H). ^{13}C NMR (101 MHz, DMSO-d_6) δ 11.5, 35.7, 44.5, 111.1, 116.4 ($^2J_{CF}$ = 22.0 Hz), 117.3, 123.6 (d, $^4J_{CF}$ = 3.7 Hz), 125.3, 128.8, 131.0 (d, $^3J_{CF}$ = 8.8 Hz), 137.4, 144.2, 145.6, 148.8, 151.3, 152.5, 162.8 (d, $^1J_{CF}$ = 247.2 Hz), 169.5. ^{19}F NMR (282 MHz, DMSO-d_6) δ -110.9 (4-F-Phe), -74.2 (CF_3). TLC-MS (ESI) *m*/*z*: calculated for $C_{20}H_{18}FN_7O$ $[M+H]^+$ 392.2, found 392.5. HPLC: t_R = 7.25 min (method B) (96.0% purity).

***N*-(4-(4-(4-Fluorophenyl)-2-methyl-1*H*-imidazol-5-yl)pyridin-2-yl)-3-(1*H*-tetrazol-1-yl)propanamide (4b)**

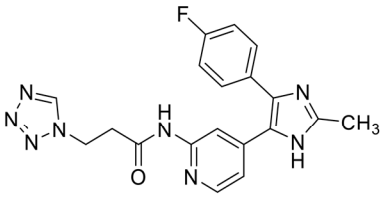

The title compound was synthesized according to **General Procedure G** starting from compound **S17** (100 mg, 0.37 mmol) and 3-(1*H*-tetrazol-1-yl)propanoic acid (75 mg, 0.53 mmol). Purification by flash chromatography (SiO_2, DCM/2M ammonia in MeOH 95:05 to 90:10) afforded 61 mg (42.3%) of an off-white solid. ^{1}H NMR (300 MHz, DMSO-d_6) δ 2.35 (s, 3H), 3.08 (t, *J* = 6.5 Hz, 2H), 4.72 (t, *J* = 6.5 Hz, 2H), 7.01 (dd, *J* = 5.2, 1.6 Hz, 1H), 7.23 (t, *J* = 8.8 Hz, 2H), 7.40 - 7.53 (m, 2H), 8.12 (d, *J* = 5.2 Hz, 1H), 8.25 (br. s., 1H), 9.34 (s, 1H), 10.53 (s, 1H), 12.33 (br. s., 1H). ^{13}C NMR (75 MHz, DMSO-d_6) δ 13.7, 35.4, 43.6, 110.5, 115.6 (d, $^2J_{CF}$ = 21.6 Hz), 116.7, 130.2 (d, $^3J_{CF}$ = 7.2 Hz), 144.2, 145.0, 147.8, 152.1, 161.6 (d, $^1J_{CF}$ = 244.9 Hz), 168.5. TLC-MS (ESI) *m*/*z*: calculated for $C_{19}H_{17}FN_8O$ $[M+H]^+$ 393.2, found 393.6. HPLC: t_R = 7.25 min (method B) (100.0% purity).

Synthesis of 4c and 4d

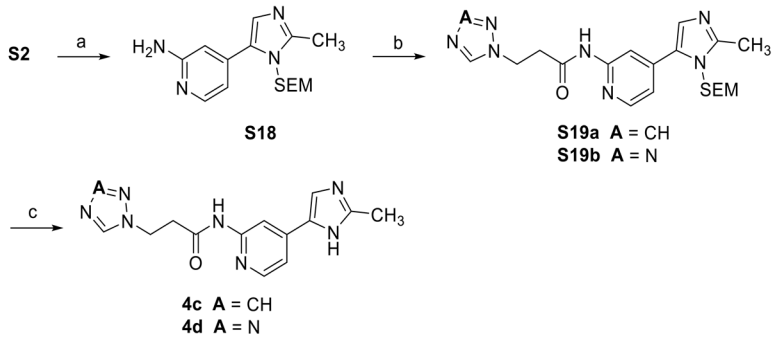

Scheme S7. *Reagents and conditions:* (a) 2-amino-4-bromopyridine, $Pd(PPh_3)_4$, 1,4-dioxane, 105 °C, 18 h, 41%; (b) carboxylic acid, HATU, DIPEA, rt, 18 h, 52-66%; (c) trifluoroacetic acid, DCM, rt, 8 h, 44-45%.

4-(2-Methyl-1-((2-(trimethylsilyl)ethoxy)methyl)-1*H*-imidazol-5-yl)pyridin-2-amine (S18)

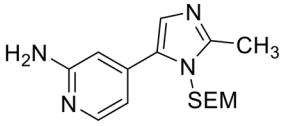

Compound **S2** (1.00 g, 2.00 mmol), 2-amino-4-bromopyridine (282 mg, 3.00 mmol) and $Pd(PPh_3)_4$ (170 mg, 0.15 mmol) were dissolved in degassed 1,4-dioxane (15 mL) under an atmosphere of argon. The reaction mixture was heated to 105 °C for 18 h before the solution was filtered through a pad of celite. The pad was washed with DCM (30 mL) and the solvents were removed under reduced pressure. Purification by flash chromatography (SiO_2, DCM/2M ammonia in MeOH 95:5) afforded 592 mg (41.3%) of an orange solid. ^{1}H NMR (300 MHz, $CDCl_3$) δ -0.04 (s, 9H), 0.80 - 0.91 (m, 2H), 2.48 (s, 3H), 3.41 - 3.52 (m, 2H), 5.19 (s, 2H), 6.66 (s, 1H), 6.72 (dd, *J* = 5.5, 1.2 Hz, 1H), 7.05 (s, 1H), 8.00 (d, *J* = 5.4 Hz, 1H). ^{13}C NMR (75 MHz, $CDCl_3$) δ -1.6, 13.6, 17.7, 66.0, 72.6, 107.0, 112.8, 127.8, 131.6, 139.6, 147.2, 148.2, 158.5. TLC-MS (ESI) *m*/*z*: calculated for $C_{15}H_{14}N_4OSi$ $[M+H]^+$ 305.2, found 305.3. HPLC: t_R = 2.56 min.

***N*-(4-(2-Methyl-1-((2-(trimethylsilyl)ethoxy)methyl)-1*H*-imidazol-5-yl)pyridin-2-yl)-3-(1*H*-1,2,4-triazol-1-yl)propanamide (S19a)**

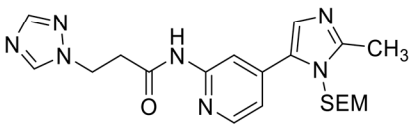

The title compound was synthesized according to **General Procedure G** starting from compound **S18** (100 mg, 0.33 mmol) and 3-(1*H*-1,2,4-triazol-1-yl)propanoic acid (67 mg, 0.47 mmol). Purification by flash chromatography (SiO_2, DCM/2M ammonia in MeOH 95:5) afforded 93 mg (66.3%) of a white solid.

^{1}H NMR (300 MHz, $CDCl_3$) δ -0.03 (s, 9H), 0.88 - 0.98 (m, 2H), 2.53 (s, 3H), 3.03 (t, *J* = 6.1 Hz, 2H), 3.48 - 3.56 (m, 2H), 4.58 (t, *J* = 6.1 Hz, 2H), 5.26 (s, 2H), 7.17 - 7.21 (m, 2H), 7.92 (s, 1H), 8.18 (s, 1H), 8.21 - 8.30 (m, 2H), 9.39 (br. s, 1H). ^{13}C NMR (75 MHz, $CDCl_3$) δ -1.5, 13.6, 17.7, 36.5, 44.7, 66.0, 72.7, 112.4, 118.6, 128.5, 131.2, 140.1, 143.9, 148.1, 148.8, 151.7, 152.0, 168.2. TLC-MS (ESI) *m*/*z*: calculated for $C_{20}H_{29}N_7O_2Si$ $[M+Na]^+$ 450.2, found 450.5. HPLC: t_R = 3.76 min.

_N_-(4-(2-Methyl-1-((2-(trimethylsilyl)ethoxy)methyl)-1_H_-imidazol-5-yl)pyridin-2-yl)-3-(1_H_-tetrazol-1-yl)propanamide (S19b)

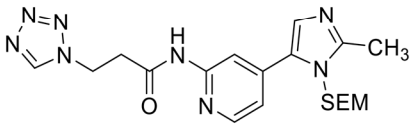

The title compound was synthesized according to **General Procedure G** starting from compound **S18** (150 mg, 0.49 mmol) and 3-(1*H*-tetrazol-1-yl)propanoic acid (100 mg, 0.70 mmol). Purification by flash chromatography (SiO_2, DCM/2M ammonia in MeOH 95:5) afforded 110 mg (52.4%) of a white solid. ^{1}H NMR (300 MHz, $CDCl_3$) δ -0.02 (s, 9H), 0.89 - 0.99 (m, 2H), 2.56 (s, 3H), 3.15 (t, *J* = 5.8 Hz, 2H), 3.51 - 3.59 (m, 2H), 4.85 (t, *J* = 6.0 Hz, 2H), 5.28 (s, 2H), 7.20 (s, 1H), 7.23 (dd, *J* = 5.2, 1.6 Hz, 1H), 8.21 (br. s., 1H), 8.28 (dd, *J* = 5.2, 0.6 Hz, 1H), 8.86 (s, 1H), 8.90 (br. s., 1H). ^{13}C NMR (75 MHz, $CDCl_3$) δ -1.5, 13.5, 17.8, 36.2, 43.5, 66.2, 72.9, 112.4, 118.8, 127.9, 131.4, 139.9, 143.7, 148.3, 148.7, 151.4, 167.7. TLC-MS (ESI) *m*/*z*: calculated for $C_{19}H_{28}N_8O_2Si$ $[M+Na]^+$ 451.2, found 451.6. HPLC: t_R = 3.49 min.

_N_-(4-(2-Methyl-1_H_-imidazol-5-yl)pyridin-2-yl)-3-(1_H_-1,2,4-triazol-1-yl)propanamide (4c)

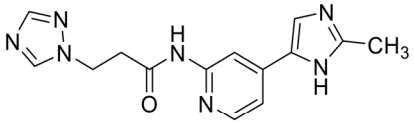

Compound **S19a** (93 mg, 0.22 mmol) was dissolved in a 1:5 mixture of trifluoroacetic acid in DCM and stirred at rt for 8 h. The solvent was evaporated and the crude product was purified by flash chromatography (SiO_2, DCM/2M ammonia in MeOH 95:5) to yield 29 mg (44.9%) of a yellow solid. ^{1}H NMR (300 MHz, $CDCl_3$) δ 2.63 (s, 3H), 3.06 (t, *J* = 6.4 Hz, 2H), 4.51 (t, *J* = 6.5 Hz, 2H), 7.47 (dd, *J* = 5.2, 1.5 Hz, 1H), 8.01 (s, 1H), 8.20 (s, 1H), 8.36 (s, 1H), 8.39 (d, *J* = 5.2 Hz, 1H), 8.57 (s, 1H), 10.81 (s, 1H). ^{13}C NMR (101 MHz, DMSO-d_6) δ 13.8, 35.8, 44.6, 108.0, 114.7, 116.3, 136.6, 143.7, 144.3, 145.4, 147.8, 151.4, 152.3, 169.0. TLC-MS (ESI) *m*/*z*: calculated for $C_{14}H_{15}N_7O$ $[M+H]^+$ 298.1, found 298.2. HPLC: t_R = 1.09 min t_R = 4.14 min (method B) (95.1% purity).

_N_-(4-(2-Methyl-1_H_-imidazol-5-yl)pyridin-2-yl)-3-(1_H_-tetrazol-1-yl)propanamide TFA salt (4d)

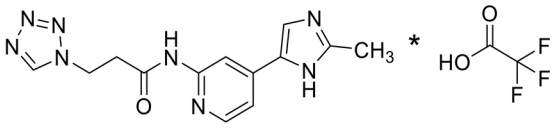

Compound **S19b** (93 mg, 0.22 mmol) was dissolved in a 1:5 mixture of trifluoroacetic acid in DCM and stirred at rt for 8 h. As the product was highly soluble in water, the solvents were evaporated and the crude product was directly purified by flash chromatography (SiO_2, DCM/2M ammonia in MeOH 90:10). Subsequent purification by RP-18 flash chromatography (MeCN:H_2O [8:2]/H_2O + 0.1% TFA) afforded 40 mg (44.1%) of the TFA salt. ^{1}H NMR (400 MHz, DMSO-d_6) δ 2.33 (s, 3H), 3.11 (t, *J* = 6.4 Hz, 2H), 4.64 - 4.80 (m, 2H), 7.36 (dd, *J* = 5.2, 1.4 Hz, 1H), 7.65 (s, 1H), 8.18 (d, *J* = 5.3 Hz, 1H), 8.35 (br. s., 1H), 9.40 (s, 1H), 10.51 (s, 1H). ^{13}C NMR (101 MHz, DMSO-d_6) δ 13.7, 35.4, 43.6, 108.0, 114.8, 116.5, 136.2, 143.4, 144.3, 145.4, 147.9, 152.2, 168.6. ^{19}F NMR (282 MHz, DMSO-d_6) δ -73.4. TLC-MS (ESI) *m*/*z*: calculated for $C_{13}H_{14}N_8O$ $[M+Na]^+$ 321.1, found 321.2. HPLC: t_R = 3.77 min (method B) (97.5% purity).

Synthesis of 5a,6a and 7

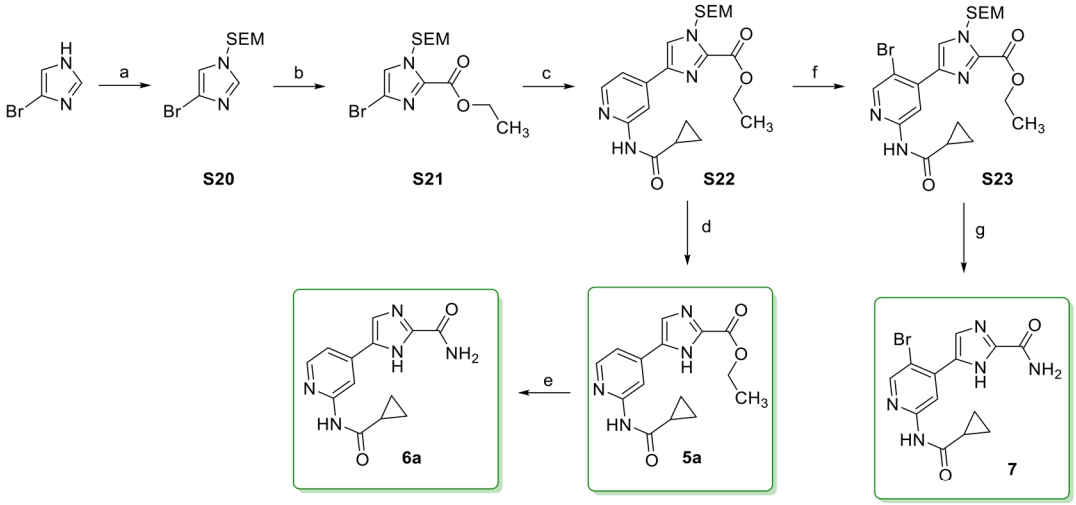

Scheme S8. *Reagents and conditions:* (a) NaH, SEM-Cl, THF, 0 °C then rt, 18 h, 91%; (b) 2.0 M LDA solution in THF/heptane/ethylbenzene, ethyl chloroformate, THF, -78 °C, 2 h, 52%; (c) **S11**, KF, XPhos, $Pd(OAc)_2$, 1,4-dioxane/H_2O, 110 °C, 18 h, 65% *or* K_2CO_3, $Pd(dppf)Cl_2$·DCM, DMF, 85 °C, 18 h, 82%; (d) trifluoroacetic acid, DCM, rt, 6 h, 94%; (e) 7 M ammonia in MeOH, 45 °C, 18 h, 66-74%.(f) NBS, MeCN, -20 °C to rt, 3 h, 70%; (g) 7 M ammonia in MeOH, 45 °C, 48 h *followed by* trifluoroacetic acid, DCM/EtOH, 45 °C, 48 h, 62% (*over 2 steps*)

4-Bromo-1-((2-(trimethylsilyl)ethoxy)methyl)-1*H*-imidazole (S20)

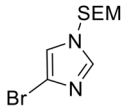

4-Bromo-1*H*-imidazole (5.00 g, 34.02 mmol) was dissolved in THF (50 mL) under an atmosphere of argon while being cooled to 0 °C. NaH 60% dispersion in mineral oil (1.77 g, 44.22 mmol) was added portionwise over 10 min and the resulting suspension was stirred for 20 more min. Then 2-(trimethylsilyl)ethoxymethyl chloride (6.37 mL, 36 mmol) was slowly added and the resulting mixture was stirred at rt for 18 h. H_2O (150 mL) was added, the organic layer was separated and the aqueous layer was further extracted with DCM (3x). The combined organic layers were dried over anhydrous Na_2SO_4 before the solvent was removed under reduced pressure. Purification by flash chromatography (SiO_2, *n*-hexane:EtOAc 90:10) afforded 8.61 g (91.3%) of a light orange oil. ^{1}H NMR (300 MHz, DMSO-d_6) δ -0.04 (s, 9H), 0.80 - 0.87 (m, 2H), 3.43 - 3.51 (m, 2H), 5.30 (s, 2H), 7.44 (d, *J* = 1.6 Hz, 1H), 7.79 (d, *J* = 1.5 Hz, 1H). ^{13}C NMR (75 MHz, DMSO-d_6) δ -1.4, 17.1, 65.5, 75.3, 114.3, 118.8, 138.1. TLC-MS (ESI) *m*/*z*: calculated for $C_9H_{17}BrN_2OSi$ [M+Na]$^+$ 299.0/301.0, found 299.1/301.1. HPLC: t_R = 7.93 min (*218 nm*).

Ethyl 4-bromo-1-((2-(trimethylsilyl)ethoxy)methyl)-1*H*-imidazole-2-carboxylate (S21)

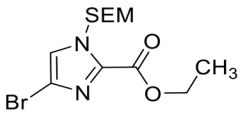

Compound **S20** (3.25 g, 11.72 mmol) was dissolved in THF (40 mL) under an atmosphere of argon and the solution was cooled to -78 °C. Lithium diisopropylamide 2.0M solution in THF/heptane/ethylbenzene (6.00 mL, 12.0 mmol) was added dropwise over 30 min. The red solution was stirred further for 30 min at -78 °C. In the meantime, a second flask was evacuated and backfilled with argon (3x). Ethyl chloroformate (3.36 mL, 35.17 mmol) and THF (5 mL) were added and then also cooled to -78 °C. Then the imidazole solution was added dropwise to the ethyl chloroformate solution and after complete addition the solution was further stirred at -78 °C for 30 min before it was quenched by the addition of H_2O (150 mL). The organic layer was separated and the aqueous layer was further extracted with EtOAc (3x). The combined organic layers were dried over anhydrous Na_2SO_4 before the solvent was removed under reduced pressure. Purification by flash chromatography (SiO_2, *n*-hexane:EtOAc 90:10) afforded 2.14 g (52.3%) of an orange wax. ^{1}H NMR (300 MHz, DMSO-d_6) δ -0.07 (s, 9H), 0.79 - 0.87 (m, 2H), 1.30 (t, *J* = 7.1 Hz, 3H), 3.48 - 3.57 (m, 2H), 4.30 (q, *J* = 7.2 Hz, 2H), 5.66 (s, 2H), 7.84 (s, 1H). ^{13}C NMR (75 MHz, DMSO-d_6) δ -1.5, 14.0, 17.1, 61.3, 66.1, 76.3, 114.6, 125.5, 135.6, 157.4. TLC-MS (ESI) *m*/*z*: calculated for $C_{12}H_{21}BrN_2O_3Si$ [M+Na]$^+$ 371.0/373.0, found 371.0/372.9. HPLC: t_R = 9.93 min.

Ethyl 4-(2-(cyclopropanecarboxamido)pyridin-4-yl)-1-((2-(trimethylsilyl)ethoxy)methyl)-1*H*-imidazole-2-carboxylate (S22)

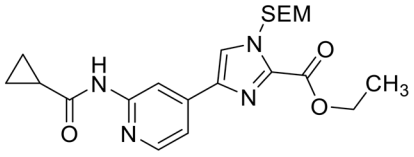

Compound **S21** (100 mg, 0.29 mmol), **S11** (148 mg, 0.52 mmol), K_2CO_3 (119 mg, 0.86 mmol) and Pd(dppf)Cl_2·DCM was dissolved in degassed DMF (3 mL) under an atmosphere of argon. The reaction mixture was heated to 85 °C for 18 h. After cooling to rt, sat. aq. NH_4Cl solution (40 mL) was added and it was extracted with EtOAc (3x). The combined organic layers were dried over anhydrous Na_2SO_4 before the solvent was removed under reduced pressure. Purification by flash chromatography (SiO_2, DCM:EtOH 97:3) afforded 101 mg (82.0%) of a white solid. *Alternative prep.:* Compound **S21** (500 mg, 1.43 mmol), **S22** (825 mg, 2.86 mmol), KF (333 mg, 5.73 mmol), XPhos (68 mg, 0.143 mmol) and $Pd(OAc)_2$ (16 mg, 0.072 mmol) were dissolved in a mix of degassed 1,4-dioxane (8.6 mL) and degassed H_2O (4.1 mL) under an atmosphere of argon. The reaction mixture was heated to 110 °C for 18 h. After cooling to rt, H_2O (40 mL) was added and it was extracted with EtOAc (3x). The combined organic layers were washed with brine and dried over anhydrous Na_2SO_4 before the solvent was removed under reduced pressure. Purification by flash chromatography (SiO_2, *n*-hexane:EtOAc 50:50 to 30:70) afforded 401 mg (65.1%) of a white solid. ^{1}H NMR (300 MHz, $CDCl_3$) δ -0.01 (s, 9H), 0.84 - 0.91 (m, 2H), 0.91 - 0.98 (m, 2H), 1.08 - 1.16 (m, 2H), 1.46 (t, *J* = 7.1 Hz, 3H), 1.56 - 1.66 (m, 1H), 3.53 - 3.63 (m, 2H), 4.47 (q, *J* = 7.2 Hz, 2H), 5.80 (s, 2H), 7.68 (dd, *J* = 5.3, 1.5 Hz, 1H), 7.78 (s, 1H), 8.29 (dd, *J* = 5.3, 0.6 Hz, 1H), 8.52 (d, *J* = 0.6 Hz, 1H), 8.99 (s, 1H). ^{13}C NMR (75 MHz, $CDCl_3$) δ -1.5, 8.4, 14.2, 15.8, 17.8, 62.0, 67.2, 77.1, 109.6, 116.1, 122.5, 136.9, 139.7, 142.8, 148.0, 152.0, 159.0, 172.7. TLC-MS (ESI) *m*/*z*: calculated for $C_{21}H_{30}N_4O_4Si$ $[M+Na]^+$ 453.2, found 453.5. HPLC: t_R = 9.55 min.

Ethyl 5-(2-(cyclopropanecarboxamido)pyridin-4-yl)-1*H*-imidazole-2-carboxylate (5a)

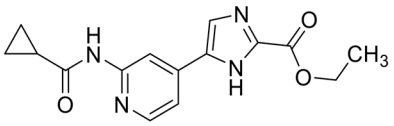

Compound **S22** (110 mg, 0.26 mmol) was treated according to **General Procedure E** and stirred at rt for 18 h. Sat. aq. $NaHCO_3$ solution was added until the aqueous phase was adjusted to pH 7. The organic phase was collected and the aqueous layer was extracted with DCM (2x). The combined organic layers were washed with brine and dried over anhydrous Na_2SO_4 before the solvent was removed under reduced pressure. Purification by flash chromatography (SiO_2, DCM:EtOH 95:5) afforded 72 mg (93.9%) of a white solid. ^{1}H NMR (300 MHz, DMSO-d_6) δ 0.74 - 0.90 (m, 4H), 1.34 (t, *J* = 7.1 Hz, 3H), 1.93 - 2.09 (m, 1H), 4.35 (q, *J* = 7.1 Hz, 2H), 7.49 (dd, *J* = 5.2, 1.4 Hz, 1H), 8.06 (s, 1H), 8.27 (d, *J* = 5.2 Hz, 1H), 8.54 (s, 1H), 10.74 (s, 1H), 13.65 (br. s., 1H). ^{13}C NMR (75 MHz, DMSO-d_6) δ 7.6, 14.2, 14.2, 61.0, 108.6, 115.1, 119.9, 137.9, 140.2, 142.7, 148.1, 152.8, 158.3, 172.6. TLC-MS (ESI) *m*/*z*: calculated for $C_{15}H_{16}N_4O_3$ $[M+H]^+$ 301.1, found 301.3. HPLC: t_R = 2.20 min (100.0% purity).

5-(2-(Cyclopropanecarboxamido)pyridin-4-yl)-1*H*-imidazole-2-carboxamide (6a)

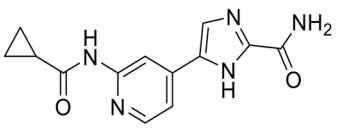

Compound **5a** (70 mg, 0.23 mmol) was dissolved in 7 M ammonia in MeOH (5 mL) and heated to 45 °C for 18 h. The solvent was removed under reduced pressure and purification by flash chromatography (SiO_2, DCM:EtOH 95:05 to 90:10) afforded 46 mg (73.5%) of a white solid. ^{1}H NMR (300 MHz, DMSO-d_6) δ 0.76 - 0.95 (m, 4H), 2.02 (quin, *J* = 6.1 Hz, 1H), 7.58 (dd, *J* = 5.5, 1.3 Hz, 1H), 7.63 (br. s., 1H), 7.80 (br. s., 1H), 7.99 (s, 1H), 8.27 (d, *J* = 5.5 Hz, 1H), 8.37 (s, 1H), 11.10 (br. s., 1H). ^{13}C NMR (75 MHz, DMSO-d_6) d 8.1, 14.4, 108.8, 115.3, 120.6, 138.0, 142.4, 144.2, 146.2, 151.7, 159.9, 173.2. TLC-MS (ESI) *m*/*z*: calculated for $C_{13}H_{13}N_5O_2$ $[M+H]^+$ 271.2, found 272.2. HPLC: t_R = 1.39 min (95.3% purity).

Ethyl 4-(5-bromo-2-(cyclopropanecarboxamido)pyridin-4-yl)-1-((2-(trimethylsilyl)ethoxy)methyl)-1*H*-imidazole-2-carboxylate (S23)

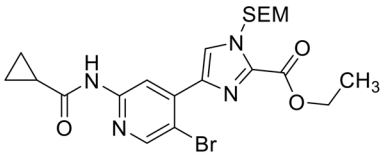

Compound **S22** (101 mg, 0.24 mmol) was dissolved in MeCN (2 mL) at -30 °C. *N*-Bromosuccinimide (44 mg, 0.25 mmol) was added in one portion and the solution was stirred at -30 °C. Reaction control after 10, 30 and 120 min showed no conversion so the solution was slowly brought to rt and stirred overnight. Reaction control now showed full conversion and the reaction was quenched with sat. aq. Na_2SO_3 solution and extracted with EtOAc (3x). The combined organic layers were washed with brine and dried over anhydrous Na_2SO_4 before the solvent was removed under reduced pressure. Purification by flash chromatography (SiO_2, *n*-hexane:EtOAc 80:20 to 20:80) afforded 83 mg (69.5%) of an off-white solid. ^{1}H NMR (300 MHz, $CDCl_3$) δ -0.02 (s, 9H), 0.84 - 0.92 (m, 2H), 0.92 - 0.99 (m, 2H), 1.11 (dd, *J* = 4.3, 3.0 Hz, 2H), 1.44 (t, *J* = 7.2 Hz, 3H), 1.54 - 1.65 (m, 1H), 3.57 - 3.66 (m, 2H), 4.44 (q, *J* = 7.1 Hz, 2H), 5.83 (s, 2H), 8.06 (s, 1H), 8.38 (s, 1H), 8.70 (s, 1H), 8.78 (s, 1H). ^{13}C NMR (75 MHz, $CDCl_3$) δ -1.5, 8.4, 14.2, 15.7, 17.8, 61.9, 67.1, 77.1, 112.4, 114.6, 124.9, 136.3, 137.5, 142.7, 150.1, 150.7, 159.1, 172.1. TLC-MS (ESI) *m*/*z*: calculated for $C_{21}H_{29}BrN_4O_4Si$ $[M+Na]^+$ 531.1/533.1, found 531.0/533.0. HPLC: t_R = 11.24 min.

5-(5-Bromo-2-(cyclopropanecarboxamido)pyridin-4-yl)-1*H*-imidazole-2-carboxamide (7)

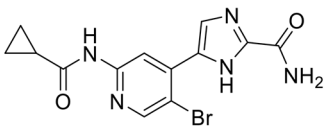

Compound **S23** (80 mg, 0.167 mmol) was suspended in 7 M ammonia in MeOH (3 mL) and stirred at 45 °C for 48 h. The solvent was removed under reduced pressure and the crude product was dissolved in a mix of DCM (4 mL), EtOH (2 mL) and trifluoroacetic acid (1 mL). The reaction was stirred at 45 °C for 48 h. Sat. aq. $NaHCO_3$ solution was added until the aqueous phase was adjusted to pH 7. The forming precipitate was collected by suction filtration and the aqueous phase was further extracted with EtOAc (2x) and DCM (2x). The organic layers were dried over anhydrous Na_2SO_4 and the solvent was removed under reduced pressure. The combined fractions were purified by flash chromatography (SiO_2,

DCM:EtOH 97:3 to 90:10) to afford 36 mg (61.7%) of a yellow solid which was poorly soluble in most organic solvents (MeOH, THF, MeCN, EtOAc, DCM, *n*-hexane). ^{1}H NMR (300 MHz, DMSO-d_6) δ 0.77 - 0.89 (m, 4H), 1.95 - 2.07 (m, 1H), 7.66 (br. s., 1H), 7.73 (br. s., 1H), 8.02 (s, 1H), 8.48 (s, 1H), 8.71 (s, 1H), 10.88 (s, 1H), 13.48 (br. s., 1H). ^{13}C NMR (75 MHz, DMSO-d_6) δ 7.8, 14.2, 111.2, 113.4, 121.0, 136.7, 141.5, 142.6, 150.4, 151.4, 159.7, 172.6. TLC-MS (ESI) *m*/*z*: calculated for $C_{13}H_{12}BrN_5O_2$ $[M+Na]^+$ 372.0/374.0, found 371.9/373.9. HPLC: t_R = 2.93 min (97.1% purity).

Synthesis of 6b

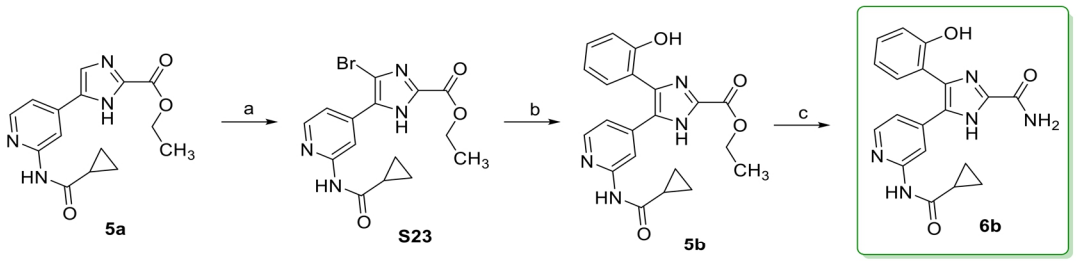

Scheme S9. *Reagents and conditions:* (a) NBS, MeCN, -20 °C, 1 h, 75%; (b) arylboronic acid, KF, Pd(dppf)Cl_2·DCM, 1,4-dioxane/H_2O, 85 °C, 18 h, 93%; (c) 7 M ammonia in MeOH, 45 °C, 18 h, 66-74%.

Ethyl 4-bromo-5-(2-(cyclopropanecarboxamido)pyridin-4-yl)-1*H*-imidazole-2-carboxylate (S23)

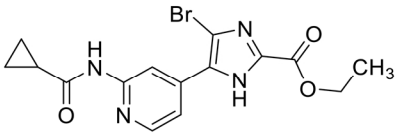

Compound **5a** (410 mg, 1.37 mmol) was dissolved in MeCN (2 mL) at -20 °C and *N*-bromosuccinimide (243 mg, 1.37 mmol) was added in one portion. The mixture was stirred at -20 °C for 1 h before it was quenched with. The aqueous phase was extracted with EtOAc (3x) and the combined organic layers were dried over anhydrous Na_2SO_4 and the solvent was removed under reduced pressure. Purification by flash chromatography (SiO_2, DCM:EtOH 97:3 to 95:5) afforded 389 mg (75.1%) of a pale white solid. ^{1}H NMR (300 MHz, DMSO-d_6) δ 0.75 - 0.88 (m, 4H), 1.27 - 1.37 (m, 3H), 1.97 - 2.09 (m, 1H), 4.35 (q, *J* = 7.2 Hz, 2H), 7.43 - 7.56 (m, 1H), 8.39 (d, *J* = 5.2 Hz, 1H), 8.64 (s, 1H), 10.89 (s, 1H), 14.37 (br. s., 1H). ^{13}C NMR (75 MHz, DMSO-d_6) δ 7.7, 14.1, 14.3, 61.4, 110.8, 116.8, 138.1, 148.3, 152.5, 157.6, 172.8. TLC-MS (ESI) *m*/*z*: calculated for $C_{15}H_{15}BrN_4O_3$ $[M+Na]^+$ 401.0/403.0, found 401.0/402.9. HPLC: t_R = 4.49 min.

Ethyl 5-(2-(cyclopropanecarboxamido)pyridin-4-yl)-4-(2-hydroxyphenyl)-1*H*-imidazole-2-carboxylate (5b)

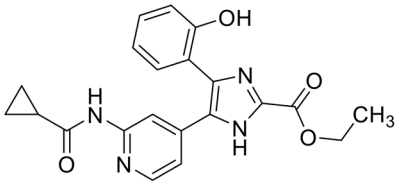

Compound **S23** (100 mg, 0.26 mmol), 2-hydroxyphenylboronic acid (73 mg, 0.53 mmol) and Pd(dppf)Cl_2·DCM were dissolved in degassed 1,4-dioxane (7 mL) under an atmosphere of argon and degassed 0.25 M aq. KF solution (3.25 mL) was added. The reaction was stirred at 90 °C for 18 h. Work-up was performed according to **General Procedure D**. Purification by flash chromatography (SiO_2, DCM:EtOH 97:3 to 95:5) afforded 96 mg (92.8%) of a solid. ^{1}H NMR (400 MHz, MeOD) δ 0.82 - 0.88 (m, 2H), 0.91 - 0.97 (m, 2H), 1.42 (t, *J* = 7.2 Hz, 3H), 1.78 - 1.89 (m, 1H), 4.44 (q, *J* = 7.1 Hz, 2H), 6.88 (t, *J* = 7.5 Hz, 1H), 6.93 (d, *J* = 8.1 Hz, 1H), 7.13 (d, *J* = 4.3 Hz, 1H), 7.21 (d, *J* = 7.5 Hz, 1H), 7.28 (t, *J* = 7.5 Hz, 1H), 8.12 (d, *J* = 4.3 Hz, 1H), 8.22 (br. s., 1H). TLC-MS (ESI) *m*/*z*: calculated for $C_{21}H_{20}N_4O_4$ $[M+H]^+$ 392.2, found 393.3. HPLC: t_R = 3.58 min.

5-(2-(Cyclopropanecarboxamido)pyridin-4-yl)-4-(2-hydroxyphenyl)-1*H*-imidazole-2-carboxamide (6b)

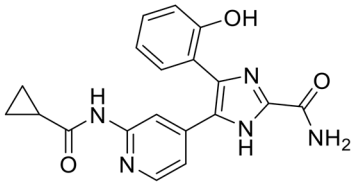

Compound **5b** (96 mg, 0.24 mmol) was dissolved in 7 M ammonia in MeOH (5 mL) and heated to 45 °C for 18 h. The solvent was removed under reduced pressure and the product was purified by flash chromatography (SiO_2, DCM:EtOH 95:5 to 90:10) to afford 59 mg (66.4%) of a beige-brown solid. ^{1}H NMR (400 MHz, DMSO-d_6) δ 0.69 - 0.84 (m, 4H), 1.83 - 2.12 (m, 1H), 6.81 - 6.91 (m, 2H), 6.95 (d, *J* = 8.1 Hz, 1H), 7.19 (d, *J* = 7.2 Hz, 1H), 7.27 (t, *J* = 7.3 Hz, 1H), 7.55 (br. s., 1H), 7.71 (br. s., 1H), 8.06 (d, *J* = 4.9 Hz, 1H), 8.40 (s, 1H), 9.70 (s, 1H), 10.60 (br. s., 1H), 13.17 (br. s., 1H). ^{13}C NMR (101 MHz, DMSO-d_6) δ 7.5, 14.2, 110.6, 115.9, 116.1, 117.2, 119.0, 129.6, 130.4, 131.5, 135.2, 140.7, 144.2, 147.2, 152.4, 155.5, 160.0, 172.2. TLC-MS (ESI) *m*/*z*: calculated for $C_{19}H_{17}N_5O_3$ $[M+H]^+$ 364.1, found 364.3. HPLC: t_R = 2.12 min (100.0% purity).

Synthesis of 5c and 6c-f

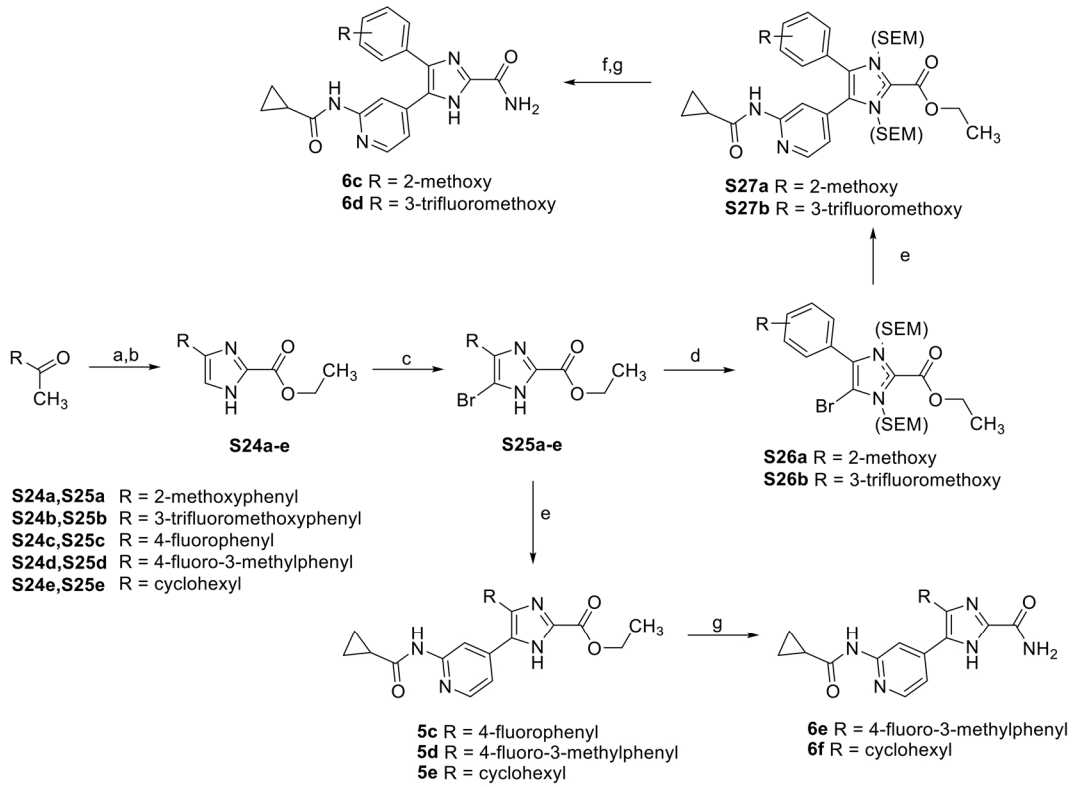

Scheme S10. *Reagents and conditions:* (a) 48% aq. HBr/DMSO, 55 °C, 18 h *or in case of* **S24e**: SeO_2, dioxane/H_2O (15:1), 110 °C; (b) ethyl glyoxylate (polymer form ~50% in toluene), NH_4OAc, MeOH/MeCN, rt, 1.5 h, 41-71%; (c) NBS, MeCN, 0 °C, 1 h, 53-74% *or in case of* **S25a**: Br_2, DCM/2M aq. Na_2CO_3, 0 °C to rt, 14 h, 63%; (d) SEM-Cl, K_2CO_3, DMF, 0 °C to rt, 3.5-6.5 h, 62-86%; (e) **S11**, K_2CO_3, Pd(dppf)Cl_2·DCM, DMF, 80 °C, 18 h, 71-84% *or in case of* **S26a**: **S11**, KF, Xphos, $Pd(OAc)_2$, 1,4-dioxane/H_2O (3:1), 110 °C, 18 h, 44%; (f) 7 M ammonia in MeOH, rt *or* 45 °C, 18-96 h, 59-78% (for **6c** & **6d**); (g) trifluoroacetic acid, DCM, rt, 48 h 45-70% (*over 2 steps* for **6d** and **6e**).

Ethyl 4-(2-methoxyphenyl)-1*H*-imidazole-2-carboxylate (S24a)

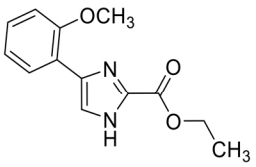

2'-Methoxyacetophenone (826 mg, 5.50 mmol) was treated according to **General Procedure C**. Purification by flash chromatography (SiO_2, DCM:EtOH 97:3 to 90:10) afforded 763 mg (56.3%) of a red oil. ^{1}H NMR (300 MHz, DMSO-d_6) δ 1.34 (t, *J* = 7.1 Hz, 3H), 3.91 (s, 3H), 4.35 (q, *J* = 7.2 Hz, 2H), 7.01 (td, *J* = 7.5, 1.0 Hz, 1H), 7.08 (d, *J* = 8.1 Hz, 1H), 7.21 - 7.30 (m, 1H), 7.69 (br. s., 1H), 8.07 (br. s., 1H),

13.39 (br. s., 1H). TLC-MS (ESI) *m*/*z*: calculated for $C_{13}H_{14}N_2O_3$ $[M+Na]^+$ 269.1, found 269.4. HPLC: t_R = 4.18 min.

Ethyl 4-(4-fluoro-3-methylphenyl)-1*H*-imidazole-2-carboxylate (S24b)

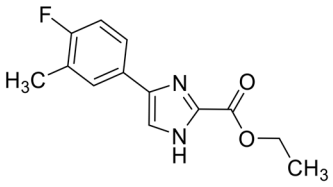

4'-Fluoro-3'-methylacetophenone (500 mg, 3.29 mmol) was treated according to **General Procedure C**. Purification by flash chromatography (SiO_2, DCM:EtOH 97:3) afforded 582 mg (71.4%) of a red oil. ^{1}H NMR (300 MHz, $CDCl_3$) δ 1.34 (t, *J* = 7.2 Hz, 3H), 2.26 (d, *J* = 1.7 Hz, 3H), 4.40 (q, *J* = 7.2 Hz, 2H), 6.99 (t, *J* = 8.9 Hz, 1H), 7.45 (s, 1H), 7.48 - 7.56 (m, 1H), 7.61 (d, *J* = 7.1 Hz, 1H). ^{13}C NMR (75 MHz, $CDCl_3$) δ 14.0, 14.4 (d, $^3J_{CF}$ = 3.3 Hz), 61.8, 115.2 (d, $^2J_{CF}$ = 22.7 Hz), 124.3 (d, $^3J_{CF}$ = 7.7 Hz), 125.1 (d, $^2J_{CF}$ = 17.7 Hz), 128.6 (d, $^3J_{CF}$ = 5.5 Hz), 137.8, 159.1, 160.9 (d, $^1J_{CF}$ = 246.0 Hz). TLC-MS (ESI) *m*/*z*: calculated for $C_{13}H_{13}FN_2O_2$ $[M+Na]^+$ 271.1, found 271.1. HPLC: t_R = 6.13 min.

Ethyl 4-(4-fluorophenyl)-1*H*-imidazole-2-carboxylate (S24c)

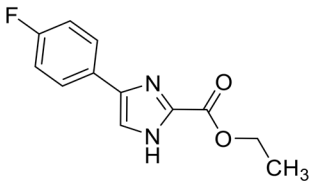

4'-Fluoroacetophenone (863 mg, 6.25 mmol) was treated according to **General Procedure C**. Purification by flash chromatography (SiO_2, DCM:EtOH 97:3) afforded 606 mg (41.4%) of a red oil. ^{1}H NMR (300 MHz, DMSO-d_6) δ 1.34 (t, *J* = 7.1 Hz, 3H), 4.35 (q, *J* = 7.1 Hz, 2H), 7.22 (t, *J* = 8.8 Hz, 2H), 7.79 - 7.95 (m, 3H), 13.46 (br. s., 1H). ^{13}C NMR (75 MHz, DMSO-d_6) δ 14.2, 60.8, 115.4 (d, $^2J_{CF}$ = 22.1 Hz), 117.3, 126.6 (d, $^3J_{CF}$ = 7.7 Hz), 130.3 (d, $^4J_{CF}$ = 2.8 Hz), 137.2, 141.6, 158.4, 161.4 (d, $^1J_{CF}$ = 246.0 Hz). TLC-MS (ESI) *m*/*z*: calculated for $C_{12}H_{11}FN_2O_2$ $[M-H]^-$ 233.1, found 233.1. HPLC: t_R = 4.59 min.

Ethyl 4-(3-(trifluoromethoxy)phenyl)-1*H*-imidazole-2-carboxylate (S24d)

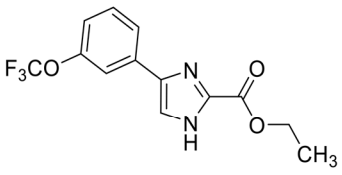

3'-(Trifluoromethoxy)acetophenone (866 mg, 3.67 mmol) was treated according to **General Procedure C**. Purification by flash chromatography (SiO_2, *n*-hexane:EtOAc 70:30 to 50:50) afforded 580 mg 2(52.7%) of a red oil. ^{1}H NMR (300 MHz, $CDCl_3$) δ 1.33 (t, *J* = 7.1 Hz, 3H), 4.41 (q, *J* = 7.1 Hz, 2H), 7.13

(d, *J* = 8.2 Hz, 1H), 7.38 (t, *J* = 8.0 Hz, 1H), 7.56 (s, 1H), 7.63 - 7.76 (m, 2H), 10.43 (br. s., 1H). TLC-MS (ESI) *m*/*z*: calculated for $C_{13}H_{11}F_3N_2O_3$ $[M+H]^+$ 301.1, found 300.9. HPLC: t_R = 7.47 min.

Ethyl 4-cyclohexyl-1*H*-imidazole-2-carboxylate (S24e)

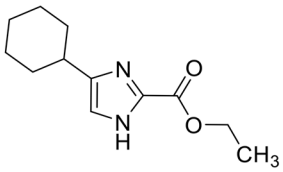

Cyclohexyl methyl ketone (500 mg, 3.96 mmol) was oxidized with selenium dioxide (484 mg, 4.36 mmol) according to a literature procedure[6] and then treated further according to **General Procedure C**. Purification by flash chromatography (SiO_2, DCM:EtOH 97:3) afforded 385 mg (43.7%) of an orange solid. ^{1}H NMR (300 MHz, $CDCl_3$) δ 1.24 - 1.48 (m, 8H), 1.65 - 1.85 (m, 3H), 1.98 - 2.09 (m, 2H), 2.59 - 2.72 (m, 1H), 4.38 (q, *J* = 7.2 Hz, 2H), 6.96 (d, *J* = 0.6 Hz, 1H). ^{13}C NMR (75 MHz, $CDCl_3$) δ 13.7, 25.6, 25.8, 32.4, 35.7, 60.9, 121.2, 136.2, 145.0, 159.0. TLC-MS (ESI) *m*/*z*: calculated for $C_{12}H_{18}N_2O_2$ $[M+H]^+$ 223.1, found 223.1. HPLC: t_R = 3.64 min.

Ethyl 5-bromo-4-(2-methoxyphenyl)-1*H*-imidazole-2-carboxylate (S25a)

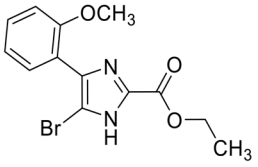

Compound **S24a** (400 mg, 1.62 mmol) was dissolved in DCM (5 mL) and 2M aq. Na_2CO_3 solution (5 mL). The mixture was cooled to 0 °C and bromine (100 µL, 1.95 mmol) was added dropwise. The reaction was further stirred at rt overnight before sat. aq. NaS_2O_3 solution was added and it was extracted with DCM (3x). The combined organic layers were dried over anhydrous Na_2SO_4 and the solvent was removed under reduced pressure. Purification by flash chromatography (SiO_2, *n*-hexane:EtOAc 60:40) afforded 333 mg (63.1%) of a yellow solid. ^{1}H NMR (300 MHz, $CDCl_3$) δ 1.40 (t, *J* = 7.2 Hz, 3H), 3.92 (s, 3H), 4.42 (q, *J* = 7.2 Hz, 2H), 7.01 (d, *J* = 8.4 Hz, 1H), 7.08 (td, *J* = 7.6, 1.0 Hz, 1H), 7.37 (ddd, *J* = 8.3, 7.5, 1.7 Hz, 1H), 8.08 (dd, *J* = 7.8, 1.6 Hz, 1H), 11.15 (br. s., 1H). ^{13}C NMR (75 MHz, $CDCl_3$) δ 14.2, 55.8, 62.0, 111.3, 115.6, 115.9, 121.0, 128.4, 129.2, 130.4, 135.5, 155.7, 158.3. TLC-MS (ESI) *m*/*z*: calculated for $C_{13}H_{13}BrN_2O_3$ $[M+Na]^+$ 247.0/249.0, found 347.2/349.2. HPLC: t_R = 5.89 min.

Ethyl 5-bromo-4-(3-(trifluoromethoxy)phenyl)-1*H*-imidazole-2-carboxylate (S25b)

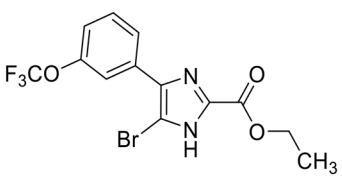

Compound **S24b** (580 mg, 1.93 mmol) was dissolved in MeCN, cooled to 0 °C and *N*-bromosuccinimide (344 mg, 1.93 mmol) was added in one portion. The mixture was stirred for 1 h at 0 °C before the reaction was quenched with sat. aq. Na_2SO_3 solution. The aqueous phase was extracted with EtOAc (3x) and the combined organic layers were dried over anhydrous Na_2SO_4 and the solvent was removed under reduced pressure. Purification by flash chromatography (SiO_2, *n*-hexane:EtOAc 90:10) afforded 541 mg (73.9%) of the title compound. ^{1}H NMR (300 MHz, $CDCl_3$) δ 1.30 (t, *J* = 7.2 Hz, 3H), 4.35 (q, *J* = 7.2 Hz, 2H), 7.22 - 7.28 (m, 1H), 7.48 (t, *J* = 8.1 Hz, 1H), 7.70 (s, 1H), 7.77 (d, *J* = 7.9 Hz, 1H), 12.11 (br. s., 1H). ^{13}C NMR (75 MHz, $CDCl_3$) δ 13.9, 62.6, 119.9, 120.4 (d, $^1J_{OCF3}$ = 258.2 Hz), 121.0, 125.6, 130.2, 137.1, 149.4, 158.6. TLC-MS (ESI) *m*/*z*: calculated for $C_{13}H_{10}BrF_3N_2O_3$ $[M+Na]^+$ 401.0/403.0, found 400.8/402.7. HPLC: t_R = 9.61 min.

Ethyl 5-bromo-4-(4-fluorophenyl)-1*H*-imidazole-2-carboxylate (S25c)

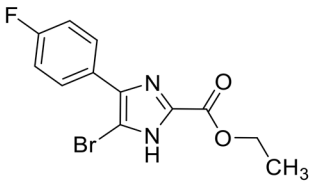

The title compound was prepared following the procedure as described for compound **S25b** starting from compound **S24c** (540 mg, 2.31 mmol) and *N*-bromosuccinimide (410 mg, 2.31 mmol). Purification by flash chromatography (SiO_2, *n*-hexane:EtOAc 80:20) afforded 430 mg (59.4%) of a white solid. ^{1}H NMR (300 MHz, $CDCl_3$) δ 1.28 (t, *J* = 7.2 Hz, 3H), 4.31 (q, *J* = 7.2 Hz, 2H), 7.13 (t, *J* = 8.6 Hz, 2H), 7.71 - 7.83 (m, 2H), 12.02 (br. s, 1H). ^{13}C NMR (75 MHz, $CDCl_3$) δ 14.0, 62.4, 115.8 (d, $^2J_{CF}$ = 21.6 Hz), 129.4 (d, $^3J_{CF}$ = 8.8 Hz), 136.6, 158.7, 162.8 (d, $^1J_{CF}$ = 246.0 Hz). TLC-MS (ESI) *m*/*z*: calculated for $C_{12}H_{10}BrFN_2O_2$ $[M+Na]^+$ 335.0/337.0, found 335.2/337.2. HPLC: t_R = 6.84 min.

Ethyl 5-bromo-4-(4-fluoro-3-methylphenyl)-1*H*-imidazole-2-carboxylate (S25d)

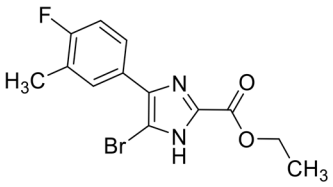

The title compound was prepared following the procedure as described for compound **S25b** starting from compound **S24d** (470 mg, 1.89 mmol) and *N*-bromosuccinimide (337 mg, 1.89 mmol). Purification by flash chromatography (SiO_2, *n*-hexane:EtOAc 80:20) afforded 384 mg (52.8%) of a yellow solid. ^{1}H NMR (300 MHz, $CDCl_3$) δ 1.29 (t, *J* = 7.1 Hz, 3H), 2.31 (s, 3H), 4.31 (q, *J* = 7.1 Hz, 2H), 7.06 (t, *J* = 8.8 Hz, 1H), 7.48 - 7.66 (m, 2H), 11.71 (br. s., 1H). ^{13}C NMR (75 MHz, $CDCl_3$) δ 14.0, 14.6 (d, $^3J_{CF}$ = 3.3 Hz), 62.3, 115.4 (d, $^2J_{CF}$ = 23.2 Hz), 125.5 (d, $^2J_{CF}$ = 17.7 Hz), 126.7 (d, $^3J_{CF}$ = 8.3 Hz), 130.7 (d, $^3J_{CF}$ = 5.5 Hz), 136.5, 158.6, 161.5 (d, $^1J_{CF}$ = 249.3 Hz). TLC-MS (ESI) *m*/*z*: calculated for $C_{13}H_{12}BrFN_2O_2$ $[M+Na]^+$ 349.0/351.0, found 349.2/351.2. HPLC: t_R = 8.14 min.

Ethyl 4-cyclohexyl-1*H*-imidazole-2-carboxylate (S25e)

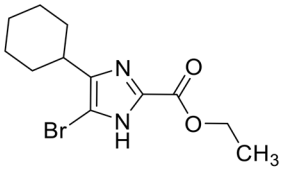

The title compound was prepared following the procedure as described for compound **S25b** starting from compound **S24e** (380 mg, 1.71 mmol) and *N*-bromosuccinimide (304 mg, 1.71 mmol). Purification by flash chromatography (SiO_2, *n*-hexane:EtOAc 80:20) afforded 299 mg (58.1%) of a white solid. ^{1}H NMR (300 MHz, $CDCl_3$) δ 1.17 - 1.59 (m, 5H), 1.36 (t, *J* = 7.2 Hz, 3H), 1.71 - 1.97 (m, 5H), 2.78 (tt, *J* = 11.8, 3.3 Hz, 1H), 4.40 (q, *J* = 7.2 Hz, 2H), 10.98 (br. s., 1H). ^{13}C NMR (75 MHz, $CDCl_3$) δ 13.7, 25.4, 26.0, 31.3, 34.9, 61.5, 114.0, 135.3, 138.2, 158.3. TLC-MS (ESI) *m*/*z*: calculated for $C_{12}H_{17}BrN_2O_2$ $[M+Na]^+$ 323.0/325.0, found 323.2/325.2. HPLC: t_R = 8.31 min.

Ethyl 5(4)-bromo-4(5)-(2-methoxyphenyl)-1-((2-(trimethylsilyl)ethoxy)methyl)-1*H*-imidazole-2-carboxylate (S26a)

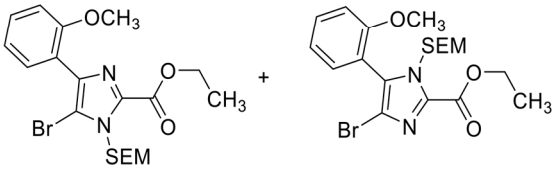

Compound **S25a** (326 mg, 1.00 mmol) was dissolved in DMF (3 mL) and cooled to 0 °C before K_2CO_3 (180 mg, 1.10 mmol) was added. After stirring for 30 min, SEM-Cl (195 µL, 1.30 mmol) was added and the reaction was further stirred at rt for 3 h. H_2O (35 mL) was added and it was extracted with EtOAc (3x). The combined organic layers were dried over anhydrous Na_2SO_4 and the solvent was removed under reduced pressure. Purification by flash chromatography (SiO_2, *n*-hexane:EtOAc 90:10 to 50:50) afforded 280 mg (61.5%) of a clear oil, containing both regioisomers. TLC-MS (ESI) *m*/*z*: calculated for $C_{19}H_{27}N_2O_4Si$ $[M+Na]^+$ 477.1/479.1, found 476.8/478.8.

Ethyl 4(5)-bromo-5(4)-(3-(trifluoromethoxy)phenyl)-1-((2-(trimethylsilyl)ethoxy)methyl)-1*H*-imidazole-2-carboxylate (S26b)

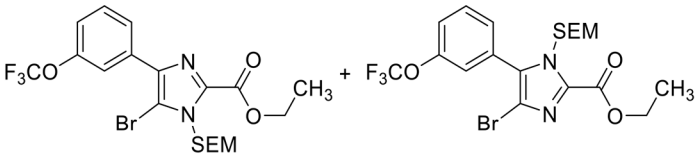

Compound **S25b** (490 mg, 1.30 mmol) was dissolved in DMF (3 mL) and cooled to 0 °C before K_2CO_3 (215 mg, 1.56 mmol) was added. After stirring for 30 min, SEM-Cl (259 µL, 1.57 mmol) was added and the reaction was further stirred at rt for 6 h. H_2O (35 mL) was added and it was extracted with EtOAc (3x). The combined organic layers were dried over anhydrous Na_2SO_4 and the solvent was removed under reduced pressure. Purification by flash chromatography (SiO_2, *n*-hexane:EtOAc 95:05 to 85:05)

afforded 565 mg (85.6%) of a mix of regioisomers (ratio 4.3:1). *isomer 1:* ^{1}H NMR (300 MHz, $CDCl_3$) δ 0.00 (s, 9H), 0.83 - 1.05 (m, 2H), 1.46 (t, *J* = 7.2 Hz, 3H), 3.66 (dd, *J* = 8.7, 7.7 Hz, 2H), 4.49 (q, *J* = 7.1 Hz, 2H), 5.96 (s, 2H), 7.21 (ddt, *J* = 8.2, 2.3, 1.0 Hz, 1H), 7.46 (t, *J* = 8.0 Hz, 1H), 7.87 (s, 1H), 7.94 (dt, *J* = 7.8, 1.2 Hz, 1H). *isomer 2:* ^{1}H NMR (300 MHz, $CDCl_3$) δ 0.00 (s, 9H), 0.86 - 0.94 (m, 2H), 1.45 (t, *J* = 7.2 Hz, 3H), 3.54 - 3.62 (m, 2H), 4.47 (q, *J* = 7.1 Hz, 2H), 5.66 (s, 2H), 7.35 (dd, *J* = 6.7, 1.0 Hz, 1H), 7.47 - 7.56 (m, 3H). TLC-MS (ESI) *m*/*z*: calculated for $C_{19}H_{24}BrF_3N_2O_4Si$ $[M+Na]^+$ 531.1/533.1, found 530.8/532.9. HPLC: t_R = 12.55 min & 14.27 min.

Ethyl 5(4)-(2-(cyclopropanecarboxamido)pyridin-4-yl)-4(5)-(2-methoxyphenyl)-1-((2-(trimethylsilyl)ethoxy)methyl)-1*H*-imidazole-2-carboxylate (S27a)

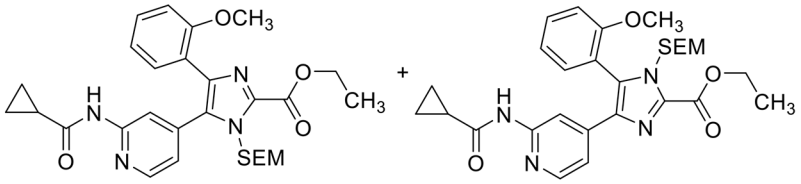

Compound **S26a** (265 mg, 0.70 mmol), **S11** (406 mg, 1.41 mmol), KF (164 mg, 2.82 mmol), XPhos (34 mg, 0.070 mmol) and $Pd(OAc)_2$ (8 mg, 0.035 mmol) were dissolved in a mix of degassed 1,4-dioxane (6 mL) and degassed H_2O (2 mL) under an atmosphere of argon. The reaction mixture was heated to 110 °C for 18 h. After cooling to rt, H_2O (40 mL) was added and it was extracted with EtOAc (3x). The combined organic layers were washed with brine and dried over anhydrous Na_2SO_4 before the solvent was removed under reduced pressure. Purification by flash chromatography (SiO_2, *n*-hexane:EtOAc 70:30 to 50:50) afforded 165 mg (43.7%) of a mix of regioisomers which could not be separated completely by column chromatograpy. *example NMR for one pure isomer:* ^{1}H NMR (300 MHz, $CDCl_3$) δ -0.11 (s, 9H), 0.68 - 0.80 (m, 4H), 0.95 - 1.03 (m, 2H), 1.44 (t, *J* = 7.1 Hz, 3H), 1.49 - 1.57 (m, 1H), 3.26 - 3.37 (m, 2H), 3.70 (s, 3H), 4.46 (q, *J* = 7.1 Hz, 2H), 5.22 (d, *J* = 10.2 Hz, 1H), 5.88 (d, *J* = 10.3 Hz, 1H), 6.98 - 7.09 (m, 3H), 7.21 (d, *J* = 6.8 Hz, 1H), 7.47 (t, *J* = 7.5 Hz, 1H), 8.04 (d, *J* = 5.3 Hz, 1H), 8.29 (s, 1H), 9.31 (s, 1H). ^{13}C NMR (75 MHz, $CDCl_3$) δ -1.6, 7.9, 14.2, 15.4, 17.7, 55.4, 61.6, 66.1, 73.8, 111.5, 111.8, 117.1, 117.2, 121.0, 131.6, 132.6, 132.7, 136.8, 136.9, 143.8, 146.8, 151.9, 157.7, 159.2, 171.8. TLC-MS (ESI) *m*/*z*: calculated for $C_{28}H_{36}N_4O_5Si$ $[M+H]^+$ 537.3, found 537.3.

Ethyl 4-(2-(cyclopropanecarboxamido)pyridin-4-yl)-5-(3-(trifluoromethoxy)phenyl)-1-((2-(trimethylsilyl)ethoxy)methyl)-1*H*-imidazole-2-carboxylate or ethyl 5-(2-(cyclopropanecarboxamido)pyridin-4-yl)-4-(3-(trifluoromethoxy)phenyl)-1-((2-(trimethylsilyl)ethoxy)methyl)-1*H*-imidazole-2-carboxylate (S27b)

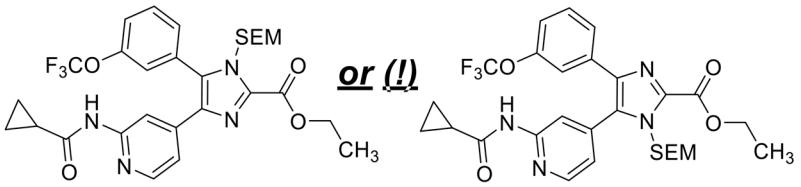

The title compound was synthesized according to **General Procedure F** starting from one (*not closer characterized*) pure regioisomer of **S26b** (250 mg, 0.49 mmol), **S11** (219 mg, 0.76 mmol), potassium carbonate (203 mg, 1.47 mmol) and $Pd(dppf)Cl_2$·DCM (40 mg, 0.049 mmol). Purification by flash chromatography (SiO_2, *n*-hexane:EtOAc 70:30) afforded 213 mg (73.5%) of the title compound. ^{1}H NMR (300 MHz, $CDCl_3$) δ -0.02 (s, 9H), 0.84 - 0.97 (m, 4H), 1.07 - 1.16 (m, 2H), 1.50 (t, *J* = 7.1 Hz, 3H), 1.58 - 1.68 (m, 1H), 3.47 - 3.59 (m, 2H), 4.53 (q, *J* = 7.1 Hz, 2H), 5.74 (s, 2H), 7.04 - 7.13 (m, 2H), 7.28 - 7.35 (m, 2H), 7.49 (dt, *J* = 7.9, 1.2 Hz, 1H), 8.34 - 8.41 (m, 2H), 8.92 (s, 1H). ^{13}C NMR (75 MHz, $CDCl_3$) δ -1.5, 8.5, 14.3, 15.7, 17.7, 62.1, 66.4, 73.7, 115.4, 120.3, 120.0, 120.2 (d, $^1J_{OCF3}$ = 257.1 Hz), 121.2, 126.1, 129.7, 131.7, 134.7, 137.3, 138.7, 139.6, 148.3, 149.1, 152.4, 159.1, 172.4. TLC-MS (ESI) *m*/*z*: calculated for $C_{28}H_{33}F_3N_4O_5Si$ $[M+Na]^+$ 613.2, found 613.0.

5-(2-(Cyclopropanecarboxamido)pyridin-4-yl)-4-(2-methoxyphenyl)-1*H*-imidazole-2-carboxamide (6c)

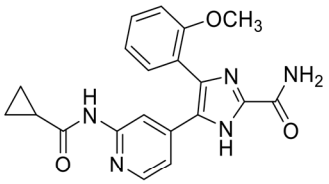

Compound **S27a** (160 mg, 0.30 mmol) was dissolved in 7 M ammonia in MeOH (5 mL) and stirred at 45 °C for 48 h. The solvent was removed under reduced pressure and the crude product was redissolved in DCM (3 mL) and trifluoroacetic acid (3 mL). The solution was stirred at rt for 48 h and work-up was performed according to **General Procedure E**. Purification by flash chromatography (SiO_2, DCM:EtOH 99:1 to 95:5) afforded 51 mg (45.3%) of a tan white solid. ^{1}H NMR (300 MHz, DMSO-d_6) δ 0.70 - 0.88 (m, 4H), 1.97 (quin, *J* = 6.2 Hz, 1H), 3.60 (s, 3H), 6.89 (dd, *J* = 5.3, 1.3 Hz, 1H), 7.00 (t, *J* = 7.3 Hz, 1H), 7.10 (d, *J* = 8.3 Hz, 1H), 7.27 (d, *J* = 6.4 Hz, 1H), 7.39 - 7.48 (m, 1H), 7.57 (br. s., 1H), 7.75 (br. s., 1H), 8.07 (d, *J* = 5.3 Hz, 1H), 8.29 (s, 1H), 10.66 (s, 1H), 13.27 (br. s., 1H). ^{13}C NMR (75 MHz, DMSO-d_6) δ 7.6, 14.2, 55.2, 110.5, 111.7, 116.1, 120.4, 130.6, 131.4, 141.0, 147.0, 152.2, 157.0, 160.0, 172.3. TLC-MS (ESI) *m*/*z*: calculated for $C_{20}H_{19}N_5O_3$ $[M+Na]^+$ 400.1, found 400.0. HPLC: t_R = 2.08 min (98.5%).

5-(2-(Cyclopropanecarboxamido)pyridin-4-yl)-4-(3-(trifluoromethoxy)phenyl)-1*H*-imidazole-2-carboxamide (6d)

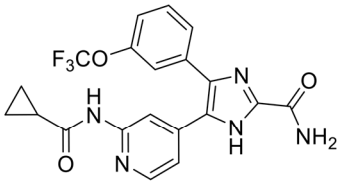

Compound **S27b** (213 mg, 0.36 mmol) was dissolved in 7 M ammonia in MeOH (4 mL) and stirred at rt for 96 h. The solvent was removed under reduced pressure and the crude product was redissolved in DCM (3 mL) and trifluoroacetic acid (3 mL). The solution was stirred at rt for 48 h and work-up was performed according to **General Procedure E**. Purification by flash chromatography (SiO_2, DCM:EtOH

95:5) afforded 109 mg (70.1%) of a white solid. ^{1}H NMR (300 MHz, DMSO-d_6) δ 0.70 - 0.85 (m, 4H), 1.91 - 2.06 (m, 1H), 6.97 - 7.43 (m, 3H), 7.52 (br. s., 2H), 7.64 (s, 1H), 7.89 (br. s., 1H), 8.12 - 8.37 (m, 2H), 10.57 - 10.96 (m, 1H), 13.71 (br. s., 1H). ^{13}C NMR (75 MHz, DMSO-d_6) δ 7.6, 14.1, 111.6, 117.5, 119.7, 120.0 (d, $^{1}J_{OCF3}$ = 256.5 Hz), 120.9, 127.8, 130.6, 141.9, 143.5, 147.8, 148.3, 152.6, 159.8, 172.4. TLC-MS (ESI) *m*/*z*: calculated for $C_{20}H_{16}F_3N_5O_3$ [M-H]$^-$ 430.1, found 429.8. HPLC: t_R = 6.30 min (100.0%).

Ethyl 5-(2-(cyclopropanecarboxamido)pyridin-4-yl)-4-(4-fluorophenyl)-1*H*-imidazole-2-carboxylate (5c)

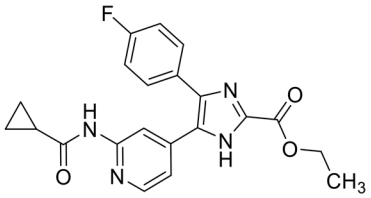

The title compound was synthesized according to **General Procedure F** starting from compound **S25c** (200 mg, 0.64 mmol), **S11** (239 mg, 0.83 mmol), potassium carbonate (265 mg, 1.92 mmol) and Pd(dppf)Cl_2·DCM (31 mg, 0.038 mmol). Purification by flash chromatography (SiO_2, DCM:EtOH 97:3) afforded 198 mg (78.7%) of a white solid. ^{1}H NMR (300 MHz, $CDCl_3$) δ 0.80 - 0.92 (m, 2H), 0.99 - 1.09 (m, 2H), 1.39 (t, *J* = 7.1 Hz, 3H), 1.53 - 1.71 (m, 1H), 4.42 (q, *J* = 7.1 Hz, 2H), 7.05 (t, *J* = 8.4 Hz, 3H), 7.36 - 7.54 (m, 2H), 7.91 (d, *J* = 5.1 Hz, 1H), 8.36 (s, 1H), 9.14 (br. s., 1H), 12.25 (br. s., 1H). ^{13}C NMR (75 MHz, $CDCl_3$) δ 8.5, 14.2, 15.6, 62.2, 112.2, 115.9, 118.0, 130.6, 137.8, 147.3, 151.9, 159.4, 163.0, 172.6. TLC-MS (ESI) *m*/*z*: calculated for $C_{21}H_{19}FN_4O_3$ [M+Na]$^+$ 417.1, found 417.4. HPLC: t_R = 4.85 min (97.6% purity).

Ethyl 5-(2-(cyclopropanecarboxamido)pyridin-4-yl)-4-(4-fluoro-3-methylphenyl)-1*H*-imidazole-2-carboxylate (5d)

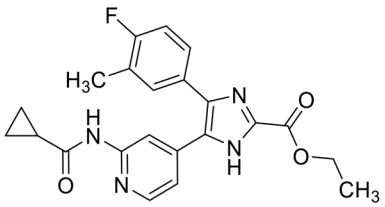

The title compound was synthesized according to **General Procedure F** starting from compound **S25d** (200 mg, 0.61 mmol), **S11** (229 mg, 0.79 mmol), potassium carbonate (265 mg, 1.83 mmol) and Pd(dppf)Cl_2·DCM (30 mg, 0.037 mmol). Purification by flash chromatography (SiO_2, DCM:EtOH 97:3) afforded 208 mg (83.5%) of a white solid. ^{1}H NMR (300 MHz, $CDCl_3$) δ 0.84 (d, *J* = 3.7 Hz, 2H), 1.03 (br. s., 2H), 1.39 (t, *J* = 7.0 Hz, 3H), 1.63 (br. s., 1H), 2.21 (s, 3H), 4.42 (q, *J* = 6.9 Hz, 2H), 6.95 (t, *J* = 8.6 Hz, 1H), 7.03 - 7.24 (m, 2H), 7.33 (br. s., 1H), 7.91 (d, *J* = 3.3 Hz, 1H), 8.38 (s, 1H), 9.23 (br. s., 1H), 12.39 (br. s., 1H). TLC-MS (ESI) *m*/*z*: calculated for $C_{22}H_{21}FN_4O_3$ [M+Na]$^+$ 431.2, found 431.4. HPLC: t_R = 6.49 min.

Ethyl 4-cyclohexyl-5-(2-(cyclopropanecarboxamido)pyridin-4-yl)-1*H*-imidazole-2-carboxylate (5e)

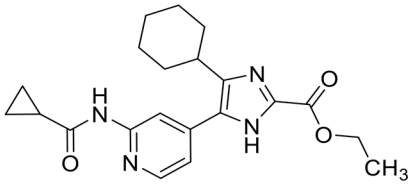

The title compound was synthesized according to **General Procedure F** starting from compound **S25e** (200 mg, 0.66 mmol), **S11** (287 mg, 1.00 mmol), potassium carbonate (277 mg, 2.00 mmol) and Pd(dppf)Cl_2·DCM (43 mg, 0.053 mmol). Purification by flash chromatography (SiO_2, DCM:EtOH 95:05) afforded 179 mg (70.5%) of a white solid. ^{1}H NMR (300 MHz, $CDCl_3$) δ 0.79 - 0.89 (m, 2H), 1.03 - 1.12 (m, 2H), 1.38 (t, *J* = 7.2 Hz, 3H), 1.41 - 1.58 (m, 3H), 1.60 - 1.66 (m, 1H), 1.69 - 2.05 (m, 5H), 2.60 (br. s., 2H), 3.09 (br. s., 1H), 4.41 (q, *J* = 7.1 Hz, 2H), 7.44 (dd, *J* = 5.1, 1.7 Hz, 1H), 8.24 (d, *J* = 5.2 Hz, 1H), 8.43 (s, 1H), 9.27 (br. s., 1H), 11.15 (br. s., 1H). TLC-MS (ESI) *m*/*z*: calculated for $C_{21}H_{26}N_4O_3$ $[M+Na]^+$ 405.2, found 405.6. HPLC: t_R = 6.93 min.

5-(2-(Cyclopropanecarboxamido)pyridin-4-yl)-4-(4-fluoro-3-methylphenyl)-1*H*-imidazole-2-carboxamide (6e)

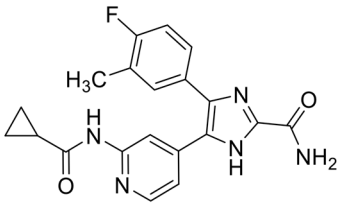

Compound **5d** (190 mg, 0.47 mmol) was dissolved in 7 M ammonia in MeOH (4 mL) and stirred at rt for 18 h. The solvent was removed under reduced pressure and purification by flash chromatography (SiO_2, DCM:EtOH 97:3 to 95:5) afforded 104 mg (58.9%) of a white solid. ^{1}H NMR (300 MHz, DMSO-d_6) δ 0.66 - 0.87 (m, 4H), 1.88 - 2.08 (m, 1H), 2.22 (s, 3H), 7.05 (d, *J* = 5.0 Hz, 1H), 7.12 - 7.31 (m, 2H), 7.43 (d, *J* = 7.2 Hz, 1H), 7.59 (s, 1H), 7.79 (br. s., 1H), 8.16 (d, *J* = 5.2 Hz, 1H), 8.34 (s, 1H), 10.68 (s, 1H), 13.45 (br. s., 1H). ^{13}C NMR (75 MHz, DMSO-d_6) δ 7.6, 14.1 (d, $^3J_{CF}$ = 3.3 Hz), 14.2, 111.2, 115.2 (d, $^2J_{CF}$ = 22.1 Hz), 117.2, 124.6, 125.6, 128.5, 131.4, 132.3, 134.7, 141.2, 143.8, 147.6, 152.5, 159.9, 160.7 (d, $^1J_{CF}$ = 246.2 Hz), 172.4. TLC-MS (ESI) *m*/*z*: calculated for $C_{20}H_{18}FN_5O_2$ $[M+Na]^+$ 402.1, found 402.3. HPLC: t_R = 4.85 min (99.0%).

4-Cyclohexyl-5-(2-(cyclopropanecarboxamido)pyridin-4-yl)-1*H*-imidazole-2-carboxamide (6f)

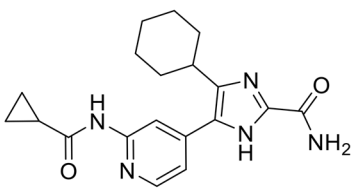

Compound **5e** (170 mg, 0.44 mmol) was dissolved in 7 M ammonia in MeOH (4 mL) and stirred at rt for 18 h. The solvent was removed under reduced pressure and purification by flash chromatography (SiO_2, DCM:EtOH 95:5 to 90:10) afforded 123 mg (78.3%) of a white solid. ^{1}H NMR (300 MHz, DMSO-d_6) δ 0.77 - 0.86 (m, 4H), 1.14 - 1.43 (m, 3H), 1.62 - 1.86 (m, 7H), 1.97 - 2.07 (m, 1H), 2.90 - 3.03 (m, 1H), 7.30 (dd, *J* = 5.2, 1.5 Hz, 1H), 7.47 (br. s., 1H), 7.68 (br. s., 1H), 8.29 (d, *J* = 5.2 Hz, 1H), 8.33 (s, 1H), 10.74 (s, 1H), 12.98 (s, 1H). ^{13}C NMR (75 MHz, DMSO-d_6) δ 7.6, 14.3, 25.2, 26.1, 31.5, 34.8, 111.0, 117.2, 133.6, 138.5, 140.3, 144.0, 147.9, 152.4, 160.1, 172.6. TLC-MS (ESI) *m*/*z*: calculated for $C_{19}H_{23}N_5O_2$ $[M+H]^+$ 354.2, found 354.5. HPLC: t_R = 5.19 min (99.5% purity).

Synthesis of 6g

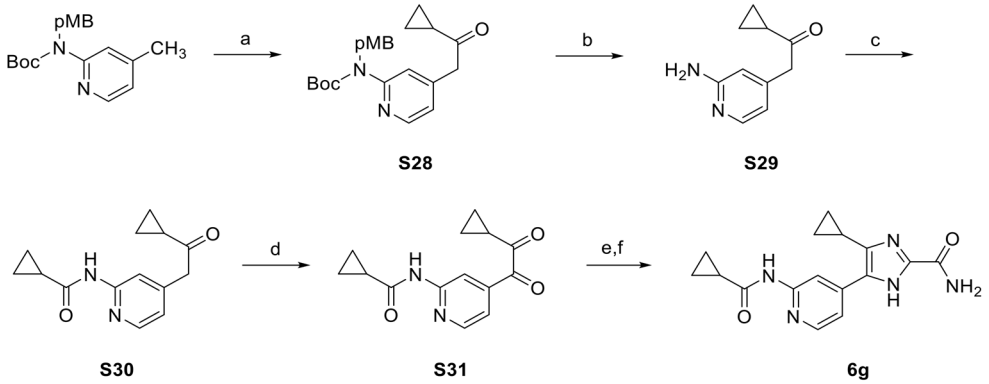

Scheme S11. *Reagents and conditions:* (a) 2.0M NaHMDS in THF, ethyl cyclopropanecarboxylate, THF, 0 °C then rt, 2 h, 68%; (b) trifluoroacetic acid, DCM, 55 °C, 48 h, 78%; (c) cyclopropanecarbonyl chloride, pyridine, DCM, 0 °C then rt, 18 h, 85%; (d) SeO_2, acetic acid, 70 °C, 3 h, 38%; (e) ethyl glyoxylate (polymer form ~50% in toluene), NH_4OAc, THF/MeOH, rt, 18 h, 38%; (f) 7 M ammonia in MeOH, 45 °C, 72 h, 65%.

tert-Butyl (4-(2-cyclopropyl-2-oxoethyl)pyridin-2-yl)(4-methoxybenzyl)carbamate (S28)

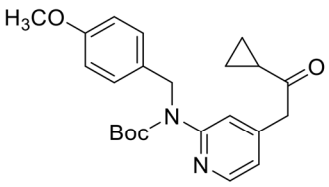

tert-Butyl (4-methoxybenzyl)(4-methylpyridin-2-yl)carbamate (1500 mg, 4.66 mmol) was dissolved in THF (60 mL) under an atmosphere of argon. The solution was cooled to 0 °C before 2M sodium bis(trimethylsilyl)amide in THF (4.75 mL, 9.50 mmol) was added via syringe over 10 min and the resulting mixture was stirred for 45 min while still being cooled to 0 °C. Then ethyl

cyclopropanecarboxylate (783 mg, 6.88 mmol) dissolved in THF (5 mL) was added in one portion and the reaction was further stirred for 2 h at rt. H_2O (150 mL) was added, the organic layer was separated, and it was extracted with EtOAc (3x). The combined organic layers were dried over anhydrous Na_2SO_4 and the solvent was removed under reduced pressure. Purification by flash chromatography (SiO_2, *n*-hexane:EtOAc 75:25) afforded 1.23 g (67.8%) of the title compound. ^{1}H NMR (300 MHz, $CDCl_3$) δ 0.83 - 0.94 (m, 2H), 1.01 - 1.11 (m, 2H), 1.42 (s, 9H), 1.89 - 2.00 (m, 1H), 3.77 (s, 3H), 3.82 (s, 2H), 5.12 (s, 2H), 6.75 - 6.83 (m, 2H), 6.88 (dd, *J* = 5.0, 1.4 Hz, 1H), 7.18 - 7.25 (m, 2H), 7.57 (s, 1H), 8.33 (d, *J* = 5.0 Hz, 1H). ^{13}C NMR (75 MHz, $CDCl_3$) δ 11.6, 20.4, 28.2, 49.4, 49.8, 55.2, 81.3, 113.5, 120.4, 120.6, 128.7, 131.5, 144.2, 147.5, 154.2, 154.8, 158.4, 206.5. TLC-MS (ESI) *m*/*z*: calculated for $C_{23}H_{28}N_2O_3$ $[M+Na]^+$ 419.2, found 419.3. HPLC: t_R = 8.28 min.

2-(2-Aminopyridin-4-yl)-1-cyclopropylethan-1-one (S29)

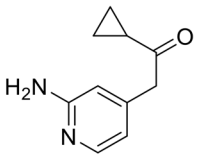

Compound **S28** (1.23 g, 3.16 mmol) was dissolved in DCM (2 mL) and trifluoroacetic acid (2 mL) and heated to 55 °C for 48 h. The solvent was evaporated and the product was redissolved in EtOAc and then washed with sat. aq. $NaHCO_3$ solution (2x). The organic layer was removed under reduced pressure to afford 435 mg (78.1%) of the title compound. ^{1}H NMR (300 MHz, $CDCl_3$) δ 0.80 - 0.93 (m, 2H), 1.00 - 1.11 (m, 2H), 1.95 (tt, *J* = 7.8, 4.5 Hz, 1H), 3.70 (s, 2H), 4.34 (br. s., 2H), 6.37 (d, *J* = 0.6 Hz, 1H), 6.52 (dd, *J* = 5.2, 1.5 Hz, 1H), 8.00 (dd, *J* = 5.3, 0.4 Hz, 1H). ^{13}C NMR (75 MHz, $CDCl_3$) δ 11.6, 20.3, 49.8, 109.2, 115.3, 144.9, 148.2, 158.7, 206.9. TLC-MS (ESI) *m*/*z*: calculated for $C_{10}H_{12}N_2O$ $[M+H]^+$ 177.1, found 177.1. HPLC: t_R = 1.13 min.

***N*-(4-(2-Cyclopropyl-2-oxoethyl)pyridin-2-yl)cyclopropanecarboxamide (S30)**

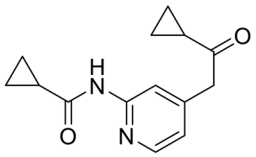

Compound **S29** (435 mg, 2.36 mmol) was dissolved in DCM (10 mL), cooled to 0 °C and pyridine (242 µL, 2.94 mmol) was added slowly. After 5 min, cyclopropanecarbonyl chloride (195 µL, 2.60 mmol) was added dropwise and the resulting solution was stirred at rt for 18 h. The solvents were removed under reduced pressure and purification by flash chromatography (SiO_2, DCM:EtOH 97:3) afforded 490 mg (85.0%) of a clear oil. ^{1}H NMR (300 MHz, $CDCl_3$) δ 0.76 - 0.92 (m, 4H), 0.99 - 1.13 (m, 4H), 1.54 - 1.68 (m, 1H), 1.96 (tt, *J* = 7.8, 4.6 Hz, 1H), 3.83 (s, 2H), 6.88 (dd, *J* = 5.2, 1.5 Hz, 1H), 8.15 (s, 1H), 8.19 (d, *J* = 5.1 Hz, 1H), 9.83 (br. s., 1H). ^{13}C NMR (75 MHz, $CDCl_3$) δ 8.2, 11.5, 15.4, 20.5, 49.8, 115.4, 120.6, 145.9, 147.2, 152.2, 172.7, 206.3. TLC-MS (ESI) *m*/*z*: calculated for $C_{14}H_{16}N_2O_2$ $[M+Na]^+$ 267.1, found 267.1. HPLC: t_R = 1.67 min.

***N*-(4-(2-Cyclopropyl-2-oxoacetyl)pyridin-2-yl)cyclopropanecarboxamide (S31)**

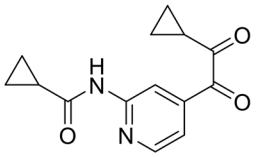

Compound **S30** (450 mg, 1.84 mmol) was dissolved in glacial acetic acid (10 mL) and selenium dioxide (232 mg, 2.09 mmol) was added. The mixture was heated to 70 °C for 3 h. After cooling to rt, the solution was filtered over celite, the solvent was removed in vacuo and redissolved in DCM. The organic phase was washed with sat. aq. $NaHCO_3$ solution (2x) and then removed under reduced pressure. Purification by flash chromatography (SiO_2, *n*-hexane:EtOAc 60:40) afforded 180 mg (37.8%) of a yellow-orange oil. ^{1}H NMR (300 MHz, $CDCl_3$) δ 0.84 - 0.99 (m, 4H), 1.07 - 1.18 (m, 4H), 1.61 - 1.70 (m, 1H), 2.64 (tt, *J* = 7.8, 4.6 Hz, 1H), 7.52 (dd, *J* = 5.2, 1.5 Hz, 1H), 8.40 (dd, *J* = 5.2, 0.7 Hz, 1H), 8.73 (s, 1H), 9.27 (br. s., 1H). ^{13}C NMR (75 MHz, $CDCl_3$) δ 8.7, 13.9, 15.7, 18.0, 114.4, 118.3, 141.3, 148.1, 152.7, 172.8, 190.0, 200.1. TLC-MS (ESI) *m*/*z*: calculated for $C_{14}H_{14}N_2O_3$ $[M-H]^-$ 257.1, found 257.1. HPLC: t_R = 2.60 min.

5-(2-(Cyclopropanecarboxamido)pyridin-4-yl)-4-cyclopropyl-1*H*-imidazole-2-carboxamide (6g)

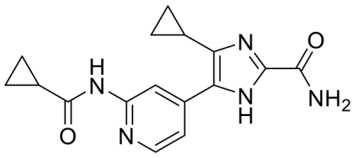

Compound **S31** (180 mg, 0.70 mmol) was dissolved in THF (5 mL) and ethyl glyoxylate (polymer form ~50% in toluene; 428 µL, 2.10 mmol) was added in one portion. A previously prepared solution of NH_4OAc (540 mg, 7.00 mmol) in MeOH (3 mL) was now added and the solution was stirred at rt for 18 h. The solvent was removed under reduced pressure and H_2O (40 mL) was added before it was extracted with EtOAc (3x). The combined organic layers were dried over anhydrous Na_2SO_4 and the solvent was removed under reduced pressure. The crude product was dissolved in 7 M ammonia in MeOH (4 mL) and the mixture was heated to 45 °C for 18 h. The solvent was removed under reduced pressure and purification by flash chromatography (SiO_2, DCM:EtOH 90:10) afforded 17 mg (7.8%) of a white solid. ^{1}H NMR (400 MHz, DMSO-*d*$_6$) δ 0.78 - 0.84 (m, 4H), 0.87 - 0.92 (m, 2H), 0.98 - 1.06 (m, 2H), 1.99 - 2.07 (m, 2H), 7.48 (br. s., 1H), 7.55 (dd, *J* = 5.3, 1.5 Hz, 1H), 7.66 (br. s., 1H), 8.28 (dd, *J* = 5.3, 0.5 Hz, 1H), 8.64 (s, 1H), 10.71 (s, 1H), 12.84 (s, 1H). ^{13}C NMR (101 MHz, DMSO-*d*$_6$) δ 7.1, 7.6, 7.8, 14.3, 110.2, 116.4, 135.2, 135.4, 139.4, 143.7, 147.7, 152.4, 160.0, 172.5. TLC-MS (ESI) *m*/*z*: calculated for $C_{16}H_{17}N_5O_2$ $[M+Na]^+$ 334.1, found 334.4. HPLC: t_R = 1.95 min (98.8% purity).

Synthesis of 8 and 6h

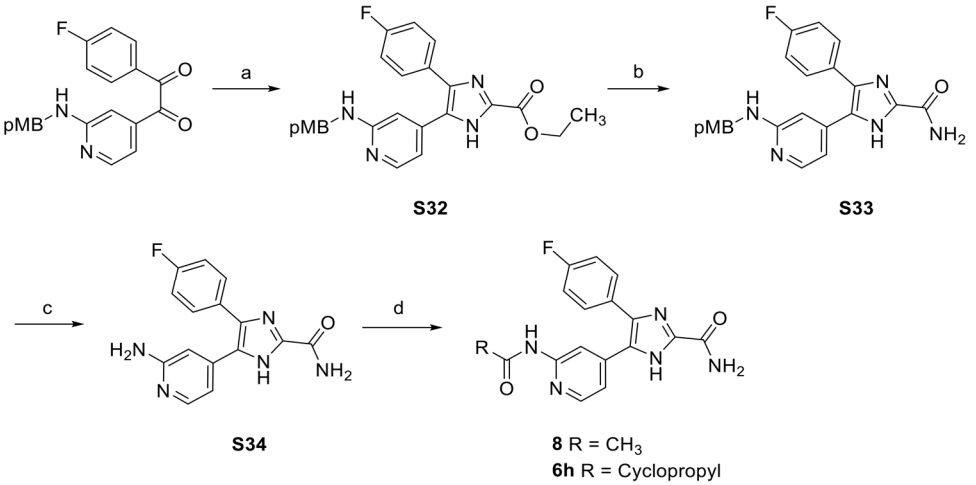

Scheme S12. *Reagents and conditions:* (a) ethyl glyoxylate (polymer form ~50% in toluene), NH_4OAc, MeOH, rt, 18 h, 38%; (b) 7 M ammonia in MeOH, 45 °C, 72 h, 65%; (c) trifluoroacetic acid, DCM, 55 °C, 6 h, 91%; (d) cyclopropanecarbonyl chloride *or* acetyl chloride, pyridine, 0 °C then rt, 18 h, 39-49%.

Ethyl 4-(4-fluorophenyl)-5-(2-((4-methoxybenzyl)amino)pyridin-4-yl)-1*H*-imidazole-2-carboxylate (S32)

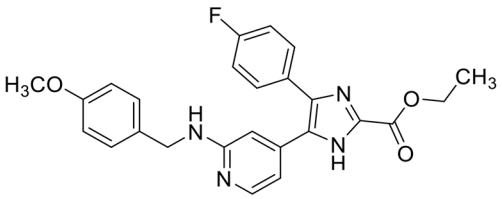

1-(4-Fluorophenyl)-2-(2-((4-methoxybenzyl)amino)pyridin-4-yl)ethane-1,2-dione[2] (500 mg, 1.37 mmol) was dissolved in THF (7 mL) and ethyl glyoxylate (polymer form ~50% in toluene; 841 µL, 4.12 mmol) was added in one portion. A previously prepared solution of NH_4OAc (1.06 g, 13.72 mmol) in MeOH (5 mL) was now added and the solution was stirred at rt for 18 h. The solvent was removed under reduced pressure and H_2O (40 mL) was added before it was extracted with EtOAc (3x). The combined organic layers were dried over anhydrous Na_2SO_4 and the solvent was removed under reduced pressure. Purification by flash chromatography (SiO_2, *n*-hexane:EtOAc 50:50 to 0:100) afforded 230 mg (37.6%) of a yellow resin. ^{1}H NMR (300 MHz, $CDCl_3$) δ 1.32 (t, *J* = 7.1 Hz, 3H), 3.76 (s, 3H), 4.22 (s, 2H), 4.36 (q, *J* = 7.2 Hz, 2H), 5.81 (br. s, 1H), 6.57 (br. s., 1H), 6.65 (d, *J* = 5.4 Hz, 1H), 6.77 - 6.82 (m, 2H), 6.96 - 7.04 (m, 2H), 7.12 (d, *J* = 8.6 Hz, 2H), 7.41 (dd, *J* = 8.4, 5.4 Hz, 2H), 7.80 (d, *J* = 5.5 Hz, 1H). ^{13}C NMR (75 MHz, $CDCl_3$) δ 14.1, 45.6, 55.2, 62.1, 104.7, 111.5, 113.9, 115.7 (d, $^2J_{CF}$ = 21.6 Hz), 128.4, 130.4, 130.6 (d, $^3J_{CF}$ = 8.3 Hz), 137.5, 147.0, 158.6, 158.8, 159.2, 162.8 (d, $^1J_{CF}$ = 249.3 Hz). TLC-MS (ESI) *m*/*z*: calculated for $C_{25}H_{23}FN_4O_3$ $[M+H]^+$ 447.2, found 447.0. HPLC: t_R = 6.38 min.

4-(4-Fluorophenyl)-5-(2-((4-methoxybenzyl)amino)pyridin-4-yl)-1*H*-imidazole-2-carboxamide (S33)

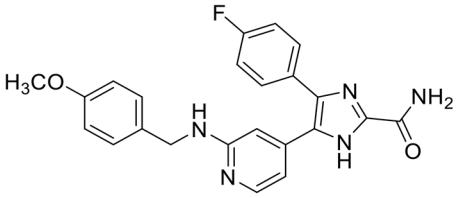

Compound **S32** (330 mg, 0.74 mmol) was dissolved in 7 M ammonia in MeOH (4 mL) and the mixture was heated to 45 °C for 72 h. The solvent was evaporated and H_2O (10 mL) was added before it was extracted with EtOAc (3x). The combined organic layers were dried over anhydrous Na_2SO_4 before the solvent was removed under reduced pressure to yield 200 mg (64.8%) of a cream-colored solid. ^{1}H NMR (300 MHz, DMSO-d_6) δ 3.72 (s, 3H), 4.28 - 4.39 (m, 2H), 6.48 - 6.66 (m, 2H), 6.86 (dd, *J* = 8.6, 3.5 Hz, 2H), 7.13 - 7.31 (m, 4H), 7.44 - 7.60 (m, 3H), 7.66 - 8.03 (m, 3H), 13.43 (br. s., 1H). TLC-MS (ESI) *m*/*z*: calculated for $C_{23}H_{20}FN_5O_2$ $[M+H]^+$ 418.2, found 418.1. HPLC: t_R = 4.60 min.

5-(2-Aminopyridin-4-yl)-4-(4-fluorophenyl)-1*H*-imidazole-2-carboxamide (S34)

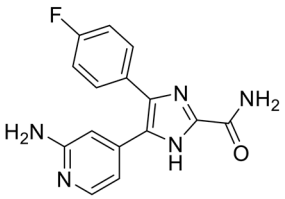

Compound **S33** (190 mg, 0.46 mmol) was dissolved in DCM (3 mL) and trifluoroacetic acid (3 mL). The solution was heated to 55 °C for 6 h before the reaction was quenched with sat. aq. $NaHCO_3$ solution and it was extracted with DCM (3x). Purification by flash chromatography (SiO_2, DCM:EtOH 97:3 to 95:5) afforded 124 mg (90.5%) of an off-white solid. ^{1}H NMR (300 MHz, DMSO-d_6) δ 5.89 (br. s., 2H), 6.50 (dd, *J* = 5.3, 1.5 Hz, 1H), 6.57 (s, 1H), 7.25 (t, *J* = 8.7 Hz, 2H), 7.47 - 7.55 (m, 2H), 7.57 (br. s., 1H), 7.80 (br. s., 1H), 7.84 (d, *J* = 5.2 Hz, 1H), 12.28 (br. s., 1H). TLC-MS (ESI) *m*/*z*: calculated for $C_{15}H_{12}FN_5O$ $[M+H]^+$ 298.1, found 298.0. HPLC: t_R = 2.19 min.

5-(2-(Cyclopropanecarboxamido)pyridin-4-yl)-4-(4-fluorophenyl)-1*H*-imidazole-2-carboxamide (6h)

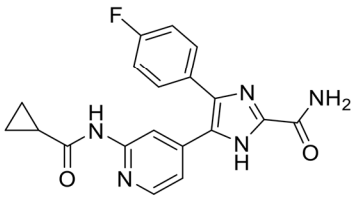

Compound **S34** (35 mg, 0.12 mmol) was dissolved in pyridine (4 mL) and cooled to 0 °C. Cyclopropanecarbonyl chloride (11.75 µL, 0.13 mmol) was added and the mixture was stirred at rt for

18 h. The solvent was removed in vacuo and purification by flash chromatography (SiO_2, DCM:EtOH 95:5) afforded 21 mg (48.8%) of a sand-colored solid. ^{1}H NMR (300 MHz, DMSO-d_6) δ 0.73 - 0.84 (m, 4H), 1.91 - 2.04 (m, 1H), 7.04 (dd, J = 5.2, 1.6 Hz, 1H), 7.24 (t, J = 8.9 Hz, 2H), 7.49 (dd, J = 8.9, 5.5 Hz, 2H), 7.60 (br. s, 1H), 7.84 (br. s., 1H), 8.20 (d, J = 5.2 Hz, 1H), 8.25 (s, 1H), 10.77 (s, 1H). ^{13}C NMR (75 MHz, DMSO-d_6) δ 7.8, 14.3, 111.7, 115.6 (d, $^2J_{CF}$ = 21.6 Hz), 117.6, 130.9 (d, $^3J_{CF}$ = 8.3 Hz), 141.5, 147.6, 152.4, 160.0, 162.1 (d, $^1J_{CF}$ = 246.5 Hz), 172.6. TLC-MS (ESI) m/z: calculated for $C_{19}H_{16}FN_5O_2$ $[M+Na]^+$ 388.1, found 388.1. HPLC: t_R = 3.95 min (96.8% purity).

5-(2-Acetamidopyridin-4-yl)-4-(4-fluorophenyl)-1*H*-imidazole-2-carboxamide (8)

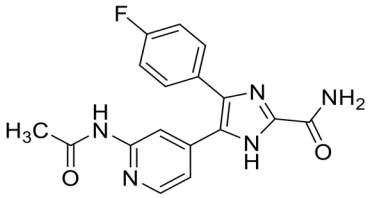

The title compound was prepared following the procedure as described for compound **6h** starting from compound **S34** (150 mg, 0.50 mmol) and acetyl chloride (47 µL, 0.66 mmol). Purification by flash chromatography (SiO_2, DCM:EtOH 95:5 to 90:10) afforded 64 mg (37.4%) of an orange solid. ^{1}H NMR (300 MHz, DMSO-d_6) δ 2.05 (s, 3H), 7.10 (dd, J = 5.2, 1.6 Hz, 1H), 7.23 (t, J = 8.8 Hz, 2H), 7.50 (dd, J = 8.8, 5.5 Hz, 2H), 7.61 (s, 1H), 7.85 (s, 1H), 8.20 (d, J = 5.3 Hz, 1H), 8.23 (s, 1H), 10.42 (s, 1H), 13.51 (br. s, 1H). ^{13}C NMR (75 MHz, DMSO-d_6) δ 23.9, 111.4, 115.6 (d, $^2J_{CF}$ = 22.1 Hz), 117.6, 130.8 (d, $^3J_{CF}$ = 8.3 Hz), 141.4, 147.8, 152.4, 159.9, 162.0 (d, $^1J_{CF}$ = 246.6 Hz), 169.1. TLC-MS (ESI) m/z: calculated for $C_{17}H_{14}FN_5O_2$ $[M+Na]^+$ 362.1, found 362.2. HPLC: t_R = 2.14 min (98.1% purity).

Synthesis of 6i

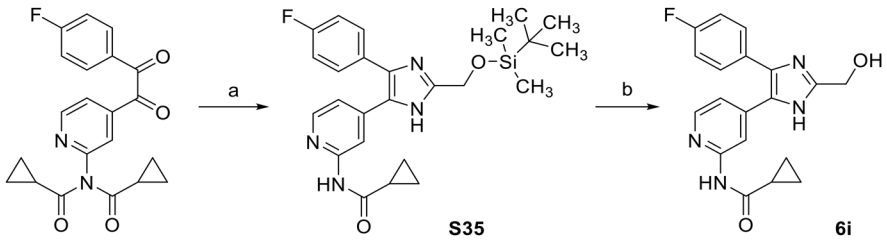

Scheme S13. *Reagents and conditions:* (a) (*tert*-butyldimethylsilyloxy)acetaldehyde, NH_4OAc, MeOH, 80 °C, 4 h, 20%; (b) Tetrabutylammonium fluoride in THF, rt, 5 h, 46%.

_N_-(4-(2-(((tert-Butyldimethylsilyl)oxy)methyl)-4-(4-fluorophenyl)-1_H_-imidazol-5-yl)pyridin-2-yl)cyclopropanecarboxamide (S35)

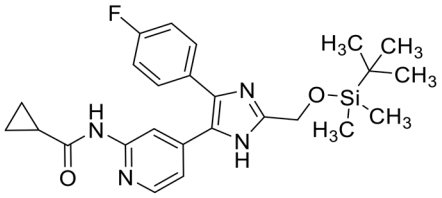

_N_-(Cyclopropanecarbonyl)-_N_-(4-(2-(4-fluorophenyl)-2-oxoacetyl)pyridin-2-yl)cyclo-propanecarbox-amide[2] (313 mg, 0.82 mmol), 2-((_tert_-butyldimethylsilyl)oxy)acetaldehyde (251 µL, 1.32 mmol) and NH_4OAc (1.27 g, 16.46 mmol) were dissolved in MeOH (8 mL). The reaction mixture was heated to 80 °C for 4 h. Work-up was performed according to **General Procedure A**. Purification by flash chromatography (SiO_2, _n_-hexane:EtOAc 80:20 to 0:100) afforded 78 mg (20.3%) of a brown solid. ^{1}H NMR (300 MHz, $CDCl_3$) δ 0.14 (s, 6H), 0.81 - 0.88 (m, 2H), 0.94 (s, 9H), 1.01 - 1.10 (m, 2H), 1.50 - 1.65 (m, 1H), 4.86 (s, 2H), 6.96 - 7.11 (m, 3H), 7.39 - 7.49 (m, 2H), 8.07 (d, _J_ = 5.4 Hz, 1H), 8.33 (br. s, 1H), 9.10 (s, 1H). TLC-MS (ESI) _m/z_: calculated for $C_{25}H_{31}FN_4O_2Si$ $[M+H]^+$ 467.2, found 467.7. HPLC: t_R = 9.95 min.

_N_-(4-(4-(4-Fluorophenyl)-2-(hydroxymethyl)-1_H_-imidazol-5-yl)pyridin-2-yl)cyclopropanecarboxamide (6i)

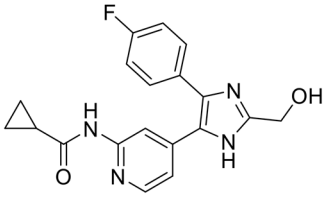

Compound **S35** (78 mg, 0.67 mmol) was dissolved in 1.0M TBAF in THF (5 mL) and stirred at rt for 5 h. Purification by flash chromatography (SiO_2, DCM:EtOH 95:5) afforded 27 mg (45.8%) of a yellow-orange solid. ^{1}H NMR (300 MHz, MeOD) δ 0.14 (s, 6H), 0.81 - 0.88 (m, 2H), 0.94 (s, 9H), 1.01 - 1.10 (m, 2H), 1.50 - 1.65 (m, 1H), 4.86 (s, 2H), 6.96 - 7.11 (m, 3H), 7.39 - 7.49 (m, 2H), 8.07 (d, _J_ = 5.4 Hz, 1H), 8.33 (br. s, 1H), 9.10 (s, 1H). ^{13}C NMR (75 MHz, MeOD) δ 8.6, 15.7, 58.3, 113.6, 116.8 (d, $^2J_{CF}$ = 22.1 Hz), 119.1, 129.5 (d, $^4J_{CF}$ = 3.3 Hz), 131.8 (d, $^3J_{CF}$ = 8.3 Hz), 144.5, 149.1, 150.6, 153.6, 164.2 (d, $^1J_{CF}$ = 246.6 Hz), 175.3. TLC-MS (ESI) _m/z_: calculated for $C_{19}H_{17}FN_4O_2$ $[M+H]^+$ 353.1, found 353.4. HPLC: t_R = 2.78 min (95.9% purity).

Synthesis of 6j

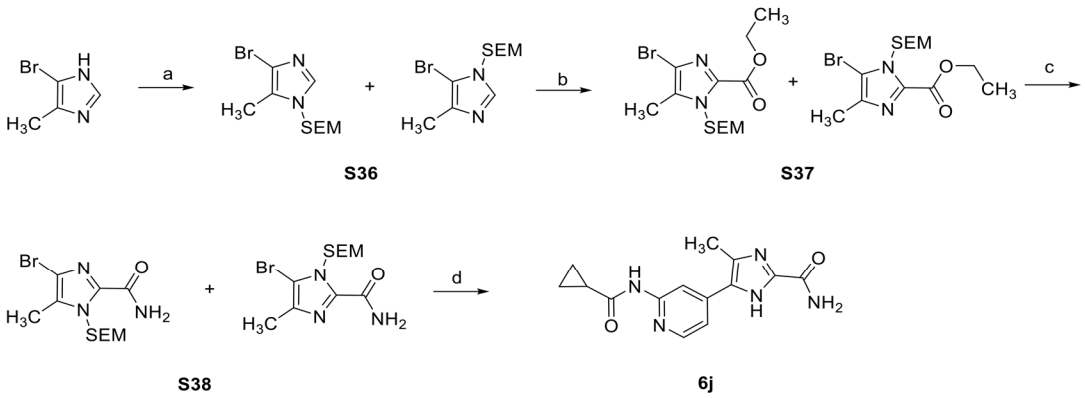

Scheme S14. *Reagents and conditions:* (a) NaH, SEM-Cl, THF, 0 °C then rt, 18 h, 98%; (b) 2.0 M Lithium diisopropylamide solution in THF/heptane/ethylbenzene, ethyl chloroformate, THF, -78 °C, 2 h, 32%; (c) 7 M ammonia in MeOH, rt, 18 h, 88%; (d) **S11**, Na_2CO_3, cataCXium® A, $Pd(OAc)_2$, DME/H2O, 90 °C, 18 h, 40%.

Ethyl 4(5)-bromo-5(4)-methyl-1*H*-imidazole-2-carboxylate (S36)

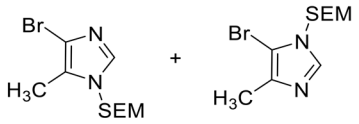

The title compound was prepared following the procedure as described for compound **S20** starting from 4-bromo-5-methyl-1*H*-imidazole (820 mg, 5.09 mmol), NaH 60% dispersion in mineral oil (305 mg, 7.64 mmol) and 2-(trimethylsilyl)ethoxymethyl chloride (991 µL, 5.60 mmol). Purification by flash chromatography (SiO_2, *n*-hexane:EtOAc 90:10 to 60:40) afforded 1.46 g (98.3%) of a clear oil (mix of both regioisomers). ^{1}H NMR (300 MHz, DMSO-d_6) δ -0.03 (s, 18H, *2x (CH₃)₃ of SEM*), 0.74 - 0.91 (m, 4H, *2x CH₂ of SEM*), 2.06 (s, 3H, *CH₃[1]*), 2.15 (s, 3H, *CH₃[2]*), 3.39 - 3.51 (m, 4H, *2x CH₂ of SEM*), 5.24 (s, 2H, *CH₂ of SEM[1]*), 5.29 (s, 2H, *CH₂ of SEM[2]*), 7.75 (s, 1H, *Imid.-CH[1]*), 7.90 (s, 1H, *Imid.-CH[2]*). TLC-MS (ESI) *m/z*: calculated for $C_{10}H_{19}BrN_2OSi$ $[M+H]^+$ 291.0/293.0, found 291.0/293.1. HPLC: t_R = 7.57 min + 8.90 min.

Ethyl 4(5)-bromo-5(4)-methyl-1-((2-(trimethylsilyl)ethoxy)methyl)-1*H*-imidazole-2-carboxylate (S37)

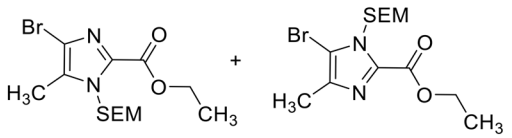

The title compound was prepared following the procedure as described for compound **S21** starting from **S36** (550 mg, 1.88 mmol), lithium diisopropylamide 2.0M solution in THF/heptane/ethylbenzene (944 µL, 1.88 mmol) and ethyl chloroformate (550 µL, 5.76 mmol). Work-up was performed according to the synthesis of **S21**. Purification by flash chromatography (SiO_2, *n*-hexane:EtOAc 90:10 to 50:50) afforded 220 mg (32.1%) of a mix of regioisomers which could not be separated completely by column chromatograpy. *example NMR for one pure isomer:* ^{1}H NMR (300 MHz, $CDCl_3$) δ -0.01 (s, 9H), 0.85 - 0.94 (m, 2H), 1.39 (t, *J* = 7.2 Hz, 3H), 2.33 (s, 3H), 3.51 - 3.61 (m, 2H), 4.40 (q, *J* = 7.1 Hz, 2H), 5.82 (s, 2H). ^{13}C NMR (75 MHz, $CDCl_3$) δ -1.5, 9.6, 14.2, 17.7, 61.8, 66.3, 74.0, 116.3, 132.5, 135.3, 158.4. TLC-MS (ESI) *m*/*z*: calculated for $C_{13}H_{23}BrN_2O_3Si$ $[M+Na]^+$ 385.1/387.1, found 385.2/387.2. HPLC: t_R = 10.14 min & 10.37 min.

4(5)-Bromo-5(4)-methyl-1-((2-(trimethylsilyl)ethoxy)methyl)-1H-imidazole-2-carboxamide (S38)

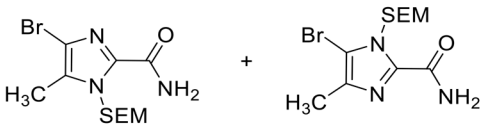

A mixture of regioisomers **S37** (220 mg, 0.61 mmol) was dissolved in 7 M ammonia in MeOH (5 mL) and stirred at rt for 18 h. The solvent was evaporated and purification by flash chromatography (SiO_2, *n*-hexane:EtOAc 50:50 to 0:100) afforded 178 mg (87.9%) of a mix of regioisomers which could not be separated by column chromatography. TLC-MS (ESI) *m*/*z*: calculated for $C_{11}H_{20}BrN_3O_2Si$ $[M+H]^+$ 334.1/336.1, found 334.4/336.4. HPLC: t_R = 9.14 min.

5-(2-(Cyclopropanecarboxamido)pyridin-4-yl)-4-methyl-1*H*-imidazole-2-carboxamide (6j)

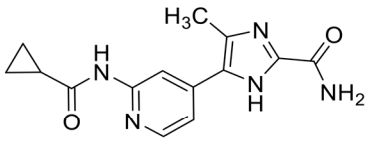

Compound **S38** (60 mg, 0.18 mmol), **S11** (78 mg, 0.27 mmol), Na_2CO_3 (57 mg, 0.54 mmol), cataCXium® A (13 mg, 0.036 mmol) and $Pd(OAc)_2$ (6 mg, 0.027 mmol) were dissolved in a degassed 3:1 mixture of DME/H_2O (4 mL) under an atmosphere of argon. The mixture was heated to 90 °C under an atmosphere of argon for 18 h. The reaction mixture was allowed to cool to rt and more H_2O was added. It was extracted with EtOAc (3x) and the combined organic layers were dried over anhydrous Na_2SO_4. The solvent was removed under reduced pressure and the crude product was dissolved in DCM (4 mL) and trifluoroacetic acid (4 mL). After stirring for 24 h, the solution was neutralized with sat. aq. $NaHCO_3$ to pH 7. The organic layer was separated and the aqueous layer was extracted with EtOAc (3x). The combined organic layers were dried over anhydrous Na_2SO_4 and the solvent was removed under reduced pressure. Purification by flash chromatography (SiO_2, DCM/2M ammonia in MeOH 99:1 to 95:5) afforded 20 mg (40.0%) of a white solid. ^{1}H NMR (300 MHz, DMSO-d_6) δ 0.73 - 0.89 (m, 4H), 1.96 - 2.08 (m, 1H), 2.46 (s, 3H), 7.43 (dd, *J* = 5.3, 1.3 Hz, 1H), 7.49 (br. s., 1H), 7.67 (br. s., 1H), 8.27 (d, *J* = 5.2 Hz, 1H), 8.44 (s, 1H), 10.73 (s, 1H), 13.11 (br. s., 1H). ^{13}C NMR (75 MHz, DMSO-d_6) δ 7.6, 11.4,

14.2, 109.6, 116.0, 129.4, 134.1, 139.5, 143.8, 147.8, 152.5, 160.0, 172.6 TLC-MS (ESI) *m*/*z*: calculated for $C_{14}H_{15}N_5O_2$ $[M+H]^+$ 286.1, found 286.2. HPLC: t_R = 6.31 min (method B) (100.0% purity).

2. ESI-QTOF assay

We followed the method reported in our previous paper.[7]

Materials: GSK3β enzyme and synthetic peptide GSM were purchased from Merck Millipore (Darmstadt, Germany). Adenosine triphosphate (ATP) disodium salt hydrate, ammonium acetate, ammonium hydroxide, dimethyl sulfoxide (DMSO), magnesium acetate tetrahydrate, formic acid, were purchased from Sigma–Aldrich (St. Louis, MO, USA). All other reagents were of analytical grade and filtered by nylon membrane filters 0.40 µm from Merck Millipore (Darmstadt, Germany). Ultrapure water was obtained on a Purite LTD water purification system (Thame, UK). Stock solutions of ATP (1 mM) were prepared in pH 7.4, 6 mM ammonium acetate and 1.6 mM magnesium acetate buffer. Stock solutions of GSM (1 mM) and 100 ng/L GSK3β were prepared in the same buffer and stored in aliquots at −80 °C. Further dilutions were prepared with fresh buffer before carrying out the assay. The inhibitors stock solutions (10 mM) were diluted with DMSO to achieve the concentration of 1 mM and then they were further diluted to the desired concentration with buffer. The percentage of DMSO was kept below 1%.

Inhibition assay by ESI-QTOF: The inhibition studies were performed by setting the assay solutions composed of 2.5 ng/L GSK3β, 62.5 µM GSM substrate, 250 µM ATP and inhibitors. Enzymatic reactions were carried out in the Eppendorf ThermoMixer (Hamburg, Germany) at 37 °C for 30 min. The sample solutions were analyzed by flow injection into the electrospray ionization (ESI) source at a 10 µL/min flow rate in positive ion mode (+ESI) with Micromass QTOF Ultima Global (Manchester, UK) equipped with an ESI source, and operating with a QTOF mass analyzer. Instrument control, data acquisition and processing were performed with Waters MassLynx 4.1 software (Manchester, UK). The ESI-QTOF source temperature was set at 80 °C, the capillary voltage at 3.0 kV and the cone voltage at 80 V. The scan time was set at 1 s, the inter scan time at 0.1 s and the desolvation gas was 200 L/h. Mass chromatograms were recorded in total ion current (TIC) mode in the mass range 100–1200 m/z. The spectra (m/z 370–815) deconvolution was carried out onto a true mass scale using the maximum entropy (MaxEnt1)-based software supplied with MassLynx 4.1 software. Output parameters were set as follows: mass range 2000–5000 Da; resolution 0.50 Da/channel. The uniform Gaussian model was used with 0.75 Da width at half height. The abundance of phosporylated muscle glycogen synthase P-GSM, as ion product of enzymatic reaction, was expressed as the ratio between the intensity of its diphosphorylated ion form and the amount of both the intensities of diphosphorylated and monophosphorilated GSM most abundant ion form, expressed as percentage. The applied formula is reported in Eq. (1). Data were analyzed by Microsoft Excel software.

Eq. (1) $$\frac{\mathrm{P-GSM}}{(\mathrm{P-GSM+GSM})}\cdot 100$$

The % of inhibition at different inhibitors concentrations, was calculated by the following formula reported in Eq. (2).

Eq. (2) $$100-(\frac{\mathrm{Ai}}{\mathrm{A0}}\cdot 100)$$

A_i is the intensity percent obtained in the presence of inhibitor and A_0 is the intensity percent obtained in the absence of inhibitor. Inhibition curves were obtained for compound **3a** by plotting the % inhibition versus the logarithm of inhibitor concentrations in the assay solution. The linear regression parameters were determined and an IC_{50} value of 0.034 µM was extrapolated (GraphPad Prism 4.0, GraphPad Software Inc.).

Compounds **3i**, **6a** and **6h** were tested at single concentration corresponding to their IC_{50} previously determined by luminometric assay. Compound **1** was tested at 0.7 µM. The obtained percentages of inhibition are reported in Table 1.

Table S1. Comparison of ESI-QTOF and ADO-Glo™ results.

	ESI-QTOF assay results	ADP-Glo™ assay results
Cpd	**% inhibition**	**IC_{50} ± SEM [µM]**
1	0% @ 0.700 µM	1.684 ± 0.120
3i	27.85% @ 0.059 µM	0.059 ± 0.007
6a	29.80% @ 0.047 µM	0.047 ± 0.020
6h	25.41% @ 0.039 µM	0.039 ± 0.017

For these compounds, the IC_{50} values were derived by applying the Eq. (3) reported by Kornacker and coworkers,[8] where [I] is the concentration of the tested inhibitor and "% inhibition" is the observed inhibition percentage. The derived IC_{50} values are reported in Table S2.

Eq. (3) $$IC_{50} = [I] \cdot \frac{100}{(\%\ \text{inhibition} - 1)}$$

Table S2. Comparison of ESI-QTOF and ADO-Glo™ IC_{50} values.

	ESI-QTOF assay results	ADP-Glo™ assay results
Cpd	**IC_{50}[µM][a]**	**IC_{50} ± SEM [µM]**
1	> 0.700	1.684 ± 0.120
3a	0.034	0.011 ± 0.001
3i	0.220	0.059 ± 0.007
6a	0.163	0.047 ± 0.020
6h	0.159	0.039 ± 0.017

[a]mean value of two independent experiments. RSD below 5%

The IC_{50} values obtained by both ADP-Glo™ method and by ESI-QTOF method are in good agreement as shown by the following correlation graph.

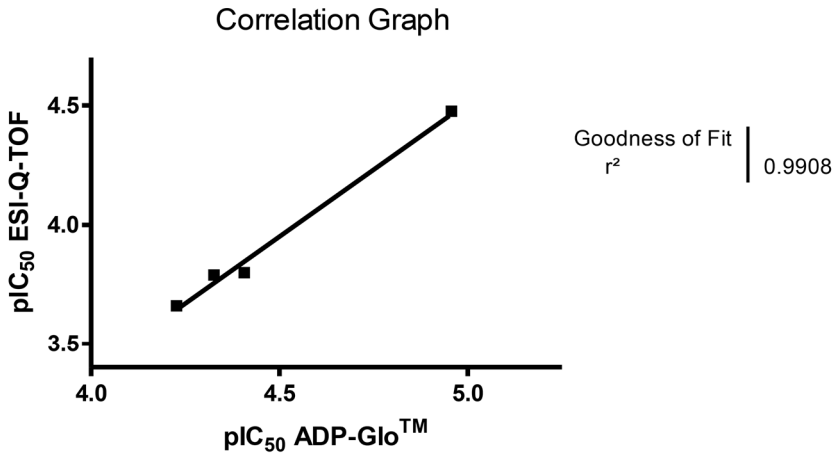

Figure S1. Correlation plot for inhibitory potency (pIC_{50}) of tested inhibitors obtained by ESI-QTOF assay and the ADP-Glo™ assay.

3. Molecular modeling, QM calculations and MD simulations

All the modeling was conducted with Maestro Small-Molecule Drug Discovery Suite 2018-4 (Schrödinger, LLC) with OPLS3e force field,[9-10] unless otherwise stated. The figures were prepared with PyMOL 2.2.3 (Schrödinger, LLC).

QM Conformer & Tautomer Prediction

For the tautomer prediction, we used the QM Conformer & Tautomer Predictor tool of Maestro (Schrödinger, LLC, New York, NY, 2018) that utilizes Jaguar[11] in the QM calculations. In brief, the workflow is the following:

The proton donor and acceptor atoms are identified, and protons are redistributed among these to form a list of tautomers (protons can also be added to or subtracted from the input molecule). The generated tautomers were next ranked by their semiempirical PM3 heat of formation, and the high-energy tautomers were then discarded. For the surviving tautomers, a set of conformers were generated with MacroModel and the high-energy structures were eliminated by their semiempirical PM3 heat of formation. Subsequently, DFT geometry optimizations were performed on the surviving structures, using the B3LYP-D3/LACVP** level of theory. Finally, the structures were ranked using single-point energies at the M06-2X/cc-pVTZ(-f) calculated at the optimal geometries from the previous step. The Boltzmann populations were calculated based on the Solution phase energy at the temperature of 298.15 K.

Table S3 Results of QM Conformer & Tautomer Prediction

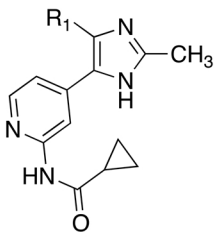

Tautomer A ("acceptor")

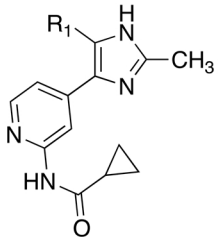

Tautomer B ("donor")

Note: The conformations highlighted with yellow (e.g. **3a-I**) are shown on the right.

Conform.	Solution phase energy	Tautomer	Boltzmann population
3a-I	-1104.296602	A	44.472
3a-II	-1104.296234	A	30.106
3a-III	-1104.295322	B	11.457
3a-IV	-1104.294701	A	5.934
3a-V	-1104.294536	A	4.982
3a-VI	-1104.293568	B	1.788
3a-VII	-1104.293228	B	1.248
3a-VIII	-1104.288470	A	0.008
3a-IX	-1104.287568	A	0.003
3a-X	-1104.287402	A	0.003

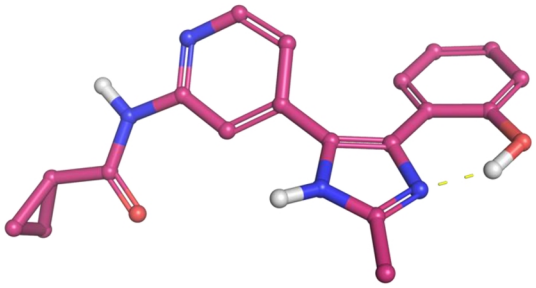

GSK3β: IC_{50} ± SEM [μM]= **0.011 ± 0.001**
Tautomer A total pop: 85.508%

Conform.	Solution phase energy	Tautomer	Boltzmann population
3f-I	-1143.578678	B	38.173
3f-II	-1143.578454	B	30.113
3f-III	-1143.578256	A*	24.408
3f-IV	-1143.577047	A*	6.782
3f-V	-1143.573711	B	0.198
3f-VI	-1143.573631	B	0.182
3f-VII	-1143.573149	B	0.109
3f-VIII	-1143.572068	B	0.035

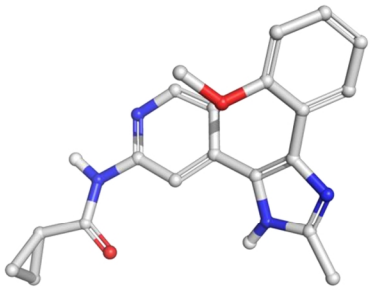

GSK3β: IC_{50} ± SEM [μM] = **> 10 μM**
Tautomer A total pop: 31.19%
*Tautomer A appears only in a conformation where the methoxy-group folds on top of the pyridinyl ring (non-binding conformation)

Conform.	Solution phase energy	Tautomer	Boltzmann population
3d-I	-1349.830260	A	33.202
3d-II	-1349.830196	A	31.018
3d-III	-1349.829072	B	9.433
3d-IV	-1349.829046	B	9.178
3d-V	-1349.828982	A	8.575
3d-VI	-1349.828974	A	8.503
3d-VII	-1349.823891	B	0.039
3d-VIII	-1349.823712	B	0.032
3d-IX	-1349.822647	A	0.010
3d-X	-1349.822568	A	0.010

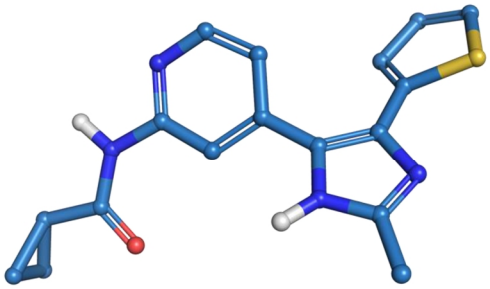

GSK3β: IC_{50} ± SEM [μM] = **0.069 ± 0.000**
Tautomer A total pop: 81.318%

Conform.	Solution phase energy	Tautomer	Boltzmann population
3c-I	-1104.295629	B	35.763
3c-II	-1104.295420	B	28.660
3c-III	-1104.295204	B	22.803
3c-IV	-1104.293884	A	5.631
3c-V	-1104.293827	A	5.302
3c-VI	-1104.292269	A	1.019
3c-VII	-1104.291961	A	0.735
3c-VIII	-1104.288925	B	0.029
3c-IX	-1104.288924	B	0.029
3c-X	-1104.288892	B	0.028

GSK3β: IC_{50} ± SEM [μM] = **0.893 ± 0.001**
Tautomer A total pop: 12.687%

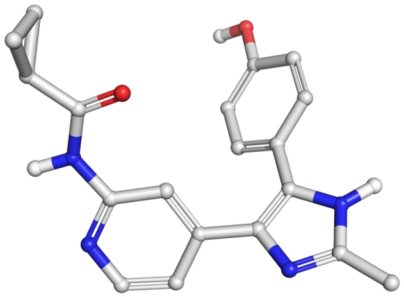

Conform.	Solution phase energy	Tautomer	Boltzmann population
3g-I	-1061.148029	A	21.208
3g-II	-1061.147961	A	19.717
3g-III	-1061.147922	A	18.917
3g-IV	-1061.147245	A	9.244
3g-V	-1061.147183	A	8.652
3g-VI	-1061.147127	A	8.154
3g-VII	-1061.146353	B	3.593
3g-VIII	-1061.146340	B	3.543
3g-IX	-1061.146333	B	3.515
3g-X	-1061.146317	B	3.457

GSK3β: IC_{50} ± SEM [μM] **> 10 μM**
Tautomer A total pop: 85.892%
Note: Pyrimidine is unsuitable for hydrophobic pocket.

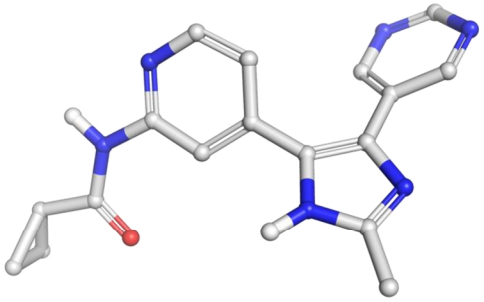

Conform.	Solution phase energy	Tautomer	Boltzmann population
1-I	-1128.306260	B	24.865
1-II	-1128.306193	B	23.180
1-III	-1128.305582	A	12.136
1-IV	-1128.305315	A	9.144
1-V	-1128.305114	B	7.389
1-VI	-1128.305110	B	7.360
1-VII	-1128.304984	B	6.437
1-VIII	-1128.304611	A	4.337
1-IX	-1128.304478	A	3.769
1-X	-1128.303533	B	1.385

GSK3β: IC_{50} ± SEM [μM] = **0.053 ± 0.012**[a]
Tautomer A total pop: 29.386%

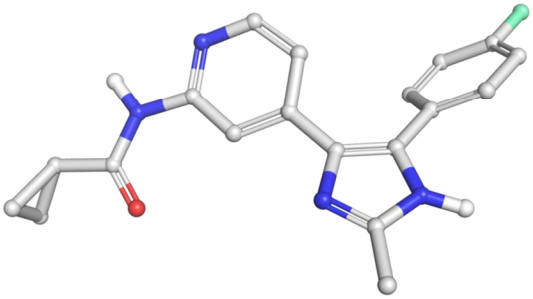

Conform.	Solution phase energy	Tautomer	Boltzmann population	Boltzmann population[a]
3b-I	-1104.297522	B*	96.981	-
3b-II	-1104.293541	A	1.431	47.390
3b-III	-1104.293523	A	1.403	46.495
3b-IV	-1104.290784	B	0.077	2.556
3b-V	-1104.290191	B	0.041	1.364
3b-VI	-1104.289543	B	0.021	0.686
3b-VII	-1104.289482	B	0.019	0.644
3b-VIII	-1104.289403	B	0.018	0.592
3b-IX	-1104.288674	B	0.008	0.273
3b-X	-1104.283337	B	0.000	0.001

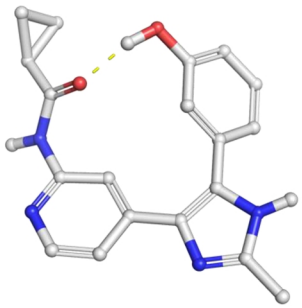

GSK3β: IC_{50} ± SEM [μM] = **0.043 ± 0.005**
Tautomer A total pop: 2.834% (93.885% when intramolecular H-bond conformation **16-I** is excluded)
*intramolecular H-bond
[a] population distribution excluding the intramolecular bond conformation

Conform.	Solution phase energy	Tautomer	Boltzmann population
3e-I	-1026.847726	A	27.085
3e-II	-1026.847633	A	24.544
3e-III	-1026.847341	B	18.016
3e-IV	-1026.846808	B	10.237
3e-V	-1026.846805	A	10.210
3e-VI	-1026.846746	A	9.590
3e-VII	-1026.842545	B	0.112
3e-VIII	-1026.842530	B	0.110
3e-IX	-1026.841911	B	0.057
3e-X	-1026.841532	A	0.038

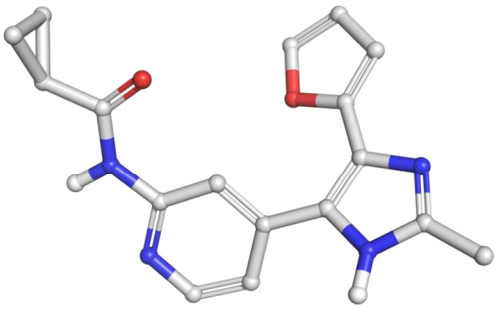

GSK3β: IC_{50} ± SEM [μM] = **0.099 ± 0.033**
Tautomer A total pop: 71.467%

Conform.	Solution phase energy	Tautomer	Boltzmann population
3k-I	-954.022095	B	28.389
3k-II	-954.022069	B	27.632
3k-III	-954.021732	B	19.337
3k-IV	-954.021454	B	14.403
3k-V	-954.020006	A	3.106
3k-VI	-954.019877	A	2.710
3k-VII	-954.019871	A	2.693
3k-VIII	-954.019448	A	1.720
3k-IX	-954.014328	B	0.008
3k-X	-954.013155	B	0.002

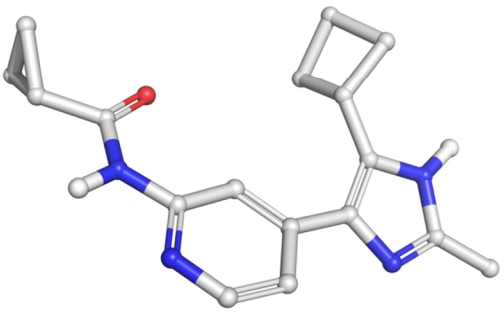

GSK3β: IC_{50} ± SEM [μM] = **4.114 ± 0.191**
Tautomer A total pop: 10.229%

Conform.	Solution phase energy	Tautomer	Boltzmann population
3l-I	-993.357257	B	28.091
3l-II	-993.357103	B	23.843
3l-III	-993.356732	B	16.095
3l-IV	-993.356680	B	15.237
3l-V	-993.355688	A	5.329
3l-VI	-993.355552	A	4.612
3l-VII	-993.355282	A	3.467
3l-VIII	-993.355232	A	3.286
3l-IX	-993.351037	A	0.039
3l-X	-993.347911	A	0.001

GSK3β: IC_{50} ± SEM [μM] = **5.456 ± 0.006**
Tautomer A total pop: 16.734%

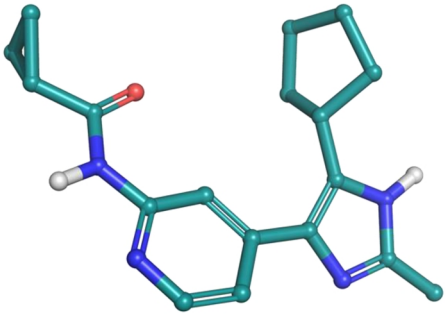

Conform.	Solution phase energy	Tautomer	Boltzmann population
3h-I	-1182.687499	B	51.856
3h-II	-1182.686104	B	11.833
3h-III	-1182.685564	B	6.681
3h-IV	-1182.685365	A	5.411
3h-V	-1182.685277	A	4.931
3h-VI	-1182.685252	B	4.802
3h-VII	-1182.685199	B	4.539
3h-VIII	-1182.684985	A	3.617
3h-IX	-1182.684886	A	3.257
3h-X	-1182.684831	A	3.073

GSK3β: IC_{50} ± SEM [μM] = **> 10 μM**
Tautomer A total pop: 20.289%

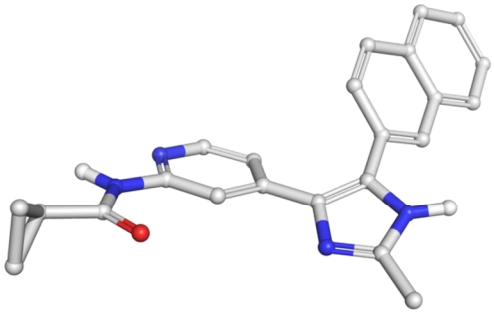

Conform.	Solution phase energy	Tautomer	Boltzmann population
3j-I	-914.716713	B	20.118
3j-II	-914.716682	B	19.469
3j-III	-914.716653	B	18.864
3j-IV	-914.716572	B	17.327
3j-V	-914.716067	B	10.144
3j-VI	-914.715850	B	8.063
3j-VII	-914.714501	A	1.932
3j-VIII	-914.714341	A	1.630
3j-IX	-914.714283	A	1.534
3j-X	-914.713799	A	0.918

GSK3β: IC_{50} ± SEM [μM] = **3.085 ± 0.304**
Tautomer A total pop: 6.014%

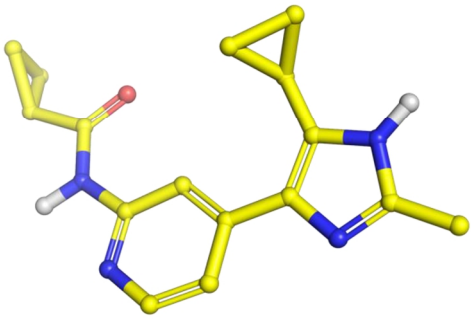

Conform.	Solution phase energy	Tautomer	Boltzmann population
6g-I	-1044.125829	B	21.528
6g-II	-1044.125800	B	20.867
6g-III	-1044.125748	B	19.762
6g-IV	-1044.125613	B	17.132
6g-V	-1044.125424	B	14.023
6g-VI	-1044.124012	A	3.142
6g-VII	-1044.123911	A	2.823
6g-VIII	-1044.121999	A	0.372
6g-IX	-1044.121940	A	0.350
6g-X	-1044.115771	A	0.001

GSK3β: IC_{50} ± SEM [μM] = **0.003 ± 0.000**
Tautomer A total pop: 6.688%

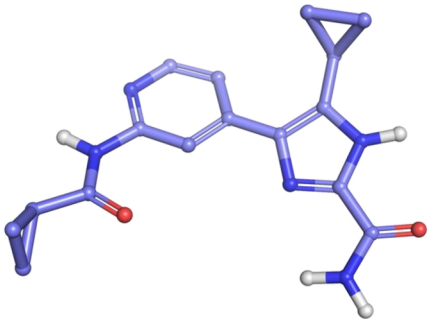

Conform.	Solution phase energy	Tautomer	Boltzmann population
3m-I	-1032.674226	B	38.531
3m-II	-1032.673584	B	19.524
3m-III	-1032.673014	B	10.676
3m-IV	-1032.672765	B	8.199
3m-V	-1032.672547	B	6.511
3m-VI	-1032.672202	A	4.514
3m-VII	-1032.672180	A	4.414
3m-VIII	-1032.672106	A	4.078
3m-IX	-1032.671974	A	3.546
3m-X	-1032.666049	B	0.007

GSK3β: IC_{50} ± SEM [μM] = **4.644 ± 1.159**
Tautomer A total pop: 16.552%

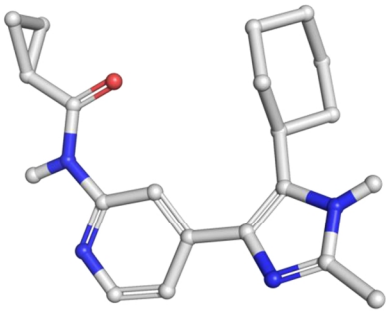

Conform.	Solution phase energy	Tautomer	Boltzmann population
6f-I	-1162.082426	B	29.067
6f-II	-1162.082186	B	22.549
6f-III	-1162.082042	B	19.362
6f-IV	-1162.081962	B	17.784
6f-V	-1162.080625	A	4.317
6f-VI	-1162.080347	A	3.216
6f-VII	-1162.080159	A	2.634
6f-VIII	-1162.079229	A	0.984
6f-IX	-1162.076626	B	0.062
6f-X	-1162.075806	B	0.026

GSK3β: IC_{50} ± SEM [μM] = **0.003 ± 0.000**
Tautomer A total pop: 11.151%

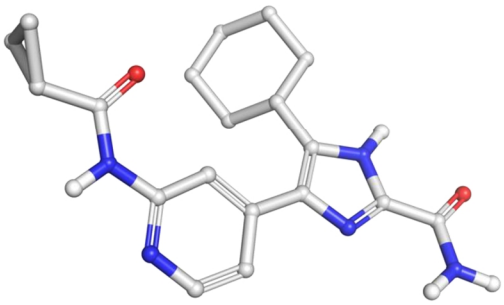

MD simulations

For the MD simulations we used the structures 6GN1[12] and 4PTC[4] (for the additional simulations of **3a**, **3j**, **6b** and **6g**), which were prepared with Protein Preparation Wizard (default settings).[13] The initial coordinates for the ligand-protein complexes were obtained by Induced Fit Docking (IFD),[14-16] using default settings, except the Glide redocking was conducted with XP.[17] The grid box was defined by the co-crystalized ligand. Before the docking, the small-molecules were prepared with LipPrep (default settings) using Epik.[18-19] The tautomeric state of a compound used in the simulations was chosen based on the QM Conformer & Tautomer Predictor results. The MD simulations were conducted with Desmond.[20]

For the compounds **3a**, **3j**, **6b** and **6g**, the systems were solvated in a cubic box (edges 14 Å from the protein) and neutralized with counterions (Cl^-) with 0.15M NaCl salt. The water was described with TIP3P water model.[21] The final 6GN1 systems consisted of 65,545; 65,405; 65,561 and 65,460 atoms. The 4PTC systems consisted of 74,622; 74,642; 74,632 and 74,631 atoms. The default relaxation protocol of Desmond was used before the 1,000 ns production simulations, which were conducted in NPT ensemble (310 K, thermostat: Nosé-Hoover chain; 1.01325 bar, barostat: Martyna-Tobias-Klein). The default timestep of 2 fs and cutoff radius of 9.0 Å for Coulombic interactions were used. The total simulation time was 8 μs (4 x 2 x 1,000 ns).

The compounds **4a** and **4b** were solvated in an orthorhombic box (edges 13 Å from the protein) with counterions (Cl^-) without salt, resulting in systems of 56,176 and 56,445 atoms. After the default relaxation protocol, the systems were simulated for 200 ns with the above-mentioned settings.

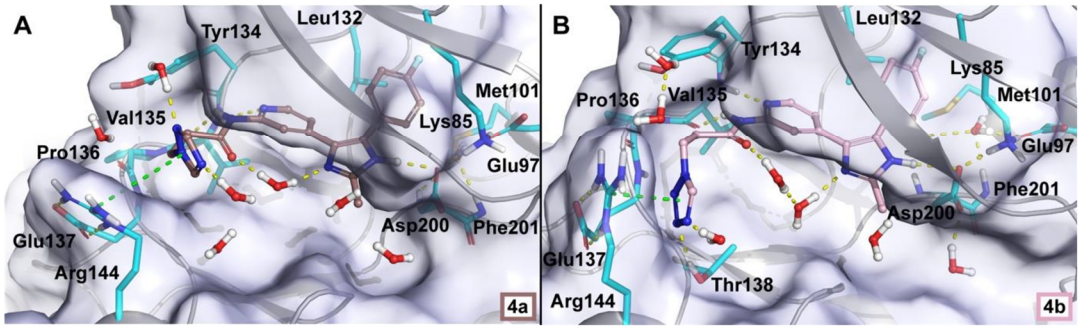

Figure S2. The output conformations of compounds **4a** (**A**) and **4b** (**B**) after 200 ns MD simulations. The most important interacting residues and the closest water molecules are shown. The H-bonds are displayed with yellow and the cation-π interaction with green dashed line.

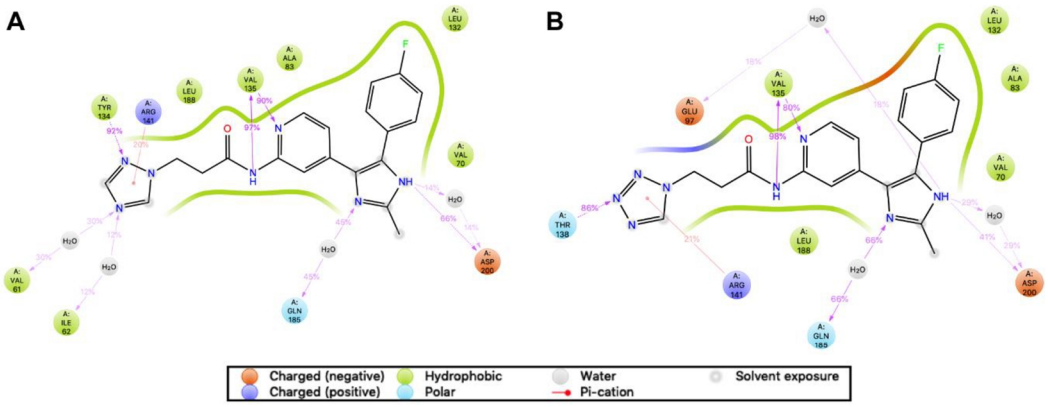

Figure S3. The simulation interactions of compound **4a** (**A**) and **4b** (**B**). In the solvent exposed area near the HR II, compound **4a** displays interaction to Tyr134, π-cation interaction to Arg141 and water mediated interactions, whereas **4b** interacts with Thr138 and Arg141. Interactions that appear >10% frequency in the simulation are shown.

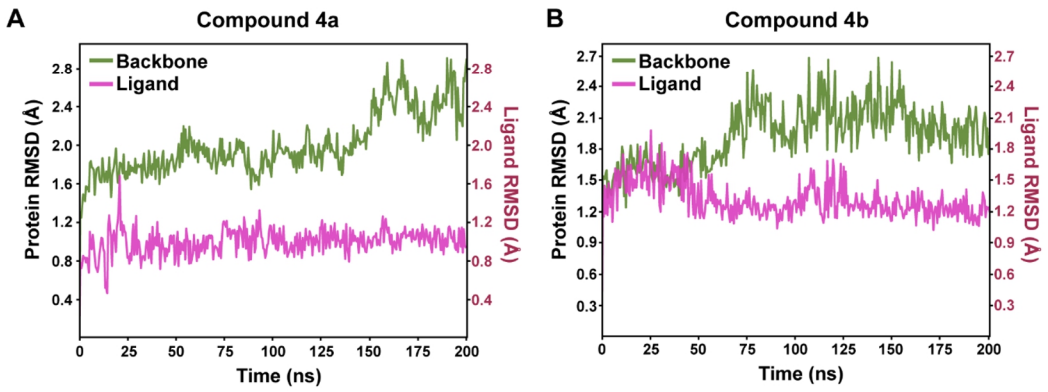

Figure S4. The RMSD of protein backbone and ligand in the simulations of compound **4a** (**A**) and **4b** (**B**).

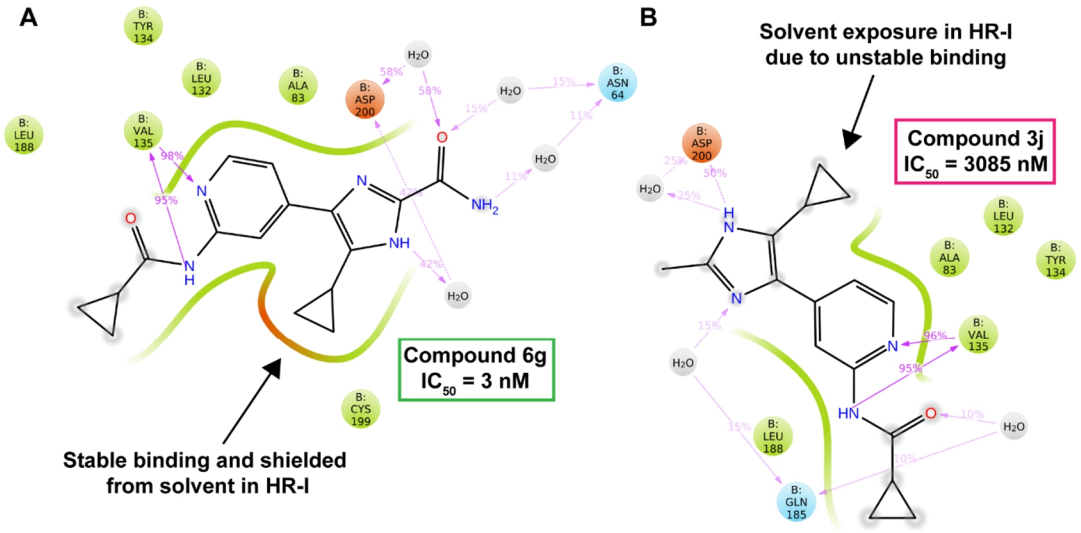

Figure S5. The simulation interactions of compound **6g** (**A**) and **3j** (**B**) in 6GN1 simulations. The instability of compound **3j** binding can be observed from the solvent exposure of the cyclopropyl moiety in the HR-I region. The amide residue (compound **6g**) stabilizes the solvent interaction networks and shields HR-I from solvent enabling stable binding. Interactions that appear >10% frequency in the simulation are shown. See interaction legend from **Figure S3.**

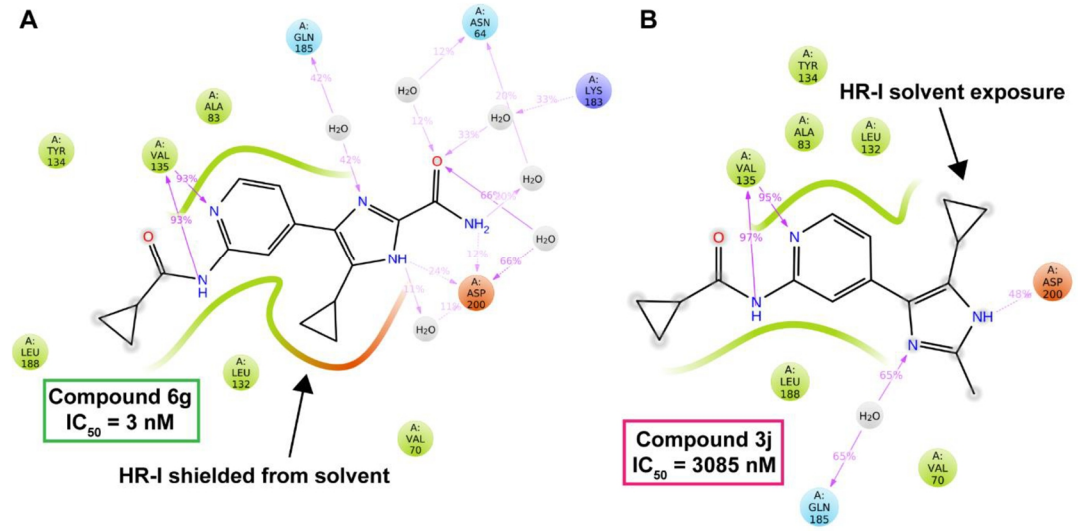

Figure S6. The simulation interactions of compound **6g** (**A**) and **3j** (**B**) in 4PTC simulations. Identical interactions are observed as in **Figure S5**, with the solvent exposure of the cyclopropyl with compound **3j** (**B**). Interactions that appear >10% frequency in the simulation are shown. See interaction legend from **Figure S3.**

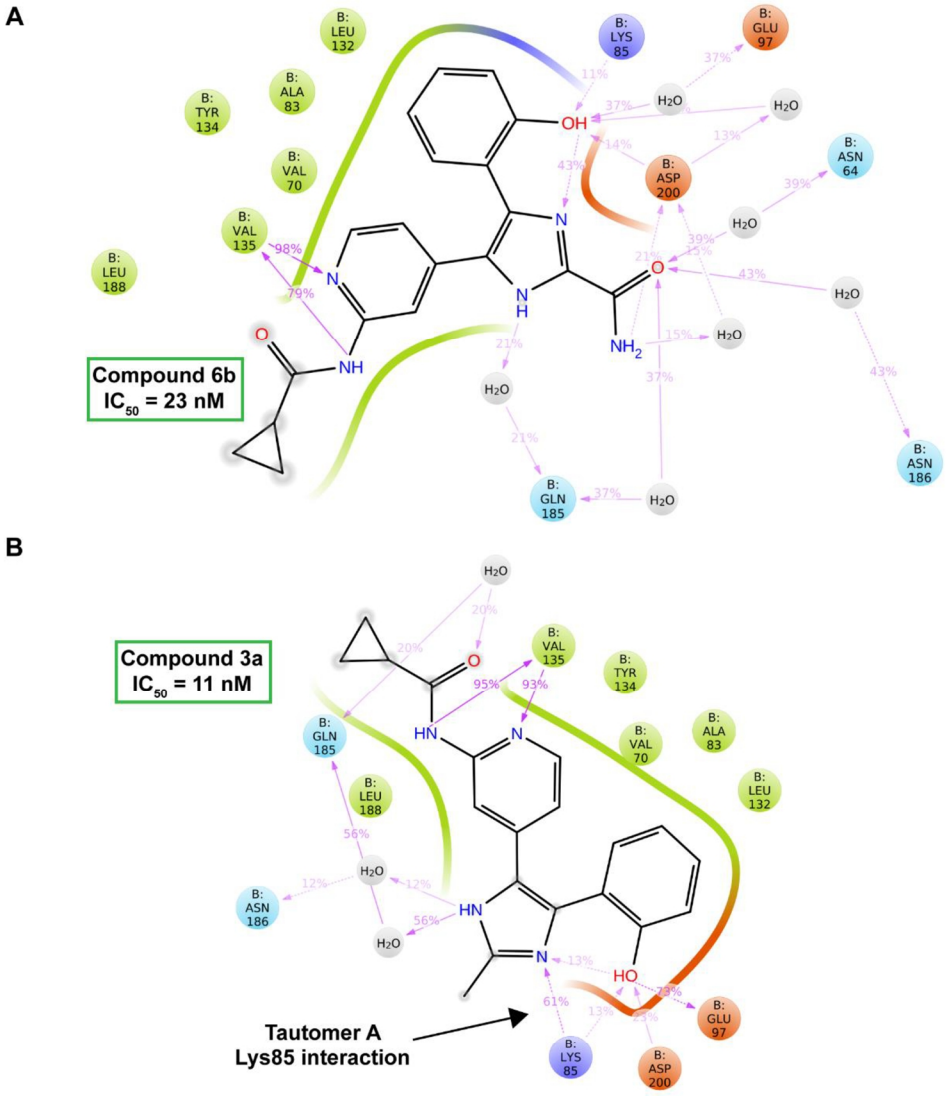

Figure S7. The simulation interactions of compound **6b** (**A**) and **3a** (**B**) in 6GN1 simulations. The tautomer A with the methyl derivative (compound **15**) forms a direct interaction to the Lys85 (61%). Interactions that appear >10% frequency in the simulation are shown. See interaction legend from **Figure S3**.

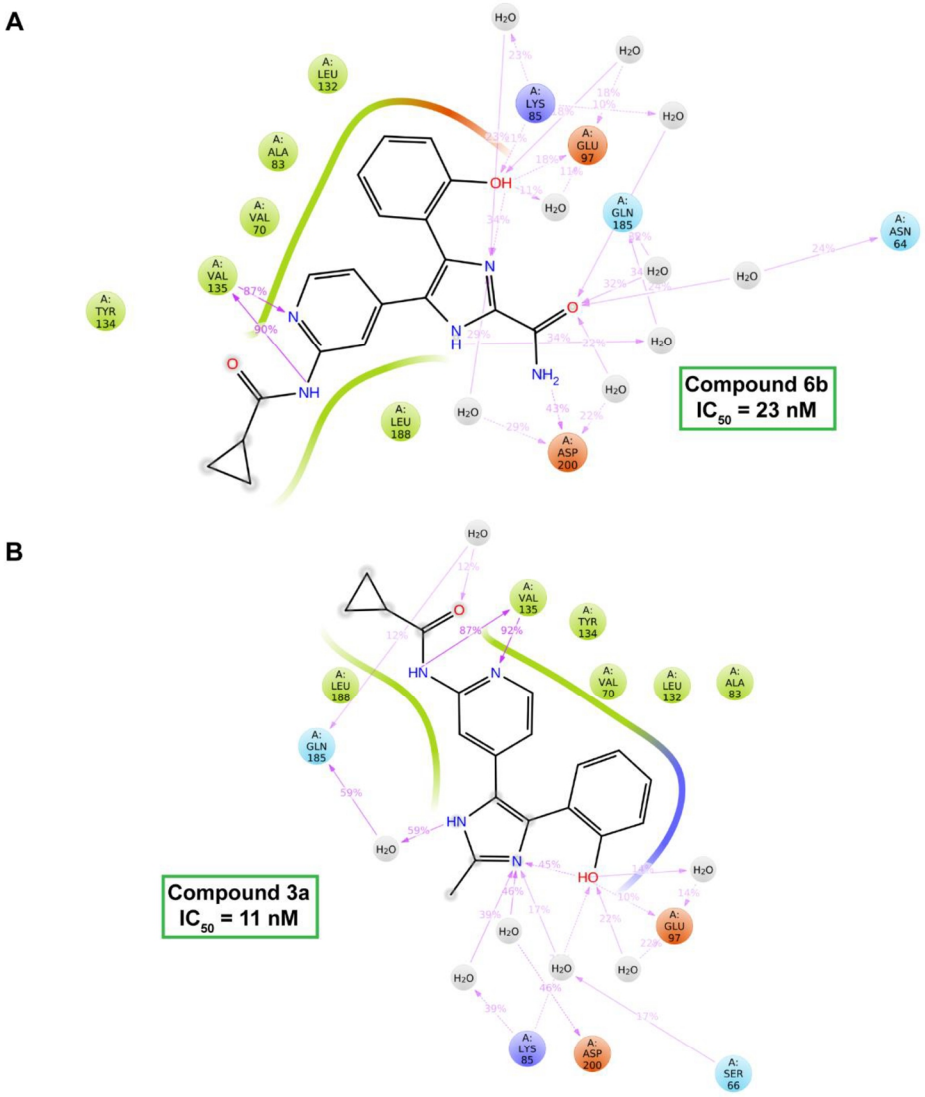

Figure S8. The simulation interactions of compound **6b** (**A**) and **3a** (**B**) in 4PTC simulations. The tautomer A with the methyl derivative (compound **3a**) forms a water mediated interactions to the Lys85 and more frequent intramolecular interaction to the hydroxyl-group compared to **Figure S7**. The lipophilic part of the 2-hydroxyphenyl is shielded from water as in **Figure S7**. Interactions that appear >10% frequency in the simulation are shown. See interaction legend from **Figure S3**.

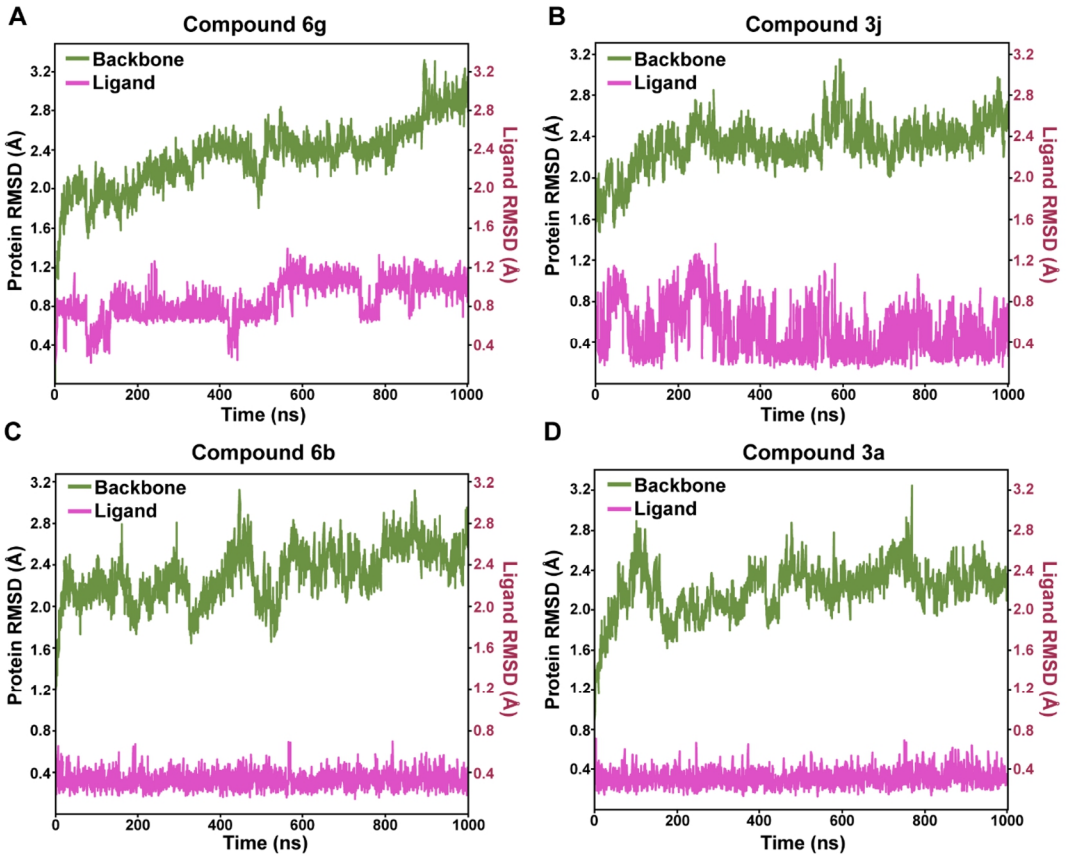

Figure S9. The RMSD of protein backbone and ligand in the 6GN1 simulations of compound **6g** (**A**), **3j** (**B**), **6b** (**C**) and **3a** (**D**).

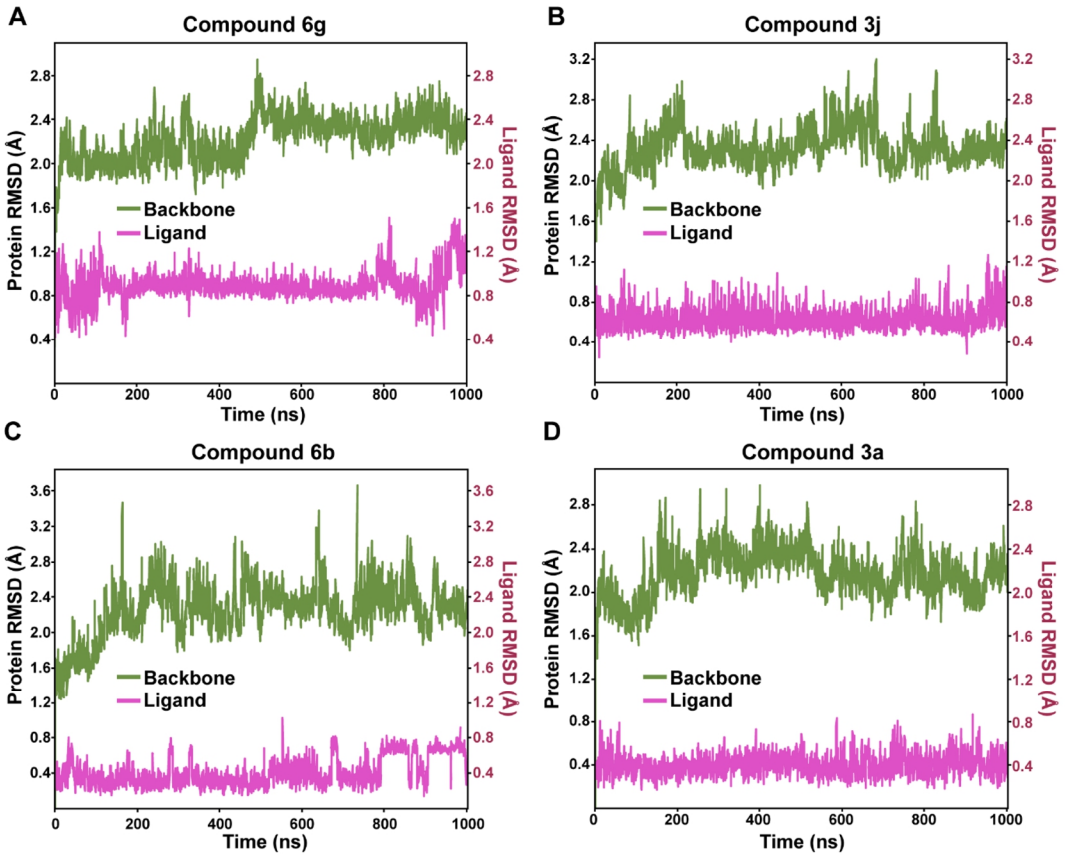

Figure S10. The RMSD of protein backbone and ligand in the 4PTC simulations of compound **6g** (**A**), **3j** (**B**), **6b** (**C**) and **3a** (**D**).

4. Metabolic stability in human liver microsomes

Microsomes from liver, pooled from human (male and female) (Lot: SLBQ7487V) were purchased from Merck (Schnelldorf, Germany). The incubations of compounds **3a** and **6g** were made in the presence of an NADPH-regenerating system (5 mM Glucose-6-phosphate, 5 U/mL Glucose-6-phosphate dehydrogenase and 1 mM $NADP^+$). The substrate (100 µM), the NADPH-regenerating system and 4 mM $MgCl_2 \cdot 6\ H_2O$ in 0.1 M Tris buffer (pH 7.4) were preincubated for 5 min at 37 °C and 750 rpm. The incubation mix was split into aliquots (50 µL) and the reaction was started by the addition of HLM. The reaction was quenched at selected time points (0, 10, 20, 30, 60, 120, 180 and 240 min) by adding 100 µL internal standard at a concentration of 22.5 µM in MeCN. The samples were vortexed for 30 s and centrifuged (19,800 relative centrifugal force/4 °C/10 min). The supernatant was directly used for LC-MS analysis (see below). All incubations were conducted in triplicates and a limit of 1% organic solvent was not exceeded. Propranolol was used as a positive control.

The metabolite formation was analyzed with an Alliance 2695 Separations Module (Waters GmbH, Eschborn). Samples were maintained at 4 °C, the column temperature was set to 40 °C and injection volume was 10 µL. The chromatographic separation for all analytes was performed on a Dr Maisch Nucleosil 100 C18 column (53 x 4.6 mm; 5 µm). The following gradient of solvent A (90% H_2O, 10% ACN, 0.1% formic acid) and solvent B (MeOH, 0.1% formic acid) at a flow rate of 400 µL/min was used:

gradient

time [min]	A [%]	B [%]
0	90	10
2	90	10
10	0	100
12	0	100
14	90	10

The detection was performed on a Micromass Quattro micro triple quadrupole mass spectrometer (Waters GmbH, Eschborn) using the electrospray ionization in the positive-mode. Spray voltage was set to 4.5 kV. The heated capillary operated at 250 °C and the desolvation gas flow worked at 600 L/h.

Table S4 Metabolic degradation of **3a**.

time [min]	#1 [%]	#2 [%]	#3 [%]	AVERAGE [%]	SD
0	100.00	100.00	100.00	100.00	0.00
10	100.31	109.91	96.72	102.31	6.82
20	93.29	109.27	95.71	99.42	8.62
30	100.84	103.72	99.25	101.27	2.26
60	101.84	106.23	102.17	103.41	2.44
120	100.10	99.27	96.03	98.47	2.15
180	107.06	102.81	100.14	103.34	3.49
240	101.91	103.72	100.48	102.04	1.63

Table S5 Metabolic degradation of **6g**.

time [min]	#1 [%]	#2 [%]	#3 [%]	AVERAGE [%]	SD
0	100.00	100.00	100.00	100.00	0.00
10	104.45	102.45	97.33	101.41	3.67
20	99.26	103.68	95.42	99.45	4.13
30	103.95	99.37	100.85	101.39	2.33
60	99.75	102.88	101.58	101.40	1.57
120	105.62	100.03	100.14	101.93	3.20
180	94.73	97.80	105.70	99.41	5.66
240	98.49	99.30	105.62	101.14	3.90

5. Kinome selectivity screening

Compound **6g** was tested at Eurofins Cerep SA (Celle-L'Evescault, France) in enzymatic radioactive assays in a panel of 68 different kinases (including GSK3β) from diverse families.

Table S6 Kinome selectivity screening

	residual activity in % using 0.5 µM of **6g**		residual activity in % using 0.5 µM of **6g**
Abl(h)	68	MAPK2(h) (ERK2)	95
ALK(h)	85	MAP4K4(h) (HGK)	47
AMPKα1(h)	102	MAPKAP-K2(h)	33
ASK1(h)	85	MEK1(h)	102
Aurora-A(h)	38	MLK1(h)	12
CaMKI(h)	124	Mnk2(h)	65
CDK1/cyclinB(h)	36	MSK2(h)	95
CDK2/cyclinA(h)	11	MST1(h)	77
CDK6/cyclinD3(h)	98	mTOR(h)	111
CDK7/cyclinH/MAT1(h)	82	NEK2(h)	109
CDK9/cyclin T1(h)	6	p70S6K(h)	95
CHK1(h)	84	PAK2(h)	47
CK1γ1(h)	68	PDGFRβ(h)	108
CK2α2(h)	55	Pim-1(h)	79
c-RAF(h)	109	PKA(h)	111
DRAK1(h)	52	PKBα(h)	105
eEF-2K(h)	122	PKCα(h)	67
EGFR(h)	109	PKCθ(h)	98
EphA5(h)	89	PKG1α(h)	113
EphB4(h)	82	Plk3(h)	114
FGFR3(h)	87	PRAK(h)	52
Fyn(h)	74	ROCK-I(h)	105
GSK3β(h)	1	Rse(h)	116
IGF-1R(h)	108	Rsk1(h)	73
IKKα(h)	47	SAPK2a(h) (p38α)	102
IRAK4(h)	57	SAPK2b(h) (p38β)	91
JAK2(h)	77	SAPK3(h) (p38γ)	48
JNK1α1(h)	31	SAPK4(h) (p38δ)	64
JNK2α2(h)	78	SRPK1(h)	108
JNK3(h)	7	TAK1(h)	83
KDR (h) (VEGFR2)	26	PI3 Kinase (p110b/p85a)(h)	100
LOK(h)	39	PI3 Kinase (p120g)(h)	100
Lyn(h)	67	PI3 Kinase (p110d/p85a)(h)	96
MAPK1(h) (ERK1)	85	PI3 Kinase (p110a/p85a)(h)	102

6. Inhibition of CYP450 isoenzymes

CYP inhibition assays were performed by Eurofins Panlabs Inc. (St Charles, MO, USA).

CYP inhibition assay (fluorimetric detection) was performed at 10 µM inhibitor concentration in single dose duplicate mode with human recombinant CYP enzyme and the appropriate CYP substrates: CYP1A2, 3-cyano-7-ethoxycoumarin (CFC); CYP2C9, CFC; CYP2C19, 7-methoxy-4-trifluoromethyl-coumarin (MFC); CYP2D6, MFC; CYP3A4 7-benzyloxy-trifluoromethylcoumarin (BFC)

7. Investigation of cell toxicity on six different cell lines

Maintenance of cell culture

The experiments were performed in an *in vitro* model of cell cytotoxicity analyses on hepatocellular carcinoma (HepG2), human prostate cancer (LNCap), human breast adenocarcinoma (MCF7), human lung fibroblast (MRC5), chinese hamster ovary (CHO-K1) and murine macrophages (RAW 264.7). The cells lines were cultured in appropriate medium, supplemented with 10% (v/v) of fetal bovine serum (FBS) and 1 % antibiotic/antimycotic solution. For subculture, cells were dissociated with trypsin-EDTA (Cultilab), split into a 1:3 ratio and subculture into Petri dishes with 25 cm^2 growth area. Raw 264.7 cells were dissociated using a scrapper. Culture medium was replaced every 2 days until the cells reached the total confluence after 4-5 days of initial seeding. Cells were maintained in the following controlled conditions: 95% of humidified atmosphere, 5% of CO_2 and constant temperature of 37ºC.

Cytotoxicity

The assessment of cell viability was performed according to the MTT colorimetric assay on 6 different cells lines. Cells were treated with different concentrations of **6g** for 48 h. The effects were estimated by colorimetric assay based on the conversion of tetrazolium salts (MTT) after 3 h of incubation to a blue formazan product by active mitochondria. The absorbance was read at 570 nm using a Spectramax i5 microplate reader. Results were expressed as percentage of control.

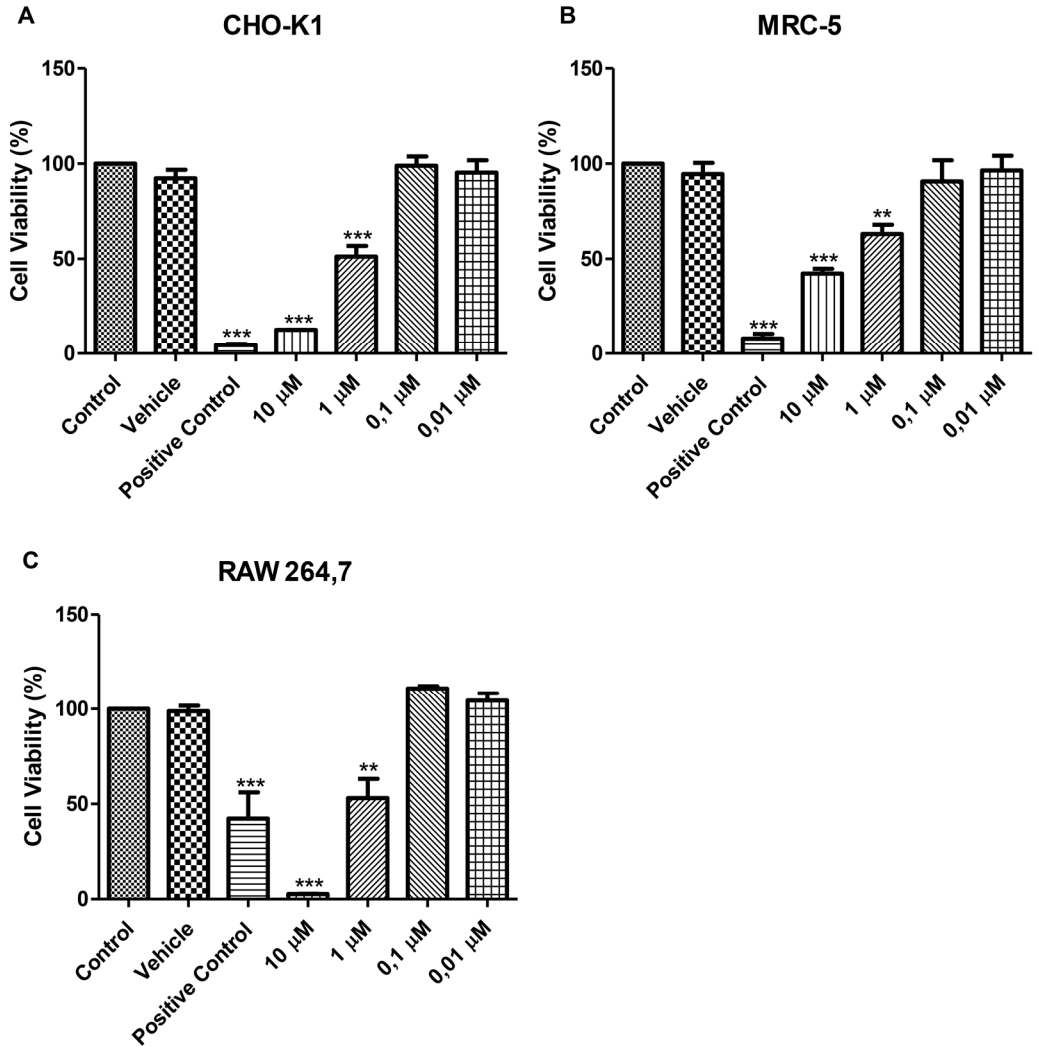

Figure S11. Evaluation of the cytotoxic potential of **6g** in non-tumorigenic cells lines. (A) Chinese hamster ovary cells CHO-K1, (B) human lung fibroblast cell line MRC-5, and (C) murine macrophages RAW 264.7.

Cell viability was evaluated by MTT assay, after 48h treatment with **6g**. Mean values ± SEM are shown. ***p<0.001 compared with control. Vehicle (DMSO); Positive Control (hydrogen peroxide).

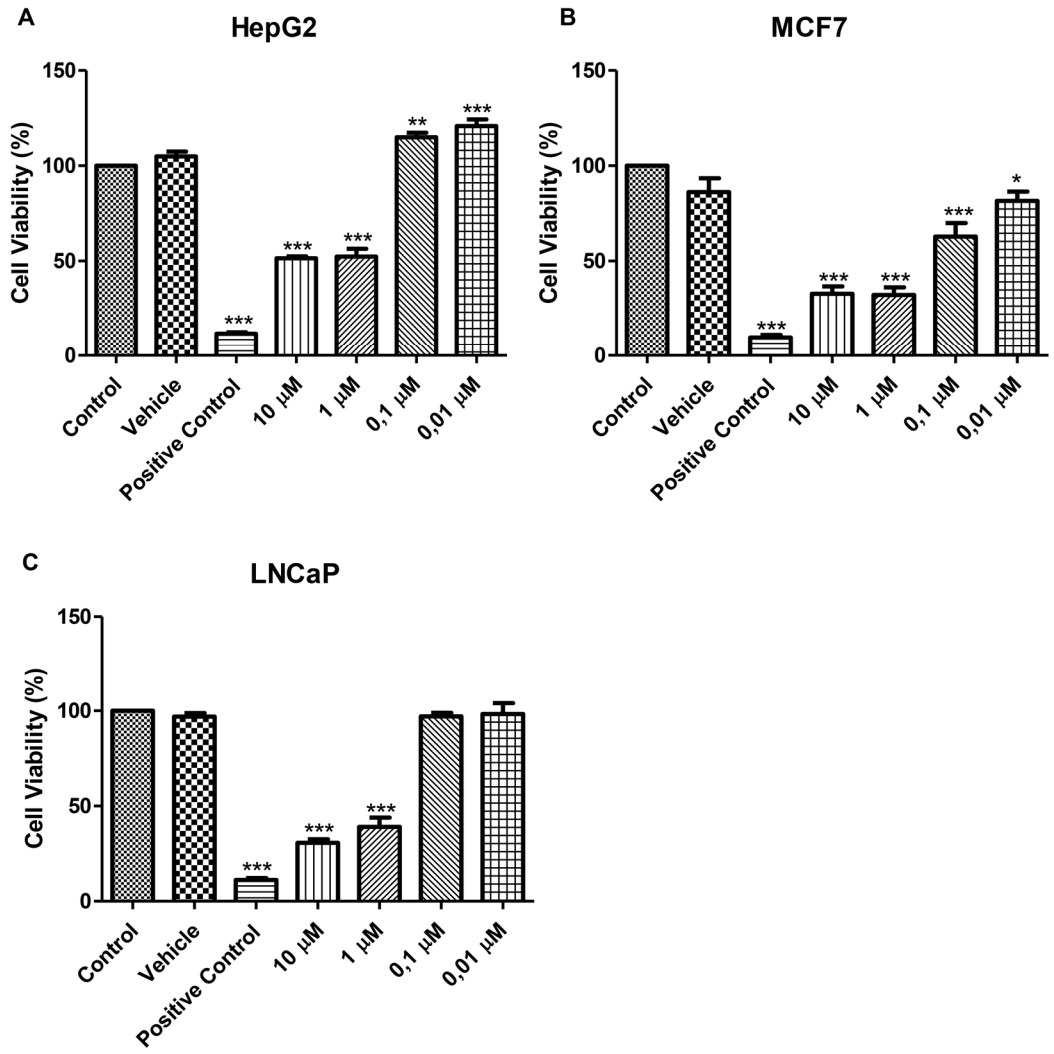

Figure S12. Evaluation of the cytotoxic potential of **6g** in tumorigenic cells lines. (A) Hepatocellular carcinoma cell line HepG2 , (B) human breast adenocarcinoma cell line MCF7, and (C) human prostate cancer cell line LNCaP.

Cell viability was evaluated by MTT assay, after 48h treatment with **6g**. Mean values ± SEM are shown. ***p<0.001 compared with control. Vehicle (DMSO); Positive Control (hydrogen peroxide).

8. Inhibition of GSK3β in SH-SY5Y cells

Material and Methods

Cell culture

Human neuronal SH-SY5Y cells were routinely grown in Dulbecco's modified Eagle's Medium supplemented with 10% fetal bovine serum, 2 mM L-glutamine, 50 U/mL penicillin and 50 µg/mL streptomycin at 37°C in a humidified incubator with 5% CO_2.

Western Blotting

SH-SY5Y cells were seeded in 60 mm dishes at 2 × 10^6 cells/dish, incubated for 24 h and subsequently treated with compound **6g** [1 µM] for 1 h at 37°C in 5% CO_2. At the end of incubation, cells were lysed by addition of ice-cold lysis buffer containing leupeptin 2 µg/mL and PMSF 100 µg/mL. An aliquot was used for protein analysis with the Bradford assay for protein quantification. Cell lysates (50 µg per sample) were separated by SDS-polyacrylamide gels and transferred onto nitrocellulose membranes, which were probed with primary phospho-GSK3α/β (Ser21/9) (1:1000; Cell Signaling Technology, Danvers, MA, USA) and secondary antibodies. ECL reagents (Pierce, Rockford, IL, USA) were utilized to detect targeted bands. The same membrane was stripped and reprobed with total GSK3β (1:1000; Cell Signaling Technology) and β-Actin (1:1000; Sigma Aldrich, St. Louis, MO, USA) antibodies. Data were analysed by densitometry, using Quantity One software (Bio-Rad, Hercules, CA, USA). Data are expressed as ratio between phospho-GSK3α/β and total GSK3β levels normalized against β-Actin.

9. References

1. Floyd, M. B.; Du, M. T.; Fabio, P. F.; Jacob, L. A.; Johnson, B. D., The oxidation of acetophenones to arylglyoxals with aqueous hydrobromic acid in dimethyl sulfoxide. *J. Org. Chem.* **1985**, *50*, 5022–5027.

2. Heider, F.; Ansideri, F.; Tesch, R.; Pantsar, T.; Haun, U.; Döring, E.; Kudolo, M.; Poso, A.; Albrecht, W.; Laufer, S. A.; Koch, P., Pyridinylimidazoles as dual glycogen synthase kinase 3β/p38α mitogen-activated protein kinase inhibitors. *Eur. J. Med. Chem.* **2019**, *175*, 309-329.

3. Markey, M. D.; Kelly, T. R., Synthesis of cribrostatin 6. *J. Org. Chem.* **2008**, *73*, 7441–7443.

4. Sivaprakasam, P.; Han, X.; Civiello, R. L.; Jacutin-Porte, S.; Kish, K.; Pokross, M.; Lewis, H. A.; Ahmed, N.; Szapiel, N.; Newitt, J. A.; Baldwin, E. T.; Xiao, H.; Krause, C. M.; Park, H.; Nophsker, M.; Lippy, J. S.; Burton, C. R.; Langley, D. R.; Macor, J. E.; Dubowchik, G. M., Discovery of new acylaminopyridines as GSK-3 inhibitors by a structure guided in-depth exploration of chemical space around a pyrrolopyridinone core. *Bioorg. Med. Chem. Lett.* **2015**, *25*, 1856–1863.

5. Joo, J. M.; Touré, B. B.; Sames, D., C-H bonds as ubiquitous functionality: a general approach to complex arylated imidazoles via regioselective sequential arylation of all three C-H bonds and regioselective N-alkylation enabled by SEM-group transposition. *J. Org. Chem.* **2010**, *75*, 4911–4920.

6. Wagner, G. K.; Kotschenreuther, D.; Zimmermann, W.; Laufer, S. A., Identification of regioisomers in a series of N-substituted pyridin-4-yl imidazole derivatives by regiospecific synthesis, GC/MS, and 1H NMR. *J. Org. Chem.* **2003**, *68*, 4527–4530.

7. De Simone, A.; Fiori, J.; Naldi, M.; D'Urzo, A.; Tumiatti, V.; Milelli, A.; Andrisano, V., Application of an ESI-QTOF method for the detailed characterization of GSK-3β inhibitors. *J. Pharm. Biomed. Anal.* **2017**, *144*, 159-166.

8. Kornacker, M. G.; Lai, Z.; Witmer, M.; Ma, J.; Hendrick, J.; Lee, V. G.; Riexinger, D. J.; Mapelli, C.; Metzler, W.; Copeland, R. A., An inhibitor binding pocket distinct from the catalytic active site on human β-APP cleaving enzyme. *Biochemistry* **2005**, *44*, 11567-73.

9. Harder, E.; Damm, W.; Maple, J.; Wu, C. J.; Reboul, M.; Xiang, J. Y.; Wang, L. L.; Lupyan, D.; Dahlgren, M. K.; Knight, J. L.; Kaus, J. W.; Cerutti, D. S.; Krilov, G.; Jorgensen, W. L.; Abel, R.; Friesner, R. A., OPLS3: A Force Field Providing Broad Coverage of Drug-like Small Molecules and Proteins. *J. Chem. Theory Comput.* **2016**, *12*, 281-296.

10. Roos, K.; Wu, C. J.; Damm, W.; Reboul, M.; Stevenson, J. M.; Lu, C.; Dahlgren, M. K.; Mondal, S.; Chen, W.; Wang, L. L.; Abel, R.; Friesner, R. A.; Harder, E. D., OPLS3e: Extending Force Field Coverage for Drug-Like Small Molecules. *J. Chem. Theory Comput.* **2019**, *15*, 1863-1874.

11. Bochevarov, A. D.; Harder, E.; Hughes, T. F.; Greenwood, J. R.; Braden, D. A.; Philipp, D. M.; Rinaldo, D.; Halls, M. D.; Zhang, J.; Friesner, R. A., Jaguar: A high-performance quantum chemistry software program with strengths in life and materials sciences. *International Journal of Quantum Chemistry* **2013**, *113*, 2110–2142.

12. Tesch, R.; Becker, C.; Muller, M. P.; Beck, M. E.; Quambusch, L.; Getlik, M.; Lategahn, J.; Uhlenbrock, N.; Costa, F. N.; Poleto, M. D.; Pinheiro, P. D. M.; Rodrigues, D. A.; Sant'Anna, C. M. R.; Ferreira, F. F.; Verli, H.; Fraga, C. A. M.; Rauh, D., An Unusual Intramolecular Halogen Bond Guides Conformational Selection. *Angew. Chem. Int. Ed.* **2018**, *57*, 9970-9975.

13. Sastry, G. M.; Adzhigirey, M.; Day, T.; Annabhimoju, R.; Sherman, W., Protein and ligand preparation: parameters, protocols, and influence on virtual screening enrichments. *J. Comput. Aid. Mol. Des.* **2013**, *27*, 221-234.

14. Farid, R.; Day, T.; Friesner, R. A.; Pearlstein, R. A., New insights about HERG blockade obtained from protein modeling, potential energy mapping, and docking studies. *Bioorg. Med. Chem.* **2006**, *14*, 3160-3173.

15. Sherman, W.; Beard, H. S.; Farid, R., Use of an induced fit receptor structure in virtual screening. *Chem. Biol. Drug Des.* **2006**, *67*, 83-4.

16. Sherman, W.; Day, T.; Jacobson, M. P.; Friesner, R. A.; Farid, R., Novel procedure for modeling ligand/receptor induced fit effects. *J. Med. Chem.* **2006**, *49*, 534-553.

17. Friesner, R. A.; Murphy, R. B.; Repasky, M. P.; Frye, L. L.; Greenwood, J. R.; Halgren, T. A.; Sanschagrin, P. C.; Mainz, D. T., Extra precision glide: Docking and scoring incorporating a model of hydrophobic enclosure for protein-ligand complexes. *J. Med. Chem.* **2006**, *49*, 6177-6196.

18. Greenwood, J. R.; Calkins, D.; Sullivan, A. P.; Shelley, J. C., Towards the comprehensive, rapid, and accurate prediction of the favorable tautomeric states of drug-like molecules in aqueous solution. *J. Comput. Aid. Mol. Des.* **2010**, *24*, 591-604.

19. Shelley, J. C.; Cholleti, A.; Frye, L. L.; Greenwood, J. R.; Timlin, M. R.; Uchimaya, M., Epik: a software program for pK (a) prediction and protonation state generation for drug-like molecules. *J. Comput. Aid. Mol. Des.* **2007**, *21*, 681-691.

20. Bowers, K. J. E., C.; Xu, H.; Dror, R. O.; Eastwood, M. P.; Gregerson, B. A.; Klepeis, J. L.; Kolossvary, I.; Moraes, M. A.; Sacerdoti, F. D.; Salmon, J. K.; Shan, Y.; Shaw, D. E., Algorithms for Molecular Dynamics Simulations on Commodity Clusters. Proceedings of the ACM/IEEE Conference on Supercomputing (SC06), Tampa, Florida. **2006**, November 11-17.

21. Jorgensen, W. L.; Chandrasekhar, J.; Madura, J. D.; Impey, R. W.; Klein, M. L., Comparison of Simple Potential Functions for Simulating Liquid Water. *J. Chem. Phys.* **1983**, *79*, 926-935.

List of synthesized compounds

ID	Structure	ID	Structure
PIT02 03001	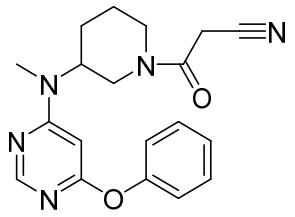	**PIT02 03007**	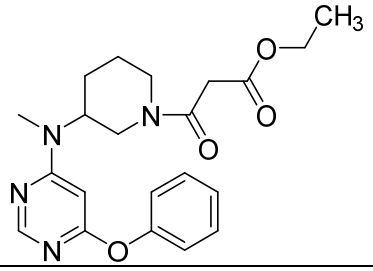
PIT02 03002	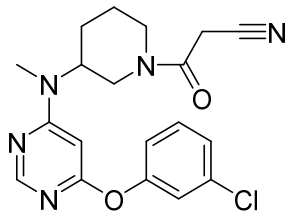	**PIT02 03008**	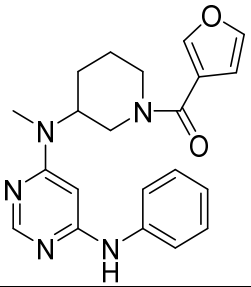
PIT02 03003	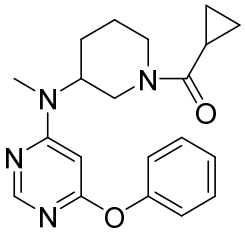	**PIT02 03009**	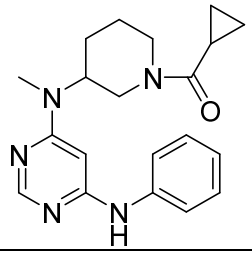
PIT02 03004	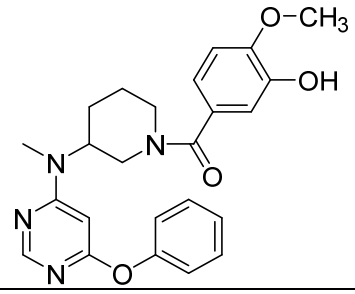	**PIT02 03010**	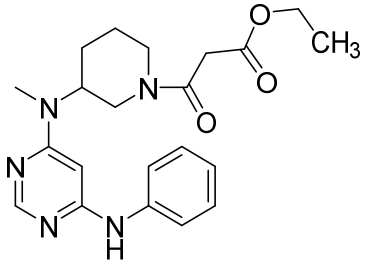
PIT02 03005	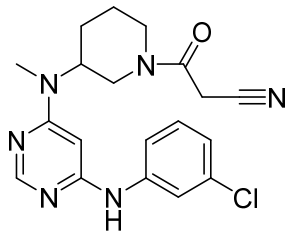	**PIT02 03011**	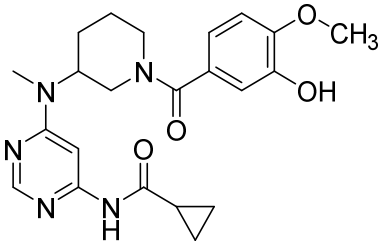
PIT02 03006	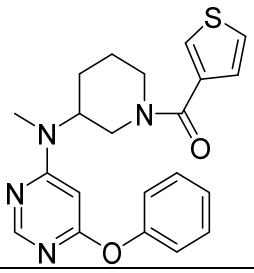	**PIT02 03012**	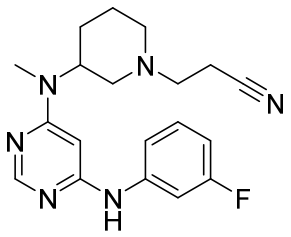

ID	Structure	ID	Structure
PIT02 03013	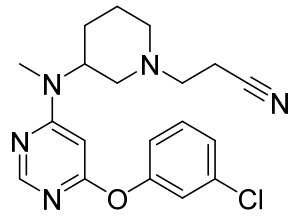	**PIT02 03020**	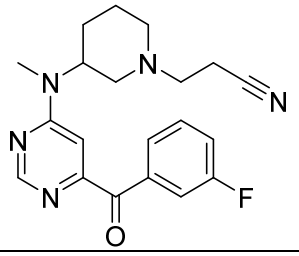
PIT02 03014	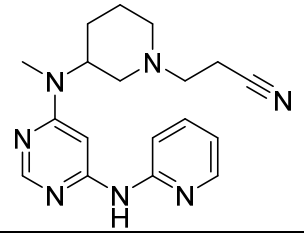	**PIT02 03021**	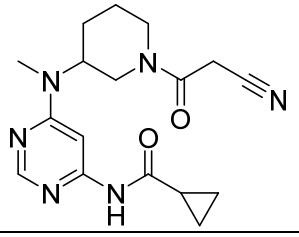
PIT02 03015	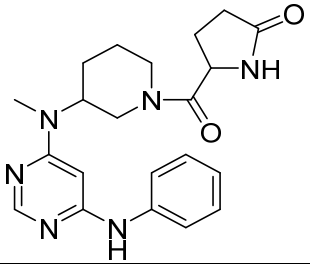	**PIT02 03022**	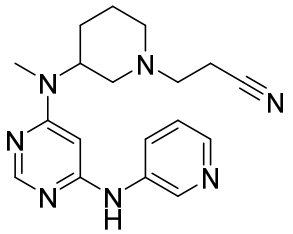
PIT02 03016	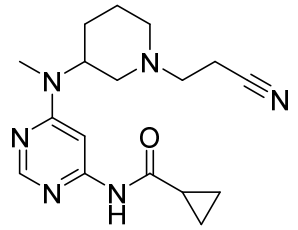	**PIT02 03023**	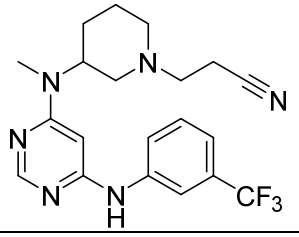
PIT02 03017	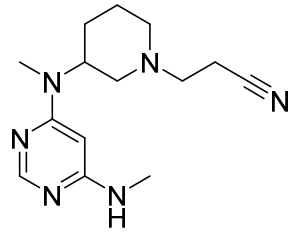	**PIT02 03024**	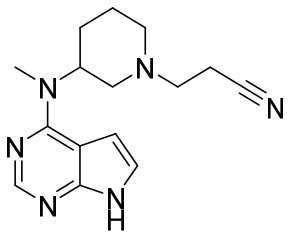
PIT02 03018	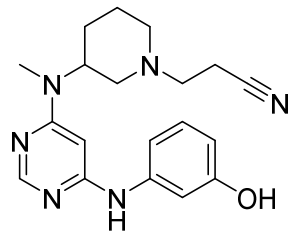	**PIT02 03025**	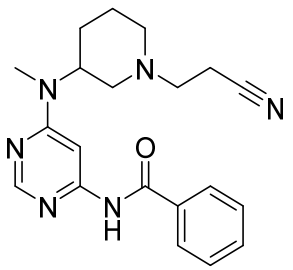
PIT02 03019	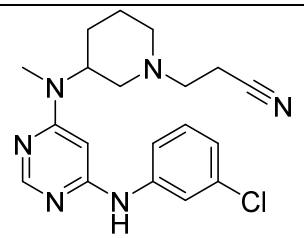	**PIT02 03026**	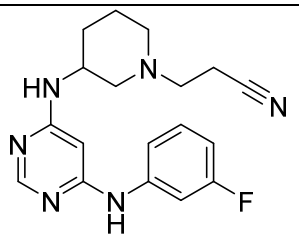

ID	Structure	ID	Structure
PIT02 03027	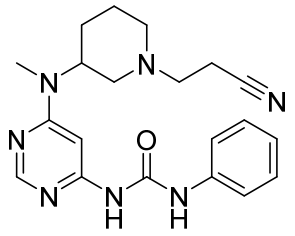	**PIT02 03034**	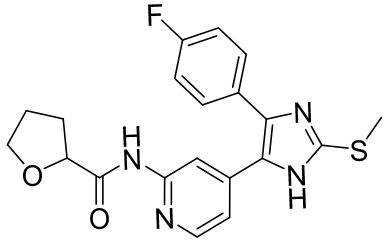
PIT02 03028	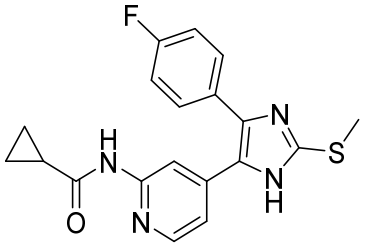	**PIT02 03035**	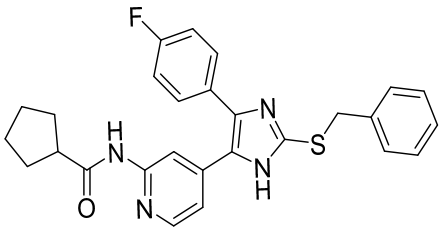
PIT02 03029	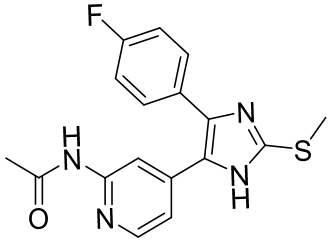	**PIT02 03036**	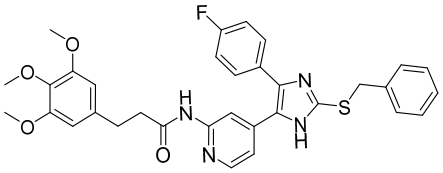
PIT02 03030	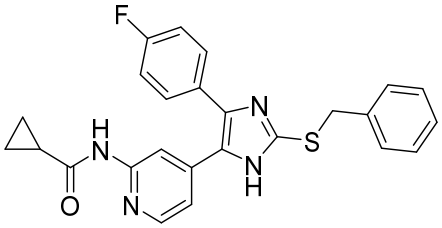	**PIT02 03037**	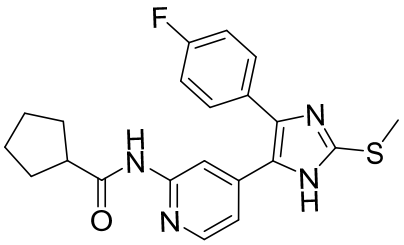
PIT02 03031	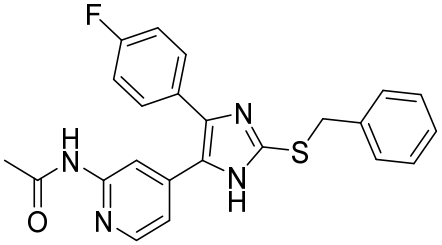	**PIT02 03038**	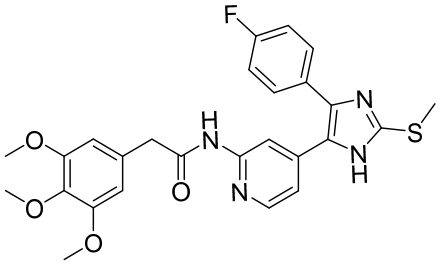
PIT02 03032	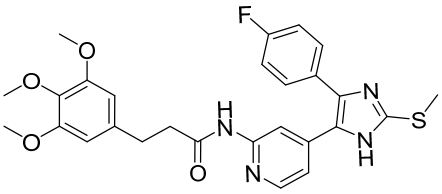	**PIT02 03039**	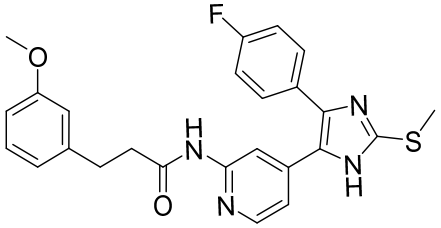
PIT02 03033	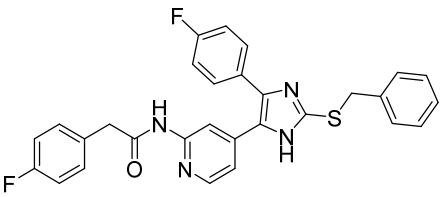	**PIT02 03040**	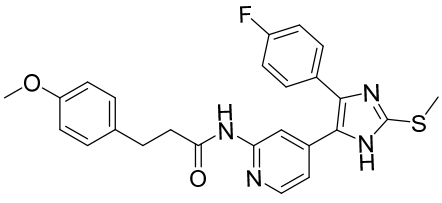

ID	Structure	ID	Structure
PIT02 03041	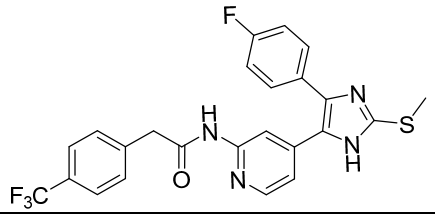	**PIT02 03049**	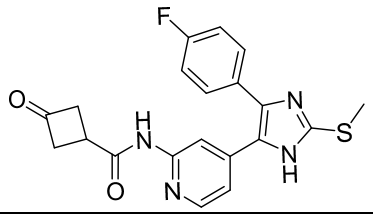
PIT02 03042	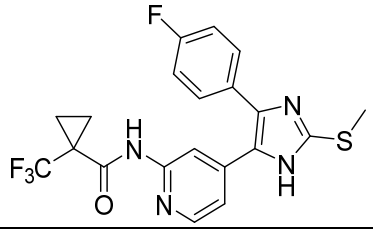	**PIT02 03051**	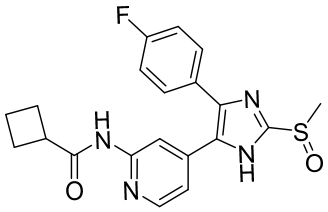
PIT02 03043	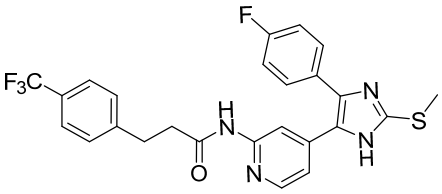	**PIT02 03052**	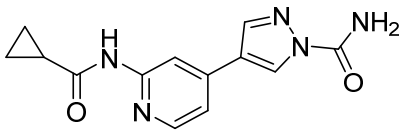
PIT02 03044	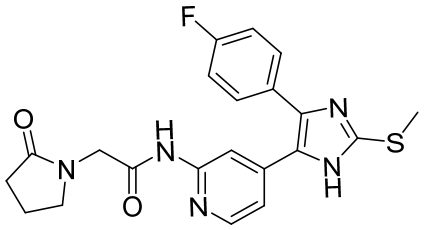	**PIT02 03053**	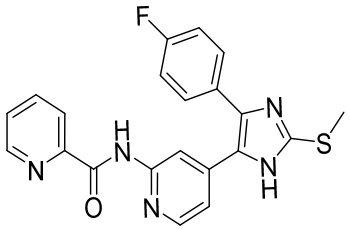
PIT02 03045	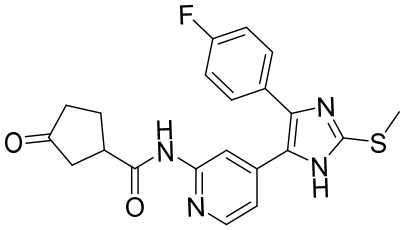	**PIT02 03054**	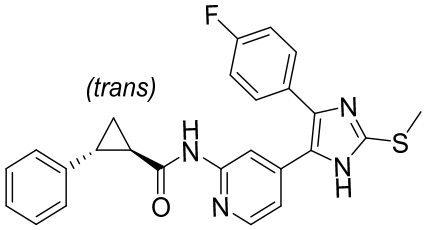
PIT02 03046	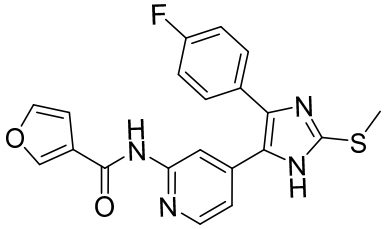	**PIT02 03055**	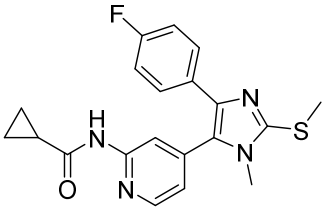
PIT02 03047	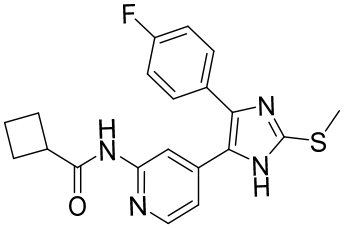	**PIT02 03056**	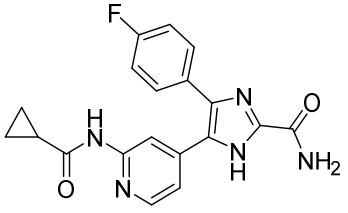
PIT02 03048	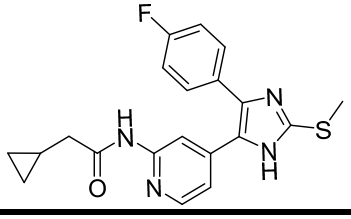	**PIT02 03057**	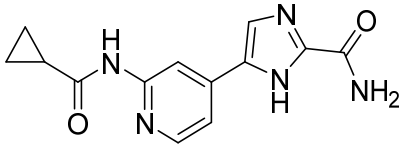

ID	Structure	ID	Structure
PIT02 03058	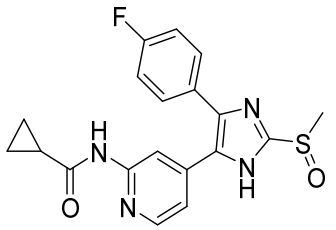	**PIT02 03065**	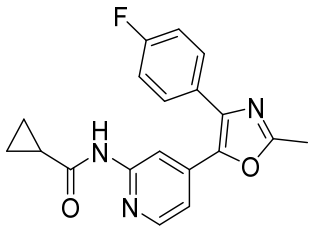
PIT02 03059	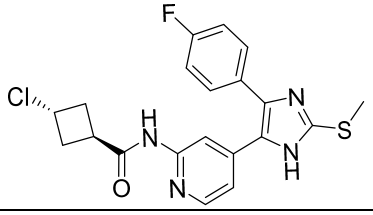	**PIT02 03066**	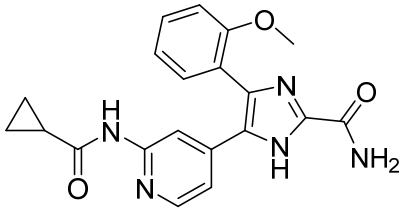
PIT02 03060	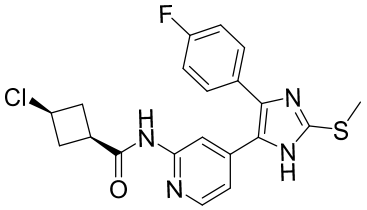	**PIT02 03068**	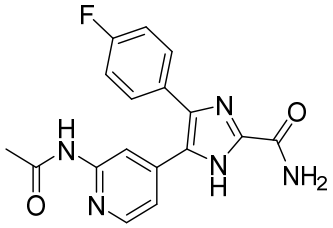
PIT02 03061	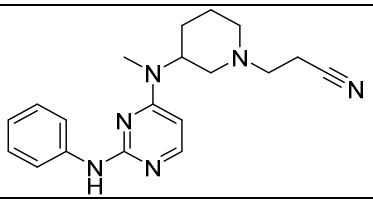	**PIT02 03069**	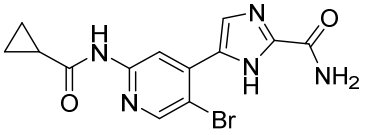
PIT02 03062	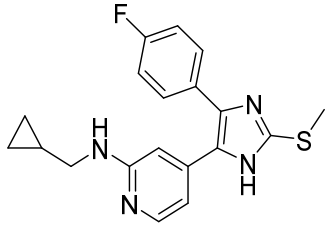	**PIT02 03070**	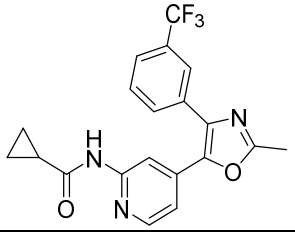
PIT02 03063	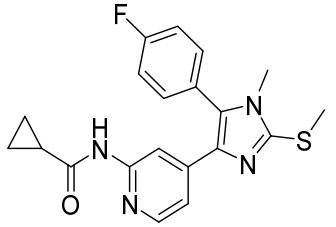	**PIT02 03071**	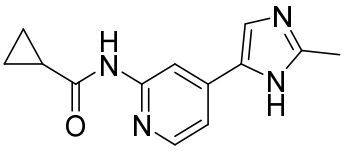
PIT02 03064	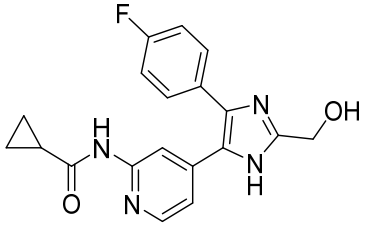	**PIT02 03072**	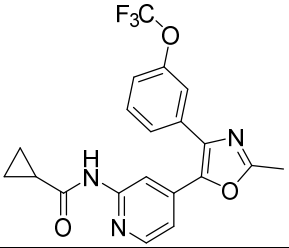
PIT02 03073	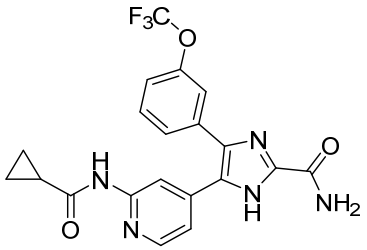	**PIT02 03081**	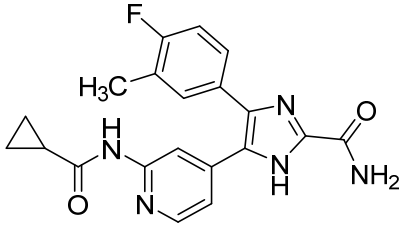

ID	Structure	ID	Structure
PIT02 03074	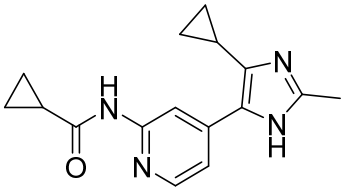	**PIT02 03082**	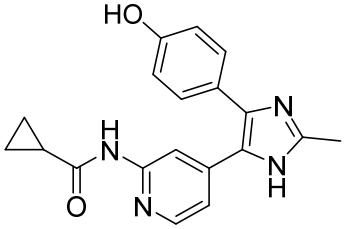
PIT02 03075	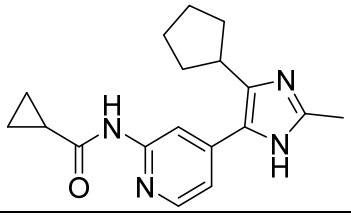	**PIT02 03083**	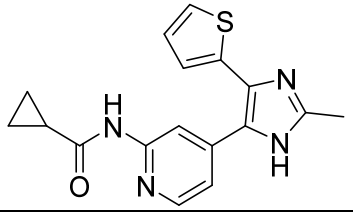
PIT02 03076	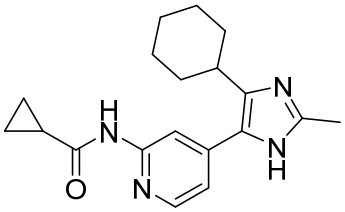	**PIT02 03084**	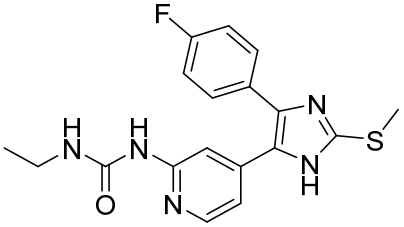
PIT02 03077	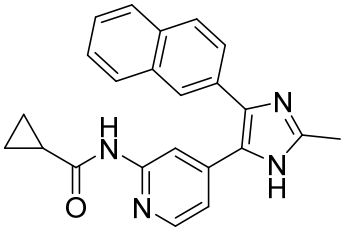	**PIT02 03085**	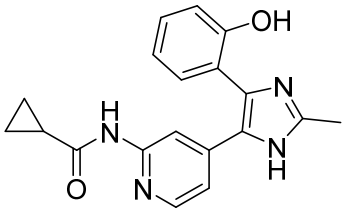
PIT02 03078	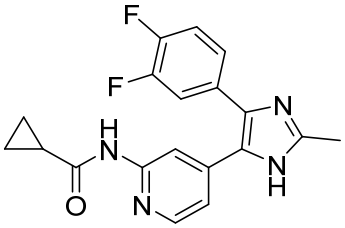	**PIT02 03086**	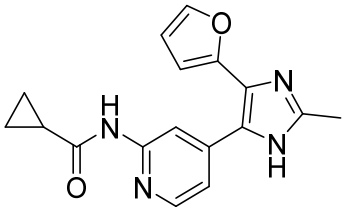
PIT02 03079	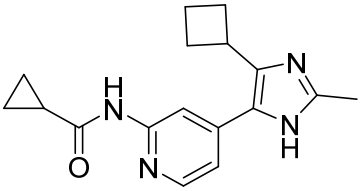	**PIT02 03087**	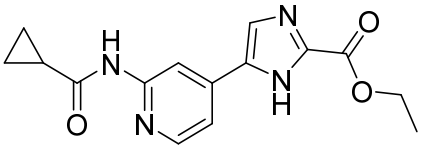
PIT02 03080	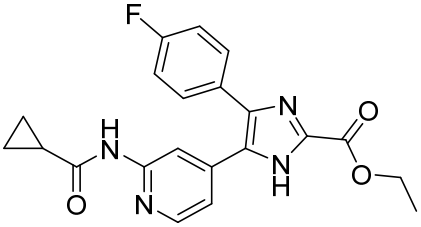	**PIT02 03088**	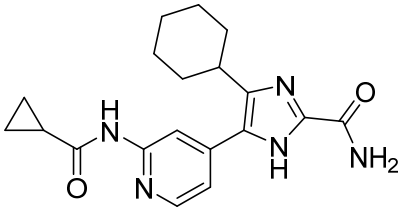
PIT02 03089	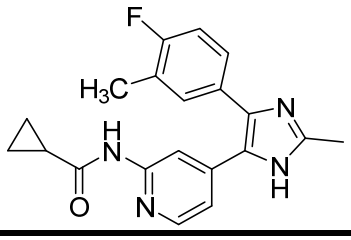	**PIT02 03095**	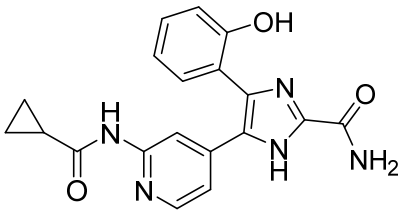

ID	Structure	ID	Structure
PIT02 03090	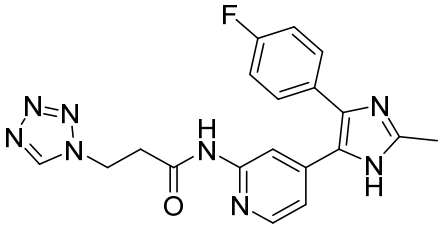	**PIT02 03096**	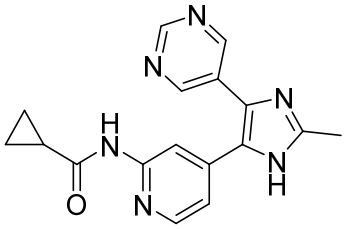
PIT02 03091	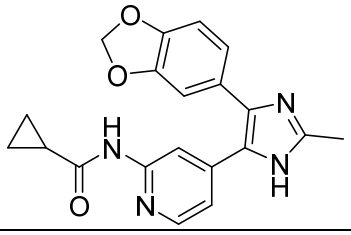	**PIT02 03097**	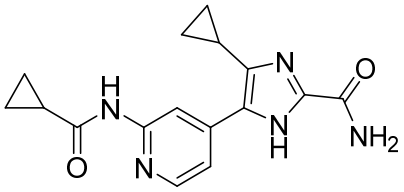
PIT02 03092	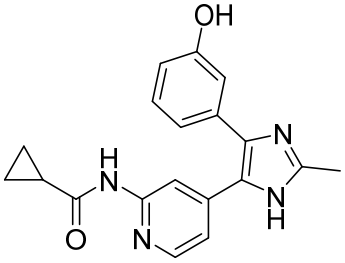	**PIT02 03098**	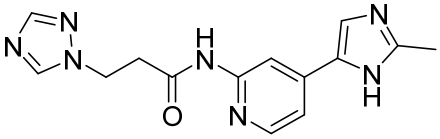
PIT02 03093	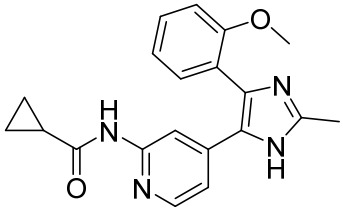	**PIT02 03099**	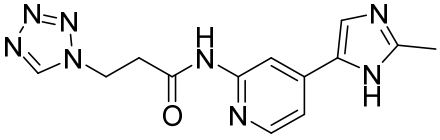
PIT02 03094	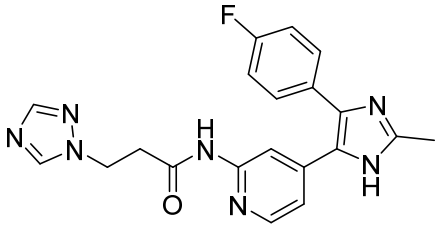	**PIT02 03100**